Annexes

AI

Annex I: Atlas of Global and Regional Climate Projections

Editorial Team:
Geert Jan van Oldenborgh (Netherlands), Matthew Collins (UK), Julie Arblaster (Australia), Jens Hesselbjerg Christensen (Denmark), Jochem Marotzke (Germany), Scott B. Power (Australia), Markku Rummukainen (Sweden), Tianjun Zhou (China)

Advisory Board:
David Wratt (New Zealand), Francis Zwiers (Canada), Bruce Hewitson (South Africa)

Review Editor Team:
Pascale Delecluse (France), John Fyfe (Canada), Karl Taylor (USA)

This annex should be cited as:
IPCC, 2013: Annex I: Atlas of Global and Regional Climate Projections [van Oldenborgh, G.J., M. Collins, J. Arblaster, J.H. Christensen, J. Marotzke, S.B. Power, M. Rummukainen and T. Zhou (eds.)]. In: *Climate Change 2013: The Physical Science Basis. Contribution of Working Group I to the Fifth Assessment Report of the Intergovernmental Panel on Climate Change* [Stocker, T.F., D. Qin, G.-K. Plattner, M. Tignor, S.K. Allen, J. Boschung, A. Nauels, Y. Xia, V. Bex and P.M. Midgley (eds.)]. Cambridge University Press, Cambridge, United Kingdom and New York, NY, USA.

Table of Contents

Introduction and Scope

This Annex presents a series of figures showing global and regional patterns of climate change computed from global climate model output gathered as part of the Coupled Model Intercomparison Project Phase 5 (CMIP5; Taylor et al., 2012). Maps of surface air temperature change and relative precipitation change (i.e., change expressed as a percentage of mean precipitation) in different seasons are presented for the globe and for a number of different sub-continental-scale regions. Twenty-year average changes for the near term (2016–2035), for the mid term (2046–2065) and for the long term (2081–2100) are given, relative to a reference period of 1986–2005. Time series for temperature and relative precipitation changes are shown for global land and sea averages, the 26 sub-continental SREX (IPCC Special Report on Managing the Risks of Extreme Events and Disasters to Advance Climate Change Adaptation) regions (IPCC, 2012) augmented with polar regions and the Caribbean, two Indian Ocean and three Pacific Ocean regions. In total this Annex gives projections for 35 regions, 2 variables and 2 seasons. The projections are made under the Representative Concentration Pathway (RCP) scenarios, which are introduced in Chapter 1 with more technical detail given in Section 12.3 (also note the discussion of near-term biases in Sections 11.3.5.1 and 11.3.6.1). Maps are shown only for the RCP4.5 scenario; however, the time series presented show how the area-average response varies among the RCP2.6, RCP4.5, RCP6.0 and RCP8.5 scenarios. Spatial maps for the other RCP scenarios and additional seasons are presented in the Annex I Supplementary Material. Figures AI.1 and AI.2 give a graphical explanation of aspects of both the time series plots and the spatial maps. While some of the background to the information presented is given here, discussion of the maps and time series, as well as important additional background, is provided in Chapters 9, 11, 12 and 14. Figure captions on each page of the Atlas reference the specific sub-sections in the report relevant to the regions considered on that page.

The projection of future climate change involves the careful evaluation of models, taking into account uncertainties in observations and consideration of the physical basis of the findings, in order to characterize the credibility of the projections and assess their sensitivity to uncertainties. As discussed in Chapter 9, different climate models have varying degrees of success in simulating past climate variability and mean state when compared to observations. Verification of regional trends is discussed in Box 11.2 and provides further information on the credibility of model projections. The information presented in this Annex is based entirely on all available CMIP5 model output with equal weight given to each model or version with different parameterizations.

Complementary methods for making quantitative projections, in which model output is combined with information about model performance using statistical techniques, exist and should be considered in impacts studies (see Sections 9.8.3, 11.3.1 and 12.2.2 to 12.2.3). Although results from the application of such methods can be assessed alongside the projections from CMIP5 presented here, it is beyond the scope of this Annex. Nor do the simple maps provided represent a robust estimate of the uncertainty associated with the projections. Here the range of model spread is provided as a simple, albeit imperfect, guide to the range of possible futures (including the effect of natural variability). Alternative approaches used to estimate projection uncertainty are discussed in Sections 11.3.1 and 12.2.2 to 12.2.3. The reliability of past trends is assessed in Box 11.2, which concludes that the time series and maps cannot be interpreted literally as probability density functions. They should not be interpreted as 'forecasts'.

Projections of future climate change are conditional on assumptions of climate forcing, affected by shortcomings of climate models and inevitably also subject to internal variability when considering specific periods. Projected patterns of climate change may differ from one climate model generation to the next due to improvements in models. Some model-inadequacies are common to all models, but so are many patterns of change across successive generations of models, which gives some confidence in projections. The information presented is intended to be only a starting point for anyone interested in more detailed information on projections of future climate change and complements the assessment in Chapters 11, 12 and 14.

Technical Notes

Data and Processing: The figures have been constructed using the CMIP5 model output available at the time of the AR5 cut-off for accepted papers (15 March 2013). This data set comprises 32/42/25/39 scenario experiments for RCP2.6/4.5/6.0/8.5 from 42 climate models (Table AI.1). Only concentration-driven experiments are used (i.e., those in which concentrations rather than emissions of greenhouse gases are prescribed) and only one ensemble member from each model is selected, even if multiple realizations exist with different initial conditions and different realizations of natural variability. Hence each model is given equal weight. Maps from only one scenario (RCP4.5) are shown but time series are included from all four RCPs. Maps from other RCPs are presented in the Annex I Supplementary Material.

Reference Period: Projections are expressed as anomalies with respect to the reference period of 1986–2005 for both time series and spatial maps (i.e., differences between the future period and the reference period). Thus the changes are relative to the climate change that has already occurred since the pre-industrial period and which is discussed in Chapters 2 and 10. For quantities where the trend is larger than the natural variability such as large-area temperature changes, a more recent reference period would give better estimates (see Section 11.3.6.1); for quantities where the natural variability is much larger than the trend a longer reference period would be preferable.

Equal Model Weighting: Model evaluation uses a multitude of techniques (see Chapter 9) and there is no consensus in the community about how to use this information to assign likelihood to different model projections. Consequently, the different CMIP5 models used for the projections in the Atlas are all considered to give equally likely projections in the sense of 'one model, one vote'. Models with variations in physical parameterization schemes are treated as distinct models.

Variables: Two variables have been plotted: surface air temperature change and relative precipitation change. The relative precipitation change is defined as the percentage change from the 1986–2005 reference period in each ensemble member. For the time series, the variables are first averaged over the domain and then the changes from the reference period are computed. This implies that in regions with

large climatological precipitation gradients, the change is generally dominated by the areas with the most precipitation.

Seasons: For temperature, the standard meteorological seasons June to August and December to February are shown, as these often correspond roughly with the warmest and coldest seasons. The annual mean and remaining seasons, March to May and September to October can be found in the Annex I Supplementary Material. For precipitation, the half-years April to September and October to March are shown so that in most monsoon areas the local rain seasons are entirely contained within the seasonal range plotted. Because the seasonal average is computed first, followed by the percentile change, these numbers are dominated by the rainy months within the half-year. The annual means are included in the Supplementary Material.

Regions: In addition to the global maps, the areas defined in the SREX (IPCC, 2012) are plotted with the addition of six regions containing the Caribbean, Indian Ocean and Pacific Island States and land and sea areas of the two polar regions. For regions containing large land-areas, averages are computed only over land grid points only. For ocean regions, averages are computed over both land and ocean grid points (see figure captions). A grid box is considered land if the land fraction is larger than 50% and sea if it is smaller than this. SREX regions with long coastlines (west coast of South America, North Europe, South-east Asia) therefore include some influence of the ocean. Note that temperature and precipitation over islands may be very different from those over the surrounding sea.

Time Series: For each of the resulting areas the areal mean is computed on the original model grid using land, sea or all points, depending on the definition of the region (see above). As an indication of the model uncertainty and natural variability, the time series of each model and scenario over the common period 1900–2100 are shown on the top of the page as anomalies relative to 1986–2005 (the seasons December to February and October to March are counted towards the second year in the interval). The multi-model ensemble means are also shown. Finally, for the period 2081–2100, the 20-year means are computed and the box-and-whisker plots show the 5th, 25th, 50th (median), 75th and 95th percentiles sampled over the distribution of the 20-year means of the model time series indicated in Table AI.1, including both natural variability and model spread. In the 20-year means the natural variability is suppressed relative to the annual values in the time series whereas the model uncertainty is the same. Note that owing to a smaller number of models, the box-and-whisker plots for the RCP2.6 scenario and especially the RCP6.0 scenario are less certain than those for RCP4.5 and RCP8.5.

Spatial Maps: The maps in the Atlas show, for an area encompassing two or three regions, the difference between the periods 2016–2035, 2046–2065 and 2081–2100 and the reference period 1986–2005. As local projections of climate change are uncertain, a measure of the range of model projections is shown in addition to the median response of the model ensemble interpolated to a common 2.5° grid (the interpolation was done bilinearly for surface air temperature and first order conservatively for precipitation). It should again be emphasized (see above) that this range does not represent the full uncertainty in the projection. On the left, the 25th percentile of the distribution of ensemble members is shown, on the right the 75th percentile. The median is shown in the middle (different from similar plots in Chapters 11 and 12 and the time series which show the multi-model mean). The distribution combines the effects of natural variability and model spread. The colour scale is kept constant over all maps.

Hatching: Hatching indicates regions where the magnitude of the change of the 20-year mean is less than 1 standard deviation of model-estimated present-day natural variability of 20-year mean differences. The natural variability is estimated using all pre-industrial control runs which are at least 500 years long. The first 100 years of the pre-industrial are ignored. The natural variability is then calculated for every grid point as the standard deviation of non-overlapping 20-year means after a quadratic fit is subtracted at every grid point to eliminate model drift. This is multiplied by the square root of 2, a factor that arises as the comparison is between two distributions of numbers. The median across all models of that quantity is used. This characterizes the typical difference between two 20-year averages that would be expected due to unforced internal variability. The hatching is applied to all maps so, for example, if the 25th percentile of the distribution of model projections is less than 1 standard deviation of natural variability, it is hatched.

The hatching can be interpreted as some indication of the strength of the future anomalies from present-day climate, when compared to the strength of present day internal 20-year variability. It either means that the change is relatively small or that there is little agreement between models on the sign of the change. It is presented only as a guide to assessing the strength of change as the difference between two 20-year intervals. Using other measures of natural variability would give smaller or larger hatched areas, but the colours underneath the hatching would not be very different. Other methods of hatching and stippling are possible (see Box 12.1) and, in cases where such information is critical, it is recommended that thorough attention is paid to assessing significance using a statistical test appropriate to the problem being considered.

Scenarios: Spatial patterns of changes for scenarios other than RCP4.5 can be found in the Annex I Supplementary Material.

References

IPCC, 2012: *Managing the Risks of Extreme Events and Disasters to Advance Climate Change Adaptation.* A Special Report of Working Groups I and II of the Intergovernmental Panel on Climate Change [C. B. Field, V. Baros, T. F. Stocker, D. Qin, D. J. Dokken, K. L. Ebi, M. D. Mastrandrea, K .J. Mach, G.-K. Plattner, S. K. Allen, M. Tignor and P. M. Midgley (eds.)]. Cambridge University Press, Cambridge, United Kingdom, and New York, NY, USA, 582 pp.

Taylor, K. E., R. J. Stouffer, and G. A. Meehl, 2012: A summary of the CMIP5 experiment design. *Bull. Am. Meteorol. Soc.*, **93**, 485–498.

Table AI.1 | The CMIP5 models used in this Annex for each of the historical and RCP scenario experiments. A number in each column is the identifier of the single ensemble member from that model that is used. A blank indicates no run was used, usually because that scenario run was not available. For the pre-industrial control column (piControl), a 'tas' indicates that those control simulations are used in the estimate of internal variability of surface air temperature and a 'pr' indicates that those control simulations are used in the estimate of precipitation internal variability.

CMIP5 Model Name	piControl	Historical	RCP2.6	RCP4.5	RCP6.0	RCP8.5
ACCESS1-0	tas/pr	1		1		1
ACCESS1-3	tas/pr	1		1		1
bcc-csm1-1	tas/pr	1	1	1	1	1
bcc-csm1-1-m		1	1	1	1	
BNU-ESM	tas/pr	1	1	1		1
CanESM2	tas/pr	1	1	1		1
CCSM4	tas/pr	1	1	1	1	1
CESM1-BGC	tas/pr	1		1		1
CESM1-CAM5		1	1	1	1	1
CMCC-CM		1		1		1
CMCC-CMS	tas/pr	1		1		1
CNRM-CM5	tas/pr	1	1	1		1
CSIRO-Mk3-6-0	tas/pr	1	1	1	1	1
EC-EARTH		8	8	8		8
FGOALS-g2	tas/pr	1	1	1		1
FIO-ESM	tas/pr	1	1	1	1	1
GFDL-CM3	tas/pr	1	1	1	1	1
GFDL-ESM2G	tas/pr	1	1	1	1	1
GFDL-ESM2M	tas/pr	1	1	1	1	1
GISS-E2-H p1		1	1	1	1	1
GISS-E2-H p2	tas/pr	1	1	1	1	1
GISS-E2-H p3	tas/pr	1	1	1	1	1
GISS-E2-H-CC		1		1		
GISS-E2-R p1		1	1	1	1	1
GISS-E2-R p2	pr	1	1	1	1	1
GISS-E2-R p3	pr	1	1	1	1	1
GISS-E2-R-CC		1		1		
HadGEM2-AO		1	1	1	1	1
HadGEM2-CC		1		1		1
HadGEM2-ES		2	2	2	2	2
inmcm4	tas/pr	1		1		1
IPSL-CM5A-LR	tas/pr	1	1	1	1	1
IPSL-CM5A-MR		1	1	1	1	1
IPSL-CM5B-LR		1		1		1
MIROC5	tas/pr	1	1	1	1	1
MIROC-ESM	tas/pr	1	1	1	1	1
MIROC-ESM-CHEM		1	1	1	1	1
MPI-ESM-LR	tas/pr	1	1	1		1
MPI-ESM-MR	tas/pr	1	1	1		1
MPI-ESM-P	tas/pr					
MRI-CGCM3	tas/pr	1	1	1	1	1
NorESM1-M	tas/pr	1	1	1	1	1
NorESM1-ME		1	1	1	1	1
Number of models		42	32	42	25	39

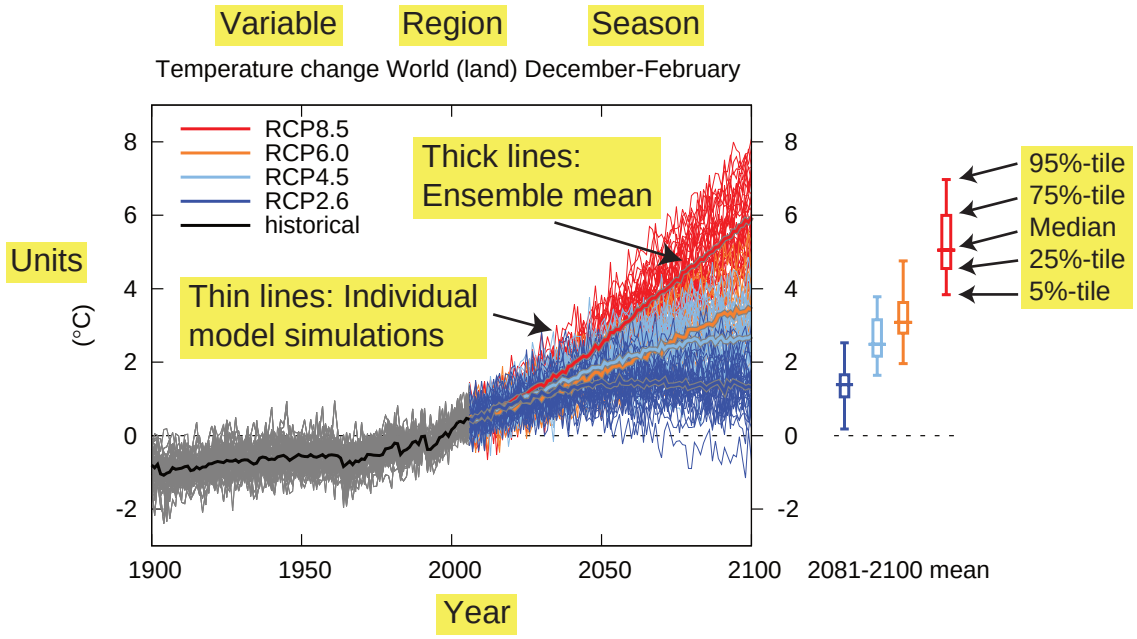

Figure AI.1 | Explanation of the features of a typical time series figure presented in Annex I.

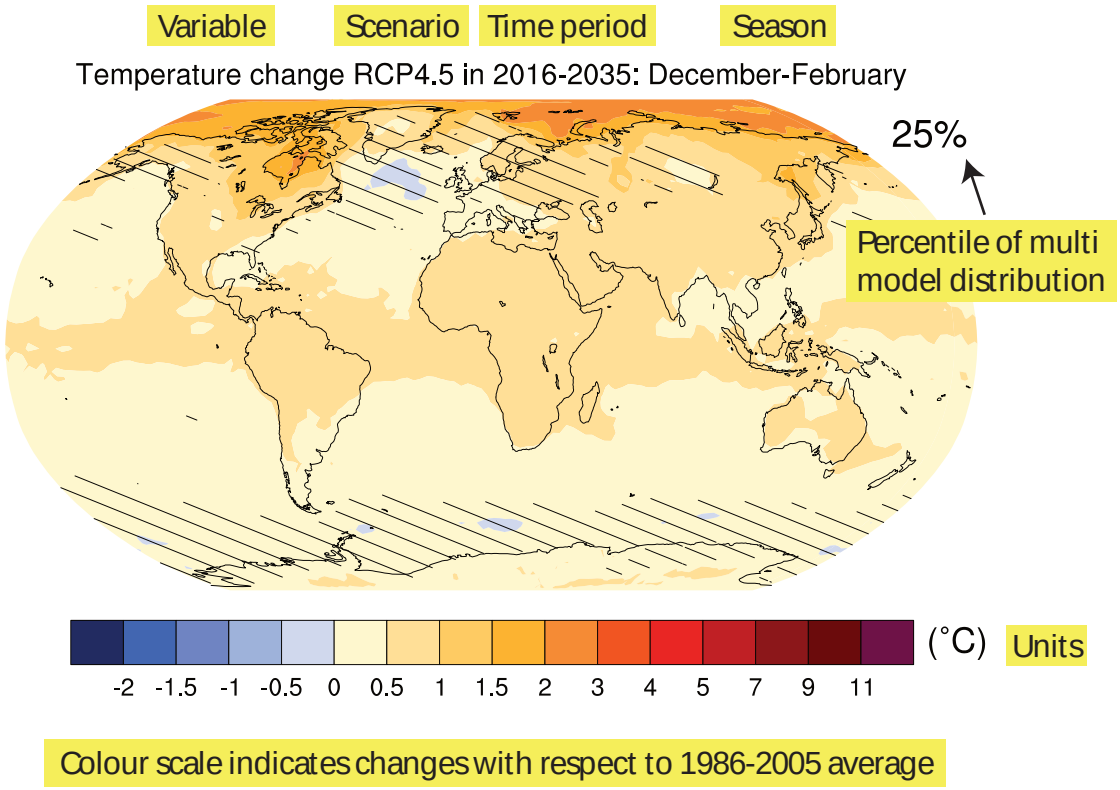

Figure AI.2 | Explanation of the features of a typical spatial map presented in Annex I. Hatching indicates regions where the magnitude of the 25th, median or 75th percentile of the 20-year mean change is less than 1 standard deviation of model-estimated natural variability of 20-year mean differences.

Atlas

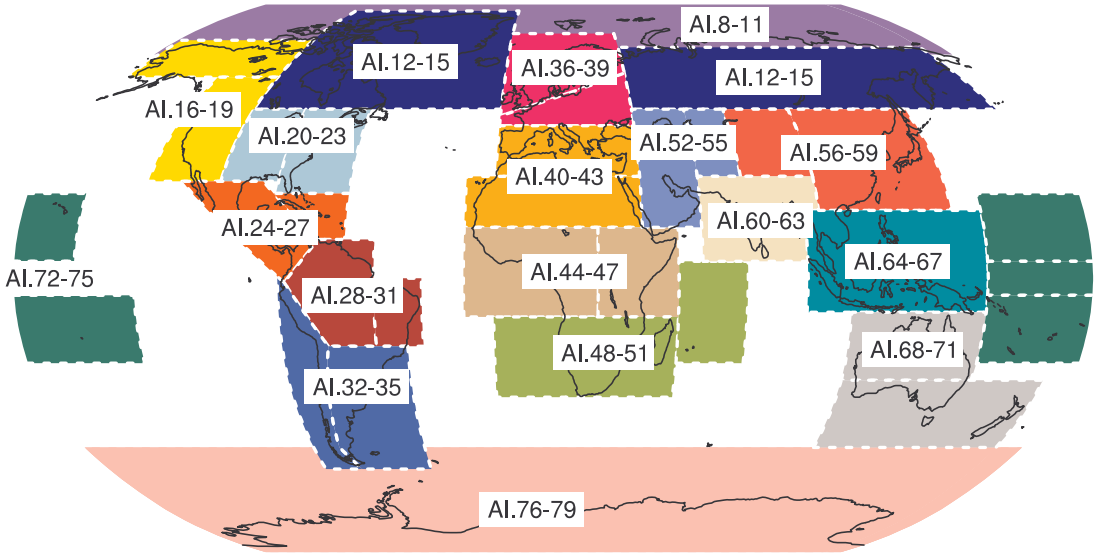

Figure AI.3 | Overview of the SREX, ocean and polar regions used.

Figures AI.4 to AI.7: World
Figures AI.8 to AI.11: Arctic
Figures AI.12 to AI.15: High latitudes
Figures AI.16 to AI.19: North America (West)
Figures AI.20 to AI.23: North America (East)
Figures AI.24 to AI.27: Central America and Caribbean
Figures AI.28 to AI.31: Northern South America
Figures AI.32 to AI.35: Southern South America
Figures AI.36 to AI.39: North and Central Europe
Figures AI.40 to AI.43: Mediterranean and Sahara
Figures AI.44 to AI.47: West and East Africa
Figures AI.48 to AI.51: Southern Africa and West Indian Ocean
Figures AI.52 to AI.55: West and Central Asia
Figures AI.56 to AI.59: Eastern Asia and Tibetan Plateau
Figures AI.60 to AI.63: South Asia
Figures AI.64 to AI.67: Southeast Asia
Figures AI.68 to AI.71: Australia and New Zealand
Figures AI.72 to AI.75: Pacific Islands region
Figures AI.76 to AI.79: Antarctica

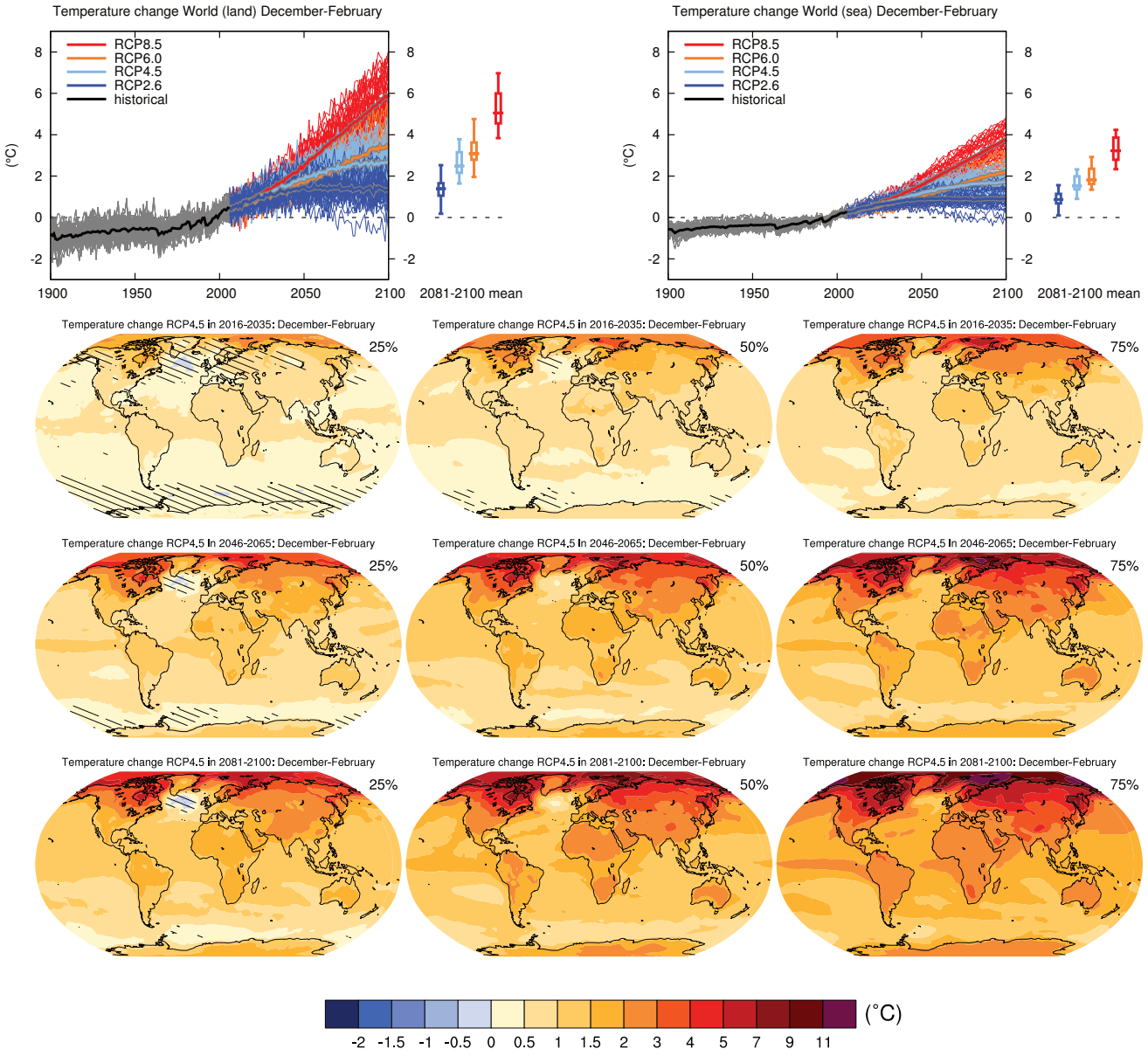

Figure AI.4 | (Top left) Time series of temperature change relative to 1986–2005 averaged over land grid points over the globe in December to February. (Top right) Same for sea grid points. Thin lines denote one ensemble member per model, thick lines the CMIP5 multi-model mean. On the right-hand side the 5th, 25th, 50th (median), 75th and 95th percentiles of the distribution of 20-year mean changes are given for 2081–2100 in the four RCP scenarios.

(Below) Maps of temperature changes in 2016–2035, 2046–2065 and 2081–2100 with respect to 1986–2005 in the RCP4.5 scenario. For each point, the 25th, 50th and 75th percentiles of the distribution of the CMIP5 ensemble are shown; this includes both natural variability and inter-model spread. Hatching denotes areas where the 20-year mean differences of the percentiles are less than the standard deviation of model-estimated present-day natural variability of 20-year mean differences.

Sections 9.4.1.1, 9.6.1.1, 10.3.1.1.4, 11.3.2.1.2, 11.3.3.1, Box 11.2, 12.4.3.1 and 12.4.7 contain relevant information regarding the evaluation of models in this region, the model spread in the context of other methods of projecting changes and the role of modes of variability and other climate phenomena.

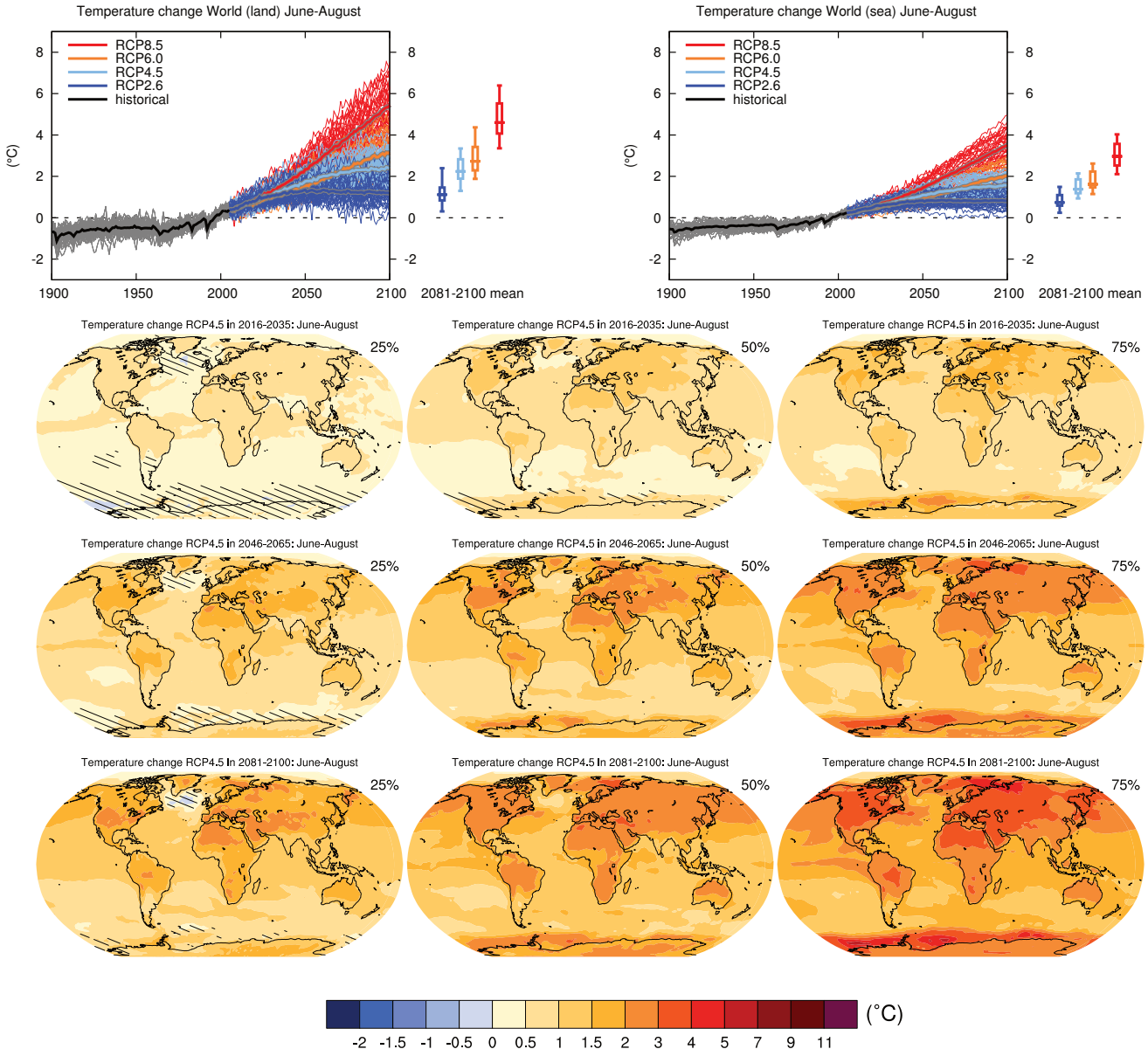

Figure AI.5 | (Top left) Time series of temperature change relative to 1986–2005 averaged over land grid points over the globe in June to August. (Top right) Same for sea grid points. Thin lines denote one ensemble member per model, thick lines the CMIP5 multi-model mean. On the right-hand side the 5th, 25th, 50th (median), 75th and 95th percentiles of the distribution of 20-year mean changes are given for 2081–2100 in the four RCP scenarios.

(Below) Maps of temperature changes in 2016–2035, 2046–2065 and 2081–2100 with respect to 1986–2005 in the RCP4.5 scenario. For each point, the 25th, 50th and 75th percentiles of the distribution of the CMIP5 ensemble are shown; this includes both natural variability and inter-model spread. Hatching denotes areas where the 20-year mean differences of the percentiles are less than the standard deviation of model-estimated present-day natural variability of 20-year mean differences.

Sections 9.4.1.1, 9.6.1.1, 10.3.1.1.4, 11.3.2.1.2, 11.3.3.1, Box 11.2, 12.4.3.1 and 12.4.7 contain relevant information regarding the evaluation of models in this region, the model spread in the context of other methods of projecting changes and the role of modes of variability and other climate phenomena.

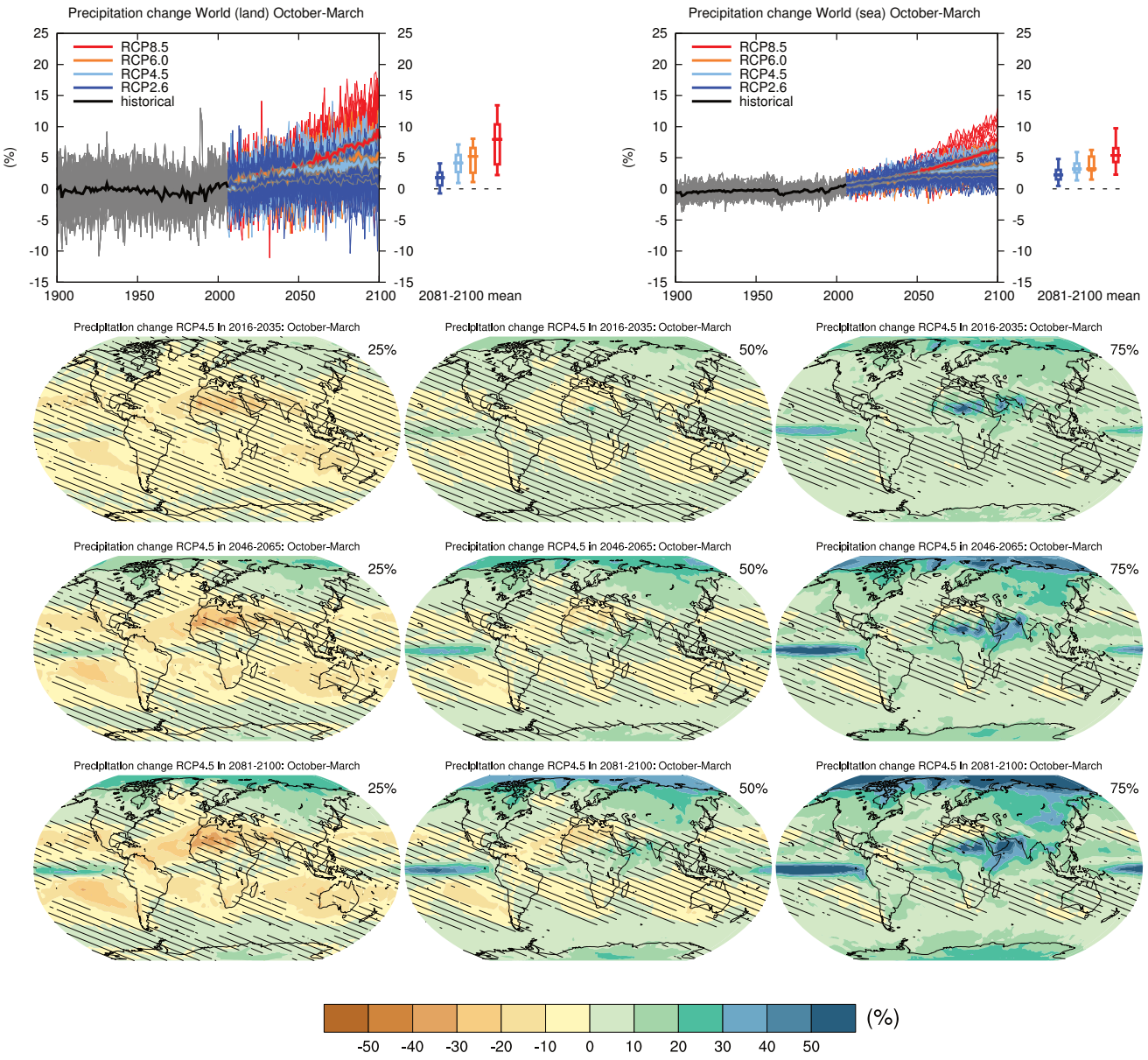

Figure AI.6 | (Top left) Time series of relative change relative to 1986–2005 in precipitation averaged over land grid points over the globe in October to March. (Top right) Same for sea grid points. Thin lines denote one ensemble member per model, thick lines the CMIP5 multi-model mean. On the right-hand side the 5th, 25th, 50th (median), 75th and 95th percentiles of the distribution of 20-year mean changes are given for 2081–2100 in the four RCP scenarios.

(Below) Maps of precipitation changes in 2016–2035, 2046–2065 and 2081–2100 with respect to 1986–2005 in the RCP4.5 scenario. For each point, the 25th, 50th and 75th percentiles of the distribution of the CMIP5 ensemble are shown; this includes both natural variability and inter-model spread. Hatching denotes areas where the 20-year mean differences of the percentiles are less than the standard deviation of model-estimated present-day natural variability of 20-year mean differences.

Sections 9.4.1.1, 9.6.1.1, 10.3.2.2, 11.3.2.3.1, Box 11.2, 12.4.5.2, 14.2 contain relevant information regarding the evaluation of models in this region, the model spread in the context of other methods of projecting changes and the role of modes of variability and other climate phenomena.

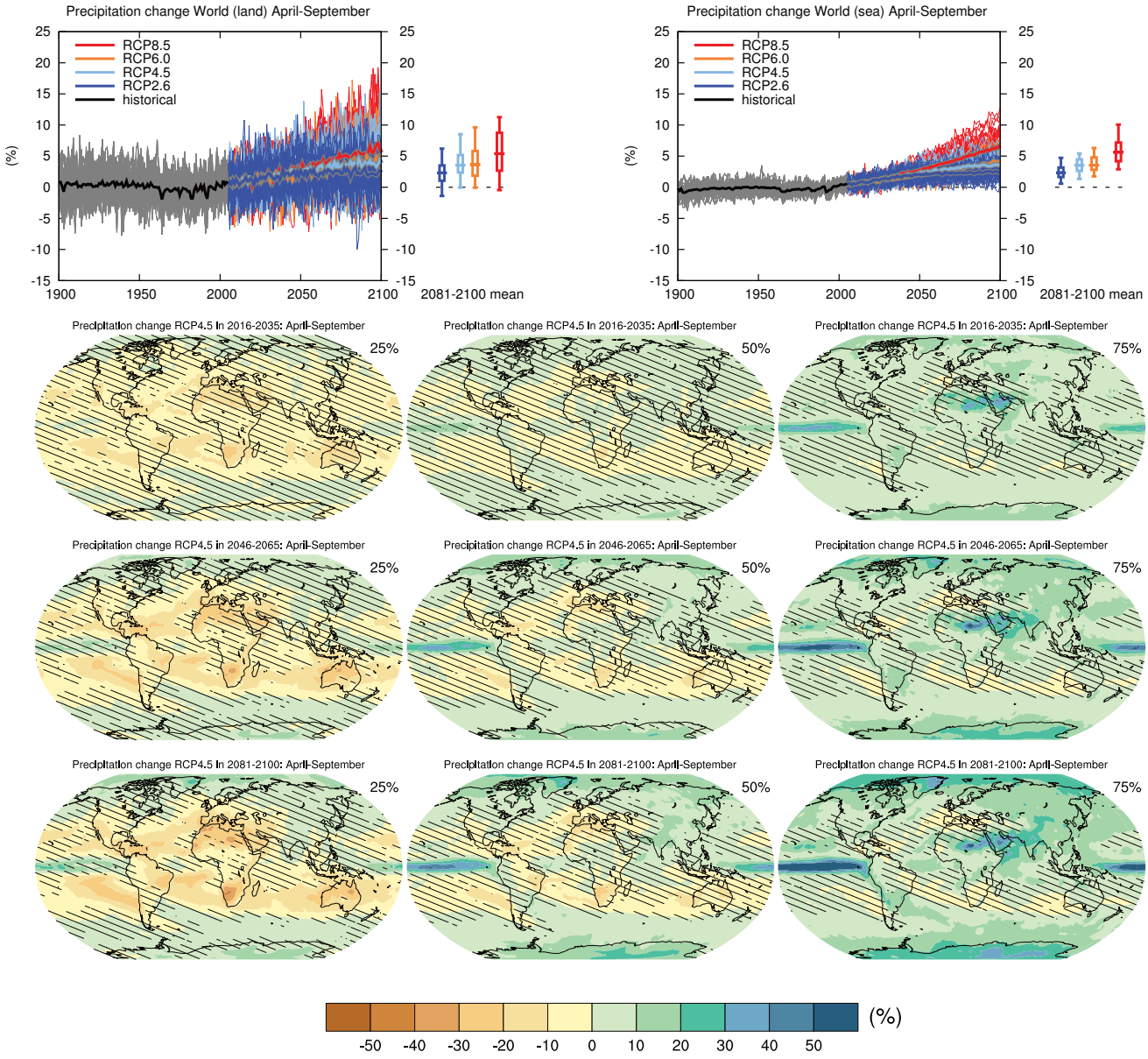

Figure AI.7 | (Top left) Time series of relative change relative to 1986–2005 in precipitation averaged over land grid points over the globe in April to September. (Top right) Same for sea grid points. Thin lines denote one ensemble member per model, thick lines the CMIP5 multi-model mean. On the right-hand side the 5th, 25th, 50th (median), 75th and 95th percentiles of the distribution of 20-year mean changes are given for 2081–2100 in the four RCP scenarios.

(Below) Maps of precipitation changes in 2016–2035, 2046–2065 and 2081–2100 with respect to 1986–2005 in the RCP4.5 scenario. For each point, the 25th, 50th and 75th percentiles of the distribution of the CMIP5 ensemble are shown; this includes both natural variability and inter-model spread. Hatching denotes areas where the 20-year mean differences of the percentiles are less than the standard deviation of model-estimated present-day natural variability of 20-year mean differences.

Sections 9.4.1.1, 9.6.1.1, 10.3.2.2, 11.3.2.3.1, Box 11.2, 12.4.5.2, 14.2 contain relevant information regarding the evaluation of models in this region, the model spread in the context of other methods of projecting changes and the role of modes of variability and other climate phenomena.

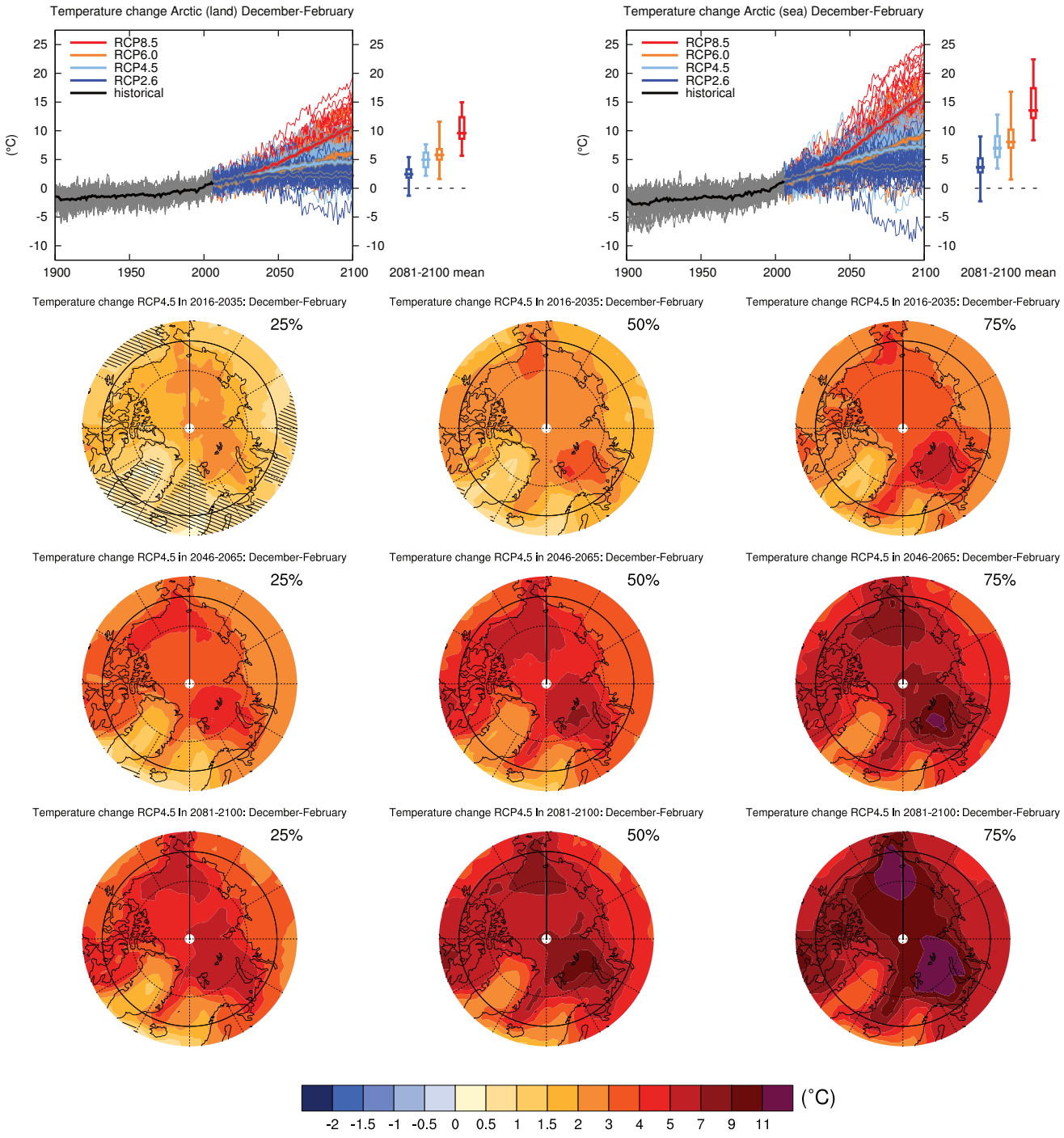

Figure AI.8 | (Top left) Time series of temperature change relative to 1986–2005 averaged over land grid points in the Arctic (67.5°N to 90°N) in December to February. (Top right) Same for sea grid points. Thin lines denote one ensemble member per model, thick lines the CMIP5 multi-model mean. On the right-hand side the 5th, 25th, 50th (median), 75th and 95th percentiles of the distribution of 20-year mean changes are given for 2081–2100 in the four RCP scenarios.

(Below) Maps of temperature changes in 2016–2035, 2046–2065 and 2081–2100 with respect to 1986–2005 in the RCP4.5 scenario. For each point, the 25th, 50th and 75th percentiles of the distribution of the CMIP5 ensemble are shown; this includes both natural variability and inter-model spread. Hatching denotes areas where the 20-year mean differences of the percentiles are less than the standard deviation of model-estimated present-day natural variability of 20-year mean differences.

Sections 9.4.1.1, 9.6.1.1, 10.3.1.1.4, 11.3.2.1.2, Box 11.2, 12.4.3.1, 14.8.2 contain relevant information regarding the evaluation of models in this region, the model spread in the context of other methods of projecting changes and the role of modes of variability and other climate phenomena.

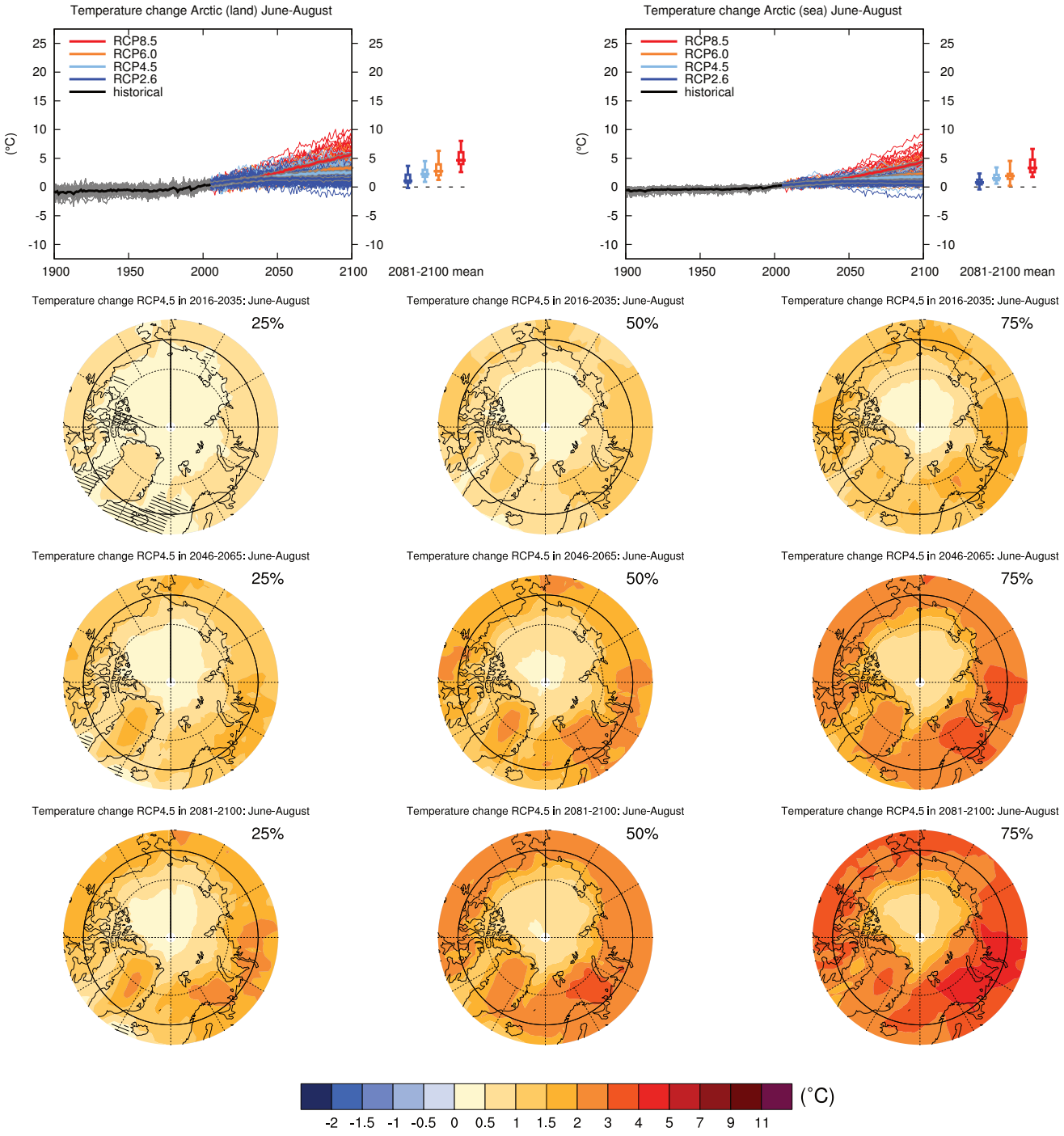

Figure AI.9 | (Top left) Time series of temperature change relative to 1986–2005 averaged over land grid points in the Arctic (67.5°N to 90°N) in June to August. (Top right) Same for sea grid points. Thin lines denote one ensemble member per model, thick lines the CMIP5 multi-model mean. On the right-hand side the 5th, 25th, 50th (median), 75th and 95th percentiles of the distribution of 20-year mean changes are given for 2081–2100 in the four RCP scenarios.

(Below) Maps of temperature changes in 2016–2035, 2046–2065 and 2081–2100 with respect to 1986–2005 in the RCP4.5 scenario. For each point, the 25th, 50th and 75th percentiles of the distribution of the CMIP5 ensemble are shown; this includes both natural variability and inter-model spread. Hatching denotes areas where the 20-year mean differences of the percentiles are less than the standard deviation of model-estimated present-day natural variability of 20-year mean differences.

Sections 9.4.1.1, 9.6.1.1, 10.3.1.1.4, 11.3.2.1.2, Box 11.2, 12.4.3.1, 14.8.2 contain relevant information regarding the evaluation of models in this region, the model spread in the context of other methods of projecting changes and the role of modes of variability and other climate phenomena.

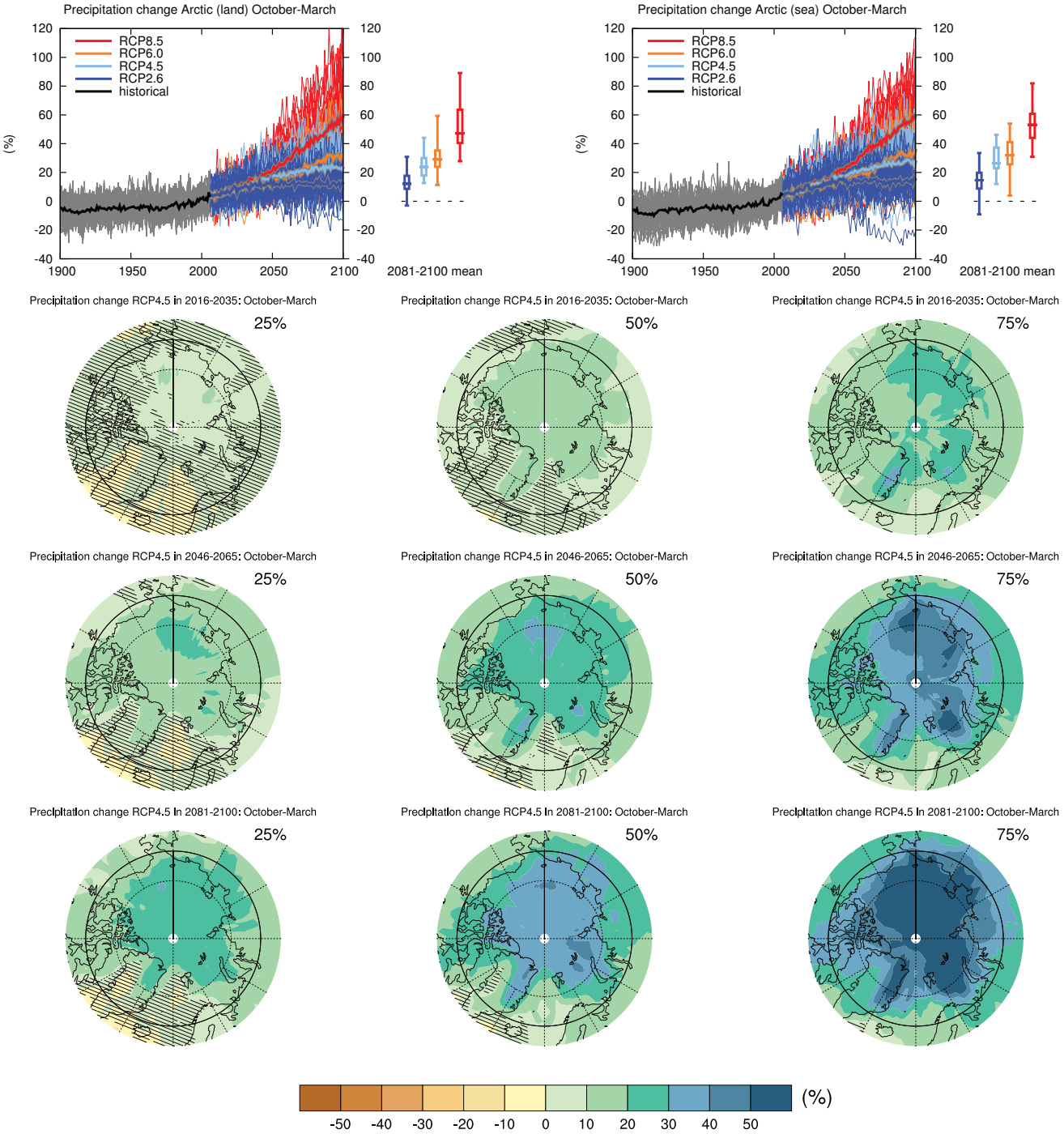

Figure AI.10 | (Top left) Time series of relative change relative to 1986–2005 in precipitation averaged over land grid points in the Arctic (67.5°N to 90°N) in October to March. (Top right) Same for sea grid points. Thin lines denote one ensemble member per model, thick lines the CMIP5 multi-model mean. On the right-hand side the 5th, 25th, 50th (median), 75th and 95th percentiles of the distribution of 20-year mean changes are given for 2081–2100 in the four RCP scenarios.

(Below) Maps of precipitation changes in 2016–2035, 2046–2065 and 2081–2100 with respect to 1986–2005 in the RCP4.5 scenario. For each point, the 25th, 50th and 75th percentiles of the distribution of the CMIP5 ensemble are shown; this includes both natural variability and inter-model spread. Hatching denotes areas where the 20-year mean differences of the percentiles are less than the standard deviation of model-estimated present-day natural variability of 20-year mean differences.

Sections 9.4.1.1, 9.6.1.1, 11.3.2.3.1, Box 11.2, 12.4.5.2, 14.8.2 contain relevant information regarding the evaluation of models in this region, the model spread in the context of other methods of projecting changes and the role of modes of variability and other climate phenomena.

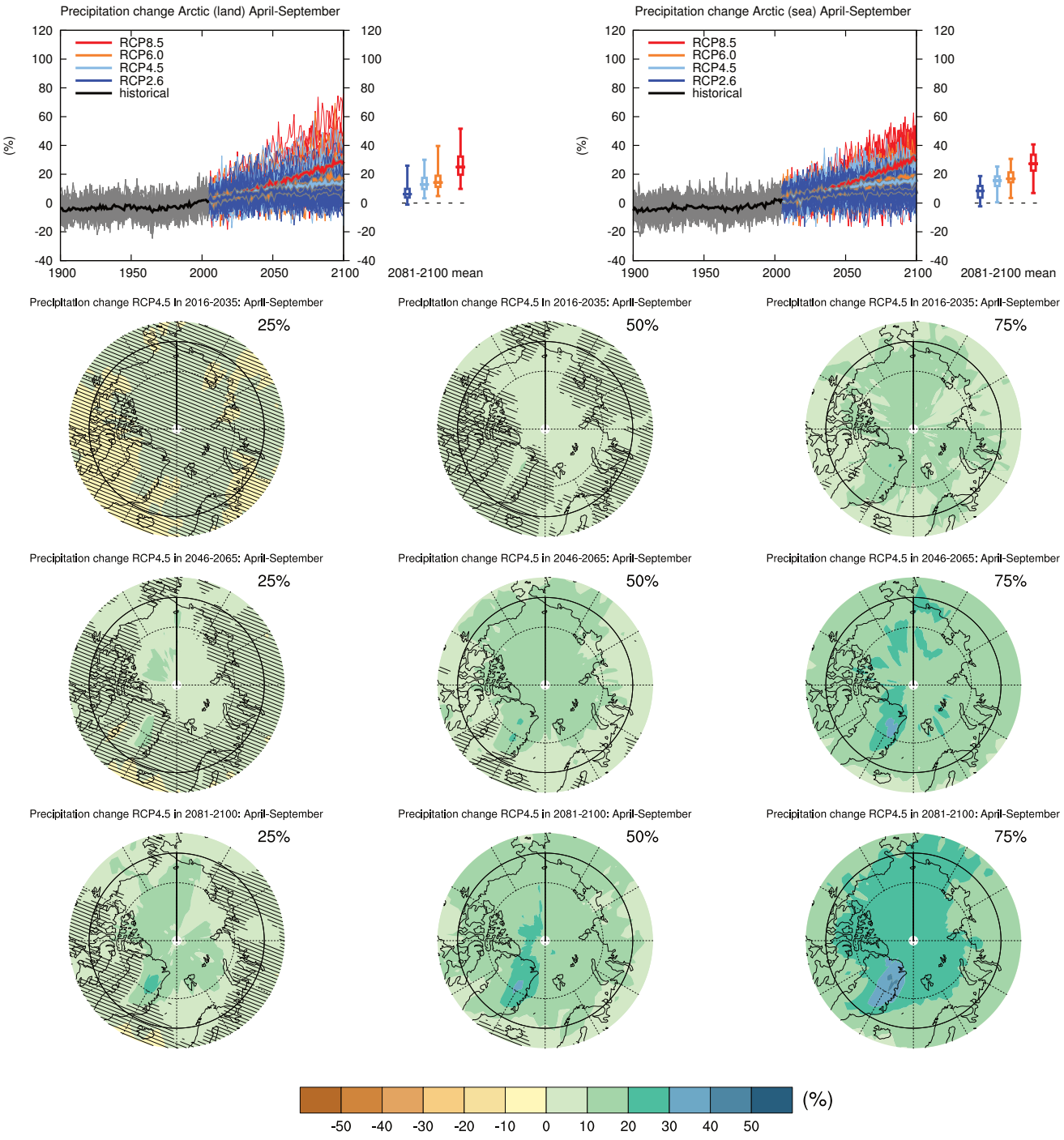

Figure AI.11 | (Top left) Time series of relative change relative to 1986–2005 in precipitation averaged over land grid points in the Arctic (67.5°N to 90°N) in April to September. (Top right) Same for sea grid points. Thin lines denote one ensemble member per model, thick lines the CMIP5 multi-model mean. On the right-hand side the 5th, 25th, 50th (median), 75th and 95th percentiles of the distribution of 20-year mean changes are given for 2081–2100 in the four RCP scenarios.

(Below) Maps of precipitation changes in 2016–2035, 2046–2065 and 2081–2100 with respect to 1986–2005 in the RCP4.5 scenario. For each point, the 25th, 50th and 75th percentiles of the distribution of the CMIP5 ensemble are shown; this includes both natural variability and inter-model spread. Hatching denotes areas where the 20-year mean differences of the percentiles are less than the standard deviation of model-estimated present-day natural variability of 20-year mean differences.

Sections 9.4.1.1, 9.6.1.1, 11.3.2.3.1, Box 11.2, 12.4.5.2, 14.8.2 contain relevant information regarding the evaluation of models in this region, the model spread in the context of other methods of projecting changes and the role of modes of variability and other climate phenomena.

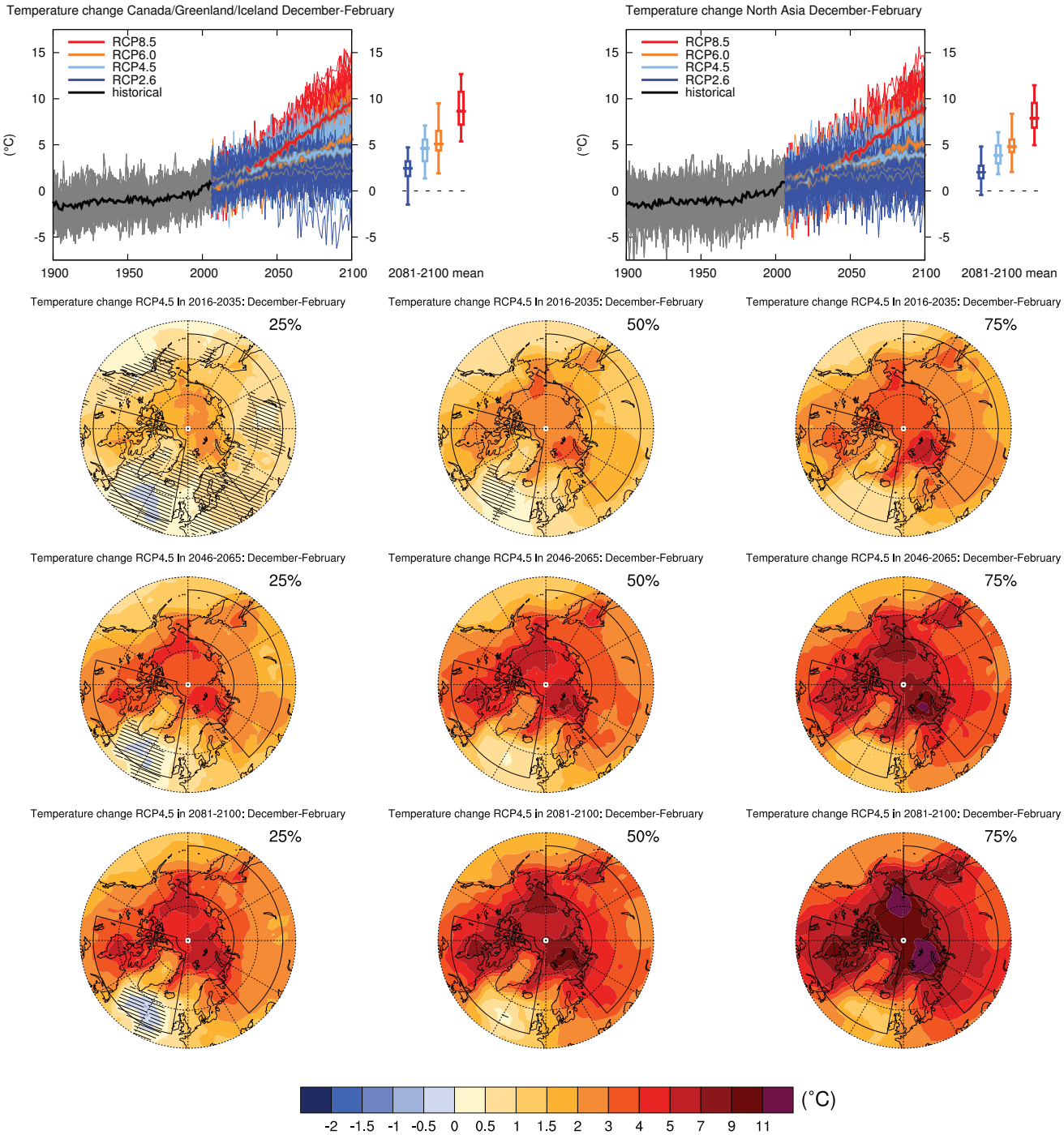

Figure AI.12 | (Top left) Time series of temperature change relative to 1986–2005 averaged over land grid points in Canada/Greenland/Iceland (50°N to 85°N, 105°W to 10°W) in December to February. (Top right) Same for land grid points in North Asia (50°N to 70°N, 40°E to 180°E). Thin lines denote one ensemble member per model, thick lines the CMIP5 multi-model mean. On the right-hand side the 5th, 25th, 50th (median), 75th and 95th percentiles of the distribution of 20-year mean changes are given for 2081–2100 in the four RCP scenarios.

(Below) Maps of temperature changes in 2016–2035, 2046–2065 and 2081–2100 with respect to 1986–2005 in the RCP4.5 scenario. For each point, the 25th, 50th and 75th percentiles of the distribution of the CMIP5 ensemble are shown; this includes both natural variability and inter-model spread. Hatching denotes areas where the 20-year mean differences of the percentiles are less than the standard deviation of model-estimated present-day natural variability of 20-year mean differences.

Sections 9.4.1.1, 9.6.1.1, 10.3.1.1.4, 11.3.2.1.2, Box 11.2, 14.8.2, 14.8.8 contain relevant information regarding the evaluation of models in this region, the model spread in the context of other methods of projecting changes and the role of modes of variability and other climate phenomena.

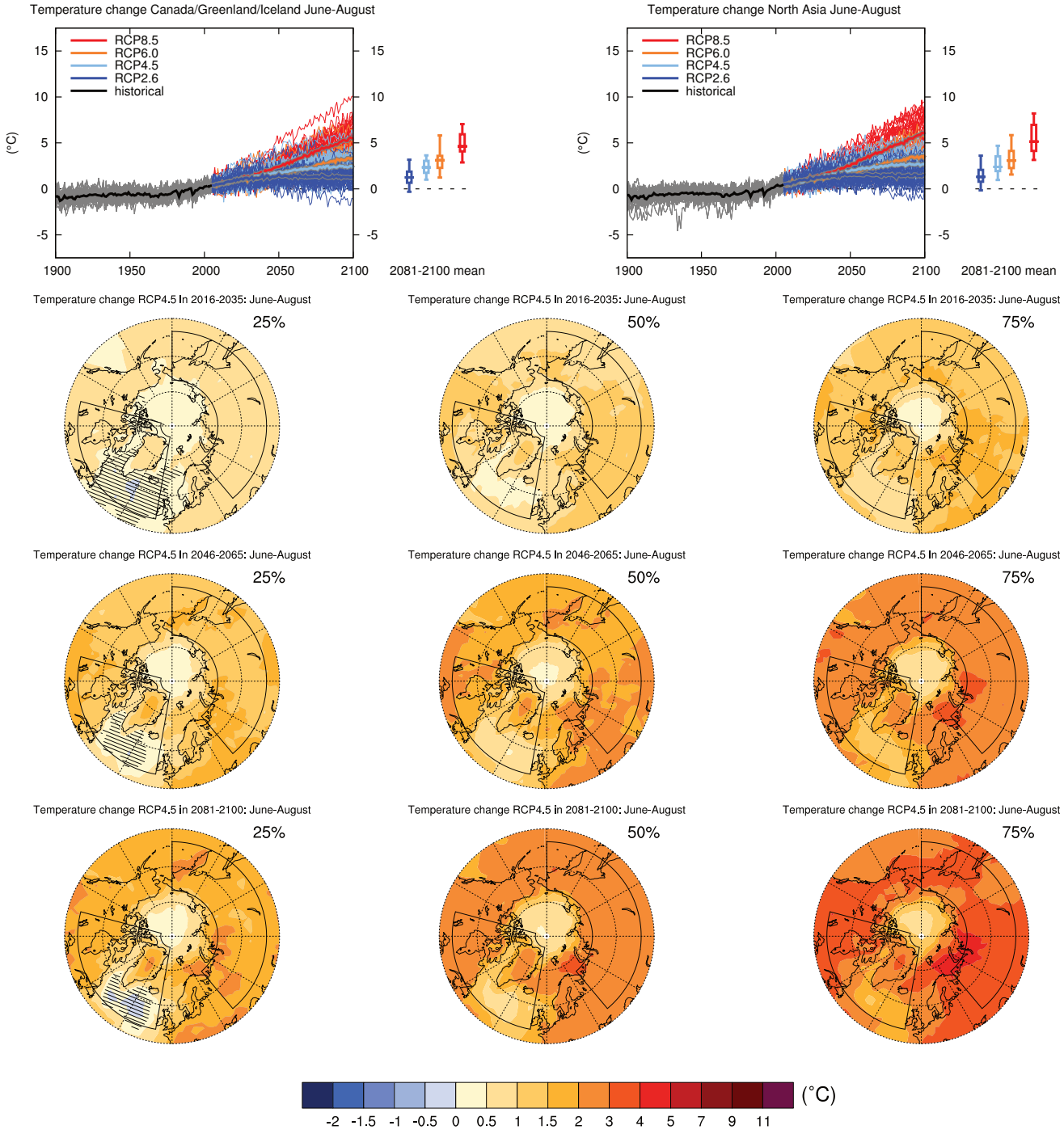

Figure AI.13 | (Top left) Time series of temperature change relative to 1986–2005 averaged over land grid points in Canada/Greenland/Iceland (50°N to 85°N, 105°W to 10°W) in June to August. (Top right) Same for land grid points in North Asia (50°N to 70°N, 40°E to 180°E). Thin lines denote one ensemble member per model, thick lines the CMIP5 multi-model mean. On the right-hand side the 5th, 25th, 50th (median), 75th and 95th percentiles of the distribution of 20-year mean changes are given for 2081–2100 in the four RCP scenarios.

(Below) Maps of temperature changes in 2016–2035, 2046–2065 and 2081–2100 with respect to 1986–2005 in the RCP4.5 scenario. For each point, the 25th, 50th and 75th percentiles of the distribution of the CMIP5 ensemble are shown; this includes both natural variability and inter-model spread. Hatching denotes areas where the 20-year mean differences of the percentiles are less than the standard deviation of model-estimated present-day natural variability of 20-year mean differences.

Sections 9.4.1.1, 9.6.1.1, 10.3.1.1.4, 11.3.2.1.2, Box 11.2, 14.8.2, 14.8.8 contain relevant information regarding the evaluation of models in this region, the model spread in the context of other methods of projecting changes and the role of modes of variability and other climate phenomena.

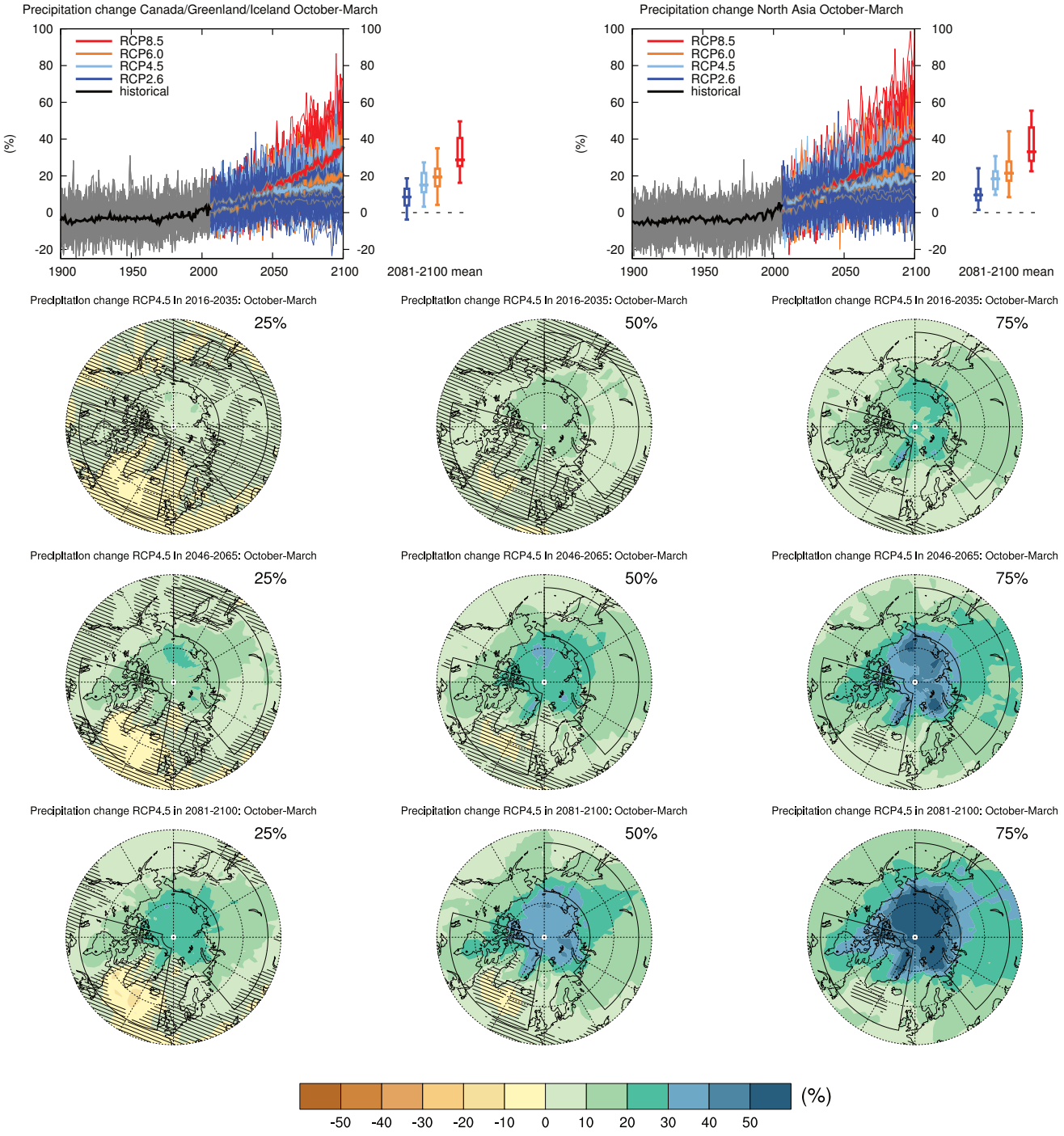

Figure AI.14 | (Top left) Time series of relative change relative to 1986–2005 in precipitation averaged over land grid points in Canada/Greenland/Iceland (50°N to 85°N, 105°W to 10°W) in October to March. (Top right) Same for land grid points in North Asia (50°N to 70°N, 40°E to 180°E). Thin lines denote one ensemble member per model, thick lines the CMIP5 multi-model mean. On the right-hand side the 5th, 25th, 50th (median), 75th and 95th percentiles of the distribution of 20-year mean changes are given for 2081–2100 in the four RCP scenarios.

(Below) Maps of precipitation changes in 2016–2035, 2046–2065 and 2081–2100 with respect to 1986–2005 in the RCP4.5 scenario. For each point, the 25th, 50th and 75th percentiles of the distribution of the CMIP5 ensemble are shown; this includes both natural variability and inter-model spread. Hatching denotes areas where the 20-year mean differences of the percentiles are less than the standard deviation of model-estimated present-day natural variability of 20-year mean differences.

Sections 9.4.1.1, 9.6.1.1, 10.3.2.2, 11.3.2.3.1, Box 11.2, 12.4.5.2, 14.8.2, 14.8.8 contain relevant information regarding the evaluation of models in this region, the model spread in the context of other methods of projecting changes and the role of modes of variability and other climate phenomena.

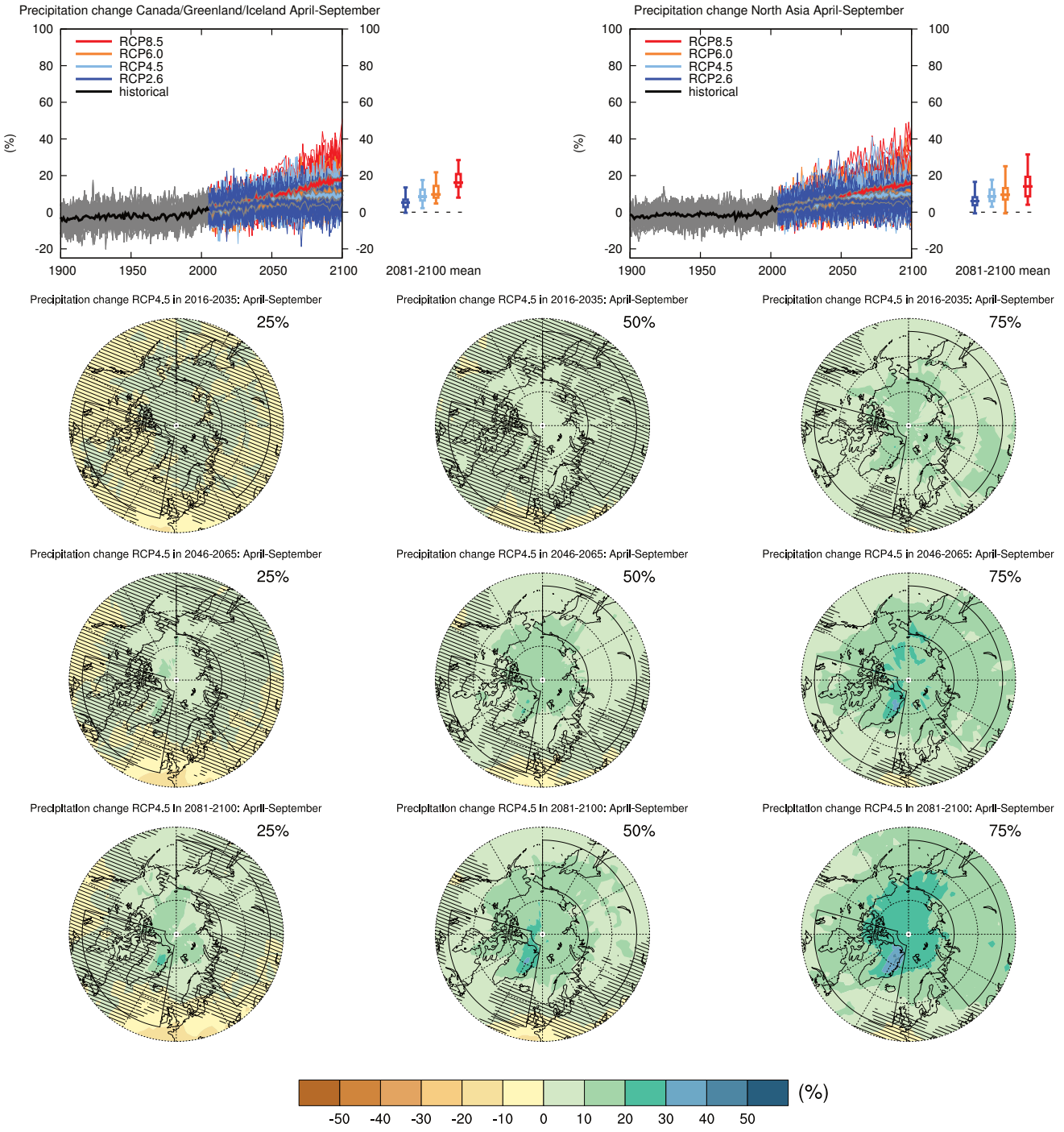

Figure AI.15 | (Top left) Time series of relative change relative to 1986–2005 in precipitation averaged over land grid points in Canada/Greenland/Iceland (50°N to 85°N, 105°W to 10°W) in April to September. (Top right) Same for land grid points in North Asia (50°N to 70°N, 40°E to 180°E). Thin lines denote one ensemble member per model, thick lines the CMIP5 multi-model mean. On the right-hand side the 5th, 25th, 50th (median), 75th and 95th percentiles of the distribution of 20-year mean changes are given for 2081–2100 in the four RCP scenarios.

(Below) Maps of precipitation changes in 2016–2035, 2046–2065 and 2081–2100 with respect to 1986–2005 in the RCP4.5 scenario. For each point, the 25th, 50th and 75th percentiles of the distribution of the CMIP5 ensemble are shown; this includes both natural variability and inter-model spread. Hatching denotes areas where the 20-year mean differences of the percentiles are less than the standard deviation of model-estimated present-day natural variability of 20-year mean differences.

Sections 9.4.1.1, 9.6.1.1, 10.3.2.2, 11.3.2.3.1, Box 11.2, 12.4.5.2, 14.8.2, 14.8.8 contain relevant information regarding the evaluation of models in this region, the model spread in the context of other methods of projecting changes and the role of modes of variability and other climate phenomena.

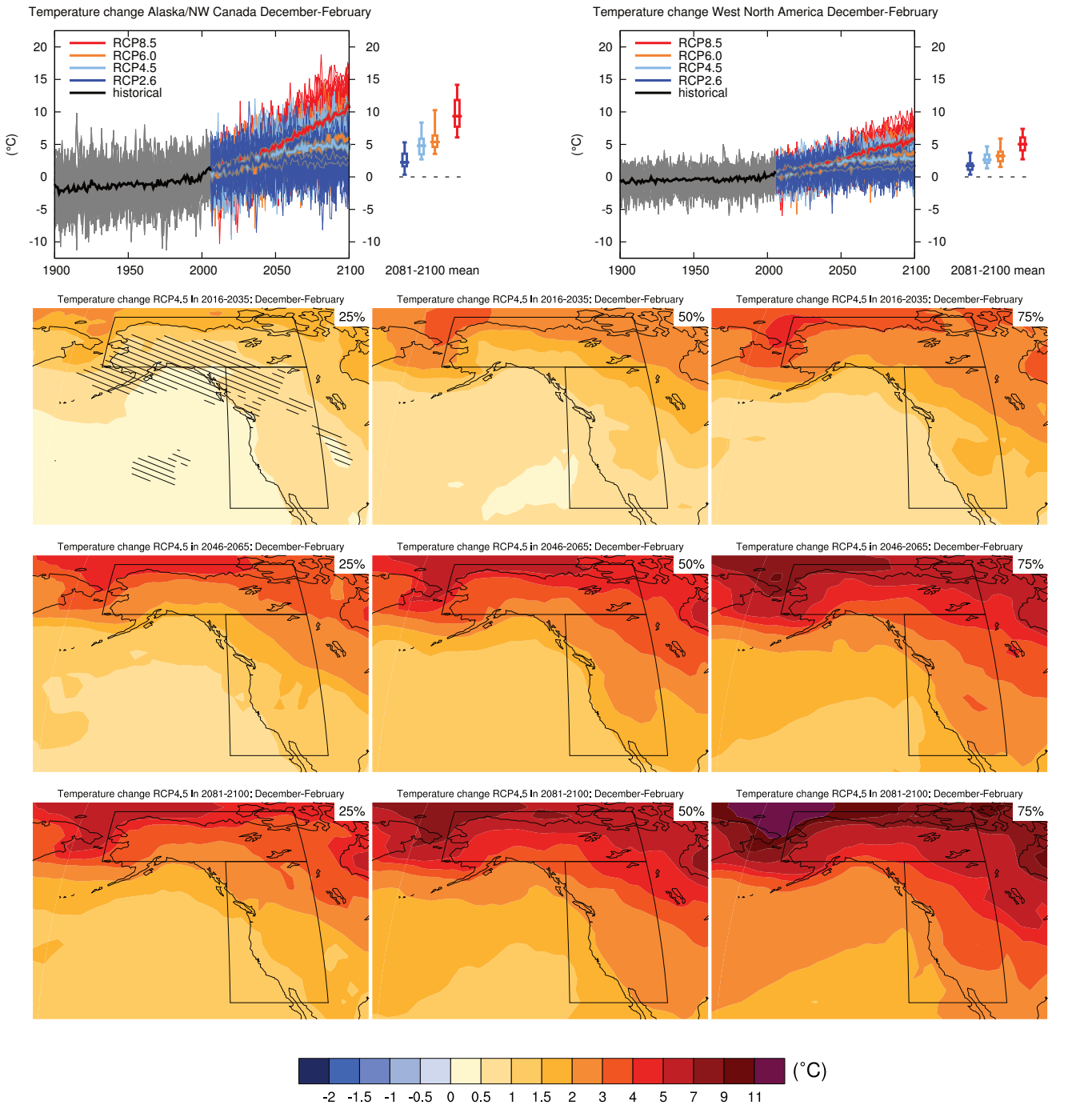

Figure AI.16 | (Top left) Time series of temperature change relative to 1986–2005 averaged over land grid points in Alaska/NW Canada (60°N to 72.6°N, 168°W to 105°W) in December to February. (Top right) Same for land grid points in West North America (28.6°N to 60°N, 130°W to 105°W). Thin lines denote one ensemble member per model, thick lines the CMIP5 multi-model mean. On the right-hand side the 5th, 25th, 50th (median), 75th and 95th percentiles of the distribution of 20-year mean changes are given for 2081–2100 in the four RCP scenarios.

(Below) Maps of temperature changes in 2016–2035, 2046–2065 and 2081–2100 with respect to 1986–2005 in the RCP4.5 scenario. For each point, the 25th, 50th and 75th percentiles of the distribution of the CMIP5 ensemble are shown; this includes both natural variability and inter-model spread. Hatching denotes areas where the 20-year mean differences of the percentiles are less than the standard deviation of model-estimated present-day natural variability of 20-year mean differences.

Sections 9.4.1.1, 9.6.1.1, 10.3.1.1.4, Box 11.2, 14.8.3 contain relevant information regarding the evaluation of models in this region, the model spread in the context of other methods of projecting changes and the role of modes of variability and other climate phenomena.

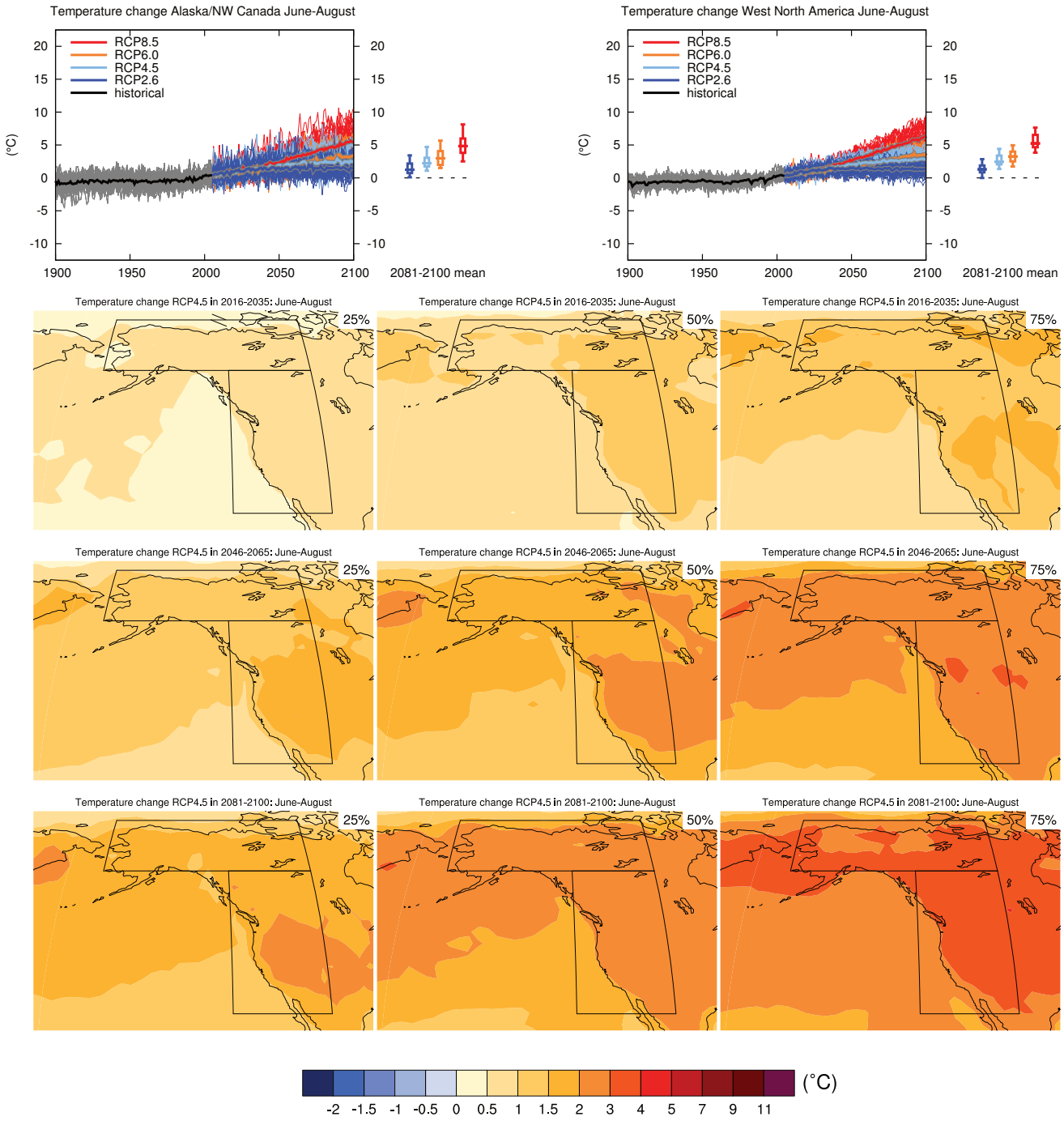

Figure AI.17 | (Top left) Time series of temperature change relative to 1986–2005 averaged over land grid points in Alaska/NW Canada (60°N to 72.6°N, 168°W to 105°W) in June to August. (Top right) Same for land grid points in West North America (28.6°N to 60°N, 130°W to 105°W). Thin lines denote one ensemble member per model, thick lines the CMIP5 multi-model mean. On the right-hand side the 5th, 25th, 50th (median), 75th and 95th percentiles of the distribution of 20-year mean changes are given for 2081–2100 in the four RCP scenarios.

(Below) Maps of temperature changes in 2016–2035, 2046–2065 and 2081–2100 with respect to 1986–2005 in the RCP4.5 scenario. For each point, the 25th, 50th and 75th percentiles of the distribution of the CMIP5 ensemble are shown; this includes both natural variability and inter-model spread. Hatching denotes areas where the 20-year mean differences of the percentiles are less than the standard deviation of model-estimated present-day natural variability of 20-year mean differences.

Sections 9.4.1.1, 9.6.1.1, 10.3.1.1.4, Box 11.2, 14.8.3 contain relevant information regarding the evaluation of models in this region, the model spread in the context of other methods of projecting changes and the role of modes of variability and other climate phenomena.

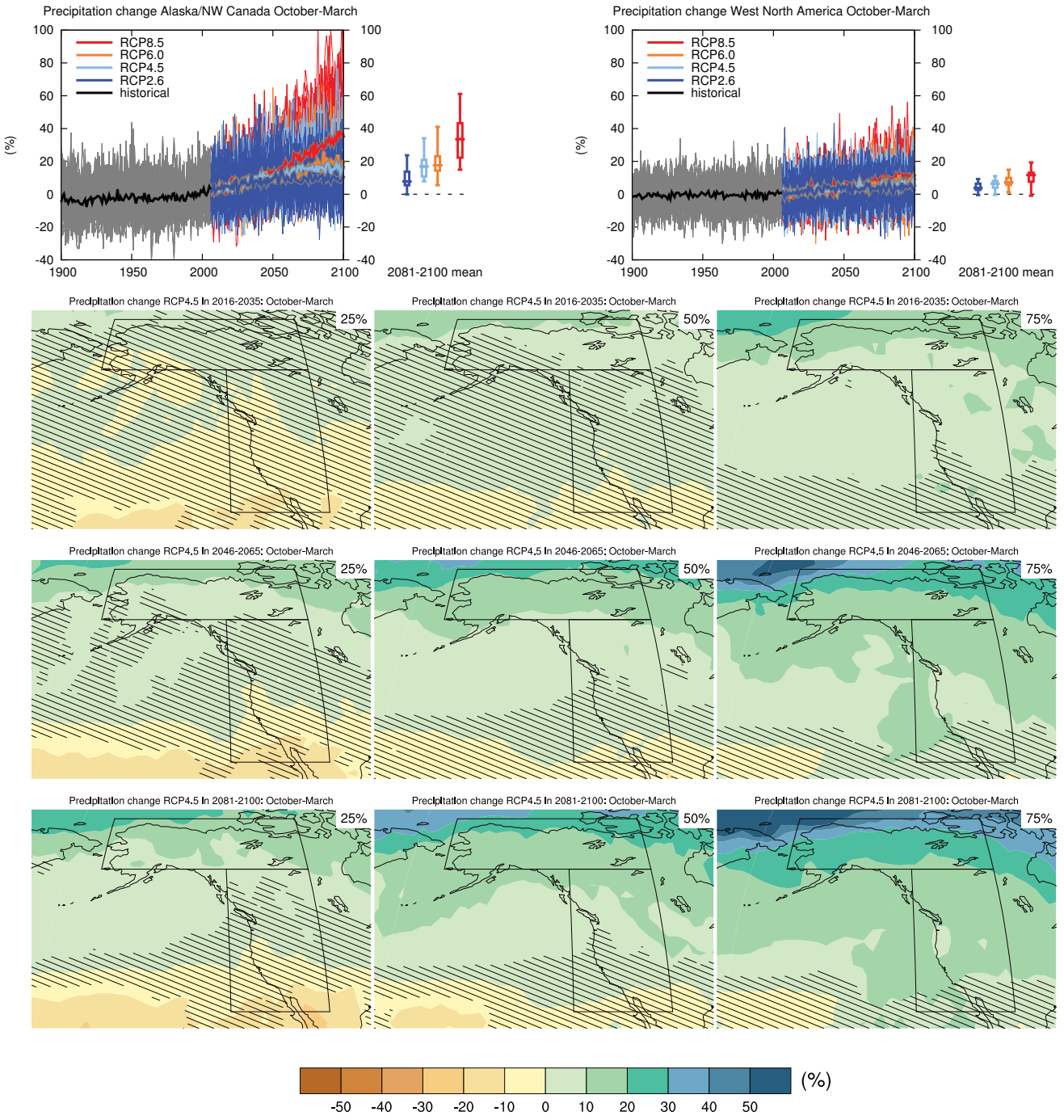

Figure AI.18 | (Top left) Time series of relative change relative to 1986–2005 in precipitation averaged over land grid points in Alaska/NW Canada (60°N to 72.6°N, 168°W to 105°W) in October to March. (Top right) Same for land grid points in West North America (28.6°N to 60°N, 130°W to 105°W). Thin lines denote one ensemble member per model, thick lines the CMIP5 multi-model mean. On the right-hand side the 5th, 25th, 50th (median), 75th and 95th percentiles of the distribution of 20-year mean changes are given for 2081–2100 in the four RCP scenarios.

(Below) Maps of precipitation changes in 2016–2035, 2046–2065 and 2081–2100 with respect to 1986–2005 in the RCP4.5 scenario. For each point, the 25th, 50th and 75th percentiles of the distribution of the CMIP5 ensemble are shown; this includes both natural variability and inter-model spread. Hatching denotes areas where the 20-year mean differences of the percentiles are less than the standard deviation of model-estimated present-day natural variability of 20-year mean differences.

Sections 9.4.1.1, 9.6.1.1, Box 11.2, 12.4.5.2, 14.2.3.1, 14.8.3 contain relevant information regarding the evaluation of models in this region, the model spread in the context of other methods of projecting changes and the role of modes of variability and other climate phenomena.

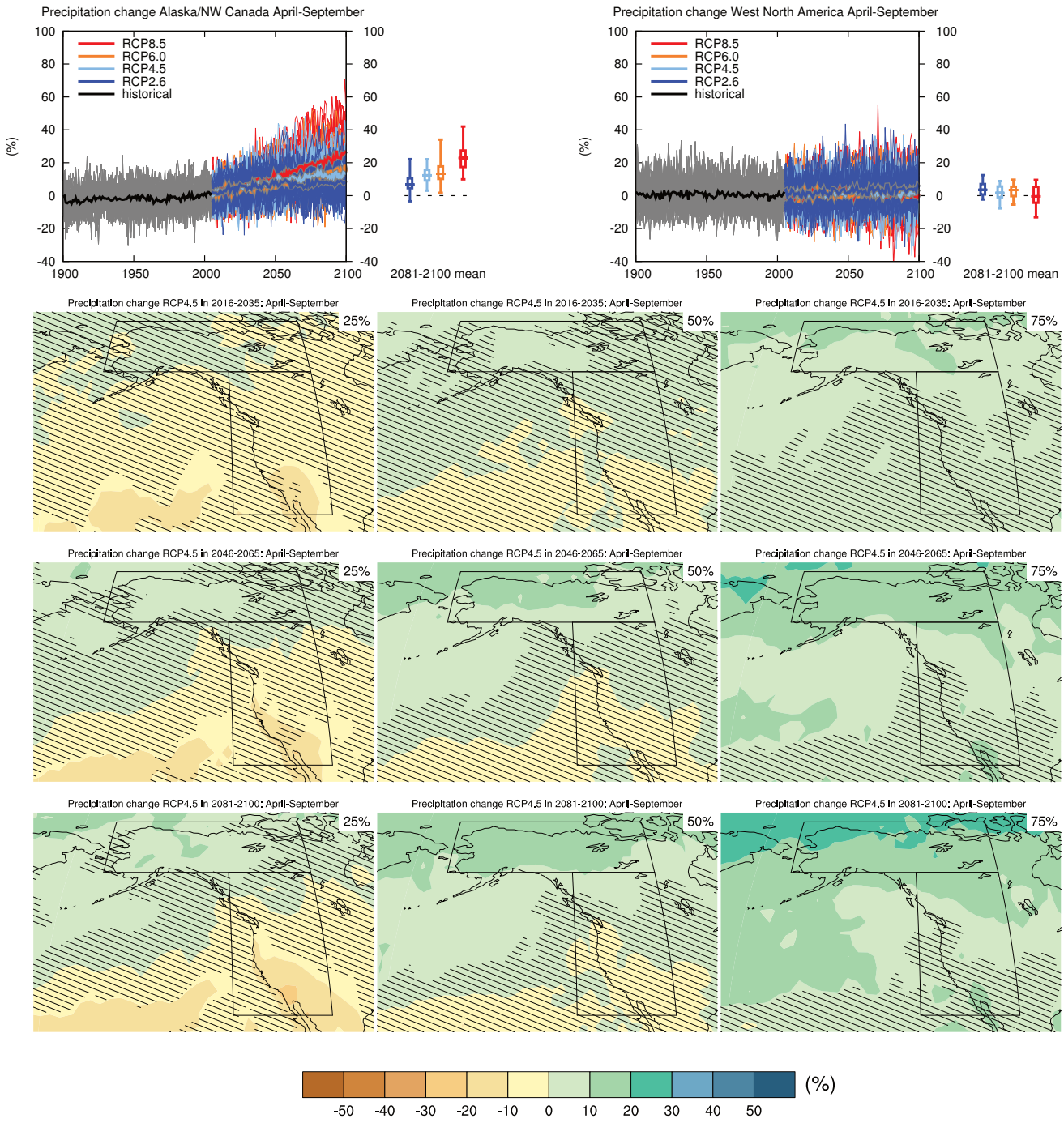

Figure AI.19 | (Top left) Time series of relative change relative to 1986–2005 in precipitation averaged over land grid points in Alaska/NW Canada (60°N to 72.6°N, 168°W to 105°W) in April to September. (Top right) Same for land grid points in West North America (28.6°N to 60°N, 130°W to 105°W). Thin lines denote one ensemble member per model, thick lines the CMIP5 multi-model mean. On the right-hand side the 5th, 25th, 50th (median), 75th and 95th percentiles of the distribution of 20-year mean changes are given for 2081–2100 in the four RCP scenarios.

(Below) Maps of precipitation changes in 2016–2035, 2046–2065 and 2081–2100 with respect to 1986–2005 in the RCP4.5 scenario. For each point, the 25th, 50th and 75th percentiles of the distribution of the CMIP5 ensemble are shown; this includes both natural variability and inter-model spread. Hatching denotes areas where the 20-year mean differences of the percentiles are less than the standard deviation of model-estimated present-day natural variability of 20-year mean differences.

Sections 9.4.1.1, 9.6.1.1, Box 11.2, 12.4.5.2, 14.2.3.1, 14.8.3 contain relevant information regarding the evaluation of models in this region, the model spread in the context of other methods of projecting changes and the role of modes of variability and other climate phenomena.

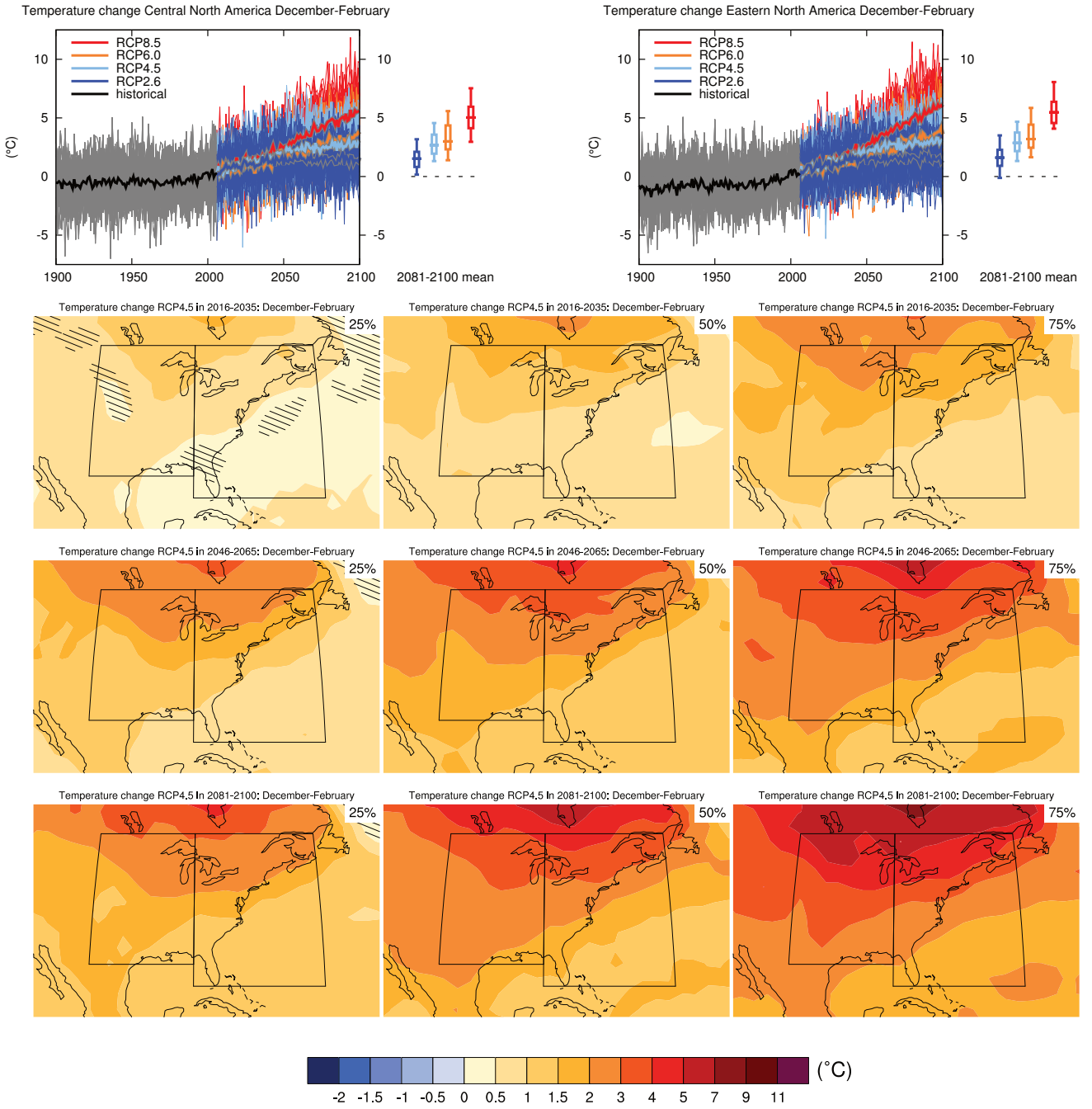

Figure AI.20 | (Top left) Time series of temperature change relative to 1986–2005 averaged over land grid points in Central North America (28.6°N to 50°N, 105°W to 85°W) in December to February. (Top right) Same for land grid points in Eastern North America (25°N to 50°N, 85°W to 60°W). Thin lines denote one ensemble member per model, thick lines the CMIP5 multi-model mean. On the right-hand side the 5th, 25th, 50th (median), 75th and 95th percentiles of the distribution of 20-year mean changes are given for 2081–2100 in the four RCP scenarios.

(Below) Maps of temperature changes in 2016–2035, 2046–2065 and 2081–2100 with respect to 1986–2005 in the RCP4.5 scenario. For each point, the 25th, 50th and 75th percentiles of the distribution of the CMIP5 ensemble are shown; this includes both natural variability and inter-model spread. Hatching denotes areas where the 20-year mean differences of the percentiles are less than the standard deviation of model-estimated present-day natural variability of 20-year mean differences.

Sections 9.4.1.1, 9.6.1.1, 10.3.1.1.4, Box 11.2, 14.8.3 contain relevant information regarding the evaluation of models in this region, the model spread in the context of other methods of projecting changes and the role of modes of variability and other climate phenomena.

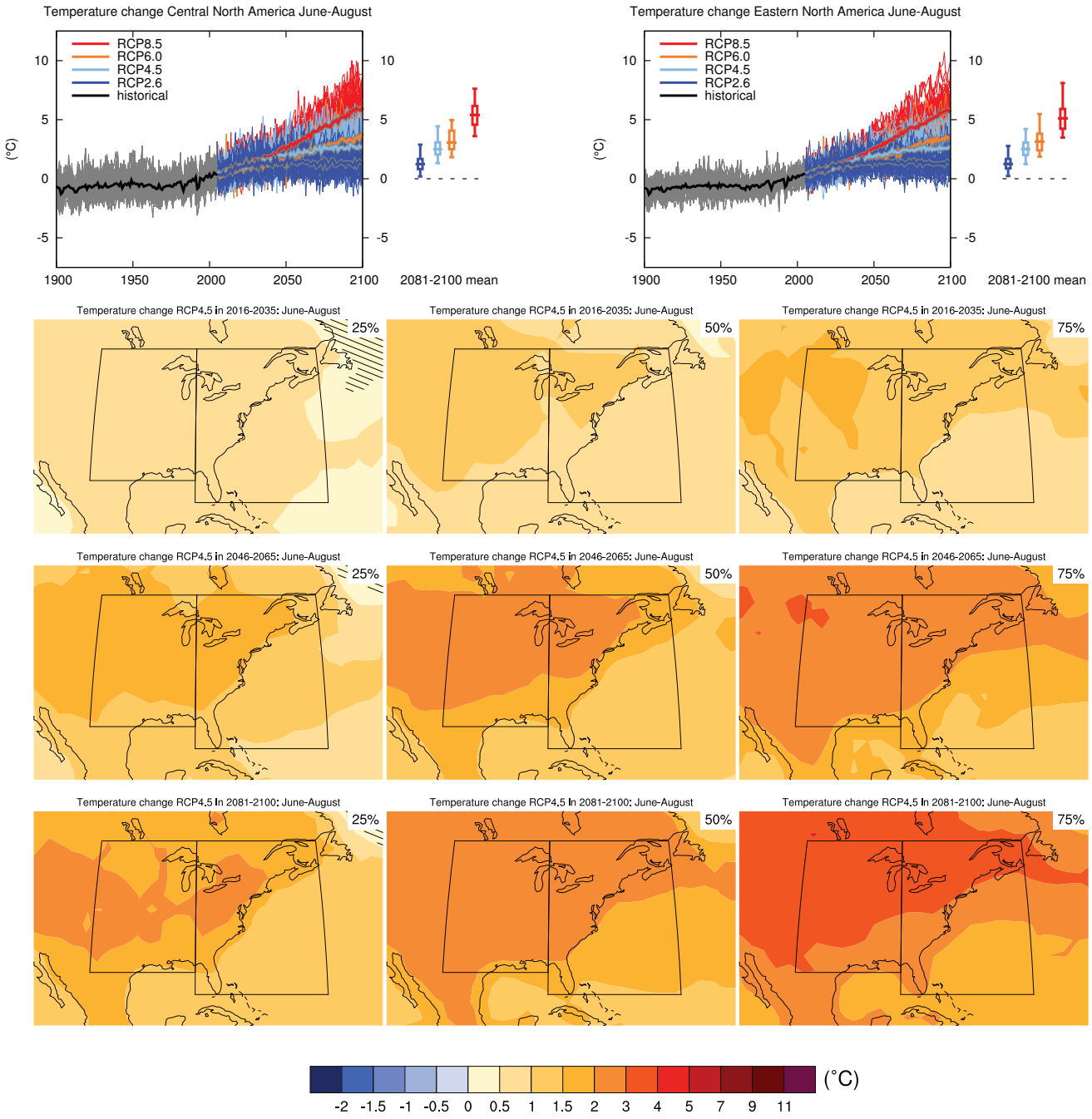

Figure AI.21 | (Top left) Time series of temperature change relative to 1986–2005 averaged over land grid points in Central North America (28.6°N to 50°N, 105°W to 85°W) in June to August. (Top right) Same for land grid points in Eastern North America (25°N to 50°N, 85°W to 60°W). Thin lines denote one ensemble member per model, thick lines the CMIP5 multi-model mean. On the right-hand side the 5th, 25th, 50th (median), 75th and 95th percentiles of the distribution of 20-year mean changes are given for 2081–2100 in the four RCP scenarios.

(Below) Maps of temperature changes in 2016–2035, 2046–2065 and 2081–2100 with respect to 1986–2005

in the RCP4.5 scenario. For each point, the 25th, 50th and 75th percentiles of the distribution of the CMIP5 ensemble are shown; this includes both natural variability and inter-model spread. Hatching denotes areas where the 20-year mean differences of the percentiles are less than the standard deviation of model-estimated present-day natural variability of 20-year mean differences.

Sections 9.4.1.1, 9.6.1.1, 10.3.1.1.4, Box 11.2, 14.8.3 contain relevant information regarding the evaluation of models in this region, the model spread in the context of other methods of projecting changes and the role of modes of variability and other climate phenomena.

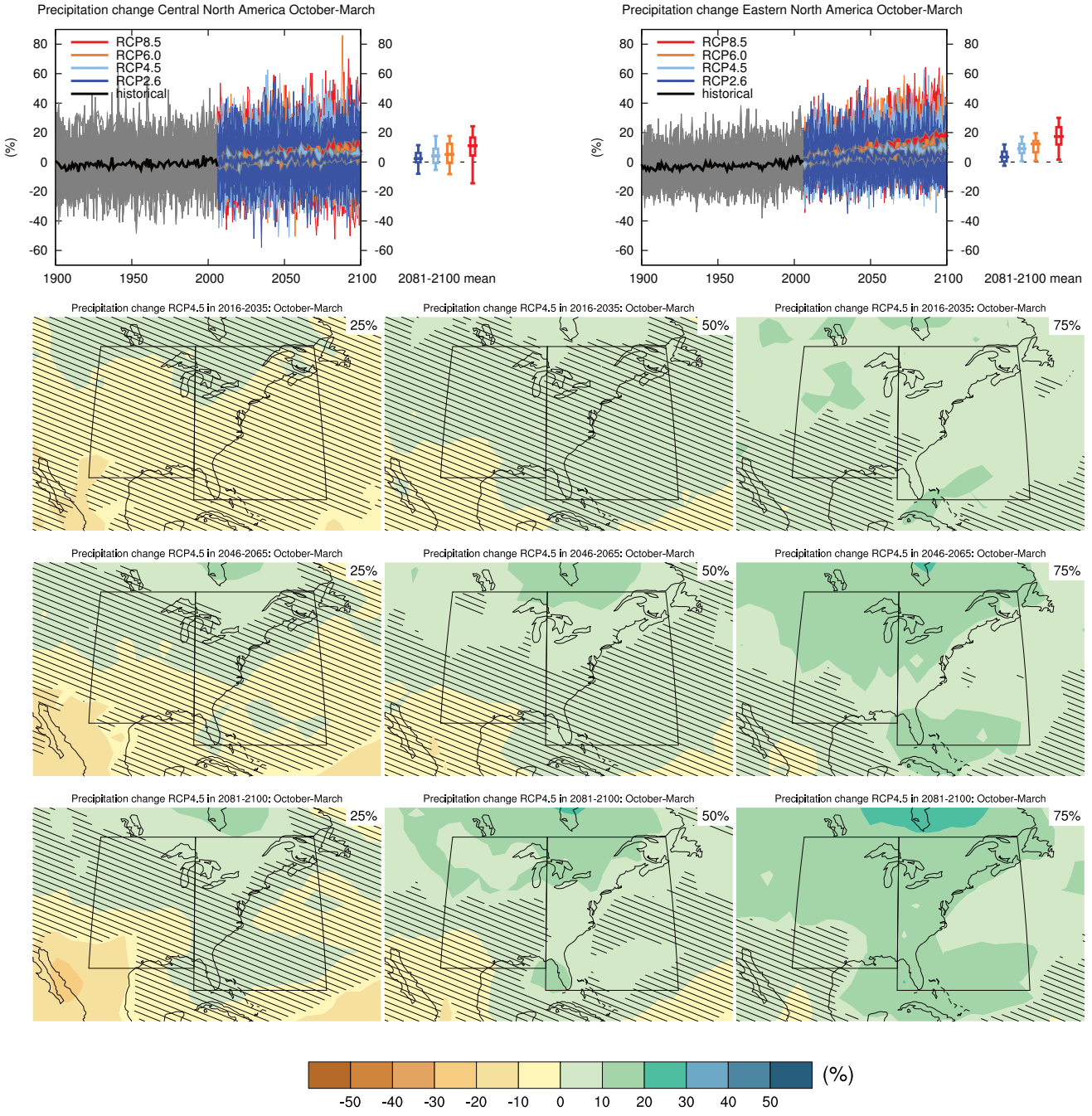

Figure AI.22 | (Top left) Time series of relative change relative to 1986–2005 in precipitation averaged over land grid points in Central North America (28.6°N to 50°N, 105°W to 85°W) in October to March. (Top right) Same for land grid points in Eastern North America (25°N to 50°N, 85°W to 60°W). Thin lines denote one ensemble member per model, thick lines the CMIP5 multi-model mean. On the right-hand side the 5th, 25th, 50th (median), 75th and 95th percentiles of the distribution of 20-year mean changes are given for 2081–2100 in the four RCP scenarios.

(Below) Maps of precipitation changes in 2016–2035, 2046–2065 and 2081–2100 with respect to 1986–2005 in the RCP4.5 scenario. For each point, the 25th, 50th and 75th percentiles of the distribution of the CMIP5 ensemble are shown; this includes both natural variability and inter-model spread. Hatching denotes areas where the 20-year mean differences of the percentiles are less than the standard deviation of model-estimated present-day natural variability of 20-year mean differences.

Sections 9.4.1.1, 9.6.1.1, Box 11.2, 14.8.3 contain relevant information regarding the evaluation of models in this region, the model spread in the context of other methods of projecting changes and the role of modes of variability and other climate phenomena.

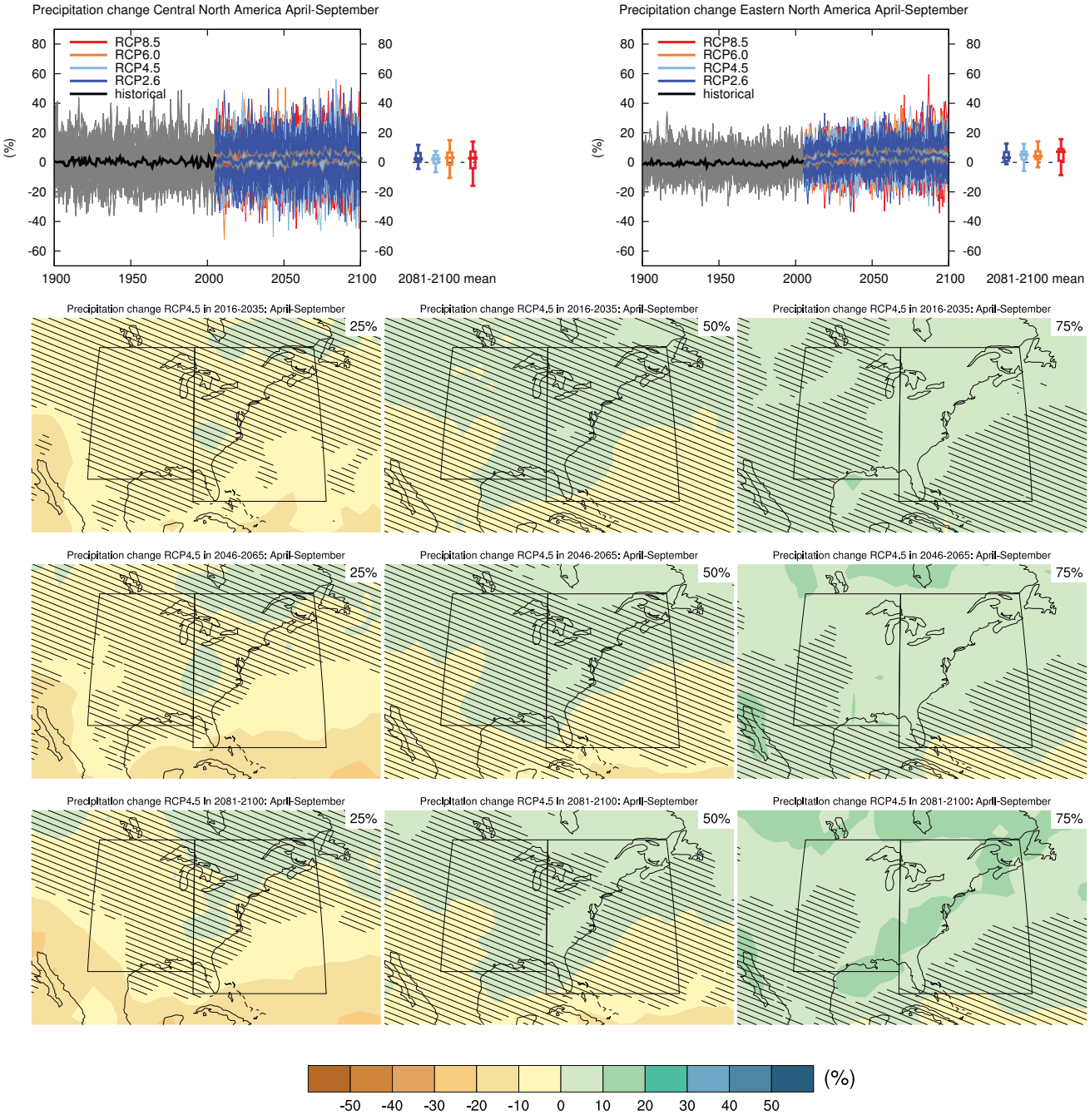

Figure AI.23 | (Top left) Time series of relative change relative to 1986–2005 in precipitation averaged over land grid points in Central North America (28.6°N to 50°N, 105°W to 85°W) in April to September. (Top right) Same for land grid points in Eastern North America (25°N to 50°N, 85°W to 60°W). Thin lines denote one ensemble member per model, thick lines the CMIP5 multi-model mean. On the right-hand side the 5th, 25th, 50th (median), 75th and 95th percentiles of the distribution of 20-year mean changes are given for 2081–2100 in the four RCP scenarios.

(Below) Maps of precipitation changes in 2016–2035, 2046–2065 and 2081–2100 with respect to 1986–2005 in the RCP4.5 scenario. For each point, the 25th, 50th and 75th percentiles of the distribution of the CMIP5 ensemble are shown; this includes both natural variability and inter-model spread. Hatching denotes areas where the 20-year mean differences of the percentiles are less than the standard deviation of model-estimated present-day natural variability of 20-year mean differences.

Sections 9.4.1.1, 9.6.1.1, Box 11.2, 14.8.3 contain relevant information regarding the evaluation of models in this region, the model spread in the context of other methods of projecting changes and the role of modes of variability and other climate phenomena.

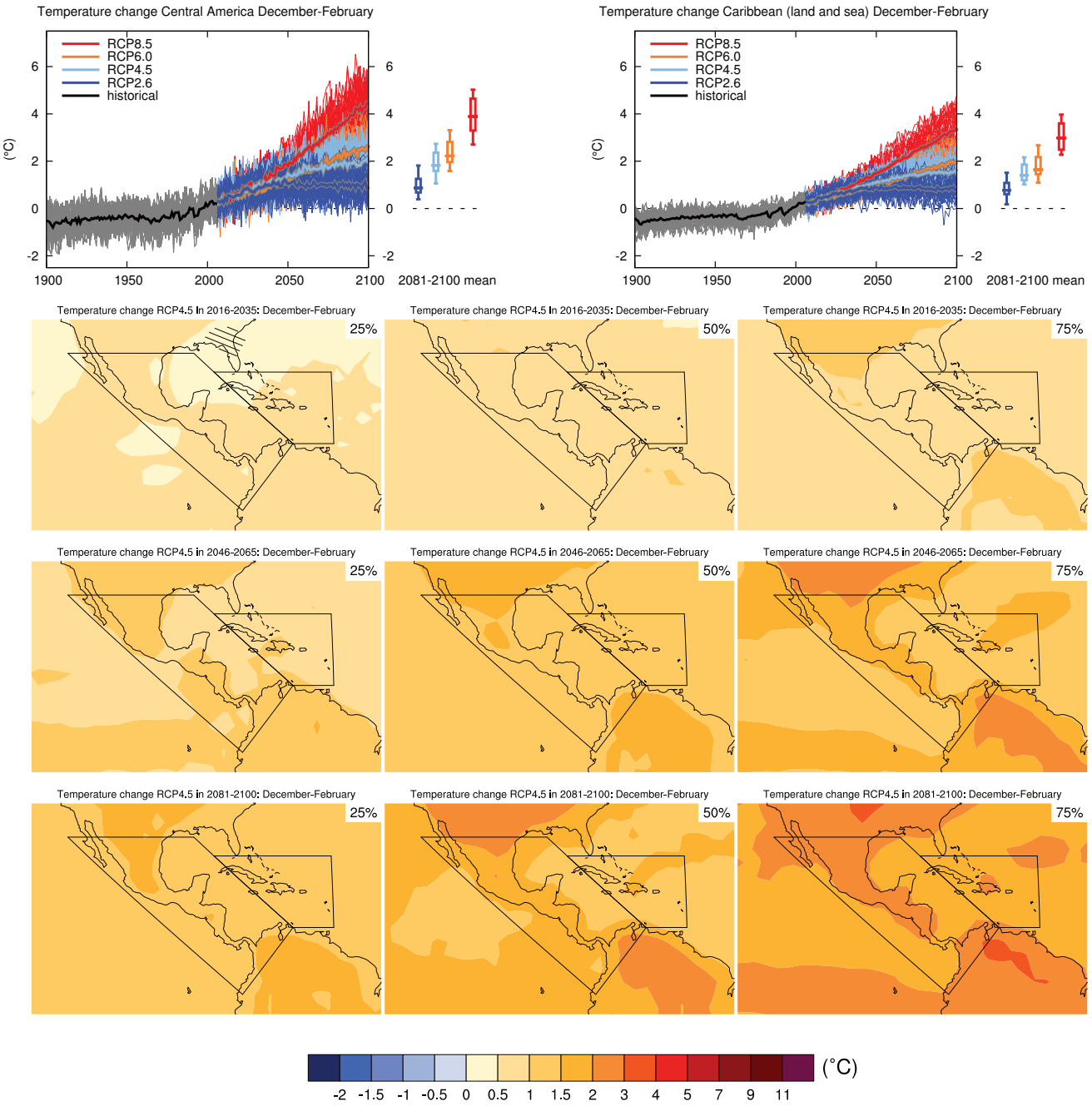

Figure AI.24 | (Top left) Time series of temperature change relative to 1986–2005 averaged over land grid points in Central America (68.8°W, 11.4°N; 79.7°W, 1.2°S; 116.3°W, 28.6°N; 90.3°W, 28.6°N) in December to February. (Top right) Same for all grid points in Caribbean (land and sea) (68.8°W, 11.4°N; 85.8°W, 25°N, 60°W, 25°N, 60°W, 11.44°N). Thin lines denote one ensemble member per model, thick lines the CMIP5 multi-model mean. On the right-hand side the 5th, 25th, 50th (median), 75th and 95th percentiles of the distribution of 20-year mean changes are given for 2081–2100 in the four RCP scenarios.

(Below) Maps of temperature changes in 2016–2035, 2046–2065 and 2081–2100 with respect to 1986–2005 in the RCP4.5 scenario. For each point, the 25th, 50th and 75th percentiles of the distribution of the CMIP5 ensemble are shown; this includes both natural variability and inter-model spread. Hatching denotes areas where the 20-year mean differences of the percentiles are less than the standard deviation of model-estimated present-day natural variability of 20-year mean differences.

Sections 9.4.1.1, 9.6.1.1, 10.3.1.1.4, Box 11.2, 14.8.4 contain relevant information regarding the evaluation of models in this region, the model spread in the context of other methods of projecting changes and the role of modes of variability and other climate phenomena.

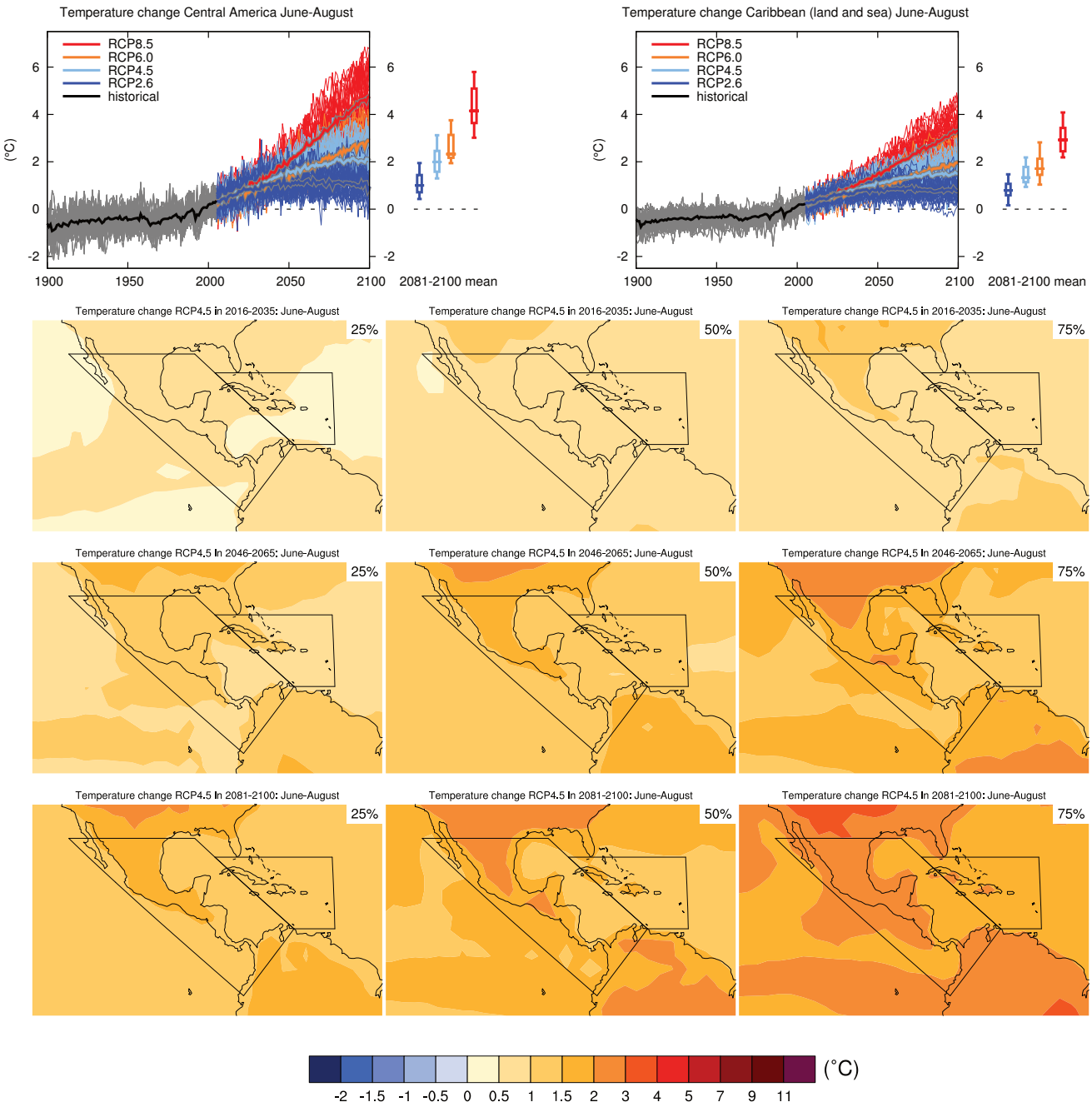

Figure AI.25 | (Top left) Time series of temperature change relative to 1986–2005 averaged over land grid points in Central America (68.8°W, 11.4°N; 79.7°W, 1.2°S; 116.3°W, 28.6°N; 90.3°W, 28.6°N) in June to August. (Top right) Same for all grid points in Caribbean (land and sea) (68.8°W, 11.4°N; 85.8°W, 25°N, 60°W, 25°N, 60°W, 11.44°N). Thin lines denote one ensemble member per model, thick lines the CMIP5 multi-model mean. On the right-hand side the 5th, 25th, 50th (median), 75th and 95th percentiles of the distribution of 20-year mean changes are given for 2081–2100 in the four RCP scenarios.

(Below) Maps of temperature changes in 2016–2035, 2046–2065 and 2081–2100 with respect to 1986–2005 in the RCP4.5 scenario. For each point, the 25th, 50th and 75th percentiles of the distribution of the CMIP5 ensemble are shown; this includes both natural variability and inter-model spread. Hatching denotes areas where the 20-year mean differences of the percentiles are less than the standard deviation of model-estimated present-day natural variability of 20-year mean differences.

Sections 9.4.1.1, 9.6.1.1, 10.3.1.1.4, Box 11.2, 14.8.4 contain relevant information regarding the evaluation of models in this region, the model spread in the context of other methods of projecting changes and the role of modes of variability and other climate phenomena.

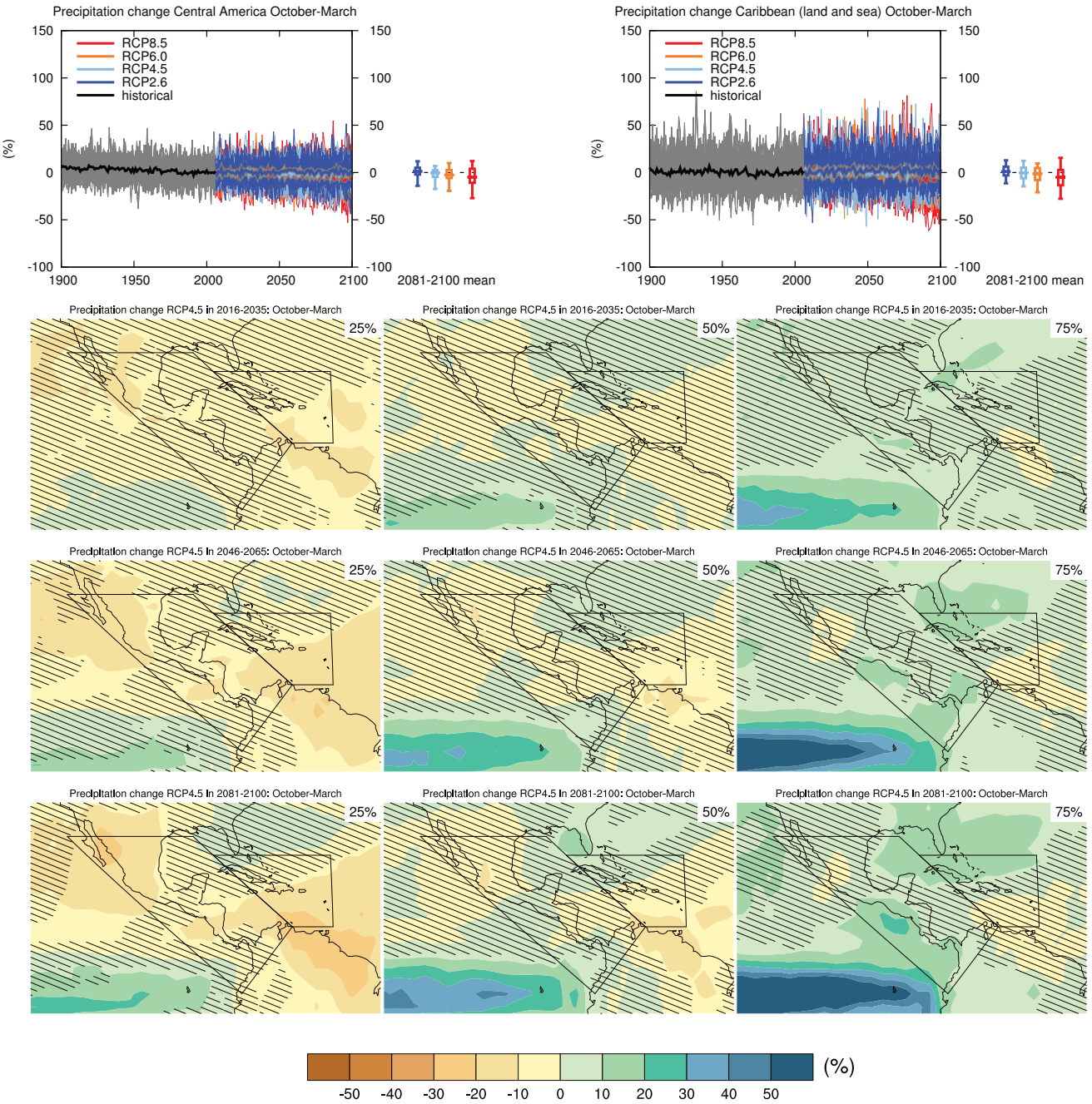

Figure AI.26 | (Top left) Time series of relative change relative to 1986–2005 in precipitation averaged over land grid points in Central America (68.8°W,11.4°N; 79.7°W, 1.2°S; 116.3°W,28.6°N; 90.3°W,28.6°N) in October to March. (Top right) Same for all grid points in Caribbean (land and sea) (68.8°W, 11.4°N; 85.8°W, 25°N, 60°W, 25°N, 60°W, 11.44°N). Thin lines denote one ensemble member per model, thick lines the CMIP5 multi-model mean. On the right-hand side the 5th, 25th, 50th (median), 75th and 95th percentiles of the distribution of 20-year mean changes are given for 2081–2100 in the four RCP scenarios.

(Below) Maps of precipitation changes in 2016–2035, 2046–2065 and 2081–2100 with respect to 1986–2005 in the RCP4.5 scenario. For each point, the 25th, 50th and 75th percentiles of the distribution of the CMIP5 ensemble are shown; this includes both natural variability and inter-model spread. Hatching denotes areas where the 20-year mean differences of the percentiles are less than the standard deviation of model-estimated present-day natural variability of 20-year mean differences.

Sections 9.4.1.1, 9.6.1.1, Box 11.2, 12.4.5.2, 14.2.3.1, 14.8.4 contain relevant information regarding the evaluation of models in this region, the model spread in the context of other methods of projecting changes and the role of modes of variability and other climate phenomena.

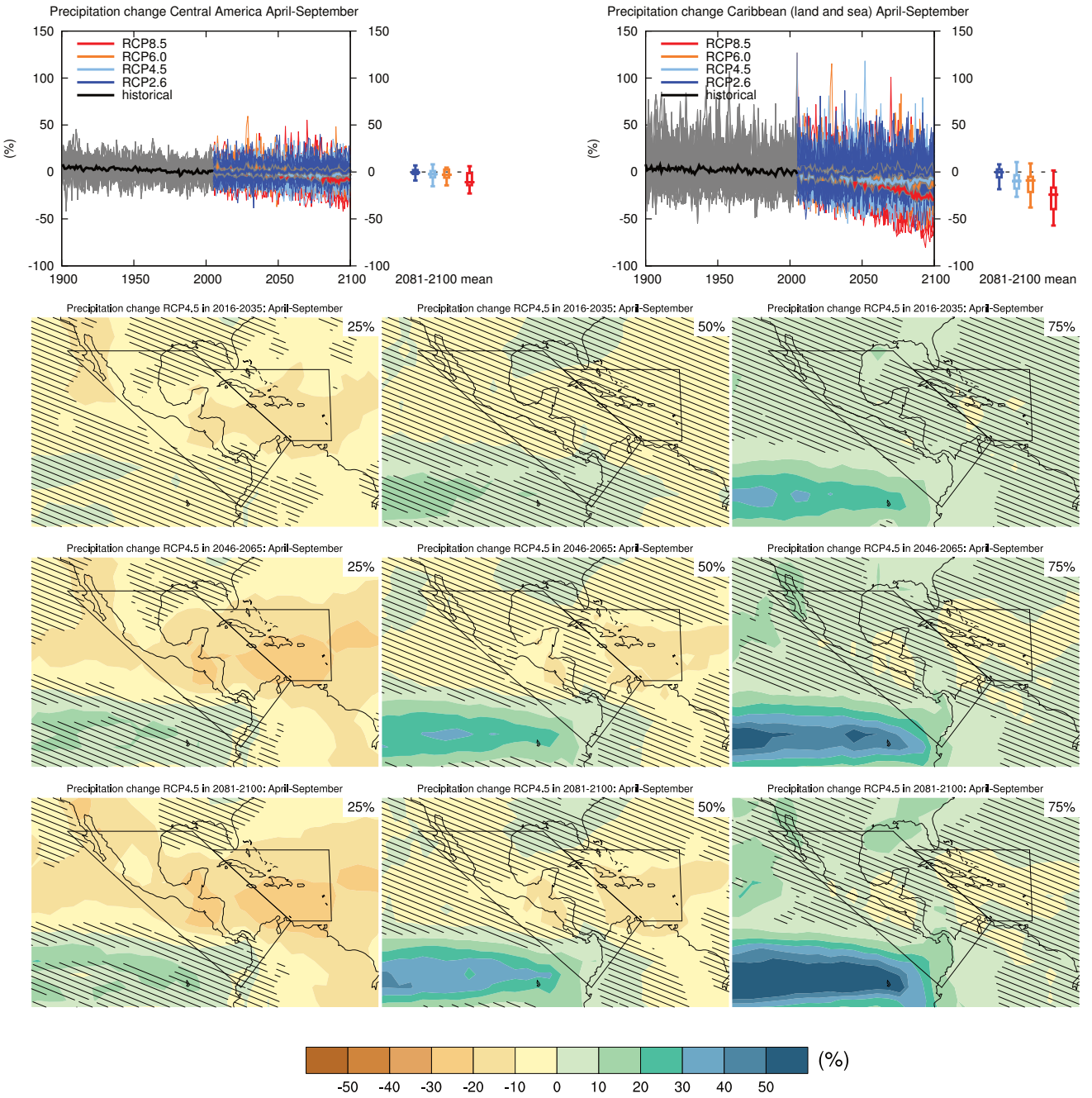

Figure AI.27 | (Top left) Time series of relative change relative to 1986–2005 in precipitation averaged over land grid points in Central America (68.8°W, 11.4°N; 79.7°W, 1.2°S; 116.3°W, 28.6°N; 90.3°W, 28.6°N) in April to September. (Top right) Same for all grid points in Caribbean (land and sea) (68.8°W, 11.4°N; 85.8°W, 25°N, 60°W, 25°N, 60°W, 11.44°N). Thin lines denote one ensemble member per model, thick lines the CMIP5 multi-model mean. On the right-hand side the 5th, 25th, 50th (median), 75th and 95th percentiles of the distribution of 20-year mean changes are given for 2081–2100 in the four RCP scenarios.

(Below) Maps of precipitation changes in 2016–2035, 2046–2065 and 2081–2100 with respect to 1986–2005 in the RCP4.5 scenario. For each point, the 25th, 50th and 75th percentiles of the distribution of the CMIP5 ensemble are shown; this includes both natural variability and inter-model spread. Hatching denotes areas where the 20-year mean differences of the percentiles are less than the standard deviation of model-estimated present-day natural variability of 20-year mean differences.

Sections 9.4.1.1, 9.6.1.1, Box 11.2, 12.4.5.2, 14.2.3.1, 14.8.4 contain relevant information regarding the evaluation of models in this region, the model spread in the context of other methods of projecting changes and the role of modes of variability and other climate phenomena.

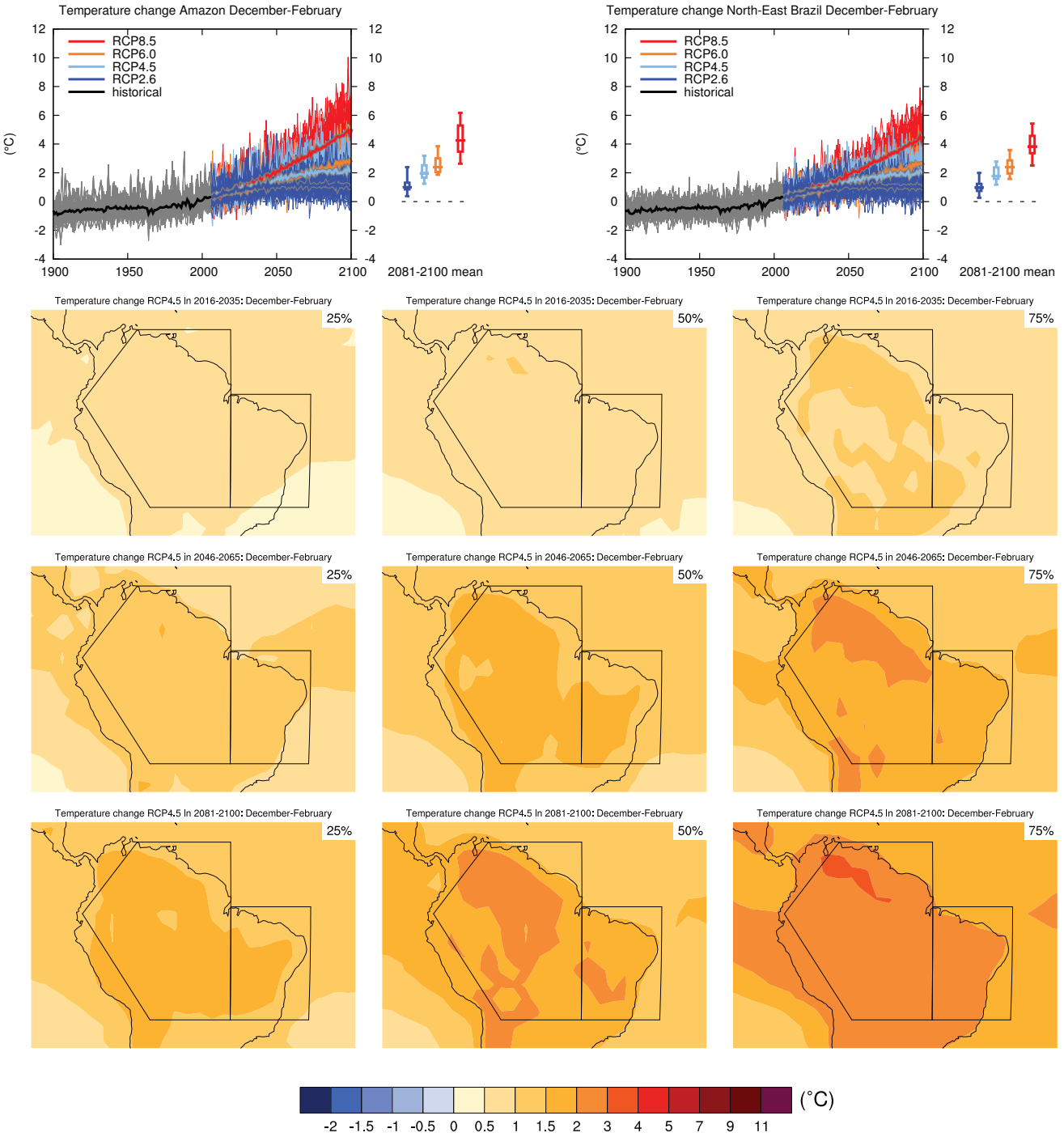

Figure AI.28 | (Top left) Time series of temperature change relative to 1986–2005 averaged over land grid points in the Amazon (20°S, 66.4°W; 1.24°S, 79.7°W; 11.44°N, 68.8°W; 11.44°N, 50°W; 20°S, 50°W) in December-February. (Top right) Same for land grid points in northeast Brazil (20°S to EQ, 50°W to 34°W). Thin lines denote one ensemble member per model, thick lines the CMIP5 multi-model mean. On the right-hand side the 5th, 25th, 50th (median), 75th and 95th percentiles of the distribution of 20-year mean changes are given for 2081–2100 in the four RCP scenarios.

(Below) Maps of temperature changes in 2016–2035, 2046–2065 and 2081–2100 with respect to 1986–2005 in the RCP4.5 scenario. For each point, the 25th, 50th and 75th percentiles of the distribution of the CMIP5 ensemble are shown; this includes both natural variability and inter-model spread. Hatching denotes areas where the 20-year mean differences of the percentiles are less than the standard deviation of model-estimated present-day natural variability of 20-year mean differences.

Sections 9.4.1.1, 9.6.1.1, 10.3.1.1.4, Box 11.2, 14.8.5 contain relevant information regarding the evaluation of models in this region, the model spread in the context of other methods of projecting changes and the role of modes of variability and other climate phenomena.

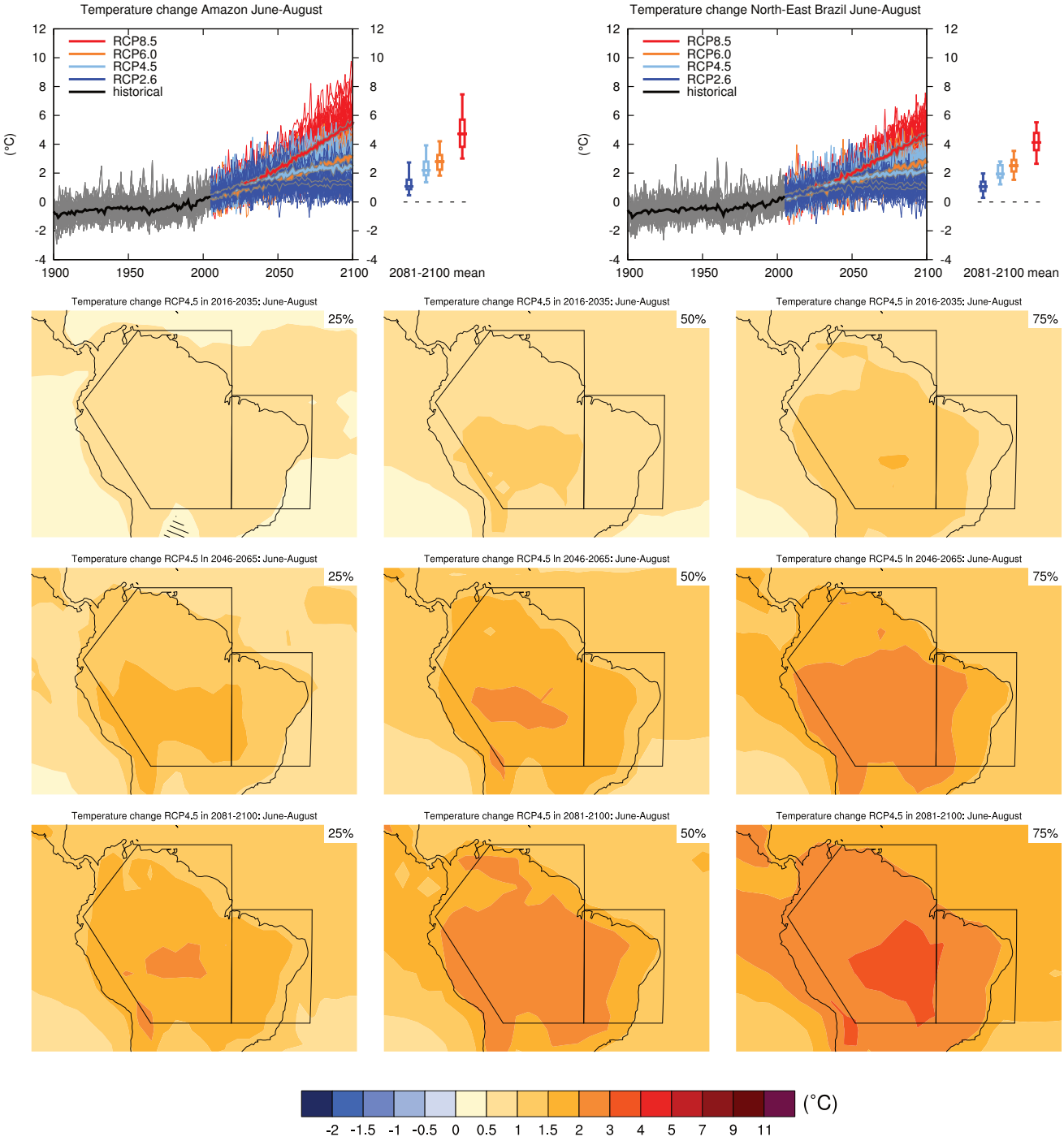

Figure AI.29 | (Top left) Time series of temperature change relative to 1986–2005 averaged over land grid points in the Amazon (20°S, 66.4°W; 1.24°S, 79.7°W; 11.44°N, 68.8°W; 11.44°N, 50°W; 20°S, 50°W) in June to August. (Top right) Same for land grid points in northeast Brazil (20°S to EQ, 50°W to 34°W). Thin lines denote one ensemble member per model, thick lines the CMIP5 multi-model mean. On the right-hand side the 5th, 25th, 50th (median), 75th and 95th percentiles of the distribution of 20-year mean changes are given for 2081–2100 in the four RCP scenarios.

(Below) Maps of temperature changes in 2016–2035, 2046–2065 and 2081–2100 with respect to 1986–2005 in the RCP4.5 scenario. For each point, the 25th, 50th and 75th percentiles of the distribution of the CMIP5 ensemble are shown; this includes both natural variability and inter-model spread. Hatching denotes areas where the 20-year mean differences of the percentiles are less than the standard deviation of model-estimated present-day natural variability of 20-year mean differences.

Sections 9.4.1.1, 9.6.1.1, 10.3.1.1.4, Box 11.2, 14.8.5 contain relevant information regarding the evaluation of models in this region, the model spread in the context of other methods of projecting changes and the role of modes of variability and other climate phenomena.

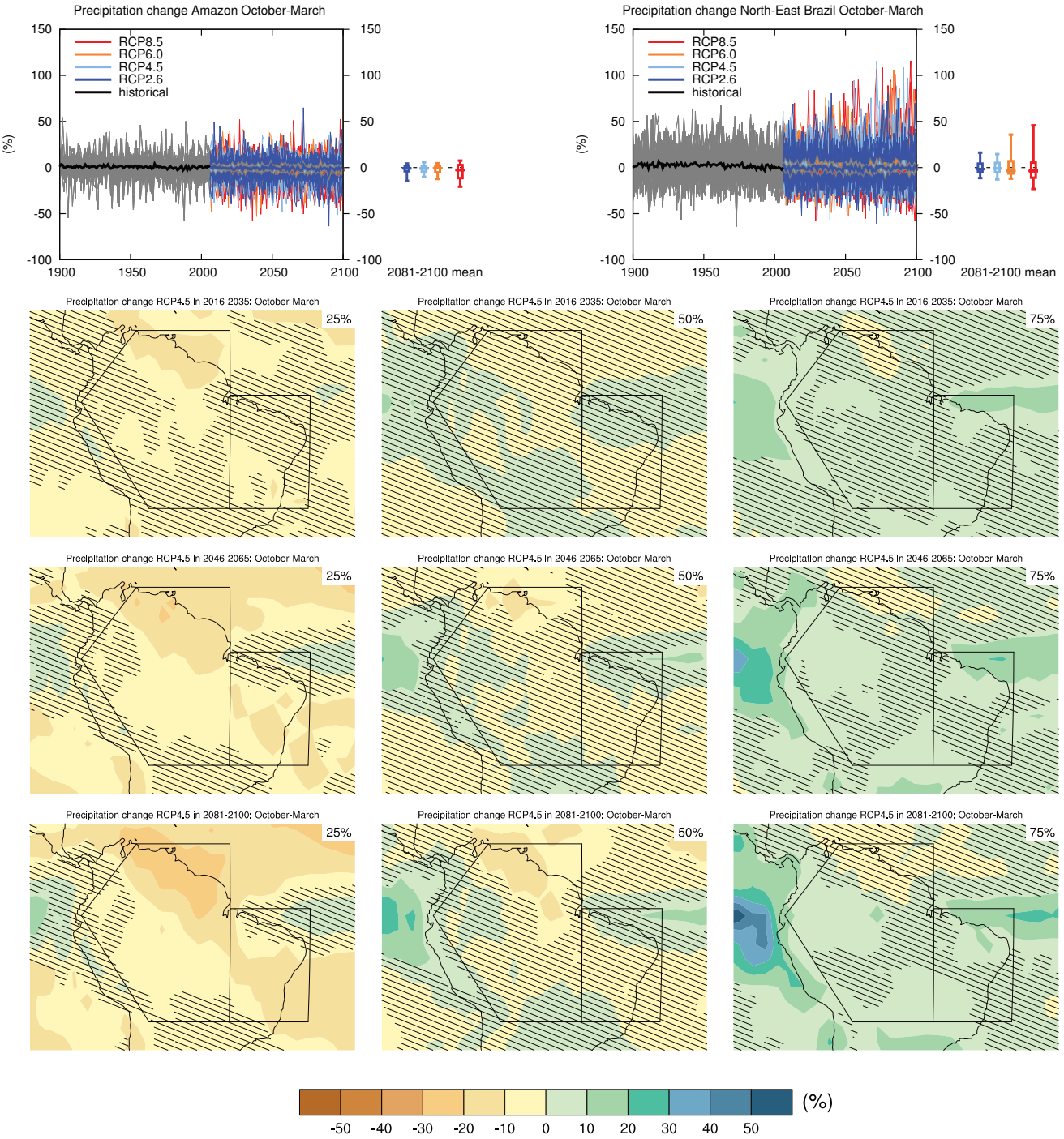

Figure AI.30 | (Top left) Time series of relative change relative to 1986–2005 in precipitation averaged over land grid points in the Amazon (20°S, 66.4°W; 1.24°S, 79.7°W; 11.44°N, 68.8°W; 11.44°N, 50°W; 20°S, 50°W) in October to March. (Top right) Same for land grid points in northeast Brazil (20°S to EQ, 50°W to 34°W). Thin lines denote one ensemble member per model, thick lines the CMIP5 multi-model mean. On the right-hand side the 5th, 25th, 50th (median), 75th and 95th percentiles of the distribution of 20-year mean changes are given for 2081–2100 in the four RCP scenarios.

(Below) Maps of precipitation changes in 2016–2035, 2046–2065 and 2081–2100 with respect to 1986–2005 in the RCP4.5 scenario. For each point, the 25th, 50th and 75th percentiles of the distribution of the CMIP5 ensemble are shown; this includes both natural variability and inter-model spread. Hatching denotes areas where the 20-year mean differences of the percentiles are less than the standard deviation of model-estimated present-day natural variability of 20-year mean differences.

Sections 9.4.1.1, 9.6.1.1, 11.3.2.1.2, Box 11.2, 14.2.3.2, 14.8.5 contain relevant information regarding the evaluation of models in this region, the model spread in the context of other methods of projecting changes and the role of modes of variability and other climate phenomena.

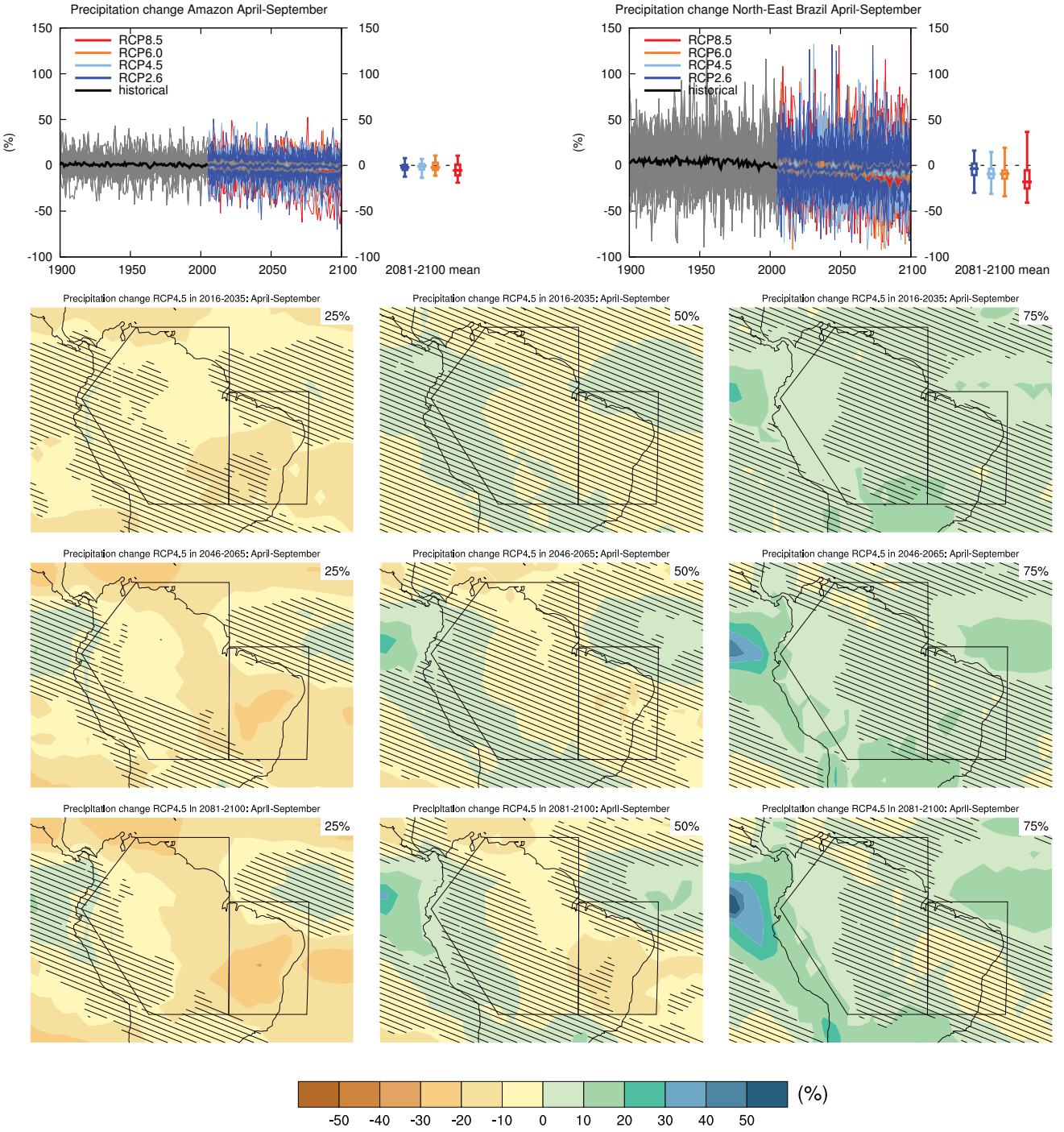

Figure AI.31 | (Top left) Time series of relative change relative to 1986–2005 in precipitation averaged over land grid points in the Amazon (20°S, 66.4°W; 1.24°S, 79.7°W; 11.44°N, 68.8°W; 11.44°N, 50°W; 20°S, 50°W) in April to September. (Top right) Same for land grid points in northeast Brazil (20°S to EQ, 50°W to 34°W). Thin lines denote one ensemble member per model, thick lines the CMIP5 multi-model mean. On the right-hand side the 5th, 25th, 50th (median), 75th and 95th percentiles of the distribution of 20-year mean changes are given for 2081–2100 in the four RCP scenarios.

(Below) Maps of precipitation changes in 2016–2035, 2046–2065 and 2081–2100 with respect to 1986–2005 in the RCP4.5 scenario. For each point, the 25th, 50th and 75th percentiles of the distribution of the CMIP5 ensemble are shown; this includes both natural variability and inter-model spread. Hatching denotes areas where the 20-year mean differences of the percentiles are less than the standard deviation of model-estimated present-day natural variability of 20-year mean differences.

Sections 9.4.1.1, 9.6.1.1, 11.3.2.1.2, Box 11.2, 14.2.3.2, 14.8.5 contain relevant information regarding the evaluation of models in this region, the model spread in the context of other methods of projecting changes and the role of modes of variability and other climate phenomena.

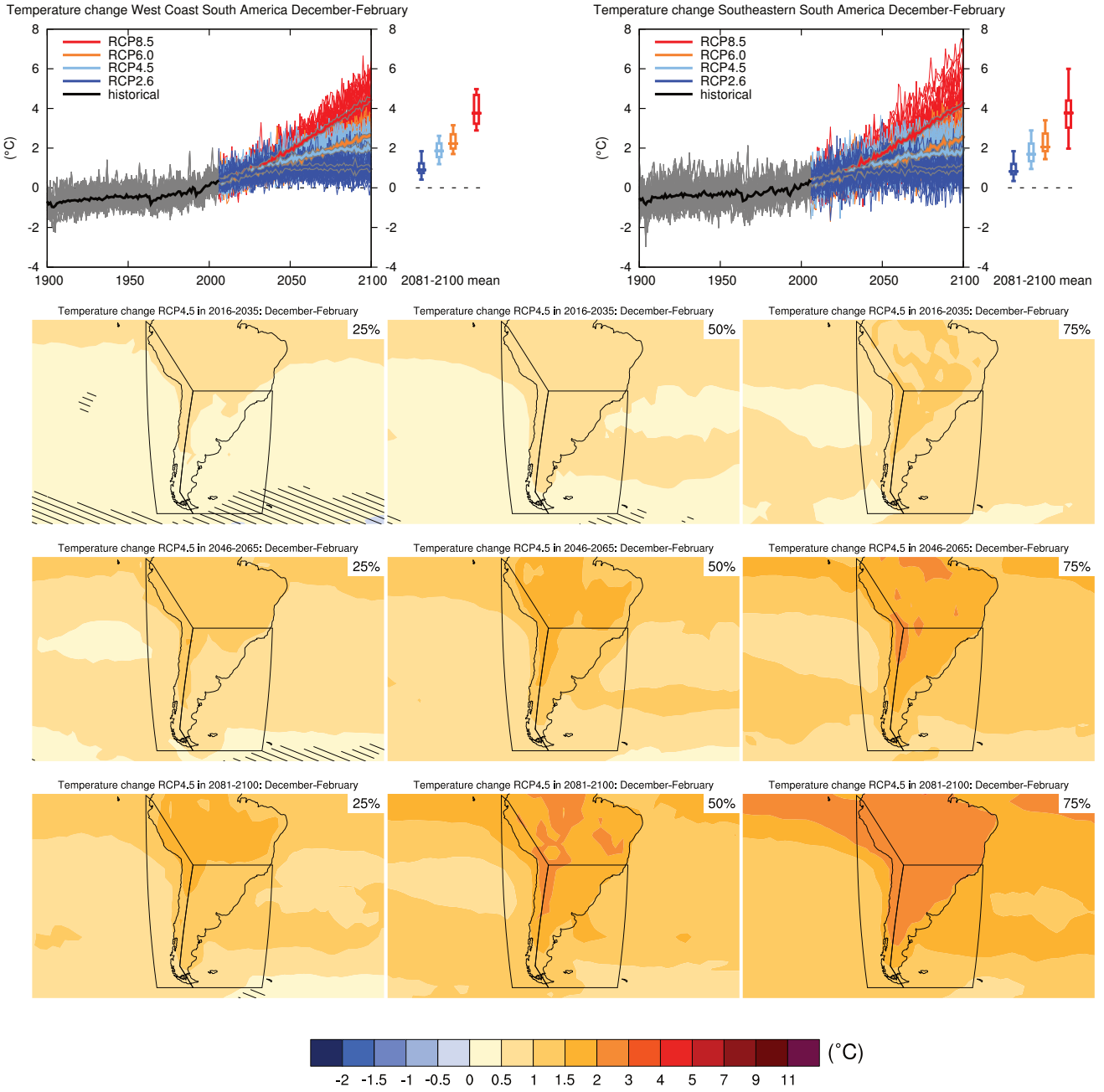

Figure AI.32 | (Top left) Time series of temperature change relative to 1986–2005 averaged over land grid points in the west coast of South America (79.7°W, 1.2°S; 66.4°W, 20°S; 72.1°W, 50°S; 67.3°W, 56.7°S; 82.0°W, 56.7°S; 82.2°W, 0.5°N) in December to February. (Top right) Same for land grid points in southeastern South America (39.4°W, 20°S; 39.4°W, 56.6°S; 67.3°W, 56.7°S; 72.1°W, 50°S; 66°W, 20°S). Thin lines denote one ensemble member per model, thick lines the CMIP5 multi-model mean. On the right-hand side the 5th, 25th, 50th (median), 75th and 95th percentiles of the distribution of 20-year mean changes are given for 2081–2100 in the four RCP scenarios.

(Below) Maps of temperature changes in 2016–2035, 2046–2065 and 2081–2100 with respect to 1986–2005 in the RCP4.5 scenario. For each point, the 25th, 50th and 75th percentiles of the distribution of the CMIP5 ensemble are shown; this includes both natural variability and inter-model spread. Hatching denotes areas where the 20-year mean differences of the percentiles are less than the standard deviation of model-estimated present-day natural variability of 20-year mean differences.

Sections 9.4.1.1, 9.6.1.1, 10.3.1.1.4, Box 11.2, 14.8.5 contain relevant information regarding the evaluation of models in this region, the model spread in the context of other methods of projecting changes and the role of modes of variability and other climate phenomena.

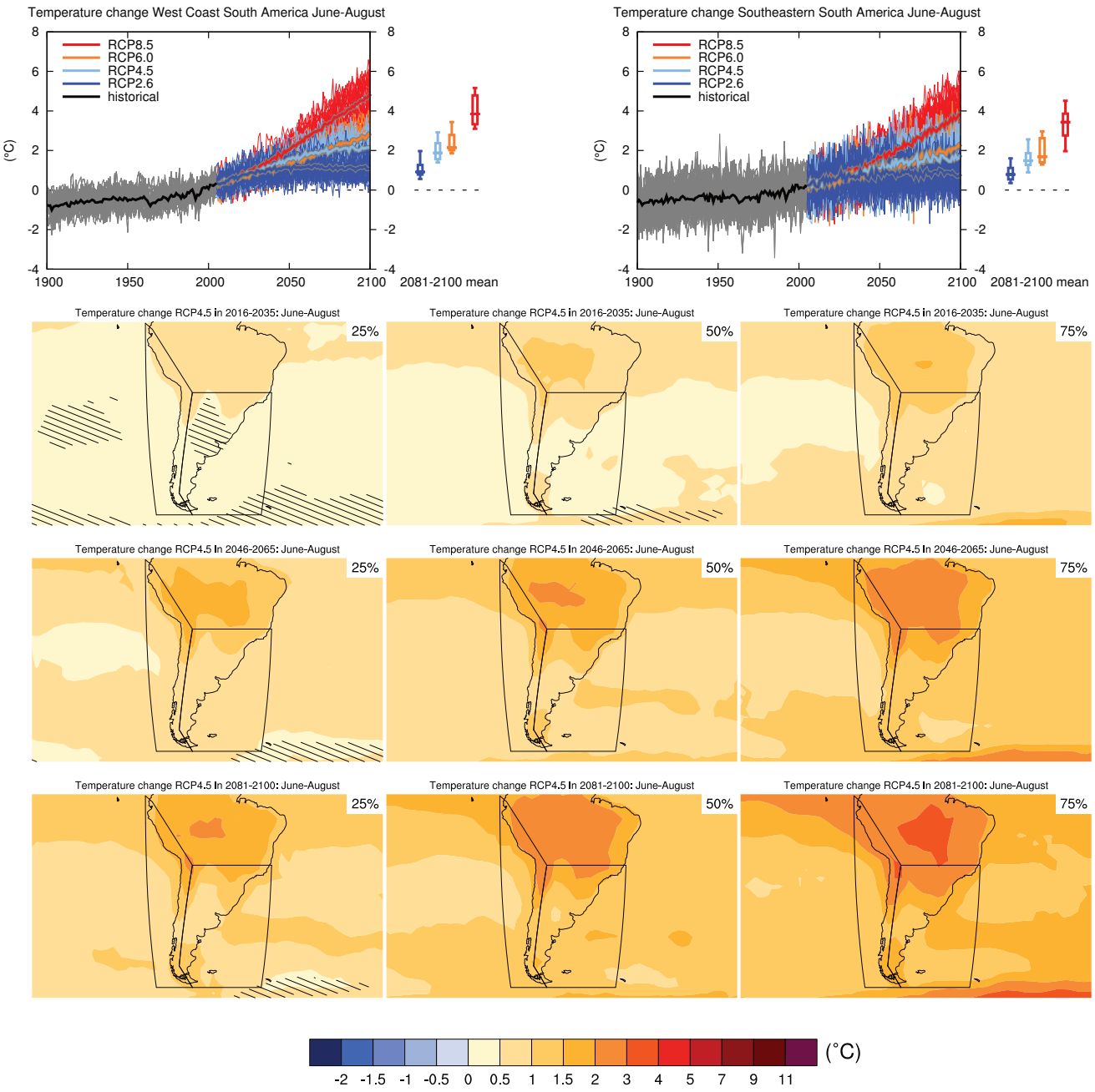

Figure AI.33 | (Top left) Time series of temperature change relative to 1986–2005 averaged over land grid points in the west coast of South America (79.7°W, 1.2°S; 66.4°W, 20°S; 72.1°W, 50°S; 67.3°W, 56.7°S; 82.0°W, 56.7°S; 82.2°W, 0.5°N) in June to August. (Top right) Same for land grid points in southeastern South America (39.4°W, 20°S; 39.4°W, 56.6°S; 67.3°W, 56.7°S; 72.1°W, 50°S; 66°W, 20°S). Thin lines denote one ensemble member per model, thick lines the CMIP5 multi-model mean. On the right-hand side the 5th, 25th, 50th (median), 75th and 95th percentiles of the distribution of 20-year mean changes are given for 2081–2100 in the four RCP scenarios.

(Below) Maps of temperature changes in 2016–2035, 2046–2065 and 2081–2100 with respect to 1986–2005 in the RCP4.5 scenario. For each point, the 25th, 50th and 75th percentiles of the distribution of the CMIP5 ensemble are shown; this includes both natural variability and inter-model spread. Hatching denotes areas where the 20-year mean differences of the percentiles are less than the standard deviation of model-estimated present-day natural variability of 20-year mean differences.

Sections 9.4.1.1, 9.6.1.1, 10.3.1.1.4, Box 11.2, 14.8.5 contain relevant information regarding the evaluation of models in this region, the model spread in the context of other methods of projecting changes and the role of modes of variability and other climate phenomena.

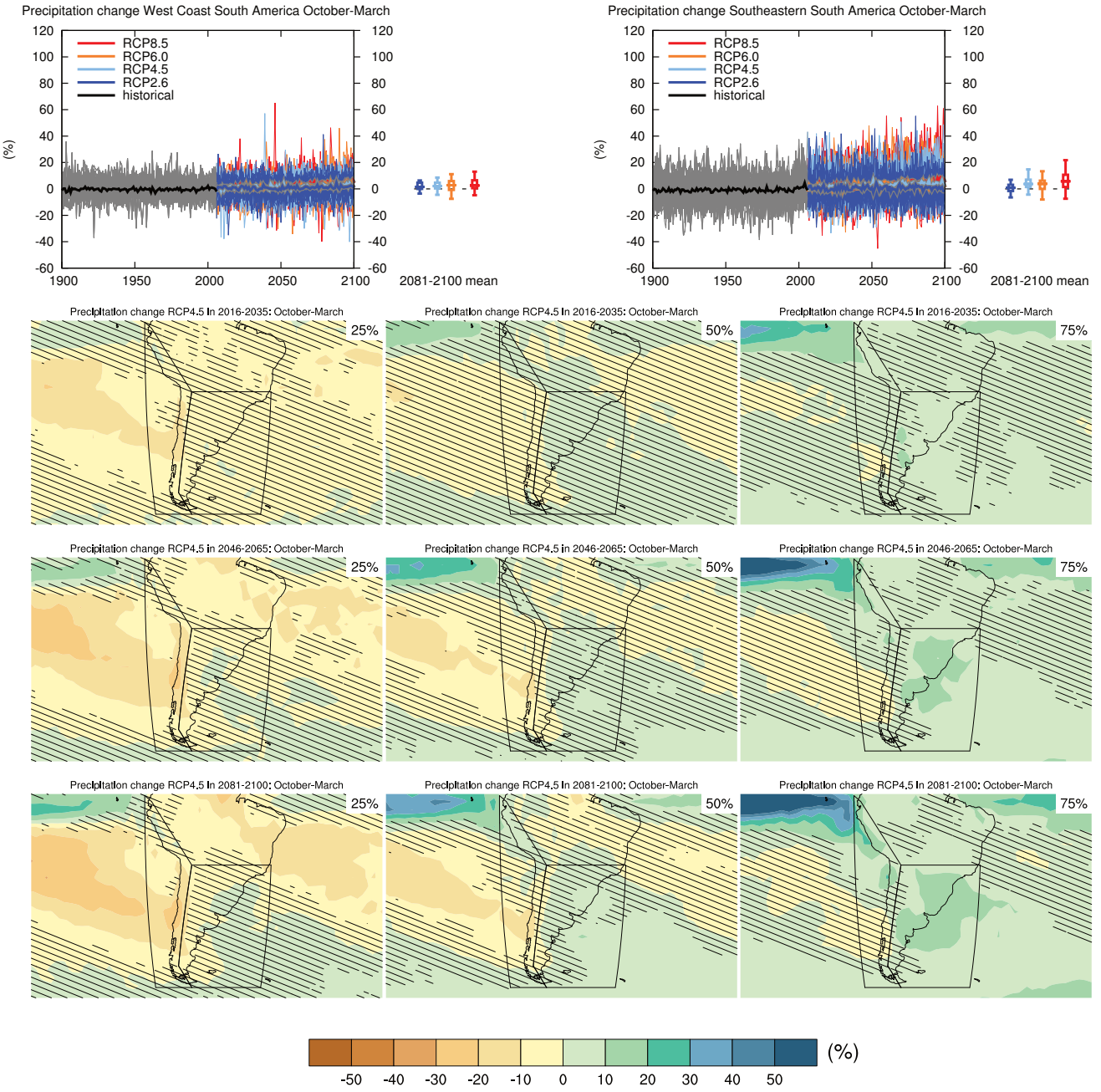

Figure AI.34 | (Top left) Time series of relative change relative to 1986–2005 in precipitation averaged over land grid points in the west coast of South America (79.7°W, 1.2°S; 66.4°W, 20°S; 72.1°W, 50°S; 67.3°W, 56.7°S; 82.0°W, 56.7°S; 82.2°W, 0.5°N) in October to March. (Top right) Same for land grid points in southeastern South America (39.4°W, 20°S; 39.4°W, 56.6°S; 67.3°W, 56.7°S; 72.1°W, 50°S; 66°W, 20°S). Thin lines denote one ensemble member per model, thick lines the CMIP5 multi-model mean. On the right-hand side the 5th, 25th, 50th (median), 75th and 95th percentiles of the distribution of 20-year mean changes are given for 2081–2100 in the four RCP scenarios.

(Below) Maps of precipitation changes in 2016–2035, 2046–2065 and 2081–2100 with respect to 1986–2005 in the RCP4.5 scenario. For each point, the 25th, 50th and 75th percentiles of the distribution of the CMIP5 ensemble are shown; this includes both natural variability and inter-model spread. Hatching denotes areas where the 20-year mean differences of the percentiles are less than the standard deviation of model-estimated present-day natural variability of 20-year mean differences.

Sections 9.4.1.1, 9.6.1.1, Box 11.2, 12.4.5.2, 14.8.5 contain relevant information regarding the evaluation of models in this region, the model spread in the context of other methods of projecting changes and the role of modes of variability and other climate phenomena.

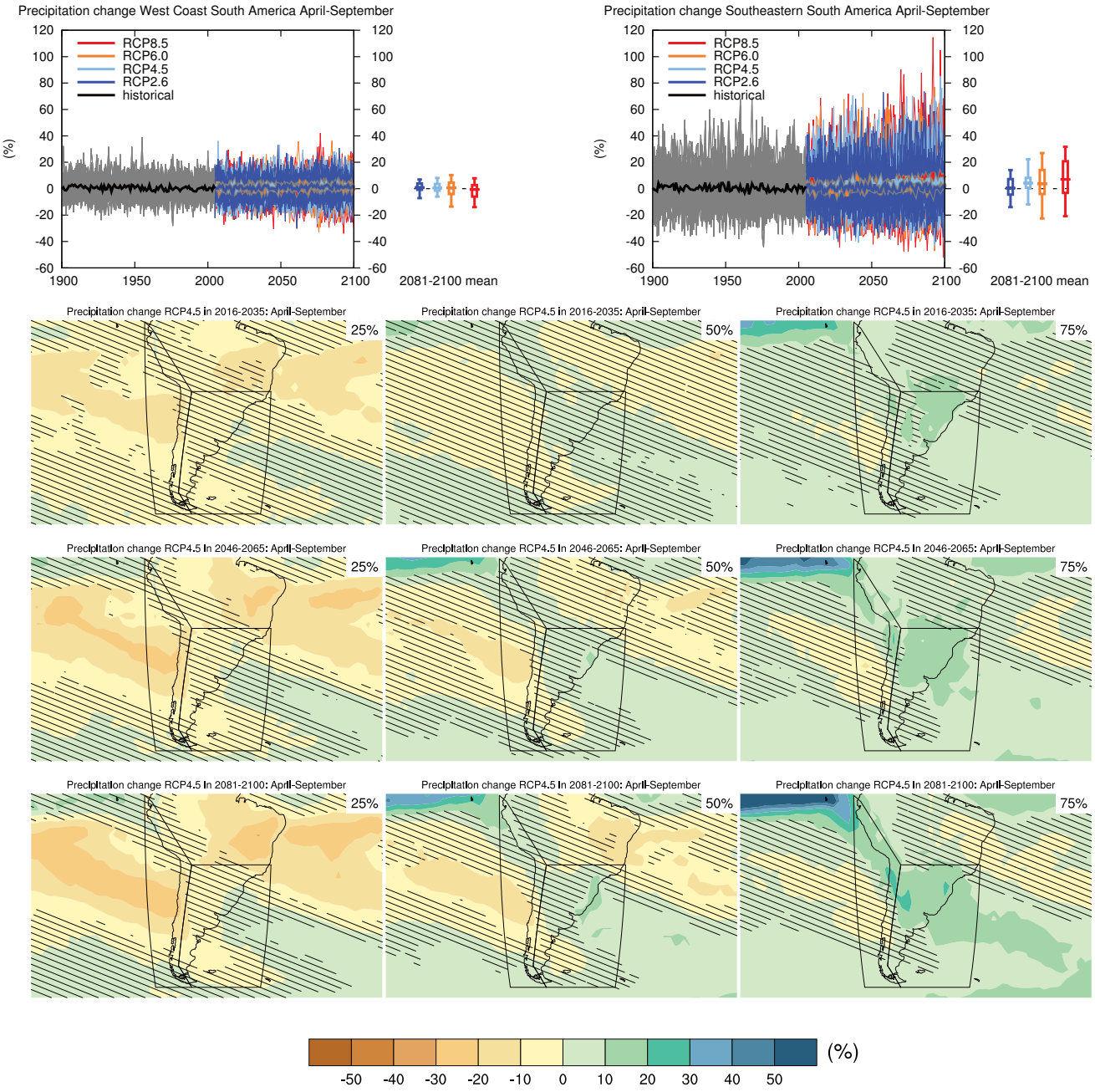

Figure AI.35 | (Top left) Time series of relative change relative to 1986–2005 in precipitation averaged over land grid points in the west coast of South America (79.7°W, 1.2°S; 66.4°W, 20°S; 72.1°W, 50°S; 67.3°W, 56.7°S; 82.0°W, 56.7°S; 82.2°W, 0.5°N) in April to September. (Top right) Same for land grid points in southeastern South America (39.4°W, 20°S; 39.4°W, 56.6°S; 67.3°W, 56.7°S; 72.1°W, 50°S; 66°W, 20°S). Thin lines denote one ensemble member per model, thick lines the CMIP5 multi-model mean. On the right-hand side the 5th, 25th, 50th (median), 75th and 95th percentiles of the distribution of 20-year mean changes are given for 2081–2100 in the four RCP scenarios.

(Below) Maps of precipitation changes in 2016–2035, 2046–2065 and 2081–2100 with respect to 1986–2005 in the RCP4.5 scenario. For each point, the 25th, 50th and 75th percentiles of the distribution of the CMIP5 ensemble are shown; this includes both natural variability and inter-model spread. Hatching denotes areas where the 20-year mean differences of the percentiles are less than the standard deviation of model-estimated present-day natural variability of 20-year mean differences.

Sections 9.4.1.1, 9.6.1.1, Box 11.2, 12.4.5.2, 14.8.5 contain relevant information regarding the evaluation of models in this region, the model spread in the context of other methods of projecting changes and the role of modes of variability and other climate phenomena.

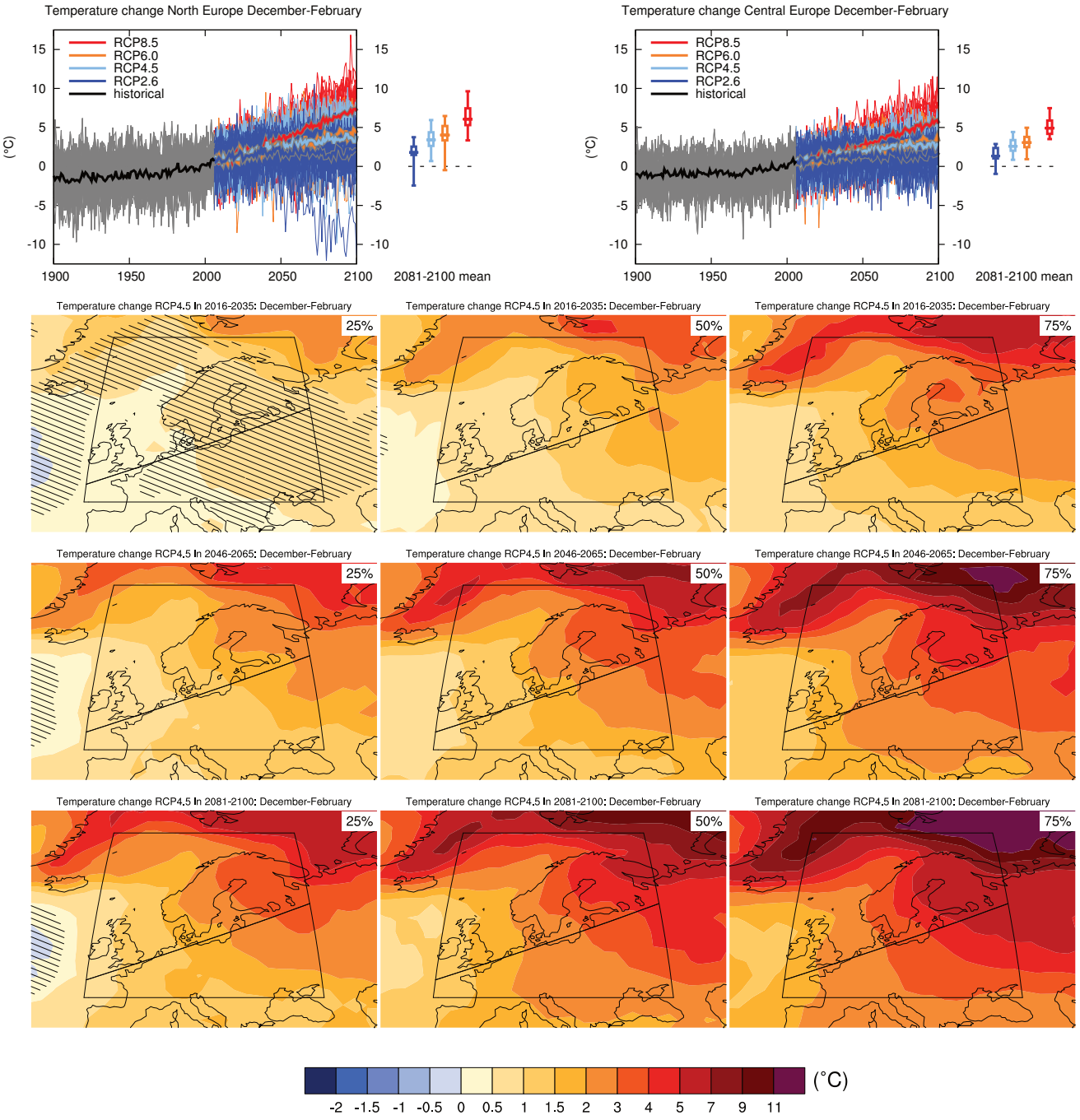

Figure AI.36 | (Top left) Time series of temperature change relative to 1986–2005 averaged over land grid points in North Europe (10°W, 48°N; 10°W, 75°N; 40°E, 75°N; 40°E, 61.3°N) in December to February. (Top right) Same for land grid points in Central Europe (10°W, 45°N; 10°W, 48°N; 40°E, 61.3°N; 40°E, 45°N). Thin lines denote one ensemble member per model, thick lines the CMIP5 multi-model mean. On the right-hand side the 5th, 25th, 50th (median), 75th and 95th percentiles of the distribution of 20-year mean changes are given for 2081–2100 in the four RCP scenarios.

(Below) Maps of temperature changes in 2016–2035, 2046–2065 and 2081–2100 with respect to 1986–2005 in the RCP4.5 scenario. For each point, the 25th, 50th and 75th percentiles of the distribution of the CMIP5 ensemble are shown; this includes both natural variability and inter-model spread. Hatching denotes areas where the 20-year mean differences of the percentiles are less than the standard deviation of model-estimated present-day natural variability of 20-year mean differences.

Sections 9.4.1.1, 9.6.1.1, 10.3.1.1.4, 10.3, Box 11.2, 14.8.6 contain relevant information regarding the evaluation of models in this region, the model spread in the context of other methods of projecting changes and the role of modes of variability and other climate phenomena.

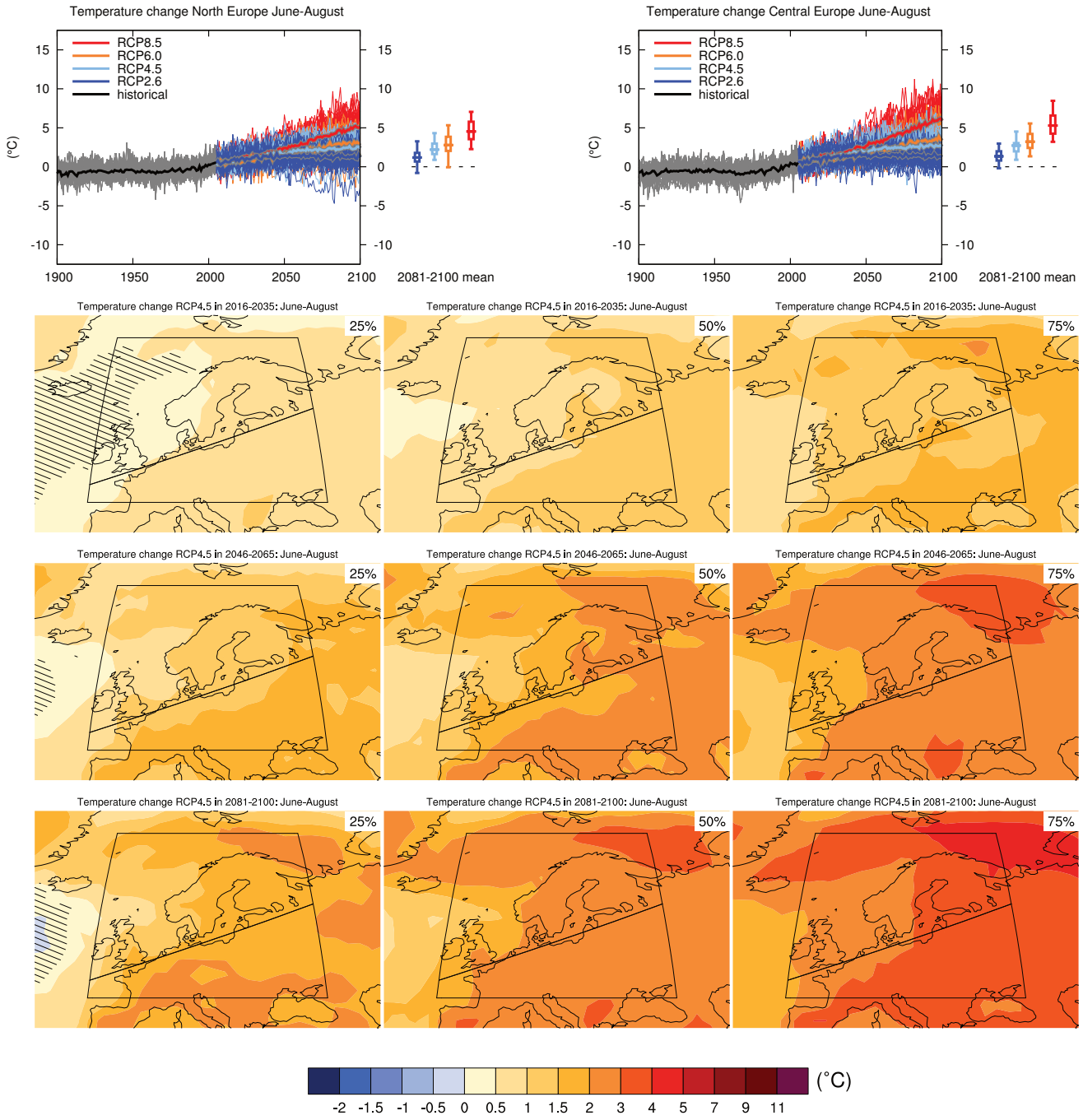

Figure AI.37 | (Top left) Time series of temperature change relative to 1986–2005 averaged over land grid points in North Europe (10°W, 48°N; 10°W, 75°N; 40°E, 75°N; 40°E, 61.3°N) in June to August. (Top right) Same for land grid points in Central Europe (10°W, 45°N; 10°W, 48°N; 40°E, 61.3°N; 40°E, 45°N). Thin lines denote one ensemble member per model, thick lines the CMIP5 multi-model mean. On the right-hand side the 5th, 25th, 50th (median), 75th and 95th percentiles of the distribution of 20-year mean changes are given for 2081–2100 in the four RCP scenarios.

(Below) Maps of temperature changes in 2016–2035, 2046–2065 and 2081–2100 with respect to 1986–2005 in the RCP4.5 scenario. For each point, the 25th, 50th and 75th percentiles of the distribution of the CMIP5 ensemble are shown; this includes both natural variability and inter-model spread. Hatching denotes areas where the 20-year mean differences of the percentiles are less than the standard deviation of model-estimated present-day natural variability of 20-year mean differences.

Sections 9.4.1.1, 9.6.1.1, 10.3.1.1.4, 10.3, Box 11.2, 14.8.6 contain relevant information regarding the evaluation of models in this region, the model spread in the context of other methods of projecting changes and the role of modes of variability and other climate phenomena.

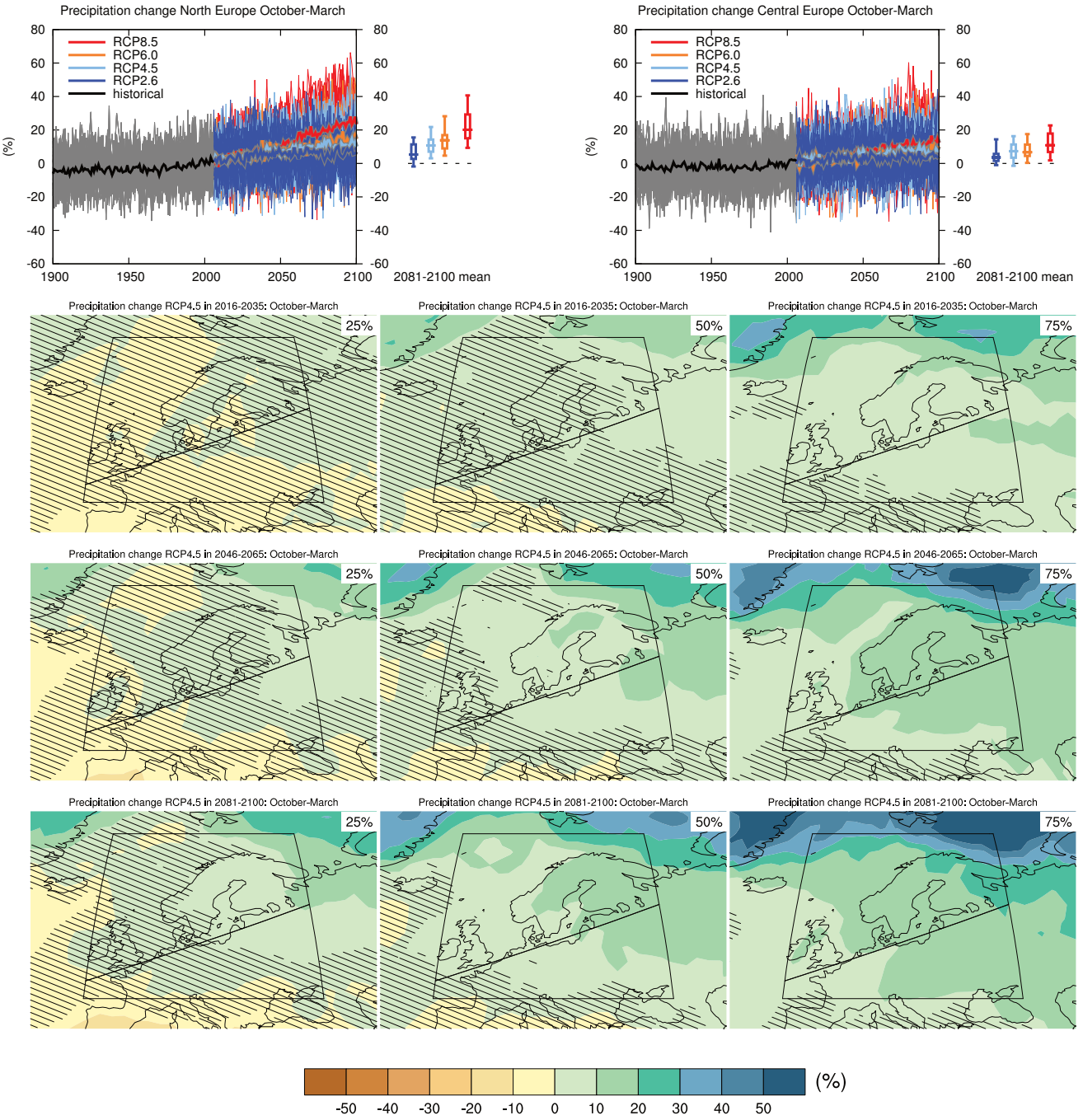

Figure AI.38 | (Top left) Time series of relative change relative to 1986–2005 in precipitation averaged over land grid points in North Europe (10°W, 48°N; 10°W, 75°N; 40°E, 75°N; 40°E, 61.3°N) in October to March. (Top right) Same for land grid points in Central Europe (10°W, 45°N; 10°W, 48°N; 40°E, 61.3°N; 40°E, 45°N). Thin lines denote one ensemble member per model, thick lines the CMIP5 multi-model mean. On the right-hand side the 5th, 25th, 50th (median), 75th and 95th percentiles of the distribution of 20-year mean changes are given for 2081–2100 in the four RCP scenarios.

(Below) Maps of precipitation changes in 2016–2035, 2046–2065 and 2081–2100 with respect to 1986–2005 in the RCP4.5 scenario. For each point, the 25th, 50th and 75th percentiles of the distribution of the CMIP5 ensemble are shown; this includes both natural variability and inter-model spread. Hatching denotes areas where the 20-year mean differences of the percentiles are less than the standard deviation of model-estimated present-day natural variability of 20-year mean differences.

Sections 9.4.1.1, 9.6.1.1, Box 11.2, 12.4.5.2, 14.8.6 contain relevant information regarding the evaluation of models in this region, the model spread in the context of other methods of projecting changes and the role of modes of variability and other climate phenomena.

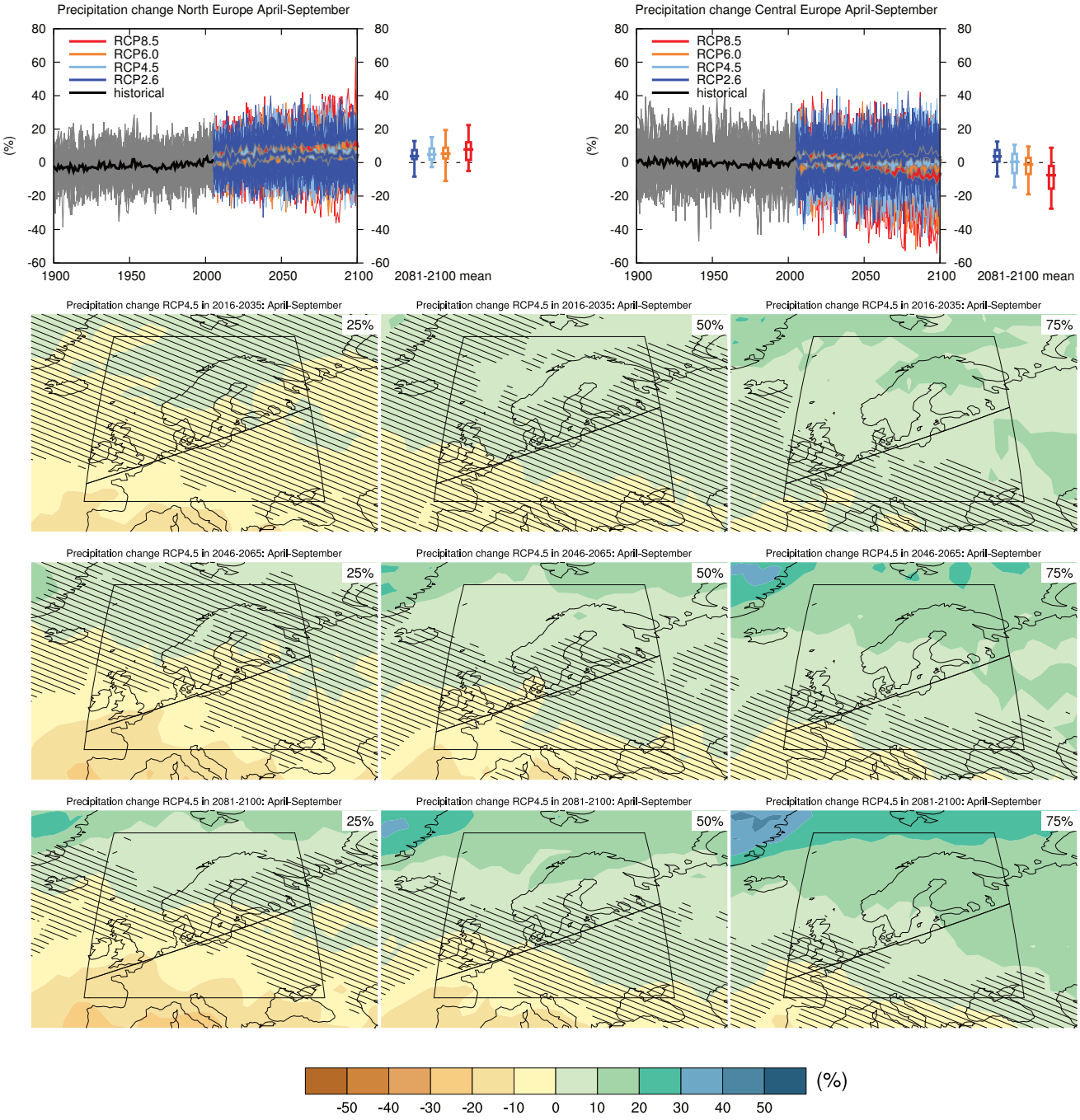

Figure AI.39 | (Top left) Time series of relative change relative to 1986–2005 in precipitation averaged over land grid points in North Europe (10°W, 48°N; 10°W, 75°N; 40°E, 75°N; 40°E, 61.3°N) in April to September. (Top right) Same for land grid points in Central Europe (10°W, 45°N; 10°W, 48°N; 40°E, 61.3°N; 40°E, 45°N). Thin lines denote one ensemble member per model, thick lines the CMIP5 multi-model mean. On the right-hand side the 5th, 25th, 50th (median), 75th and 95th percentiles of the distribution of 20-year mean changes are given for 2081–2100 in the four RCP scenarios.

(Below) Maps of precipitation changes in 2016–2035, 2046–2065 and 2081–2100 with respect to 1986–2005 in the RCP4.5 scenario. For each point, the 25th, 50th and 75th percentiles of the distribution of the CMIP5 ensemble are shown; this includes both natural variability and inter-model spread. Hatching denotes areas where the 20-year mean differences of the percentiles are less than the standard deviation of model-estimated present-day natural variability of 20-year mean differences.

Sections 9.4.1.1, 9.6.1.1, Box 11.2, 12.4.5.2, 14.8.6 contain relevant information regarding the evaluation of models in this region, the model spread in the context of other methods of projecting changes and the role of modes of variability and other climate phenomena.

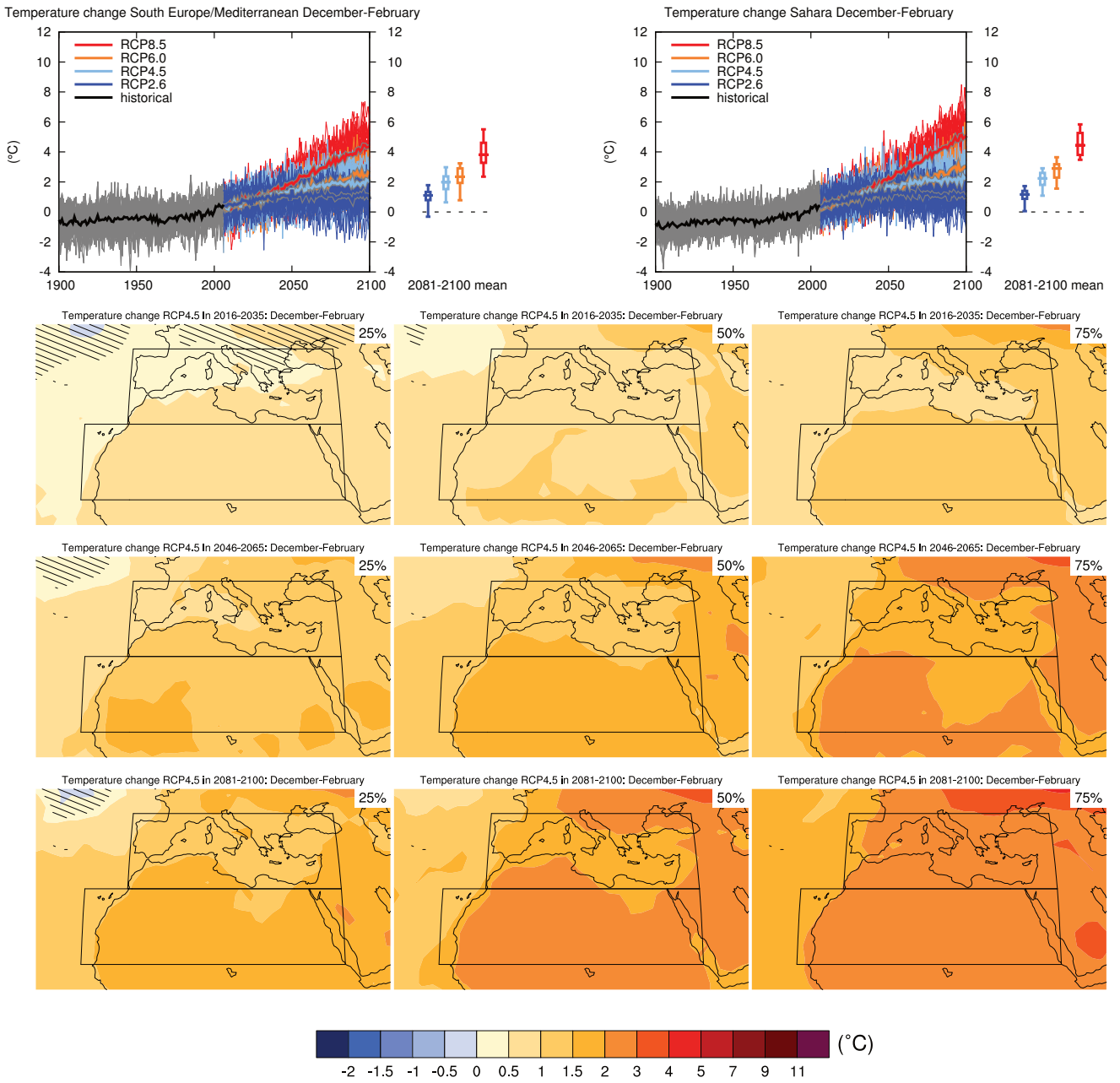

Figure AI.40 | (Top left) Time series of temperature change relative to 1986–2005 averaged over land grid points in the region South Europe/Mediterranean (30°N to 45°N, 10°W to 40°E) in December to February. (Top right) Same for land grid points in the Sahara (15°N to 30°N, 20°W to 40°E). Thin lines denote one ensemble member per model, thick lines the CMIP5 multi-model mean. On the right-hand side the 5th, 25th, 50th (median), 75th and 95th percentiles of the distribution of 20-year mean changes are given for 2081–2100 in the four RCP scenarios.

(Below) Maps of temperature changes in 2016–2035, 2046–2065 and 2081–2100 with respect to 1986–2005 in the RCP4.5 scenario. For each point, the 25th, 50th and 75th percentiles of the distribution of the CMIP5 ensemble are shown; this includes both natural variability and inter-model spread. Hatching denotes areas where the 20-year mean differences of the percentiles are less than the standard deviation of model-estimated present-day natural variability of 20-year mean differences.

Sections 9.4.1.1, 9.6.1.1, 10.3.1.1.4, Box 11.2, 14.8.6, 14.8.7 contain relevant information regarding the evaluation of models in this region, the model spread in the context of other methods of projecting changes and the role of modes of variability and other climate phenomena.

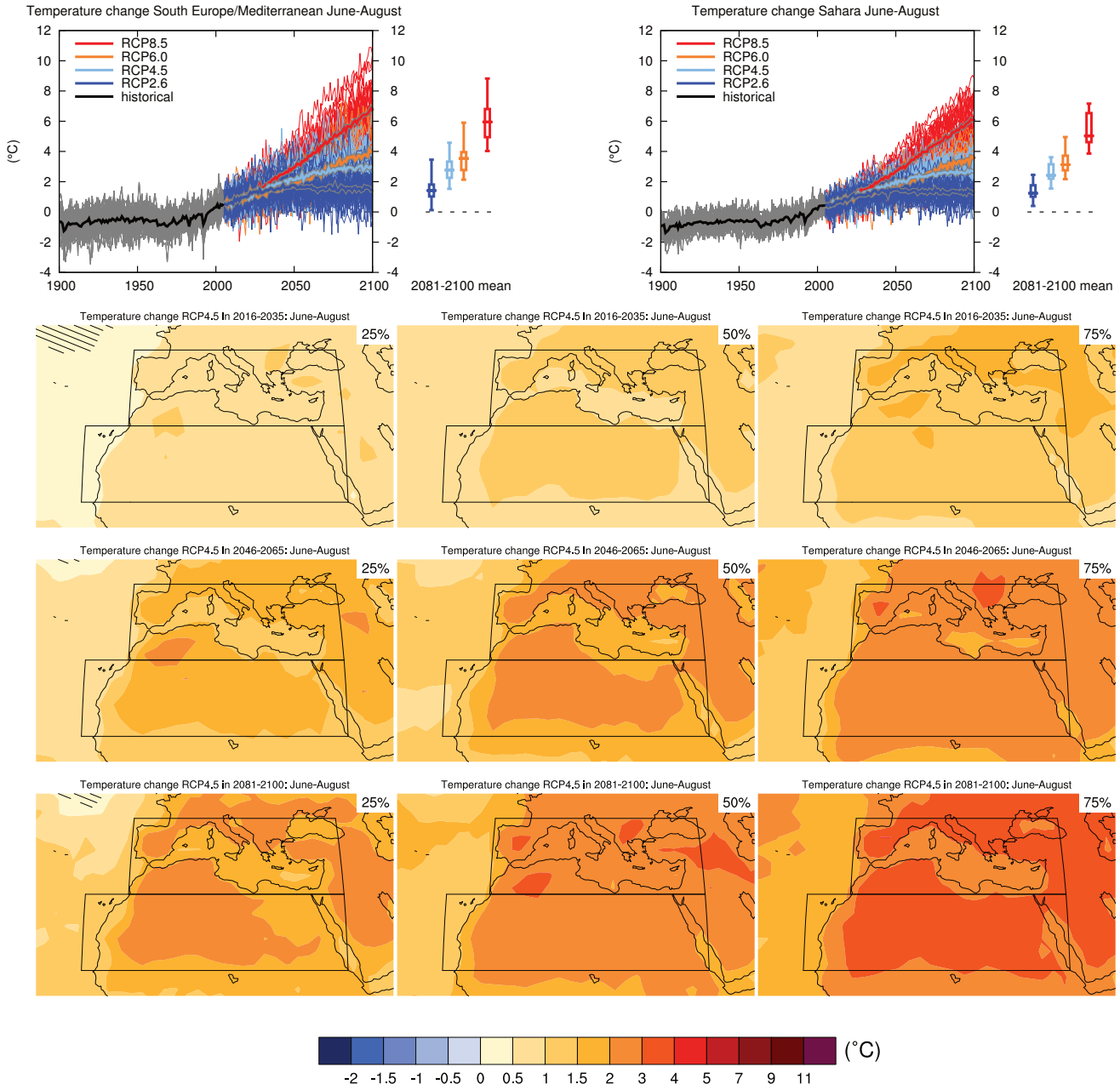

Figure AI.41 | (Top left) Time series of temperature change relative to 1986–2005 averaged over land grid points in the region South Europe/Mediterranean (30°N to 45°N, 10°W to 40°E) in June to August. (Top right) Same for land grid points in the Sahara (15°N to 30°N, 20°W to 40°E). Thin lines denote one ensemble member per model, thick lines the CMIP5 multi-model mean. On the right-hand side the 5th, 25th, 50th (median), 75th and 95th percentiles of the distribution of 20-year mean changes are given for 2081–2100 in the four RCP scenarios.

(Below) Maps of temperature changes in 2016–2035, 2046–2065 and 2081–2100 with respect to 1986–2005 in the RCP4.5 scenario. For each point, the 25th, 50th and 75th percentiles of the distribution of the CMIP5 ensemble are shown; this includes both natural variability and inter-model spread. Hatching denotes areas where the 20-year mean differences of the percentiles are less than the standard deviation of model-estimated present-day natural variability of 20-year mean differences.

Sections 9.4.1.1, 9.6.1.1, 10.3.1.1.4, Box 11.2, 14.8.6, 14.8.7 contain relevant information regarding the evaluation of models in this region, the model spread in the context of other methods of projecting changes and the role of modes of variability and other climate phenomena.

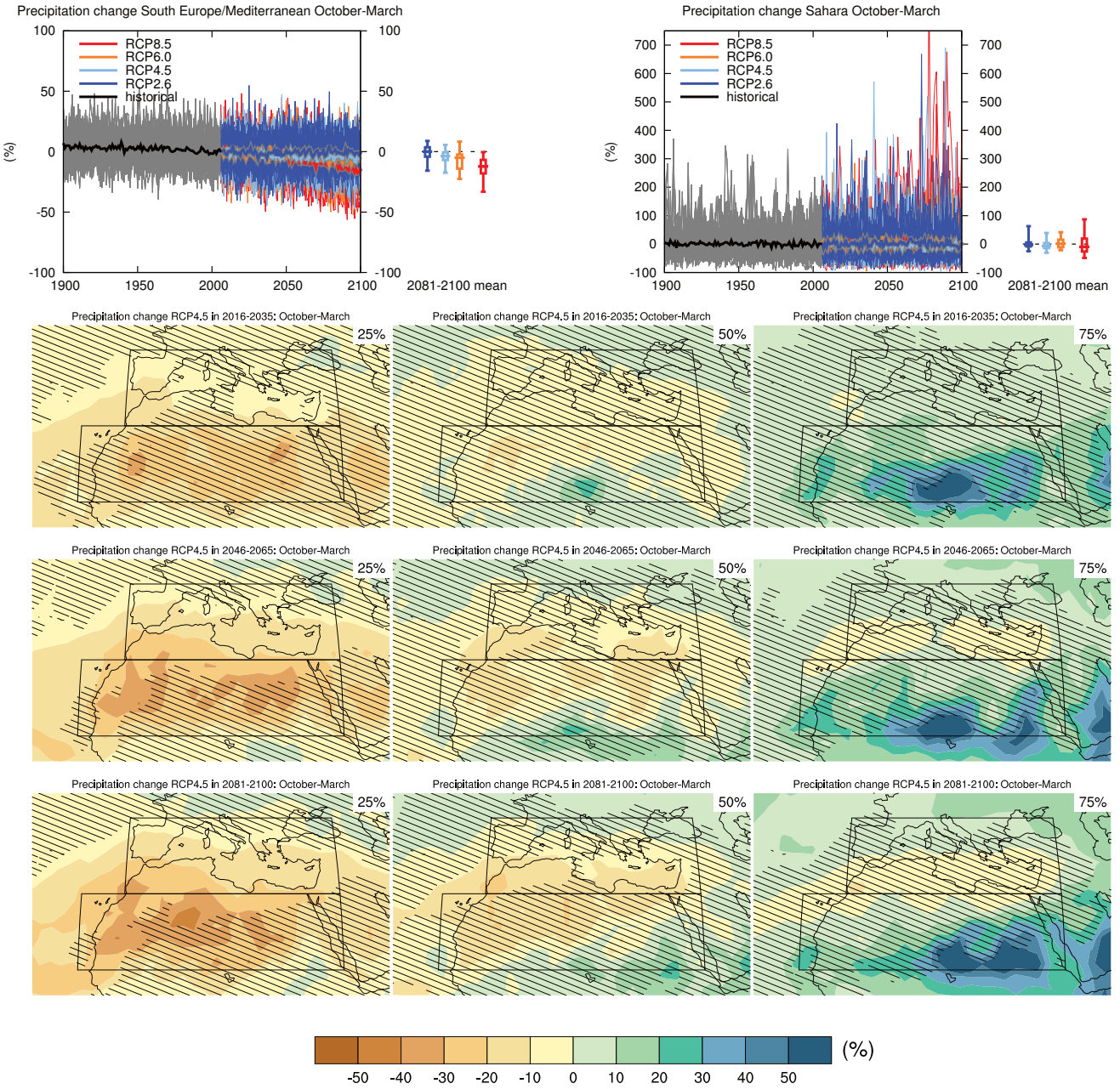

Figure AI.42 | (Top left) Time series of relative change relative to 1986–2005 in precipitation averaged over land grid points in the region South Europe/Mediterranean (30°N to 45°N, 10°W to 40°E) in October to March. (Top right) Same for land grid points in the Sahara (15°N to 30°N, 20°W to 40°E). Thin lines denote one ensemble member per model, thick lines the CMIP5 multi-model mean. On the right-hand side the 5th, 25th, 50th (median), 75th and 95th percentiles of the distribution of 20-year mean changes are given for 2081–2100 in the four RCP scenarios. Note different scales.

(Below) Maps of precipitation changes in 2016–2035, 2046–2065 and 2081–2100 with respect to 1986–2005 in the RCP4.5 scenario. For each point, the 25th, 50th and 75th percentiles of the distribution of the CMIP5 ensemble are shown; this includes both natural variability and inter-model spread. Hatching denotes areas where the 20-year mean differences of the percentiles are less than the standard deviation of model-estimated present-day natural variability of 20-year mean differences.

Sections 9.4.1.1, 9.6.1.1, Box 11.2, 12.4.5.2, 14.8.6, 14.8.7 contain relevant information regarding the evaluation of models in this region, the model spread in the context of other methods of projecting changes and the role of modes of variability and other climate phenomena.

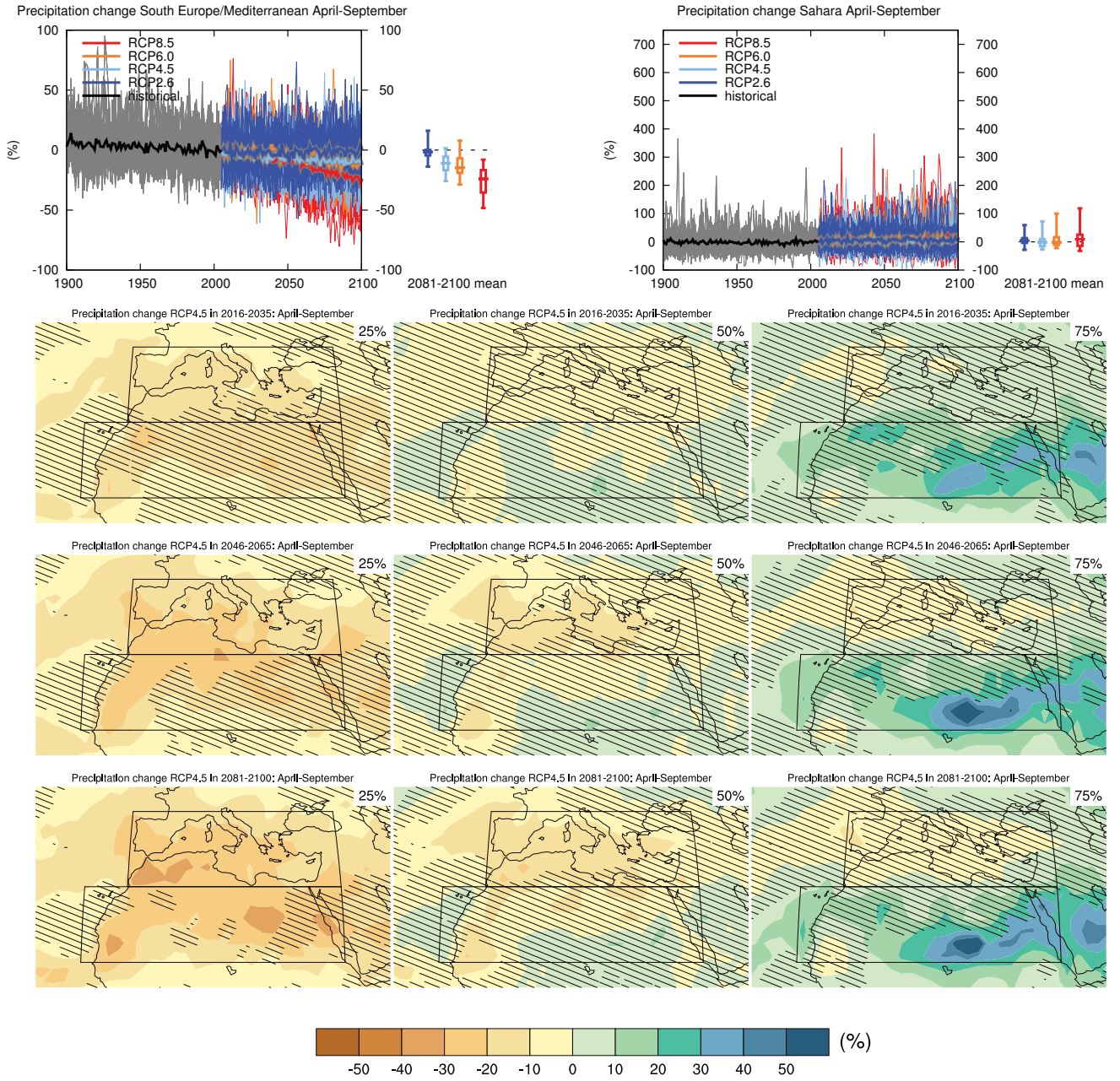

Figure AI.43 | (Top left) Time series of relative change relative to 1986–2005 in precipitation averaged over land grid points in the region South Europe/Mediterranean (30°N to 45°N, 10°W to 40°E) in April to September. (Top right) Same for land grid points in the Sahara (15°N to 30°N, 20°W to 40°E). Thin lines denote one ensemble member per model, thick lines the CMIP5 multi-model mean. On the right-hand side the 5th, 25th, 50th (median), 75th and 95th percentiles of the distribution of 20-year mean changes are given for 2081–2100 in the four RCP scenarios. Note different scales.

(Below) Maps of precipitation changes in 2016–2035, 2046–2065 and 2081–2100 with respect to 1986–2005 in the RCP4.5 scenario. For each point, the 25th, 50th and 75th percentiles of the distribution of the CMIP5 ensemble are shown; this includes both natural variability and inter-model spread. Hatching denotes areas where the 20-year mean differences of the percentiles are less than the standard deviation of model-estimated present-day natural variability of 20-year mean differences.

Sections 9.4.1.1, 9.6.1.1, Box 11.2, 12.4.5.2, 14.8.6, 14.8.7 contain relevant information regarding the evaluation of models in this region, the model spread in the context of other methods of projecting changes and the role of modes of variability and other climate phenomena.

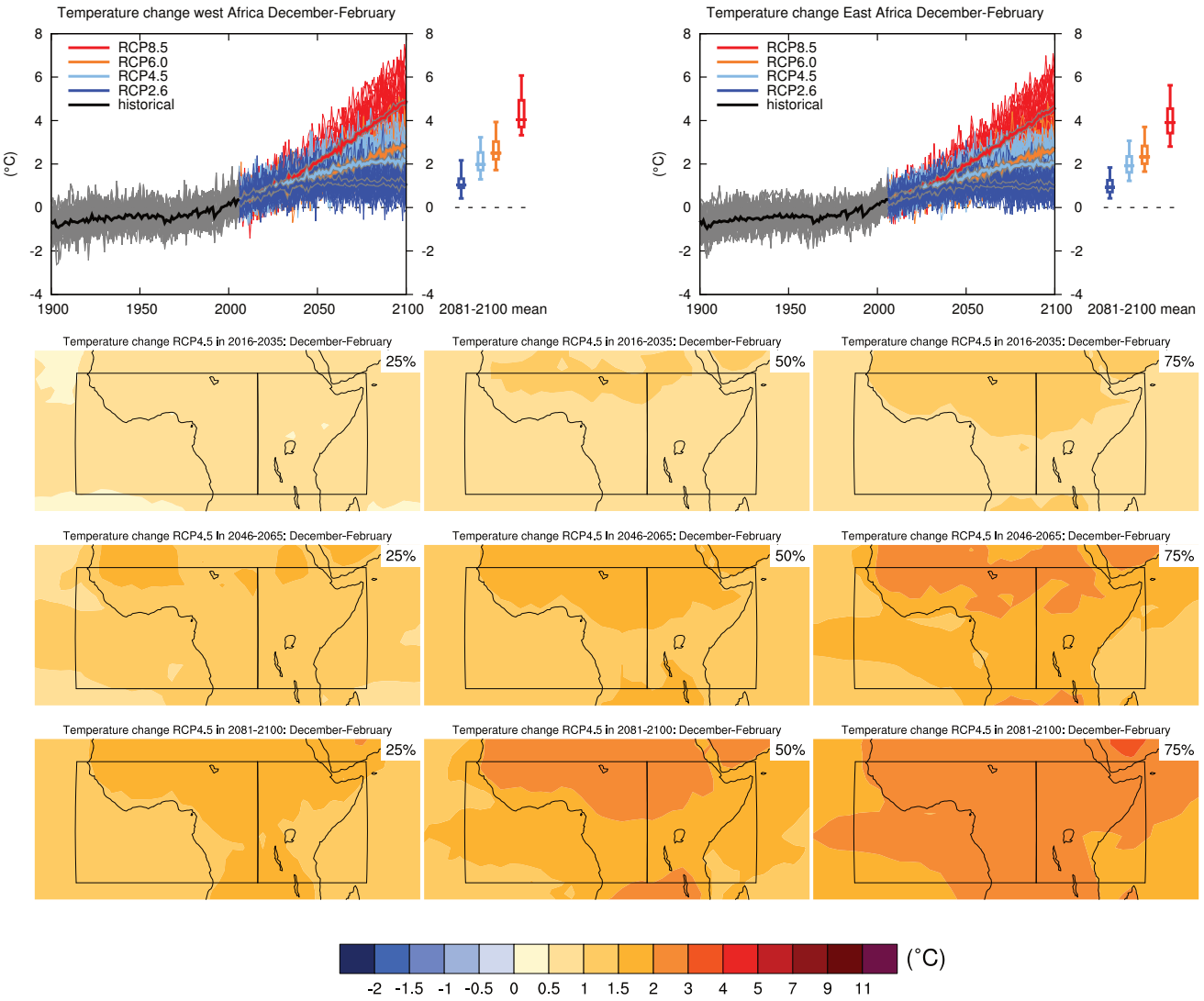

Figure AI.44 | (Top left) Time series of temperature change relative to 1986–2005 averaged over land grid points in West Africa (11.4°S to 15°N, 20°W to 25°E) in December to February. (Top right) Same for land grid points in East Africa (11.3°S to 15°N, 25°E to 52°E). Thin lines denote one ensemble member per model, thick lines the CMIP5 multi-model mean. On the right-hand side the 5th, 25th, 50th (median), 75th and 95th percentiles of the distribution of 20-year mean changes are given for 2081–2100 in the four RCP scenarios.

(Below) Maps of temperature changes in 2016–2035, 2046–2065 and 2081–2100 with respect to 1986–2005 in the RCP4.5 scenario. For each point, the 25th, 50th and 75th percentiles of the distribution of the CMIP5 ensemble are shown; this includes both natural variability and inter-model spread. Hatching denotes areas where the 20-year mean differences of the percentiles are less than the standard deviation of model-estimated present-day natural variability of 20-year mean differences.

Sections 9.4.1.1, 9.6.1.1, 10.3.1.1.4, Box 11.2, 14.8.7 contain relevant information regarding the evaluation of models in this region, the model spread in the context of other methods of projecting changes and the role of modes of variability and other climate phenomena.

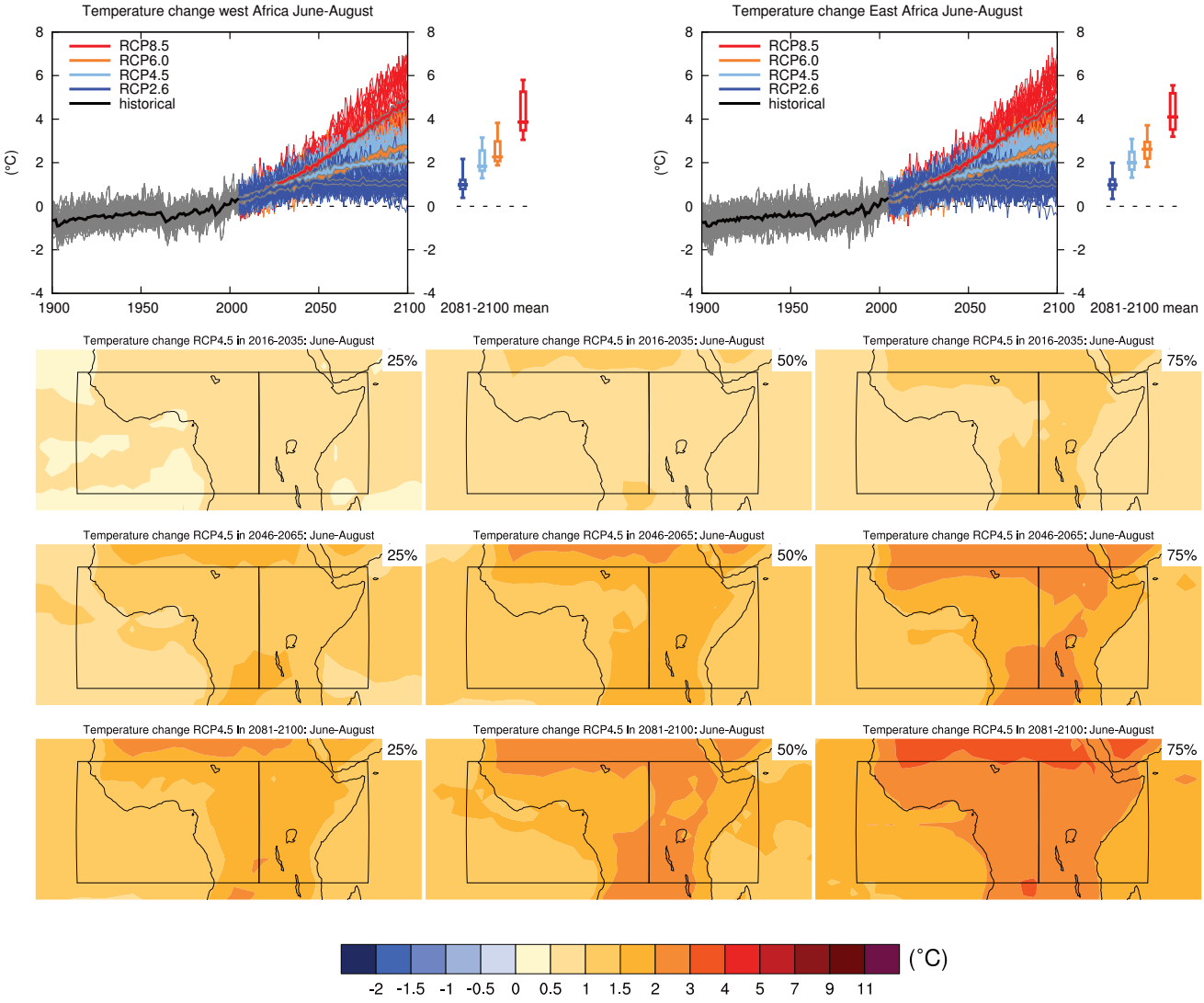

Figure AI.45 | (Top left) Time series of temperature change relative to 1986–2005 averaged over land grid points in West Africa (11.4°S to 15°N, 20°W to 25°E) in June to August. (Top right) Same for land grid points in East Africa (11.3°S to 15°N, 25°E to 52°E). Thin lines denote one ensemble member per model, thick lines the CMIP5 multi-model mean. On the right-hand side the 5th, 25th, 50th (median), 75th and 95th percentiles of the distribution of 20-year mean changes are given for 2081–2100 in the four RCP scenarios.

(Below) Maps of temperature changes in 2016–2035, 2046–2065 and 2081–2100 with respect to 1986–2005 in the RCP4.5 scenario. For each point, the 25th, 50th and 75th percentiles of the distribution of the CMIP5 ensemble are shown; this includes both natural variability and inter-model spread. Hatching denotes areas where the 20-year mean differences of the percentiles are less than the standard deviation of model-estimated present-day natural variability of 20-year mean differences.

Sections 9.4.1.1, 9.6.1.1, 10.3.1.1.4, Box 11.2, 14.8.7 contain relevant information regarding the evaluation of models in this region, the model spread in the context of other methods of projecting changes and the role of modes of variability and other climate phenomena.

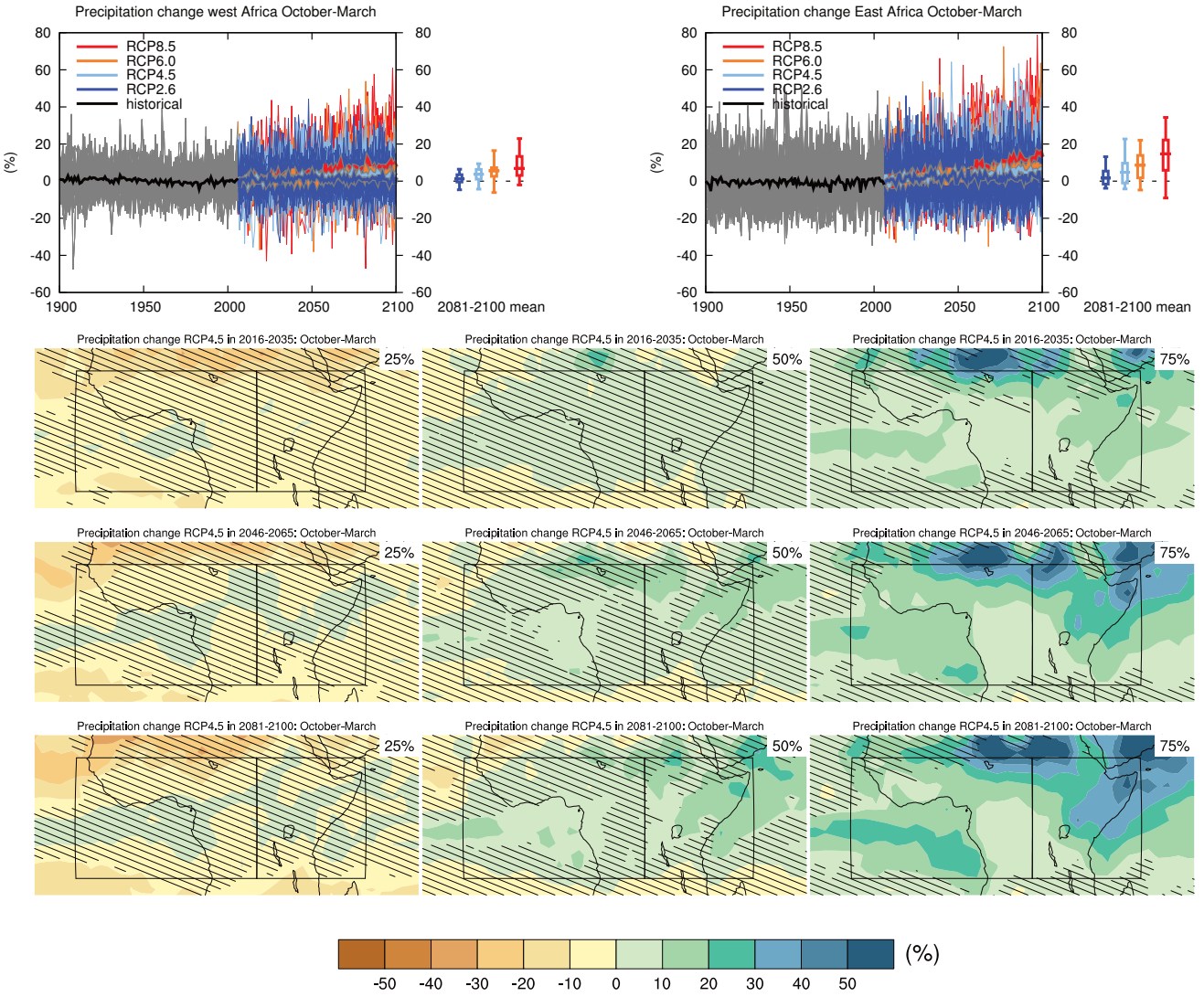

Figure AI.46 | (Top left) Time series of relative change relative to 1986–2005 in precipitation averaged over land grid points in West Africa (11.4°S to 15°N, 20°W to 25°E) in October to March. (Top right) Same for land grid points in East Africa (11.3°S to 15°N, 25°E to 52°E). Thin lines denote one ensemble member per model, thick lines the CMIP5 multi-model mean. On the right-hand side the 5th, 25th, 50th (median), 75th and 95th percentiles of the distribution of 20-year mean changes are given for 2081–2100 in the four RCP scenarios.

(Below) Maps of precipitation changes in 2016–2035, 2046–2065 and 2081–2100 with respect to 1986–2005 in the RCP4.5 scenario. For each point, the 25th, 50th and 75th percentiles of the distribution of the CMIP5 ensemble are shown; this includes both natural variability and inter-model spread. Hatching denotes areas where the 20-year mean differences of the percentiles are less than the standard deviation of model-estimated present-day natural variability of 20-year mean differences.

Sections 9.4.1.1, 9.6.1.1, 11.3.2.1.2, Box 11.2, 12.4.5.2, 14.2.4, 14.8.7 contain relevant information regarding the evaluation of models in this region, the model spread in the context of other methods of projecting changes and the role of modes of variability and other climate phenomena.

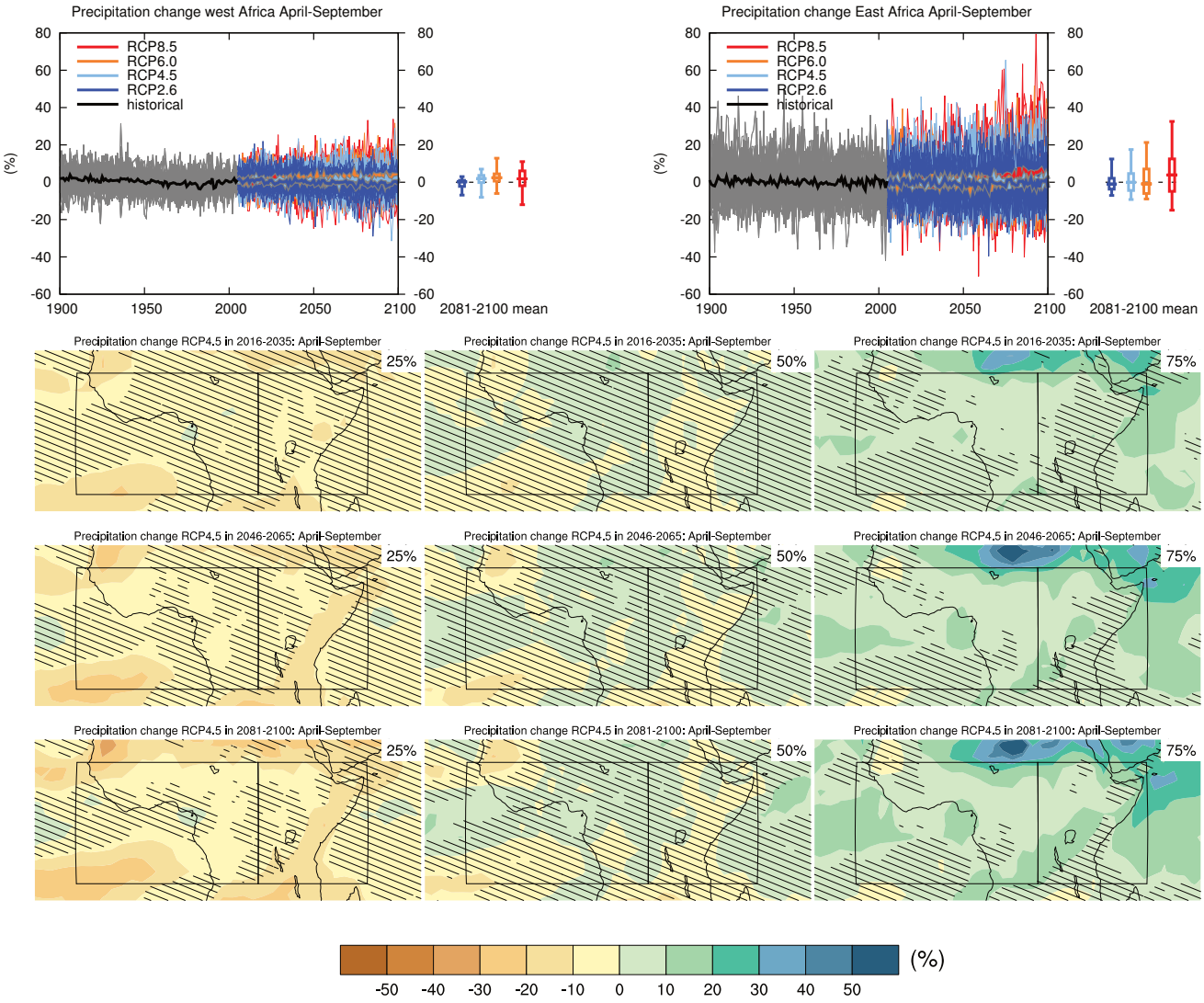

Figure AI.47 | (Top left) Time series of relative change relative to 1986–2005 in precipitation averaged over land grid points in West Africa (11.4°S to 15°N, 20°W to 25°E) in April to September. (Top right) Same for land grid points in East Africa (11.3°S to 15°N, 25°E to 52°E). Thin lines denote one ensemble member per model, thick lines the CMIP5 multi-model mean. On the right-hand side the 5th, 25th, 50th (median), 75th and 95th percentiles of the distribution of 20-year mean changes are given for 2081–2100 in the four RCP scenarios.

(Below) Maps of precipitation changes in 2016–2035, 2046–2065 and 2081–2100 with respect to 1986–2005 in the RCP4.5 scenario. For each point, the 25th, 50th and 75th percentiles of the distribution of the CMIP5 ensemble are shown; this includes both natural variability and inter-model spread. Hatching denotes areas where the 20-year mean differences of the percentiles are less than the standard deviation of model-estimated present-day natural variability of 20-year mean differences.

Sections 9.4.1.1, 9.6.1.1, 11.3.2.1.2, Box 11.2, 12.4.5.2, 14.2.4, 14.8.7 contain relevant information regarding the evaluation of models in this region, the model spread in the context of other methods of projecting changes and the role of modes of variability and other climate phenomena.

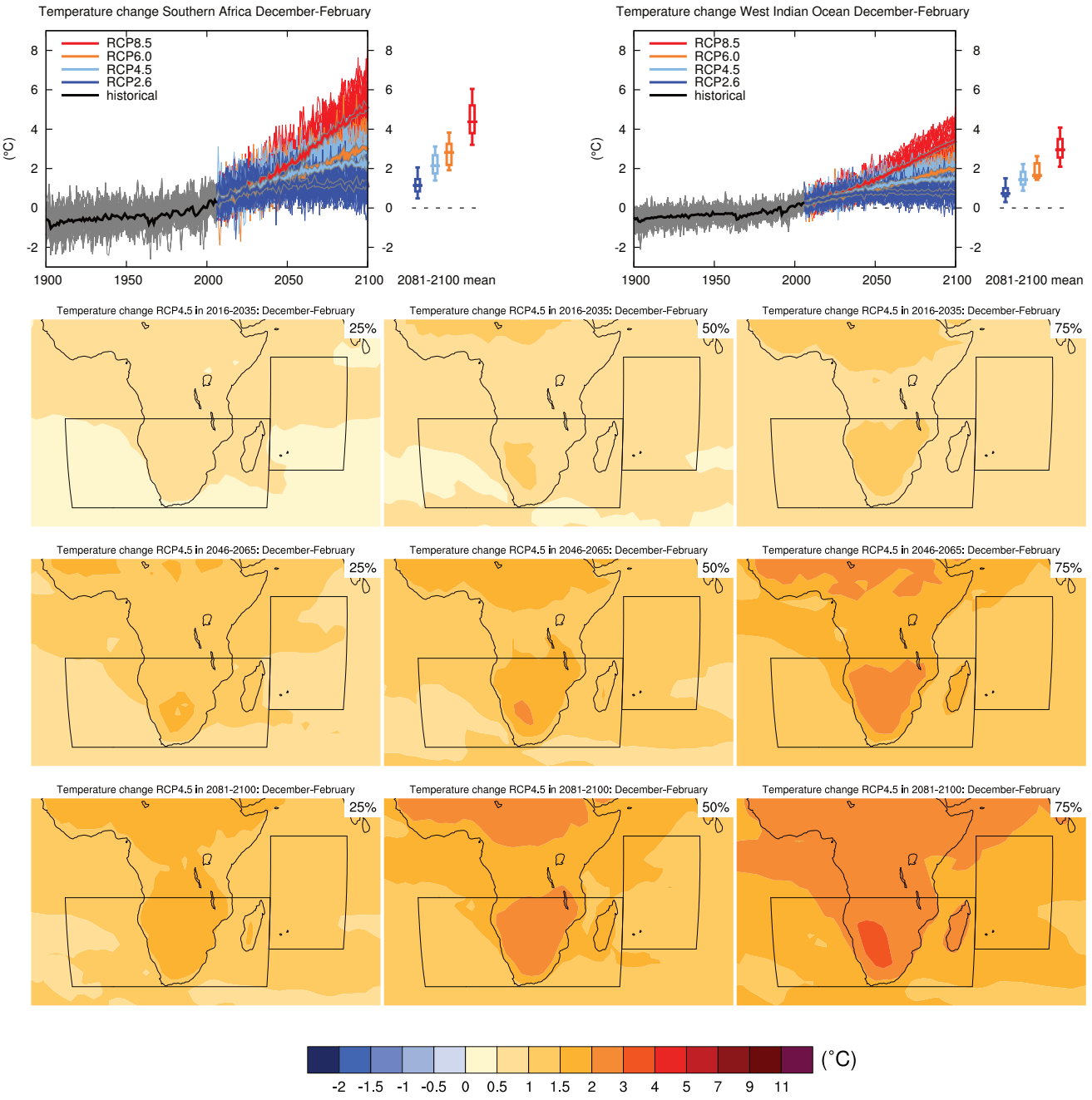

Figure AI.48 | (Top left) Time series of temperature change relative to 1986–2005 averaged over land grid points in Southern Africa (35°S to 11.4°S, 10°W to 52°E) in December to February. (Top right) Same for sea grid points in the West Indian Ocean (25°S to 5°N, 52°E to 75°E). Thin lines denote one ensemble member per model, thick lines the CMIP5 multi-model mean. On the right-hand side the 5th, 25th, 50th (median), 75th and 95th percentiles of the distribution of 20-year mean changes are given for 2081–2100 in the four RCP scenarios.

(Below) Maps of temperature changes in 2016–2035, 2046–2065 and 2081–2100 with respect to 1986–2005 in the RCP4.5 scenario. For each point, the 25th, 50th and 75th percentiles of the distribution of the CMIP5 ensemble are shown; this includes both natural variability and inter-model spread. Hatching denotes areas where the 20-year mean differences of the percentiles are less than the standard deviation of model-estimated present-day natural variability of 20-year mean differences.

Sections 9.4.1.1, 9.6.1.1, 10.3.1.1.4, Box 11.2, 14.8.7 contain relevant information regarding the evaluation of models in this region, the model spread in the context of other methods of projecting changes and the role of modes of variability and other climate phenomena.

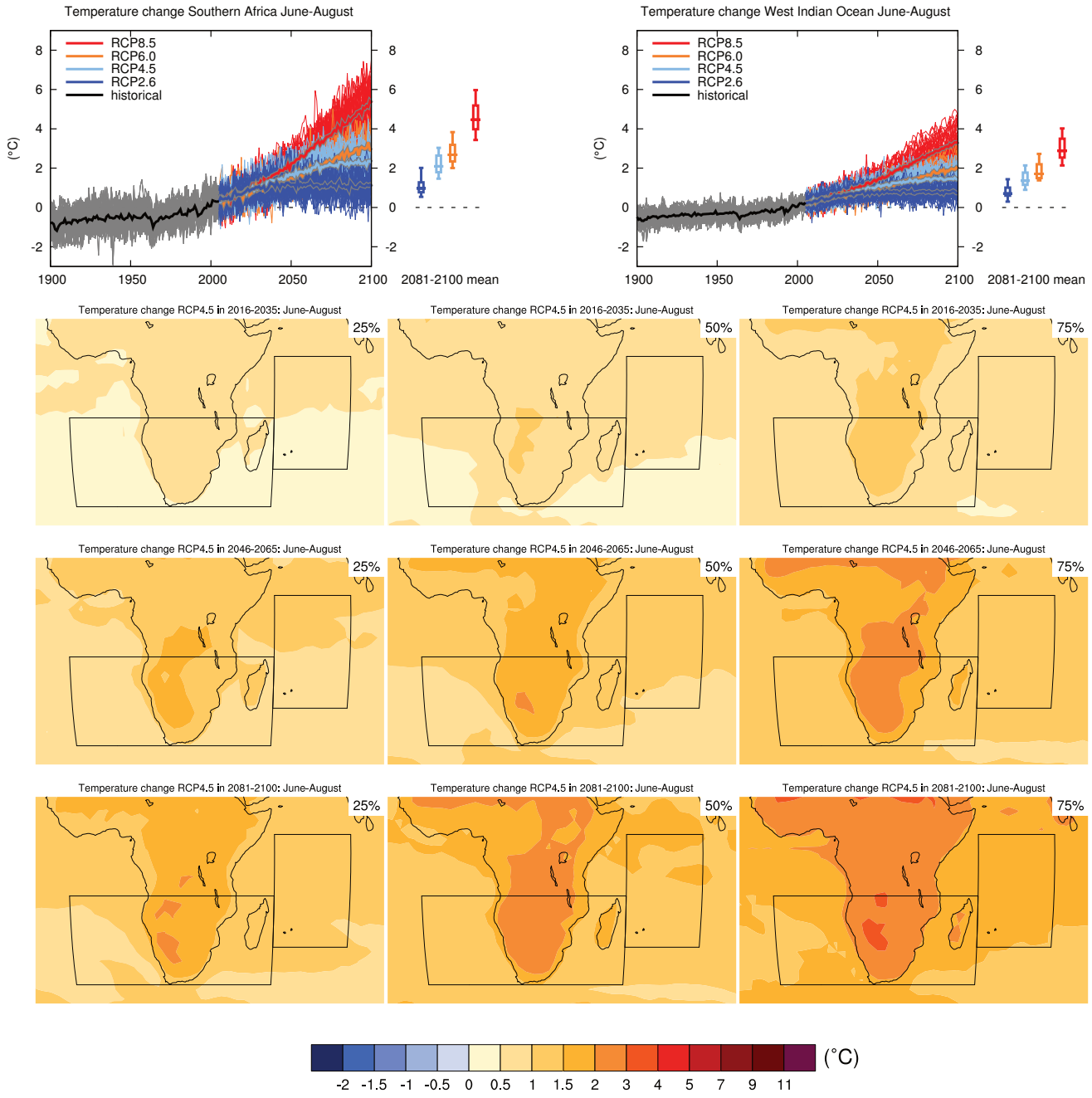

Figure AI.49 | (Top left) Time series of temperature change relative to 1986–2005 averaged over land grid points in Southern Africa (35°S to 11.4°S, 10°W to 52°E) in June to August. (Top right) Same for sea grid points in the West Indian Ocean (25°S to 5°N, 52°E to 75°E). Thin lines denote one ensemble member per model, thick lines the CMIP5 multi-model mean. On the right-hand side the 5th, 25th, 50th (median), 75th and 95th percentiles of the distribution of 20-year mean changes are given for 2081–2100 in the four RCP scenarios.

(Below) Maps of temperature changes in 2016–2035, 2046–2065 and 2081–2100 with respect to 1986–2005 in the RCP4.5 scenario. For each point, the 25th, 50th and 75th percentiles of the distribution of the CMIP5 ensemble are shown; this includes both natural variability and inter-model spread. Hatching denotes areas where the 20-year mean differences of the percentiles are less than the standard deviation of model-estimated present-day natural variability of 20-year mean differences.

Sections 9.4.1.1, 9.6.1.1, 10.3.1.1.4, Box 11.2, 14.8.7 contain relevant information regarding the evaluation of models in this region, the model spread in the context of other methods of projecting changes and the role of modes of variability and other climate phenomena.

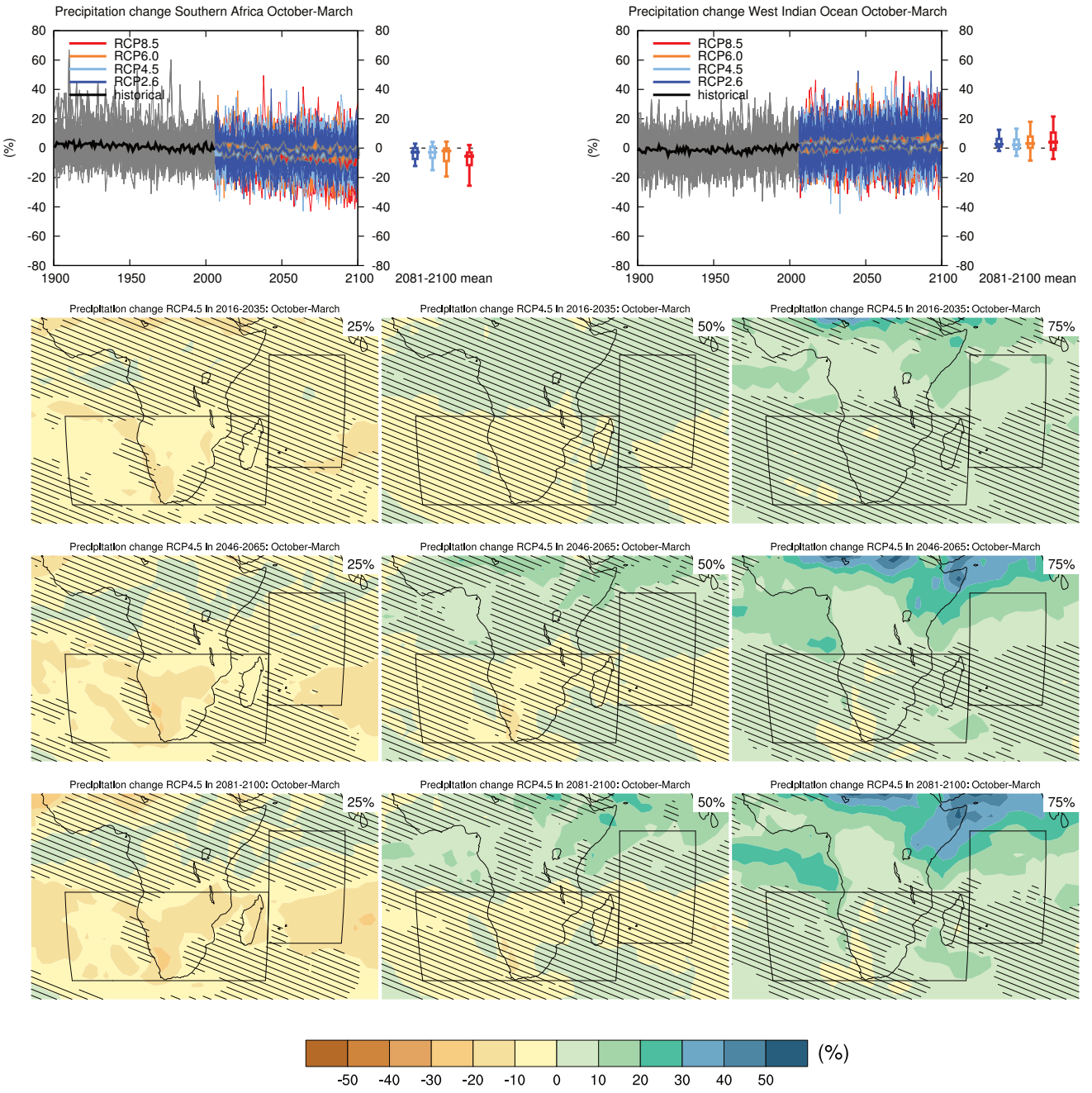

Figure AI.50 | (Top left) Time series of relative change relative to 1986–2005 in precipitation averaged over land grid points in Southern Africa (35°S to 11.4°S, 10°W to 52°E) in October to March. (Top right) Same for sea grid points in the West Indian Ocean (25°S to 5°N, 52°E to 75°E). Thin lines denote one ensemble member per model, thick lines the CMIP5 multi-model mean. On the right-hand side the 5th, 25th, 50th (median), 75th and 95th percentiles of the distribution of 20-year mean changes are given for 2081–2100 in the four RCP scenarios.

(Below) Maps of precipitation changes in 2016–2035, 2046–2065 and 2081–2100 with respect to 1986–2005 in the RCP4.5 scenario. For each point, the 25th, 50th and 75th percentiles of the distribution of the CMIP5 ensemble are shown; this includes both natural variability and inter-model spread. Hatching denotes areas where the 20-year mean differences of the percentiles are less than the standard deviation of model-estimated present-day natural variability of 20-year mean differences.

Sections 9.4.1.1, 9.6.1.1, Box 11.2, 12.4.5.2, 14.8.7 contain relevant information regarding the evaluation of models in this region, the model spread in the context of other methods of projecting changes and the role of modes of variability and other climate phenomena.

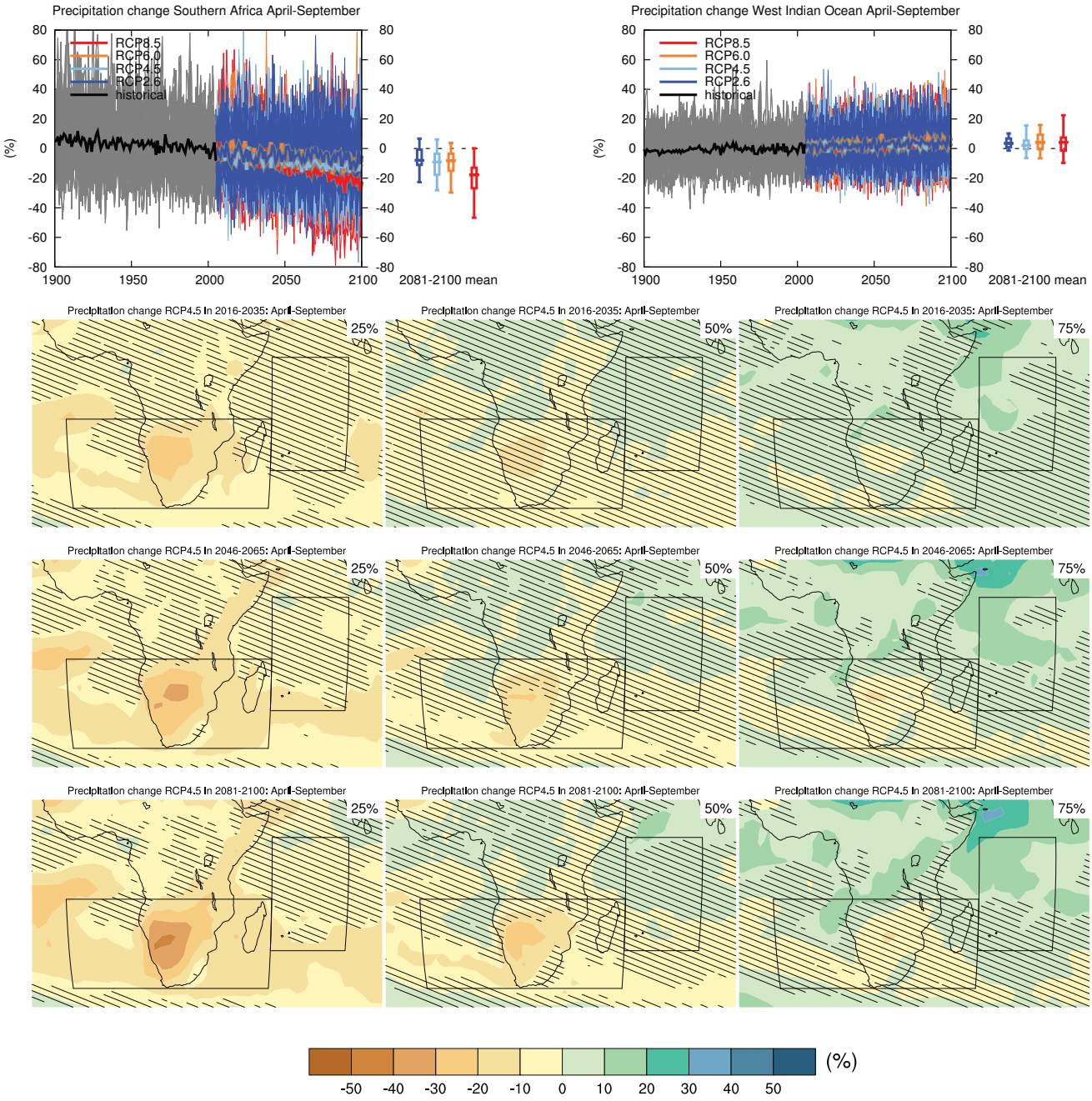

Figure AI.51 | (Top left) Time series of relative change relative to 1986–2005 in precipitation averaged over land grid points in Southern Africa (35°S to 11.4°S, 10°W to 52°E) in April to September. (Top right) Same for sea grid points in the West Indian Ocean (25°S to 5°N, 52°E to 75°E). Thin lines denote one ensemble member per model, thick lines the CMIP5 multi-model mean. On the right-hand side the 5th, 25th, 50th (median), 75th and 95th percentiles of the distribution of 20-year mean changes are given for 2081–2100 in the four RCP scenarios.

(Below) Maps of precipitation changes in 2016–2035, 2046–2065 and 2081–2100 with respect to 1986–2005 in the RCP4.5 scenario. For each point, the 25th, 50th and 75th percentiles of the distribution of the CMIP5 ensemble are shown; this includes both natural variability and inter-model spread. Hatching denotes areas where the 20-year mean differences of the percentiles are less than the standard deviation of model-estimated present-day natural variability of 20-year mean differences.

Sections 9.4.1.1, 9.6.1.1, Box 11.2, 12.4.5.2, 14.8.7 contain relevant information regarding the evaluation of models in this region, the model spread in the context of other methods of projecting changes and the role of modes of variability and other climate phenomena.

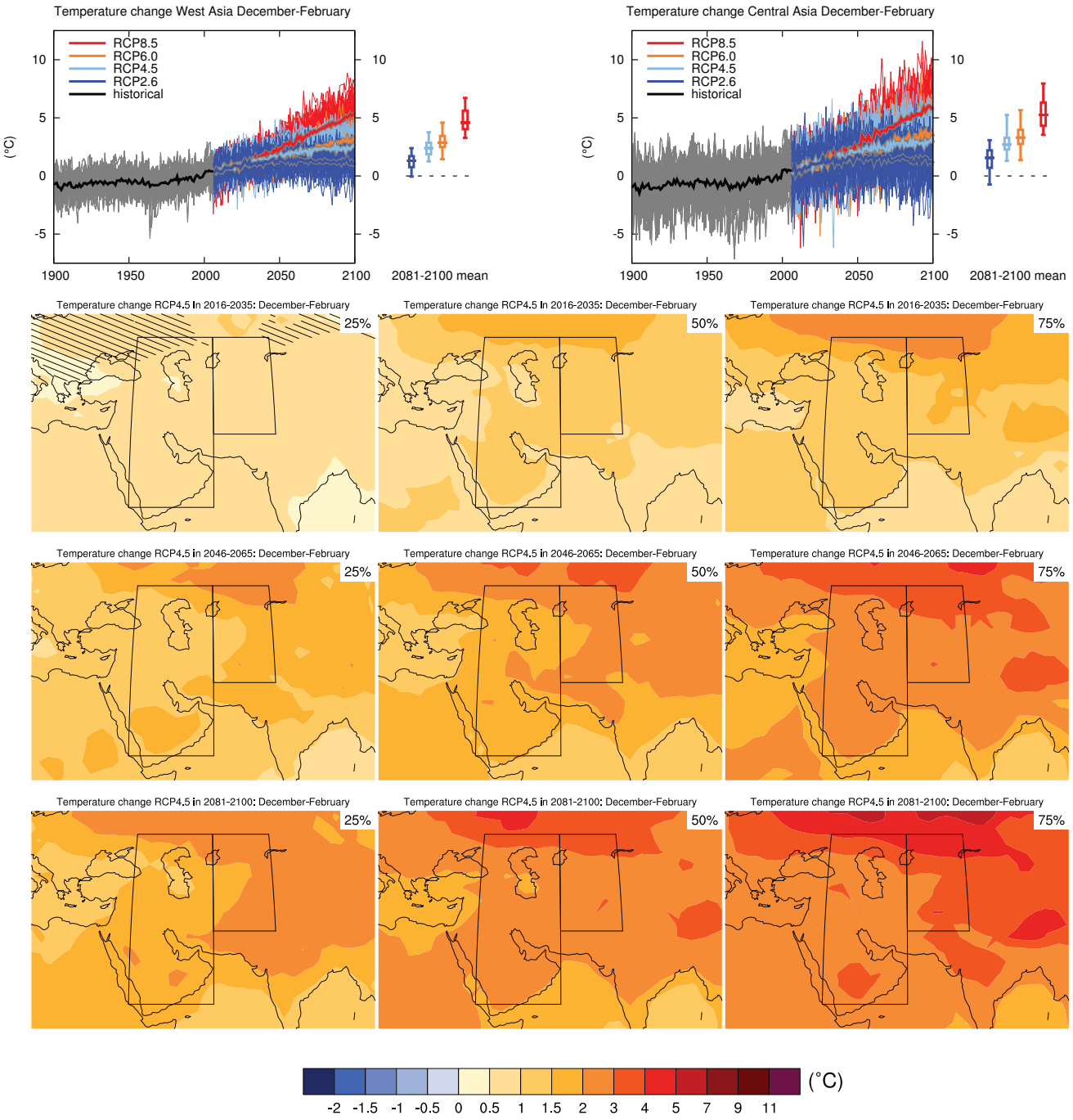

Figure AI.52 | (Top left) Time series of temperature change relative to 1986–2005 averaged over land grid points in West Asia (15°N to 50°N, 40°E to 60°E) in December to February. (Top right) Same for land grid points in Central Asia (30°N to 50°N, 60°E to 75°E). Thin lines denote one ensemble member per model, thick lines the CMIP5 multi-model mean. On the right-hand side the 5th, 25th, 50th (median), 75th and 95th percentiles of the distribution of 20-year mean changes are given for 2081–2100 in the four RCP scenarios.

(Below) Maps of temperature changes in 2016–2035, 2046–2065 and 2081–2100 with respect to 1986–2005 in the RCP4.5 scenario. For each point, the 25th, 50th and 75th percentiles of the distribution of the CMIP5 ensemble are shown; this includes both natural variability and inter-model spread. Hatching denotes areas where the 20-year mean differences of the percentiles are less than the standard deviation of model-estimated present-day natural variability of 20-year mean differences.

Sections 9.4.1.1, 9.6.1.1, 10.3.1.1.4, Box 11.2, 14.8.8, 14.8.10 contain relevant information regarding the evaluation of models in this region, the model spread in the context of other methods of projecting changes and the role of modes of variability and other climate phenomena.

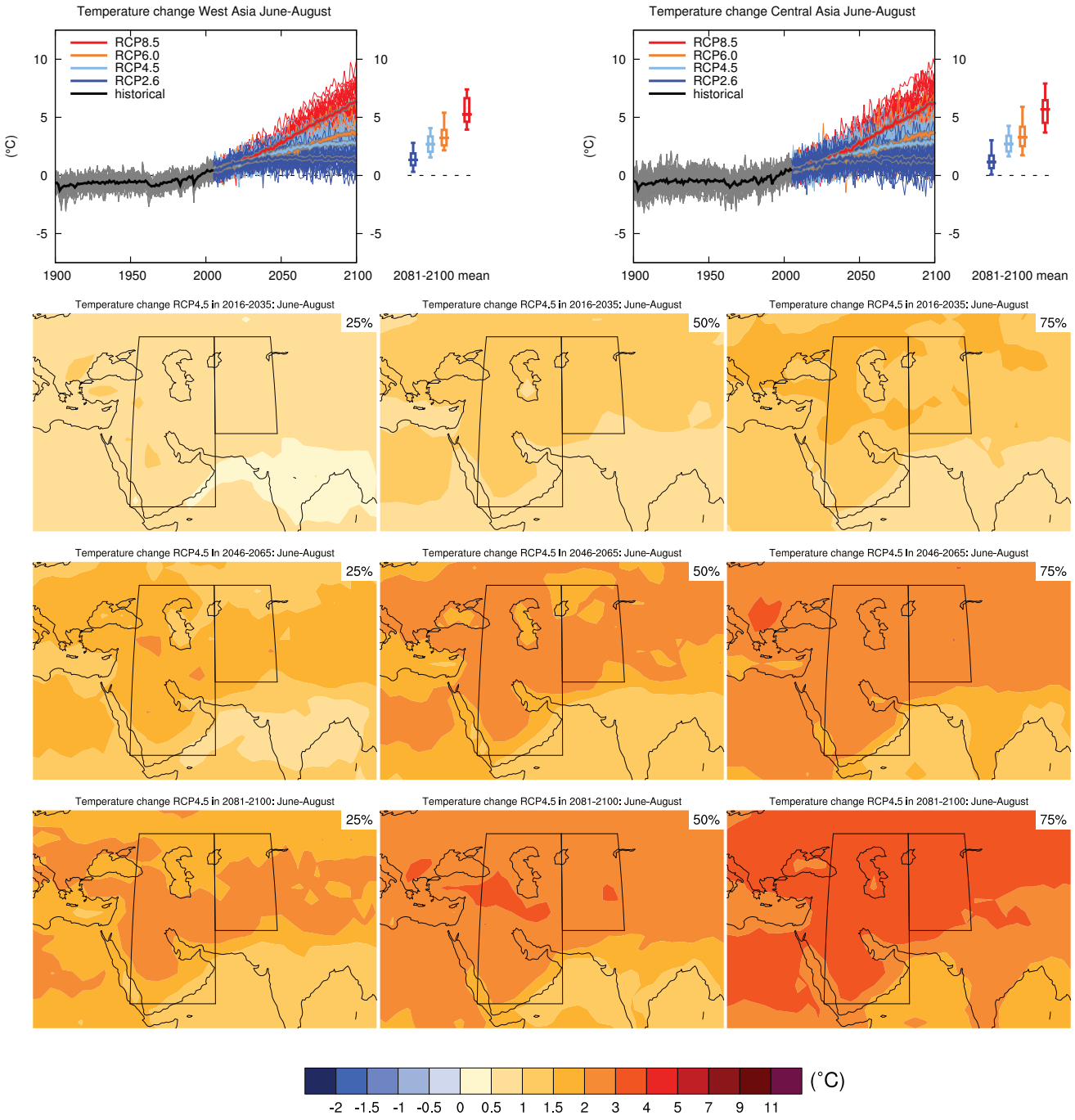

Figure AI.53 | (Top left) Time series of temperature change relative to 1986–2005 averaged over land grid points in West Asia (15°N to 50°N, 40°E to 60°E) in June to August. (Top right) Same for land grid points in Central Asia (30°N to 50°N, 60°E to 75°E). Thin lines denote one ensemble member per model, thick lines the CMIP5 multi-model mean. On the right-hand side the 5th, 25th, 50th (median), 75th and 95th percentiles of the distribution of 20-year mean changes are given for 2081–2100 in the four RCP scenarios.

(Below) Maps of temperature changes in 2016–2035, 2046–2065 and 2081–2100 with respect to 1986–2005 in the RCP4.5 scenario. For each point, the 25th, 50th and 75th percentiles of the distribution of the CMIP5 ensemble are shown; this includes both natural variability and inter-model spread. Hatching denotes areas where the 20-year mean differences of the percentiles are less than the standard deviation of model-estimated present-day natural variability of 20-year mean differences.

Sections 9.4.1.1, 9.6.1.1, 10.3.1.1.4, Box 11.2, 14.8.8, 14.8.10 contain relevant information regarding the evaluation of models in this region, the model spread in the context of other methods of projecting changes and the role of modes of variability and other climate phenomena.

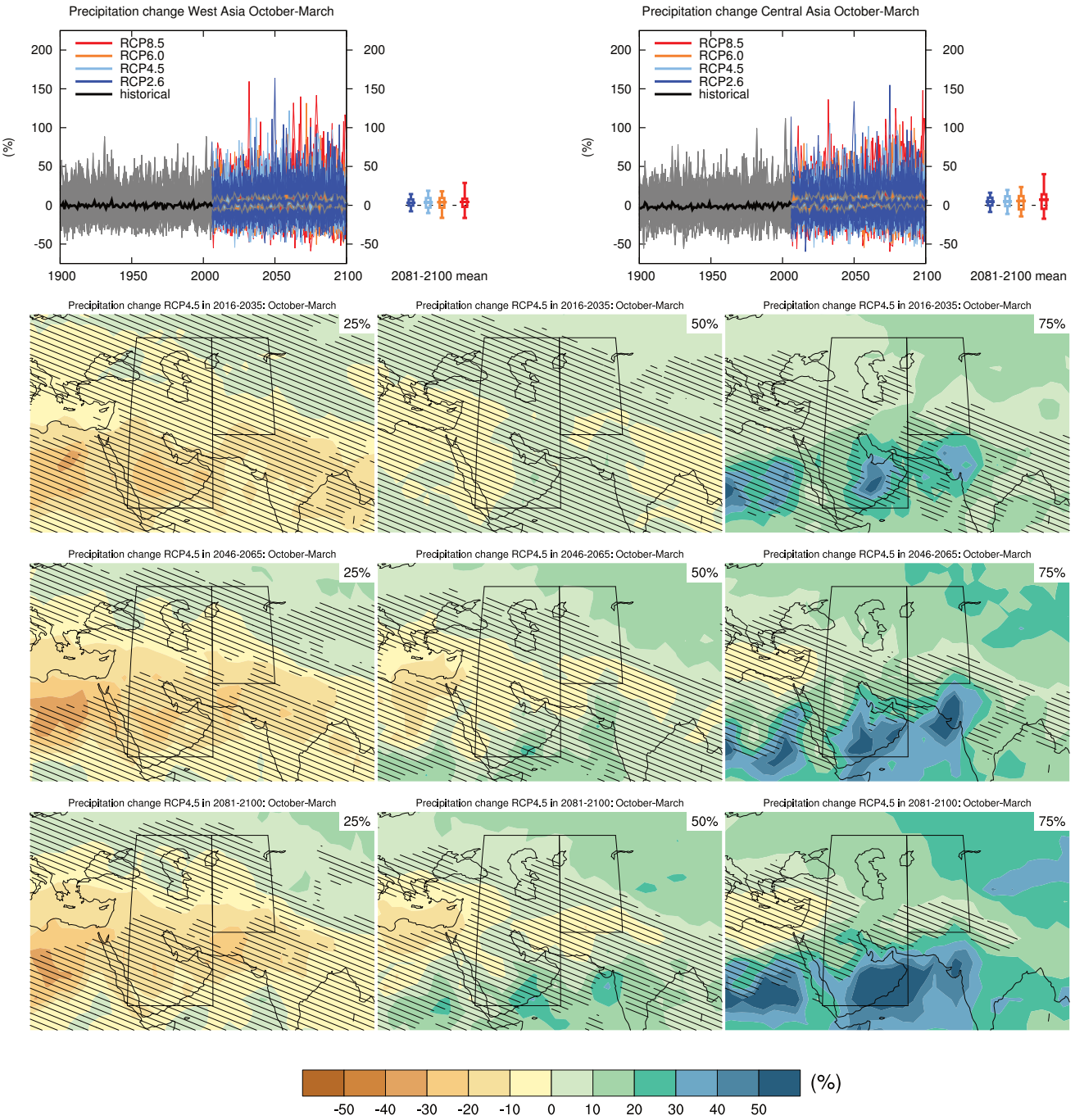

Figure AI.54 | (Top left) Time series of relative change relative to 1986–2005 in precipitation averaged over land grid points in West Asia (15°N to 50°N, 40°E to 60°E) in October to March. (Top right) Same for land grid points in Central Asia (30°N to 50°N, 60°E to 75°E). Thin lines denote one ensemble member per model, thick lines the CMIP5 multi-model mean. On the right-hand side the 5th, 25th, 50th (median), 75th and 95th percentiles of the distribution of 20-year mean changes are given for 2081–2100 in the four RCP scenarios.

(Below) Maps of precipitation changes in 2016–2035, 2046–2065 and 2081–2100 with respect to 1986–2005 in the RCP4.5 scenario. For each point, the 25th, 50th and 75th percentiles of the distribution of the CMIP5 ensemble are shown; this includes both natural variability and inter-model spread. Hatching denotes areas where the 20-year mean differences of the percentiles are less than the standard deviation of model-estimated present-day natural variability of 20-year mean differences.

Sections 9.4.1.1, 9.6.1.1, Box 11.2, 12.4.5.2, 14.8.8, 14.8.10 contain relevant information regarding the evaluation of models in this region, the model spread in the context of other methods of projecting changes and the role of modes of variability and other climate phenomena.

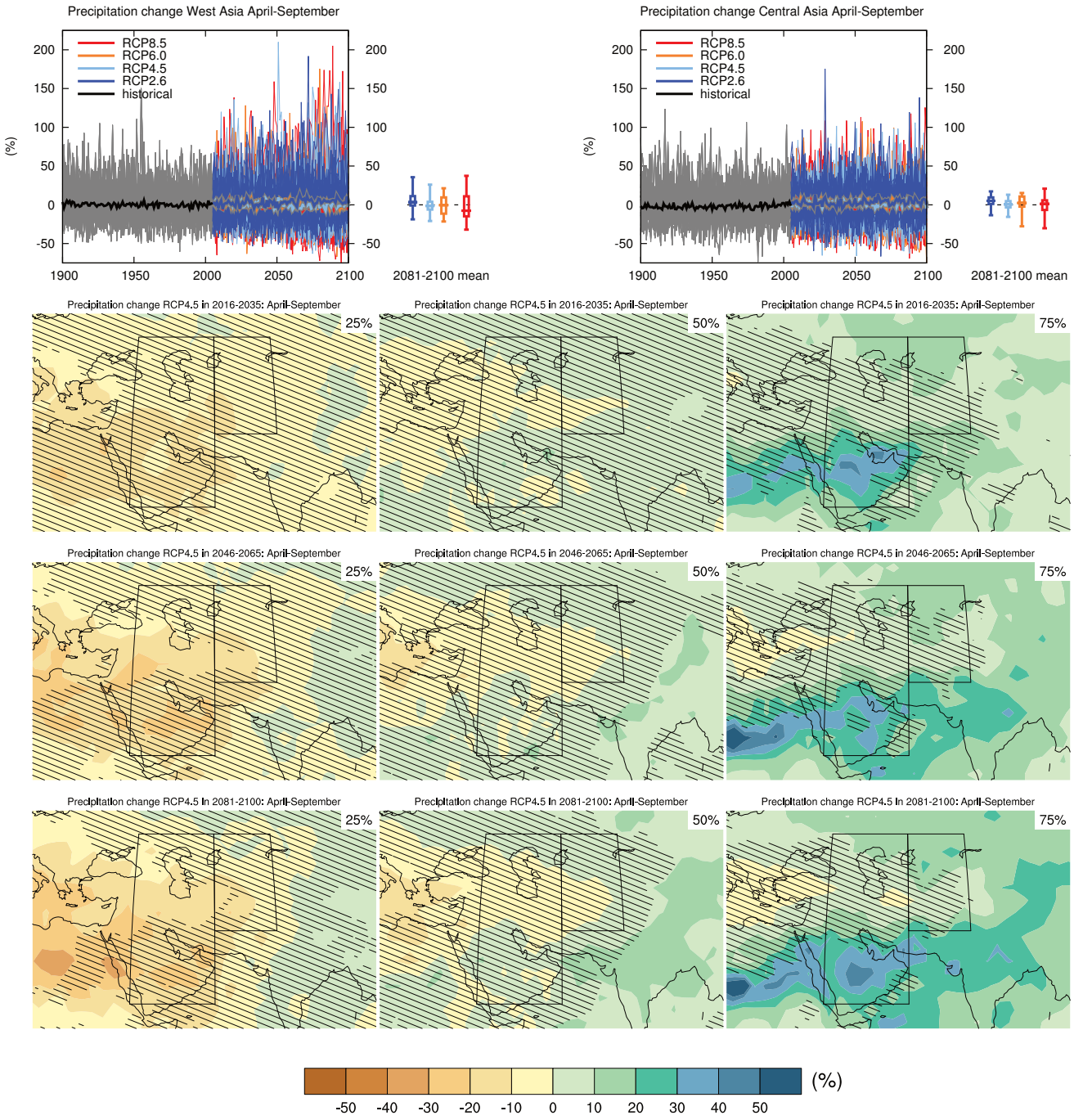

Figure AI.55 | (Top left) Time series of relative change relative to 1986–2005 in precipitation averaged over land grid points in West Asia (15°N to 50°N, 40°E to 60°E) in April to September. (Top right) Same for land grid points in Central Asia (30°N to 50°N, 60°E to 75°E). Thin lines denote one ensemble member per model, thick lines the CMIP5 multi-model mean. On the right-hand side the 5th, 25th, 50th (median), 75th and 95th percentiles of the distribution of 20-year mean changes are given for 2081–2100 in the four RCP scenarios.

(Below) Maps of precipitation changes in 2016–2035, 2046–2065 and 2081–2100 with respect to 1986–2005 in the RCP4.5 scenario. For each point, the 25th, 50th and 75th percentiles of the distribution of the CMIP5 ensemble are shown; this includes both natural variability and inter-model spread. Hatching denotes areas where the 20-year mean differences of the percentiles are less than the standard deviation of model-estimated present-day natural variability of 20-year mean differences.

Sections 9.4.1.1, 9.6.1.1, Box 11.2, 12.4.5.2, 14.8.8, 14.8.10 contain relevant information regarding the evaluation of models in this region, the model spread in the context of other methods of projecting changes and the role of modes of variability and other climate phenomena.

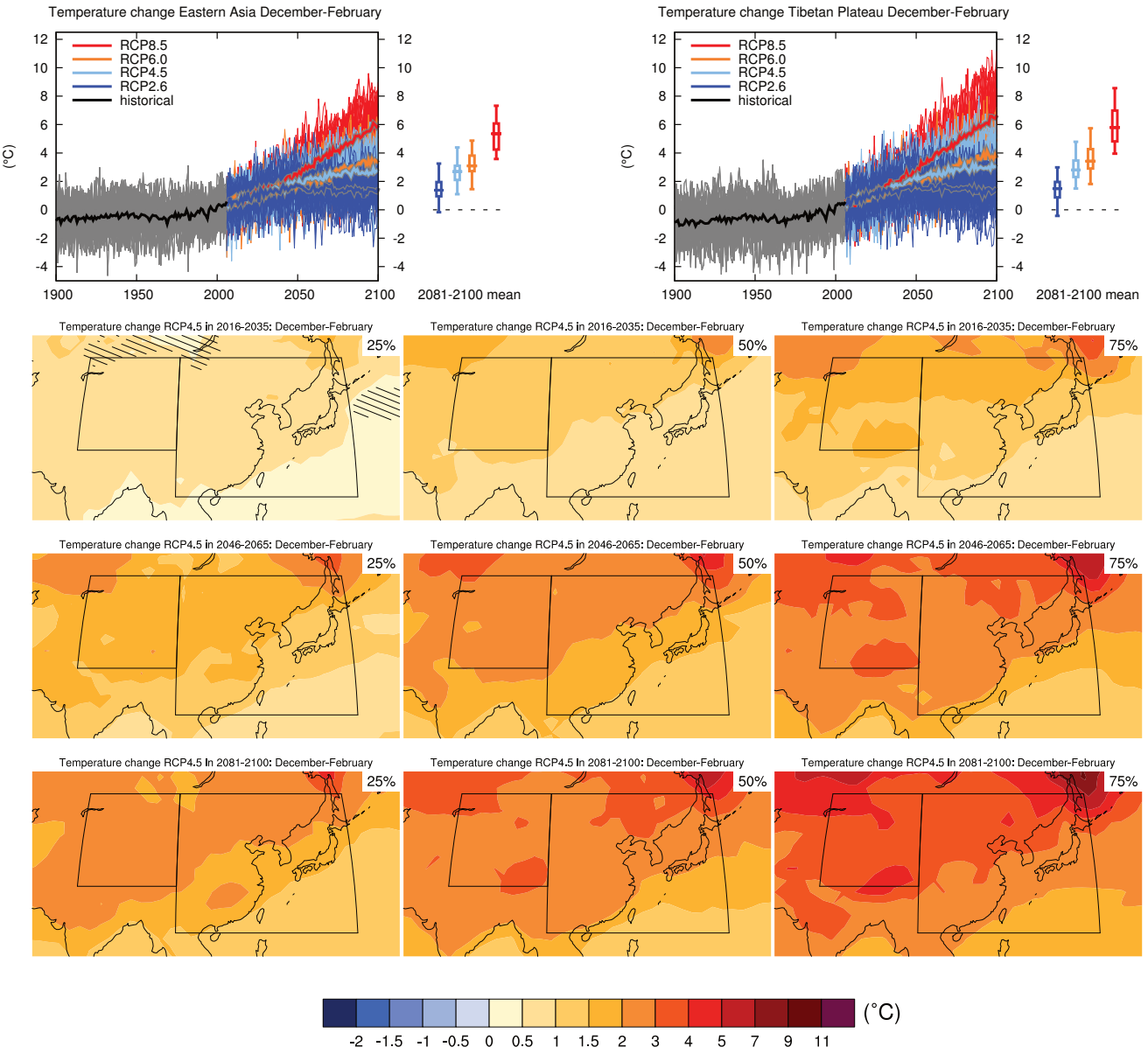

Figure AI.56 | (Top left) Time series of temperature change relative to 1986–2005 averaged over land grid points in Eastern Asia (20°N to 50°N, 100°E to 145°E) in December to February. (Top right) Same for land grid points on the Tibetan Plateau (30°N to 50°N, 75°E to 100°E). Thin lines denote one ensemble member per model, thick lines the CMIP5 multi-model mean. On the right-hand side the 5th, 25th, 50th (median), 75th and 95th percentiles of the distribution of 20-year mean changes are given for 2081–2100 in the four RCP scenarios.

(Below) Maps of temperature changes in 2016–2035, 2046–2065 and 2081–2100 with respect to 1986–2005 in the RCP4.5 scenario. For each point, the 25th, 50th and 75th percentiles of the distribution of the CMIP5 ensemble are shown; this includes both natural variability and inter-model spread. Hatching denotes areas where the 20-year mean differences of the percentiles are less than the standard deviation of model-estimated present-day natural variability of 20-year mean differences.

Sections 9.4.1.1, 9.6.1.1, 10.3.1.1.4, Box 11.2, 14.8.8, 14.8.9 contain relevant information regarding the evaluation of models in this region, the model spread in the context of other methods of projecting changes and the role of modes of variability and other climate phenomena.

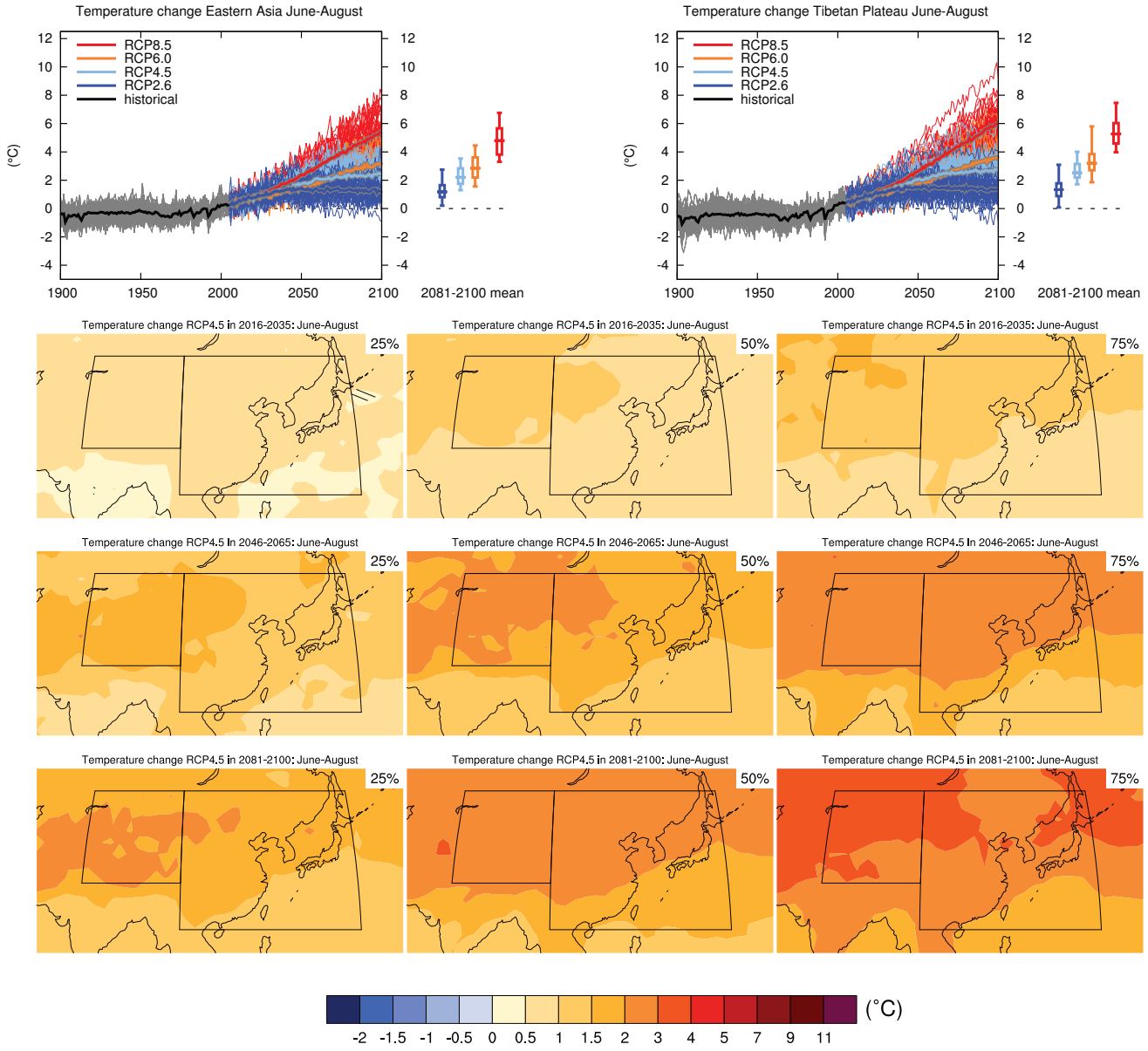

Figure AI.57 | (Top left) Time series of temperature change relative to 1986–2005 averaged over land grid points in Eastern Asia (20°N to 50°N, 100°E to 145°E) in June to August. (Top right) Same for land grid points on the Tibetan Plateau (30°N to 50°N, 75°E to 100°E). Thin lines denote one ensemble member per model, thick lines the CMIP5 multi-model mean. On the right-hand side the 5th, 25th, 50th (median), 75th and 95th percentiles of the distribution of 20-year mean changes are given for 2081–2100 in the four RCP scenarios.

(Below) Maps of temperature changes in 2016–2035, 2046–2065 and 2081–2100 with respect to 1986–2005 in the RCP4.5 scenario. For each point, the 25th, 50th and 75th percentiles of the distribution of the CMIP5 ensemble are shown; this includes both natural variability and inter-model spread. Hatching denotes areas where the 20-year mean differences of the percentiles are less than the standard deviation of model-estimated present-day natural variability of 20-year mean differences.

Sections 9.4.1.1, 9.6.1.1, 10.3.1.1.4, Box 11.2, 14.8.8, 14.8.9 contain relevant information regarding the evaluation of models in this region, the model spread in the context of other methods of projecting changes and the role of modes of variability and other climate phenomena.

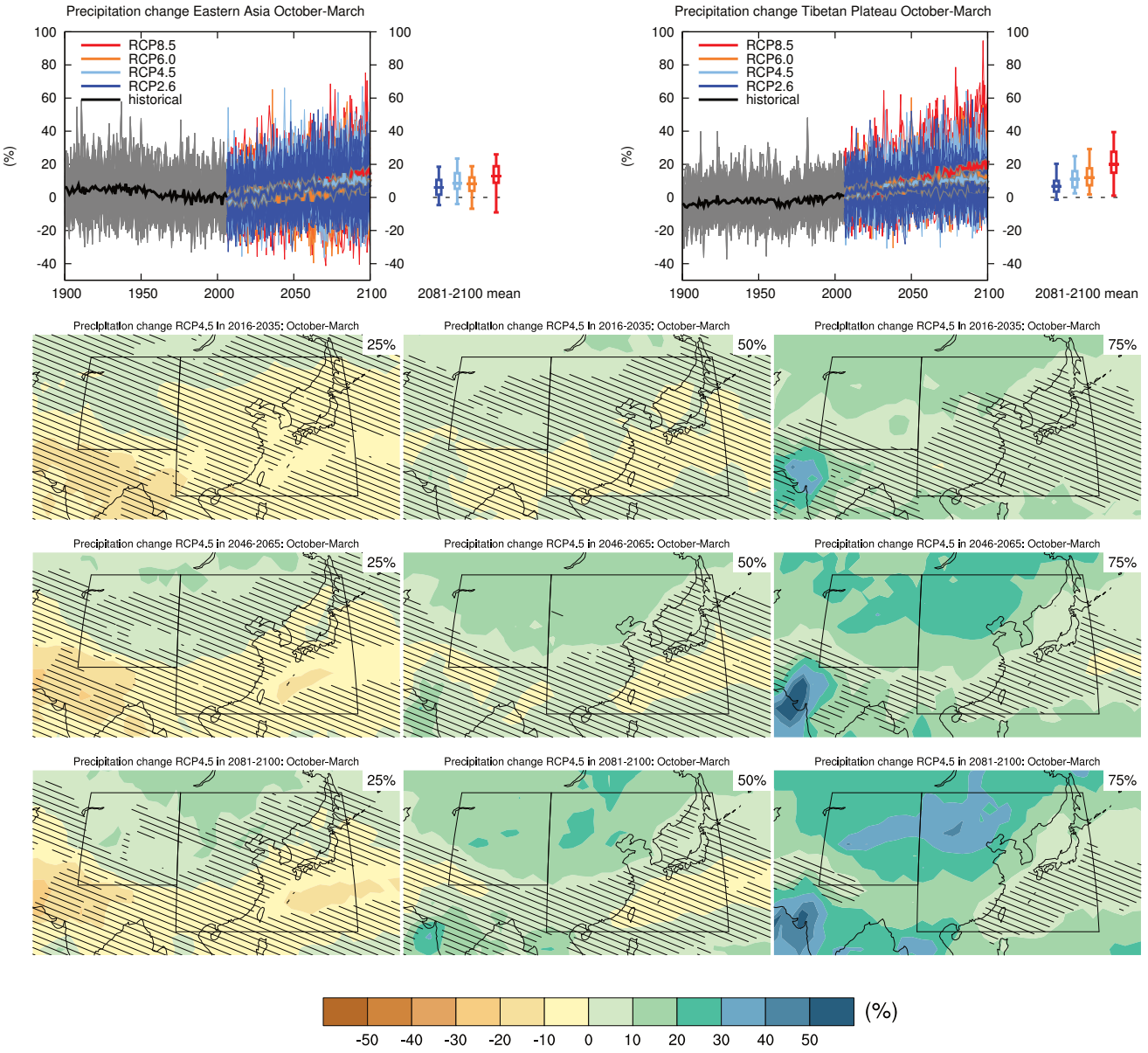

Figure AI.58 | (Top left) Time series of relative change relative to 1986–2005 in precipitation averaged over land grid points in Eastern Asia (20°N to 50°N, 100°E to 145°E) in October to March. (Top right) Same for land grid points on the Tibetan Plateau (30°N to 50°N, 75°E to 100°E). Thin lines denote one ensemble member per model, thick lines the CMIP5 multi-model mean. On the right-hand side the 5th, 25th, 50th (median), 75th and 95th percentiles of the distribution of 20-year mean changes are given for 2081–2100 in the four RCP scenarios.

(Below) Maps of precipitation changes in 2016–2035, 2046–2065 and 2081–2100 with respect to 1986–2005 in the RCP4.5 scenario. For each point, the 25th, 50th and 75th percentiles of the distribution of the CMIP5 ensemble are shown; this includes both natural variability and inter-model spread. Hatching denotes areas where the 20-year mean differences of the percentiles are less than the standard deviation of model-estimated present-day natural variability of 20-year mean differences.

Sections 9.4.1.1, 9.6.1.1, Box 11.2, 14.2.2.2, 14.8.8, 14.8.9 contain relevant information regarding the evaluation of models in this region, the model spread in the context of other methods of projecting changes and the role of modes of variability and other climate phenomena.

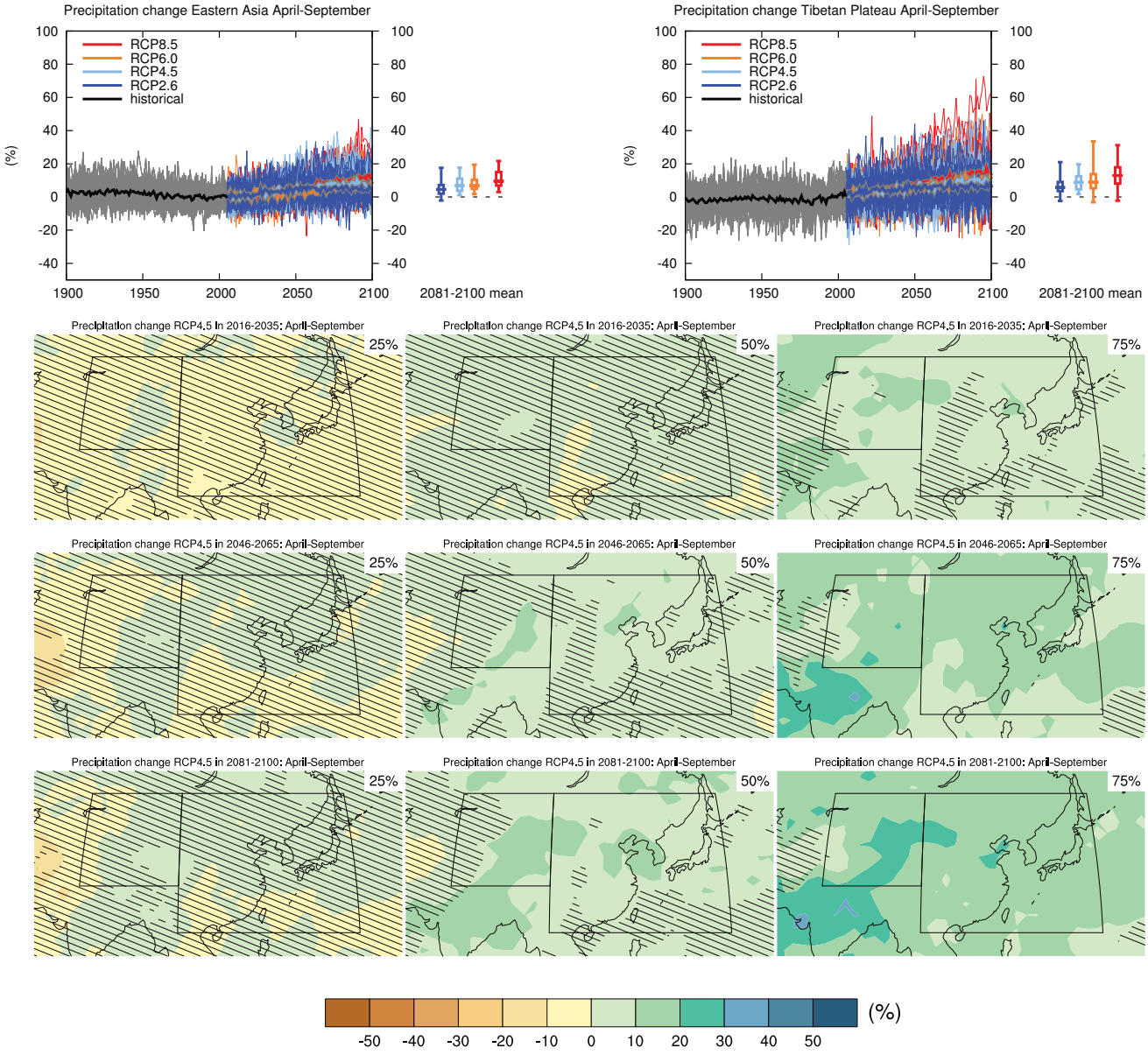

Figure AI.59 | (Top left) Time series of relative change relative to 1986–2005 in precipitation averaged over land grid points in Eastern Asia (20°N to 50°N, 100°E to 145°E) in April to September. (Top right) Same for land grid points on the Tibetan Plateau (30°N to 50°N, 75°E to 100°E). Thin lines denote one ensemble member per model, thick lines the CMIP5 multi-model mean. On the right-hand side the 5th, 25th, 50th (median), 75th and 95th percentiles of the distribution of 20-year mean changes are given for 2081–2100 in the four RCP scenarios.

(Below) Maps of precipitation changes in 2016–2035, 2046–2065 and 2081–2100 with respect to 1986–2005 in the RCP4.5 scenario. For each point, the 25th, 50th and 75th percentiles of the distribution of the CMIP5 ensemble are shown; this includes both natural variability and inter-model spread. Hatching denotes areas where the 20-year mean differences of the percentiles are less than the standard deviation of model-estimated present-day natural variability of 20-year mean differences.

Sections 9.4.1.1, 9.6.1.1, Box 11.2, 14.2.2.2, 14.8.8, 14.8.9 contain relevant information regarding the evaluation of models in this region, the model spread in the context of other methods of projecting changes and the role of modes of variability and other climate phenomena.

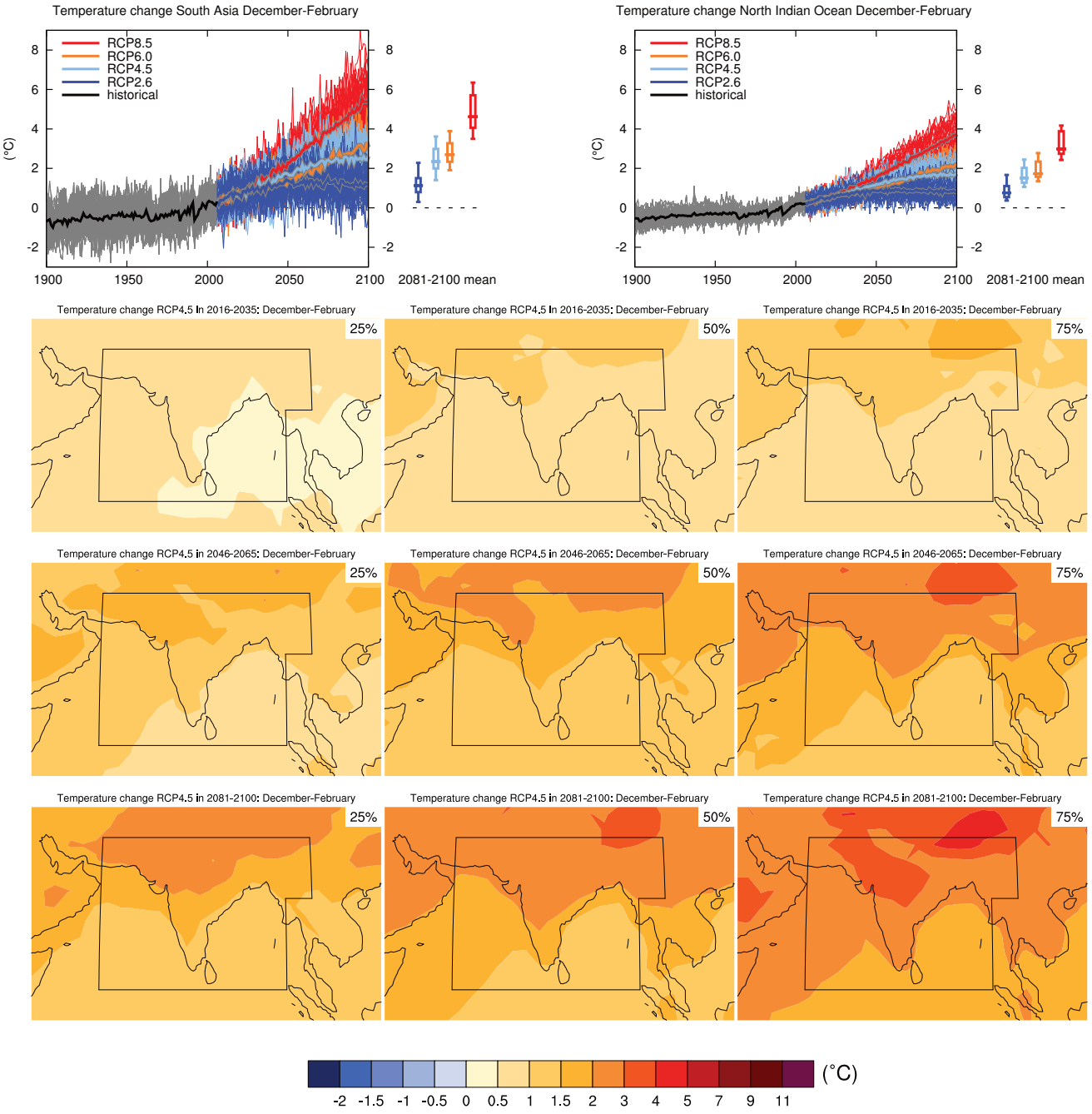

Figure AI.60 | (Top left) Time series of temperature change relative to 1986–2005 averaged over land grid points in South Asia (60°E, 5°N; 60°E, 30°N; 100°E, 30°N; 100°E, 20°E; 95°E, 20°N; 95°E, 5°N) in December to February. (Top right) Same for sea grid points in the North Indian Ocean (5°N to 30°N, 60°E to 95°E). Thin lines denote one ensemble member per model, thick lines the CMIP5 multi-model mean. On the right-hand side the 5th, 25th, 50th (median), 75th and 95th percentiles of the distribution of 20-year mean changes are given for 2081–2100 in the four RCP scenarios.

(Below) Maps of temperature changes in 2016–2035, 2046–2065 and 2081–2100 with respect to 1986–2005 in the RCP4.5 scenario. For each point, the 25th, 50th and 75th percentiles of the distribution of the CMIP5 ensemble are shown; this includes both natural variability and inter-model spread. Hatching denotes areas where the 20-year mean differences of the percentiles are less than the standard deviation of model-estimated present-day natural variability of 20-year mean differences.

Sections 9.4.1.1, 9.6.1.1, 10.3.1.1.4, Box 11.2, 14.8.11 contain relevant information regarding the evaluation of models in this region, the model spread in the context of other methods of projecting changes and the role of modes of variability and other climate phenomena.

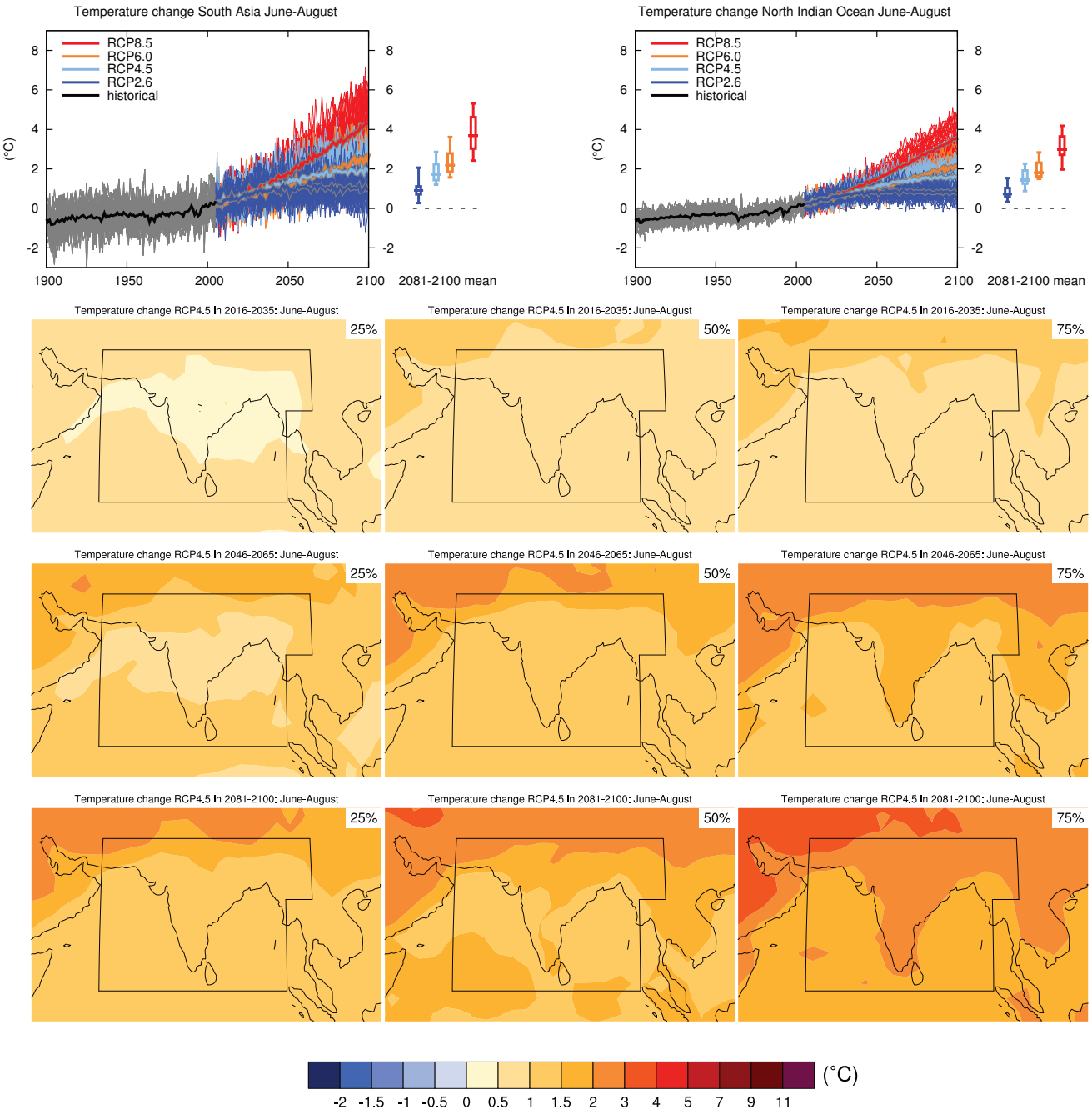

Figure AI.61 | (Top left) Time series of temperature change relative to 1986–2005 averaged over land grid points in South Asia (60°E, 5°N; 60°E, 30°N; 100°E, 30°N; 100°E, 20°E; 95°E, 20°N; 95°E, 5°N) in June to August. (Top right) Same for sea grid points in the North Indian Ocean (5°N to 30°N, 60°E to 95°E). Thin lines denote one ensemble member per model, thick lines the CMIP5 multi-model mean. On the right-hand side the 5th, 25th, 50th (median), 75th and 95th percentiles of the distribution of 20-year mean changes are given for 2081–2100 in the four RCP scenarios.

(Below) Maps of temperature changes in 2016–2035, 2046–2065 and 2081–2100 with respect to 1986–2005 in the RCP4.5 scenario. For each point, the 25th, 50th and 75th percentiles of the distribution of the CMIP5 ensemble are shown; this includes both natural variability and inter-model spread. Hatching denotes areas where the 20-year mean differences of the percentiles are less than the standard deviation of model-estimated present-day natural variability of 20-year mean differences.

Sections 9.4.1.1, 9.6.1.1, 10.3.1.1.4, Box 11.2, 14.8.11 contain relevant information regarding the evaluation of models in this region, the model spread in the context of other methods of projecting changes and the role of modes of variability and other climate phenomena.

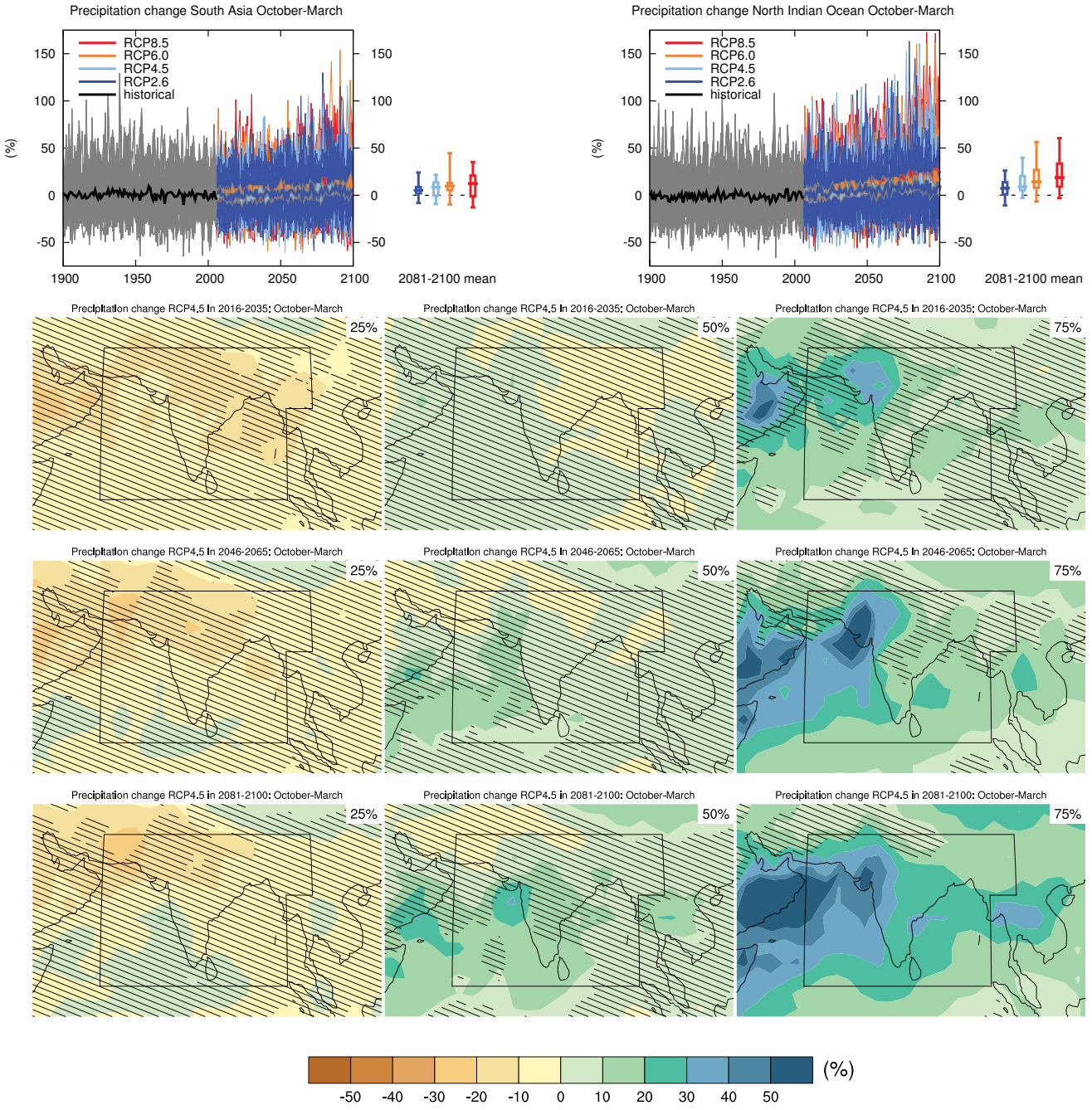

Figure AI.62 | (Top left) Time series of relative change relative to 1986–2005 in precipitation averaged over land grid points in South Asia (60°E, 5°N; 60°E, 30°N; 100°E, 30°N; 100°E, 20°E; 95°E, 20°N; 95°E, 5°N) in October to March. (Top right) Same for sea grid points in the North Indian Ocean (5°N to 30°N, 60°E to 95°E). Thin lines denote one ensemble member per model, thick lines the CMIP5 multi-model mean. On the right-hand side the 5th, 25th, 50th (median), 75th and 95th percentiles of the distribution of 20-year mean changes are given for 2081–2100 in the four RCP scenarios.

(Below) Maps of precipitation changes in 2016–2035, 2046–2065 and 2081–2100 with respect to 1986–2005 in the RCP4.5 scenario. For each point, the 25th, 50th and 75th percentiles of the distribution of the CMIP5 ensemble are shown; this includes both natural variability and inter-model spread. Hatching denotes areas where the 20-year mean differences of the percentiles are less than the standard deviation of model-estimated present-day natural variability of 20-year mean differences.

Sections 9.4.1.1, 9.6.1.1, Box 11.2, 14.2.2.1, 14.8.11 contain relevant information regarding the evaluation of models in this region, the model spread in the context of other methods of projecting changes and the role of modes of variability and other climate phenomena.

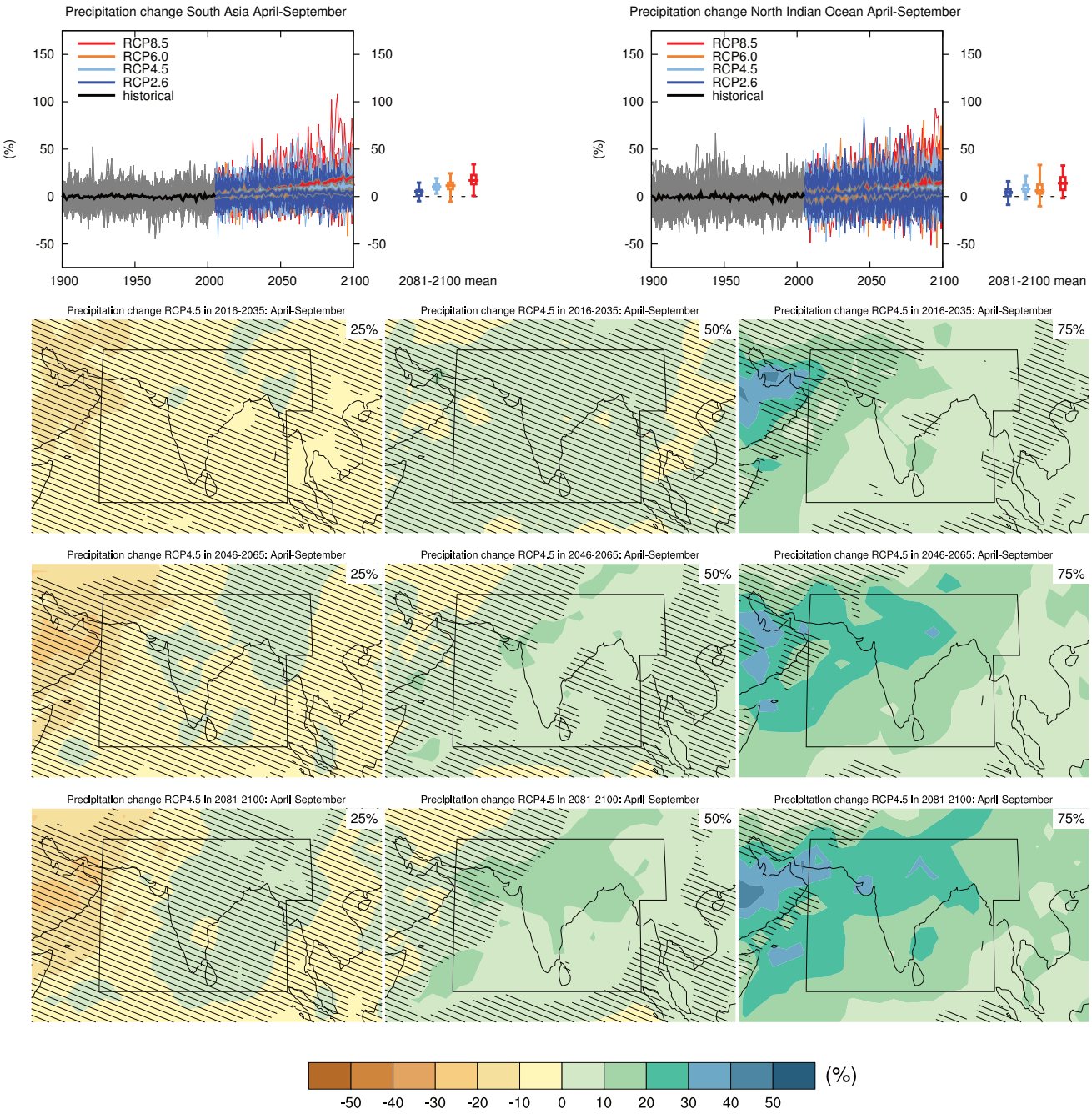

Figure AI.63 | (Top left) Time series of relative change relative to 1986–2005 in precipitation averaged over land grid points in South Asia (60°E, 5°N; 60°E, 30°N; 100°E, 30°N; 100°E, 20°E; 95°E, 20°N; 95°E, 5°N) in April to September. (Top right) Same for sea grid points in the North Indian Ocean (5°N to 30°N, 60°E to 95°E). Thin lines denote one ensemble member per model, thick lines the CMIP5 multi-model mean. On the right-hand side the 5th, 25th, 50th (median), 75th and 95th percentiles of the distribution of 20-year mean changes are given for 2081–2100 in the four RCP scenarios.

(Below) Maps of precipitation changes in 2016–2035, 2046–2065 and 2081–2100 with respect to 1986–2005 in the RCP4.5 scenario. For each point, the 25th, 50th and 75th percentiles of the distribution of the CMIP5 ensemble are shown; this includes both natural variability and inter-model spread. Hatching denotes areas where the 20-year mean differences of the percentiles are less than the standard deviation of model-estimated present-day natural variability of 20-year mean differences.

Sections 9.4.1.1, 9.6.1.1, Box 11.2, 14.2.2.1, 14.8.11 contain relevant information regarding the evaluation of models in this region, the model spread in the context of other methods of projecting changes and the role of modes of variability and other climate phenomena.

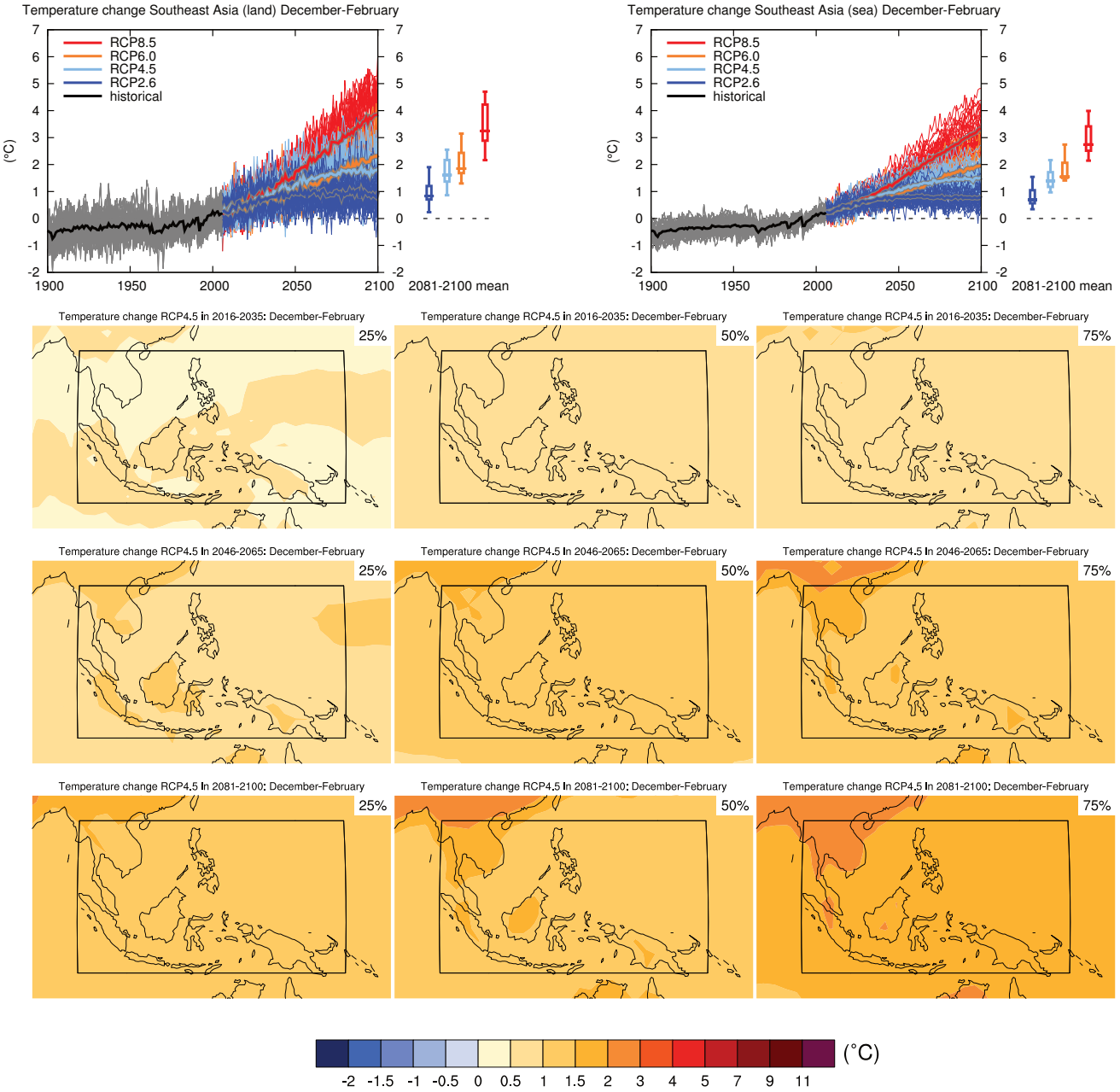

Figure AI.64 | (Top left) Time series of temperature change relative to 1986–2005 averaged over land grid points in Southeast Asia (10°S to 20°N, 95°E to 155°E) in December to February. (Top right) Same for sea grid points. Thin lines denote one ensemble member per model, thick lines the CMIP5 multi-model mean. On the right-hand side the 5th, 25th, 50th (median), 75th and 95th percentiles of the distribution of 20-year mean changes are given for 2081–2100 in the four RCP scenarios.

(Below) Maps of temperature changes in 2016–2035, 2046–2065 and 2081–2100 with respect to 1986–2005 in the RCP4.5 scenario. For each point, the 25th, 50th and 75th percentiles of the distribution of the CMIP5 ensemble are shown; this includes both natural variability and inter-model spread. Hatching denotes areas where the 20-year mean differences of the percentiles are less than the standard deviation of model-estimated present-day natural variability of 20-year mean differences.

Sections 9.4.1.1, 9.6.1.1, 10.3.1.1.4, Box 11.2, 14.8.12 contain relevant information regarding the evaluation of models in this region, the model spread in the context of other methods of projecting changes and the role of modes of variability and other climate phenomena.

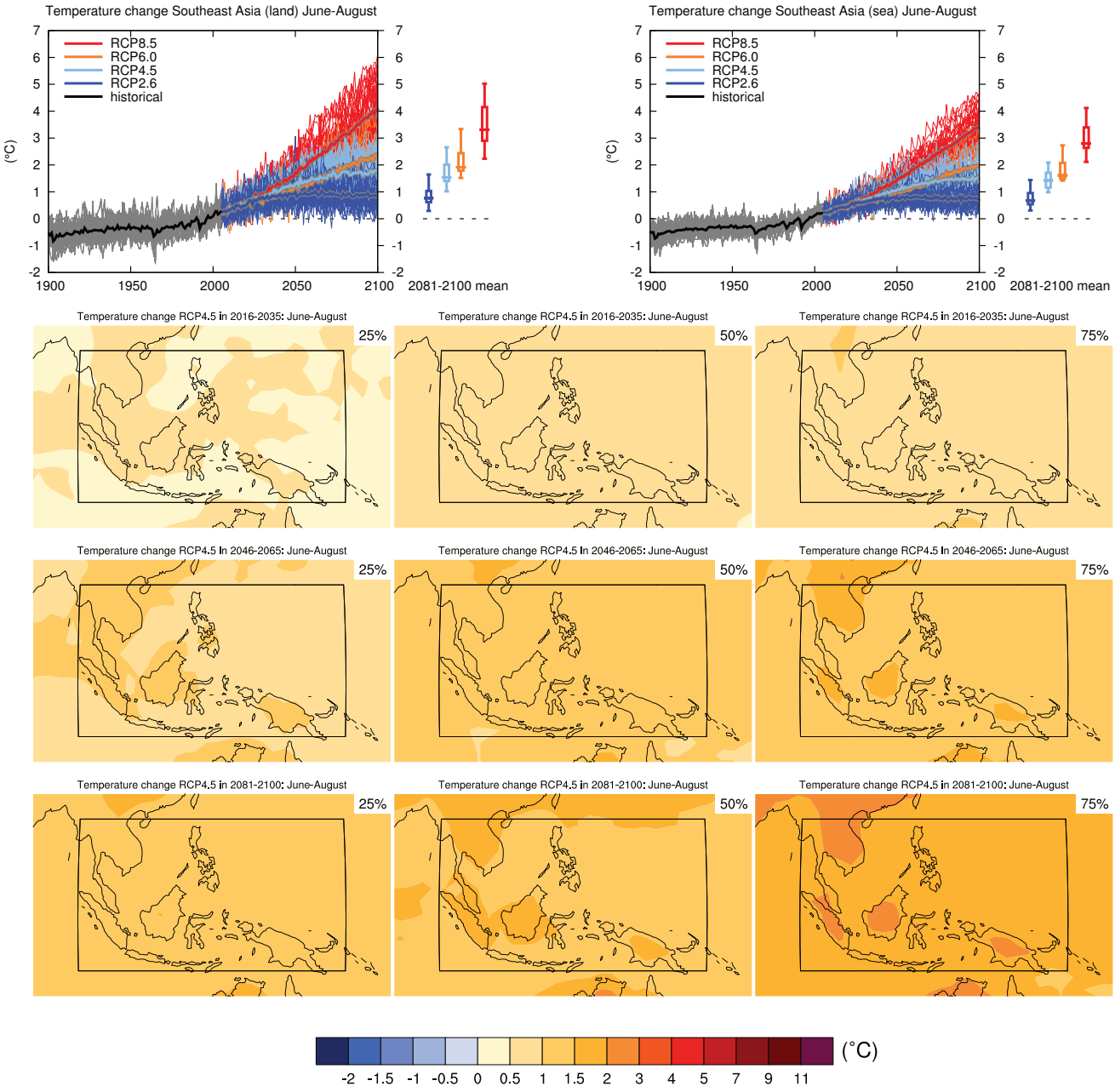

Figure AI.65 | (Top left) Time series of temperature change relative to 1986–2005 averaged over land grid points in Southeast Asia (10°S to 20°N, 95°E to 155°E) in June to August. (Top right) Same for sea grid points. Thin lines denote one ensemble member per model, thick lines the CMIP5 multi-model mean. On the right-hand side the 5th, 25th, 50th (median), 75th and 95th percentiles of the distribution of 20-year mean changes are given for 2081–2100 in the four RCP scenarios.

(Below) Maps of temperature changes in 2016–2035, 2046–2065 and 2081–2100 with respect to 1986–2005 in the RCP4.5 scenario. For each point, the 25th, 50th and 75th percentiles of the distribution of the CMIP5 ensemble are shown; this includes both natural variability and inter-model spread. Hatching denotes areas where the 20-year mean differences of the percentiles are less than the standard deviation of model-estimated present-day natural variability of 20-year mean differences.

Sections 9.4.1.1, 9.6.1.1, 10.3.1.1.4, Box 11.2, 14.8.12 contain relevant information regarding the evaluation of models in this region, the model spread in the context of other methods of projecting changes and the role of modes of variability and other climate phenomena.

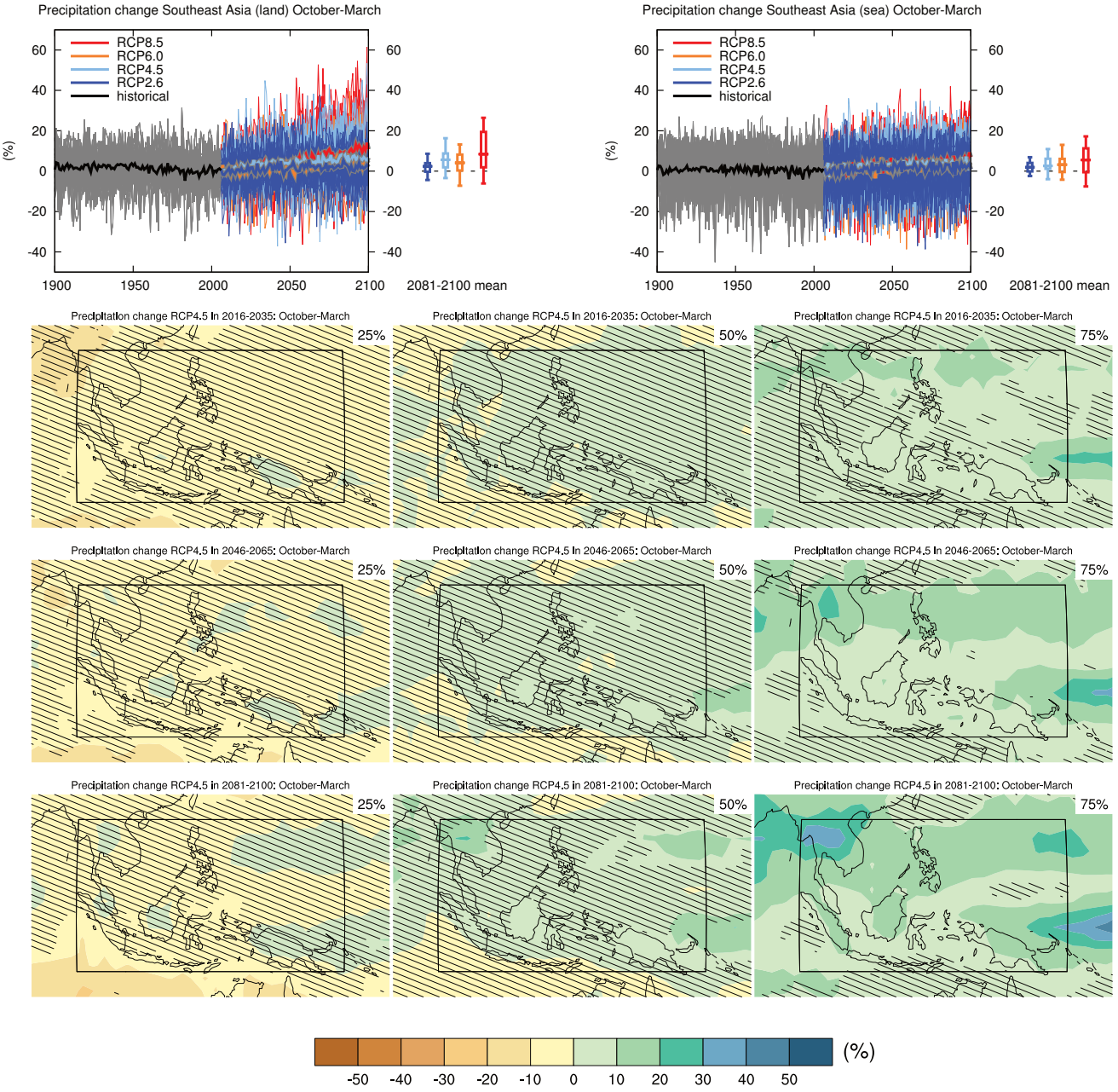

Figure AI.66 | (Top left) Time series of relative change relative to 1986–2005 in precipitation averaged over land grid points in Southeast Asia (10°S to 20°N, 95°E to 155°E) in October to March. (Top right) Same for sea grid points. Thin lines denote one ensemble member per model, thick lines the CMIP5 multi-model mean. On the right-hand side the 5th, 25th, 50th (median), 75th and 95th percentiles of the distribution of 20-year mean changes are given for 2081–2100 in the four RCP scenarios.

(Below) Maps of precipitation changes in 2016–2035, 2046–2065 and 2081–2100 with respect to 1986–2005 in the RCP4.5 scenario. For each point, the 25th, 50th and 75th percentiles of the distribution of the CMIP5 ensemble are shown; this includes both natural variability and inter-model spread. Hatching denotes areas where the 20-year mean differences of the percentiles are less than the standard deviation of model-estimated present-day natural variability of 20-year mean differences.

Sections 9.4.1.1, 9.6.1.1, Box 11.2, 14.2.2.3, 14.2.2.5, 14.8.12 contain relevant information regarding the evaluation of models in this region, the model spread in the context of other methods of projecting changes and the role of modes of variability and other climate phenomena.

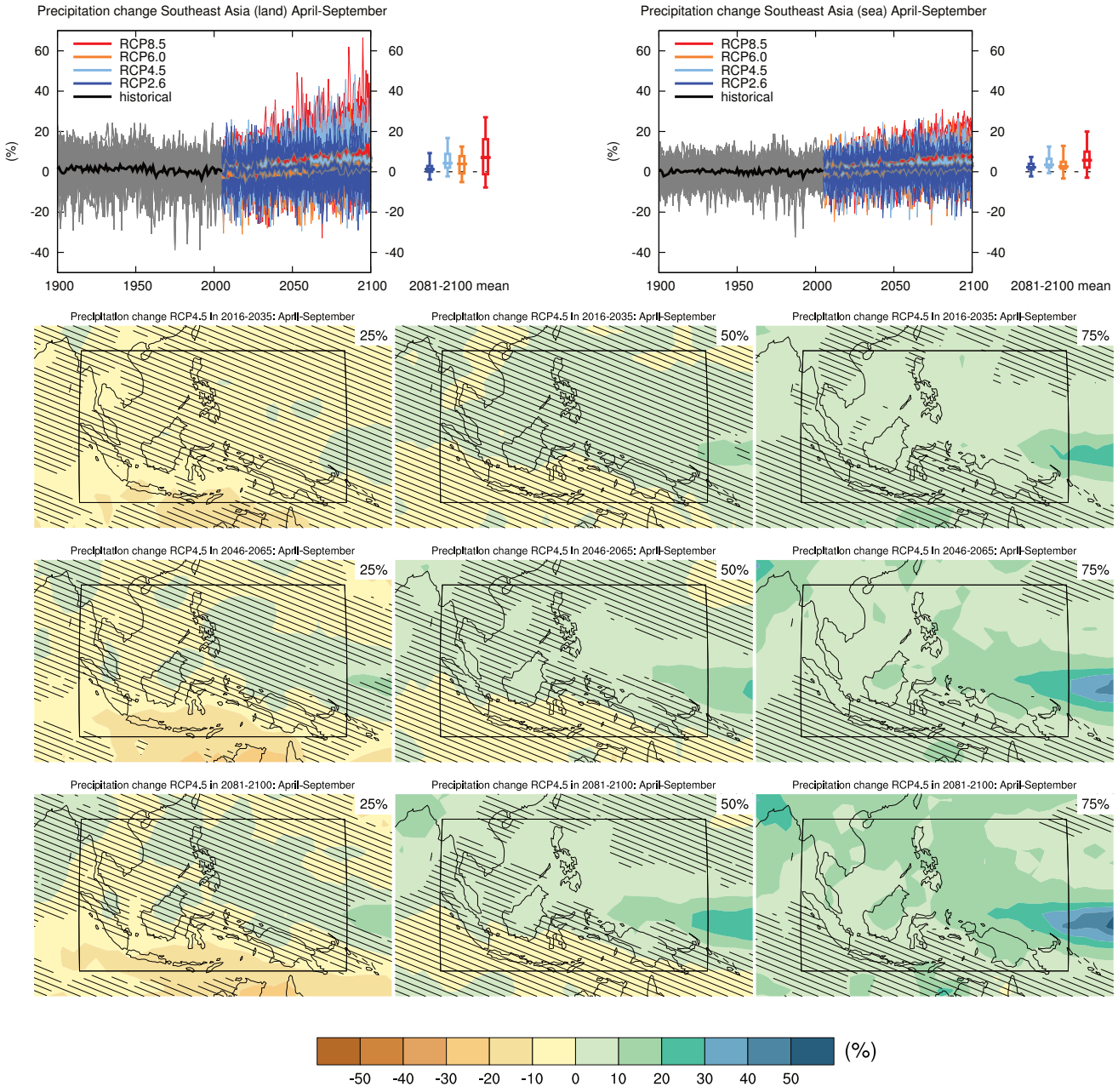

Figure AI.67 | (Top left) Time series of relative change relative to 1986–2005 in precipitation averaged over land grid points in Southeast Asia (10°S to 20°N, 95°E to 155°E) in April to September. (Top right) Same for sea grid points. Thin lines denote one ensemble member per model, thick lines the CMIP5 multi-model mean. On the right-hand side the 5th, 25th, 50th (median), 75th and 95th percentiles of the distribution of 20-year mean changes are given for 2081–2100 in the four RCP scenarios.

(Below) Maps of precipitation changes in 2016–2035, 2046–2065 and 2081–2100 with respect to 1986–2005 in the RCP4.5 scenario. For each point, the 25th, 50th and 75th percentiles of the distribution of the CMIP5 ensemble are shown; this includes both natural variability and inter-model spread. Hatching denotes areas where the 20-year mean differences of the percentiles are less than the standard deviation of model-estimated present-day natural variability of 20-year mean differences.

Sections 9.4.1.1, 9.6.1.1, Box 11.2, 14.2.2.3, 14.2.2.5, 14.8.12 contain relevant information regarding the evaluation of models in this region, the model spread in the context of other methods of projecting changes and the role of modes of variability and other climate phenomena.

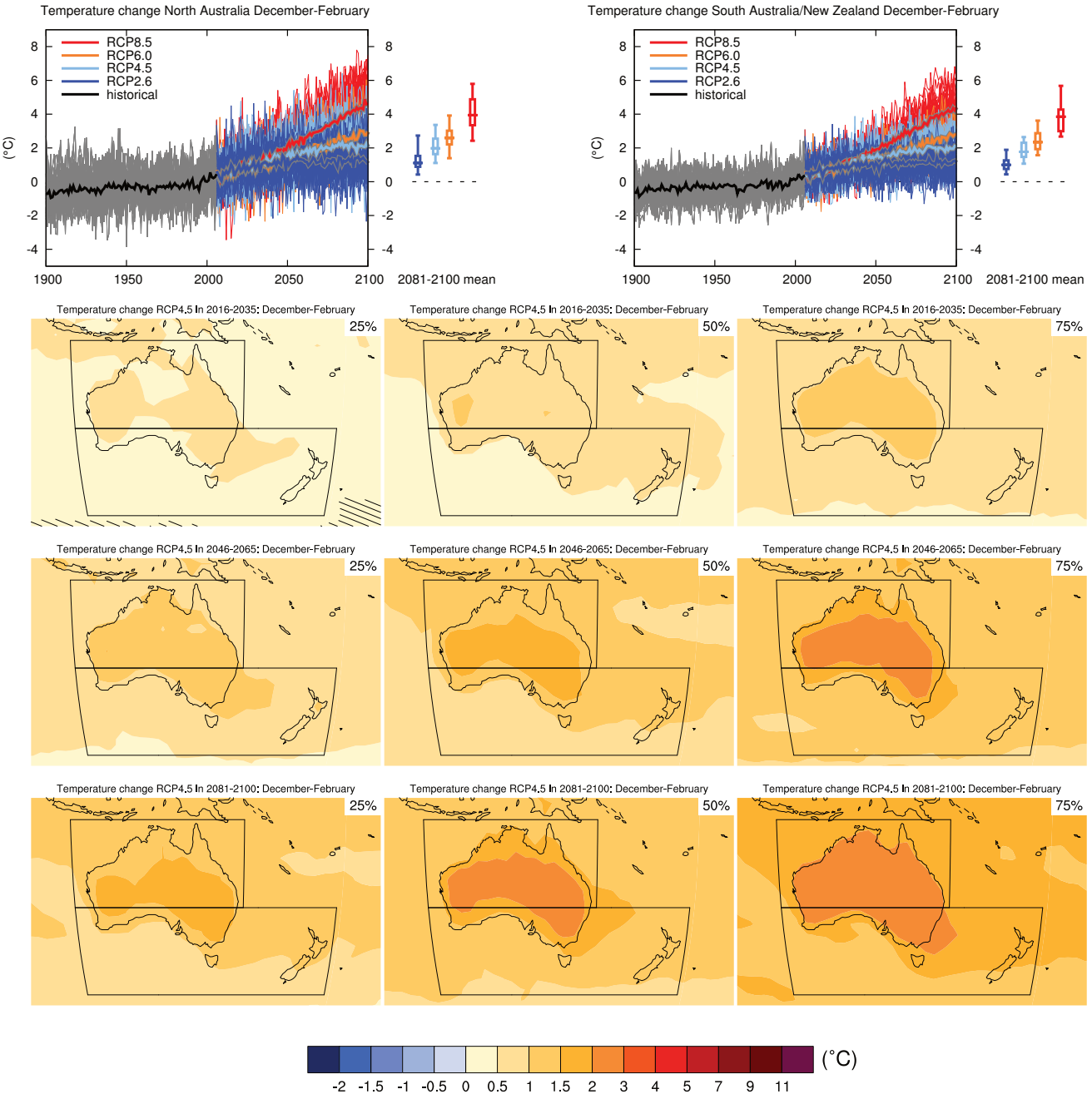

Figure AI.68 | (Top left) Time series of temperature change relative to 1986–2005 averaged over land grid points in North Australia (30°S to 10°S, 110°E to 155°E) in December to February. (Top right) Same for land grid points in South Australia/New Zealand (50°S to 30°S, 110°E to 180°E). Thin lines denote one ensemble member per model, thick lines the CMIP5 multi-model mean. On the right-hand side the 5th, 25th, 50th (median), 75th and 95th percentiles of the distribution of 20-year mean changes are given for 2081–2100 in the four RCP scenarios.

(Below) Maps of temperature changes in 2016–2035, 2046–2065 and 2081–2100 with respect to 1986–2005 in the RCP4.5 scenario. For each point, the 25th, 50th and 75th percentiles of the distribution of the CMIP5 ensemble are shown; this includes both natural variability and inter-model spread. Hatching denotes areas where the 20-year mean differences of the percentiles are less than the standard deviation of model-estimated present-day natural variability of 20-year mean differences.

Sections 9.4.1.1, 9.6.1.1, 10.3.1.1.4, Box 11.2, 14.8.13 contain relevant information regarding the evaluation of models in this region, the model spread in the context of other methods of projecting changes and the role of modes of variability and other climate phenomena.

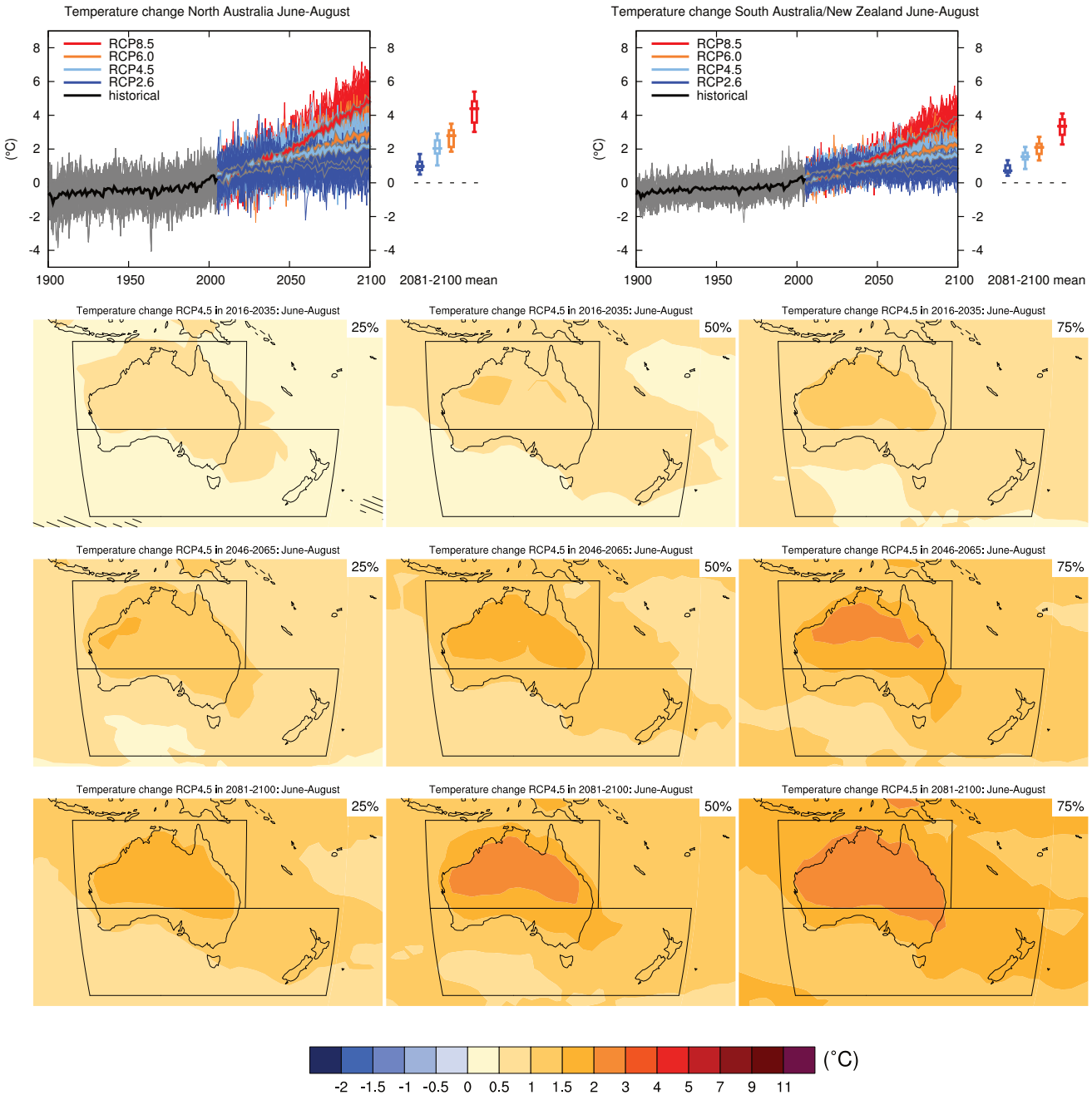

Figure AI.69 | (Top left) Time series of temperature change relative to 1986–2005 averaged over land grid points in North Australia (30°S to 10°S, 110°E to 155°E) in June to August. (Top right) Same for land grid points in South Australia/New Zealand (50°S to 30°S, 110°E to 180°E). Thin lines denote one ensemble member per model, thick lines the CMIP5 multi-model mean. On the right-hand side the 5th, 25th, 50th (median), 75th and 95th percentiles of the distribution of 20-year mean changes are given for 2081–2100 in the four RCP scenarios.

(Below) Maps of temperature changes in 2016–2035, 2046–2065 and 2081–2100 with respect to 1986–2005 in the RCP4.5 scenario. For each point, the 25th, 50th and 75th percentiles of the distribution of the CMIP5 ensemble are shown; this includes both natural variability and inter-model spread. Hatching denotes areas where the 20-year mean differences of the percentiles are less than the standard deviation of model-estimated present-day natural variability of 20-year mean differences.

Sections 9.4.1.1, 9.6.1.1, 10.3.1.1.4, Box 11.2, 14.8.13 contain relevant information regarding the evaluation of models in this region, the model spread in the context of other methods of projecting changes and the role of modes of variability and other climate phenomena.

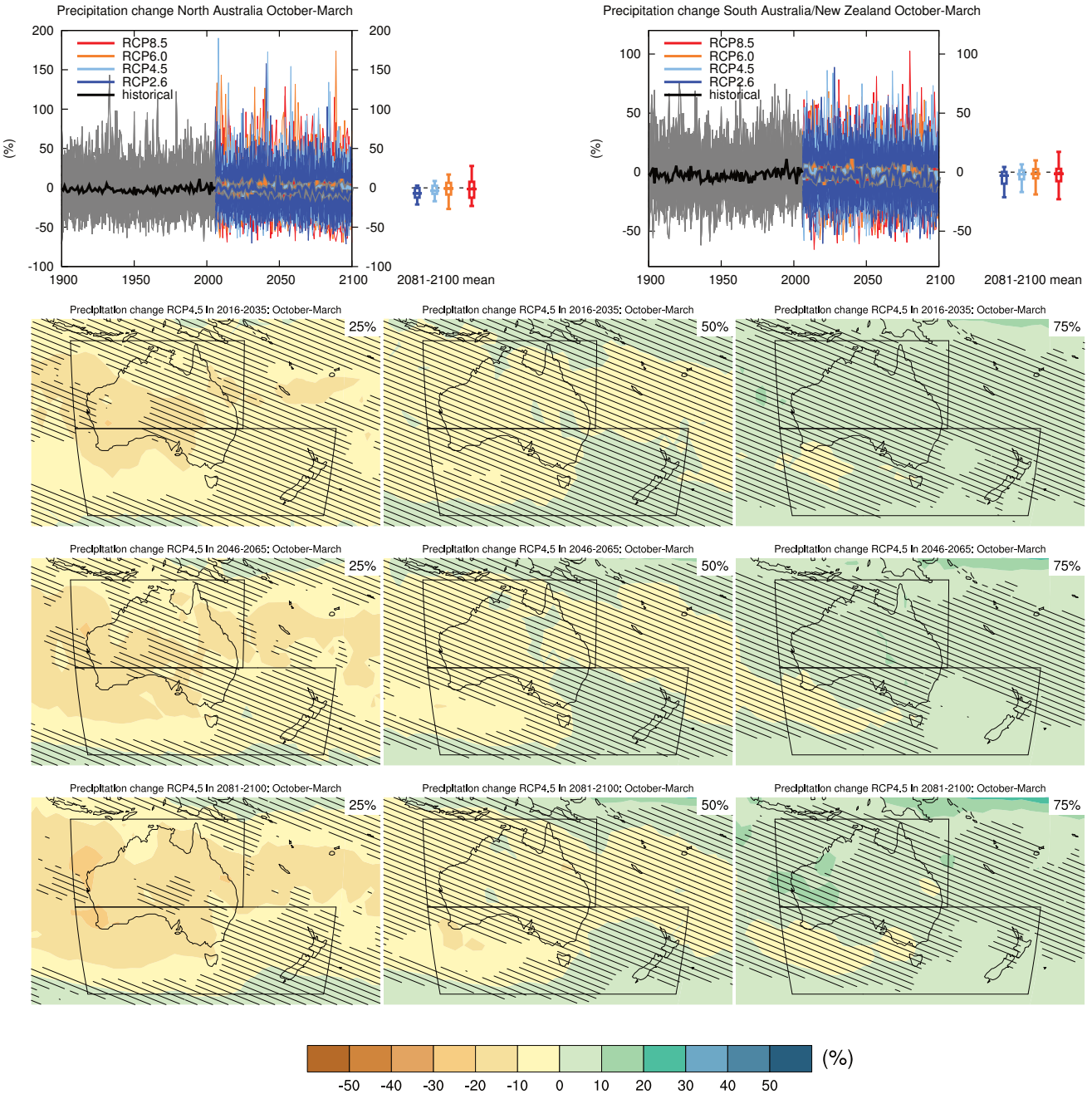

Figure AI.70 | (Top left) Time series of relative change relative to 1986–2005 in precipitation averaged over land grid points in North Australia (30°S to 10°S, 110°E to 155°E) in October to March. (Top right) Same for land grid points in South Australia/New Zealand (50°S to 30°S, 110°E to 180°E). Thin lines denote one ensemble member per model, thick lines the CMIP5 multi-model mean. On the right-hand side the 5th, 25th, 50th (median), 75th and 95th percentiles of the distribution of 20-year mean changes are given for 2081–2100 in the four RCP scenarios. Note different scales.

(Below) Maps of precipitation changes in 2016–2035, 2046–2065 and 2081–2100 with respect to 1986–2005 in the RCP4.5 scenario. For each point, the 25th, 50th and 75th percentiles of the distribution of the CMIP5 ensemble are shown; this includes both natural variability and inter-model spread. Hatching denotes areas where the 20-year mean differences of the percentiles are less than the standard deviation of model-estimated present-day natural variability of 20-year mean differences.

Sections 9.4.1.1, 9.6.1.1, Box 11.2, 14.2.2.4, 14.8.13 contain relevant information regarding the evaluation of models in this region, the model spread in the context of other methods of projecting changes and the role of modes of variability and other climate phenomena.

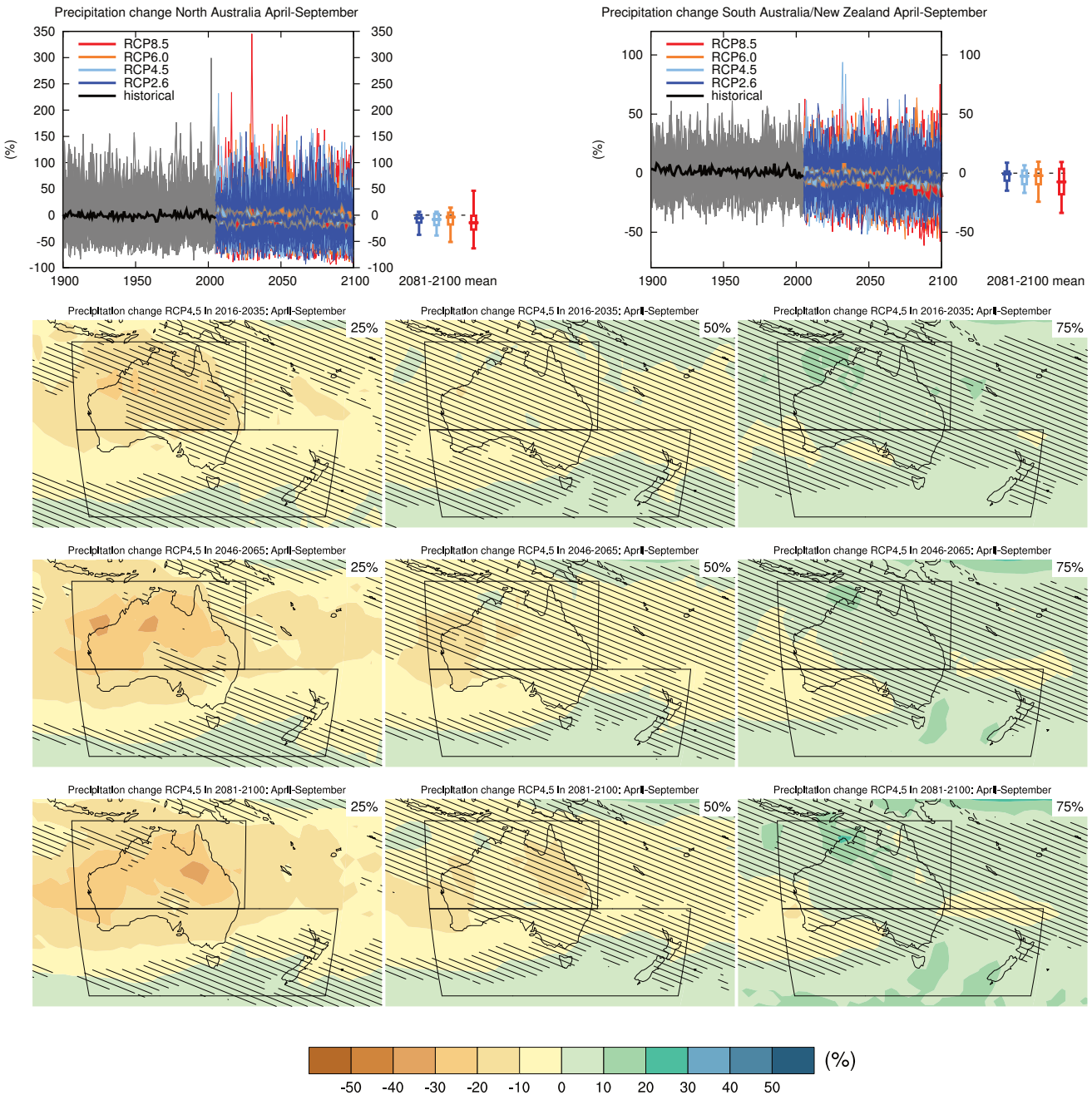

Figure AI.71 | (Top left) Time series of relative change relative to 1986–2005 in precipitation averaged over land grid points in North Australia (30°S to 10°S, 110°E to 155°E) in April to September. (Top right) Same for land grid points in South Australia/New Zealand (50°S to 30°S, 110°E to 180°E). Thin lines denote one ensemble member per model, thick lines the CMIP5 multi-model mean. On the right-hand side the 5th, 25th, 50th (median), 75th and 95th percentiles of the distribution of 20-year mean changes are given for 2081–2100 in the four RCP scenarios. Note different scales.

(Below) Maps of precipitation changes in 2016–2035, 2046–2065 and 2081–2100 with respect to 1986–2005 in the RCP4.5 scenario. For each point, the 25th, 50th and 75th percentiles of the distribution of the CMIP5 ensemble are shown; this includes both natural variability and inter-model spread. Hatching denotes areas where the 20-year mean differences of the percentiles are less than the standard deviation of model-estimated present-day natural variability of 20-year mean differences.

Sections 9.4.1.1, 9.6.1.1, Box 11.2, 14.2.2.4, 14.8.13 contain relevant information regarding the evaluation of models in this region, the model spread in the context of other methods of projecting changes and the role of modes of variability and other climate phenomena.

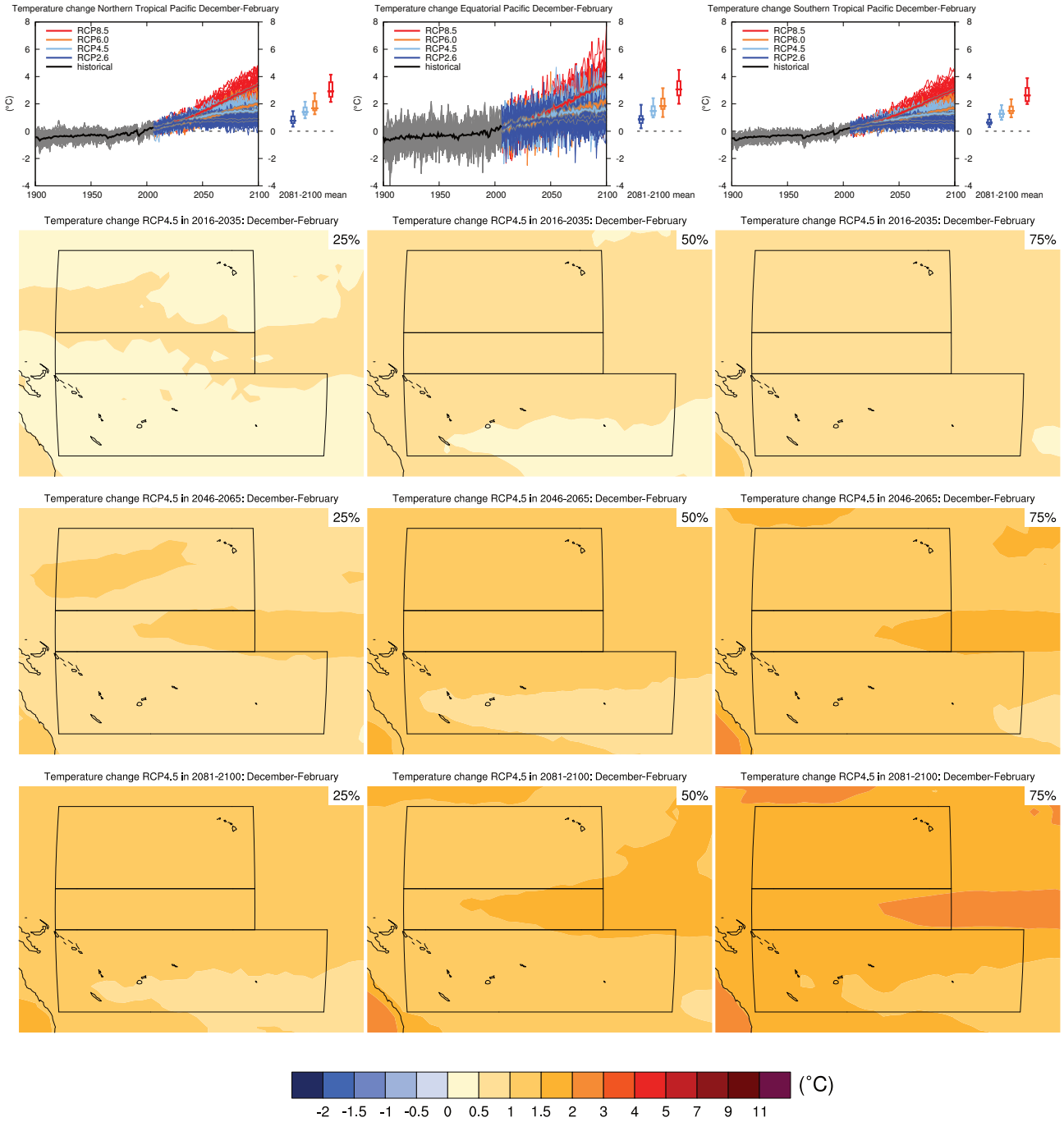

Figure AI.72 | (Top left) Time series of temperature change relative to 1986–2005 averaged over all grid points in the Northern Tropical Pacific (5°N to 25°N, 155°E to 150°W) in December to February. Top middle: same for all grid points in the Equatorial Pacific (5°S to 5°N, 155°E to 150°W). (Top right) Same for all grid points in the Southern Tropical Pacific (5°S to 5°N, 155°E to 150°W). Thin lines denote one ensemble member per model, thick lines the CMIP5 multi-model mean. On the right-hand side the 5th, 25th, 50th (median), 75th and 95th percentiles of the distribution of 20-year mean changes are given for 2081–2100 in the four RCP scenarios.

(Below) Maps of temperature changes in 2016–2035, 2046–2065 and 2081–2100 with respect to 1986–2005 in the RCP4.5 scenario. For each point, the 25th, 50th and 75th percentiles of the distribution of the CMIP5 ensemble are shown; this includes both natural variability and inter-model spread. Hatching denotes areas where the 20-year mean differences of the percentiles are less than the standard deviation of model-estimated present-day natural variability of 20-year mean differences.

Sections 9.4.1.1, 9.6.1.1, 10.3.1.1.4, Box 11.2, 12.4.3.1, 14.4.1, 14.8.14 contain relevant information regarding the evaluation of models in this region, the model spread in the context of other methods of projecting changes and the role of modes of variability and other climate phenomena.

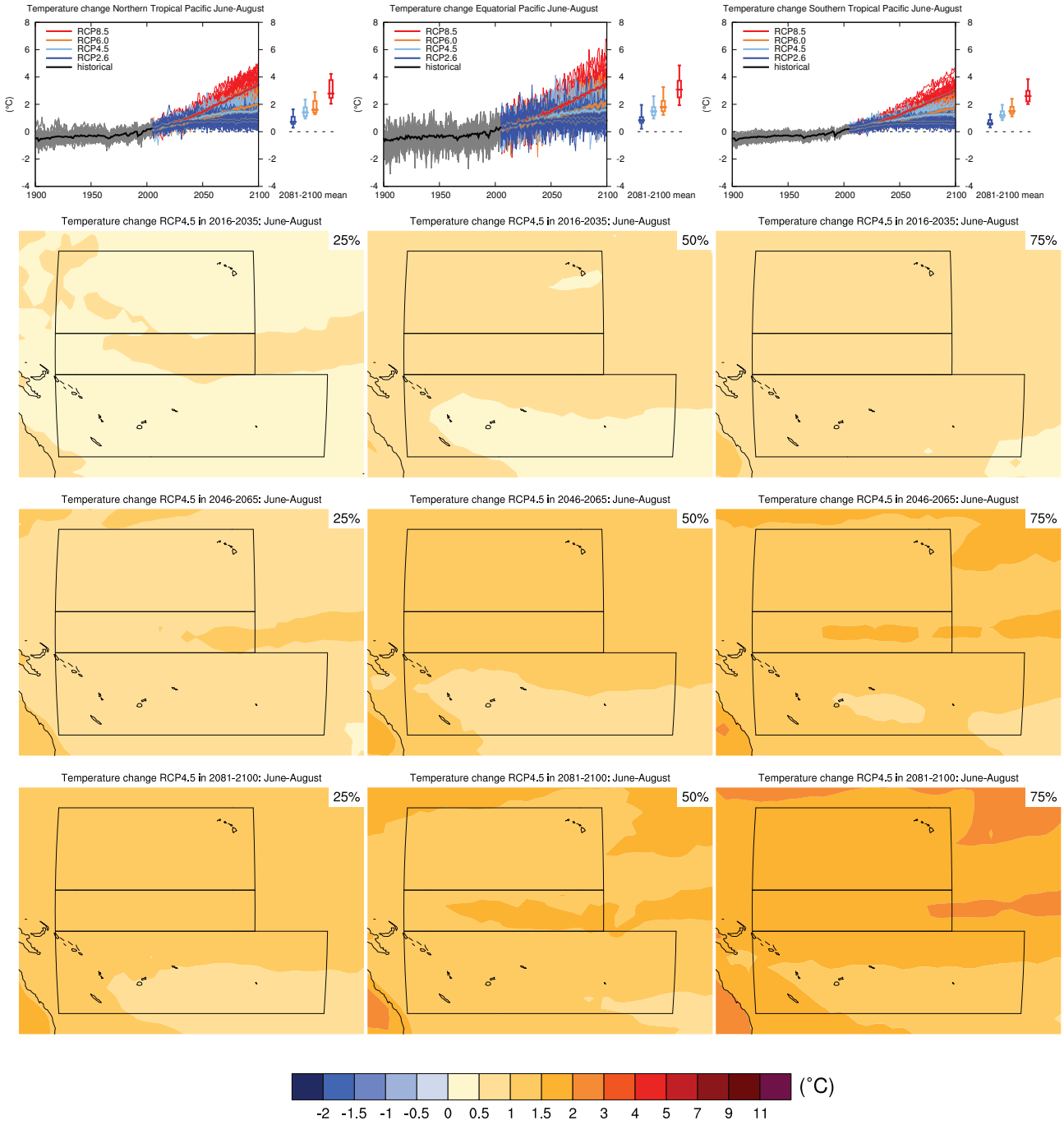

Figure AI.73 | (Top left) Time series of temperature change relative to 1986–2005 averaged over all grid points in the Northern Tropical Pacific (5°N to 25°N, 155°E to 150°W) in June to August. Top middle: same for all grid points in the Equatorial Pacific (5°S to 5°N, 155°E to 150°W). (Top right) Same for all grid points in the Southern Tropical Pacific (5°S to 5°N, 155°E to 150°W). Thin lines denote one ensemble member per model, thick lines the CMIP5 multi-model mean. On the right-hand side the 5th, 25th, 50th (median), 75th and 95th percentiles of the distribution of 20-year mean changes are given for 2081–2100 in the four RCP scenarios.

(Below) Maps of temperature changes in 2016–2035, 2046–2065 and 2081–2100 with respect to 1986–2005 in the RCP4.5 scenario. For each point, the 25th, 50th and 75th percentiles of the distribution of the CMIP5 ensemble are shown; this includes both natural variability and inter-model spread. Hatching denotes areas where the 20-year mean differences of the percentiles are less than the standard deviation of model-estimated present-day natural variability of 20-year mean differences.

Sections 9.4.1.1, 9.6.1.1, 10.3.1.1.4, Box 11.2, 12.4.3.1, 14.4.1, 14.8.14 contain relevant information regarding the evaluation of models in this region, the model spread in the context of other methods of projecting changes and the role of modes of variability and other climate phenomena.

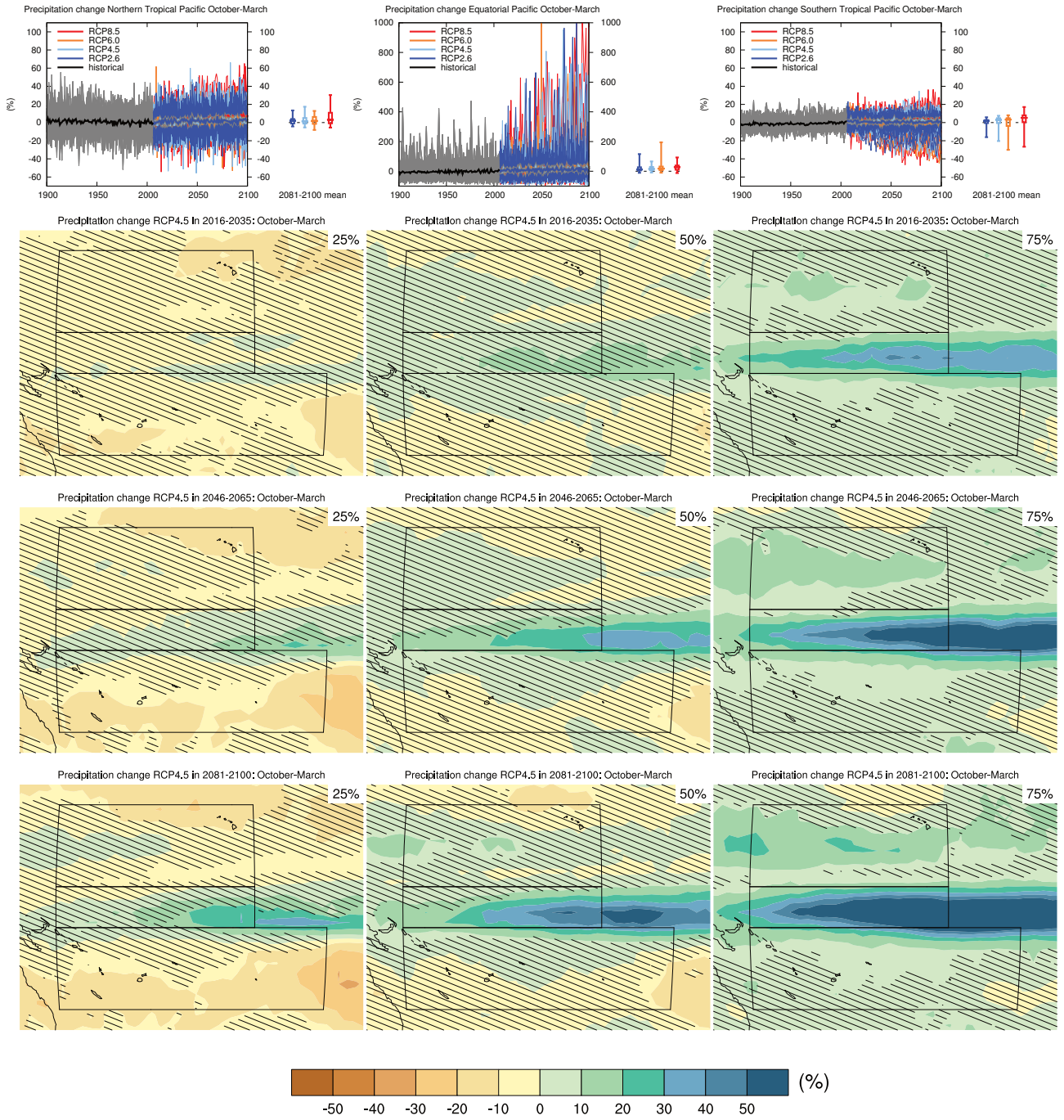

Figure AI.74 | (Top left) Time series of relative change relative to 1986–2005 in precipitation averaged over all grid points in the Northern Tropical Pacific (5°N to 25°N, 155°E to 150°W) in October to March. Top middle: same for all grid points in the Equatorial Pacific (5°S to 5°N, 155°E to 150°W). (Top right) Same for all grid points in the Southern Tropical Pacific (5°S to 5°N, 155°E to 150°W). Thin lines denote one ensemble member per model, thick lines the CMIP5 multi-model mean. On the right-hand side the 5th, 25th, 50th (median), 75th and 95th percentiles of the distribution of 20-year mean changes are given for 2081–2100 in the four RCP scenarios. Note different scales.

(Below) Maps of precipitation changes in 2016–2035, 2046–2065 and 2081–2100 with respect to 1986–2005 in the RCP4.5 scenario. For each point, the 25th, 50th and 75th percentiles of the distribution of the CMIP5 ensemble are shown; this includes both natural variability and inter-model spread. Hatching denotes areas where the 20-year mean differences of the percentiles are less than the standard deviation of model-estimated present-day natural variability of 20-year mean differences.

Sections 9.4.1.1, 9.6.1.1, 11.3.2.1.2, Box 11.2, 12.4.5.2, 14.8.14 contain relevant information regarding the evaluation of models in this region, the model spread in the context of other methods of projecting changes and the role of modes of variability and other climate phenomena.

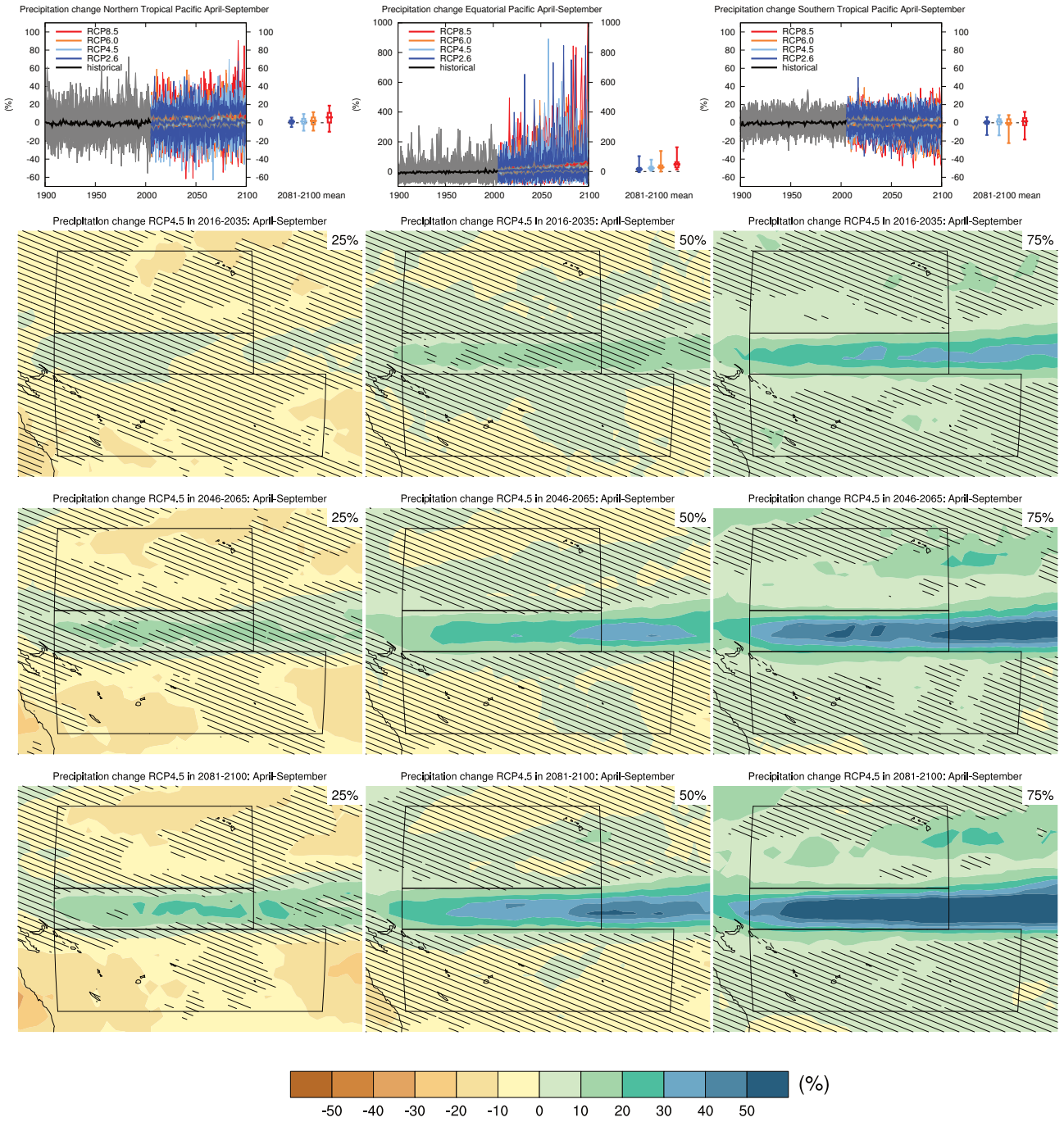

Figure AI.75 | (Top left) Time series of relative change relative to 1986–2005 in precipitation averaged over all grid points in the Northern Tropical Pacific (5°N to 25°N, 155°E to 150°W) in April to September. Top middle: same for all grid points in the Equatorial Pacific (5°S to 5°N, 155°E to 150°W). (Top right) Same for all grid points in the Southern Tropical Pacific (5°S to 5°N, 155°E to 150°W). Thin lines denote one ensemble member per model, thick lines the CMIP5 multi-model mean. On the right-hand side the 5th, 25th, 50th (median), 75th and 95th percentiles of the distribution of 20-year mean changes are given for 2081–2100 in the four RCP scenarios. Note different scales.

(Below) Maps of precipitation changes in 2016–2035, 2046–2065 and 2081–2100 with respect to 1986–2005 in the RCP4.5 scenario. For each point, the 25th, 50th and 75th percentiles of the distribution of the CMIP5 ensemble are shown; this includes both natural variability and inter-model spread. Hatching denotes areas where the 20-year mean differences of the percentiles are less than the standard deviation of model-estimated present-day natural variability of 20-year mean differences.

Sections 9.4.1.1, 9.6.1.1, 11.3.2.1.2, Box 11.2, 12.4.5.2, 14.8.14 contain relevant information regarding the evaluation of models in this region, the model spread in the context of other methods of projecting changes and the role of modes of variability and other climate phenomena.

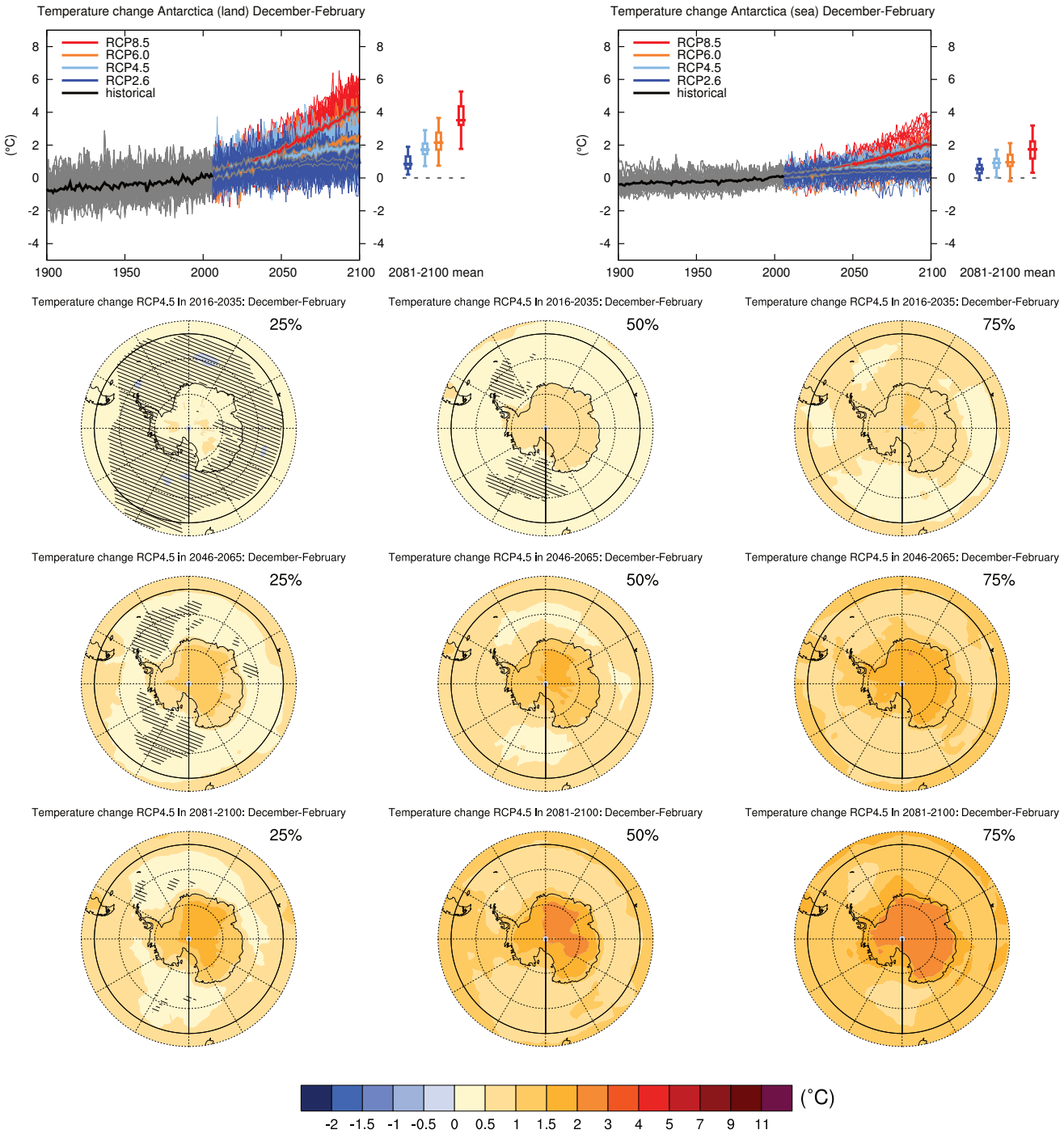

Figure AI.76 | (Top left) Time series of temperature change relative to 1986–2005 averaged over land grid points in Antarctica (90°S to 50°S) in December to February. (Top right) Same for sea grid points. Thin lines denote one ensemble member per model, thick lines the CMIP5 multi-model mean. On the right-hand side the 5th, 25th, 50th (median), 75th and 95th percentiles of the distribution of 20-year mean changes are given for 2081–2100 in the four RCP scenarios.

(Below) Maps of temperature changes in 2016–2035, 2046–2065 and 2081–2100 with respect to 1986–2005 in the RCP4.5 scenario. For each point, the 25th, 50th and 75th percentiles of the distribution of the CMIP5 ensemble are shown; this includes both natural variability and inter-model spread. Hatching denotes areas where the 20-year mean differences of the percentiles are less than the standard deviation of model-estimated present-day natural variability of 20-year mean differences.

Sections 9.4.1.1, 9.6.1.1, 10.3.1.1.4, Box 11.2, 12.4.3.1, 14.8.15 contain relevant information regarding the evaluation of models in this region, the model spread in the context of other methods of projecting changes and the role of modes of variability and other climate phenomena.

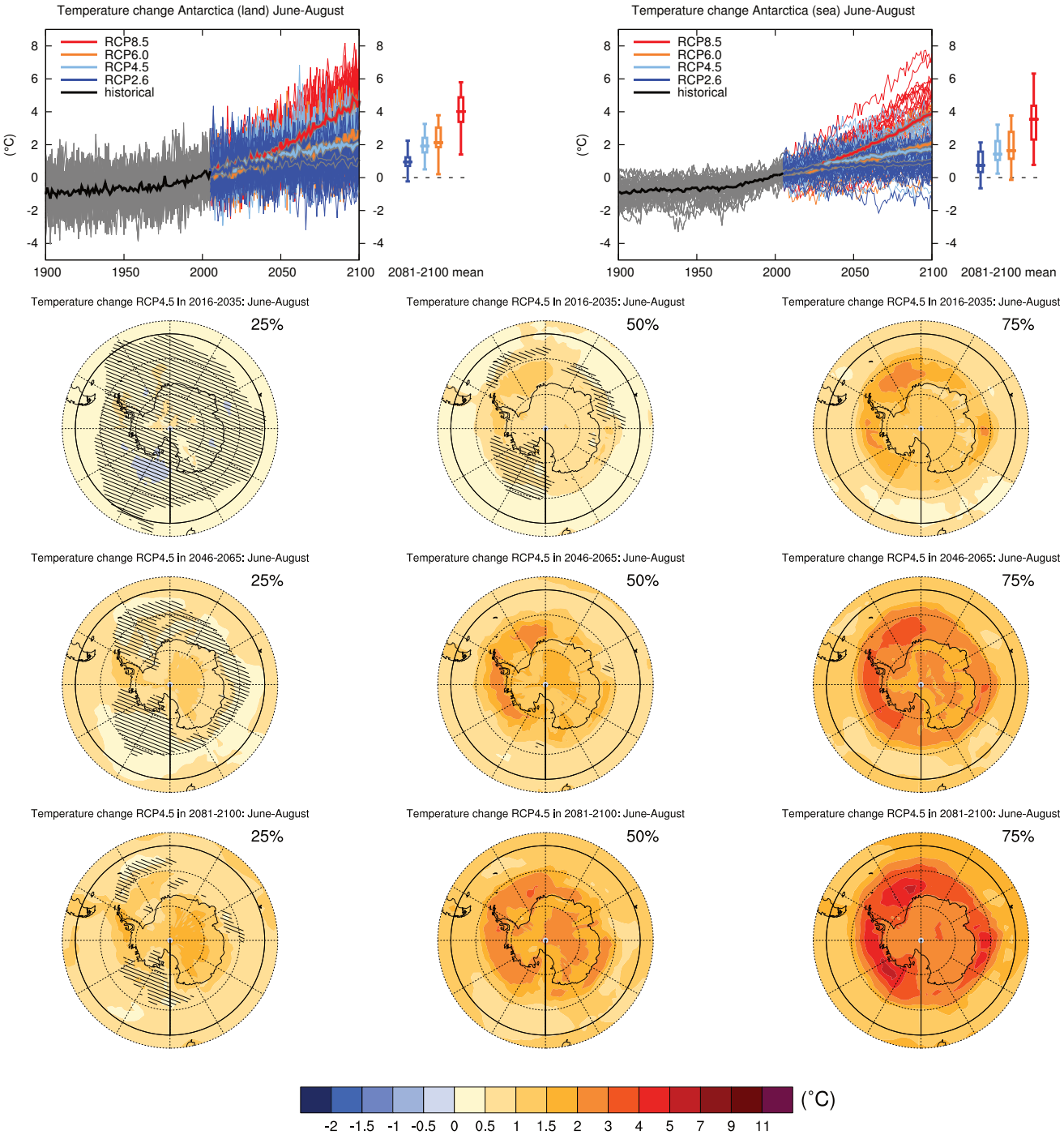

Figure AI.77 | (Top left) Time series of temperature change relative to 1986–2005 averaged over land grid points in Antarctica (90°S to 50°S) in June to August. (Top right) Same for sea grid points. Thin lines denote one ensemble member per model, thick lines the CMIP5 multi-model mean. On the right-hand side the 5th, 25th, 50th (median), 75th and 95th percentiles of the distribution of 20-year mean changes are given for 2081–2100 in the four RCP scenarios.

(Below) Maps of temperature changes in 2016–2035, 2046–2065 and 2081–2100 with respect to 1986–2005 in the RCP4.5 scenario. For each point, the 25th, 50th and 75th percentiles of the distribution of the CMIP5 ensemble are shown; this includes both natural variability and inter-model spread. Hatching denotes areas where the 20-year mean differences of the percentiles are less than the standard deviation of model-estimated present-day natural variability of 20-year mean differences.

Sections 9.4.1.1, 9.6.1.1, 10.3.1.1.4, Box 11.2, 12.4.3.1, 14.8.15 contain relevant information regarding the evaluation of models in this region, the model spread in the context of other methods of projecting changes and the role of modes of variability and other climate phenomena.

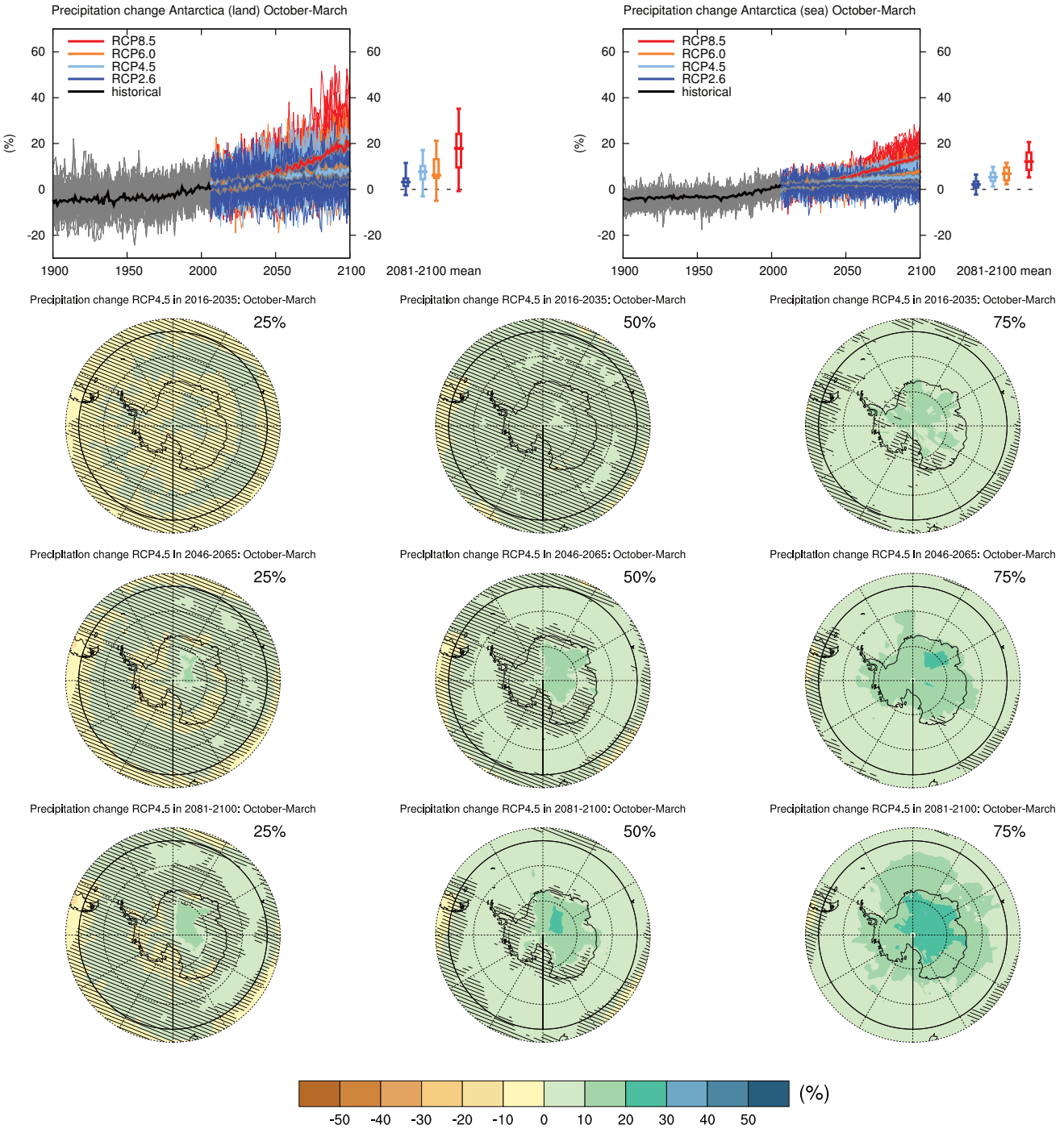

Figure AI.78 | (Top left) Time series of relative change relative to 1986–2005 in precipitation averaged over land grid points in Antarctica (90°S to 50°S) in October to March. (Top right) Same for sea grid points. Thin lines denote one ensemble member per model, thick lines the CMIP5 multi-model mean. On the right-hand side the 5th, 25th, 50th (median), 75th and 95th percentiles of the distribution of 20-year mean changes are given for 2081–2100 in the four RCP scenarios.

(Below) Maps of precipitation changes in 2016–2035, 2046–2065 and 2081–2100 with respect to 1986–2005 in the RCP4.5 scenario. For each point, the 25th, 50th and 75th percentiles of the distribution of the CMIP5 ensemble are shown; this includes both natural variability and inter-model spread. Hatching denotes areas where the 20-year mean differences of the percentiles are less than the standard deviation of model-estimated present-day natural variability of 20-year mean differences.

Sections 9.4.1.1, 9.6.1.1, 10.3.2.2, Box 11.2, 12.4.5.2, 14.8.15 contain relevant information regarding the evaluation of models in this region, the model spread in the context of other methods of projecting changes and the role of modes of variability and other climate phenomena.

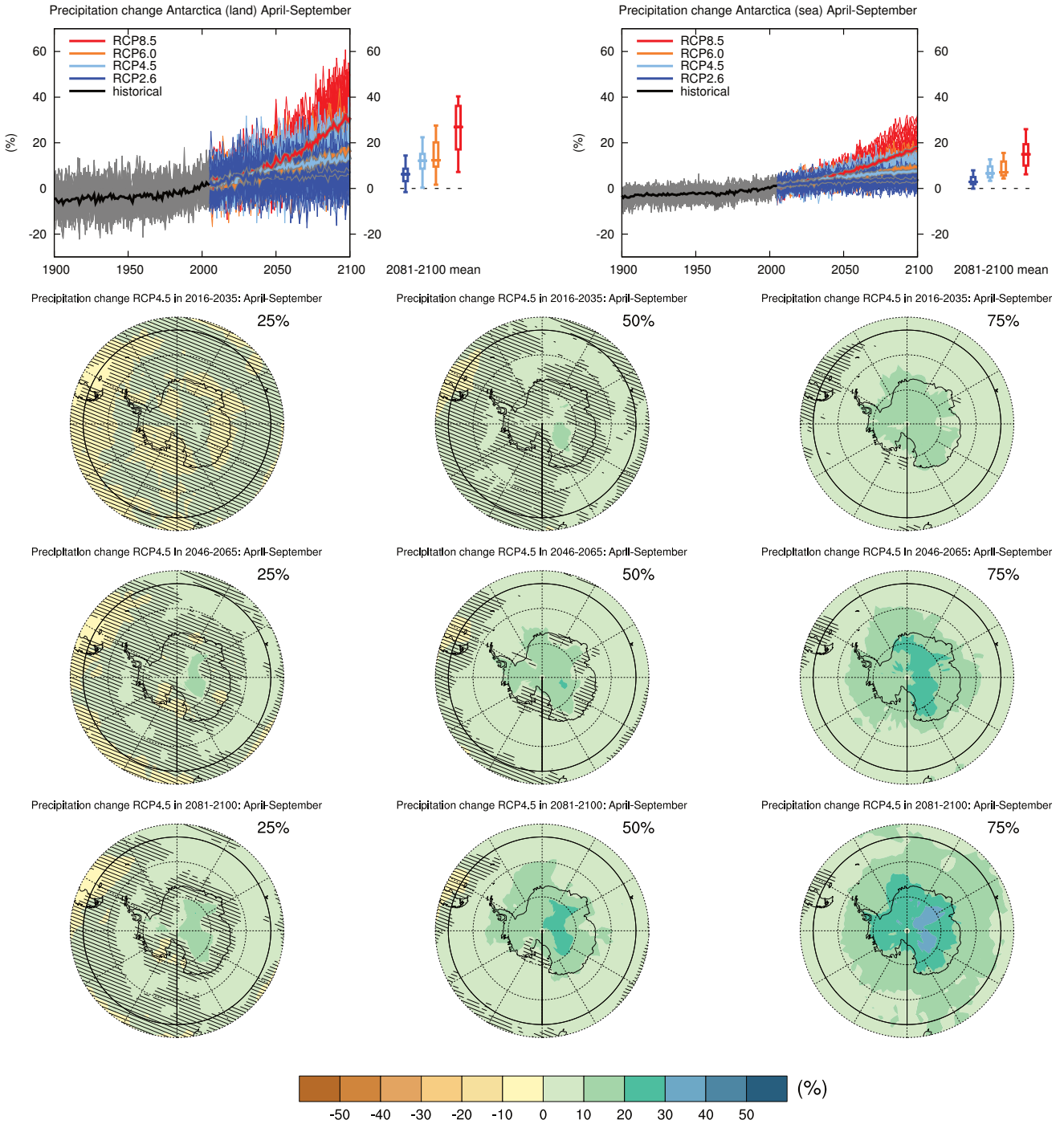

Figure AI.79 | (Top left) Time series of relative change relative to 1986–2005 in precipitation averaged over land grid points in Antarctica (90°S to 50°S) in April to September. (Top right) Same for sea grid points. Thin lines denote one ensemble member per model, thick lines the CMIP5 multi-model mean. On the right-hand side the 5th, 25th, 50th (median), 75th and 95th percentiles of the distribution of 20-year mean changes are given for 2081–2100 in the four RCP scenarios.

(Below) Maps of precipitation changes in 2016–2035, 2046–2065 and 2081–2100 with respect to 1986–2005 in the RCP4.5 scenario. For each point, the 25th, 50th and 75th percentiles of the distribution of the CMIP5 ensemble are shown; this includes both natural variability and inter-model spread. Hatching denotes areas where the 20-year mean differences of the percentiles are less than the standard deviation of model-estimated present-day natural variability of 20-year mean differences.

Sections 9.4.1.1, 9.6.1.1, 10.3.2.2, Box 11.2, 12.4.5.2, 14.8.15 contain relevant information regarding the evaluation of models in this region, the model spread in the context of other methods of projecting changes and the role of modes of variability and other climate phenomena.

AII Annex II: Climate System Scenario Tables

Editorial Team:
Michael Prather (USA), Gregory Flato (Canada), Pierre Friedlingstein (UK/Belgium), Christopher Jones (UK), Jean-François Lamarque (USA), Hong Liao (China), Philip Rasch (USA)

Contributors:
Olivier Boucher (France), François-Marie Bréon (France), Tim Carter (Finland), William Collins (UK), Frank J. Dentener (EU/Netherlands), Edward J. Dlugokencky (USA), Jean-Louis Dufresne (France), Jan Willem Erisman (Netherlands), Veronika Eyring (Germany), Arlene M. Fiore (USA), James Galloway (USA), Jonathan M. Gregory (UK), Ed Hawkins (UK), Chris Holmes (USA), Jasmin John (USA), Tim Johns (UK), Fiona Lo (USA), Natalie Mahowald (USA), Malte Meinshausen (Germany), Colin Morice (UK), Vaishali Naik (USA/India), Drew Shindell (USA), Steven J. Smith (USA), David Stevenson (UK), Peter W. Thorne (USA/Norway/UK), Geert Jan van Oldenborgh (Netherlands), Apostolos Voulgarakis (UK/Greece), Oliver Wild (UK), Donald Wuebbles (USA), Paul Young (UK)

This annex should be cited as:
IPCC, 2013: Annex II: Climate System Scenario Tables [Prather, M., G. Flato, P. Friedlingstein, C. Jones, J.-F. Lamarque, H. Liao and P. Rasch (eds.)]. In: *Climate Change 2013: The Physical Science Basis. Contribution of Working Group I to the Fifth Assessment Report of the Intergovernmental Panel on Climate Change* [Stocker, T.F., D. Qin, G.-K. Plattner, M. Tignor, S.K. Allen, J. Boschung, A. Nauels, Y. Xia, V. Bex and P.M. Midgley (eds.)]. Cambridge University Press, Cambridge, United Kingdom and New York, NY, USA.

Table of Contents

Introduction

Annex II presents, in tabulated form, data related to historical and projected changes in the climate system that are assessed in the chapters of this report (see Section 1.6). It also includes some comparisons with the Third Assessment Report (TAR) and Fourth Assessment Report (AR4) results. These data include values for emissions into the atmosphere, atmospheric abundances and burdens (integrated abundance), effective radiative forcing (ERF; includes adjusted forcing from aerosols, see Chapters 7 and 8), and global mean surface temperatures and sea level. Projections from 2010 to 2100 focus on the RCP scenarios (Moss et al., 2010; Lamarque et al., 2010; 2011; Meinshausen et al., 2011a; van Vuuren et al., 2011; see also Chapters 1, 6, 8, 11, 12 and 13). Projections also include previous IPCC scenarios (IPCC Scenarios 1992a (IS92a), Special Report on Emission Scenarios (SRES) A2 and B1, TAR Appendix II) and some alternative near-term scenarios for methane (CH_4) and short-lived pollutants that impact climate or air quality. Emissions from biomass burning are included as anthropogenic. ERF from land use change is also included in some tables.

Where uncertainties or ranges are presented here, they are noted in each table as being a recommended value or model ensemble mean/median with a 68% confidence interval (16 to 84%, $\pm 1\sigma$ for a normal distribution) or 90% confidence interval (5 to 95%, $\pm 1.645\sigma$ for a normal distribution) or statistics (standard deviation, percentiles, or minimum/maximum) of an ensemble of models. In some cases these are a formal evaluation of uncertainty as assessed in the chapters, but in other cases (specifically Tables AII.2.1, 3.1, 4.1, 5.1, 6.10, 7.1 to 7.5) they just describe the statistical results from the available models, and the referenced chapters must be consulted for the assessed uncertainty or confidence level of these results. In the case of Table AII.7.5, for example, the global mean surface temperature change (°C) relative to 1986–2005 is a statistical summary of the spread in the Coupled Model Intercomparison Project (CMIP) ensembles for each of the scenarios: model biases and model dependencies are not accounted for; the percentiles do not correspond to the assessed uncertainty derived in Chapters 11 (Section 11.3.6.3) and 12 (Section 12.4.1); and statistical spread across models cannot be interpreted in terms of calibrated language (Section 12.2).

The Representative Concentration Pathway (RCP) scenarios for emissions include only anthropogenic sources and use a single model to project from emissions to abundances to radiative forcing to climate change (Meinshausen et al., 2011a; 2011b). We include projected changes in natural carbon dioxide (CO_2) sources and sinks for 2010–2100 based on this assessment (Chapters 6 and 12). Present-day natural and anthropogenic emissions of CH_4 and nitrous oxide (N_2O) are assessed and used to scale the RCP anthropogenic emissions to be consistent with these best estimates (Chapters 6 and 11). Current model evaluations of atmospheric chemistry and the carbon cycle, including results from the CMIP5 and Atmospheric Chemistry and Climate Model Intercomparison Project (ACCMIP) projects, are used to project future composition and ERF separately from the RCP model (see Sections 6.4.3, 11.3.5 and 12.3). Thus, projected changes in greenhouse gases (GHGs), aerosols and ERF evaluated in this report may differ from the published RCPs and from what was used in the CMIP5 runs, and these are denoted RCP$^{\&}$. The CMIP5 climate projections used for the most part the RCP concentration pathways for well-mixed greenhouse gases (WMGHG) and the emissions pathways for ozone (O_3) and aerosol precursors. Such differences are discussed in the relevant chapters and noted in the tables.

For each species, the abundances (given as dry air mole fraction: ppm = micromoles per mole (10^{-6}); ppb = nanomoles per mole (10^{-9}); and ppt = picomoles per mole (10^{-12})), burdens (global total in grams, 1 Tg = 10^{12} g), average column amount (1 Dobson Unit (DU) = 2.687×10^{16} molecules per cm^2), AOD (mean aerosol optical depth at 550 nm), ERF (effective radiative forcing, W m^{-2}), and other climate system quantities are calculated for scenarios using methodologies based on the latest climate chemistry and climate carbon models (see Chapters 2, 6, 7, 8, 10, 11 and 12). Results are shown for individual years (e.g., 2010 = year 2010) and decadal averages (e.g., 2020^{d} = average of years 2016 through 2025), although some 10-year periods are different, see table notes. Year 2011 is the last year for observed quantities (denoted 2011* or 2011^{obs}). Results are shown as global mean values except for environmental data focussing on air quality (Tables AII.7.1–AII.7.4), which give regional mean surface abundances of O_3 and fine particulate matter with diameter less than 2.5 µm ($PM_{2.5}$). Results for global mean surface temperature (Tables AII.7.5 and AII.7.6) show only raw CMIP5 data or data from previous assessments. For best estimates of near-term and long-term temperature change see Chapters 11 and 12, respectively. Results for global mean sea level rise (Table AII.7.7) are assessed values with uncertainties described in Chapter 13.

Chemical Abbreviations and Symbols

Well Mixed Greenhouse Gases (WMGHG)

CO_2	carbon dioxide (KP, Kyoto Protocol gas)
CH_4	methane (KP)
N_2O	nitrous oxide (KP)
HFC	hydrofluorocarbon[1] (a class of compounds: HFC-32, HFC-134a, …) (KP)
PFC	perfluorocarbon (a class of compounds: CF_4, C_2F_6, …) (KP)
SF_6	sulphur hexafluoride (KP)
NF_3	nitrogen trifluoride (KP)
CFC	chlorofluorocarbon (a class of compounds: $CFCl_3$, CF_2Cl_2, …) (MP, Montreal Protocol gas)
HCFC	hydrochlorofluorocarbon[1] (a class of compounds: HCFC-22, HCFC-141b, …) (MP)
CCl_4	carbon tetrachloride (MP)
CH_3CCl_3	methyl chloroform (MP)

[1] A few HFCs and HCFCs are very short lived in the atmosphere and therefore not well mixed.

Ozone and Aerosols, and their Precursors

O_3	ozone (both stratospheric and tropospheric)
NO_x	sum of NO (nitric oxide) and NO_2 (nitrogen dioxide)
NH_3	ammonia
CO	carbon monoxide
NMVOC	a class of compounds comprising all non-methane volatile organic compounds (i.e., hydrocarbons that may also contain oxygen, also known as biogenic VOC or NMHC)
OH	hydroxyl radical
$PM_{2.5}$	any aerosols with diameter less than 2.5 µm
BC	black carbon aerosol
OC	organic carbon aerosol
SO_2	sulphur dioxide, a gas
SO_x	oxidized sulphur in gaseous form, including SO_2
$SO_4^=$	sulphate ion, usually as sulphuric acid or ammonium sulphate in aerosol

List of Tables

AII.1: Historical Climate System Data

AII.2: Anthropogenic Emissions

AII.3: Natural Emissions

AII.4: Abundances of the Well-Mixed Greenhouse Gases

AII.5: Column Abundances, Burdens, and Lifetimes

AII.6: Effective Radiative Forcing

AII.7: Environmental Data

Table AII.7.1: Global mean surface O_3 change (ppb)
Table AII.7.2: Surface O_3 change (ppb) for HTAP regions
Table AII.7.3: Surface O_3 change (ppb) from CMIP5/ACCMIP for continental regions
Table AII.7.4: Surface particulate matter change ($\log_{10}$[$PM_{2.5}$ (microgram/m^3)]) from CMIP5/ACCMIP for continental regions
Table AII.7.5: CMIP5 (RCP) and CMIP3 (SRES A1B) global mean surface temperature change (°C) relative to 1986–2005 reference period
Table AII.7.6: Global mean surface temperature change (°C) relative to 1990 from the TAR
Table AII.7.7: Global mean sea level rise (m) with respect to 1986–2005 at 1 January on the years indicated

References

Calvin, K., et al., 2012: The role of Asia in mitigating climate change: Results from the Asia modeling exercise. *Energy Econ*., **34**, S251–S260.

Cionni, I., V. Eyring, J. Lamarque, W. Randel, D. Stevenson, F. Wu, G. Bodeker, T. Shepherd, D. Shindell, and D. Waugh, 2011: Ozone database in support of CMIP5 simulations: Results and corresponding radiative forcing. *Atmos. Chem. Phys*., **11**, 11267–11292.

Cofala, J., M. Amann, Z. Klimont, K. Kupiainen, and L. Hoglund-Isaksson, 2007: Scenarios of global anthropogenic emissions of air pollutants and methane until 2030. *Atmos. Environ*., **41**, 8486–8499.

Dentener, F., D. Stevenson, J. Cofala, R. Mechler, M. Amann, P. Bergamaschi, F. Raes, and R. Derwent, 2005: The impact of air pollutant and methane emission controls on tropospheric ozone and radiative forcing: CTM calculations for the period 1990-2030. *Atmos. Chem. Phys*., **5**, 1731–1755.

Dentener, F., et al., 2006: The global atmospheric environment for the next generation. *Environ. Sci. Technol*., **40**, 3586–3594.

Douglass, A. and V. Fioletov, 2010: *Stratospheric Ozone and Surface Ultraviolet Radiation in Scientific Assessment of Ozone Depletion: 2010.* Global Ozone Research and Monitoring Project-Report No. 52.World Meteorological Organization, Geneva, Switzerland.

Erisman, J. W., M. A. Sutton, J. Galloway, Z. Klimont, and W. Winiwarter, 2008: How a century of ammonia synthesis changed the world. *Nature Geosci*., **1**, 636–639.

Eyring, V., et al., 2013: Long-term ozone changes and associated climate impacts in CMIP5 simulations. *J. Geophys*. *Res*., doi:10.1002/jgrd.50316.

Fiore, A. M., et al., 2012: Global air quality and climate. *Chem. Soc. Rev*., **41**, 6663–6683.

Fleming, E., C. Jackman, R. Stolarski and A. Douglass, 2011: A model study of the impact of source gas changes on the stratosphere for 1850-2100. *Atmos. Chem. Phys*., **11**, 8515–8541.

Forster, P. M., T. Andrews, P. Good, J. M. Gregory, L. S. Jackson, and M. Zelinka, 2013: Evaluating adjusted forcing and model spread for historical and future scenarios in the CMIP5 generation of climate models. *J. Geophys*. *Res.*, **118**, 1139–1150.

Friedlingstein, P., et al., 2006: Climate-carbon cycle feedback analysis: Results from the C4MIP model intercomparison. *J. Clim.*, **19**, 3337–3353.

Holmes, C. D., M. J. Prather, A.O. Søvde, and G. Myhre, 2013: Future methane, hydroxyl, and their uncertainties: Key climate and emission parameters for future predictions. *Atmos. Chem. Phys*., **13**, 285–302.

HTAP, 2010. *Hemispheric Transport of Air Pollution 2010, Part A: Ozone and Particulate Matter*. United Nations, Geneva, Switzerland.

Jones, C. D., et al., 2013: 21st Century compatible CO2 emissions and airborne fraction simulated by CMIP5 Earth System models under 4 Representative Concentration Pathways. *J. Clim*., doi:10.1175/JCLI-D-12-00554.1.

Lamarque, J. F., G. P. Kyle, M. Meinshausen, K. Riahi, S. J. Smith, D. P. Van Vuuren, A. J. Conley, and F. Vitt, 2011: Global and regional evolution of short-lived radiatively-active gases and aerosols in the Representative Concentration Pathways. *Clim. Change*, **109**, 191–212.

Lamarque, J. F., et al., 2010: Historical (1850-2000) gridded anthropogenic and biomass burning emissions of reactive gases and aerosols: methodology and application. *Atmos. Chem. Phys*., **10**, 7017–7039.

Lamarque, J. F., et al., 2013: The Atmospheric Chemistry and Climate Model Intercomparison Project (ACCMIP): Overview and description of models, simulations and climate diagnostics. *Geosci. Model Dev*., **6**, 179–206.

Meinshausen, M., T. M. L. Wigley, and S. C. B. Raper, 2011b: Emulating atmosphere-ocean and carbon cycle models with a simpler model, MAGICC6-Part 2: Applications. *Atmos. Chem. Phys*., **11**, 1457–1471.

Meinshausen, M., et al., 2011a: The RCP greenhouse gas concentrations and their extensions from 1765 to 2300. *Clim*. *Change*, **109**, 213–241.

Moss, R. H., et al., 2010: The next generation of scenarios for climate change research and assessment. *Nature*, **463**, 747–756.

Prather, M., et al., 2001: Atmospheric chemistry and greenhouse gases. In: *Climate Change 2001: The Scientific Basis. Contribution of Working Group I to the Third Assessment Report of the Intergovernmental Panel on Climate Change* [J. T. Houghton, Y. Ding, D. J. Griggs, M. Noquer, P. J. van der Linden, X. Dai, K. Maskell and C. A. Johnson (eds.)]. Cambridge University Press, Cambridge, United Kingdom and New York, NY, USA, pp. 239–287.

Prather, M., et al., 2003: Fresh air in the 21st century? *Geophys. Res. Lett*., **30**, 1100.

Prather, M. J., C. D. Holmes, and J. Hsu, 2012: Reactive greenhouse gas scenarios: Systematic exploration of uncertainties and the role of atmospheric chemistry. *Geophys. Res. Lett*., **39**, L09803.

Rogelj, J., et al., 2011: Emission pathways consistent with a 2°C global temperature limit. *Nature Clim. Change*, **1**, 413–418.

Shindell, D.T., J.-F. Lamarque, M. Schulz, M. Flanner, et al., 2013: Radiative forcing in the ACCMIP historical and future climate simulations. *Atmos. Chem. Phys*., **13**, 2939–2974.

Stevenson, D. S., et al., 2013: Tropospheric ozone changes, radiative forcing and attribution to emissions in the Atmospheric Chemistry and Climate Model Intercomparison Project (ACCMIP). *Atmos. Chem. Phys*., **13**, 3063–3085.

van Vuuren, D. P., et al., 2008: Temperature increase of 21st century mitigation scenarios. *Proc. Natl. Acad. Sci. U.S.A.*, **105**, 15258–15262.

van Vuuren, D., et al., 2011: The representative concentration pathways: An overview. *Clim. Change*, **109**, 5–31.

Voulgarakis, A., et al., 2013: Analysis of present day and future OH and methane lifetime in the ACCMIP simulations. 21 *Atmos. Chem. Phys*., **13**, 2563–2587.

Wild, O., A.M. Fiore et al., 2012: Modelling future changes in surface ozone: A parameterized approach. *Atmos. Chem. Phys.*, **12**, 2037–2054.

WMO. 2010. *Scientific Assessment of Ozone Depletion: 2010*. Global Ozone Research and Monitoring Project—Report No. 52. World Meteorological Organization, Geneva, Switzerland.

Young, P. J., et al., 2013: Pre-industrial to end 21st century projections of tropospheric ozone from the Atmospheric Chemistry and Climate Model Intercomparison Project (ACCMIP). Atmos. Chem. Phys., **13**, 2063–2090.

Tables

AII.1: Historical Climate System Data

Table AII.1.1a | Historical abundances of the Kyoto greenhouse gases

Year	CO_2 (ppm)	CH_4 (ppb)	N_2O (ppb)
PI*	278 ± 2	722 ± 25	270 ± 7
1755	276.7	723	272.8
1760	276.5	726	274.1
1765	276.6	730	274.2
1770	277.3	733	273.7
1775	278.0	736	273.1
1780	278.2	739	272.4
1785	278.6	742	271.9
1790	280.0	745	271.8
1795	281.4	748	272.1
1800	282.6	751	272.6
1805	283.6	755	272.1
1810	284.2	760	271.4
1815	284.0	765	271.5
1820	283.3	769	272.9
1825	283.1	774	274.1
1830	283.8	779	273.7
1835	283.9	784	270.5
1840	284.1	789	269.6
1845	285.8	795	270.3
1850	286.8	802	270.4
1855	286.4	808	270.6
1860	286.1	815	271.7
1865	286.3	823	272.3
1870	288.0	831	273.0
1875	289.4	839	274.7
1880	289.8	847	275.8
1885	290.9	856	277.2
1890	293.1	866	278.3
1895	295.4	877	277.7
1900	296.2	891	277.3
1905	297.4	912	279.2
1910	299.3	935	280.8
1915	301.1	961	282.7
1920	303.3	990	285.1
1925	304.7	1020	284.3
1930	306.6	1049	284.9
1935	308.4	1077	286.6
1940	310.4	1102	287.7
1945	310.9	1129	288.0
1950	311.2	1162	287.6
1955	313.4	1207	289.6
1956	314.0	1217	290.4
1957	314.6	1228	291.2
1958	315.3	1239	291.7
1959	316.0	1251	292.1
1960	316.7	1263	292.4
1961	317.4	1275	292.5
1962	318.0	1288	292.5
1963	318.5	1301	292.6
1964	319.0	319.0	292.6
1965	319.7	1328	292.7
1966	320.6	1343	292.9
1967	321.5	1357	293.3
1968	322.5	1372	293.8
1969	323.5	1388	294.4
1970	324.6	1403	295.2
1971	325.6	1419	296.0
1972	326.8	1435	296.9
1973	328.0	1451	297.8
1974	329.2	1467	298.4
1975	330.2	1483	299.0
1976	331.3	1500	299.4
1977	332.7	1516	299.8
1978	334.3	1532	300.2
1979	336.2	1549	300.7
1980	338.0	1567	301.3
1981	339.3	1587	302.0
1982	340.5	1607	303.0
1983	342.1	1626	303.9
1984	343.7	1643	304.5
1985	345.2	1657	305.5
1986	346.6	1670	305.9
1987	348.4	1682	306.3
1988	350.5	1694	306.7
1989	352.2	1704	307.8
1990	353.6	1714	308.7
1991	354.8	1725	309.3
1992	355.7	1733	309.8
1993	356.6	1738	310.1
1994	358.0	1743	310.4
1995	359.9	1747	311.0
1996	361.4	1751	311.8
1997	363.1	1757	312.7
1998	365.2	1765	313.7
1999	367.2	1771	314.7
2000	368.7	1773	315.6
2001	370.2	1773	316.3
2002	372.3	1774	317.0

(continued on next page)

Table AII.1.1a *(continued)*

Year	CO_2 (ppm)	CH_4 (ppb)	N_2O (ppb)
PI*	278 ± 2	722 ± 25	270 ± 7
2003	374.5	1776	317.6
2004	376.6	1776	318.3
2005	378.7	1776	319.1
2006	380.8	1776	319.8
2007	382.7	1781	320.6
2008	384.6	1787	321.4
2005	378.7	1776	319.1
2006	380.8	1776	319.8
2007	382.7	1781	320.6
2008	384.6	1787	321.4
2009	386.4	1792	322.3
2010	388.4	1798	323.2
2011*	390.5 ± 0.3	1803 ± 4	324 ± 1

Year	SF_6 (ppt)	CF_4 (ppt)	C_2F_6 (ppt)	C_6F_{14} (ppt)	NF_3 (ppt)
PI*	0	35	0	0	
1900	0	35	0	0	
1910	0	35	0.1	0	
1920	0	35	0.1	0	
1930	0	36	0.2	0	
1940	0	37	0.3	0	
1950	0	39	0.5	0	
1960	0.1	43	0.6	0	
1970	0.3	51	0.8	0	
1980	0.8	60	1.2	0	
1990	2.4	68	1.9	0	
2000	4.5	76	2.9	0	
2005	5.6	75	3.7	0	0.3
2010	7.0	78.3	4.1	0	
2011*	7.3 ± 0.1	79.0	4.2	0	0.6

Year	HFC-23 (ppt)	HFC-32 (ppt)	HFC-125 (ppt)	HFC-134a (ppt)	HFC-143a (ppt)	HFC-227ea (ppt)	HFC-245fa (ppt)	HFC-43-10mee (ppt)
PI*	0	0	0	0	0	0	0	0
1940	0.1	0	0	0	0	0	0	0
1950	0.3	0	0	0	0	0	0	0
1960	0.7	0	0	0	0	0	0	0
1970	1.6	0	0	0	0	0	0	0
1980	3.7	0	0	0	0.2	0	0	0
1990	7.9	0	0.1	0	0.6	0	0	0
2000	14.8	0	1.3	14	3.1	0.1	0	0
2010	23.2	4.1	8.2	58	10.9	0.6	1.1	0
2011*	24.0	4.9	9.6	63 ± 1	12.0	0.65	1.24	0

Notes:

Abundances are mole fraction of dry air for the lower, well-mixed atmosphere (ppm = micromoles per mole, ppb = nanomoles per mole, ppt = picomoles per mole). Values refer to single-year average. Uncertainties (5 to 95% confidence intervals) are given for 2011 only when more than one laboratory reports global data. Pre-industrial (PI*, taken to be 1750 for GHG) and present day (2011*) abundances are from Chapter 2, Tables 2.1 and 2.SM.1; see also Chapter 6 for Holocene variability (10 ppm CO_2, 40 ppb CH_4, 10 ppb N_2O). Intermediate data for CO_2, CH_4 and N_2O are from Chapters 2 and 8, Figure 8.6. See also Appendix 1.A. Intermediate data for the F-gases are taken from Meinshausen et al. (2011).

Table AII.1.1b | Historical abundances of the Montreal Protocol greenhouse gases (all ppt)

Year	CFC-11	CFC-12	CFC-113	CFC-114	CFC-115	CCl_4	CH_3CCl_3	HCFC-22
PI*	0	0	0	0	0	0	0	0
1960	9.5	29.5	1.9	3.8	0.0	52.1	1.5	2.1
1965	23.5	58.8	3.1	5.0	0.0	64.4	4.7	4.9
1970	52.8	114.3	5.5	6.5	0.2	75.9	16.2	12.1
1975	106.1	203.1	10.4	8.3	0.6	85.5	40.0	23.8
1980	161.9	297.4	19.0	10.7	1.3	93.3	81.6	42.5
1985	205.4	381.2	37.3	12.9	2.8	99.6	106.1	62.7
1990	256.2	477.5	67.6	15.4	4.7	106.5	127.2	88.2
1995	267.4	523.8	83.6	16.1	6.8	103.2	110.3	113.6
2000	261.7	541.0	82.3	16.5	7.9	98.6	49.7	139.5
2005	251.6	542.7	78.8	16.6	8.3	93.7	20.1	165.5
2010	240.9	532.5	75.6	16.4	8.4	87.6	8.3	206.8
2011*	238 ± 1	528±2	74.3±0.5	15.8	8.4	86±2	6.4±0.4	213±2

Year	HCFC-141b	HCFC-142b	Halon 1211	Halon 1202	Halon 1301	Halon 2402	CH_3Br	CH_3Cl
PI*	0	0	0	0	0	0		
1960	0.0	0.0	0.00	0.00	0.00	0.00	6.5	510
1965	0.0	0.0	0.00	0.00	0.00	0.00	6.7	528
1970	0.0	0.0	0.02	0.00	0.00	0.02	0.0	540
1975	0.0	0.2	0.12	0.01	0.04	0.06	7.4	546
1980	0.0	0.4	0.42	0.01	0.24	0.15	7.7	548
1985	0.0	0.7	1.04	0.02	0.74	0.26	8.2	549
1990	0.0	1.2	2.27	0.03	1.66	0.41	8.6	550
1995	2.7	6.3	3.34	0.04	2.63	0.52	9.2	550
2000	11.8	11.4	4.02	0.04	2.84	0.50	8.9	550
2005	17.5	15.1	4.26	0.02	3.03	0.48	7.9	550
2010	20.3	20.5	4.07	0.00	3.20	0.46	7.2	550
2011*	21.4±0.5	21.2±0.5	4.07	0.00	3.23	0.45	7.1	534

Notes:
See Table AII.1.1a. For present-day (2011*) see Chapter 2. Intermediate years are from Scenario A1, WMO Ozone Assessment (WMO, 2010).

Table AII.1.2 | Historical effective radiative forcing (ERF) (W m^{-2}), including land use change (LUC)

Year	CO_2	GHG Other*	O_3 (Trop)	O_3 (Strat)	Aerosol (Total)	LUC	H_2O (Strat)	BC Snow	Con–trails	Solar	Volcano
1750	0.000	0.000	0.000	0.000	0.000	0.000	0.000	0.000	0.000	0.000	–0.001
1751	–0.023	0.004	0.000	0.000	–0.002	0.000	0.000	0.000	0.000	–0.014	0.000
1752	–0.024	0.006	0.001	0.000	–0.004	–0.001	0.000	0.000	0.000	–0.029	0.000
1753	–0.024	0.007	0.001	0.000	–0.005	–0.001	0.000	0.000	0.000	–0.033	0.000
1754	–0.025	0.008	0.002	0.000	–0.007	–0.002	0.000	0.001	0.000	–0.043	0.000
1755	–0.026	0.010	0.002	0.000	–0.009	–0.002	0.000	0.001	0.000	–0.054	–0.664
1756	–0.026	0.011	0.003	0.000	–0.011	–0.002	0.000	0.001	0.000	–0.055	0.000
1757	–0.027	0.013	0.003	0.000	–0.013	–0.003	0.000	0.001	0.000	–0.048	0.000
1758	–0.028	0.014	0.003	0.000	–0.014	–0.003	0.000	0.001	0.000	–0.050	0.000
1759	–0.028	0.015	0.004	0.000	–0.016	–0.004	0.000	0.001	0.000	–0.102	0.000
1760	–0.029	0.016	0.004	0.000	–0.018	–0.004	0.000	0.001	0.000	–0.112	–0.060
1761	–0.029	0.017	0.005	0.000	–0.020	–0.004	0.000	0.002	0.000	–0.016	–1.093
1762	–0.029	0.017	0.005	0.000	–0.021	–0.005	0.001	0.002	0.000	–0.007	–0.300
1763	–0.029	0.018	0.006	0.000	–0.023	–0.005	0.001	0.002	0.000	–0.018	–0.093
1764	–0.028	0.018	0.006	0.000	–0.025	–0.006	0.001	0.002	0.000	–0.022	–0.021
1765	–0.026	0.018	0.006	0.000	–0.027	–0.006	0.001	0.002	0.000	–0.054	–0.003
1766	–0.024	0.018	0.007	0.000	–0.029	–0.006	0.001	0.002	0.000	–0.048	0.000
1767	–0.022	0.018	0.007	0.000	–0.030	–0.007	0.001	0.003	0.000	–0.036	0.000
1768	–0.020	0.018	0.008	0.000	–0.032	–0.007	0.001	0.003	0.000	0.016	0.000
1769	–0.017	0.018	0.008	0.000	–0.034	–0.008	0.001	0.003	0.000	0.050	0.000
1770	–0.014	0.018	0.009	0.000	–0.036	–0.008	0.001	0.003	0.000	0.081	0.000
1771	–0.011	0.018	0.009	0.000	–0.038	–0.008	0.001	0.003	0.000	0.055	0.000
1772	–0.008	0.018	0.009	0.000	–0.039	–0.009	0.001	0.003	0.000	0.052	–0.070
1773	–0.005	0.018	0.010	0.000	–0.041	–0.009	0.001	0.003	0.000	0.016	–0.020
1774	–0.003	0.018	0.010	0.000	–0.043	–0.010	0.001	0.004	0.000	–0.002	–0.005
1775	–0.001	0.018	0.011	0.000	–0.045	–0.010	0.001	0.004	0.000	–0.038	–0.001
1776	0.001	0.018	0.011	0.000	–0.046	–0.010	0.001	0.004	0.000	–0.045	0.000
1777	0.002	0.018	0.011	0.000	–0.048	–0.011	0.001	0.004	0.000	–0.036	0.000
1778	0.003	0.018	0.012	0.000	–0.050	–0.011	0.001	0.004	0.000	0.017	–0.067
1779	0.003	0.018	0.012	0.000	–0.052	–0.012	0.001	0.004	0.000	–0.034	–0.071
1780	0.003	0.018	0.013	0.000	–0.054	–0.012	0.002	0.004	0.000	–0.069	–0.018
1781	0.004	0.018	0.013	0.000	–0.055	–0.012	0.002	0.005	0.000	–0.057	–0.004
1782	0.004	0.018	0.014	0.000	–0.057	–0.013	0.002	0.005	0.000	–0.028	–0.001
1783	0.006	0.018	0.014	0.000	–0.059	–0.013	0.002	0.005	0.000	–0.065	–7.857
1784	0.009	0.018	0.014	0.000	–0.061	–0.014	0.002	0.005	0.000	–0.059	–0.522
1785	0.012	0.018	0.015	0.000	–0.062	–0.014	0.002	0.005	0.000	–0.046	–0.121
1786	0.017	0.018	0.015	0.000	–0.064	–0.014	0.002	0.005	0.000	–0.022	–0.027
1787	0.021	0.018	0.016	0.000	–0.066	–0.015	0.002	0.005	0.000	–0.001	–0.002
1788	0.027	0.018	0.016	0.000	–0.068	–0.015	0.002	0.006	0.000	0.034	–0.133
1789	0.033	0.019	0.017	0.000	–0.070	–0.016	0.002	0.006	0.000	–0.033	–0.041
1790	0.038	0.019	0.017	0.000	–0.071	–0.016	0.002	0.006	0.000	–0.058	–0.009
1791	0.044	0.019	0.017	0.000	–0.073	–0.016	0.002	0.006	0.000	–0.056	–0.001
1792	0.050	0.020	0.018	0.000	–0.075	–0.017	0.002	0.006	0.000	–0.051	0.000
1793	0.055	0.020	0.018	0.000	–0.077	–0.017	0.002	0.006	0.000	–0.065	0.000
1794	0.060	0.021	0.019	0.000	–0.079	–0.018	0.002	0.006	0.000	–0.064	–0.157
1795	0.066	0.022	0.019	0.000	–0.080	–0.018	0.002	0.007	0.000	–0.027	0.000
1796	0.070	0.023	0.020	0.000	–0.082	–0.018	0.002	0.007	0.000	–0.033	–0.781
1797	0.075	0.023	0.020	0.000	–0.084	–0.019	0.002	0.007	0.000	–0.043	–0.071
1798	0.079	0.024	0.020	0.000	–0.086	–0.019	0.002	0.007	0.000	–0.045	–0.016

Table AII.1.2 | *(continued)*

Year	CO_2	GHG Other*	O_3 (Trop)	O_3 (Strat)	Aerosol (Total)	LUC	H_2O (Strat)	BC Snow	Con–trails	Solar	Volcano
1799	0.084	0.025	0.021	0.000	–0.087	–0.020	0.003	0.007	0.000	–0.047	–0.002
1800	0.088	0.025	0.021	0.000	–0.089	–0.020	0.003	0.007	0.000	–0.055	0.000
1801	0.092	0.026	0.022	0.000	–0.091	–0.020	0.003	0.007	0.000	–0.021	–0.154
1802	0.096	0.026	0.022	0.000	–0.093	–0.021	0.003	0.008	0.000	–0.010	–0.048
1803	0.099	0.026	0.023	0.000	–0.095	–0.021	0.003	0.008	0.000	–0.033	–0.011
1804	0.103	0.026	0.023	0.000	–0.096	–0.022	0.003	0.008	0.000	–0.040	–0.230
1805	0.106	0.026	0.023	0.000	–0.098	–0.022	0.003	0.008	0.000	–0.046	–0.070
1806	0.109	0.026	0.024	0.000	–0.100	–0.022	0.003	0.008	0.000	–0.036	–0.016
1807	0.112	0.026	0.024	0.000	–0.102	–0.023	0.003	0.008	0.000	–0.057	–0.002
1808	0.114	0.026	0.025	0.000	–0.104	–0.023	0.003	0.008	0.000	–0.065	0.000
1809	0.116	0.026	0.025	0.000	–0.105	–0.024	0.003	0.009	0.000	–0.065	–6.947
1810	0.117	0.026	0.025	0.000	–0.107	–0.024	0.003	0.009	0.000	–0.070	–2.254
1811	0.118	0.027	0.026	0.000	–0.109	–0.024	0.003	0.009	0.000	–0.072	–0.836
1812	0.119	0.027	0.026	0.000	–0.111	–0.025	0.003	0.009	0.000	–0.072	–0.308
1813	0.118	0.028	0.027	0.000	–0.112	–0.025	0.004	0.009	0.000	–0.069	–0.109
1814	0.117	0.029	0.027	0.000	–0.114	–0.026	0.004	0.009	0.000	–0.064	0.000
1815	0.115	0.030	0.028	0.000	–0.116	–0.026	0.004	0.009	0.000	–0.062	–11.629
1816	0.113	0.031	0.028	0.000	–0.118	–0.026	0.004	0.010	0.000	–0.052	–4.553
1817	0.110	0.032	0.028	0.000	–0.120	–0.027	0.004	0.010	0.000	–0.048	–2.419
1818	0.107	0.034	0.029	0.000	–0.121	–0.027	0.004	0.010	0.000	–0.053	–0.915
1819	0.104	0.035	0.029	0.000	–0.123	–0.028	0.004	0.010	0.000	–0.054	–0.337
1820	0.101	0.037	0.030	0.000	–0.125	–0.028	0.004	0.010	0.000	–0.059	–0.039
1821	0.099	0.038	0.030	0.000	–0.127	–0.028	0.004	0.010	0.000	–0.065	0.000
1822	0.097	0.040	0.031	0.000	–0.128	–0.029	0.004	0.010	0.000	–0.066	0.000
1823	0.096	0.041	0.031	0.000	–0.130	–0.029	0.004	0.011	0.000	–0.068	0.000
1824	0.097	0.042	0.031	0.000	–0.132	–0.030	0.004	0.011	0.000	–0.059	0.000
1825	0.098	0.043	0.032	0.000	–0.134	–0.030	0.005	0.011	0.000	–0.052	0.000
1826	0.100	0.044	0.032	0.000	–0.136	–0.030	0.005	0.011	0.000	–0.044	0.000
1827	0.103	0.045	0.033	0.000	–0.137	–0.031	0.005	0.011	0.000	–0.018	0.000
1828	0.106	0.045	0.033	0.000	–0.139	–0.031	0.005	0.011	0.000	–0.008	0.000
1829	0.109	0.045	0.034	0.000	–0.141	–0.032	0.005	0.011	0.000	–0.006	0.000
1830	0.111	0.045	0.034	0.000	–0.143	–0.032	0.005	0.012	0.000	0.002	0.000
1831	0.113	0.044	0.034	0.000	–0.145	–0.032	0.005	0.012	0.000	0.002	–1.538
1832	0.114	0.043	0.035	0.000	–0.146	–0.033	0.005	0.012	0.000	–0.020	–1.229
1833	0.114	0.041	0.035	0.000	–0.148	–0.033	0.005	0.012	0.000	–0.035	–0.605
1834	0.114	0.039	0.036	0.000	–0.150	–0.034	0.005	0.012	0.000	–0.038	–0.223
1835	0.113	0.037	0.036	0.000	–0.152	–0.034	0.005	0.012	0.000	–0.033	–4.935
1836	0.112	0.036	0.037	0.000	–0.153	–0.034	0.005	0.012	0.000	0.017	–1.445
1837	0.112	0.035	0.037	0.000	–0.155	–0.035	0.006	0.013	0.000	0.055	–0.523
1838	0.112	0.035	0.037	0.000	–0.157	–0.035	0.006	0.013	0.000	0.051	–0.192
1839	0.114	0.036	0.038	0.000	–0.159	–0.036	0.006	0.013	0.000	0.028	–0.069
1840	0.117	0.037	0.038	0.000	–0.161	–0.036	0.006	0.013	0.000	0.027	–0.047
1841	0.121	0.038	0.039	0.000	–0.162	–0.036	0.006	0.013	0.000	0.007	–0.013
1842	0.127	0.040	0.039	0.000	–0.164	–0.037	0.006	0.013	0.000	–0.006	–0.003
1843	0.135	0.041	0.039	0.000	–0.166	–0.037	0.006	0.013	0.000	–0.013	–0.052
1844	0.142	0.042	0.040	0.000	–0.168	–0.038	0.006	0.014	0.000	–0.024	–0.014
1845	0.149	0.043	0.040	0.000	–0.169	–0.038	0.006	0.014	0.000	–0.026	–0.003
1846	0.155	0.044	0.041	0.000	–0.171	–0.038	0.006	0.014	0.000	–0.024	–0.071
1847	0.160	0.044	0.041	0.000	–0.173	–0.039	0.007	0.014	0.000	–0.062	–0.020
1848	0.163	0.045	0.042	0.000	–0.175	–0.039	0.007	0.014	0.000	–0.018	–0.005

Table AII.1.2 | *(continued)*

Year	CO_2	GHG Other*	O_3 (Trop)	O_3 (Strat)	Aerosol (Total)	LUC	H_2O (Strat)	BC Snow	Con–trails	Solar	Volcano
1849	0.166	0.046	0.042	0.000	–0.177	–0.040	0.007	0.014	0.000	0.043	–0.001
1850	0.167	0.046	0.042	0.000	–0.178	–0.040	0.007	0.014	0.000	0.024	–0.100
1851	0.167	0.047	0.043	0.000	–0.180	–0.040	0.007	0.015	0.000	0.016	–0.075
1852	0.166	0.048	0.044	0.000	–0.182	–0.041	0.007	0.015	0.000	0.020	–0.025
1853	0.164	0.049	0.045	0.000	–0.184	–0.041	0.007	0.015	0.000	0.011	–0.025
1854	0.162	0.050	0.046	0.000	–0.185	–0.041	0.007	0.016	0.000	–0.010	0.000
1855	0.160	0.051	0.047	0.000	–0.187	–0.042	0.007	0.016	0.000	–0.027	–0.050
1856	0.158	0.052	0.048	0.000	–0.189	–0.042	0.007	0.016	0.000	–0.037	–0.975
1857	0.156	0.054	0.049	0.000	–0.191	–0.042	0.008	0.016	0.000	–0.037	–1.500
1858	0.155	0.055	0.050	0.000	–0.192	–0.043	0.008	0.017	0.000	–0.020	–0.725
1859	0.154	0.057	0.050	0.000	–0.194	–0.043	0.008	0.017	0.000	–0.007	–0.275
1860	0.154	0.058	0.051	0.000	–0.196	–0.043	0.008	0.017	0.000	0.029	–0.125
1861	0.153	0.060	0.052	0.000	–0.198	–0.044	0.008	0.018	0.000	0.036	–0.075
1862	0.153	0.061	0.053	0.000	–0.199	–0.044	0.008	0.018	0.000	0.013	–0.350
1863	0.154	0.062	0.054	0.000	–0.201	–0.044	0.008	0.018	0.000	0.006	–0.250
1864	0.156	0.063	0.055	0.000	–0.203	–0.045	0.008	0.018	0.000	–0.017	–0.125
1865	0.158	0.064	0.056	0.000	–0.205	–0.045	0.009	0.019	0.000	–0.018	–0.050
1866	0.162	0.066	0.057	0.000	–0.206	–0.045	0.009	0.019	0.000	–0.021	–0.025
1867	0.167	0.067	0.058	0.000	–0.208	–0.046	0.009	0.019	0.000	–0.037	0.000
1868	0.173	0.068	0.059	0.000	–0.210	–0.046	0.009	0.020	0.000	–0.039	0.000
1869	0.180	0.070	0.059	0.000	–0.212	–0.046	0.009	0.020	0.000	–0.005	–0.025
1870	0.188	0.071	0.060	0.000	–0.213	–0.047	0.009	0.020	0.000	–0.028	–0.025
1871	0.195	0.073	0.061	0.000	–0.215	–0.047	0.009	0.020	0.000	0.025	–0.025
1872	0.202	0.075	0.062	0.000	–0.217	–0.047	0.009	0.021	0.000	0.012	–0.025
1873	0.208	0.077	0.063	0.000	–0.219	–0.048	0.010	0.021	0.000	0.015	–0.075
1874	0.212	0.079	0.064	0.000	–0.220	–0.048	0.010	0.021	0.000	0.000	–0.050
1875	0.215	0.081	0.065	0.000	–0.222	–0.049	0.010	0.022	0.000	–0.015	–0.025
1876	0.218	0.083	0.066	0.000	–0.224	–0.049	0.010	0.022	0.000	–0.029	–0.150
1877	0.219	0.084	0.067	0.000	–0.226	–0.049	0.010	0.022	0.000	–0.033	–0.125
1878	0.219	0.086	0.067	0.000	–0.227	–0.050	0.010	0.022	0.000	–0.041	–0.075
1879	0.221	0.088	0.068	0.000	–0.229	–0.050	0.010	0.023	0.000	–0.044	–0.050
1880	0.222	0.089	0.069	0.000	–0.231	–0.050	0.011	0.023	0.000	–0.039	–0.025
1881	0.224	0.091	0.070	0.000	–0.233	–0.051	0.011	0.023	0.000	–0.007	–0.025
1882	0.228	0.092	0.071	0.000	–0.234	–0.051	0.011	0.024	0.000	–0.019	–0.025
1883	0.232	0.094	0.072	0.000	–0.236	–0.052	0.011	0.024	0.000	–0.031	–1.175
1884	0.238	0.096	0.073	0.000	–0.238	–0.052	0.011	0.024	0.000	0.018	–3.575
1885	0.244	0.098	0.074	0.000	–0.240	–0.053	0.011	0.024	0.000	0.002	–1.575
1886	0.250	0.100	0.075	0.000	–0.241	–0.053	0.011	0.025	0.000	–0.014	–0.900
1887	0.258	0.102	0.075	0.000	–0.243	–0.053	0.012	0.025	0.000	–0.033	–0.925
1888	0.266	0.104	0.076	0.000	–0.245	–0.054	0.012	0.025	0.000	–0.037	–0.550
1889	0.274	0.106	0.077	0.000	–0.247	–0.054	0.012	0.026	0.000	–0.041	–0.725
1890	0.283	0.107	0.078	0.000	–0.248	–0.055	0.012	0.026	0.000	–0.041	–0.975
1891	0.293	0.108	0.079	0.000	–0.250	–0.055	0.012	0.026	0.000	–0.020	–0.750
1892	0.302	0.109	0.080	0.000	–0.252	–0.056	0.012	0.026	0.000	0.004	–0.550
1893	0.311	0.110	0.081	0.000	–0.254	–0.056	0.013	0.027	0.000	0.035	–0.225
1894	0.319	0.111	0.082	0.000	–0.255	–0.057	0.013	0.027	0.000	0.072	–0.100
1895	0.325	0.111	0.083	0.000	–0.257	–0.057	0.013	0.027	0.000	0.052	–0.025
1896	0.330	0.112	0.083	0.000	–0.259	–0.058	0.013	0.028	0.000	0.023	–0.450
1897	0.334	0.113	0.084	0.000	–0.261	–0.058	0.013	0.028	0.000	–0.003	–0.425
1898	0.336	0.114	0.085	0.000	–0.262	–0.059	0.014	0.028	0.000	–0.012	–0.300

Table AII.1.2 | *(continued)*

Year	CO_2	GHG Other*	O_3 (Trop)	O_3 (Strat)	Aerosol (Total)	LUC	H_2O (Strat)	BC Snow	Con–trails	Solar	Volcano
1899	0.337	0.115	0.086	0.000	–0.264	–0.059	0.014	0.028	0.000	–0.017	–0.125
1900	0.339	0.117	0.087	0.000	–0.266	–0.060	0.014	0.029	0.000	–0.028	–0.050
1901	0.341	0.120	0.088	0.000	–0.268	–0.061	0.014	0.029	0.000	–0.043	–0.025
1902	0.344	0.123	0.089	0.000	–0.270	–0.061	0.015	0.030	0.000	–0.048	–0.500
1903	0.349	0.127	0.090	0.000	–0.272	–0.062	0.015	0.030	0.000	–0.036	–1.800
1904	0.355	0.130	0.091	0.000	–0.274	–0.062	0.015	0.031	0.000	0.011	–0.800
1905	0.362	0.134	0.092	0.000	–0.276	–0.063	0.016	0.032	0.000	–0.016	–0.325
1906	0.369	0.138	0.092	0.000	–0.278	–0.063	0.016	0.032	0.000	0.028	–0.175
1907	0.376	0.141	0.093	0.000	–0.280	–0.064	0.016	0.033	0.000	–0.001	–0.225
1908	0.383	0.145	0.094	0.000	–0.282	–0.064	0.017	0.033	0.000	0.020	–0.250
1909	0.389	0.148	0.095	–0.001	–0.284	–0.065	0.017	0.034	0.000	–0.002	–0.100
1910	0.395	0.151	0.096	–0.001	–0.286	–0.065	0.017	0.035	0.000	–0.006	–0.075
1911	0.400	0.155	0.097	–0.001	–0.288	–0.066	0.018	0.035	0.000	–0.032	–0.050
1912	0.406	0.159	0.098	–0.001	–0.289	–0.066	0.018	0.035	0.000	–0.045	–0.475
1913	0.412	0.163	0.100	–0.001	–0.290	–0.067	0.019	0.035	0.000	–0.042	–0.600
1914	0.419	0.167	0.101	–0.001	–0.291	–0.068	0.019	0.035	0.000	–0.033	–0.250
1915	0.427	0.171	0.102	–0.001	–0.292	–0.068	0.019	0.035	0.000	0.013	–0.100
1916	0.436	0.175	0.103	–0.001	–0.293	–0.069	0.020	0.035	0.000	0.068	–0.075
1917	0.445	0.180	0.104	–0.001	–0.294	–0.069	0.020	0.035	0.000	0.086	–0.050
1918	0.453	0.185	0.105	–0.001	–0.296	–0.070	0.021	0.035	0.000	0.121	–0.050
1919	0.460	0.189	0.107	–0.002	–0.297	–0.071	0.021	0.035	0.000	0.073	–0.050
1920	0.466	0.193	0.108	–0.001	–0.298	–0.071	0.022	0.035	0.000	0.039	–0.225
1921	0.472	0.196	0.109	–0.001	–0.302	–0.072	0.022	0.036	0.000	0.012	–0.200
1922	0.476	0.199	0.110	–0.002	–0.305	–0.073	0.022	0.036	0.000	–0.013	–0.075
1923	0.481	0.201	0.111	–0.002	–0.309	–0.073	0.023	0.036	0.000	–0.025	–0.025
1924	0.486	0.203	0.113	–0.002	–0.313	–0.074	0.023	0.036	0.000	–0.029	–0.075
1925	0.491	0.205	0.114	–0.002	–0.317	–0.075	0.024	0.036	0.000	–0.015	–0.075
1926	0.497	0.207	0.115	–0.002	–0.321	–0.076	0.024	0.036	0.000	0.020	–0.050
1927	0.503	0.210	0.116	–0.002	–0.325	–0.076	0.025	0.036	0.000	0.063	–0.050
1928	0.510	0.214	0.117	–0.002	–0.328	–0.077	0.025	0.037	0.000	0.033	–0.125
1929	0.517	0.218	0.119	–0.002	–0.332	–0.078	0.025	0.037	0.000	0.028	–0.250
1930	0.523	0.222	0.120	–0.003	–0.336	–0.079	0.026	0.037	0.000	0.048	–0.150
1931	0.530	0.226	0.122	–0.003	–0.338	–0.080	0.026	0.037	0.000	0.009	–0.125
1932	0.536	0.230	0.124	–0.003	–0.340	–0.081	0.027	0.038	0.000	–0.016	–0.200
1933	0.542	0.234	0.126	–0.003	–0.341	–0.081	0.027	0.038	0.000	–0.029	–0.175
1934	0.548	0.237	0.128	–0.003	–0.343	–0.082	0.027	0.039	0.000	–0.027	–0.100
1935	0.555	0.241	0.130	–0.003	–0.345	–0.083	0.028	0.039	0.000	–0.008	–0.100
1936	0.563	0.244	0.133	–0.003	–0.347	–0.084	0.028	0.040	0.000	0.068	–0.075
1937	0.570	0.247	0.135	–0.003	–0.349	–0.085	0.029	0.040	0.000	0.089	–0.075
1938	0.577	0.251	0.137	–0.003	–0.350	–0.086	0.029	0.040	0.000	0.080	–0.125
1939	0.584	0.254	0.139	–0.004	–0.352	–0.087	0.029	0.041	0.000	0.094	–0.100
1940	0.590	0.257	0.141	–0.004	–0.354	–0.088	0.030	0.041	0.000	0.070	–0.075
1941	0.595	0.261	0.143	–0.004	–0.358	–0.089	0.030	0.042	0.000	0.057	–0.050
1942	0.598	0.264	0.146	–0.004	–0.362	–0.090	0.030	0.042	0.000	0.030	–0.100
1943	0.599	0.267	0.148	–0.004	–0.366	–0.092	0.031	0.043	0.000	–0.005	–0.100
1944	0.599	0.270	0.150	–0.004	–0.370	–0.093	0.031	0.043	0.001	–0.011	–0.050
1945	0.599	0.273	0.152	–0.004	–0.374	–0.094	0.032	0.043	0.001	0.019	–0.050
1946	0.599	0.276	0.154	–0.005	–0.378	–0.095	0.032	0.044	0.001	0.025	–0.050
1947	0.598	0.279	0.156	–0.005	–0.382	–0.096	0.032	0.044	0.002	0.093	–0.050
1948	0.598	0.283	0.158	–0.005	–0.386	–0.097	0.033	0.045	0.002	0.146	–0.050

Table AII.1.2 | *(continued)*

Year	CO_2	GHG Other*	O_3 (Trop)	O_3 (Strat)	Aerosol (Total)	LUC	H_2O (Strat)	BC Snow	Con–trails	Solar	Volcano
1949	0.601	0.287	0.161	–0.005	–0.390	–0.099	0.033	0.045	0.002	0.123	–0.075
1950	0.604	0.291	0.163	–0.005	–0.394	–0.100	0.034	0.046	0.002	0.110	–0.075
1951	0.608	0.296	0.168	–0.005	–0.409	–0.102	0.034	0.046	0.002	0.037	–0.050
1952	0.615	0.302	0.173	–0.006	–0.424	–0.103	0.035	0.047	0.002	0.045	–0.100
1953	0.623	0.308	0.178	–0.006	–0.439	–0.105	0.036	0.047	0.003	0.025	–0.075
1954	0.631	0.315	0.183	–0.006	–0.455	–0.106	0.036	0.048	0.003	0.003	–0.100
1955	0.641	0.323	0.188	–0.006	–0.470	–0.108	0.037	0.048	0.003	0.015	–0.050
1956	0.651	0.332	0.193	–0.007	–0.485	–0.109	0.038	0.049	0.003	0.064	–0.025
1957	0.662	0.341	0.198	–0.007	–0.500	–0.111	0.038	0.050	0.004	0.129	–0.025
1958	0.673	0.349	0.203	–0.007	–0.515	–0.112	0.039	0.050	0.004	0.194	0.000
1959	0.685	0.358	0.208	–0.008	–0.530	–0.114	0.040	0.051	0.004	0.159	0.000
1960	0.698	0.366	0.213	–0.008	–0.546	–0.116	0.041	0.051	0.004	0.151	–0.125
1961	0.709	0.374	0.218	–0.008	–0.563	–0.117	0.041	0.051	0.004	0.110	–0.275
1962	0.719	0.383	0.223	–0.009	–0.580	–0.119	0.042	0.051	0.004	0.051	–0.325
1963	0.727	0.392	0.228	–0.009	–0.598	–0.120	0.043	0.050	0.005	0.038	–1.150
1964	0.735	0.402	0.233	–0.010	–0.615	–0.122	0.044	0.050	0.005	0.019	–1.800
1965	0.748	0.412	0.239	–0.011	–0.632	–0.123	0.045	0.050	0.005	0.008	–1.075
1966	0.762	0.424	0.244	–0.011	–0.650	–0.125	0.046	0.050	0.006	0.012	–0.575
1967	0.778	0.437	0.249	–0.012	–0.667	–0.126	0.047	0.049	0.007	0.055	–0.375
1968	0.794	0.451	0.254	–0.013	–0.684	–0.127	0.048	0.049	0.008	0.086	–0.675
1969	0.811	0.466	0.259	–0.014	–0.701	–0.129	0.049	0.049	0.009	0.077	–0.850
1970	0.828	0.483	0.264	–0.014	–0.719	–0.130	0.050	0.049	0.009	0.092	–0.425
1971	0.846	0.500	0.270	–0.016	–0.722	–0.131	0.050	0.049	0.009	0.082	–0.150
1972	0.865	0.519	0.277	–0.017	–0.725	–0.132	0.051	0.049	0.009	0.076	–0.100
1973	0.885	0.538	0.284	–0.018	–0.728	–0.134	0.052	0.049	0.010	0.044	–0.200
1974	0.904	0.558	0.290	–0.019	–0.732	–0.135	0.053	0.050	0.010	0.023	–0.325
1975	0.920	0.578	0.297	–0.021	–0.735	–0.136	0.054	0.050	0.010	0.006	–0.750
1976	0.938	0.598	0.304	–0.022	–0.738	–0.137	0.055	0.050	0.010	–0.003	–0.350
1977	0.960	0.617	0.310	–0.024	–0.741	–0.138	0.056	0.050	0.011	0.040	–0.125
1978	0.987	0.636	0.317	–0.026	–0.745	–0.138	0.057	0.051	0.011	0.129	–0.200
1979	1.018	0.656	0.324	–0.027	–0.748	–0.139	0.058	0.051	0.012	0.167	–0.225
1980	1.046	0.675	0.330	–0.029	–0.751	–0.140	0.059	0.051	0.012	0.150	–0.125
1981	1.066	0.696	0.335	–0.031	–0.763	–0.141	0.061	0.051	0.012	0.147	–0.125
1982	1.085	0.717	0.339	–0.033	–0.775	–0.141	0.062	0.050	0.012	0.094	–1.325
1983	1.110	0.737	0.343	–0.035	–0.788	–0.142	0.063	0.050	0.012	0.091	–1.875
1984	1.136	0.757	0.348	–0.037	–0.800	–0.143	0.064	0.049	0.013	0.016	–0.750
1985	1.158	0.776	0.352	–0.038	–0.812	–0.143	0.065	0.049	0.014	0.011	–0.325
1986	1.180	0.795	0.356	–0.040	–0.824	–0.144	0.065	0.049	0.015	0.012	–0.350
1987	1.208	0.813	0.360	–0.042	–0.836	–0.144	0.066	0.048	0.016	0.015	–0.250
1988	1.240	0.832	0.365	–0.044	–0.848	–0.145	0.067	0.048	0.017	0.095	–0.200
1989	1.266	0.853	0.369	–0.046	–0.861	–0.145	0.067	0.047	0.018	0.151	–0.150
1990	1.287	0.872	0.373	–0.048	–0.873	–0.146	0.068	0.047	0.019	0.118	–0.150
1991	1.305	0.888	0.375	–0.050	–0.878	–0.146	0.068	0.046	0.019	0.126	–1.350
1992	1.318	0.900	0.376	–0.052	–0.883	–0.146	0.069	0.045	0.020	0.137	–3.025
1993	1.332	0.909	0.378	–0.054	–0.888	–0.147	0.069	0.045	0.022	0.063	–1.225
1994	1.354	0.916	0.379	–0.055	–0.893	–0.147	0.069	0.044	0.024	0.027	–0.500
1995	1.381	0.923	0.380	–0.056	–0.897	–0.147	0.070	0.043	0.025	0.020	–0.250
1996	1.404	0.930	0.382	–0.057	–0.902	–0.148	0.070	0.043	0.027	0.003	–0.175
1997	1.428	0.937	0.383	–0.057	–0.907	–0.148	0.070	0.042	0.028	0.016	–0.125
1998	1.459	0.944	0.385	–0.057	–0.912	–0.148	0.071	0.041	0.029	0.062	–0.075

Table AII.1.2 | *(continued)*

Year	CO_2	GHG Other*	O_3 (Trop)	O_3 (Strat)	Aerosol (Total)	LUC	H_2O (Strat)	BC Snow	Con–trails	Solar	Volcano
1999	1.489	0.952	0.386	–0.056	–0.917	–0.148	0.071	0.041	0.031	0.104	–0.050
2000	1.510	0.957	0.388	–0.056	–0.922	–0.149	0.071	0.040	0.033	0.127	–0.050
2001	1.532	0.961	0.389	–0.055	–0.920	–0.149	0.071	0.040	0.033	0.114	–0.050
2002	1.563	0.965	0.390	–0.055	–0.918	–0.149	0.071	0.040	0.033	0.108	–0.050
2003	1.594	0.969	0.391	–0.054	–0.916	–0.149	0.071	0.040	0.034	0.042	–0.075
2004	1.624	0.973	0.393	–0.053	–0.913	–0.149	0.071	0.040	0.038	0.012	–0.050
2005	1.654	0.976	0.394	–0.053	–0.911	–0.149	0.071	0.040	0.040	–0.011	–0.075
2006	1.684	0.981	0.395	–0.052	–0.909	–0.150	0.071	0.040	0.042	–0.016	–0.100
2007	1.711	0.986	0.396	–0.052	–0.907	–0.150	0.071	0.040	0.044	–0.017	–0.100
2008	1.736	0.992	0.398	–0.051	–0.904	–0.150	0.072	0.040	0.046	–0.025	–0.100
2009	1.762	0.999	0.399	–0.051	–0.902	–0.150	0.072	0.040	0.044	–0.027	–0.125
2010	1.789	1.005	0.400	–0.050	–0.900	–0.150	0.072	0.040	0.048	0.001	–0.100
2011	1.816	1.015	0.400	–0.050	–0.900	–0.150	0.073	0.040	0.050	0.030	–0.125

Notes:

See Figure 8.18, also Sections 8.1 and 11.3.6.1. To get the total ERF (effective radiative forcing) all components can be summed. Small negative values for CO_2 prior to 1800 are due to uncertainty in PI values. GHG other* includes only WMGHG. Aerosol is the sum of direct and indirect effects. LUC includes land use land cover change. Contrails combines aviation contrails (~20% of total) and contrail-induced cirrus. Values are annual average.

Table AII.1.3 | Historical global decadal mean global surface air temperature (°C) relative to 1961–1990 average

Year	HadCRUT4			GISS	NCDC
	Lower (5%)	Median (50%)	Upper (95%)	Median (50%)	Median (50%)
1850[d]	–0.404	–0.320	–0.243		
1860[d]	–0.413	–0.335	–0.263		
1870[d]	–0.326	–0.258	–0.195		
1880[d]	–0.363	–0.297	–0.237	–0.296	–0.291
1890[d]	–0.430	–0.359	–0.299	–0.361	–0.370
1900[d]	–0.473	–0.410	–0.353	–0.418	–0.434
1910[d]	–0.448	–0.387	–0.334	–0.435	–0.430
1920[d]	–0.297	–0.242	–0.193	–0.311	–0.311
1930[d]	–0.166	–0.116	–0.070	–0.172	–0.161
1940[d]	–0.047	–0.002	+0.042	–0.085	–0.063
1950[d]	–0.106	–0.061	–0.017	–0.134	–0.136
1960[d]	–0.093	–0.054	–0.014	–0.104	–0.086
1970[d]	–0.113	–0.077	–0.041	–0.058	–0.060
1980[d]	+0.052	+0.095	+0.135	+0.118	+0.109
1990[d]	+0.221	+0.270	+0.318	+0.275	+0.272
2000[d]	+0.400	+0.453	+0.508	+0.472	+0.450
1986–2005 minus 1850–1900		+0.61 ± 0.06		N/A	N/A
1986–2005 minus 1886–1905		+0.66 ± 0.06		+0.66	+0.66
1986–2005 minus 1961–1990		+0.30 ± 0.03		+0.31	+0.30
1986–2005 minus 1980–1999		+0.11 ± 0.02		+0.11	+0.11
1946–2012 minus 1880–1945		+0.38 ± 0.04		+0.40	+0.39

Notes:

Decadal average (1990[d] = 1990–1999) median global surface air temperatures from HadCRUT4, GISS and NCDC analyses. See Chapter 2, Sections 2.4.3 and 2.SM.4.3.3, Table 2.7, Figures 2.19, 2.20, 2.21 and 2.22, and also Figure 11.24a. Confidence intervals (5 to 95% for HadCRUT4 only) take into account measurement, sampling, bias and coverage uncertainties. Also shown are temperature increases between the CMIP5 reference period (1986–2005) and four earlier averaging periods, where 1850–1900 is the early instrumental temperature record. Uncertainties in these temperature differences are 5 to 95% confidence intervals.

AII.2: Anthropogenic Emissions

See discussion of Figure 8.2 and Section 11.3.5.

Table AII.2.1a | Anthropogenic CO_2 emissions from fossil fuels and other industrial sources (FF) ($PgC\ yr^{-1}$)

Year	RCP2.6	RCP4.5	RCP6.0	RCP8.5	A2	B1	IS92a	RCP2.6[&]	RCP4.5[&]	RCP6.0[&]	RCP8.5[&]
2000[d]	6.82	6.82	6.82	6.82	6.90	6.90	7.10	6.92 ± 0.80	6.98 ± 0.81	6.76 ± 0.71	6.98 ± 0.81
2010[d]	8.61	8.54	8.39	8.90	8.46	8.50	8.68	8.38 ± 1.03	8.63 ± 1.07	7.66 ± 1.64	8.27 ± 1.68
2020[d]	9.00	9.79	8.99	11.38	11.01	10.00	10.26	8.46 ± 1.38	10.24±1.69	8.33 ± 1.82	10.30 ± 1.87
2030[d]	7.21	10.83	9.99	13.79	13.53	11.20	11.62	6.81 ± 1.49	10.93±1.83	9.20 ± 1.55	12.36 ± 2.25
2040[d]	4.79	11.25	11.47	16.69	15.01	12.20	12.66	4.61 ± 1.60	11.82±1.84	10.04 ± 1.42	15.09 ± 2.15
2050[d]	3.21	10.91	13.00	20.03	16.49	11.70	13.70	2.96 ± 1.80	11.37±1.84	11.14 ± 1.55	18.15 ± 2.56
2060[d]	1.55	9.42	14.73	23.32	18.49	10.20	14.68	1.77 ± 1.06	9.96 ± 2.17	13.22 ± 2.05	21.49 ± 2.42
2070[d]	0.26	7.17	16.33	25.75	20.49	8.60	15.66	0.75 ± 0.90	7.86 ± 1.94	14.57 ± 1.88	23.62 ± 2.43
2080[d]	–0.39	4.62	16.87	27.28	22.97	7.30	17.00	–0.09 ± 0.99	5.17 ± 1.77	15.51 ± 2.29	24.47 ± 2.70
2090[d]	–0.81	4.19	14.70	28.24	25.94	6.10	18.70	–0.30 ± 1.09	5.13 ± 1.53	14.24 ± 1.81	25.30 ± 2.86
2100[d]	–0.92	4.09	13.63	28.68	28.91	5.20	20.40	–0.63 ± 1.17	4.64 ± 1.34	12.78 ± 1.35	25.28 ± 2.73

Notes:

Decadal mean values (2010[d] = average of 2005–2014) are used for emissions because linear interpolation between decadal means conserves total emissions. Data are taken from RCP database (Meinshausen et al., 2011a; http://www.iiasa.ac.at/web-apps/tnt/RcpDb) and may be different from yearly snapshots; for 2100 the average (2095–2100) is used. SRES A2 and B1 and IS92a are taken from TAR Appendix II. RCPn.n[&] values are inferred from ESMs used in CMIP5. The model mean and standard deviation is shown. ESM fossil emissions are taken from 14 models as described in Jones et al. (2013) although not every model has performed every scenario. See Chapter 6, Sections 6.4.3, and 6.4.3.3, and Figure 6.25.

Table AII.2.1b | Anthropogenic CO_2 emissions from agriculture, forestry, land use (AFOLU) ($PgC\ yr^{-1}$)

Year	RCP2.6	RCP4.5	RCP6.0	RCP8.5	SRES-A2	SRES-B1	IS92a
2000[d]	1.21	1.21	1.21	1.21	1.07	1.07	1.30
2010[d]	1.09	0.94	0.93	1.08	1.12	0.78	1.22
2020[d]	0.97	0.41	0.38	0.91	1.25	0.63	1.14
2030[d]	0.79	0.23	–0.43	0.74	1.19	–0.09	1.04
2040[d]	0.51	0.21	–0.67	0.65	1.06	–0.48	0.92
2050[d]	0.29	0.23	–0.48	0.58	0.93	–0.41	0.80
2060[d]	0.55	0.19	–0.27	0.50	0.67	–0.46	0.54
2070[d]	0.55	0.11	–0.04	0.42	0.40	–0.42	0.28
2080[d]	0.55	0.02	0.20	0.31	0.25	–0.60	0.12
2090[d]	0.59	0.03	0.24	0.20	0.21	–0.78	0.06
2100[d]	0.50	0.04	0.18	0.09	0.18	–0.97	–0.10

Notes:

See Table AII.2.1a.

Table AII.2.1c | Anthropogenic total CO_2 emissions ($PgC\ yr^{-1}$)

Year	RCP2.6	RCP4.5	RCP6.0	RCP8.5
2000[d]	8.03	8.03	8.03	8.03
2010[d]	9.70	9.48	9.32	9.98
2020[d]	9.97	10.20	9.37	12.28
2030[d]	8.00	11.06	9.57	14.53
2040[d]	5.30	11.46	10.80	17.33
2050[d]	3.50	11.15	12.52	20.61
2060[d]	2.10	9.60	14.46	23.83
2070[d]	0.81	7.27	16.29	26.17
2080[d]	0.16	4.65	17.07	27.60
2090[d]	–0.23	4.22	14.94	28.44
2100[d]	–0.42	4.13	13.82	28.77

Notes:

See Table AII.2.1a.

Table AII.2.2 | Anthropogenic CH_4 emissions (Tg yr^{-1})

Year	RCP2.6	RCP4.5	RCP6.0	RCP8.5	A2	B1	IS92a	RCP2.6[&]	RCP4.5[&]	RCP6.0[&]	RCP8.5[&]
PI								202 ± 28	202 ± 28	202 ± 28	202 ± 28
2010[total]								554 ± 56	554 ± 56	554 ± 56	554 ± 56
2010[anthrop]								352 ± 45	352 ± 45	352 ± 45	352 ± 45
2010[d]	322	322	321	345	370	349	433	352 ± 45	352 ± 45	352 ± 45	352 ± 45
2020[d]	267	334	315	415	424	377	477	268 ± 34	366 ± 47	338 ± 43	424 ± 54
2030[d]	238	338	326	484	486	385	529	246 ± 31	370 ± 47	354 ± 45	490 ± 63
2040[d]	223	337	343	573	542	381	580	235 ± 30	368 ± 47	373 ± 47	585 ± 75
2050[d]	192	331	354	669	598	359	630	198 ± 25	361 ± 46	385 ± 49	685 ± 88
2060[d]	169	318	362	738	654	342	654	174 ± 22	346 ± 44	395 ± 50	754 ± 96
2070[d]	161	301	359	779	711	324	678	169 ± 22	328 ± 42	390 ± 50	790 ±101
2080[d]	155	283	336	820	770	293	704	162 ± 21	306 ± 39	369 ± 47	832 ±106
2090[d]	149	274	278	865	829	266	733	155 ± 20	298 ± 38	293 ± 37	882 ±113
2100[d]	143	267	250	885	889	236	762	148 ± 19	290 ± 37	267 ± 34	899 ±115

Year	MFR	CLE	MFR*	CLE*	Rog^L	Rog^U	AME^L	AME^U
2000[d]	366	366	303	303				
2010[d]			193	335			332	333
2020[d]			208	383	240	390	294	350
2030[d]	339	478	229	443	217	428	293	376
2040[d]							295	404
2050[d]					178	454	291	426
2060[d]							275	434
2070[d]							254	436
2080[d]							201	430
2090[d]							183	417
2100[d]					121	385	167	406

Notes:

For all anthropogenic emissions see Box 1.1 (Figure 4), Section 8.2.2, Figure 8.2, Sections 11.3.5.1.1 to 3, 11.3.5.2, 11.3.6.1. Ten-year average values (2010[d] = average of 2005–2014; but 2100[d] = average of 2095–2100) are given for RCP-based emissions, but single-year emissions are shown for other scenarios. RCPn.n = harmonized anthropogenic emissions as reported. SRES A2 and B1 and IS92a are from TAR Appendix II. AR5 RCPn.n[&] emissions have ± 1-σ (16 to 84% confidence) uncertainties and are based on the methodology of Prather et al. (2012) updated with CMIP5 results (Holmes et al., 2013; Voulgarakis et al., 2013). Projections of CH_4 lifetimes are harmonized based on PI (1750) and PD (2010) budgets that include uncertainties in lifetimes and abundances. All projected RCP abundances for CH_4 and N_2O (Tables AII.4.2 to AII.4.3) rescale each of the RCP emissions by a fixed factor equal to the ratio of RCP to AR5 anthropogenic emissions at year 2010 to ensure harmonization between total emissions, lifetimes and observed abundances. Natural emissions are kept constant but included as additional uncertainty. Independent emission estimates are shown as follows: MFR/CLE are the maximum feasible reduction and current legislation scenarios from Dentener et al. (2005; 2006), while MFR*/CLE* are the similarly labeled scenarios from Cofala et al. (2007). REF^L/REF^U are lower/upper bounds from the reference scenario of van Vuuren et al. (2008), while POL^L/POL^U are the lower/upper bounds from their policy scenario. AME^L/AME^U are lower/upper bounds from Calvin et al. (2012). Rog^L/Rog^U are lower/upper bounds from Rogelj et et. (2011).

Table AII.2.3 | Anthropogenic N_2O emissions (TgN yr^{-1})

Year	RCP2.6	RCP4.5	RCP6.0	RCP8.5	A2	B1	IS92a	RCP2.6[&]	RCP4.5[&]	RCP6.0[&]	RCP8.5[&]
PI								9.1 ± 1.0	9.1 ± 1.0	9.1 ± 1.0	9.1 ± 1.0
2010[total]								15.7 ± 1.1	15.7 ± 1.1	15.7 ± 1.1	15.7 ± 1.1
2010[anthrop]								6.5 ± 1.3	6.5 ± 1.3	6.5 ± 1.3	6.5 ± 1.3
2010[d]	7.7	7.8	8.0	8.25	8.1	7.5	6.2	6.5 ± 1.3	6.5 ± 1.3	6.5 ± 1.3	6.5 ± 1.3
2020[d]	7.4	8.2	8.1	9.5	9.6	8.1	7.1	6.1 ± 1.2	6.8 ± 1.3	6.3 ± 1.2	7.7 ± 1.5
2030[d]	7.3	8.5	8.8	10.7	10.7	8.2	7.7	6.1 ± 1.2	7.1 ± 1.4	7.0 ± 1.4	8.6 ± 1.7
2040[d]	7.1	8.7	9.7	11.9	11.3	8.3	8.0	6.0 ± 1.2	7.2 ± 1.4	7.8 ± 1.5	9.6 ± 1.9
2050[d]	6.3	8.6	10.5	12.7	12.0	8.3	8.3	5.2 ± 1.0	7.1 ± 1.4	8.4 ± 1.6	10.3 ± 2.0
2060[d]	5.8	8.5	11.3	13.4	12.9	7.7	8.3	4.8 ± 0.9	7.1 ± 1.4	9.1 ± 1.8	10.8 ± 2.1
2070[d]	5.7	8.4	12.0	13.9	13.9	7.4	8.4	4.8 ± 0.9	7.0 ± 1.3	9.6 ± 1.9	11.2 ± 2.2
2080[d]	5.6	8.2	12.3	14.5	14.8	7.0	8.5	4.7 ± 0.9	6.8 ± 1.3	9.9 ± 1.9	11.7 ± 2.3
2090[d]	5.5	8.1	12.4	15.2	15.7	6.4	8.6	4.6 ± 0.9	6.8 ± 1.3	9.9 ± 1.9	12.3 ± 2.4
2100[d]	5.3	8.1	12.2	15.7	16.5	5.7	8.7	4.4 ± 0.9	6.7 ± 1.3	9.8 ± 1.9	12.6 ± 2.4

Notes:
See Table AII.2.2.

Table AII.2.4 | Anthropogenic SF_6 emissions (Gg yr^{-1})

Year	RCP2.6	RCP4.5	RCP6.0	RCP8.5	A2	B1
2000[d]	5.70	5.70	5.70	5.70	6.20	6.20
2010[d]	6.14	5.68	7.43	6.93	7.60	5.60
2020[d]	2.87	3.02	9.19	8.12	9.70	5.70
2030[d]	1.96	2.89	9.58	9.83	11.60	7.20
2040[d]	1.53	3.32	9.68	11.14	13.70	8.90
2050[d]	0.76	3.77	9.78	12.07	16.00	10.40
2060[d]	0.51	4.28	9.92	13.69	18.80	10.90
2070[d]	0.42	4.87	10.05	13.72	19.80	9.50
2080[d]	0.32	5.53	10.00	14.79	20.70	7.10
2090[d]	0.19	5.99	9.86	15.96	23.40	6.50
2100[d]	0.07	6.25	9.37	16.79	25.20	6.50

Notes:
For this and all following emissions tables, see Table AII.2.2. RCPn.n = harmonized anthropogenic emissions as reported by RCPs (Lamarque et al., 2010; 2011; Meinshausen et al., 2011a). SRES A2 and B1 and IS92a from TAR Appendix II.

Table AII.2.5 | Anthropogenic CF_4 emissions (Gg yr^{-1})

Year	RCP2.6	RCP4.5	RCP6.0	RCP8.5	A2	B1
2000[d]	11.62	11.62	11.62	11.62	12.60	12.60
2010[d]	13.65	10.69	19.10	11.04	20.30	14.50
2020[d]	12.07	8.77	22.84	11.67	25.20	15.70
2030[d]	7.36	8.47	23.46	12.29	31.40	16.60
2040[d]	5.06	8.68	23.77	12.22	37.90	18.50
2050[d]	2.95	9.04	23.73	12.37	45.60	20.90
2060[d]	2.24	8.95	23.70	11.89	56.00	23.10
2070[d]	2.07	9.04	23.45	11.81	63.60	22.50
2080[d]	1.52	9.51	22.91	11.58	73.20	21.30
2090[d]	1.22	10.50	21.98	11.14	82.80	22.50
2100[d]	1.11	11.05	20.56	10.81	88.20	22.20

Table AII.2.6 | Anthropogenic C_2F_6 emissions (Gg yr^{-1})

Year	RCP2.6	RCP4.5	RCP6.0	RCP8.5	A2	B1
2000[d]	2.43	2.43	2.43	2.43	1.30	1.30
2010[d]	4.29	2.34	2.62	2.50	2.00	1.50
2020[d]	4.98	1.76	2.66	2.61	2.50	1.60
2030[d]	2.33	1.80	2.69	2.75	3.10	1.70
2040[d]	1.15	1.94	2.63	2.74	3.80	1.80
2050[d]	0.55	2.03	2.56	2.79	4.60	2.10
2060[d]	0.34	2.03	2.49	2.71	5.60	2.30
2070[d]	0.26	1.99	2.50	2.74	6.40	2.20
2080[d]	0.16	1.93	2.36	2.74	7.30	2.10
2090[d]	0.10	1.97	2.26	2.68	8.30	2.20
2100[d]	0.09	2.01	2.09	2.63	8.80	2.20

Table AII.2.7 | Anthropogenic C_6F_{14} emissions (Gg yr^{-1})

Year	RCP2.6	RCP4.5	RCP6.0	RCP8.5
2000[d]	0.213	0.213	0.213	0.213
2010[d]	0.430	0.430	0.429	0.430
2020[d]	0.220	0.220	0.220	0.220
2030[d]	0.123	0.123	0.123	0.123
2040[d]	0.112	0.112	0.112	0.112
2050[d]	0.109	0.109	0.109	0.109
2060[d]	0.108	0.108	0.108	0.108
2070[d]	0.106	0.106	0.106	0.106
2080[d]	0.103	0.103	0.103	0.103
2090[d]	0.097	0.097	0.097	0.097
2100[d]	0.090	0.088	0.088	0.090

Table AII.2.8 | Anthropogenic HFC-23 emissions (Gg yr^{-1})

Year	RCP2.6	RCP4.5	RCP6.0	RCP8.5	A2	B1
2000[d]	10.4	10.4	10.4	10.4	13.0	13.0
2010[d]	9.1	9.1	9.1	9.1	15.0	15.0
2020[d]	2.4	2.4	2.4	2.4	5.0	5.0
2030[d]	0.7	0.7	0.7	0.7	2.0	2.0
2040[d]	0.4	0.4	0.4	0.4	2.0	2.0
2050[d]	0.3	0.3	0.3	0.3	1.0	1.0
2060[d]	0.1	0.1	0.1	0.1	1.0	1.0
2070[d]	0.1	0.1	0.1	0.1	1.0	1.0
2080[d]	0.0	0.0	0.0	0.0	1.0	1.0
2090[d]	0.0	0.0	0.0	0.0	1.0	1.0
2100[d]	0.0	0.0	0.0	0.0	1.0	1.0

Table AII.2.9 | Anthropogenic HFC-32 emissions (Gg yr^{-1})

Year	RCP2.6	RCP4.5	RCP6.0	RCP8.5	A2	B1
2000[d]	3.5	3.5	3.5	3.5	0.0	0.0
2010[d]	20.1	20.1	20.1	20.1	4.0	3.0
2020[d]	55.4	55.4	55.4	55.4	6.0	6.0
2030[d]	71.2	71.2	71.2	71.2	9.0	8.0
2040[d]	78.8	78.8	78.8	78.8	11.0	10.0
2050[d]	76.5	76.5	76.5	76.5	14.0	14.0
2060[d]	83.6	83.6	83.6	83.6	17.0	14.0
2070[d]	92.7	92.7	92.7	92.7	20.0	14.0
2080[d]	95.4	95.4	95.4	95.4	24.0	14.0
2090[d]	91.0	91.0	91.0	91.0	29.0	14.0
2100[d]	82.7	82.7	82.7	82.7	33.0	13.0

Table AII.2.10 | Anthropogenic HFC-125 emissions (Gg yr^{-1})

Year	RCP2.6	RCP4.5	RCP6.0	RCP8.5	A2	B1	IS92a
2000[d]	8	8	8	8	0	0	0
2010[d]	29	18	10	32	11	11	1
2020[d]	82	29	9	63	21	21	9
2030[d]	108	32	9	79	29	29	46
2040[d]	122	31	10	99	35	36	111
2050[d]	122	30	10	115	46	48	175
2060[d]	138	27	11	128	56	48	185
2070[d]	157	24	11	139	66	48	194
2080[d]	165	24	12	144	79	48	199
2090[d]	161	23	12	147	94	46	199
2100[d]	150	23	12	148	106	44	199

Table AII.2.11 | Anthropogenic HFC-134a emissions (Gg yr^{-1})

Year	RCP2.6	RCP4.5	RCP6.0	RCP8.5	A2	B1	IS92a
2000[d]	72	72	72	72	80	80	148
2010[d]	146	140	139	153	166	163	290
2020[d]	173	184	153	255	252	249	396
2030[d]	193	208	159	331	330	326	557
2040[d]	209	229	163	402	405	414	738
2050[d]	203	248	167	461	506	547	918
2060[d]	225	246	172	506	633	550	969
2070[d]	252	260	175	553	758	544	1020
2080[d]	263	299	177	602	915	533	1047
2090[d]	256	351	175	651	1107	513	1051
2100[d]	239	400	171	696	1260	486	1055

Table AII.2.12 | Anthropogenic HFC-143a emissions (Gg yr^{-1})

Year	RCP2.6	RCP4.5	RCP6.0	RCP8.5	A2	B1
2000[d]	7.5	7.5	7.5	7.5	0.0	0.0
2010[d]	23.1	14.0	7.0	23.2	9.0	8.0
2020[d]	59.1	17.4	5.4	34.1	16.0	15.0
2030[d]	74.7	20.3	6.0	38.5	22.0	21.0
2040[d]	81.8	23.1	6.6	45.1	27.0	26.0
2050[d]	79.0	25.6	7.1	49.8	35.0	35.0
2060[d]	86.1	25.9	7.7	52.3	43.0	35.0
2070[d]	94.2	28.2	8.3	54.1	51.0	35.0
2080[d]	95.1	33.5	8.7	52.7	61.0	35.0
2090[d]	88.7	39.6	9.0	50.2	73.0	34.0
2100[d]	79.2	45.1	9.1	47.3	82.0	32.0

Table AII.2.13 | Anthropogenic HFC-227ea emissions (Gg yr^{-1})

Year	RCP2.6	RCP4.5	RCP6.0	RCP8.5	A2	B1
2000[d]	1.7	1.7	1.7	1.7	0.0	0.0
2010[d]	7.0	5.3	6.9	8.5	12.0	13.0
2020[d]	2.6	1.4	2.5	2.7	17.0	18.0
2030[d]	0.9	0.3	0.8	0.7	21.0	24.0
2040[d]	0.8	0.2	0.7	0.7	26.0	30.0
2050[d]	0.4	0.1	0.3	0.4	32.0	39.0
2060[d]	0.2	0.0	0.1	0.2	40.0	40.0
2070[d]	0.1	0.0	0.1	0.1	48.0	39.0
2080[d]	0.1	0.0	0.1	0.1	58.0	38.0
2090[d]	0.1	0.0	0.0	0.1	70.0	36.0
2100[d]	0.1	0.0	0.0	0.1	80.0	34.0

Table AII.2.14 | Anthropogenic HFC-245fa emissions (Gg yr^{-1})

Year	RCP2.6	RCP4.5	RCP6.0	RCP8.5	A2	B1
2000[d]	11	11	11	11	0	0
2010[d]	42	46	53	74	59	60
2020[d]	32	86	65	143	79	80
2030[d]	7	95	67	186	98	102
2040[d]	0	97	68	181	121	131
2050[d]	0	95	69	163	149	173
2060[d]	0	87	70	150	190	173
2070[d]	0	82	71	138	228	170
2080[d]	0	80	70	129	276	166
2090[d]	0	81	68	123	334	159
2100[d]	0	83	65	130	388	150

Table AII.2.15 | Anthropogenic HFC-43-10mee emissions (Gg yr^{-1})

Year	RCP2.6	RCP4.5	RCP6.0	RCP8.5	A2	B1
2000[d]	0.6	0.6	0.6	0.6	0.0	0.0
2010[d]	5.6	5.6	5.6	5.6	7.0	6.0
2020[d]	7.2	7.2	7.2	7.2	8.0	7.0
2030[d]	8.1	8.1	8.1	8.1	8.0	8.0
2040[d]	9.4	9.4	9.4	9.1	9.0	9.0
2050[d]	10.8	10.8	10.8	10.4	11.0	11.0
2060[d]	11.1	11.1	11.1	12.1	12.0	11.0
2070[d]	11.0	11.0	11.0	13.9	14.0	11.0
2080[d]	11.0	11.0	10.9	16.2	16.0	11.0
2090[d]	10.7	10.7	10.7	18.9	19.0	11.0
2100[d]	10.5	10.5	10.5	21.4	22.0	10.0

Table AII.2.16 | Anthropogenic CO emissions (Tg yr^{-1})

Year	RCP2.6	RCP4.5	RCP6.0	RCP8.5	A2	B1	IS92a
2000[d]	1071	1071	1071	1071	877	877	1048
2010[d]	1035	1041	1045	1054	977	789	1096
2020[d]	984	997	1028	1058	1075	751	1145
2030[d]	930	986	1030	1019	1259	603	1207
2040[d]	879	948	1046	960	1344	531	1282
2050[d]	825	875	1033	907	1428	471	1358
2060[d]	779	782	996	846	1545	459	1431
2070[d]	718	678	939	799	1662	456	1504
2080[d]	668	571	879	759	1842	426	1576
2090[d]	638	520	835	721	2084	399	1649
2100[d]	612	483	798	694	2326	363	1722

Year	MFR	CLE	REF^L	REF^U	POL^L	POL^U
2000[d]	977	977	708	1197	706	1197
2010[d]			771	1408	769	1408
2020[d]			755	1629	705	1611
2030[d]	729	904	707	1865	592	1803
2040[d]			695	2165	620	2002
2050[d]			591	2487	482	2218
2060[d]			504	2787	363	2409
2070[d]			450	3052	328	2558
2080[d]			438	3279	268	2635
2090[d]			410	3510	259	2714
2100[d]			363	3735	253	2796

Table AII.2.17 | Anthropogenic NMVOC emissions (Tg yr^{-1})

Year	RCP2.6	RCP4.5	RCP6.0	RCP8.5	A2	B1	IS92a	CLE	MFR
2000[d]	213	213	213	213	141	141	126	147	147
2010[d]	216	209	215	217	155	141	142		
2020[d]	213	197	214	224	179	140	158		
2030[d]	202	201	217	225	202	131	173	146	103
2040[d]	192	201	222	218	214	123	188		
2050[d]	179	191	220	209	225	116	202		
2060[d]	167	180	214	202	238	111	218		
2070[d]	152	167	204	194	251	103	234		
2080[d]	140	152	193	189	275	99	251		
2090[d]	132	145	182	182	309	96	267		
2100[d]	126	141	174	177	342	87	283		

Table AII.2.18 | Anthropogenic NO_x emissions (TgN yr^{-1})

Year	RCP2.6	RCP4.5	RCP6.0	RCP8.5	CLE	MFR
2000[d]	38.5	38.5	38.5	38.5	53.4	53.4
2010[d]	43.5	42.4	43.1	43.5		
2020[d]	47.5	43.5	43.3	48.1		
2030[d]	50.8	45.2	46.2	52.1	69.8	69.8
2040[d]	53.2	46.3	49.8	55.6		
2050[d]	55.5	46.4	53.0	58.4		
2060[d]	58.4	46.0	56.5	60.6		
2070[d]	61.2	45.2	59.5	62.4		
2080[d]	63.3	44.3	60.9	63.8		
2090[d]	65.2	43.9	62.1	65.3		
2100[d]	67.0	43.6	61.8	66.9		

Year	MFR	CLE	REF^L	REF^U	POL^L	POL^U
2000[d]	38.0	38.0	29.1	41.6	29.1	41.6
2010[d]			26.0	50.2	23.9	50.1
2020[d]			26.3	60.4	21.6	59.2
2030[d]	23.1	42.9	24.4	71.8	16.5	67.4
2040[d]			21.5	86.3	14.1	75.3
2050[d]			17.0	101.7	11.6	83.3
2060[d]			13.2	115.7	11.4	89.8
2070[d]			12.0	127.5	10.5	94.6
2080[d]			11.5	137.2	9.6	97.2
2090[d]			12.0	146.2	8.8	100.1
2100[d]			13.0	155.0	8.0	104.0

Notes:
Odd nitrogen (NO_x) emissions occur as NO or NO_2, measured here as Tg of N.

Table AII.2.19 | Anthropogenic NH_3 emissions (TgN yr^{-1})

Year	RCP2.6	RCP4.5	RCP6.0	RCP8.5	CLE	MFR
2000[d]	38.5	38.5	38.5	38.5	53.4	53.4
2010[d]	43.5	42.4	43.1	43.5		
2020[d]	47.5	43.5	43.3	48.1		
2030[d]	50.8	45.2	46.2	52.1	69.8	69.8
2040[d]	53.2	46.3	49.8	55.6		
2050[d]	55.5	46.4	53.0	58.4		
2060[d]	58.4	46.0	56.5	60.6		
2070[d]	61.2	45.2	59.5	62.4		
2080[d]	63.3	44.3	60.9	63.8		
2090[d]	65.2	43.9	62.1	65.3		
2100[d]	67.0	43.6	61.8	66.9		

Table AII.2.20 | Anthropogenic SO_x emissions (TgS yr^{-1})

Year	RCP2.6	RCP4.5	RCP6.0	RCP8.5	A2	B1	IS92a
2000[d]	55.9	55.9	55.9	55.9	69.0	69.0	79.0
2010[d]	54.9	54.8	55.8	51.9	74.7	73.9	95.0
2020[d]	44.5	50.3	49.9	47.6	99.5	74.6	111.0
2030[d]	30.8	43.2	42.7	42.3	112.5	78.2	125.8
2040[d]	20.9	35.0	41.9	33.5	109.0	78.5	139.4
2050[d]	16.0	26.5	37.8	26.8	105.4	68.9	153.0
2060[d]	13.8	21.0	34.0	23.0	89.6	55.8	151.8
2070[d]	11.9	16.7	23.5	20.3	73.7	44.3	150.6
2080[d]	9.9	13.2	15.9	18.3	64.7	36.1	149.4
2090[d]	8.0	12.0	12.7	14.9	62.5	29.8	148.2
2100[d]	6.7	11.4	10.8	13.1	60.3	24.9	147.0

Year	MFR	CLE	REF^L	REF^U	POL^L	POL^U
2000[d]	55.6	55.6	50.6	76.4	50.6	76.4
2010[d]			53.1	81.8	52.7	78.7
2020[d]			56.9	84.8	47.7	77.8
2030[d]	17.9	58.8	60.1	86.7	29.8	76.3
2040[d]			52.5	82.9	19.0	72.0
2050[d]			44.2	72.3	12.4	61.7
2060[d]			32.8	73.9	9.5	52.9
2070[d]			30.5	77.7	7.8	49.8
2080[d]			29.6	81.1	6.2	50.5
2090[d]			22.8	84.5	5.1	52.5
2100[d]			18.0	88.0	4.0	54.0

Notes:
Anthropogenic sulphur emissions as SO_2, measured here as Tg of S.

Table AII.2.21 | Anthropogenic OC aerosols emissions (Tg yr^{-1})

Year	RCP2.6	RCP4.5	RCP6.0	RCP8.5	A2	B1	IS92a	MFR*	CLE*
2000[d]	35.6	35.6	35.6	35.6	81.4	81.4	81.4	35.0	35.0
2010[d]	36.6	34.6	36.2	35.6	89.3	74.5	85.2	29.2	34.6
2020[d]	36.6	30.8	36.1	34.5	97.0	71.5	89.0	28.6	32.6
2030[d]	35.3	29.2	36.0	33.2	111.4	59.9	93.9	27.9	30.9
2040[d]	32.3	28.0	36.4	31.6	118.1	54.2	99.8		
2050[d]	30.3	26.8	36.5	30.1	124.7	49.5	105.8		
2060[d]	29.6	25.0	35.7	28.5	133.9	48.6	111.5		
2070[d]	28.2	22.8	34.4	27.4	143.1	48.3	117.2		
2080[d]	27.0	20.7	33.4	26.4	157.2	46.0	122.9		
2090[d]	26.4	19.9	32.7	25.1	176.2	43.8	128.6		
2100[d]	25.5	19.5	32.2	24.1	195.2	41.0	134.4		

Notes:
For both MFR* and CLE* 23 Tg is added to Cofala et al. (2007) values to include biomass burning.

Table AII.2.22 | Anthropogenic BC aerosols emissions (Tg yr^{-1})

Year	RCP2.6	RCP4.5	RCP6.0	RCP8.5	A2	B1	IS92a	MFR*	CLE*
2000[d]	7.88	7.88	7.88	7.88	12.40	12.40	12.40	7.91	7.91
2010[d]	8.49	8.13	8.13	8.06	13.60	11.30	13.00	6.31	8.01
2020[d]	8.27	7.84	7.77	7.66	14.80	10.90	13.60	5.81	7.41
2030[d]	7.03	7.36	7.53	7.04	17.00	9.10	14.30	5.41	7.01
2040[d]	5.80	6.81	7.39	6.22	18.00	8.30	15.20		
2050[d]	5.00	6.21	7.07	5.67	19.00	7.50	16.10		
2060[d]	4.46	5.56	6.48	5.22	20.40	7.40	17.00		
2070[d]	3.99	4.88	5.75	4.88	21.80	7.40	17.90		
2080[d]	3.70	4.23	5.15	4.66	24.00	7.00	18.70		
2090[d]	3.55	4.01	4.70	4.43	26.80	6.70	19.60		
2100[d]	3.39	3.88	4.41	4.27	29.70	6.20	20.50		

Notes:
For both MFR* and CLE* 2.6 Tg added to Cofala et al. (2007) values to include biomass burning.

Table AII.2.23 | Anthropogenic nitrogen fixation (Tg-N yr^{-1})

Year	Historical	SRES A1 + Biofuel	SRES A2	SRES B1	SRES B2	FAO2000 Baseline[a]	FAO2000 Improved[a]	Tilman 2001[a]	Tubiello 2007[a]
1910	0.0								
1920	0.2								
1925	0.6								
1930	0.9								
1935	1.3								
1940	2.2								
1950	3.7								
1955	6.8								
1960	9.5								
1965	18.7								
1970	31.6								
1971	33.3								
1972	36.2								
1973	39.1								
1974	38.6								
1975	43.7								

Table AII.2.23 *(continued)*

Year	Historical	SRES A1 + Biofuel	SRES A2	SRES B1	SRES B2	FAO2000 Baseline[a]	FAO2000 Improved[a]	Tilman 2001[a]	Tubiello 2007[a]
1975	43.7								
1976	46.4								
1977	49.9								
1978	53.8								
1979	57.4								
1980	60.6								
1981	60.3								
1982	61.3								
1983	67.1								
1984	70.9								
1985	70.2								
1986	72.5								
1987	75.8								
1988	79.5								
1989	78.9								
1990	77.1								
1991	75.5								
1992	73.7								
1993	72.3								
1994	72.4								
1995	78.5								
1996	82.6					77.8	77.8		
1997	81.4								
1998	82.8								
1999	84.9								
2000	82.1							87.0	
2001	82.9								
2002	85.2								
2003	90.2								
2004	91.7								
2005	94.2								
2007	98.4								
2010		104.1	101.9	101.7	96.5				
2015		–	–	–	–	106.8	88.0		
2020		122.6	110.7	111.2	100.9			135.0	
2030		141.1	117.6	118.4	103.3	124.5	96.2		
2040		153.3	130.7	122.2	103.5				
2050		165.5	131.1	123.2	101.9			236.0	
2060		171.3	134.0	121.4	99.2				
2070		177.0	132.1	117.5	95.6				
2080		180.1	138.1	111.6	91.5				205
2090		186.0	146.5	108.8	91.3				
2100		192.5	149.8	104.1	91.0				

Notes:

(a) See Chapter 6, Figure 6.30 and Erisman et al. (2008) for details and sources.

AII.3: Natural Emissions

Table AII.3.1a | Net land (natural and land use) CO_2 emissions (PgC yr^{-1})

Year	RCP2.6[&]	RCP4.5[&]	RCP6.0[&]	RCP8.5[&]
2000[d]	–1.02 ± 0.87	–1.14 ± 0.87	–0.92 ± 0.93	–1.14 ± 0.87
2010[d]	–1.49 ± 1.02	–1.85 ± 0.96	–1.03 ± 1.65	–1.30 ± 1.64
2020[d]	–1.24 ± 1.35	–2.83 ± 1.47	–1.79 ± 1.95	–1.43 ± 1.82
2030[d]	–1.28 ± 1.53	–2.84 ± 1.59	–2.37 ± 1.54	–1.76 ± 2.22
2040[d]	–1.21 ± 1.33	–3.25 ± 1.58	–2.27 ± 1.46	–2.15 ± 2.13
2050[d]	–1.00 ± 1.53	–3.07 ± 1.54	–1.98 ± 1.57	–2.35 ± 2.45
2060[d]	–0.76 ± 0.83	–2.80 ± 1.83	–2.46 ± 2.01	–2.71 ± 2.38
2070[d]	–0.68 ± 0.84	–2.59 ± 1.73	–2.40 ± 2.06	–2.57 ± 2.42
2080[d]	–0.15 ± 0.81	–2.04 ± 1.48	–2.22 ± 2.12	–1.96 ± 2.64
2090[d]	–0.03 ± 0.99	–2.12 ± 1.38	–2.77 ± 1.96	–1.63 ± 2.70
2100[d]	0.36 ± 0.95	–1.54 ± 1.25	–2.13 ± 1.32	–1.27 ± 2.90

Notes:

Ten-year average values are shown (2010[d] = average of 2005–2014). CO_2 emissions are inferred from ESMs used in CMIP5 (Jones et al., 2013). See notes Table AII.2.1a and Chapter 6, Sections 6.4.3 and 6.4.3.3 and Figure 6.24.

Table AII.3.1b | Net ocean CO_2 emissions (PgC yr^{-1})

Year	RCP2.6[&]	RCP4.5[&]	RCP6.0[&]	RCP8.5[&]
2000[d]	–2.09 ± 0.19	–2.14 ± 0.32	–2.10 ± 0.17	–2.14 ± 0.32
2010[d]	–2.44 ± 0.22	–2.50 ± 0.42	–2.44 ± 0.20	–2.53 ± 0.43
2020[d]	–2.70 ± 0.26	–2.75 ± 0.46	–2.59 ± 0.22	–3.02 ± 0.51
2030[d]	–2.59 ± 0.30	–2.98 ± 0.52	–2.69 ± 0.22	–3.47 ± 0.54
2040[d]	–2.22 ± 0.32	–3.16 ± 0.56	–2.88 ± 0.27	–3.96 ± 0.67
2050[d]	–1.83 ± 0.33	–3.22 ± 0.60	–3.16 ± 0.31	–4.47 ± 0.76
2060[d]	–1.52 ± 0.30	–3.12 ± 0.63	–3.52 ± 0.36	–4.92 ± 0.84
2070[d]	–1.23 ± 0.23	–2.82 ± 0.61	–3.79 ± 0.41	–5.24 ± 0.97
2080[d]	–0.99 ± 0.27	–2.46 ± 0.59	–4.02 ± 0.44	–5.40 ± 1.14
2090[d]	–0.85 ± 0.26	–2.22 ± 0.53	–3.96 ± 0.43	–5.45 ± 1.18
2100[d]	–0.77 ± 0.26	–2.14 ± 0.47	–3.84 ± 0.42	–5.44 ± 1.22

Notes:

See Table AII.3.1.a.

AII.4: Abundances of the Well-Mixed Greenhouse Gases

Table AII.4.1 | CO_2 abundance (ppm)

Year	Observed	RCP2.6	RCP4.5	RCP6.0	RCP8.5	A2	B1	IS92a	Min	RCP8.5[&]	Max
PI	278 ± 2	278	278	278	278	278	278	278			
2011[obs]	390.5 ± 0.3										
2000		368.9	368.9	368.9	368.9	368	368	368			
2005		378.8	378.8	378.8	378.8					378.8	
2010		389.3	389.1	389.1	389.3	388	387	388	366	394	413
2020		412.1	411.1	409.4	415.8	416	411	414	386	425	449
2030		430.8	435.0	428.9	448.8	448	434	442	412	461	496
2040		440.2	460.8	450.7	489.4	486	460	472	443	504	555
2050		442.7	486.5	477.7	540.5	527	485	504	482	559	627
2060		441.7	508.9	510.6	603.5	574	506	538	530	625	713
2070		437.5	524.3	549.8	677.1	628	522	575	588	703	810
2080		431.6	531.1	594.3	758.2	690	534	615	651	790	914
2090		426.0	533.7	635.6	844.8	762	542	662	722	885	1026
2100		420.9	538.4	669.7	935.9	846	544	713	794	985 ± 97	1142

Notes:

For observations (2011[obs]) see Chapter 2; and for projections see Box 1.1 (Figure 2), Sections 6.4.3.1, 11.3.1.1, 11.3.5.1.1. RCPn.n refers to values taken directly from the published RCP scenarios using the MAGICC model (Meinshausen et al., 2011a; 2011b). These are harmonized to match observations up to 2005 (378.8 ppm) and project future abundances thereafter. RCP8.5[&] shows the average and assessed 90% confidence interval for year 2100, plus the min-max full range derived from the CMIP5 archive for all years (P. Friedlingstein, based on Friedlingstein et al., 2006). 11 ESMs participated (BCC-CSM-1, CanESM2, CESM1-BGC, GFDL-ESM2G, HadGem-2ES, INMCM4, IPSLCM5-LR, MIROC-ESM, MPI-ESM-LR, MRI-ESM1, and Nor-ESM1-ME), running the RCP8.5 anthropogenic emission scenario forced by the RCP8.5 climate change scenario (see Figure 12.36). All abundances are mid-year. Projected values for SRES A2 and B1 and IS92 are the average of reference models taken from the TAR Appendix II.

Table AII.4.2 | CH_4 abundance (ppb)

Year	RCP2.6	RCP4.5	RCP6.0	RCP8.5	A2	B1	IS92a	RCP2.6[&]	RCP4.5[&]	RCP6.0[&]	RCP8.5[&]
PI	720	720	720	720				722 ± 25	722 ± 25	722 ± 25	722 ± 25
2011[obs]								1803 ± 4	1803 ± 4	1803 ± 4	1803 ± 4
2000	1751	1751	1751	1751	1760	1760	1760				
2010	1773	1767	1769	1779	1861	1827	1855	1795 ± 18	1795 ± 18	1795 ± 18	1795 ± 18
2020	1731	1801	1786	1924	1997	1891	1979	1716 ± 23	1847 ± 21	1811 ± 22	1915 ± 25
2030	1600	1830	1796	2132	2163	1927	2129	1562 ± 38	1886 ± 28	1827 ± 28	2121 ± 44
2040	1527	1842	1841	2399	2357	1919	2306	1463 ± 50	1903 ± 37	1880 ± 36	2412 ± 74
2050	1452	1833	1895	2740	2562	1881	2497	1353 ± 60	1899 ± 47	1941 ± 48	2784 ± 116
2060	1365	1801	1939	3076	2779	1836	2663	1230 ± 71	1872 ± 59	1994 ± 61	3152 ± 163
2070	1311	1745	1962	3322	3011	1797	2791	1153 ± 78	1824 ± 72	2035 ± 77	3428 ± 208
2080	1285	1672	1940	3490	3252	1741	2905	1137 ± 88	1756 ± 87	2033 ± 94	3624 ± 250
2090	1268	1614	1819	3639	3493	1663	3019	1135 ± 98	1690 ± 100	1908 ± 111	3805 ± 293
2100	1254	1576	1649	3751	3731	1574	3136	1127 ± 106	1633 ± 110	1734 ± 124	3938 ± 334

Notes:

RCPn.n refers to values taken directly from the published RCP scenarios using the MAGICC model (Meinshausen et al., 2011b) and initialized in year 2005 at 1754 ppb. Values for SRES A2 and B1 and IS92 are from the TAR Appendix II. RCPn.n[&] values are best estimates with uncertainties (68% confidence intervals) from Chapter 11 (Section 11.3.5) based on Holmes et al. (2013) and using RCP[&] emissions and uncertainties tabulated above. For RCP[&] the PI, year 2011 and year 2010 values are based on observations. RCP models used slightly different PI abundances than recommended here (Table AII.1.1, Chapter 2).

Table AII.4.3 | N_2O abundance (ppb)

Year	RCP2.6	RCP4.5	RCP6.0	RCP8.5	A2	B1	IS92a	RCP2.6[&]	RCP4.5[&]	RCP6.0[&]	RCP8.5[&]
PI	272	272	272	272				270 ± 7	270 ± 7	270 ± 7	270 ± 7
2011[obs]								324 ± 1	324 ± 1	324 ± 1	324 ± 1
2000	316	316	316	316	316	316	316				
2010	323	323	323	323	325	324	324	323 ± 3	323 ± 3	323 ± 3	323 ± 3
2020	329	330	330	332	335	333	333	330 ± 4	331 ± 4	331 ± 4	332 ± 4
2030	334	337	337	342	347	341	343	336 ± 5	339 ± 5	338 ± 5	342 ± 6
2040	339	344	345	354	360	349	353	342 ± 6	346 ± 7	346 ± 7	353 ± 8
2050	342	351	355	367	373	357	363	346 ± 8	353 ± 9	355 ± 9	365 ± 11
2060	343	356	365	381	387	363	372	349 ± 9	360 ± 10	364 ± 11	377 ± 13
2070	344	361	376	394	401	368	381	351 ± 10	365 ± 12	374 ± 13	389 ± 16
2080	344	366	386	408	416	371	389	352 ± 11	370 ± 13	384 ± 15	401 ± 18
2090	344	369	397	421	432	374	396	353 ± 11	374 ± 14	393 ± 17	413 ± 21
2100	344	372	406	435	447	375	403	354 ± 12	378 ± 16	401 ± 19	425 ± 24

Notes:
See notes Table AII.4.2.

Table AII.4.4 | SF_6 abundance (ppt)

Year	RCP2.6	RCP4.5	RCP6.0	RCP8.5	A2	B1	Obs
2011[obs]							7.3 ± 0.1
2010	7.0	6.9	7.0	7.0	7	7	
2020	8.9	8.7	10.3	9.9	11	9	
2030	9.7	9.7	14.1	13.4	15	12	
2040	10.4	10.9	17.9	17.6	20	15	
2050	10.8	12.3	21.7	22.1	26	19	
2060	11.0	13.8	25.6	27.2	32	23	
2070	11.2	15.6	29.5	32.6	40	27	
2080	11.3	17.6	33.4	38.1	48	30	
2090	11.4	19.9	37.3	44.1	56	33	
2100	11.4	22.3	41.0	50.5	65	35	

Notes:
Projected SF_6 and PFC abundances (Tables AII.4.4 to AII.4.7) taken directly from RCPs (Meinshausen et al., 2011a). Observed values shown for year 2011.

Table AII.4.5 | CF_4 abundance (ppt)

Year	RCP2.6	RCP4.5	RCP6.0	RCP8.5	A2	B1	Obs
2011 [obs]							79.0
2010	84	83	85	83	92	91	
2020	93	90	99	91	107	101	
2030	99	95	115	99	125	111	
2040	103	101	130	107	148	122	
2050	106	107	146	115	175	135	
2060	108	113	162	123	208	150	
2070	109	119	177	131	246	164	
2080	110	125	193	138	291	179	
2090	111	131	207	146	341	193	
2100	112	138	222	153	397	208	

Table AII.4.6 | C_2F_6 abundance (ppt)

Year	RCP2.6	RCP4.5	RCP6.0	RCP8.5	A2	B1	Obs
2011 [obs]							**4.2**
2010	4.1	3.9	3.9	3.9	4	4	
2020	6.2	4.8	5.0	5.0	5	4	
2030	7.9	5.5	6.2	6.1	6	5	
2040	8.6	6.3	7.3	7.2	7	6	
2050	8.9	7.1	8.4	8.4	9	7	
2060	9.1	7.9	9.4	9.6	11	8	
2070	9.2	8.8	10.5	10.7	14	8	
2080	9.3	9.6	11.5	11.8	17	9	
2090	9.3	10.4	12.5	13.0	20	10	
2100	9.3	11.3	13.4	14.1	23	11	

Table AII.4.7 | C_6F_{14} abundance (ppt)

Year	RCP2.6	RCP4.5	RCP6.0	RCP8.5
2010	0.07	0.07	0.07	0.07
2020	0.13	0.13	0.13	0.13
2030	0.16	0.16	0.16	0.16
2040	0.18	0.18	0.18	0.18
2050	0.20	0.20	0.20	0.20
2060	0.21	0.21	0.21	0.21
2070	0.23	0.23	0.23	0.23
2080	0.25	0.25	0.25	0.25
2090	0.27	0.27	0.27	0.27
2100	0.28	0.28	0.28	0.28

Table AII.4.8 | HFC-23 abundance (ppt)

Year	RCP2.6	RCP4.5	RCP6.0	RCP8.5	A2	B1	RCP2.6[&]	RCP4.5[&]	RCP6.0[&]	RCP8.5[&]
2011[obs]							**24.0**	**24.0**	**24.0**	**24.0**
2010	22.9	22.9	22.9	22.9	26	26	23.2 ± 1	23.2 ± 1	23.2 ± 1	23.2 ± 1
2020	27.2	27.2	27.2	27.2	33	33	26.6 ± 1	26.6 ± 1	26.6 ± 1	26.6 ± 1
2030	27.0	27.0	27.1	27.1	35	35	26.3 ± 1	26.3 ± 1	26.3 ± 1	26.3 ± 1
2040	26.5	26.5	26.6	26.6	35	35	25.7 ± 1	25.8 ± 1	25.8 ± 1	25.8 ± 1
2050	25.8	25.9	25.9	26.0	35	35	24.9 ± 1	25.0 ± 1	25.1 ± 1	25.1 ± 1
2060	25.0	25.1	25.1	25.3	35	34	24.0 ± 1	24.2 ± 1	24.3 ± 1	24.4 ± 1
2070	24.1	24.2	24.4	24.6	34	34	23.0 ± 1	23.4 ± 1	23.4 ± 1	23.6 ± 1
2080	23.3	23.3	23.5	23.8	34	33	22.1 ± 1	22.5 ± 1	22.6 ± 1	22.8 ± 1
2090	22.4	22.5	22.7	23.0	34	33	21.2 ± 1	21.6 ± 1	21.8 ± 1	22.1 ± 1
2100	21.6	21.6	21.9	22.3	33	32	20.3 ± 1	20.8 ± 1	21.0 ± 1	21.3 ± 1

Notes:

RCPn.n HFC abundances (Tables AII.4.8 to AII.4.15) are as reported (Meinshausen et al., 2011a). SRES A2 and B1 and IS92a (where available) are taken from TAR Appendix II. Observed values are shown for 2011 (see Chapter 2, and Table AII.1.1). The AR5 RCPn.n[&] abundances are calculated starting with observed abundances (adopted for 2010) and future tropospheric OH changes using the methodology of Prather et al. (2012), updated for uncertainty in lifetime and scenario changes in OH using Holmes et al. (2013) and ACCMIP results (Stevenson et al., 2013; Voulgarakis et al., 2013). Projected RCP[&] abundances are best estimates with 68% confidence range as uncertainties. See also notes Tables AII.4.2 and AII.5.9.

Table AII.4.9 | HFC-32 abundance (ppt)

Year	RCP2.6	RCP4.5	RCP6.0	RCP8.5	A2	B1	RCP2.6[&]	RCP4.5[&]	RCP6.0[&]	RCP8.5[&]
2011[obs]							4.9	4.9	4.9	4.9
2010	5.7	5.7	5.7	5.7	1	1	4.1 ± 0	4.1 ± 0	4.1 ± 0	4.1 ± 0
2020	21.0	21.0	21.1	21.1	3	3	23.8 ± 2	24.0 ± 2	24.0 ± 2	24.0 ± 2
2030	34.7	35.2	35.5	35.8	4	4	38.1 ± 5	39.1 ± 5	39.1 ± 5	39.2 ± 5
2040	41.1	41.9	42.4	43.6	6	5	44.7 ± 6	46.7 ± 6	46.9 ± 6	47.8 ± 6
2050	41.9	42.8	43.9	46.2	7	7	44.3 ± 7	47.6 ± 7	48.2 ± 7	50.3 ± 8
2060	43.1	43.8	45.6	48.8	9	8	45.0 ± 7	49.6 ± 8	50.6 ± 8	53.8 ± 8
2070	47.9	48.1	50.7	54.7	11	8	49.4 ± 8	54.9 ± 8	56.8 ± 9	60.3 ± 9
2080	51.3	50.5	54.0	58.6	14	8	53.8 ± 9	58.2 ± 9	61.4 ± 10	64.7 ± 10
2090	51.0	49.6	52.8	58.2	17	8	54.0 ± 9	56.9 ±10	60.6 ± 10	64.4 ± 11
2100	47.5	45.6	47.4	53.8	20	8	50.5 ± 9	51.8 ± 9	55.2 ± 10	59.6 ± 11

Table AII.4.10 | HFC-125 abundance (ppt)

Year	RCP2.6	RCP4.5	RCP6.0	RCP8.5	A2	B1	IS92a	RCP2.6[&]	RCP4.5[&]	RCP6.0[&]	RCP8.5[&]
2011[obs]								9.6	9.6	9.6	9.6
2010	7.1	6.4	5.7	7.7	2	2	0	8.2 ± 1	8.2 ± 1	8.2 ± 1	8.2 ± 1
2020	27.4	14.3	7.6	25.7	8	8	2	30.9 ± 1	16.3 ± 1	9.6 ± 1	27.6 ± 1
2030	60.0	23.2	9.2	48.5	16	16	12	64.1 ± 3	25.2 ± 2	10.9 ± 1	51.0 ± 3
2040	90.5	29.7	10.6	72.0	24	24	40	95.5 ± 7	31.9 ± 3	12.2 ± 1	75.9 ± 5
2050	114.5	34.0	11.8	97.6	34	33	87	119.5 ± 11	36.6 ± 4	13.3 ± 2	103 ± 8
2060	133.4	36.0	12.9	122.9	45	43	137	139.0 ± 15	39.0 ± 5	14.4 ± 2	130 ± 12
2070	154.8	35.8	13.9	147.1	58	49	177	160.8 ± 20	39.4 ± 6	15.5 ± 2	156 ± 16
2080	176.2	34.8	14.8	168.7	72	54	210	183.2 ± 24	39.1 ± 6	16.6 ± 2	180 ± 20
2090	192.3	34.0	15.5	185.8	89	57	236	200.9 ± 29	38.7 ± 7	17.4 ± 3	199 ± 25
2100	200.2	33.2	15.8	198.9	107	58	255	210.5 ± 34	38.1 ± 7	18.0 ± 3	215 ± 30

Table AII.4.11 | HFC-134a abundance (ppt)

Year	RCP2.6	RCP4.5	RCP6.0	RCP8.5	A2	B1	IS92a	RCP2.6[&]	RCP4.5[&]	RCP6.0[&]	RCP8.5[&]
2011								63 ± 1	63 ± 1	63 ± 1	63 ± 1
2010	56	56	56	56	55	55	94	58 ± 3	58 ± 3	58 ± 3	58 ± 3
2020	96	95	90	112	111	108	183	97 ± 5	98 ± 5	91 ± 5	117 ± 5
2030	122	129	109	180	170	165	281	123 ± 9	132 ± 9	110 ± 8	184 ± 11
2040	142	154	121	245	231	223	401	143 ± 12	157 ± 12	122 ± 10	249 ± 17
2050	153	175	129	311	299	293	537	150 ± 15	178 ± 16	130 ± 12	314 ± 24
2060	160	187	135	370	382	352	657	155 ± 16	192 ± 19	137 ± 14	373 ± 32
2070	175	193	141	423	480	380	743	168 ± 18	200 ± 21	143 ± 15	427 ± 39
2080	191	205	144	471	594	391	807	184 ± 21	216 ± 23	148 ± 16	476 ± 47
2090	200	229	144	517	729	390	850	193 ± 23	242 ± 26	150 ± 18	524 ± 56
2100	199	262	141	561	877	379	878	192 ± 25	275 ± 30	148 ± 19	570 ± 64

Table AII.4.12 | HFC-143a abundance (ppt)

Year	RCP2.6	RCP4.5	RCP6.0	RCP8.5	A2	B1	RCP2.6[&]	RCP4.5[&]	RCP6.0[&]	RCP8.5[&]
2011							12.0	12.0	12.0	12.0
2010	10.2	9.4	8.4	10.8	3	2	11 ± 1	11 ± 1	11 ± 1	11 ± 1
2020	33.9	17.8	10.1	28.2	10	9	37 ± 1	19 ± 1	12 ± 1	29 ± 1
2030	72.1	26.8	12.1	46.8	20	18	75 ± 2	28 ± 1	14 ± 1	48 ± 1
2040	109.9	36.0	14.0	65.6	32	29	13 ± 4	38 ± 1	16 ± 1	67 ± 2
2050	142.1	45.4	16.0	85.7	45	43	144 ± 6	47 ± 2	18 ± 1	88 ± 3
2060	168.6	54.0	18.1	105.2	62	57	170 ± 8	56 ± 3	20 ± 1	107 ± 4
2070	196.1	61.4	20.1	123.2	81	68	197 ± 11	64 ± 3	22 ± 1	126 ± 6
2080	222.2	69.7	22.2	138.7	103	77	223 ± 14	73 ± 4	24 ± 2	142 ± 8
2090	242.0	80.2	24.0	150.2	129	85	243 ± 17	85 ± 5	26 ± 2	154 ± 9
2100	252.9	92.6	25.6	157.9	157	90	254 ± 20	98 ± 6	28 ± 2	163 ± 11

Table AII.4.13 | HFC-227ea abundance (ppt)

Year	RCP2.6	RCP4.5	RCP6.0	RCP8.5	A2	B1	RCP2.6[&]	RCP4.5[&]	RCP6.0[&]	RCP8.5[&]
2011							0.65	0.65	0.65	0.65
2010	1.43	1.28	1.42	1.56	2	2	0.6 ± 0.1	0.6 ± 0.1	0.6 ± 0.1	0.6 ± 0.1
2020	2.81	2.10	2.78	3.30	5	6	2.0 ± 0.1	1.5 ± 0.1	2.0 ± 0.1	2.4 ± 0.1
2030	2.48	1.71	2.44	2.77	10	10	2.0 ± 0.1	1.3 ± 0.1	2.0 ± 0.1	2.2 ± 0.1
2040	2.09	1.35	2.04	2.29	14	15	1.8 ± 0.1	1.1 ± 0.1	1.8 ± 0.1	2.0 ± 0.2
2050	1.74	1.06	1.68	1.92	19	21	1.6 ± 0.2	1.0 ± 0.1	1.6 ± 0.2	1.8 ± 0.2
2060	1.35	0.81	1.31	1.55	25	27	1.3 ± 0.2	0.8 ± 0.1	1.3 ± 0.2	1.5 ± 0.2
2070	1.04	0.61	1.01	1.23	32	31	1.1 ± 0.2	0.6 ± 0.1	1.1 ± 0.2	1.3 ± 0.2
2080	0.81	0.45	0.78	0.99	40	34	0.9 ± 0.2	0.5 ± 0.1	0.9 ± 0.2	1.1 ± 0.2
2090	0.63	0.34	0.59	0.79	49	35	0.8 ± 0.2	0.4 ± 0.1	0.8 ± 0.2	0.9 ± 0.2
2100	1.43	1.28	1.42	1.56	2	2	0.6 ± 0.2	0.3 ± 0.1	0.6 ± 0.2	0.8 ± 0.2

Table AII.4.14 | HFC-245fa abundance (ppt)

Year	RCP2.6	RCP4.5	RCP6.0	RCP8.5	A2	B1	RCP2.6[&]	RCP4.5[&]	RCP6.0[&]	RCP8.5[&]
2011							1.24	1.24	1.24	1.24
2010	7.5	7.3	8.2	9.5	8	8	1 ± 0.2	1 ± 0.2	1 ± 0.2	1 ± 0.2
2020	12.1	19.3	18.1	31.5	17	17	10.2 ± 1	18.9 ± 2	16.4 ± 2	31.0 ± 4
2030	7.4	28.2	21.3	51.2	23	23	6.6 ± 1.5	29.2 ± 4	21.6 ± 3	53.1 ± 8
2040	2.3	31.2	22.6	61.7	29	29	2.2 ± 1.0	33.0 ± 6	23.7 ± 4	63.8 ± 10
2050	0.6	31.9	23.3	62.0	36	38	0.7 ± 0.5	34.1 ± 7	24.6 ± 5	64.4 ± 12
2060	0.2	30.6	23.8	59.1	46	43	0.2 ± 0.2	32.9 ± 7	25.3 ± 5	61.7 ± 13
2070	0.0	28.2	24.2	55.3	58	44	0.1 ± 0.1	30.8 ± 7	25.9 ± 5	58.1 ± 13
2080	0.0	26.4	24.3	51.5	72	43	0.0 ± 0.1	29.3 ± 7	26.4 ± 6	54.4 ± 12
2090	0.0	25.8	23.6	48.0	88	42	0.0 ± 0.0	28.6 ± 6	26.0 ± 6	51.0 ± 12
2100	0.0	26.0	22.3	47.3	105	40	0.0 ± 0.0	28.6 ± 6	24.9 ± 6	50.6 ± 11

Table AII.4.15 | HFC-43-10mee abundance (ppt)

Year	RCP2.6	RCP4.5	RCP6.0	RCP8.5	A2	B1	RCP2.6[&]	RCP4.5[&]	RCP6.0[&]	RCP8.5[&]
2011							—	—	—	—
2010	0.52	0.52	0.52	0.52	1	1	0.0 ± 0.0	0.0 ± 0.0	0.0 ± 0.0	0.0 ± 0.0
2020	1.46	1.46	1.46	1.47	2	1	1.2 ± 0.1	1.2 ± 0.1	1.2 ± 0.1	1.2 ± 0.1
2030	2.09	2.11	2.12	2.14	2	2	2.0 ± 0.2	2.1 ± 0.2	2.1 ± 0.2	2.1 ± 0.2
2040	2.61	2.64	2.66	2.68	3	2	2.7 ± 0.3	2.8 ± 0.3	2.8 ± 0.3	2.8 ± 0.3
2050	3.13	3.17	3.22	3.23	3	3	3.3 ± 0.4	3.4 ± 0.4	3.4 ± 0.4	3.4 ± 0.4
2060	3.56	3.61	3.70	3.83	4	3	3.7 ± 0.6	3.9 ± 0.6	4.0 ± 0.6	4.1 ± 0.6
2070	3.78	3.81	3.96	4.52	4	4	3.9 ± 0.7	4.3 ± 0.7	4.3 ± 0.7	4.9 ± 0.7
2080	3.89	3.88	4.08	5.27	5	4	4.1 ± 0.8	4.4 ± 0.8	4.6 ± 0.8	5.8 ± 0.9
2090	3.93	3.87	4.10	6.14	6	4	4.2 ± 0.8	4.5 ± 0.8	4.7 ± 0.9	6.7 ± 1.0
2100	3.91	3.81	3.99	7.12	7	4	4.2 ± 0.9	4.4 ± 0.9	4.6 ± 0.9	7.9 ± 1.2

Table AII.4.16 | Montreal Protocol greenhouse gas abundances (ppt)

Year	CFC-11	CFC-12	CFC-113	CFC-114	CFC-115	CCl_4	CH_3CCl_3	HCFC-22
2011*	238 ± 1	528 ± 2	74.5 ± 0.5	15.8	8.4	86 ± 2	6.4 ± 0.4	213 ± 2
2010	240.9	532.5	75.6	16.4	8.4	87.6	8.3	206.8
2020	213.0	492.8	67.4	15.8	8.4	70.9	1.5	301.8
2030	182.6	448.0	59.9	15.1	8.4	54.4	0.2	265.4
2040	153.5	405.8	53.3	14.4	8.4	40.3	0.0	151.0
2050	127.2	367.3	47.4	13.6	8.4	29.2	0.0	71.1
2060	104.4	332.4	42.1	12.9	8.3	20.0	0.0	31.5
2070	85.2	300.7	37.4	12.3	8.3	13.6	0.0	13.7
2080	69.1	272.1	33.3	11.6	8.2	9.3	0.0	5.9
2090	55.9	246.2	29.6	11.1	8.2	6.3	0.0	2.6
2100	45.1	222.8	26.3	10.5	8.1	4.3	0.0	1.1

Year	HCFC-141b	HCFC-142b	Halon 1211	Halon 1202	Halon 1301	Halon 2402	CH_3Br	CH_3Cl
2011*	21.4 ± 0.5	21.2 ± 0.5	4.07	0.00	3.23	0.45	7.1	534
2010	20.3	20.5	4.07	0.00	3.20	0.46	7.2	550
2020	30.9	30.9	3.08	0.00	3.29	0.38	7.1	550
2030	34.4	31.2	2.06	0.00	3.19	0.27	7.1	550
2040	27.9	23.3	1.30	0.00	2.97	0.18	7.1	550
2050	19.3	14.9	0.78	0.00	2.71	0.12	7.1	550
2060	12.4	9.0	0.46	0.00	2.43	0.07	7.1	550
2070	7.7	5.2	0.26	0.00	2.16	0.05	7.1	550
2080	4.7	3.0	0.15	0.00	1.90	0.03	7.1	550
2090	2.9	1.7	0.08	0.00	1.66	0.02	7.1	550
2100	1.7	0.9	0.05	0.00	1.44	0.01	7.1	550

Notes:
Present day (2011*) is from Chapter 2; projections are from Scenario A1, WMO Ozone Assessment (WMO 2010).

AII.5: Column Abundances, Burdens, and Lifetimes

Table AII.5.1 | Stratospheric O_3 column changes (DU)

Year	Obs	RCP2.6	RCP4.5	RCP6.0	RCP8.5
1850		17	17	17	17
1980	11	15	15	15	15
2000	**269 ± 8**	**276 ± 9**	**276 ± 9**	**276 ± 9**	**276 ± 9**
2010	0	2	–1	1	–2
2020		4	0	3	2
2030		8	4	7	5
2040		9	7	10	9
2050		12	10	13	12
2060		13	12	14	15
2070		13	11	15	16
2080		12	11	16	15
2090		13	12	16	18
2100		15	13	17	20

Notes:

Observed O_3 columns and trends taken from WMO (Douglass and Filetov, 2010), subtracting tropospheric column O_3 (Table AII.5.2) with uncertainty estimates driven by polar variability. CMIP5 RCP results are from Eyring et al. (2013). The multi-model mean is derived from the CMIP5 models with predictive (interactive or semi-offline) stratospheric and tropospheric ozone chemistry. The absolute value is shown for year 2000. All other years are differences relative to (minus) year 2000. The multi-model standard deviation is shown only for year 2000; it does not change much over time; and, representing primarily the spread in absolute O_3 column, it is larger than the standard deviation of the changes (not evaluated here). All models used the same projections for ozone-depleting substances. Near-term differences in projected O_3 columns across scenarios reflect model sampling (i.e., different sets of models contributing to each RCP), while long-term changes reflect changes in N_2O, CH_4 and climate. See Section 11.3.5.1.2.

Table AII.5.2 | Tropospheric O_3 column changes (DU)

Year	CMIP5				ACCMIP			
	RCP2.6	RCP4.5	RCP6.0	RCP8.5	RCP2.6	RCP4.5	RCP6.0	RCP8.5
1850	–10.2	–10.2	–10.2	–10.2	–8.9	–8.9	–8.9	–8.9
1980	–2.0	–2.0	–2.0	–2.0	–1.3	–1.3	–1.3	–1.3
2000	**31.1 ± 3.3**	**31.1 ± 3.3**	**31.1 ± 3.3**	**31.1 ± 3.3**	**30.8 ± 2.1**	**30.8 ± 2.1**	**30.8 ± 2.1**	**30.8 ± 2.1**
2010	1.1	0.6	0.8	0.8				
2020	1.0	0.9	1.0	2.1				
2030	0.6	1.5	1.4	3.5	–1.3	1.0	–0.1	1.8
2040	0.5	1.6	2.1	4.5				
2050	0.0	1.7	2.4	5.7				
2060	–0.7	1.3	2.6	7.1				
2070	–1.6	0.5	2.3	8.1				
2080	–2.5	–0.1	2.0	8.9				
2090	–2.8	–0.4	1.5	9.5				
2100	–3.1	–0.5	1.1	10.2	–5.4	–2.2	–2.6	5.3

(continued on next page)

Table AII.5.2 *(continued)*

Year	A2	B1	IS92a	CLE	MFR
1850					
1980					
2000	**34.0**	**34.0**	**34.0**	**32.6**	**32.6**
2010	1.7	0.8	1.5		
2020	4.2	1.6	3.1		
2030	6.8	1.9	4.7	1.5 ± 0.8	–1.4 ± 0.4
2040	8.6	1.8	6.1		
2050	10.2	1.0	7.6		
2060	11.7	0.0	8.9		
2070	13.2	–0.9	10.0		
2080	15.3	–1.9	11.1		
2090	18.0	–2.8	12.1		
2100	20.8	–3.9	13.2		

Notes:

RCP results from CMIP5 (Eyring et al., 2013) and ACCMIP (Young et al., 2013). For ACCMIP all models have interactive tropospheric ozone chemistry and are included, in contrast to the CMIP5 multi-model mean which includes only those models with predictive (interactive or semi-offline) stratospheric and tropospheric ozone chemistry. The absolute value is shown for year 2000. All other years are differences relative to (minus) year 2000. The multi-model standard deviation is shown only for year 2000; it does not change much over time; and, representing primarily the spread in absolute O_3 columns, it is larger than the standard deviation of the changes across individual models (not evaluated here). SRES values are from TAR Appendix II. CLE/MFR scenarios are from Dentener et al. (2005, 2006): CLE includes climate change, MFR does not. See Section 11.3.5.1.2.

Table AII.5.3 | Total aerosol optical depth (AOD)

Year	(Min)	Historical	(Max)	RCP2.6	RCP4.5	RCP6.0	RCP8.5
1860[d]	0.056	0.101	0.161	0.094	0.101	0.092	0.100
1870[d]	0.058	0.102	0.162	0.095	0.102	0.094	0.101
1180[d]	0.058	0.102	0.163	0.095	0.102	0.094	0.101
1890[d]	0.059	0.104	0.164	0.098	0.104	0.096	0.103
1900[d]	0.058	0.105	0.166	0.099	0.105	0.097	0.104
1910[d]	0.059	0.107	0.169	0.101	0.107	0.099	0.106
1920[d]	0.060	0.108	0.170	0.102	0.108	0.100	0.107
1930[d]	0.061	0.110	0.173	0.104	0.110	0.101	0.109
1940[d]	0.061	0.111	0.175	0.105	0.111	0.103	0.110
1950[d]	0.060	0.115	0.181	0.108	0.115	0.106	0.113
1960[d]	0.064	0.122	0.192	0.116	0.122	0.113	0.120
1970[d]	0.065	0.130	0.204	0.123	0.130	0.120	0.128
1980[d]	0.066	0.135	0.221	0.127	0.135	0.124	0.133
1990[d]	0.068	0.138	0.231	0.129	0.138	0.126	0.135
2000[d]	0.068	0.136	0.232	0.127	0.136	0.124	0.134
2010[d]				0.127	0.137	0.124	0.133
2020[d]				0.123	0.134	0.122	0.132
2030[d]				0.117	0.130	0.119	0.130
2040[d]				0.111	0.126	0.118	0.126
2050[d]				0.108	0.123	0.117	0.124
2060[d]				0.106	0.119	0.116	0.121
2070[d]				0.105	0.116	0.110	0.120
2080[d]				0.103	0.114	0.107	0.118
2090[d]				0.102	0.112	0.106	0.118
2100[d]				0.101	0.111	0.105	0.117
Number of models		21		15	21	13	19

Notes:

Multi-model decadal global means (2030[d] = 2025–2034, 2100[d] = 2095–2100) from CMIP5 models reporting AOD. The numbers of models for each experiment are indicated in the bottom row. The full range of models (given only for historical period for AOD and AAOD) is large and systematic in that models tend to scale relative to one another. Historical estimates for different RCPs vary because of the models included. RCP4.5 included the full set of CMIP5 models contributing aerosol results (21). The standard deviation of the models is 28% (AOD) and 62% (AAOD) (N. Mahowald, CMIP5 archive; Lamarque et al., 2013; Shindell et al., 2013). See Sections 11.3.5.1.3 and 11.3.6.1.

Table AII.5.4 | Absorbing aerosol optical depth (AAOD)

Year	(Min)	Historical	(Max)	RCP2.6	RCP4.5	RCP6.0	RCP8.5
1860[d]	0.00050	0.0035	0.0054	0.0033	0.0035	0.0031	0.0035
1870[d]	0.00060	0.0035	0.0054	0.0033	0.0035	0.0032	0.0036
1180[d]	0.00060	0.0036	0.0054	0.0034	0.0036	0.0032	0.0036
1890[d]	0.00060	0.0036	0.0055	0.0035	0.0036	0.0033	0.0037
1900[d]	0.00070	0.0037	0.0056	0.0035	0.0037	0.0033	0.0038
1910[d]	0.00070	0.0038	0.0057	0.0036	0.0038	0.0034	0.0038
1920[d]	0.00070	0.0038	0.0058	0.0036	0.0038	0.0034	0.0039
1930[d]	0.00070	0.0038	0.0057	0.0036	0.0038	0.0034	0.0038
1940[d]	0.00070	0.0038	0.0057	0.0036	0.0038	0.0034	0.0039
1950[d]	0.00070	0.0038	0.0058	0.0036	0.0038	0.0034	0.0039
1960[d]	0.00080	0.0040	0.0059	0.0038	0.0040	0.0036	0.0040
1970[d]	0.00090	0.0042	0.0065	0.0040	0.0042	0.0038	0.0043
1980[d]	0.00100	0.0046	0.0073	0.0044	0.0046	0.0042	0.0046
1990[d]	0.00110	0.0049	0.0079	0.0047	0.0049	0.0044	0.0049
2000[d]	0.00120	0.0050	0.0084	0.0048	0.0050	0.0045	0.0051
2010[d]				0.0050	0.0051	0.0046	0.0051
2020[d]				0.0050	0.0050	0.0045	0.0050
2030[d]				0.0047	0.0049	0.0045	0.0049
2040[d]				0.0043	0.0048	0.0044	0.0047
2050[d]				0.0041	0.0046	0.0044	0.0046
2060[d]				0.0039	0.0044	0.0043	0.0045
2070[d]				0.0037	0.0042	0.0041	0.0044
2080[d]				0.0037	0.0040	0.0039	0.0043
2090[d]				0.0036	0.0039	0.0038	0.0043
2100[d]				0.0036	0.0039	0.0038	0.0042
Number of models		14		11	14	10	12

Notes:
See notes Table AII.5.3.

Table AII.5.5 | Sulphate aerosol atmospheric burden (TgS)

Year	(Min)	Historical	(Max)	RCP2.6	RCP4.5	RCP6.0	RCP8.5
1860[d]	0.09	0.61	1.42	0.60	0.61	0.57	0.60
1870[d]	0.10	0.62	1.45	0.62	0.62	0.59	0.61
1180[d]	0.12	0.65	1.49	0.64	0.65	0.61	0.64
1890[d]	0.16	0.68	1.57	0.67	0.68	0.64	0.66
1900[d]	0.21	0.73	1.65	0.73	0.73	0.70	0.72
1910[d]	0.23	0.79	1.80	0.79	0.79	0.76	0.78
1920[d]	0.23	0.83	1.84	0.83	0.83	0.80	0.81
1930[d]	0.24	0.87	1.94	0.88	0.87	0.85	0.86
1940[d]	0.25	0.93	2.05	0.95	0.93	0.91	0.92
1950[d]	0.27	1.03	2.21	1.05	1.03	1.01	1.01
1960[d]	0.31	1.25	2.67	1.29	1.25	1.24	1.23
1970[d]	0.35	1.48	3.14	1.52	1.48	1.45	1.47
1980[d]	0.37	1.58	3.33	1.62	1.58	1.54	1.58
1990[d]	0.37	1.59	3.31	1.63	1.59	1.55	1.60
2000[d]	0.37	1.55	3.17	1.59	1.55	1.53	1.56

(continued on next page)

Table AII.5.5 | *(continued)*

Year	(Min)	Historical	(Max)	RCP2.6	RCP4.5	RCP6.0	RCP8.5
2010[d]				1.57	1.59	1.52	1.54
2020[d]				1.43	1.54	1.43	1.51
2030[d]				1.21	1.44	1.33	1.44
2040[d]				1.03	1.31	1.34	1.31
2050[d]				0.94	1.16	1.29	1.20
2060[d]				0.90	1.05	1.24	1.13
2070[d]				0.86	0.96	1.06	1.08
2080[d]				0.81	0.88	0.92	1.05
2090[d]				0.76	0.85	0.86	0.98
2100[d]				0.71	0.83	0.80	0.94
Number of models		18		12	18	10	16

Notes:
See notes Table AII.5.3. The standard deviation of the models is about 50% for sulphate, OC and BC aerosol loadings (N. Mahowald, CMIP5 archive; Lamarque et al., 2013; Shindell et al., 2013).

Table AII.5.6 | OC aerosol atmospheric burden (Tg)

Year	(Min)	Historical	(Max)	RCP2.6	RCP4.5	RCP6.0	RCP8.5
1860[d]	0.34	1.08	2.7	1.09	1.08	1.13	1.12
1870[d]	0.35	1.09	2.7	1.10	1.09	1.14	1.13
1180[d]	0.36	1.09	2.7	1.11	1.09	1.15	1.14
1890[d]	0.35	1.10	2.8	1.12	1.10	1.16	1.15
1900[d]	0.36	1.11	2.8	1.12	1.11	1.16	1.15
1910[d]	0.33	1.10	2.8	1.11	1.10	1.15	1.15
1920[d]	0.34	1.08	2.7	1.09	1.08	1.12	1.13
1930[d]	0.33	1.07	2.6	1.07	1.07	1.11	1.12
1940[d]	0.33	1.07	2.6	1.07	1.07	1.11	1.12
1950[d]	0.36	1.08	2.6	1.08	1.08	1.11	1.12
1960[d]	0.41	1.13	2.7	1.13	1.13	1.17	1.17
1970[d]	0.46	1.20	2.9	1.22	1.20	1.26	1.24
1980[d]	0.54	1.28	3.1	1.32	1.28	1.36	1.33
1990[d]	0.53	1.38	3.3	1.44	1.38	1.48	1.43
2000[d]	0.53	1.41	3.5	1.47	1.41	1.52	1.46
2010[d]				1.59	1.21	1.55	1.29
2020[d]				1.59	1.12	1.56	1.26
2030[d]				1.56	1.08	1.55	1.25
2040[d]				1.47	1.06	1.57	1.22
2050[d]				1.41	1.04	1.57	1.20
2060[d]				1.40	1.01	1.56	1.17
2070[d]				1.36	0.96	1.55	1.14
2080[d]				1.33	0.92	1.55	1.13
2090[d]				1.32	0.90	1.54	1.10
2100[d]				1.30	0.89	1.55	1.09
Number of models		19		12	19	10	17

Notes:
See notes Table AII.5.5.

Table AII.5.7 | BC aerosol atmospheric burden (Tg)

Year	(Min)	Historical	(Max)	RCP2.6	RCP4.5	RCP6.0	RCP8.5
1860[d]	0.037	0.059	0.127	0.058	0.059	0.057	0.059
1870[d]	0.039	0.063	0.133	0.062	0.063	0.061	0.064
1180[d]	0.040	0.068	0.139	0.066	0.068	0.065	0.069
1890[d]	0.043	0.075	0.149	0.070	0.075	0.070	0.076
1900[d]	0.045	0.082	0.156	0.076	0.082	0.075	0.083
1910[d]	0.048	0.089	0.167	0.081	0.089	0.081	0.091
1920[d]	0.049	0.092	0.167	0.083	0.092	0.082	0.095
1930[d]	0.049	0.090	0.161	0.082	0.090	0.081	0.092
1940[d]	0.051	0.091	0.162	0.082	0.091	0.082	0.093
1950[d]	0.053	0.094	0.165	0.085	0.094	0.085	0.096
1960[d]	0.061	0.102	0.179	0.094	0.102	0.094	0.105
1970[d]	0.071	0.115	0.201	0.107	0.115	0.107	0.117
1980[d]	0.088	0.141	0.245	0.130	0.141	0.130	0.144
1990[d]	0.098	0.157	0.274	0.146	0.157	0.145	0.161
2000[d]	0.101	0.164	0.293	0.153	0.164	0.152	0.169
2010[d]				0.170	0.174	0.157	0.170
2020[d]				0.169	0.174	0.152	0.164
2030[d]				0.144	0.166	0.147	0.153
2040[d]				0.120	0.155	0.144	0.138
2050[d]				0.103	0.141	0.138	0.127
2060[d]				0.091	0.126	0.127	0.118
2070[d]				0.081	0.110	0.113	0.110
2080[d]				0.075	0.094	0.101	0.106
2090[d]				0.071	0.087	0.092	0.102
2100[d]				0.068	0.084	0.087	0.099
Number of models		19		13	19	11	17

Notes:
See notes Table AII.5.5.

Table AII.5.8 | CH_4 atmospheric lifetime (yr) against loss by tropospheric OH

Year	RCP2.6[&]	RCP4.5[&]	RCP6.0[&]	RCP8.5[&]	RCP2.6^	RCP4.5^	RCP6.0^	RCP8.5^
2000	11.2 ± 1.3	11.2 ± 1.3	11.2 ± 1.3	11.2 ± 1.3	11.2 ± 1.3	11.2 ± 1.3	11.2 ± 1.3	11.2 ± 1.3
2010	11.2 ± 1.3	11.2 ± 1.3	11.2 ± 1.3	11.2 ± 1.3				
2020	11.0 ± 1.3	11.2 ± 1.3	11.2 ± 1.3	11.2 ± 1.3				
2030	10.8 ± 1.3	11.3 ± 1.4	11.3 ± 1.4	11.4 ± 1.4	10.6 ± 1.4	11.4 ± 2.1	11.1 ± 1.4	11.2 ± 1.4
2040	10.6 ± 1.3	11.3 ± 1.4	11.4 ± 1.4	11.8 ± 1.4				
2050	10.2 ± 1.3	11.3 ± 1.4	11.5 ± 1.4	12.2 ± 1.5				
2060	9.9 ± 1.3	11.2 ± 1.4	11.6 ± 1.4	12.6 ± 1.6				
2070	9.9 ± 1.4	11.2 ± 1.5	11.8 ± 1.5	12.6 ± 1.7				
2080	10.4 ± 1.5	11.1 ± 1.5	11.9 ± 1.6	12.6 ± 1.8				
2090	10.4 ± 1.6	10.9 ± 1.6	11.7 ± 1.7	12.6 ± 1.8				
2100	10.6 ± 1.6	10.7 ± 1.6	11.4 ± 1.8	12.5 ± 1.9	10.7 ± 1.6	10.1 ± 1.5	11.1 ± 1.8	12.1 ± 2.0

Notes:
RCPn.n[&] lifetimes based on best estimate with uncertainty for 2000–2010 (Prather et al., 2012) and then projecting changes in key factors (Holmes et al., 2013). All uncertainties are 68% confidence intervals. RCPn.n^ lifetimes are from ACCMIP results (Voulgarakis et al., 2013) scaled to 11.2 ± 1.3 yr for year 2000; the ACCMIP mean and standard deviation in 2000 are 9.8 ± 1.5 yr. Projected ACCMIP values combine the present day uncertainty with the model standard deviation of future change. Note that the total atmospheric lifetime of CH_4 must include other losses (e.g., stratosphere, surface, tropospheric chlorine), and for 2010 it is 9.1 ± 0.9 yr, see Chapter 8, Section 11.3.5.1.1.

Table AII.5.9 | N_2O atmospheric lifetime (yr)

Year	RCP2.6[&]	RCP4.5[&]	RCP6.0[&]	RCP8.5[&]
2010	131 ± 10	131 ± 10	131 ± 10	131 ± 10
2020	130 ± 10	131 ± 10	131 ± 10	131 ± 10
2030	130 ± 10	130 ± 10	130 ± 10	130 ± 10
2040	130 ± 10	130 ± 10	130 ± 10	129 ± 10
2050	129 ± 10	129 ± 10	129 ± 10	129 ± 10
2060	129 ± 10	129 ± 10	129 ± 10	128 ± 10
2070	129 ± 11	128 ± 11	128 ± 10	128 ± 11
2080	128 ± 11	128 ± 11	128 ± 11	127 ± 11
2090	128 ± 11	128 ± 11	127 ± 11	127 ± 11
2100	128 ± 11	127 ± 11	127 ± 11	126 ± 11

Notes:
RCPn.n[&] lifetimes based on projections from Fleming et al. (2011) and Prather et al. (2012). All uncertainties are 68% confidence intervals.

AII.6: Effective Radiative Forcing

Table AII.6.1 | ERF from CO_2 (W m^{-2})

Year	RCP2.6	RCP4.5	RCP6.0	RCP8.5	A2	B1	IS92a
2000	1.51	1.51	1.51	1.51	1.50	1.50	1.50
2010	1.80	1.80	1.80	1.80	1.78	1.77	1.78
2020	2.11	2.09	2.07	2.15	2.16	2.09	2.13
2030	2.34	2.40	2.32	2.56	2.55	2.38	2.48
2040	2.46	2.70	2.58	3.03	2.99	2.69	2.83
2050	2.49	2.99	2.90	3.56	3.42	2.98	3.18
2060	2.48	3.23	3.25	4.15	3.88	3.20	3.53
2070	2.43	3.39	3.65	4.76	4.36	3.37	3.89
2080	2.35	3.46	4.06	5.37	4.86	3.49	4.25
2090	2.28	3.49	4.42	5.95	5.39	3.57	4.64
2100	2.22	3.54	4.70	6.49	5.95	3.59	5.04

Notes:
RCPn.n ERF based on RCP published projections (Tables AII.4.1 to AII.4.3) and TAR formula for RF. See Chapter 8, Figure 8.18, Section 11.3.5, 11.3.6.1, Figure 12.3. SRES A2 and B1 and IS92a calculated from abundances in Tables AII.4.1 to AII.4.3.

Table AII.6.2 | ERF from CH_4 (W m^{-2})

Year	RCP2.6	RCP4.5	RCP6.0	RCP8.5	A2	B1	IS92a
2000	0.47	0.47	0.47	0.47	0.48	0.48	0.48
2010	0.48	0.48	0.48	0.48	0.51	0.50	0.51
2020	0.47	0.49	0.49	0.54	0.56	0.53	0.56
2030	0.42	0.50	0.49	0.61	0.62	0.54	0.61
2040	0.39	0.51	0.51	0.70	0.68	0.54	0.67
2050	0.36	0.50	0.53	0.80	0.75	0.52	0.73
2060	0.32	0.49	0.54	0.90	0.81	0.51	0.78
2070	0.30	0.47	0.55	0.97	0.88	0.49	0.82
2080	0.29	0.44	0.54	1.01	0.95	0.47	0.85
2090	0.28	0.42	0.50	1.05	1.01	0.44	0.88
2100	0.27	0.41	0.44	1.08	1.07	0.41	0.92

Notes:
See notes Table AII.6.1.

Table AII.6.3 | ERF from N_2O (W m^{-2})

Year	RCP2.6	RCP4.5	RCP6.0	RCP8.5	A2	B1	IS92a
2000	0.15	0.15	0.15	0.15	0.15	0.15	0.15
2010	0.17	0.17	0.17	0.17	0.17	0.17	0.17
2020	0.19	0.19	0.19	0.19	0.20	0.20	0.20
2030	0.20	0.21	0.21	0.23	0.24	0.22	0.23
2040	0.22	0.23	0.24	0.26	0.28	0.25	0.26
2050	0.23	0.25	0.26	0.30	0.32	0.27	0.29
2060	0.23	0.27	0.29	0.34	0.36	0.29	0.32
2070	0.23	0.28	0.33	0.38	0.40	0.30	0.34
2080	0.23	0.30	0.36	0.42	0.44	0.31	0.37
2090	0.23	0.31	0.39	0.46	0.49	0.32	0.39
2100	0.23	0.32	0.41	0.49	0.53	0.32	0.41

Notes:
See notes Table AII.6.1.

Table AII.6.4 | ERF from all HFCs (W m^{-2})

Year	Historical	RCP2.6	RCP4.5	RCP6.0	RCP8.5
2011*	0.019				
2010		0.019	0.019	0.019	0.020
2020		0.038	0.034	0.030	0.044
2030		0.056	0.046	0.036	0.069
2040		0.071	0.055	0.040	0.091
2050		0.083	0.061	0.042	0.110
2060		0.092	0.064	0.044	0.128
2070		0.104	0.066	0.046	0.144
2080		0.116	0.069	0.047	0.159
2090		0.124	0.074	0.047	0.171
2100		0.126	0.080	0.046	0.182

Notes:
See Table 8.3, 8.A.1, Section 11.3.5.1.1. ERF is calculated from RCP published abundances (Meinshausen et al., 2011a; http://www.iiasa.ac.at/web-apps/tnt/RcpDb) and AR5 radiative efficiencies (Chapter 8).

Table AII.6.5 | ERF from all PFCs and SF_6 (W m^{-2})

Year	Historical	RCP2.6	RCP4.5	RCP6.0	RCP8.5
2011*	0.009				
2010		0.009	0.009	0.010	0.009
2020		0.012	0.011	0.013	0.012
2030		0.014	0.013	0.017	0.015
2040		0.015	0.014	0.021	0.019
2050		0.015	0.016	0.025	0.022
2060		0.016	0.017	0.029	0.026
2070		0.016	0.019	0.033	0.031
2080		0.016	0.021	0.038	0.035
2090		0.016	0.023	0.042	0.039
2100		0.016	0.026	0.045	0.044

Notes:
See notes Table AII.6.4.

Table AII.6.6 | ERF from Montreal Protocol greenhouse gases (W m^{-2})

Year	Historical	WMO A1
2011*	0.328	
2020		0.33 ± 0.01
2030		0.29 ± 0.01
2040		0.24 ± 0.01
2050		0.20 ± 0.01
2060		0.17 ± 0.02
2070		0.15 ± 0.02
2080		0.13 ± 0.02
2090		0.11 ± 0.02
2100		0.10 ± 0.02

Notes:

See Table 8.3, 8.A.1. ERF is calculated from AR5 radiative efficiency and projected abundances in Scenario A1 of WMO/UNEP assessment (WMO 2010). The 68% confidence interval shown is approximated by combining uncertainty in the radiative efficiency of each gas (±6.1%) and the decay of each gas since 2010 from Table AII.4.16 (±15%). All sources of uncertainty are assumed to be independent (see Chapters 2 and 8).

Table AII.6.7a | ERF from stratospheric O_3 changes since 1850 (W m^{-2})

Year	AR5	CCMVal-2
1960		0.0
1980		–0.033
2000		–0.079
2011*	–0.05	
2050		–0.055
2100		–0.075

Notes:

AR5 results are from Chapter 8, see also Sections 11.3.5.1.2, 11.3.6.1. CCMVal-2 results (Cionni et al. 2011) are the multi-model average (13 chemistry–climate models) running a single scenario for stratospheric change: REF-B2 scenario of CCMVal-2 with SRES A1B climate scenario.

Table AII.6.7b | ERF from tropospheric O_3 changes since 1850 (W m^{-2})

Year	AR5	RCP2.6	RCP4.5	RCP6.0	RCP8.5
1980		0.31 ± 0.05	0.31 ± 0.05	0.31 ± 0.05	0.31 ± 0.05
2000		0.36	0.36	0.36	0.36
2011*	0.40				
2030		0.32	0.38	0.36	0.44
2100		0.17	0.27	0.27	0.60 ± 0.11

Notes:

AR5 results from Chapter 8; see also Sections 11.3.5.1.2, 11.3.6.1. Model mean results from ACCMIP (Stevenson et al., 2013) using a consistent model set (FGKN), which is similar to the all-model mean. Standard deviation across models shown for 1980s decade is similar for all scenarios except for RCP8.5 at 2100, which is twice as large.

Table AII.6.8: Total anthropogenic ERF from published RCPs and SRES (W m^{-2})

Year	RCP2.6	RCP4.5	RCP6.0	RCP8.5	A2	A1B	B1	IS92a	AR5 Historical
1850	0.12	0.12	0.12	0.12					0.06
1990	1.23	1.23	1.23	1.23	1.03	1.03	1.03	1.03	1.60
2000	1.45	1.45	1.45	1.45	1.33	1.33	1.33	1.31	1.87
2010	1.81	1.81	1.78	1.84	1.74	1.65	1.73	1.63	2.25
2020	2.25	2.25	2.15	2.32	2.04	2.16	2.15	2.00	
2030	2.52	2.67	2.52	2.91	2.56	2.84	2.56	2.40	
2040	2.65	3.07	2.82	3.61	3.22	3.61	2.93	2.82	
2050	2.64	3.42	3.20	4.37	3.89	4.16	3.30	3.25	
2060	2.55	3.67	3.58	5.13	4.71	4.79	3.65	3.76	
2070	2.47	3.84	4.11	5.89	5.56	5.28	3.92	4.24	
2080	2.41	3.90	4.60	6.60	6.40	5.62	4.09	4.74	
2090	2.35	3.91	4.93	7.32	7.22	5.86	4.18	5.26	
2100	2.30	3.94	5.15	7.97	8.07	6.05	4.19	5.79	

Notes:

Derived from RCP published CO_2-eq concentrations that aggregate all anthropogenic forcings including greenhouse gases plus aerosols. These results may not be directly comparable to ERF values used in AR5 because of how aerosol indirect effects are included, but results are similar to those derived using ERF in Chapter 12 (see Figure 12.4). Comparisons with the TAR Appendix II (SRES A2 and B1) may not be equivalent because those total RF values (TAR II.3.11) were made using the TAR Chapter 9 Simple Model, not always consistent with the individual components in that appendix (TAR II.3.1 to 9). See Chapter 1, Sections 11.3.6.1, 12.3.1.3 and 12.3.1.4, Figures 1.15 and 12.3. For AR5 Historical, see Table AII.1.2 and Chapter 8.

Table AII.6.9: ERF components relative to 1850 (W m^{-2}) derived from ACCMIP

Year		WMGHG	Ozone	Aerosol	ERF Net
1930		0.58 ± 0.04	0.09 ± 0.03	–0.24 ± 0.06	0.44 ± 0.07
1980		1.56 ± 0.10	0.30 ± 0.10	–0.90 ± 0.22	1.00 ± 0.26
2000		2.30 ± 0.14	0.33 ± 0.11	–1.17 ± 0.28	1.51 ± 0.33
2030	RCP8.5	3.64 ± 0.22	0.43 ± 0.12	–0.91 ± 0.22	3.20 ± 0.33
2100	RCP2.6	2.83 ± 0.17	0.14 ± 0.07	–0.12 ± 0.06*	2.86 ± 0.19
2100	RCP4.5	4.33 ± 0.26	0.23 ± 0.09	–0.12 ± 0.06*	4.44 ± 0.28
2100	RCP6.0	5.60 ± 0.34	0.25 ± 0.05	–0.12 ± 0.06*	5.74 ± 0.35
2100	RCP8.5	8.27 ± 0.50	0.55 ± 0.18	–0.12 ± 0.03	8.71 ± 0.53

Notes:

Radiative forcing and adjusted forcing from the ACCMIP results (Shindell et al., 2013) are given for all well-mixed greenhouse gases (WMGHG), ozone, aerosols, and the net. Original 90% confidence intervals have been reduced to 68% confidence to compare with the CMIP5 model standard deviations in Table AII.6.10. Some uncertainty ranges (*) are estimated from the 2100 RCP8.5 results (see Chapter 12). See Sections 11.3.5.1.3 and 11.3.6.1, Figure 12.4.

Table AII.6.10 | Total anthropogenic plus natural ERF (W m^{-2}) from CMIP5 and CMIP3, including historical

Year	SRES A1B	RCP2.6[&]	RCP4.5[&]	RCP6.0[&]	RCP8.5[&]
1850s[H]	–0.19 ± 0.19	–0.12 ± 0.07			
1986–2005[H]	1.51 ± 0.44	1.34 ± 0.50			
1986–2005	1.51 ± 0.44	1.31 ± 0.47	1.30 ± 0.48	1.29 ± 0.51	1.30 ± 0.47
2010[d]	2.18 ± 0.53	1.97 ± 0.50	1.91 ± 0.53	1.90 ± 0.54	1.96 ± 0.53
2020[d]	2.58 ± 0.57	2.33 ± 0.47	2.27 ± 0.51	2.16 ± 0.55	2.43 ± 0.52
2030[d]	3.15 ± 0.60	2.50 ± 0.51	2.61 ± 0.54	2.41 ± 0.60	2.92 ± 0.57
2040[d]	3.77 ± 0.72	2.64 ± 0.47	2.98 ± 0.55	2.72 ± 0.58	3.52 ± 0.60
2050[d]	4.32 ± 0.73	2.65 ± 0.47	3.25 ± 0.56	3.07 ± 0.61	4.21 ± 0.63
2060[d]	4.86 ± 0.74	2.57 ± 0.50	3.50 ± 0.59	3.40 ± 0.60	4.97 ± 0.68
2070[d]	5.32 ± 0.79	2.51 ± 0.50	3.65 ± 0.58	3.90 ± 0.65	5.70 ± 0.76
2080[d]	5.71 ± 0.81	2.40 ± 0.46	3.71 ± 0.55	4.27 ± 0.69	6.31 ± 0.81
2090[d]	6.00 ± 0.83	2.44 ± 0.49	3.78 ± 0.58	4.64 ± 0.71	7.13 ± 0.89
2081–2100	5.99 ± 0.78	2.40 ± 0.46	3.73 ± 0.56	4.56 ± 0.70	7.02 ± 0.92

Notes:

CMIP5 historical and RCP results (Forster et al., 2013) are shown with CMIP3 SRES A1B results (Forster and Taylor, 2006). The alternative results for 1986–2005 with CMIP5 are derived from: all models contributing historical experiments (1986–2005[H]), and the subsets of models contributing to each RCP experiment (next line, 1986–2005). For SRES A1B the same set of models is used from 1850 to 2100. Values are 10-year averages (2090[d] = 2086–2095) and show multi-model means and standard deviations. See Chapter 12, Section 12.3 and discussion of Figure 12.4, also Sections 8.1, 9.3.2.2, 11.3.6.1 and 11.3.6.3. Due to lack of reporting, for RCP8.5 the 2081–2100 result contains one fewer model than the 2090d decade, and for A1B the 1850s result has just 5 models and the 2081–2100 result has 3 fewer models than the 2090[d] decade.

AII.7: Environmental Data

Table AII.7.1 | Global mean surface O_3 change (ppb)

	HTAP				SRES			
Year	RCP2.6	RCP4.5	RCP6.0	RCP8.5	A2	B1	CLE	MFR
2000	27.2 ± 2.9	27.2 ± 2.9	27.2 ± 2.9	27.2 ± 2.9	27.2 ± 2.9	27.2 ± 2.9	28.7	28.7
2010	0.1	0.1	0.0	0.1	1.2	0.6		
2020	–0.3	–0.2	–0.2	0.6	2.8	1.1		
2030	–1.1	–0.1	–0.3	1.0	4.4	1.3	0.7 ± 1.4	–2.3 ± 1.1
2040	–1.5	–0.3	–0.3	1.2	5.3	1.3		
2050	–1.9	–0.8	–0.4	1.5	6.2	0.8		
2060	–2.4	–1.3	–0.5	1.8	7.1	0.2		
2070	–3.0	–1.9	–1.0	1.9	8.0	–0.5		
2080	–3.5	–2.5	–1.5	1.9	9.2	–1.1		
2090	–3.8	–2.8	–2.1	1.9	10.6	–1.7		
2100	–4.2	–3.0	–2.8	1.9	11.9	–2.5		

	CMIP5				ACCMIP			
Year	RCP2.6	RCP4.5	RCP6.0	RCP8.5	RCP2.6	RCP4.5	RCP6.0	RCP8.5
2000	30.0 ± 4.2	30.0 ± 4.2	30.0 ± 4.2	30.0 ± 4.2	28.1 ± 3.1	28.1 ± 3.2	28.1± 3.1	28.1 ± 3.1
2010	–0.4	–0.2	–0.6	–0.1				
2020	–0.9	–0.3	–0.9	0.7				
2030	–1.8	–0.2	–1.1	1.5	–1.4	0.3	–0.6	1.7
2040	–2.3	–0.3	–1.2	2.0				
2050	–2.9	–0.9	–1.5	2.5				
2060	–4.0	–1.7	–1.9	2.9				
2070	–5.4	–2.8	–2.8	3.1				
2080	–6.4	–3.7	–3.9	3.0				
2090	–6.9	–4.1	–4.8	2.8				
2100	–7.2	–4.3	–5.6	2.7	–6.3	–3.5	–4.9	3.4

Notes:

HTAP results are from Wild et al. (2012) and use the published O_3 sensitivities to regional emissions from the HTAP multi-model study (HTAP 2010) and scale those O_3 changes to the RCP emission scenarios. The ±1 standard deviation (68% confidence interval) over the range of 14 parametric models is shown for year 2000 and is similar for all years. Results from the SRES A2 and B1 scenarios are from the TAR OxComp studies diagnosed by Wild (Prather et al., 2001; 2003). CLE and MFR results (Dentener et al., 2005; 2006) include uncertainty (standard deviation of model results) in the change since year 2000, and CLE alone includes climate effects. The CMIP5 and ACCMIP results are from V. Naik and A. Fiore based on Fiore et al. (2012) and include the standard deviation over the models in year 2000, which is similar for following years. This does not necessarily reflect the uncertainty in the projected change, which may be smaller, see Fiore et al. (2012). The difference in year 2000 between CMIP5 (4 models) and ACCMIP (12 models) reflect different model biases. Even though ACCMIP only has three decades (2000, 2030, 2100), the greater number of models (5 to 11 depending on time slice and scenario) makes this a more robust estimate. See Chapter 11, ES, Section 11.3.5.2.2.

Table AII.7.2 | Surface O_3 change (ppb) for HTAP regions

North America						
Year	**RCP2.6**	**RCP4.5**	**RCP6.0**	**RCP8.5**	**A2**	**B1**
2000	36.1 ± 3.2	36.1 ± 3.2	36.1 ± 3.2	36.1 ± 3.2	36.1 ± 3.2	36.1 ± 3.2
2010	–0.8	–1.1	–0.1	–1.5	1.5	0.4
2020	–1.9	–2.3	–0.9	–1.4	3.6	0.5
2030	–3.7	–2.7	–1.5	–1.1	5.3	–0.1
2040	–4.6	–3.2	–1.9	–1.1	6.2	–0.8
2050	–5.6	–3.9	–2.4	–0.9	6.9	–1.9
2060	–6.5	–4.6	–3.0	–0.7	7.9	–2.9
2070	–7.5	–5.3	–4.0	–0.7	8.8	–3.8
2080	–8.2	–6.1	–4.9	–0.7	10.3	–4.5
2090	–8.5	–6.4	–5.7	–0.8	12.2	–5.2
2100	–8.9	–6.6	–6.7	–0.9	13.9	–6.1

Europe						
Year	**RCP2.6**	**RCP4.5**	**RCP6.0**	**RCP8.5**	**A2**	**B1**
2000	37.8 ± 3.7	37.8 ± 3.7	37.8 ± 3.7	37.8 ± 3.7	37.8 ± 3.7	37.8 ± 3.7
2010	–0.5	–0.3	–0.1	–0.7	1.5	0.3
2020	–1.4	–1.3	–0.7	–0.2	3.7	0.6
2030	–3.0	–1.4	–1.1	0.1	5.7	0.2
2040	–3.8	–1.9	–1.5	0.1	6.7	–0.3
2050	–4.6	–2.7	–2.0	0.3	7.7	–1.2
2060	–5.6	–3.5	–2.6	0.4	8.8	–2.1
2070	–6.6	–4.3	–3.3	0.4	9.8	–3.0
2080	–7.5	–5.1	–4.2	0.2	11.3	–3.8
2090	–8.0	–5.6	–5.2	–0.1	13.4	–4.6
2100	–8.5	–6.0	–6.4	–0.2	15.1	–5.6

South Asia						
Year	**RCP2.6**	**RCP4.5**	**RCP6.0**	**RCP8.5**	**A2**	**B1**
2000	39.6 ± 3.4	39.6 ± 3.4	39.6 ± 3.4	39.6 ± 3.4	39.6 ± 3.4	39.6 ± 3.4
2010	1.5	1.4	0.3	1.4	2.7	1.8
2020	1.6	2.2	0.0	3.9	6.1	3.3
2030	0.5	3.4	–0.6	5.0	8.9	3.9
2040	0.3	3.5	–0.1	5.5	10.4	4.1
2050	0.2	2.9	0.0	5.2	11.7	2.9
2060	–0.1	1.1	0.4	5.1	12.7	1.5
2070	–1.0	–1.2	–0.2	4.9	13.6	–0.1
2080	–2.6	–3.9	–1.7	4.9	14.5	–1.5
2090	–4.4	–5.0	–3.0	4.1	15.1	–3.0
2100	–6.8	–6.0	–4.7	4.0	15.0	–4.6

(continued on next page)

Table AII.7.2 | *(continued)*

East Asia						
Year	**RCP2.6**	**RCP4.5**	**RCP6.0**	**RCP8.5**	**A2**	**B1**
2000	35.6 ± 2.7	35.6 ± 2.7	35.6 ± 2.7	35.6 ± 2.7	35.6 ± 2.7	35.6 ± 2.7
2010	1.0	0.6	0.5	1.3	2.0	1.1
2020	0.5	0.6	0.4	2.5	4.6	1.9
2030	–1.4	0.2	0.6	2.8	6.8	2.1
2040	–2.7	–0.8	1.4	1.8	8.0	2.0
2050	–3.8	–2.5	1.4	1.4	9.1	0.9
2060	–4.8	–3.6	0.9	1.4	10.2	–0.3
2070	–6.0	–4.6	–0.7	1.2	11.2	–1.4
2080	–6.9	–5.5	–2.2	1.0	12.5	–2.4
2090	–7.4	–5.8	–3.5	0.7	13.9	–3.4
2100	–8.0	–6.0	–4.9	0.5	14.9	–4.6

Notes:
HTAP results from Wild et al. (2012); see Table AII.7.1.

Table AII.7.3 | Surface O_3 change (ppb) from CMIP5/ACCMIP for continental regions

Africa								
	CMIP5				**ACCMIP**			
Year	**RCP2.6**	**RCP4.5**	**RCP6.0**	**RCP8.5**	**RCP2.6**	**RCP4.5**	**RCP6.0**	**RCP8.5**
2000	33.8 ± 4.3	33.8 ± 4.3	33.8 ± 4.3	33.8 ± 4.3	33.1 ± 4.1	33.1 ± 4.1	33.1 ± 4.1	33.1 ± 4.1
2010	–0.7	–0.1	–1.2	–0.2				
2020	–1.0	0.2	–1.5	0.9				
2030	–1.9	0.5	–1.8	1.7	–1.4	0.9	–1.3	2.4
2040	–2.0	0.6	–1.8	2.6				
2050	–2.3	0.2	–2.0	3.2				
2060	–2.6	–0.3	–2.2	3.7				
2070	–3.2	–1.2	–2.8	4.0				
2080	–3.6	–2.3	–3.7	4.1				
2090	–4.1	–3.0	–4.5	4.1				
2100	–4.8	–3.3	–5.2	4.1	–4.9	–2.9	–4.9	5.0

Australia								
	CMIP5				**ACCMIP**			
Year	**RCP2.6**	**RCP4.5**	**RCP6.0**	**RCP8.5**	**RCP2.6**	**RCP4.5**	**RCP6.0**	**RCP8.5**
2000	23.3 ± 4.6	23.3 ± 4.6	23.3 ± 4.6	23.3 ± 4.6	23.7 ± 3.5	23.7 ± 3.5	23.7 ± 3.5	23.7 ± 3.5
2010	–1.3	–1.1	–0.8	–0.9				
2020	–1.7	–1.4	–1.0	–0.6				
2030	–2.3	–1.3	–1.4	0.0	–1.8	–0.4	–1.4	0.9
2040	–2.6	–1.2	–1.7	0.5				
2050	–3.0	–1.5	–1.9	0.9				
2060	–3.7	–1.9	–2.0	1.5				
2070	–4.4	–2.4	–2.5	1.8				
2080	–5.0	–2.9	–3.1	1.9				
2090	–5.0	–3.1	–3.5	1.9				
2100	–5.2	–3.2	–4.0	2.0	–4.3	–2.5	–4.0	3.1

(continued on next page)

Table AII.7.3 | *(continued)*

Central Eurasia								
	CMIP5				ACCMIP			
Year	RCP2.6	RCP4.5	RCP6.0	RCP8.5	RCP2.6	RCP4.5	RCP6.0	RCP8.5
2000	38.7 ± 5.3	38.7 ± 5.3	38.7 ± 5.3	38.7 ± 5.3	32.5 ± 6.2	32.5 ± 6.2	32.5 ± 6.2	32.5 ± 6.2
2010	–0.6	–0.6	–0.6	–0.5				
2020	–1.6	–1.2	–1.2	0.5				
2030	–3.2	–1.3	–1.4	1.4	–1.9	–0.1	–0.3	1.8
2040	–4.5	–1.9	–1.7	1.6				
2050	–5.7	–2.9	–2.2	1.8				
2060	–7.2	–4.2	–3.0	2.8				
2070	–9.1	–5.4	–4.3	3.0				
2080	–10.6	–6.5	–6.0	2.9				
2090	–11.2	–6.8	–7.2	2.6				
2100	–11.5	–7.0	–8.1	2.6	–8.5	–3.8	–5.6	4.3

Europe								
	CMIP5				ACCMIP			
Year	RCP2.6	RCP4.5	RCP6.0	RCP8.5	RCP2.6	RCP4.5	RCP6.0	RCP8.5
2000	40.4 ± 6.0	40.4 ± 6.0	40.4 ± 6.0	40.4 ± 6.0	33.6 ± 5.2	33.6 ± 5.2	33.6 ± 5.2	33.6 ± 5.2
2010	–0.4	–0.5	–0.5	–0.4				
2020	–1.5	–1.3	–1.2	0.3				
2030	–3.2	–1.7	–1.7	1.1	–1.6	0.6	–0.4	2.3
2040	–4.6	–2.4	–2.3	1.4				
2050	–6.1	–3.5	–3.0	1.8				
2060	–8.0	–4.9	–4.1	2.4				
2070	–10.4	–6.3	–5.8	2.6				
2080	–12.2	–7.6	–7.6	2.3				
2090	–13.0	–8.0	–9.2	2.1				
2100	–13.4	–8.1	–10.3	2.0	–9.4	–3.5	–7.2	4.9

East Asia								
	CMIP5				ACCMIP			
Year	RCP2.6	RCP4.5	RCP6.0	RCP8.5	RCP2.6	RCP4.5	RCP6.0	RCP8.5
2000	46.3 ± 4.9	46.3 ± 4.9	46.3 ± 4.9	46.3 ± 4.9	41.0 ± 5.5	41.0 ± 5.5	41.0 ± 5.5	41.0 ± 5.5
2010	0.8	0.6	0.1	1.1				
2020	–0.1	0.8	–0.1	2.7				
2030	–2.3	0.5	0.4	3.8	–1.8	1.0	0.4	3.2
2040	–3.9	–0.9	1.1	3.8				
2050	–5.8	–3.3	1.0	3.7				
2060	–8.0	–5.4	0.2	3.9				
2070	–10.2	–7.3	–1.6	3.6				
2080	–12.1	–8.8	–4.0	3.3				
2090	–13.2	–9.4	–6.3	2.9				
2100	–13.9	–9.6	–8.0	2.8	–11.4	–5.9	–6.6	4.6

(continued on next page)

Table AII.7.3 | *(continued)*

Middle East								
	CMIP5				ACCMIP			
Year	RCP2.6	RCP4.5	RCP6.0	RCP8.5	RCP2.6	RCP4.5	RCP6.0	RCP8.5
2000	45.9 ± 3.1	45.9 ± 3.1	45.9 ± 3.1	45.9 ± 3.1	45.7 ± 5.4	45.7 ± 5.4	45.7 ± 5.4	45.7 ± 5.4
2010	–0.4	0.5	–0.7	0.5				
2020	–1.5	0.4	–1.4	2.5				
2030	–3.3	0.6	–1.6	3.8	–2.8	0.9	–1.1	4.1
2040	–3.6	0.2	–2.0	4.4				
2050	–4.6	–0.9	–2.6	4.7				
2060	–6.0	–2.7	–3.5	5.2				
2070	–8.1	–4.9	–4.2	5.1				
2080	–9.9	–7.1	–5.9	5.1				
2090	–11.3	–8.4	–8.2	4.8				
2100	–12.4	–9.0	–9.9	4.6	–11.7	–7.5	–9.8	5.0

North America								
	CMIP5				ACCMIP			
Year	RCP2.6	RCP4.5	RCP6.0	RCP8.5	RCP2.6	RCP4.5	RCP6.0	RCP8.5
2000	40.7 ± 5.1	40.7 ± 5.1	40.7 ± 5.1	40.7 ± 5.1	34.3 ± 5.5	34.3 ± 5.5	34.3 ± 5.5	34.3 ± 5.5
2010	–0.9	–1.2	–0.6	–1.0				
2020	–2.1	–2.4	–1.4	–0.5				
2030	–4.3	–2.8	–1.8	0.1	–2.5	–0.7	–0.8	1.3
2040	–5.7	–3.6	–2.5	0.3				
2050	–7.2	–4.6	–3.1	0.6				
2060	–9.1	–5.8	–4.4	1.0				
2070	–11.4	–7.1	–6.2	1.2				
2080	–13.2	–8.3	–8.1	1.2				
2090	–13.8	–8.5	–9.6	1.0				
2100	–14.1	–8.8	–10.9	0.9	–10.5	–4.7	–8.7	3.4

South America								
	CMIP5				ACCMIP			
Year	RCP2.6	RCP4.5	RCP6.0	RCP8.5	RCP2.6	RCP4.5	RCP6.0	RCP8.5
2000	25.3 ± 4.2	25.3 ± 4.2	25.3 ± 4.2	25.3 ± 4.2	23.7 ± 3.9	23.7 ± 3.9	23.7 ± 3.9	23.7 ± 3.9
2010	–1.4	–0.6	–1.2	–0.3				
2020	–2.1	–1.2	–1.8	0.3				
2030	–2.9	–1.2	–2.1	0.6	–2.3	–0.6	–1.8	1.2
2040	–2.9	–1.3	–2.3	1.1				
2050	–3.2	–1.7	–2.6	1.3				
2060	–3.6	–2.5	–2.9	1.5				
2070	–4.3	–3.6	–3.5	1.5				
2080	–5.1	–4.5	–4.2	1.1				
2090	–5.5	–5.0	–4.7	0.7				
2100	–5.7	–5.2	–5.3	0.4	–5.0	–4.0	–5.2	2.0

(continued on next page)

Table AII.7.3 | *(continued)*

South Asia								
	CMIP5				ACCMIP			
Year	RCP2.6	RCP4.5	RCP6.0	RCP8.5	RCP2.6	RCP4.5	RCP6.0	RCP8.5
2000	34.4 ± 3.9	34.4 ± 3.9	34.4 ± 3.9	34.4 ± 3.9	33.7 ± 4.6	33.7 ± 4.6	33.7 ± 4.6	33.7 ± 4.6
2010	1.3	0.9	–0.1	1.3				
2020	1.4	1.6	–0.2	3.1				
2030	0.7	2.7	–0.1	3.9	0.6	2.3	–0.4	4.6
2040	0.6	2.8	0.3	4.0				
2050	0.4	1.6	0.4	3.6				
2060	–0.5	–0.7	0.3	3.2				
2070	–2.0	–3.2	–0.5	2.9				
2080	–3.9	–5.7	–2.0	2.7				
2090	–5.7	–6.7	–3.3	2.2				
2100	–7.1	–7.3	–4.5	1.9	–7.2	–6.1	–4.5	3.6

Notes:
See notes for Table AII.7.1. For definition of regions, see Figure 11.23 and Fiore et al. (2012).

Table AII.7.4 | Surface particulate matter change ($\log_{10}$[$PM_{2.5}$ (microgram/m^3)]) from CMIP5/ACCMIP for continental regions

Africa				
Year	RCP2.6	RCP4.5	RCP6.0	RCP8.5
2000	1.17 ± 0.23			
2030	0.00	0.04	–0.01	0.01
2050	–0.02		–0.02	0.01
2100	0.00	–0.01	–0.03	–0.02

Australia				
Year	RCP2.6	RCP4.5	RCP6.0	RCP8.5
2000	0.65 ± 0.32			
2030	–0.04	0.03	–0.01	0.01
2050	–0.06		–0.02	–0.04
2100	0.00	0.00	–0.03	–0.01

Central Eurasia				
Year	RCP2.6	RCP4.5	RCP6.0	RCP8.5
2000	0.59 ± 0.17			
2030	–0.07	–0.01	–0.05	–0.06
2050	–0.12		–0.08	–0.09
2100	–0.13	–0.11	–0.11	–0.12

Europe				
Year	RCP2.6	RCP4.5	RCP6.0	RCP8.5
2000	0.81 ± 0.09			
2030	–0.20	–0.10	–0.13	–0.24
2050	–0.31		–0.25	–0.33
2100	–0.32	–0.28	–0.37	–0.38

(continued on next page)

Table AII.7.4 | *(continued)*

East Asia				
Year	**RCP2.6**	**RCP4.5**	**RCP6.0**	**RCP8.5**
2000	1.04 ± 0.16			
2030	–0.04	–0.02	0.01	0.01
2050	–0.24		0.07	–0.17
2100	–0.31	–0.33	–0.21	–0.30

Middle East				
Year	**RCP2.6**	**RCP4.5**	**RCP6.0**	**RCP8.5**
2000	1.10 ± 0.27			
2030	–0.06	–0.02	–0.05	–0.03
2050	–0.08		–0.06	–0.03
2100	–0.11	–0.11	–0.10	–0.12

North America				
Year	**RCP2.6**	**RCP4.5**	**RCP6.0**	**RCP8.5**
2000	0.51 ± 0.15			
2030	–0.16	–0.10	–0.10	–0.15
2050	–0.20		–0.16	–0.17
2100	–0.20	–0.19	–0.24	–0.21

South America				
Year	**RCP2.6**	**RCP4.5**	**RCP6.0**	**RCP8.5**
2000	0.71 ± 0.11			
2030	–0.05	–0.04	–0.04	–0.03
2050	–0.10		–0.05	–0.07
2100	–0.11	–0.11	–0.09	–0.12

South Asia				
Year	**RCP2.6**	**RCP4.5**	**RCP6.0**	**RCP8.5**
2000	1.02 ± 0.11			
2030	0.04	0.02	0.03	0.05
2050	–0.05		0.07	0.00
2100	–0.16	–0.24	–0.06	–0.11

Notes:

Decadal average of the $\log_{10}[PM_{2.5}]$ values are given only where results include at least four models from either ACCMIP or CMIP5. Results are from A. Fiore and V. Naik based on Fiore et al. (2012) using the CMIP5/ACCMIP archive. Due to the very large systematic spread across models, the statistics were calculated for the log values, but Figure 11.23 shows statistics for direct $PM_{2.5}$ values. Owing to the large spatial variations no global average is given. Model mean and standard deviation are shown for year 2000; differences in $\log_{10}[PM_{2.5}]$ are shown for 2030, 2050 and 2100. See notes for Table AII.7.3 and Figure 11.23 for regions; see also Chapter 11, ES.

Table AII.7.5 | CMIP5 (RCP) and CMIP3 (SRES A1B) global mean surface temperature change (°C) relative to 1986–2005 reference period. Results here are a statistical summary of the spread in the CMIP ensembles for each of the scenarios. They do not account for model biases and model dependencies, and the percentiles do not correspond to the assessed uncertainty in Chapters 11 (11.3.6.3) and 12 (12.4.1). The statistical spread across models cannot be interpreted as uncertainty ranges or in terms of calibrated language (Section 12.2).

	RCP2.6					RCP4.5				
Years	**5%**	**17%**	**50%**	**83%**	**95%**	**5%**	**17%**	**50%**	**83%**	**95%**
1850–1990			–0.61					–0.61		
1986–2005			0.00					0.00		
2010d	0.19	0.33	0.36	0.52	0.62	0.22	0.26	0.36	0.48	0.59
2020d	0.36	0.45	0.55	0.81	1.07	0.39	0.48	0.59	0.74	0.83
2030d	0.47	0.56	0.74	1.02	1.24	0.56	0.69	0.82	1.10	1.22
2040d	0.51	0.68	0.88	1.25	1.50	0.64	0.86	1.04	1.35	1.57
2050d	0.49	0.71	0.94	1.37	1.65	0.84	1.05	1.24	1.63	1.97
2060d	0.36	0.69	0.93	1.48	1.71	0.90	1.13	1.44	1.90	2.19
2070d	0.20	0.70	0.89	1.49	1.71	0.98	1.20	1.54	2.07	2.32
2080d	0.15	0.62	0.94	1.44	1.79	0.98	1.27	1.62	2.25	2.54
2090d	0.18	0.58	0.94	1.53	1.79	1.06	1.33	1.68	2.29	2.59

	RCP6.0					RCP8.5				
Years	**5%**	**17%**	**50%**	**83%**	**95%**	**5%**	**17%**	**50%**	**83%**	**95%**
1850–1990			–0.61					–0.61		
1986–2005			0.00					0.00		
2010d	0.21	0.26	0.36	0.47	0.64	0.23	0.29	0.37	0.47	0.62
2020d	0.33	0.40	0.55	0.70	0.90	0.37	0.51	0.66	0.84	0.99
2030d	0.40	0.59	0.74	0.92	1.17	0.65	0.77	0.94	1.29	1.39
2040d	0.59	0.73	0.95	1.21	1.41	0.93	1.13	1.29	1.68	1.77
2050d	0.69	0.92	1.15	1.52	1.81	1.20	1.48	1.70	2.19	2.37
2060d	0.88	1.08	1.32	1.78	2.18	1.55	1.88	2.16	2.74	2.99
2070d	1.08	1.28	1.58	2.14	2.52	1.96	2.25	2.60	3.31	3.61
2080d	1.33	1.56	1.81	2.58	2.88	2.31	2.65	3.05	3.93	4.22
2090d	1.51	1.72	2.03	2.92	3.24	2.63	2.96	3.57	4.45	4.81

	SRES A1B				
Years	**5%**	**17%**	**50%**	**83%**	**95%**
1850–1990			–0.61		
1986–2005			0.00		
2010d	0.15	0.22	0.34	0.44	0.62
2020d	0.27	0.37	0.52	0.76	0.91
2030d	0.47	0.59	0.82	1.04	1.38
2040d	0.65	0.90	1.11	1.36	1.79
2050d	0.92	1.14	1.55	1.65	2.14
2060d	1.12	1.40	1.75	1.98	2.67
2070d	1.40	1.60	2.14	2.39	3.12
2080d	1.61	1.80	2.30	2.75	3.47
2090d	1.76	1.96	2.54	3.05	3.84

Notes:

This spread in the model ensembles (as shown in Figures 11.26a and 12.5, and discussed in Section 11.3.6) is not a measure of uncertainty. For the AR5 assessment of global mean surface temperature changes and uncertainties see: Section 11.3.6.3 and Figure 11.25 for the near-term (2016–2035) temperatures; and Section 12.4.1 and Tables 12.2–3 for the long term (2081–2100). See discussion about uncertainty and ensembles in Section 12.2, which explains how model spread is not equivalent to uncertainty. Results here are shown for the CMIP5 archive (Annex I, frozen as of March 15, 2013) for the RCPs and the similarly current CMIP3 archive for SRES A1B, which is not the same set of models used in AR4 (Figure SPM.5). Ten-year averages are shown (2030d = 2026–2035). Temperature changes are relative to the reference period (1986–2005, defined as zero in this table), using CMIP5 for all four RCPs (G. J. van Oldenborgh, http://climexp.knmi.nl/t; see Annex I for listing of models included) and CMIP3 for SRES A1B (22 models). The warming from early instrumental record (1850–1900) to the modern reference period (1986–2005) is derived from HadCRUT4 observations as 0.61°C (C. Morice; see Chapter 2 and Table AII.1.3).

Table AII.7.6 | Global mean surface temperature change (°C) relative to 1990 from the TAR

Years	A1B	A1T	A1FI	A2	B1	B2	IS92a	A1B
PI*	–0.33	–0.33	–0.33	–0.33	–0.33	–0.33	–0.33	–0.33
1990	0.00	0.00	0.00	0.00	0.00	0.00	0.00	0.00
2000	0.16	0.16	0.16	0.16	0.16	0.16	0.15	0.16
2010	0.30	0.40	0.32	0.35	0.34	0.39	0.27	0.30
2020	0.52	0.71	0.55	0.50	0.55	0.66	0.43	0.52
2030	0.85	1.03	0.85	0.73	0.77	0.93	0.61	0.85
2040	1.26	1.41	1.27	1.06	0.98	1.18	0.80	1.26
2050	1.59	1.75	1.86	1.42	1.21	1.44	1.00	1.59
2060	1.97	2.04	2.50	1.85	1.44	1.69	1.26	1.97
2070	2.30	2.25	3.10	2.33	1.63	1.94	1.52	2.30
2080	2.56	2.41	3.64	2.81	1.79	2.20	1.79	2.56
2090	2.77	2.49	4.09	3.29	1.91	2.44	2.08	2.77
2100	2.95	2.54	4.49	3.79	1.98	2.69	2.38	2.95

Notes:

Single-year estimates of mean surface air temperature warming relative to the reference period 1990 for the SRES scenarios evaluated in the TAR. The pre-industrial estimates are for 1750, and all results are based on a simple climate model. See TAR Appendix II.

Table AII.7.7 | Global mean sea level rise (m) with respect to 1986–2005 at 1 January on the years indicated. Values shown as median and *likely* range; see Section 13.5.1.

Year	SRES A1B	RCP2.6	RCP4.5	RCP6.0	RCP8.5
2007	0.03 [0.02 to 0.04]	0.03 [0.02 to 0.04]	0.03 [0.02 to 0.04]	0.03 [0.02 to 0.04]	0.03 [0.02 to 0.04]
2010	0.04 [0.03 to 0.05]	0.04 [0.03 to 0.05]	0.04 [0.03 to 0.05]	0.04 [0.03 to 0.05]	0.04 [0.03 to 0.05]
2020	0.08 [0.06 to 0.10]	0.08 [0.06 to 0.10]	0.08 [0.06 to 0.10]	0.08 [0.06 to 0.10]	0.08 [0.06 to 0.11]
2030	0.12 [0.09 to 0.16]	0.13 [0.09 to 0.16]	0.13 [0.09 to 0.16]	0.12 [0.09 to 0.16]	0.13 [0.10 to 0.17]
2040	0.17 [0.13 to 0.22]	0.17 [0.13 to 0.22]	0.17 [0.13 to 0.22]	0.17 [0.12 to 0.21]	0.19 [0.14 to 0.24]
2050	0.23 [0.17 to 0.30]	0.22 [0.16 to 0.28]	0.23 [0.17 to 0.29]	0.22 [0.16 to 0.28]	0.25 [0.19 to 0.32]
2060	0.30 [0.21 to 0.38]	0.26 [0.18 to 0.35]	0.28 [0.21 to 0.37]	0.27 [0.19 to 0.35]	0.33 [0.24 to 0.42]
2070	0.37 [0.26 to 0.48]	0.31 [0.21 to 0.41]	0.35 [0.25 to 0.45]	0.33 [0.24 to 0.43]	0.42 [0.31 to 0.54]
2080	0.44 [0.31 to 0.58]	0.35 [0.24 to 0.48]	0.41 [0.28 to 0.54]	0.40 [0.28 to 0.53]	0.51 [0.37 to 0.67]
2090	0.52 [0.36 to 0.69]	0.40 [0.26 to 0.54]	0.47 [0.32 to 0.62]	0.47 [0.33 to 0.63]	0.62 [0.45 to 0.81]
2100	0.60 [0.42 to 0.80]	0.44 [0.28 to 0.61]	0.53 [0.36 to 0.71]	0.55 [0.38 to 0.73]	0.74 [0.53 to 0.98]

AIII

Annex III: Glossary

Editor:
Serge Planton (France)

This annex should be cited as:
IPCC, 2013: Annex III: Glossary [Planton, S. (ed.)]. In: *Climate Change 2013: The Physical Science Basis. Contribution of Working Group I to the Fifth Assessment Report of the Intergovernmental Panel on Climate Change* [Stocker, T.F., D. Qin, G.-K. Plattner, M. Tignor, S.K. Allen, J. Boschung, A. Nauels, Y. Xia, V. Bex and P.M. Midgley (eds.)]. Cambridge University Press, Cambridge, United Kingdom and New York, NY, USA.

This glossary defines some specific terms as the Lead Authors intend them to be interpreted in the context of this report. Red, italicized words indicate that the term is defined in the Glossary.

Abrupt climate change A large-scale change in the *climate system* that takes place over a few decades or less, persists (or is anticipated to persist) for at least a few decades and causes substantial disruptions in human and natural systems.

Active layer The layer of ground that is subject to annual thawing and freezing in areas underlain by *permafrost*.

Adjustment time See *Lifetime*. See also *Response time*.

Advection Transport of water or air along with its properties (e.g., temperature, chemical tracers) by winds or currents. Regarding the general distinction between advection and *convection*, the former describes transport by large-scale motions of the *atmosphere* or ocean, while convection describes the predominantly vertical, locally induced motions.

Aerosol A suspension of airborne solid or liquid particles, with a typical size between a few nanometres and 10 µm that reside in the *atmosphere* for at least several hours. For convenience the term *aerosol*, which includes both the particles and the suspending gas, is often used in this report in its plural form to mean *aerosol particles*. Aerosols may be of either natural or *anthropogenic* origin. Aerosols may influence *climate* in several ways: directly through scattering and absorbing radiation (see *Aerosol–radiation interaction*) and indirectly by acting as *cloud condensation nuclei* or *ice nuclei*, modifying the optical properties and *lifetime* of clouds (see *Aerosol–cloud interaction*).

Aerosol–cloud interaction A process by which a perturbation to *aerosol* affects the microphysical properties and evolution of clouds through the aerosol role as *cloud condensation nuclei* or ice nuclei, particularly in ways that affect radiation or precipitation; such processes can also include the effect of clouds and precipitation on aerosol. The aerosol perturbation can be *anthropogenic* or come from some natural *source*. The *radiative forcing* from such interactions has traditionally been attributed to numerous *indirect aerosol effects*, but in this report, only two levels of radiative forcing (or effect) are distinguished:

Radiative forcing (or effect) due to aerosol–cloud interactions (RFaci) The radiative forcing (or *radiative effect*, if the perturbation is internally generated) due to the change in number or size distribution of cloud droplets or ice crystals that is the proximate result of an aerosol perturbation, with other variables (in particular total cloud water content) remaining equal. In liquid clouds, an increase in cloud droplet concentration and surface area would increase the cloud *albedo*. This effect is also known as the *cloud albedo effect*, *first indirect effect,* or *Twomey effect*. It is a largely theoretical concept that cannot readily be isolated in observations or comprehensive process models due to the rapidity and ubiquity of *rapid adjustments*.

Effective radiative forcing (or effect) due to aerosol–cloud interactions (ERFaci) The final radiative forcing (or effect) from the aerosol perturbation including the rapid adjustments to the initial change in droplet or crystal formation rate. These adjustments include changes in the strength of *convection*, precipitation efficiency, cloud fraction, *lifetime* or water content of clouds, and the formation or suppression of clouds in remote areas due to altered circulations.

The total effective radiative forcing due to both aerosol–cloud and aerosol–radiation interactions is denoted *aerosol effective radiative forcing (ERFari+aci).* See also *Aerosol–radiation interaction*.

Aerosol–radiation interaction An interaction of *aerosol* directly with radiation produce *radiative effects*. In this report two levels of radiative forcing (or effect) are distinguished:

Radiative forcing (or effect) due to aerosol–radiation interactions (RFari) The *radiative forcing* (or radiative effect, if the perturbation is internally generated) of an aerosol perturbation due directly to aerosol–radiation interactions, with all environmental variables remaining unaffected. Traditionally known in the literature as the *direct aerosol forcing (or effect)*.

Effective radiative forcing (or effect) due to aerosol-radiation interactions (ERFari) The final radiative forcing (or effect) from the aerosol perturbation including the *rapid adjustments* to the initial change in radiation. These adjustments include changes in cloud caused by the impact of the radiative heating on convective or larger-scale atmospheric circulations, traditionally known as *semi-direct aerosol forcing (or effect)*.

The total effective radiative forcing due to both aerosol–cloud and aerosol–radiation interactions is denoted *aerosol effective radiative forcing (ERFari+aci).* See also *Aerosol–cloud interaction*.

Afforestation Planting of new *forests* on lands that historically have not contained forests. For a discussion of the term *forest* and related terms such as *afforestation*, *reforestation* and *deforestation*, see the IPCC Special Report on Land Use, Land-Use Change and Forestry (IPCC, 2000). See also the report on Definitions and Methodological Options to Inventory Emissions from Direct Human-induced Degradation of Forests and Devegetation of Other Vegetation Types (IPCC, 2003).

Airborne fraction The fraction of total CO_2 emissions (from fossil fuel and land use change) remaining in the *atmosphere*.

Air mass A widespread body of air, the approximately homogeneous properties of which (1) have been established while that air was situated over a particular *region* of the Earth's surface, and (2) undergo specific modifications while in transit away from the source region (AMS, 2000).

Albedo The fraction of *solar radiation* reflected by a surface or object, often expressed as a percentage. Snow-covered surfaces have a high albedo, the albedo of soils ranges from high to low, and vegetation-covered surfaces and oceans have a low albedo. The Earth's planetary albedo varies mainly through varying cloudiness, snow, ice, leaf area and and cover changes.

Alkalinity A measure of the capacity of an aqueous solution to neutralize acids.

Altimetry A technique for measuring the height of the Earth's surface with respect to the geocentre of the Earth within a defined terrestrial reference frame (geocentric sea level).

Annular modes See *Northern Annular Mode (NAM)* and *Southern Annular Mode (SAM)*.

Anthropogenic Resulting from or produced by human activities.

Atlantic Multi-decadal Oscillation/Variability (AMO/AMV) A multi-decadal (65- to 75-year) fluctuation in the North Atlantic, in which *sea surface temperatures* showed warm phases during roughly 1860 to 1880 and 1930 to 1960 and cool phases during 1905 to 1925 and 1970 to 1990 with a range of approximately 0.4°C. See AMO Index, Box 2.5.

Atmosphere The gaseous envelope surrounding the Earth. The dry atmosphere consists almost entirely of nitrogen (78.1% *volume mixing ratio*) and oxygen (20.9% volume mixing ratio), together with a number of trace gases, such as argon (0.93% volume mixing ratio), helium and radiatively active *greenhouse gases* such as *carbon dioxide* (0.035%

volume mixing ratio) and *ozone*. In addition, the atmosphere contains the greenhouse gas water vapour, whose amounts are highly variable but typically around 1% volume mixing ratio. The atmosphere also contains clouds and *aerosols*.

Atmosphere–Ocean General Circulation Model (AOGCM) See *Climate model*.

Atmospheric boundary layer The atmospheric layer adjacent to the Earth's surface that is affected by friction against that boundary surface, and possibly by transport of heat and other variables across that surface (AMS, 2000). The lowest 100 m of the boundary layer (about 10% of the boundary layer thickness), where mechanical generation of turbulence is dominant, is called the *surface boundary layer* or *surface layer*.

Atmospheric lifetime See *Lifetime*.

Attribution See *Detection and attribution*.

Autotrophic respiration *Respiration* by *photosynthetic* (see *photosynthesis*) organisms (e.g., plants and algaes).

Basal lubrication Reduction of friction at the base of an *ice sheet* or *glacier* due to lubrication by meltwater. This can allow the glacier or ice sheet to slide over its base. Meltwater may be produced by pressure-induced melting, friction or geothermal heat, or surface melt may drain to the base through holes in the ice.

Baseline/reference The baseline (or reference) is the state against which change is measured. A *baseline period* is the period relative to which anomalies are computed. The baseline concentration of a trace gas is that measured at a location not influenced by local *anthropogenic* emissions.

Bayesian method/approach A Bayesian method is a method by which a statistical analysis of an unknown or uncertain quantity(ies) is carried out in two steps. First, a prior probability distribution for the uncertain quantity(ies) is formulated on the basis of existing knowledge (either by eliciting expert opinion or by using existing data and studies). At this first stage, an element of subjectivity may influence the choice, but in many cases, the prior probability distribution can be chosen as neutrally as possible, in order not to influence the final outcome of the analysis. In the second step, newly acquired data are used to update the prior distribution into a posterior distribution. The update is carried out either through an analytic computation or though numeric approximation, using a theorem formulated by and named after the British mathematician Thomas Bayes (1702–1761).

Biological pump The process of transporting carbon from the ocean's surface layers to the deep ocean by the primary production of marine phytoplankton, which converts dissolved inorganic carbon (DIC) and nutrients into organic matter through *photosynthesis*. This natural cycle is limited primarily by the availability of light and nutrients such as phosphate, nitrate and silicic acid, and micronutrients, such as iron. See also *Solubility pump*.

Biomass The total mass of living organisms in a given area or volume; dead plant material can be included as dead biomass. *Biomass burning* is the burning of living and dead vegetation.

Biome A biome is a major and distinct regional element of the *biosphere*, typically consisting of several *ecosystems* (e.g., *forests*, rivers, ponds, swamps within a *region*). Biomes are characterized by typical communities of plants and animals.

Biosphere (terrestrial and marine) The part of the Earth system comprising all *ecosystems* and living organisms, in the *atmosphere*, on land (*terrestrial biosphere*) or in the oceans (*marine biosphere*), including derived dead organic matter, such as litter, soil organic matter and oceanic detritus.

Black carbon (BC) Operationally defined *aerosol* species based on measurement of light absorption and chemical reactivity and/or thermal stability. It is sometimes referred to as *soot*.

Blocking Associated with persistent, slow-moving high-pressure systems that obstruct the prevailing westerly winds in the middle and high latitudes and the normal eastward progress of extratropical transient storm systems. It is an important component of the intraseasonal *climate variability* in the extratropics and can cause long-lived weather conditions such as cold spells in winter and summer *heat waves*.

Brewer–Dobson circulation The meridional overturning circulation of the *stratosphere* transporting air upward in the tropics, poleward to the winter hemisphere, and downward at polar and subpolar latitudes. The Brewer–Dobson circulation is driven by the interaction between upward propagating planetary waves and the mean flow.

Burden The total mass of a gaseous substance of concern in the *atmosphere*.

^{13}C Stable *isotope* of carbon having an atomic weight of approximately 13. Measurements of the ratio of $^{13}C/^{12}C$ in *carbon dioxide* molecules are used to infer the importance of different *carbon cycle* and climate processes and the size of the terrestrial carbon *reservoir*.

^{14}C Unstable *isotope* of carbon having an atomic weight of approximately 14, and a half-life of about 5700 years. It is often used for dating purposes going back some 40 kyr. Its variation in time is affected by the magnetic fields of the Sun and Earth, which influence its production from cosmic rays (see *Cosmogenic radioisotopes*).

Calving The breaking off of discrete pieces of ice from a *glacier*, *ice sheet* or an *ice shelf* into lake or seawater, producing icebergs. This is a form of mass loss from an ice body. See also *Mass balance/budget (of glaciers or ice sheets)*.

Carbonaceous aerosol *Aerosol* consisting predominantly of organic substances and *black carbon*.

Carbon cycle The term used to describe the flow of carbon (in various forms, e.g., as *carbon dioxide*) through the *atmosphere*, ocean, terrestrial and marine *biosphere* and *lithosphere*. In this report, the reference unit for the global carbon cycle is GtC or equivalently PgC (10^{15}g).

Carbon dioxide (CO_2) A naturally occurring gas, also a by-product of burning fossil fuels from fossil carbon deposits, such as oil, gas and coal, of *burning biomass*, of *land use* changes and of industrial processes (e.g., cement production). It is the principal *anthropogenic greenhouse gas* that affects the Earth's radiative balance. It is the reference gas against which other greenhouse gases are measured and therefore has a *Global Warming Potential* of 1.

Carbon dioxide (CO_2) fertilization The enhancement of the growth of plants as a result of increased atmospheric *carbon dioxide (CO_2)* concentration.

Carbon Dioxide Removal (CDR) Carbon Dioxide Removal methods refer to a set of techniques that aim to remove CO_2 directly from the *atmosphere* by either (1) increasing natural *sinks* for carbon or (2) using chemical engineering to remove the CO_2, with the intent of reducing the atmospheric CO_2 concentration. CDR methods involve the ocean, land and technical systems, including such methods as *iron fertilization*, large-scale *afforestation* and direct capture of CO_2 from the atmosphere using engineered chemical means. Some CDR methods fall under the category of *geoengineering*, though this may not be the case for others, with the distinction being based on the magnitude, scale, and impact of the particular CDR activities. The boundary between CDR and *mitigation* is not clear and

there could be some overlap between the two given current definitions (IPCC, 2012, p. 2). See also *Solar Radiation Management (SRM)*.

CFC See *Halocarbons*.

Chaotic A *dynamical system* such as the *climate system*, governed by nonlinear deterministic equations (see *Nonlinearity*), may exhibit erratic or chaotic behaviour in the sense that very small changes in the initial state of the system in time lead to large and apparently unpredictable changes in its temporal evolution. Such chaotic behaviour limits the *predictability* of the state of a nonlinear dynamical system at specific future times, although changes in its statistics may still be predictable given changes in the system parameters or boundary conditions.

Charcoal Material resulting from charring of *biomass*, usually retaining some of the microscopic texture typical of plant tissues; chemically it consists mainly of carbon with a disturbed graphitic structure, with lesser amounts of oxygen and hydrogen.

Chronology Arrangement of events according to dates or times of occurrence.

Clathrate (methane) A partly frozen slushy mix of *methane* gas and ice, usually found in sediments.

Clausius–Clapeyron equation/relationship The thermodynamic relationship between small changes in temperature and vapour pressure in an equilibrium system with condensed phases present. For trace gases such as water vapour, this relation gives the increase in equilibrium (or saturation) water vapour pressure per unit change in air temperature.

Climate Climate in a narrow sense is usually defined as the average weather, or more rigorously, as the statistical description in terms of the mean and variability of relevant quantities over a period of time ranging from months to thousands or millions of years. The classical period for averaging these variables is 30 years, as defined by the World Meteorological Organization. The relevant quantities are most often surface variables such as temperature, precipitation and wind. Climate in a wider sense is the state, including a statistical description, of the *climate system*.

Climate–carbon cycle feedback A *climate feedback* involving changes in the properties of land and ocean *carbon cycle* in response to *climate change*. In the ocean, changes in oceanic temperature and circulation could affect the *atmosphere*–ocean CO_2 flux; on the continents, climate change could affect plant *photosynthesis* and soil microbial *respiration* and hence the flux of CO_2 between the atmosphere and the land *biosphere*.

Climate change Climate change refers to a change in the state of the *climate* that can be identified (e.g., by using statistical tests) by changes in the mean and/or the variability of its properties, and that persists for an extended period, typically decades or longer. Climate change may be due to natural internal processes or *external forcings* such as modulations of the *solar cycles*, volcanic eruptions and persistent *anthropogenic* changes in the composition of the *atmosphere* or in *land use*. Note that the *Framework Convention on Climate Change (UNFCCC)*, in its Article 1, defines climate change as: 'a change of climate which is attributed directly or indirectly to human activity that alters the composition of the global atmosphere and which is in addition to natural *climate variability* observed over comparable time periods'. The UNFCCC thus makes a distinction between climate change attributable to human activities altering the atmospheric composition, and climate variability attributable to natural causes. See also *Climate change commitment*, *Detection and Attribution*.

Climate change commitment Due to the thermal inertia of the ocean and slow processes in the *cryosphere* and land surfaces, the *climate* would continue to change even if the atmospheric composition were held fixed at today's values. Past change in atmospheric composition leads to a *committed climate change*, which continues for as long as a radiative imbalance persists and until all components of the *climate system* have adjusted to a new state. The further change in temperature after the composition of the *atmosphere* is held constant is referred to as the *constant composition temperature commitment* or simply *committed warming* or *warming commitment*. Climate change commitment includes other future changes, for example, in the *hydrological cycle*, in *extreme weather events*, in *extreme climate events*, and in *sea level change*. The *constant emission commitment* is the committed climate change that would result from keeping *anthropogenic* emissions constant and the *zero emission commitment* is the climate change commitment when emissions are set to zero. See also *Climate change*.

Climate feedback An interaction in which a perturbation in one climate quantity causes a change in a second, and the change in the second quantity ultimately leads to an additional change in the first. A negative *feedback* is one in which the initial perturbation is weakened by the changes it causes; a positive feedback is one in which the initial perturbation is enhanced. In this Assessment Report, a somewhat narrower definition is often used in which the climate quantity that is perturbed is the *global mean surface temperature*, which in turn causes changes in the global radiation budget. In either case, the initial perturbation can either be externally forced or arise as part of *internal variability*. See also *Climate Feedback Parameter*.

Climate Feedback Parameter A way to quantify the radiative response of the *climate system* to a *global mean surface temperature* change induced by a *radiative forcing*. It varies as the inverse of the *effective climate sensitivity*. Formally, the Climate Feedback Parameter (α; units: W m^{-2} °C^{-1}) is defined as: $\alpha = (\Delta Q - \Delta F)/\Delta T$, where Q is the global mean radiative forcing, T is the global mean air surface temperature, F is the heat flux into the ocean and Δ represents a change with respect to an unperturbed *climate*.

Climate forecast See *Climate prediction*.

Climate index A time series constructed from climate variables that provides an aggregate summary of the state of the *climate system*. For example, the difference between sea level pressure in Iceland and the Azores provides a simple yet useful historical *NAO* index. Because of their optimal properties, climate indices are often defined using *principal components*—linear combinations of climate variables at different locations that have maximum variance subject to certain normalisation constraints (e.g., the *NAM* and *SAM* indices which are principal components of Northern Hemisphere and Southern Hemisphere gridded pressure anomalies, respectively). See Box 2.5 for a summary of definitions for established observational indices. See also *Climate pattern*.

Climate model (spectrum or hierarchy) A numerical representation of the *climate system* based on the physical, chemical and biological properties of its components, their interactions and *feedback* processes, and accounting for some of its known properties. The climate system can be represented by models of varying complexity, that is, for any one component or combination of components a *spectrum* or *hierarchy* of models can be identified, differing in such aspects as the number of spatial dimensions, the extent to which physical, chemical or biological processes are explicitly represented or the level at which empirical *parametrizations* are involved. Coupled *Atmosphere–Ocean General Circulation Models (AOGCMs)* provide a representation of the climate system that is near or at the most comprehensive end of the spectrum currently available. There is an evolution towards more complex models with interactive chemistry and biology. Climate models are applied as a research tool to study and simulate the *climate*, and for operational purposes, including monthly, seasonal and interannual *climate predictions*. See also *Earth System Model*, *Earth-System Model of Intermediate Complexity*, *Energy Balance Model*, *Process-based Model, Regional Climate Model* and *Semi-empirical model*.

Climate pattern A set of spatially varying coefficients obtained by "projection" (regression) of climate variables onto a *climate index* time series. When the climate index is a principal component, the climate pattern is an eigenvector of the covariance matrix, referred to as an *Empirical Orthogonal Function (EOF)* in climate science.

Climate prediction A climate prediction or *climate forecast* is the result of an attempt to produce (starting from a particular state of the *climate system*) an estimate of the actual evolution of the *climate* in the future, for example, at seasonal, interannual or decadal time scales. Because the future evolution of the climate system may be highly sensitive to initial conditions, such predictions are usually probabilistic in nature. See also *Climate projection*, *Climate scenario*, *Model initialization* and *Predictability*.

Climate projection A climate *projection* is the simulated response of the *climate system* to a *scenario* of future emission or concentration of *greenhouse gases* and *aerosols*, generally derived using *climate models*. Climate projections are distinguished from *climate predictions* by their dependence on the emission/concentration/*radiative forcing* scenario used, which is in turn based on assumptions concerning, for example, future socioeconomic and technological developments that may or may not be realized. See also *Climate scenario*.

Climate regime A state of the *climate system* that occurs more frequently than nearby states due to either more persistence or more frequent recurrence. In other words, a cluster in climate state space associated with a local maximum in the *probability density function*.

Climate response See *Climate sensitivity*.

Climate scenario A plausible and often simplified representation of the future *climate*, based on an internally consistent set of climatological relationships that has been constructed for explicit use in investigating the potential consequences of *anthropogenic climate change*, often serving as input to impact models. *Climate projections* often serve as the raw material for constructing climate scenarios, but climate scenarios usually require additional information such as the observed current climate. A *climate change scenario* is the difference between a climate scenario and the current climate. See also *Emission scenario*, *scenario*.

Climate sensitivity In IPCC reports, *equilibrium climate sensitivity* (units: °C) refers to the equilibrium (steady state) change in the annual *global mean surface temperature* following a doubling of the atmospheric *equivalent carbon dioxide concentration*. Owing to computational constraints, the equilibrium climate sensitivity in a *climate model* is sometimes estimated by running an atmospheric general circulation model coupled to a mixed-layer ocean model, because equilibrium climate sensitivity is largely determined by atmospheric processes. Efficient models can be run to equilibrium with a dynamic ocean. The *climate sensitivity parameter* (units: °C $(W\ m^{-2})^{-1}$) refers to the equilibrium change in the annual global mean surface temperature following a unit change in *radiative forcing*.

The *effective climate sensitivity* (units: °C) is an estimate of the global mean surface temperature response to doubled *carbon dioxide* concentration that is evaluated from model output or observations for evolving non-equilibrium conditions. It is a measure of the strengths of the *climate feedbacks* at a particular time and may vary with forcing history and *climate* state, and therefore may differ from equilibrium climate sensitivity.

The *transient climate response* (units: °C) is the change in the global mean surface temperature, averaged over a 20-year period, centred at the time of atmospheric carbon dioxide doubling, in a climate model simulation in which CO_2 increases at 1% yr^{-1}. It is a measure of the strength and rapidity of the surface temperature response to *greenhouse gas* forcing.

Climate sensitivity parameter See *climate sensitivity*.

Climate system The climate system is the highly complex system consisting of five major components: the *atmosphere*, the *hydrosphere*, the *cryosphere*, the *lithosphere* and the *biosphere*, and the interactions between them. The climate system evolves in time under the influence of its own internal dynamics and because of *external forcings* such as volcanic eruptions, solar variations and *anthropogenic* forcings such as the changing composition of the atmosphere and *land use change*.

Climate variability Climate variability refers to variations in the mean state and other statistics (such as standard deviations, the occurrence of extremes, etc.) of the *climate* on all *spatial and temporal scales* beyond that of individual weather events. Variability may be due to natural internal processes within the *climate system* (*internal variability*), or to variations in natural or *anthropogenic external forcing* (*external variability*). See also *Climate change*.

Cloud condensation nuclei (CCN) The subset of *aerosol* particles that serve as an initial site for the condensation of liquid water, which can lead to the formation of cloud droplets, under typical cloud formation conditions. The main factor that determines which aerosol particles are CCN at a given supersaturation is their size.

Cloud feedback A *climate feedback* involving changes in any of the properties of clouds as a response to a change in the local or *global mean surface temperature*. Understanding cloud feedbacks and determining their magnitude and sign require an understanding of how a change in *climate* may affect the spectrum of cloud types, the cloud fraction and height, the radiative properties of clouds, and finally the Earth's radiation budget. At present, cloud feedbacks remain the largest source of *uncertainty* in *climate sensitivity* estimates. See also *Cloud radiative effect*.

Cloud radiative effect The *radiative effect* of clouds relative to the identical situation without clouds. In previous IPCC reports this was called *cloud radiative forcing*, but that terminology is inconsistent with other uses of the forcing term and is not maintained in this report. See also *Cloud feedback*.

CO_2-equivalent See *Equivalent carbon dioxide*.

Cold days/cold nights Days where maximum temperature, or nights where minimum temperature, falls below the 10th *percentile*, where the respective temperature distributions are generally defined with respect to the 1961–1990 *reference* period. For the corresponding indices, see Box 2.4.

Compatible emissions *Earth System Models* that simulate the land and ocean *carbon cycle* can calculate *CO_2* emissions that are compatible with a given atmospheric CO_2 concentration trajectory. The compatible emissions over a given period of time are equal to the increase of carbon over that same period of time in the sum of the three active *reservoirs*: the *atmosphere*, the land and the ocean.

Confidence The validity of a finding based on the type, amount, quality, and consistency of evidence (e.g., mechanistic understanding, theory, data, models, expert judgment) and on the degree of agreement. Confidence is expressed qualitatively (Mastrandrea et al., 2010). See Figure 1.11 for the levels of confidence and Table 1.1 for the list of *likelihood* qualifiers. See also *Uncertainty*.

Convection Vertical motion driven by buoyancy forces arising from static instability, usually caused by near-surface cooling or increases in salinity in the case of the ocean and near-surface warming or cloud-top radiative cooling in the case of the *atmosphere*. In the atmosphere convection gives rise to cumulus clouds and precipitation and is effective at both scavenging and vertically transporting chemical species. In the ocean convection can carry surface waters to deep within the ocean.

Cosmogenic radioisotopes Rare radioactive *isotopes* that are created by the interaction of a high-energy cosmic ray particles with atoms nuclei. They are often used as indicator of *solar activity* which modulates the cosmic rays intensity or as tracers of atmospheric transport processes, and are also called *cosmogenic radionuclides*.

Cryosphere All regions on and beneath the surface of the Earth and ocean where water is in solid form, including *sea ice*, lake ice, river ice, snow cover, *glaciers* and *ice sheets*, and *frozen ground* (which includes *permafrost*).

Dansgaard–Oeschger events Abrupt events characterized in Greenland *ice cores* and in *palaeoclimate* records from the nearby North Atlantic by a cold glacial state, followed by a rapid transition to a warmer phase, and a slow cooling back to glacial conditions. Counterparts of Dansgaard–Oeschger events are observed in other regions as well.

Deforestation Conversion of *forest* to non-forest. For a discussion of the term *forest* and related terms such as *afforestation*, *reforestation*, and *deforestation* see the IPCC Special Report on Land Use, Land-Use Change and Forestry (IPCC, 2000). See also the report on Definitions and Methodological Options to Inventory Emissions from Direct Human-induced Degradation of Forests and Devegetation of Other Vegetation Types (IPCC, 2003).

Deglaciation/glacial termination Transitions from full glacial conditions (*ice age*) to warm *interglacials* characterized by global warming and sea level rise due to change in continental ice volume.

Detection and attribution *Detection of change* is defined as the process of demonstrating that *climate* or a system affected by climate has changed in some defined statistical sense, without providing a reason for that change. An identified change is detected in observations if its *likelihood* of occurrence by chance due to *internal variability* alone is determined to be small, for example, <10%. *Attribution* is defined as the process of evaluating the relative contributions of multiple causal factors to a change or event with an assignment of statistical confidence (Hegerl et al., 2010).

Diatoms Silt-sized algae that live in surface waters of lakes, rivers and oceans and form shells of opal. Their species distribution in ocean cores is often related to past *sea surface temperatures*.

Direct (aerosol) effect See *Aerosol–radiation interaction*.

Direct Air Capture Chemical process by which a pure CO_2 stream is produced by capturing CO_2 from the ambient air.

Diurnal temperature range The difference between the maximum and minimum temperature during a 24-hour period.

Dobson Unit (DU) A unit to measure the total amount of *ozone* in a vertical column above the Earth's surface (*total column ozone*). The number of Dobson Units is the thickness in units of 10^{-5} m that the ozone column would occupy if compressed into a layer of uniform density at a pressure of 1013 hPa and a temperature of 0°C. One DU corresponds to a column of ozone containing 2.69×10^{20} molecules per square metre. A typical value for the amount of ozone in a column of the Earth's *atmosphere*, although very variable, is 300 DU.

Downscaling Downscaling is a method that derives local- to regional-scale (10 to 100 km) information from larger-scale models or data analyses. Two main methods exist: *dynamical downscaling* and *empirical/statistical downscaling*. The dynamical method uses the output of *regional climate models*, global models with variable spatial *resolution* or high-resolution global models. The empirical/statistical methods develop statistical relationships that link the large-scale atmospheric variables with local/regional climate variables. In all cases, the quality of the driving model remains an important limitation on the quality of the downscaled information.

Drought A period of abnormally dry weather long enough to cause a serious hydrological imbalance. Drought is a relative term; therefore any discussion in terms of precipitation deficit must refer to the particular precipitation-related activity that is under discussion. For example, shortage of precipitation during the growing season impinges on crop production or *ecosystem* function in general (due to *soil moisture* drought, also termed *agricultural drought*), and during the *runoff* and percolation season primarily affects water supplies (*hydrological drought*). Storage changes in soil moisture and groundwater are also affected by increases in actual *evapotranspiration* in addition to reductions in precipitation. A period with an abnormal precipitation deficit is defined as a *meteorological drought*. A *megadrought* is a very lengthy and pervasive drought, lasting much longer than normal, usually a decade or more. For the corresponding indices, see Box 2.4.

Dynamical system A process or set of processes whose evolution in time is governed by a set of deterministic physical laws. The *climate system* is a dynamical system. See also *Abrupt climate change*, *Chaotic*, *Nonlinearity* and *Predictability*.

Earth System Model (ESM) A coupled *atmosphere–ocean general circulation model* in which a representation of the *carbon cycle* is included, allowing for interactive calculation of atmospheric CO_2 or *compatible emissions*. Additional components (e.g., atmospheric chemistry, *ice sheets*, dynamic vegetation, nitrogen cycle, but also urban or crop models) may be included. See also *Climate model*.

Earth System Model of Intermediate Complexity (EMIC) A *climate model* attempting to include all the most important earth system processes as in ESMs but at a lower *resolution* or in a simpler, more idealized fashion.

Earth System sensitivity The equilibrium temperature response of the coupled *atmosphere*–ocean–*cryosphere*–vegetation–*carbon cycle* system to a doubling of the atmospheric CO_2 concentration is referred to as Earth System sensitivity. Because it allows slow components (e.g., *ice sheets*, vegetation) of the *climate system* to adjust to the external perturbation, it may differ substantially from the *climate sensitivity* derived from coupled atmosphere–ocean models.

Ecosystem An ecosystem is a functional unit consisting of living organisms, their non-living environment, and the interactions within and between them. The components included in a given ecosystem and its spatial boundaries depend on the purpose for which the ecosystem is defined: in some cases they are relatively sharp, while in others they are diffuse. Ecosystem boundaries can change over time. Ecosystems are nested within other ecosystems, and their scale can range from very small to the entire *biosphere*. In the current era, most ecosystems either contain people as key organisms, or are influenced by the effects of human activities in their environment.

Effective climate sensitivity See *Climate sensitivity*.

Effective radiative forcing See *Radiative forcing*.

Efficacy A measure of how effective a *radiative forcing* from a given *anthropogenic* or natural mechanism is at changing the equilibrium *global mean surface temperature* compared to an equivalent radiative forcing from *carbon dioxide*. A carbon dioxide increase by definition has an efficacy of 1.0. Variations in climate efficacy may result from *rapid adjustments* to the applied forcing, which differ with different forcings.

Ekman pumping Frictional stress at the surface between two fluids (*atmosphere* and ocean) or between a fluid and the adjacent solid surface (the Earth's surface) forces a circulation. When the resulting mass

transport is converging, mass conservation requires a vertical flow away from the surface. This is called Ekman pumping. The opposite effect, in case of divergence, is called *Ekman suction*. The effect is important in both the atmosphere and the ocean.

Ekman transport The total transport resulting from a balance between the Coriolis force and the frictional stress due to the action of the wind on the ocean surface. See also *Ekman pumping*.

Electromagnetic spectrum Wavelength or energy range of all electromagnetic radiation. In terms of *solar radiation*, the *spectral irradiance* is the power arriving at the Earth per unit area, per unit wavelength.

El Niño-Southern Oscillation (ENSO) The term *El Niño* was initially used to describe a warm-water current that periodically flows along the coast of Ecuador and Peru, disrupting the local fishery. It has since become identified with a basin-wide warming of the tropical Pacific Ocean east of the dateline. This oceanic event is associated with a fluctuation of a global-scale tropical and subtropical surface pressure pattern called the *Southern Oscillation*. This coupled *atmosphere*–ocean phenomenon, with preferred time scales of two to about seven years, is known as the El Niño-Southern Oscillation (ENSO). It is often measured by the surface pressure anomaly difference between Tahiti and Darwin or the *sea surface temperatures* in the central and eastern equatorial Pacific. During an ENSO event, the prevailing trade winds weaken, reducing upwelling and altering ocean currents such that the sea surface temperatures warm, further weakening the trade winds. This event has a great impact on the wind, sea surface temperature and precipitation patterns in the tropical Pacific. It has climatic effects throughout the Pacific *region* and in many other parts of the world, through global *teleconnections*. The cold phase of ENSO is called *La Niña*. For the corresponding indices, see Box 2.5.

Emission scenario A plausible representation of the future development of emissions of substances that are potentially radiatively active (e.g., *greenhouse gases*, *aerosols*) based on a coherent and internally consistent set of assumptions about driving forces (such as demographic and socioeconomic development, technological change) and their key relationships. *Concentration scenarios*, derived from emission scenarios, are used as input to a *climate model* to compute *climate projections*. In IPCC (1992) a set of emission scenarios was presented which were used as a basis for the climate projections in IPCC (1996). These emission scenarios are referred to as the IS92 scenarios. In the IPCC Special Report on Emission Scenarios (Nakićenović and Swart, 2000) emission scenarios, the so-called *SRES scenarios*, were published, some of which were used, among others, as a basis for the climate projections presented in Chapters 9 to 11 of IPCC (2001) and Chapters 10 and 11 of IPCC (2007). New emission scenarios for *climate change*, the four *Representative Concentration Pathways*, were developed for, but independently of, the present IPCC assessment. See also *Climate scenario* and *Scenario*.

Energy balance The difference between the total incoming and total outgoing energy. If this balance is positive, warming occurs; if it is negative, cooling occurs. Averaged over the globe and over long time periods, this balance must be zero. Because the *climate system* derives virtually all its energy from the Sun, zero balance implies that, globally, the absorbed *solar radiation*, that is, *incoming solar radiation* minus reflected solar radiation at the top of the *atmosphere* and *outgoing longwave radiation* emitted by the climate system are equal. See also *Energy budget*.

Energy Balance Model (EBM) An energy balance model is a simplified model that analyses the *energy budget* of the Earth to compute changes in the *climate*. In its simplest form, there is no explicit spatial dimension and the model then provides an estimate of the changes in globally averaged temperature computed from the changes in radiation. This zero-dimensional energy balance model can be extended to a one-dimensional or two-dimensional model if changes to the energy budget with respect to latitude, or both latitude and longitude, are explicitly considered. See also *Climate model*.

Energy budget (of the Earth) The Earth is a physical system with an energy budget that includes all gains of incoming energy and all losses of outgoing energy. The Earth's energy budget is determined by measuring how much energy comes into the Earth system from the Sun, how much energy is lost to space, and accounting for the remainder on Earth and its *atmosphere*. *Solar radiation* is the dominant source of energy into the Earth system. Incoming solar energy may be scattered and reflected by clouds and *aerosols* or absorbed in the atmosphere. The transmitted radiation is then either absorbed or reflected at the Earth's surface. The average *albedo* of the Earth is about 0.3, which means that 30% of the incident solar energy is reflected into space, while 70% is absorbed by the Earth. Radiant solar or shortwave energy is transformed into sensible heat, latent energy (involving different water states), potential energy, and kinetic energy before being emitted as *infrared radiation*. With the average *surface temperature* of the Earth of about 15°C (288 K), the main outgoing energy flux is in the infrared part of the spectrum. See also *Energy balance*, *Latent heat flux*, *Sensible heat flux*.

Ensemble A collection of model simulations characterizing a *climate prediction* or *projection*. Differences in initial conditions and model formulation result in different evolutions of the modelled system and may give information on *uncertainty* associated with model error and error in initial conditions in the case of *climate forecasts* and on uncertainty associated with model error and with internally generated *climate variability* in the case of climate projections.

Equilibrium and transient climate experiment An *equilibrium climate experiment* is a *climate model* experiment in which the model is allowed to fully adjust to a change in *radiative forcing*. Such experiments provide information on the difference between the initial and final states of the model, but not on the time-dependent response. If the forcing is allowed to evolve gradually according to a prescribed *emission scenario*, the time-dependent response of a climate model may be analysed. Such an experiment is called a *transient climate experiment*. See also *Climate projection*.

Equilibrium climate sensitivity See *Climate sensitivity*.

Equilibrium line The spatially averaged boundary at a given moment, usually chosen as the seasonal *mass budget* minimum at the end of summer, between the region on a *glacier* where there is a net annual loss of ice mass (*ablation* area) and that where there is a net annual gain (*accumulation* area). The altitude of this boundary is referred to as equilibrium line altitude (ELA).

Equivalent carbon dioxide (CO_2) concentration The concentration of *carbon dioxide* that would cause the same *radiative forcing* as a given mixture of carbon dioxide and other forcing components. Those values may consider only *greenhouse gases*, or a combination of greenhouse gases and *aerosols*. Equivalent carbon dioxide concentration is a *metric* for comparing radiative forcing of a mix of different greenhouse gases at a particular time but does not imply equivalence of the corresponding *climate change* responses nor future forcing. There is generally no connection between *equivalent carbon dioxide emissions* and resulting equivalent carbon dioxide concentrations.

Equivalent carbon dioxide (CO_2) emission The amount of *carbon dioxide* emission that would cause the same integrated *radiative forcing*, over a given time horizon, as an emitted amount of a *greenhouse gas* or a mixture of greenhouse gases. The equivalent carbon dioxide emission is obtained by multiplying the emission of a greenhouse gas by its *Global Warming Potential* for the given time horizon. For a mix of greenhouse

gases it is obtained by summing the equivalent carbon dioxide emissions of each gas. Equivalent carbon dioxide emission is a common scale for comparing emissions of different greenhouse gases but does not imply equivalence of the corresponding *climate change* responses. See also *Equivalent carbon dioxide concentration*.

Evapotranspiration The combined process of evaporation from the Earth's surface and transpiration from vegetation.

Extended Concentration Pathways See *Representative Concentration Pathways*.

External forcing External forcing refers to a forcing agent outside the *climate system* causing a change in the climate system. Volcanic eruptions, solar variations and *anthropogenic* changes in the composition of the *atmosphere* and *land use change* are external forcings. Orbital forcing is also an external forcing as the *insolation* changes with orbital parameters eccentricity, tilt and precession of the equinox.

Extratropical cyclone A large-scale (of order 1000 km) storm in the middle or high latitudes having low central pressure and fronts with strong horizontal gradients in temperature and humidity. A major cause of extreme wind speeds and heavy precipitation especially in wintertime.

Extreme climate event See *Extreme weather event*.

Extreme sea level See *Storm surge*.

AIII

Extreme weather event An extreme weather event is an event that is rare at a particular place and time of year. Definitions of *rare* vary, but an extreme weather event would normally be as rare as or rarer than the 10th or 90th *percentile* of a *probability density function* estimated from observations. By definition, the characteristics of what is called *extreme weather* may vary from place to place in an absolute sense. When a pattern of extreme weather persists for some time, such as a season, it may be classed as an *extreme climate event*, especially if it yields an average or total that is itself extreme (e.g., *drought* or heavy rainfall over a season).

Faculae Bright patches on the Sun. The area covered by faculae is greater during periods of high *solar activity*.

Feedback See *Climate feedback*.

Fingerprint The *climate* response pattern in space and/or time to a specific forcing is commonly referred to as a fingerprint. The spatial patterns of sea level response to melting of *glaciers* or *ice sheets* (or other changes in surface loading) are also referred to as fingerprints. Fingerprints are used to detect the presence of this response in observations and are typically estimated using forced *climate model* simulations.

Flux adjustment To avoid the problem of coupled *Atmosphere–Ocean General Circulation Models (AOGCMs)* drifting into some unrealistic *climate* state, adjustment terms can be applied to the atmosphere-ocean fluxes of heat and moisture (and sometimes the surface stresses resulting from the effect of the wind on the ocean surface) before these fluxes are imposed on the model ocean and atmosphere. Because these adjustments are pre-computed and therefore independent of the coupled model integration, they are uncorrelated with the anomalies that develop during the integration.

Forest A vegetation type dominated by trees. Many definitions of the term *forest* are in use throughout the world, reflecting wide differences in biogeophysical conditions, social structure and economics. For a discussion of the term *forest* and related terms such as *afforestation*, *reforestation* and *deforestation* see the IPCC Report on Land Use, Land-Use Change and Forestry (IPCC, 2000). See also the Report on Definitions and Methodological Options to Inventory Emissions from Direct Human-induced Degradation of Forests and Devegetation of Other Vegetation Types (IPCC, 2003).

Fossil fuel emissions Emissions of *greenhouse gases* (in particular *carbon dioxide*), other trace gases and *aerosols* resulting from the combustion of fuels from fossil carbon deposits such as oil, gas and coal.

Framework Convention on Climate Change See *United Nations Framework Convention on Climate Change (UNFCCC)*.

Free atmosphere The atmospheric layer that is negligibly affected by friction against the Earth's surface, and which is above the *atmospheric boundary layer*.

Frozen ground Soil or rock in which part or all of the *pore water* is frozen. Frozen ground includes *permafrost.* Ground that freezes and thaws annually is called *seasonally frozen ground*.

General circulation The large-scale motions of the *atmosphere* and the ocean as a consequence of differential heating on a rotating Earth. General circulation contributes to the *energy balance* of the system through transport of heat and momentum.

General Circulation Model (GCM) See *Climate model*.

Geoengineering Geoengineering refers to a broad set of methods and technologies that aim to deliberately alter the *climate system* in order to alleviate the impacts of *climate change*. Most, but not all, methods seek to either (1) reduce the amount of absorbed solar energy in the climate system (*Solar Radiation Management*) or (2) increase net carbon sinks from the *atmosphere* at a scale sufficiently large to alter *climate* (*Carbon Dioxide Removal*). Scale and intent are of central importance. Two key characteristics of geoengineering methods of particular concern are that they use or affect the climate system (e.g., atmosphere, land or ocean) globally or regionally and/or could have substantive unintended effects that cross national boundaries. Geoengineering is different from weather modification and ecological engineering, but the boundary can be fuzzy (IPCC, 2012, p. 2).

Geoid The equipotential surface having the same geopotential at each latitude and longitude around the world (geodesists denoting this potential W0) that best approximates the *mean sea level*. It is the surface of reference for measurement of altitude. In practice, several variations of definitions of the geoid exist depending on the way the permanent tide (the zero-frequency gravitational tide due to the Sun and Moon) is considered in geodetic studies.

Geostrophic winds or currents A wind or current that is in balance with the horizontal pressure gradient and the Coriolis force, and thus is outside of the influence of friction. Thus, the wind or current is directly parallel to isobars and its speed is proportional to the horizontal pressure gradient.

Glacial–interglacial cycles Phase of the Earth's history marked by large changes in continental ice volume and global sea level. See also *Ice age* and *Interglacials*.

Glacial isostatic adjustment (GIA) The deformation of the Earth and its gravity field due to the response of the earth–ocean system to changes in ice and associated water loads. It is sometimes referred to as *glacio-hydro isostasy*. It includes vertical and horizontal deformations of the Earth's surface and changes in *geoid* due to the redistribution of mass during the ice–ocean mass exchange.

Glacier A perennial mass of land ice that originates from compressed snow, shows evidence of past or present flow (through internal deformation and/or sliding at the base) and is constrained by internal stress and friction at the base and sides. A glacier is maintained by accumulation of snow at high altitudes, balanced by melting at low altitudes and/or discharge into the sea. An ice mass of the same origin as glaciers, but of continental size, is called an *ice sheet*. For the purpose of simplicity in this Assessment Report, all ice masses other than ice sheets are referred to as

glaciers. See also *Equilibrium line* and *Mass balance/budget (of glaciers or ice sheets)*.

Global dimming Global dimming refers to a widespread reduction of *solar radiation* received at the surface of the Earth from about the year 1961 to around 1990.

Global mean surface temperature An estimate of the global mean surface air temperature. However, for changes over time, only anomalies, as departures from a climatology, are used, most commonly based on the area-weighted global average of the *sea surface temperature* anomaly and *land surface air temperature* anomaly.

Global Warming Potential (GWP) An index, based on radiative properties of *greenhouse gases*, measuring the *radiative forcing* following a pulse emission of a unit mass of a given greenhouse gas in the present-day *atmosphere* integrated over a chosen time horizon, relative to that of *carbon dioxide*. The GWP represents the combined effect of the differing times these gases remain in the atmosphere and their relative effectiveness in causing radiative forcing. The *Kyoto Protocol* is based on GWPs from pulse emissions over a 100-year time frame.

Greenhouse effect The infrared *radiative effect* of all infrared-absorbing constituents in the *atmosphere*. *Greenhouse gases*, clouds, and (to a small extent) *aerosols* absorb *terrestrial radiation* emitted by the Earth's surface and elsewhere in the atmosphere. These substances emit *infrared radiation* in all directions, but, everything else being equal, the net amount emitted to space is normally less than would have been emitted in the absence of these absorbers because of the decline of temperature with altitude in the *troposphere* and the consequent weakening of emission. An increase in the concentration of greenhouse gases increases the magnitude of this effect; the difference is sometimes called the enhanced greenhouse effect. The change in a greenhouse gas concentration because of *anthropogenic* emissions contributes to an *instantaneous radiative forcing*. Surface temperature and troposphere warm in response to this forcing, gradually restoring the radiative balance at the top of the atmosphere.

Greenhouse gas (GHG) Greenhouse gases are those gaseous constituents of the *atmosphere*, both natural and *anthropogenic*, that absorb and emit radiation at specific wavelengths within the spectrum of *terrestrial radiation* emitted by the Earth's surface, the atmosphere itself, and by clouds. This property causes the *greenhouse effect.* Water vapour (H_2O), *carbon dioxide (CO_2)*, *nitrous oxide (N_2O)*, *methane (CH_4)* and *ozone* (O_3) are the primary greenhouse gases in the Earth's atmosphere. Moreover, there are a number of entirely human-made greenhouse gases in the atmosphere, such as the *halocarbons* and other chlorine- and bromine-containing substances, dealt with under the *Montreal Protocol.* Beside CO_2, N_2O and CH_4, the *Kyoto Protocol* deals with the greenhouse gases sulphur hexafluoride (SF_6), hydrofluorocarbons (*HFCs*) and perfluorocarbons (PFCs). For a list of *well-mixed greenhouse gases*, see Table 2.A.1.

Gross Primary Production (GPP) The amount of carbon fixed by the autotrophs (e.g. plants and algaes).

Grounding line The junction between a *glacier* or *ice sheet* and *ice shelf*; the place where ice starts to float. This junction normally occurs over a finite zone, rather than at a line.

Gyre Basin-scale ocean horizontal circulation pattern with slow flow circulating around the ocean basin, closed by a strong and narrow (100 to 200 km wide) boundary current on the western side. The subtropical gyres in each ocean are associated with high pressure in the centre of the gyres; the subpolar gyres are associated with low pressure.

Hadley Circulation A direct, thermally driven overturning cell in the *atmosphere* consisting of poleward flow in the upper *troposphere*, subsiding air into the subtropical anticyclones, return flow as part of the trade winds near the surface, and with rising air near the equator in the so-called *Inter-Tropical Convergence Zone*.

Halocarbons A collective term for the group of partially halogenated organic species, which includes the chlorofluorocarbons (*CFCs*), hydrochlorofluorocarbons (*HCFCs*), hydrofluorocarbons (*HFCs*), halons, methyl chloride and methyl bromide. Many of the halocarbons have large *Global Warming Potentials*. The chlorine and bromine-containing halocarbons are also involved in the depletion of the *ozone layer*.

Halocline A layer in the oceanic water column in which salinity changes rapidly with depth. Generally saltier water is denser and lies below less salty water. In some high latitude oceans the surface waters may be colder than the deep waters and the halocline is responsible for maintaining water column stability and isolating the surface waters from the deep waters. See also *Thermocline.*

Halosteric See *Sea level change*.

HCFC See *Halocarbons*.

Heat wave A period of abnormally and uncomfortably hot weather. See also *Warm spell*.

Heterotrophic respiration The conversion of organic matter to *carbon dioxide* by organisms other than autotrophs.

HFC See *Halocarbons*.

Hindcast or retrospective forecast A forecast made for a period in the past using only information available before the beginning of the forecast. A sequence of hindcasts can be used to calibrate the forecast system and/or provide a measure of the average skill that the forecast system has exhibited in the past as a guide to the skill that might be expected in the future.

Holocene The Holocene Epoch is the latter of two epochs in the *Quaternary* System, extending from 11.65 ka (thousand years before 1950) to the present. It is also known as *Marine Isotopic Stage (MIS) 1* or *current interglacial*.

Hydroclimate Part of the *climate* pertaining to the hydrology of a *region*.

Hydrological cycle The cycle in which water evaporates from the oceans and the land surface, is carried over the Earth in atmospheric circulation as water vapour, condenses to form clouds, precipitates over ocean and land as rain or snow, which on land can be intercepted by trees and vegetation, provides *runoff* on the land surface, infiltrates into soils, recharges groundwater, discharges into streams and ultimately flows out into the oceans, from which it will eventually evaporate again. The various systems involved in the hydrological cycle are usually referred to as hydrological systems.

Hydrosphere The component of the *climate system* comprising liquid surface and subterranean water, such as oceans, seas, rivers, fresh water lakes, underground water, etc.

Hypsometry The distribution of land or ice surface as a function of altitude.

Ice age An ice age or *glacial period* is characterized by a long-term reduction in the temperature of the Earth's *climate*, resulting in growth of *ice sheets* and *glaciers*.

Ice–albedo feedback A *climate feedback* involving changes in the Earth's surface *albedo*. Snow and ice have an albedo much higher (up to ~0.8) than the average planetary albedo (~0.3). With increasing temperatures, it is anticipated that snow and ice extent will decrease, the Earth's overall albedo will decrease and more *solar radiation* will be absorbed, warming the Earth further.

Ice core A cylinder of ice drilled out of a *glacier* or *ice sheet*.

Ice sheet A mass of land ice of continental size that is sufficiently thick to cover most of the underlying bed, so that its shape is mainly determined by its dynamics (the flow of the ice as it deforms internally and/or slides at its base). An ice sheet flows outward from a high central ice plateau with a small average surface slope. The margins usually slope more steeply, and most ice is discharged through fast flowing *ice streams* or *outlet glaciers*, in some cases into the sea or into *ice shelves* floating on the sea. There are only two ice sheets in the modern world, one on Greenland and one on Antarctica. During glacial periods there were others.

Ice shelf A floating slab of ice of considerable thickness extending from the coast (usually of great horizontal extent with a very gently sloping surface), often filling embayments in the coastline of an *ice sheet*. Nearly all ice shelves are in Antarctica, where most of the ice discharged into the ocean flows via ice shelves.

Ice stream A stream of ice with strongly enhanced flow that is part of an *ice sheet.* It is often separated from surrounding ice by strongly sheared, crevassed margins. See also *Outlet glacier.*

Incoming solar radiation See *Insolation*.

Indian Ocean Dipole (IOD) Large–scale mode of interannual variability of *sea surface temperature* in the Indian Ocean. This pattern manifests through a zonal gradient of tropical sea surface temperature, which in one extreme phase in boreal autumn shows cooling off Sumatra and warming off Somalia in the west, combined with anomalous easterlies along the equator.

Indirect aerosol effect See *Aerosol-cloud interaction*.

Industrial Revolution A period of rapid industrial growth with far-reaching social and economic consequences, beginning in Britain during the second half of the 18th century and spreading to Europe and later to other countries including the United States. The invention of the steam engine was an important trigger of this development. The industrial revolution marks the beginning of a strong increase in the use of fossil fuels and emission of, in particular, fossil *carbon dioxide*. In this report the terms *pre-industrial* and *industrial* refer, somewhat arbitrarily, to the periods before and after 1750, respectively.

Infrared radiation See *Terrestrial radiation*.

Insolation The amount of *solar radiation* reaching the Earth by latitude and by season measured in W m^{-2}. Usually *insolation* refers to the radiation arriving at the top of the *atmosphere*. Sometimes it is specified as referring to the radiation arriving at the Earth's surface. See also *Total Solar Irradiance*.

Interglacials or interglaciations The warm periods between *ice age* glaciations. Often defined as the periods at which sea levels were close to present sea level. For the *Last Interglacial (LIG)* this occurred between about 129 and 116 ka (thousand years) before present (defined as 1950) although the warm period started in some areas a few thousand years earlier. In terms of the oxygen *isotope* record interglaciations are defined as the interval between the midpoint of the preceding termination and the onset of the next glaciation. The present interglaciation, the *Holocene*, started at 11.65 ka before present although globally sea levels did not approach their present position until about 7 ka before present.

Internal variability See *Climate variability*.

Inter-Tropical Convergence Zone (ITCZ) The Inter-Tropical Convergence Zone is an equatorial zonal belt of low pressure, strong *convection* and heavy precipitation near the equator where the northeast trade winds meet the southeast trade winds. This band moves seasonally.

Iron fertilization Deliberate introduction of iron to the upper ocean intended to enhance biological productivity which can sequester additional atmospheric *carbon dioxide* into the oceans.

Irreversibility A perturbed state of a *dynamical system* is defined as irreversible on a given timescale, if the recovery timescale from this state due to natural processes is significantly longer than the time it takes for the system to reach this perturbed state. In the context of WGI, the time scale of interest is centennial to millennial. See also *Tipping point*.

Isostatic or Isostasy Isostasy refers to the response of the earth to changes in surface load. It includes the deformational and gravitational response. This response is elastic on short time scales, as in the earth–ocean response to recent changes in mountain glaciation, or viscoelastic on longer time scales, as in the response to the last *deglaciation* following the *Last Glacial Maximum*. See also *Glacial Isostatic Adjustment (GIA)*.

Isotopes Atoms of the same chemical element that have the same the number of protons but differ in the number of neutrons. Some proton–neutron configurations are stable (stable isotopes), others are unstable undergoing spontaneous radioactive decay (*radioisotopes*). Most elements have more than one stable isotope. Isotopes can be used to trace transport processes or to study processes that change the isotopic ratio. Radioisotopes provide in addition time information that can be used for radiometric dating.

Kyoto Protocol The Kyoto Protocol to the *United Nations Framework Convention on Climate Change (UNFCCC)* was adopted in 1997 in Kyoto, Japan, at the Third Session of the Conference of the Parties (COP) to the UNFCCC. It contains legally binding commitments, in addition to those included in the UNFCCC. Countries included in Annex B of the Protocol (most Organisation for Economic Cooperation and Development countries and countries with economies in transition) agreed to reduce their *anthropogenic greenhouse gas* emissions (*carbon dioxide*, *methane*, *nitrous oxide*, hydrofluorocarbons, perfluorocarbons, and sulphur hexafluoride) by at least 5% below 1990 levels in the commitment period 2008–2012. The Kyoto Protocol entered into force on 16 February 2005.

Land surface air temperature The surface air temperature as measured in well-ventilated screens over land at 1.5 m above the ground.

Land use and Land use change *Land use* refers to the total of arrangements, activities and inputs undertaken in a certain land cover type (a set of human actions). The term *land use* is also used in the sense of the social and economic purposes for which land is managed (e.g., grazing, timber extraction and conservation). *Land use change* refers to a change in the use or management of land by humans, which may lead to a change in land cover. Land cover and land use change may have an impact on the surface *albedo*, *evapotranspiration*, *sources* and *sinks* of *greenhouse gases*, or other properties of the *climate system* and may thus give rise to *radiative forcing* and/or other impacts on *climate*, locally or globally. See also the IPCC Report on Land Use, Land-Use Change, and Forestry (IPCC, 2000).

Land water storage Water stored on land other than in *glaciers* and *ice sheets* (that is water stored in rivers, lakes, wetlands, the vadose zone, aquifers, reservoirs, snow and *permafrost*). Changes in land water storage driven by *climate* and human activities contribute to *sea level change*.

La Niña See *El Niño-Southern Oscillation*.

Lapse rate The rate of change of an atmospheric variable, usually temperature, with height. The lapse rate is considered positive when the variable decreases with height.

Last Glacial Maximum (LGM) The period during the last *ice age* when the *glaciers* and *ice sheets* reached their maximum extent, approximately

21 ka ago. This period has been widely studied because the *radiative forcings* and boundary conditions are relatively well known.

Last Interglacial (LIG) See *Interglacials*.

Latent heat flux The turbulent flux of heat from the Earth's surface to the *atmosphere* that is associated with evaporation or condensation of water vapour at the surface; a component of the surface *energy budget*.

Lifetime Lifetime is a general term used for various time scales characterizing the rate of processes affecting the concentration of trace gases. The following lifetimes may be distinguished:

Turnover time (T) (also called *global atmospheric lifetime*) is the ratio of the mass M of a *reservoir* (e.g., a gaseous compound in the *atmosphere*) and the total rate of removal S from the reservoir: $T = M/S$. For each removal process, separate turnover times can be defined. In soil carbon biology, this is referred to as *Mean Residence Time*.

Adjustment time or response time (T_a) is the time scale characterizing the decay of an instantaneous pulse input into the reservoir. The term *adjustment time* is also used to characterize the adjustment of the mass of a reservoir following a step change in the *source* strength. *Half-life* or *decay constant* is used to quantify a first-order exponential decay process. See *Response time* for a different definition pertinent to *climate* variations.

The term *lifetime* is sometimes used, for simplicity, as a surrogate for *adjustment time*.

In simple cases, where the global removal of the compound is directly proportional to the total mass of the reservoir, the adjustment time equals the turnover time: $T = T_a$. An example is *CFC*-11, which is removed from the atmosphere only by photochemical processes in the *stratosphere*. In more complicated cases, where several reservoirs are involved or where the removal is not proportional to the total mass, the equality $T = T_a$ no longer holds. *Carbon dioxide (CO_2)* is an extreme example. Its turnover time is only about 4 years because of the rapid exchange between the atmosphere and the ocean and terrestrial biota. However, a large part of that CO_2 is returned to the atmosphere within a few years. Thus, the adjustment time of CO_2 in the atmosphere is actually determined by the rate of removal of carbon from the surface layer of the oceans into its deeper layers. Although an approximate value of 100 years may be given for the adjustment time of CO_2 in the atmosphere, the actual adjustment is faster initially and slower later on. In the case of *methane (CH_4)*, the adjustment time is different from the turnover time because the removal is mainly through a chemical reaction with the hydroxyl radical (OH), the concentration of which itself depends on the CH_4 concentration. Therefore, the CH_4 removal rate S is not proportional to its total mass M.

Likelihood The chance of a specific outcome occurring, where this might be estimated probabilistically. This is expressed in this report using a standard terminology, defined in Table 1.1. See also *Confidence* and *Uncertainty*.

Lithosphere The upper layer of the solid Earth, both continental and oceanic, which comprises all crustal rocks and the cold, mainly elastic part of the uppermost mantle. Volcanic activity, although part of the lithosphere, is not considered as part of the *climate system*, but acts as an *external forcing* factor. See also *Isostatic*.

Little Ice Age (LIA) An interval during the last millennium characterized by a number of extensive expansions of mountain *glaciers* and moderate retreats in between them, both in the Northern and Southern Hemispheres. The timing of glacial advances differs between *regions* and the LIA is, therefore, not clearly defined in time. Most definitions lie in the period 1400 CE and 1900 CE. Currently available *reconstructions* of average Northern Hemisphere temperature indicate that the coolest periods at the hemispheric scale may have occurred from 1450 to 1850 CE.

Longwave radiation See *Terrestrial radiation*.

Madden–Julian Oscillation (MJO) The largest single component of tropical atmospheric intraseasonal variability (periods from 30 to 90 days). The MJO propagates eastwards at around 5 m s^{-1} in the form of a large-scale coupling between atmospheric circulation and deep *convection*. As it progresses, it is associated with large regions of both enhanced and suppressed rainfall, mainly over the Indian and western Pacific Oceans. Each MJO event lasts approximately 30 to 60 days, hence the MJO is also known as the 30- to 60-day wave, or the intraseasonal oscillation.

Marine-based ice sheet An *ice sheet* containing a substantial region that rests on a bed lying below sea level and whose perimeter is in contact with the ocean. The best known example is the West Antarctic ice sheet.

Mass balance/budget (of glaciers or ice sheets) The balance between the mass input to the ice body (*accumulation*) and the mass loss (*ablation* and iceberg *calving*) over a stated period of time, which is often a year or a season. Point mass balance refers to the mass balance at a particular location on the *glacier* or *ice sheet*. Surface mass balance is the difference between surface accumulation and surface ablation. The input and output terms for mass balance are:

Accumulation All processes that add to the mass of a glacier. The main contribution to accumulation is snowfall. Accumulation also includes deposition of hoar, freezing rain, other types of solid precipitation, gain of wind-blown snow, and avalanching.

Ablation Surface processes that reduce the mass of a glacier. The main contributor to ablation is melting with *runoff* but on some glaciers sublimation, loss of wind-blown snow and avalanching are also significant processes of ablation.

Discharge/outflow Mass loss by iceberg calving or ice discharge across the *grounding line* of a floating *ice shelf*. Although often treated as an ablation term, in this report iceberg calving and discharge is considered separately from surface ablation.

Mean sea level The surface level of the ocean at a particular point averaged over an extended period of time such as a month or year. Mean sea level is often used as a national datum to which heights on land are referred.

Medieval Climate Anomaly (MCA) See *Medieval Warm Period*.

Medieval Warm Period (MWP) An interval of relatively warm conditions and other notable *climate* anomalies such as more extensive *drought* in some continental *regions*. The timing of this interval is not clearly defined, with different records showing onset and termination of the warmth at different times, and some showing intermittent warmth. Most definitions lie within the period 900 to 1400 CE. Currently available *reconstructions* of average Northern Hemisphere temperature indicate that the warmest period at the hemispheric scale may have occurred from 950 to 1250 CE. Currently available records and temperature reconstructions indicate that average temperatures during parts of the MWP were indeed warmer in the context of the last 2 kyr, though the warmth may not have been as ubiquitous across seasons and geographical regions as the 20th century warming. It is also called *Medieval Climate Anomaly*.

Meridional Overturning Circulation (MOC) Meridional (north–south) overturning circulation in the ocean quantified by zonal (east–west) sums of mass transports in depth or density layers. In the North Atlantic, away from the subpolar *regions*, the MOC (which is in principle an observable quantity) is often identified with the *thermohaline circulation* (THC),

which is a conceptual and incomplete interpretation. It must be borne in mind that the MOC is also driven by wind, and can also include shallower overturning cells such as occur in the upper ocean in the tropics and subtropics, in which warm (light) waters moving poleward are transformed to slightly denser waters and *subducted* equatorward at deeper levels.

Metadata Information about meteorological and climatological data concerning how and when they were measured, their quality, known problems and other characteristics.

Methane (CH_4) Methane is one of the six *greenhouse gases* to be mitigated under the *Kyoto Protocol* and is the major component of natural gas and associated with all hydrocarbon fuels, animal husbandry and agriculture.

Metric A consistent measurement of a characteristic of an object or activity that is otherwise difficult to quantify. Within the context of the evaluation of *climate models*, this is a quantitative measure of agreement between a simulated and observed quantity which can be used to assess the performance of individual models.

Microwave Sounding Unit (MSU) A microwave sounder on National Oceanic and Atmospheric Administration (NOAA) polar orbiter satellites, that estimates the temperature of thick layers of the *atmosphere* by measuring the thermal emission of oxygen molecules from a complex of emission lines near 60 GHz. A series of nine MSUs began making this kind of measurement in late 1978. Beginning in mid 1998, a follow-on series of instruments, the Advanced Microwave Sounding Units (AMSUs), began operation.

Mineralization/Remineralization The conversion of an element from its organic form to an inorganic form as a result of microbial decomposition. In nitrogen mineralization, organic nitrogen from decaying plant and animal residues (proteins, nucleic acids, amino sugars and urea) is converted to ammonia (NH_3) and ammonium (NH_4^+) by biological activity.

Mitigation A human intervention to reduce the *sources* or enhance the *sinks* of *greenhouse gases*.

Mixing ratio See *Mole fraction*.

Model drift Since model *climate* differs to some extent from observed climate, *climate forecasts* will typically 'drift' from the initial observation-based state towards the model's climate. This drift occurs at different time scales for different variables, can obscure the initial-condition forecast information and is usually removed a posteriori by an empirical, usually linear, adjustment.

Model hierarchy See *Climate model (spectrum or hierarchy)*.

Model initialization A *climate forecast* typically proceeds by integrating a *climate model* forward in time from an initial state that is intended to reflect the actual state of the *climate system*. Available observations of the climate system are 'assimilated' into the model. Initialization is a complex process that is limited by available observations, observational errors and, depending on the procedure used, may be affected by *uncertainty* in the history of climate forcing. The initial conditions will contain errors that grow as the forecast progresses, thereby limiting the time for which the forecast will be useful. See also *Climate prediction*.

Model spread The range or spread in results from *climate models*, such as those assembled for Coupled Model Intercomparison Project Phase 5 (CMIP5). Does not necessarily provide an exhaustive and formal estimate of the *uncertainty* in *feedbacks*, forcing or *projections* even when expressed numerically, for example, by computing a standard deviation of the models' responses. In order to quantify uncertainty, information from observations, physical constraints and expert judgement must be combined, using a statistical framework.

Mode of climate variability Underlying space–time structure with preferred spatial pattern and temporal variation that helps account for the gross features in variance and for *teleconnections*. A mode of variability is often considered to be the product of a spatial *climate pattern* and an associated *climate index* time series.

Mole fraction Mole fraction, or *mixing ratio*, is the ratio of the number of moles of a constituent in a given volume to the total number of moles of all constituents in that volume. It is usually reported for dry air. Typical values for *well-mixed greenhouse gases* are in the order of μmol mol^{-1} (parts per million: *ppm*), nmol mol^{-1} (parts per billion: *ppb*), and fmol mol^{-1} (parts per trillion: *ppt*). Mole fraction differs from *volume mixing ratio*, often expressed in ppmv etc., by the corrections for non-ideality of gases. This correction is significant relative to measurement precision for many greenhouse gases (Schwartz and Warneck, 1995).

Monsoon A monsoon is a tropical and subtropical seasonal reversal in both the surface winds and associated precipitation, caused by differential heating between a continental-scale land mass and the adjacent ocean. Monsoon rains occur mainly over land in summer.

Montreal Protocol The Montreal Protocol on Substances that Deplete the *Ozone Layer* was adopted in Montreal in 1987, and subsequently adjusted and amended in London (1990), Copenhagen (1992), Vienna (1995), Montreal (1997) and Beijing (1999). It controls the consumption and production of chlorine- and bromine-containing chemicals that destroy stratospheric *ozone*, such as chlorofluorocarbons, methyl chloroform, carbon tetrachloride and many others.

Near-surface permafrost A term frequently used in *climate model* applications to refer to *permafrost* at depths close to the ground surface (typically down to 3.5 m). In modelling studies, near-surface permafrost is usually diagnosed from 20 or 30 year climate averages, which is different from the conventional definition of permafrost. Disappearance of near-surface permafrost in a location does not preclude the longer-term persistence of permafrost at greater depth. See also *Active layer*, *Frozen ground* and *Thermokarst*.

Near-term climate forcers (NTCF) Near-term climate forcers (NTCF) refer to those compounds whose impact on *climate* occurs primarily within the first decade after their emission. This set of compounds is primarily composed of those with short *lifetimes* in the atmosphere compared to *well-mixed greenhouse gases*, and has been sometimes referred to as short lived climate forcers or short-lived climate pollutants. However, the common property that is of greatest interest to a climate assessment is the timescale over which their impact on climate is felt. This set of compounds includes *methane*, which is also a well-mixed greenhouse gas, as well as *ozone* and *aerosols*, or their *precursors*, and some halogenated species that are not well-mixed greenhouse gases. These compounds do not accumulate in the atmosphere at decadal to centennial timescales, and so their effect on climate is predominantly in the near term following their emission.

Nitrogen deposition Nitrogen deposition is defined as the nitrogen transferred from the *atmosphere* to the Earth's surface by the processes of wet deposition and dry deposition.

Nitrous oxide (N_2O) One of the six *greenhouse gases* to be mitigated under the *Kyoto Protocol*. The main *anthropogenic source* of nitrous oxide is agriculture (soil and animal manure management), but important contributions also come from sewage treatment, combustion of fossil fuel, and chemical industrial processes. Nitrous oxide is also produced naturally from a wide variety of biological sources in soil and water, particularly microbial action in wet tropical *forests*.

Nonlinearity A process is called *nonlinear* when there is no simple proportional relation between cause and effect. The *climate system* contains many such nonlinear processes, resulting in a system with potentially very complex behaviour. Such complexity may lead to *abrupt climate change*. See also *Chaotic* and *Predictability*.

North Atlantic Oscillation (NAO) The North Atlantic Oscillation consists of opposing variations of surface pressure near Iceland and near the Azores. It therefore corresponds to fluctuations in the strength of the main westerly winds across the Atlantic into Europe, and thus to fluctuations in the embedded *extratropical cyclones* with their associated frontal systems. See NAO Index, Box 2.5.

Northern Annular Mode (NAM) A winter fluctuation in the amplitude of a pattern characterized by low surface pressure in the Arctic and strong mid-latitude westerlies. The NAM has links with the northern polar vortex into the *stratosphere*. Its pattern has a bias to the North Atlantic and its index has a large correlation with the *North Atlantic Oscillation* index. See NAM Index, Box 2.5.

Ocean acidification Ocean acidification refers to a reduction in the *pH* of the ocean over an extended period, typically decades or longer, which is caused primarily by *uptake* of *carbon dioxide* from the *atmosphere*, but can also be caused by other chemical additions or subtractions from the ocean. *Anthropogenic ocean acidification* refers to the component of pH reduction that is caused by human activity (IPCC, 2011, p. 37).

Ocean heat uptake efficiency This is a measure (W m^{-2} $°C^{-1}$) of the rate at which heat storage by the global ocean increases as *global mean surface temperature* rises. It is a useful parameter for *climate change* experiments in which the *radiative forcing* is changing monotonically, when it can be compared with the *Climate Feedback Parameter* to gauge the relative importance of *climate response* and ocean heat *uptake* in determining the rate of climate change. It can be estimated from such an experiment as the ratio of the rate of increase of ocean heat content to the global mean surface air temperature change.

Organic aerosol Component of the *aerosol* that consists of organic compounds, mainly carbon, hydrogen, oxygen and lesser amounts of other elements. See also *Carbonaceous aerosol*.

Outgoing longwave radiation Net outgoing radiation in the infrared part of the spectrum at the top of the *atmosphere*. See also *Terrestrial radiation*.

Outlet glacier A *glacier*, usually between rock walls, that is part of, and drains an *ice sheet*. See also *Ice stream*.

Ozone Ozone, the triatomic form of oxygen (O_3), is a gaseous atmospheric constituent. In the *troposphere*, it is created both naturally and by photochemical reactions involving gases resulting from human activities (*smog*). Tropospheric ozone acts as a *greenhouse gas*. In the *stratosphere*, it is created by the interaction between solar ultraviolet radiation and molecular oxygen (O_2). Stratospheric ozone plays a dominant role in the stratospheric radiative balance. Its concentration is highest in the *ozone layer*.

Ozone hole See *Ozone layer*.

Ozone layer The *stratosphere* contains a layer in which the concentration of *ozone* is greatest, the so-called ozone layer. The layer extends from about 12 to 40 km above the Earth's surface. The ozone concentration reaches a maximum between about 20 and 25 km. This layer has been depleted by human emissions of chlorine and bromine compounds. Every year, during the Southern Hemisphere spring, a very strong depletion of the ozone layer takes place over the Antarctic, caused by *anthropogenic* chlorine and bromine compounds in combination with the specific meteorological conditions of that *region*. This phenomenon is called the *Ozone hole*. See also *Montreal Protocol*.

Pacific Decadal Oscillation (PDO) The pattern and time series of the first empirical orthogonal function of *sea surface temperature* over the North Pacific north of 20°N. The PDO broadened to cover the whole Pacific Basin is known as the Inter-decadal Pacific Oscillation. The PDO and IPO exhibit similar temporal evolution. See also *Pacific Decadal Variability*.

Pacific decadal variability Coupled decadal-to-inter-decadal variability of the atmospheric circulation and underlying ocean in the Pacific Basin. It is most prominent in the North Pacific, where fluctuations in the strength of the winter Aleutian Low pressure system co-vary with North Pacific *sea surface temperatures*, and are linked to decadal variations in atmospheric circulation, sea surface temperatures and ocean circulation throughout the whole Pacific Basin. Such fluctuations have the effect of modulating the *El Niño-Southern Oscillation* cycle. Key measures of Pacific decadal variability are the *North Pacific Index (NPI)*, the *Pacific Decadal Oscillation (PDO)* index and the *Inter-decadal Pacific Oscillation (IPO)* index, all defined in Box 2.5.

Pacific–North American (PNA) pattern An atmospheric large-scale wave pattern featuring a sequence of tropospheric high and low pressure anomalies stretching from the subtropical west Pacific to the east coast of North America. See PNA pattern index, Box 2.5.

Paleoclimate *Climate* during periods prior to the development of measuring instruments, including historic and geologic time, for which only *proxy* climate records are available.

Parameterization In *climate models*, this term refers to the technique of representing processes that cannot be explicitly resolved at the spatial or temporal *resolution* of the model (sub-grid scale processes) by relationships between model-resolved larger-scale variables and the area- or time-averaged effect of such subgrid scale processes.

Percentiles The set of partition values which divides the total population of a distribution into 100 equal parts, the 50th percentile corresponding to the *median* of the population.

Permafrost Ground (soil or rock and included ice and organic material) that remains at or below 0°C for at least two consecutive years. See also *Near-surface permafrost*.

pH pH is a dimensionless measure of the acidity of water (or any solution) given by its concentration of hydrogen ions (H^+). pH is measured on a logarithmic scale where $pH = -\log_{10}(H^+)$. Thus, a pH decrease of 1 unit corresponds to a 10-fold increase in the concentration of H^+, or acidity.

Photosynthesis The process by which plants take *carbon dioxide* from the air (or bicarbonate in water) to build carbohydrates, releasing oxygen in the process. There are several pathways of photosynthesis with different responses to atmospheric carbon dioxide concentrations. See also *Carbon dioxide fertilization*.

Plankton Microorganisms living in the upper layers of aquatic systems. A distinction is made between *phytoplankton*, which depend on *photosynthesis* for their energy supply, and *zooplankton*, which feed on phytoplankton.

Pleistocene The Pleistocene Epoch is the earlier of two epochs in the *Quaternary* System, extending from 2.59 Ma to the beginning of the *Holocene* at 11.65 ka.

Pliocene The Plionece Epoch is the last epoch of the *Neogene* System and extends from 5.33 Ma to the beginning of the *Pleistocene* at 2.59 Ma.

Pollen analysis A technique of both relative dating and environmental *reconstruction*, consisting of the identification and counting of pollen types preserved in peat, lake sediments and other deposits. See also *Proxy*.

Precipitable water The total amount of atmospheric water vapour in a vertical column of unit cross-sectional area. It is commonly expressed in terms of the height of the water if completely condensed and collected in a vessel of the same unit cross section.

Precursors Atmospheric compounds that are not *greenhouse gases* or *aerosols*, but that have an effect on greenhouse gas or aerosol concentrations by taking part in physical or chemical processes regulating their production or destruction rates.

Predictability The extent to which future states of a system may be predicted based on knowledge of current and past states of the system. Because knowledge of the *climate system*'s past and current states is generally imperfect, as are the models that utilize this knowledge to produce a *climate prediction*, and because the climate system is inherently *nonlinear* and *chaotic*, predictability of the climate system is inherently limited. Even with arbitrarily accurate models and observations, there may still be limits to the predictability of such a nonlinear system (AMS, 2000).

Prediction quality/skill Measures of the success of a *prediction* against observationally based information. No single measure can summarize all aspects of forecast quality and a suite of *metrics* is considered. Metrics will differ for forecasts given in deterministic and probabilistic form. See also *Climate prediction*.

Pre-industrial See *Industrial Revolution*.

Probability Density Function (PDF) A probability density function is a function that indicates the relative chances of occurrence of different outcomes of a variable. The function integrates to unity over the domain for which it is defined and has the property that the integral over a sub-domain equals the probability that the outcome of the variable lies within that sub-domain. For example, the probability that a temperature anomaly defined in a particular way is greater than zero is obtained from its PDF by integrating the PDF over all possible temperature anomalies greater than zero. Probability density functions that describe two or more variables simultaneously are similarly defined.

Process-based Model Theoretical concepts and computational methods that represent and simulate the behaviour of real-world systems derived from a set of functional components and their interactions with each other and the system environment, through physical and mechanistic processes occurring over time. See also *Climate model*.

Projection A projection is a potential future evolution of a quantity or set of quantities, often computed with the aid of a model. Unlike predictions, projections are conditional on assumptions concerning, for example, future socioeconomic and technological developments that may or may not be realized. See also *Climate prediction* and *Climate projection*.

Proxy A proxy *climate* indicator is a record that is interpreted, using physical and biophysical principles, to represent some combination of climate-related variations back in time. Climate-related data derived in this way are referred to as proxy data. Examples of proxies include *pollen analysis*, *tree ring* records, speleothems, characteristics of corals and various data derived from marine sediments and *ice cores*. Proxy-data can be calibrated to provide quantitative climate information.

Quasi-Biennal Oscillation (QBO) A near-periodic oscillation of the equatorial zonal wind between easterlies and westerlies in the tropical *stratosphere* with a mean period of around 28 months. The alternating wind maxima descend from the base of the mesosphere down to the *tropopause*, and are driven by wave energy that propagates up from the *troposphere*.

Quaternary The Quaternary System is the latter of three systems that make up the *Cenozoic Era* (65 Ma to present), extending from 2.59 Ma to the present, and includes the *Pleistocene* and *Holocene* epochs.

Radiative effect The impact on a radiation flux or heating rate (most commonly, on the downward flux at the top of *atmosphere*) caused by the interaction of a particular constituent with either the *infrared* or *solar radiation* fields through absorption, scattering and emission, relative to an otherwise identical atmosphere free of that constituent. This quantifies the impact of the constituent on the *climate system*. Examples include the *aerosol–radiation interactions*, *cloud radiative effect*, and *greenhouse effect*. In this report, the portion of any top-of-atmosphere radiative effect that is due to *anthropogenic* or other external influences (e.g., volcanic eruptions or changes in the sun) is termed the *instantaneous radiative forcing*.

Radiative forcing Radiative forcing is the change in the net, downward minus upward, radiative flux (expressed in W m^{-2}) at the *tropopause* or top of *atmosphere* due to a change in an external driver of *climate change*, such as, for example, a change in the concentration of *carbon dioxide* or the output of the Sun. Sometimes internal drivers are still treated as forcings even though they result from the alteration in *climate*, for example *aerosol* or *greenhouse gas* changes in *paleoclimates*. The traditional radiative forcing is computed with all tropospheric properties held fixed at their unperturbed values, and after allowing for stratospheric temperatures, if perturbed, to readjust to radiative-dynamical equilibrium. Radiative forcing is called *instantaneous* if no change in stratospheric temperature is accounted for. The radiative forcing once *rapid adjustments* are accounted for is termed the *effective radiative forcing.* For the purposes of this report, radiative forcing is further defined as the change relative to the year 1750 and, unless otherwise noted, refers to a global and annual average value. Radiative forcing is not to be confused with *cloud radiative forcing*, which describes an unrelated measure of the impact of clouds on the radiative flux at the top of the atmosphere.

Rapid adjustment The response to an agent perturbing the *climate system* that is driven directly by the agent, independently of any change in the *global mean surface temperature*. For example, *carbon dioxide* and *aerosols*, by altering internal heating and cooling rates within the *atmosphere*, can each cause changes to cloud cover and other variables thereby producing a *radiative effect* even in the absence of any surface warming or cooling. Adjustments are *rapid* in the sense that they begin to occur right away, before *climate feedbacks* which are driven by warming (although some adjustments may still take significant time to proceed to completion, for example those involving vegetation or *ice sheets*). It is also called the *rapid response* or *fast adjustment*. For further explanation on the concept, see Sections 7.1 and 8.1.

Rapid climate change See *Abrupt climate change*.

Rapid dynamical change (of glaciers or ice sheets) Changes in *glacier* or *ice sheet* mass controlled by changes in flow speed and *discharge* rather than by *accumulation* or *ablation*. This can result in a rate of mass change larger than that due to any imbalance between accumulation and ablation. Rapid dynamical change may be initiated by a climatic trigger, such as incursion of warm ocean water beneath an *ice shelf*, or thinning of a grounded tidewater terminus, which may lead to reactions within the glacier system, that may result in rapid ice loss. See also *Mass balance/budget (of glaciers or ice sheets)*.

Reanalysis Reanalyses are estimates of historical atmospheric temperature and wind or oceanographic temperature and current, and other quantities, created by processing past meteorological or oceanographic data using fixed state-of-the-art weather forecasting or ocean circulation models with data assimilation techniques. Using fixed data assimilation avoids effects from the changing analysis system that occur in operational analyses. Although continuity is improved, global reanalyses still suffer from changing coverage and biases in the observing systems.

Rebound effect When CO_2 is removed from the *atmosphere*, the CO_2 concentration gradient between atmospheric and land/ocean carbon *reservoirs* is reduced. This leads to a reduction or reversal in subsequent inherent rate of removal of CO_2 from the atmosphere by natural *carbon cycle* processes on land and ocean.

Reconstruction (of climate variable) Approach to reconstructing the past temporal and spatial characteristics of a climate variable from predictors. The predictors can be instrumental data if the reconstruction is used to infill missing data or *proxy* data if it is used to develop *paleoclimate* reconstructions. Various techniques have been developed for this purpose: linear multivariate regression based methods and nonlinear *Bayesian* and analog methods.

Reforestation Planting of *forests* on lands that have previously contained forests but that have been converted to some other use. For a discussion of the term *forest* and related terms such as *afforestation*, *reforestation* and *deforestation*, see the IPCC Report on Land Use, Land-Use Change and Forestry (IPCC, 2000). See also the Report on Definitions and Methodological Options to Inventory Emissions from Direct Human-induced Degradation of Forests and Devegetation of Other Vegetation Types (IPCC, 2003).

Region A region is a territory characterized by specific geographical and climatological features. The *climate* of a region is affected by regional and local scale features like topography, *land use* characteristics and lakes, as well as remote influences from other regions. See also *Teleconnection*.

Regional Climate Model (RCM) A *climate model* at higher *resolution* over a limited area. Such models are used in *downscaling* global *climate* results over specific regional domains.

Relative humidity The relative humidity specifies the ratio of actual water vapour pressure to that at saturation with respect to liquid water or ice at the same temperature. See also *Specific humidity*.

Relative sea level Sea level measured by a *tide gauge* with respect to the land upon which it is situated. See also *Mean sea level* and *Sea level change*.

Representative Concentration Pathways (RCPs) *Scenarios* that include time series of emissions and concentrations of the full suite of *greenhouse gases* and *aerosols* and chemically active gases, as well as *land use*/land cover (Moss et al., 2008). The word *representative* signifies that each RCP provides only one of many possible scenarios that would lead to the specific *radiative forcing* characteristics. The term *pathway* emphasizes that not only the long-term concentration levels are of interest, but also the trajectory taken over time to reach that outcome. (Moss et al., 2010).

RCPs usually refer to the portion of the concentration pathway extending up to 2100, for which Integrated Assessment Models produced corresponding *emission scenarios*. *Extended Concentration Pathways (ECPs)* describe extensions of the RCPs from 2100 to 2500 that were calculated using simple rules generated by stakeholder consultations, and do not represent fully consistent scenarios.

Four RCPs produced from Integrated Assessment Models were selected from the published literature and are used in the present IPCC Assessment as a basis for the *climate predictions* and *projections* presented in Chapters 11 to 14:

RCP2.6 One pathway where radiative forcing peaks at approximately 3 W m^{-2} before 2100 and then declines (the corresponding ECP assuming constant emissions after 2100)

RCP4.5 and RCP6.0 Two intermediate *stabilization pathways* in which radiative forcing is stabilized at approximately 4.5 W m^{-2} and 6.0 W m^{-2} after 2100 (the corresponding ECPs assuming constant concentrations after 2150)

RCP8.5 One high pathway for which radiative forcing reaches greater than 8.5 W m^{-2} by 2100 and continues to rise for some amount of time (the corresponding ECP assuming constant emissions after 2100 and constant concentrations after 2250)

For further description of future scenarios, see Box 1.1.

Reservoir A component of the *climate system*, other than the *atmosphere*, which has the capacity to store, accumulate or release a substance of concern, for example, carbon, a *greenhouse gas* or a *precursor*. Oceans, soils and *forests* are examples of reservoirs of carbon. *Pool* is an equivalent term (note that the definition of pool often includes the atmosphere). The absolute quantity of the substance of concern held within a reservoir at a specified time is called the *stock*.

Resolution In *climate models*, this term refers to the physical distance (metres or degrees) between each point on the grid used to compute the equations. *Temporal resolution* refers to the time step or time elapsed between each model computation of the equations.

Respiration The process whereby living organisms convert organic matter to *carbon dioxide*, releasing energy and consuming molecular oxygen.

Response time The response time or *adjustment time* is the time needed for the *climate system* or its components to re-equilibrate to a new state, following a forcing resulting from external processes. It is very different for various components of the climate system. The response time of the *troposphere* is relatively short, from days to weeks, whereas the *stratosphere* reaches equilibrium on a time scale of typically a few months. Due to their large heat capacity, the oceans have a much longer response time: typically decades, but up to centuries or millennia. The response time of the strongly coupled surface–troposphere system is, therefore, slow compared to that of the stratosphere, and mainly determined by the oceans. The *biosphere* may respond quickly (e.g., to *droughts*), but also very slowly to imposed changes. See *lifetime* for a different definition of response time pertinent to the rate of processes affecting the concentration of trace gases.

Return period An estimate of the average time interval between occurrences of an event (e.g., flood or extreme rainfall) of (or below/above) a defined size or intensity. See also *Return value*.

Return value The highest (or, alternatively, lowest) value of a given variable, on average occurring once in a given period of time (e.g., in 10 years). See also *Return period*.

River discharge See *Streamflow*.

Runoff That part of precipitation that does not evaporate and is not transpired, but flows through the ground or over the ground surface and returns to bodies of water. See also *Hydrological cycle*.

Scenario A plausible description of how the future may develop based on a coherent and internally consistent set of assumptions about key driving forces (e.g., rate of technological change, prices) and relationships. Note that scenarios are neither predictions nor forecasts, but are useful to provide a view of the implications of developments and actions. See also *Climate scenario*, *Emission scenario*, *Representative Concentration Pathways* and *SRES scenarios*.

Sea ice Ice found at the sea surface that has originated from the freezing of seawater. Sea ice may be discontinuous pieces (ice floes) moved on the ocean surface by wind and currents (pack ice), or a motionless sheet attached to the coast (land-fast ice). *Sea ice concentration* is the fraction of the ocean covered by ice. Sea ice less than one year old is called *first-year ice*. *Perennial ice* is sea ice that survives at least one summer. It may be subdivided into *second-year ice* and *multi-year ice*, where multiyear ice has survived at least two summers.

Sea level change Sea level can change, both globally and locally due to (1) changes in the shape of the ocean basins, (2) a change in ocean volume as a result of a change in the mass of water in the ocean, and (3) changes in ocean volume as a result of changes in ocean water density. Global *mean sea level* change resulting from change in the mass of the ocean is called *barystatic*. The amount of barystatic sea level change due to the addition or removal of a mass of water is called its *sea level equivalent (SLE)*. Sea level changes, both globally and locally, resulting from changes in water density are called *steric*. Density changes induced by temperature changes only are called *thermosteric*, while density changes induced by salinity changes are called *halosteric*. Barystatic and steric sea level changes do not include the effect of changes in the shape of ocean basins induced by the change in the ocean mass and its distribution. See also *Relative Sea Level* and *Thermal expansion*.

Sea level equivalent (SLE) The sea level equivalent of a mass of water (ice, liquid or vapour) is that mass, converted to a volume using a density of 1000 kg m^{-3}, and divided by the present-day ocean surface area of 3.625×10^{14} m^2. Thus, 362.5 Gt of water mass added to the ocean will cause 1 mm of global *mean sea level* rise. See also *Sea level change*.

Seasonally frozen ground See *Frozen ground*.

Sea surface temperature (SST) The sea surface temperature is the subsurface bulk temperature in the top few metres of the ocean, measured by ships, buoys and drifters. From ships, measurements of water samples in buckets were mostly switched in the 1940s to samples from engine intake water. Satellite measurements of *skin temperature* (uppermost layer; a fraction of a millimetre thick) in the infrared or the top centimetre or so in the microwave are also used, but must be adjusted to be compatible with the bulk temperature.

Semi-direct (aerosol) effect See *Aerosol–radiation interaction*.

Semi-empirical model Model in which calculations are based on a combination of observed associations between variables and theoretical considerations relating variables through fundamental principles (e.g., conservation of energy). For example, in sea level studies, semi-empirical models refer specifically to transfer functions formulated to project future global *mean sea level change*, or contributions to it, from future *global mean surface temperature* change or *radiative forcing*.

Sensible heat flux The turbulent or conductive flux of heat from the Earth's surface to the *atmosphere* that is not associated with phase changes of water; a component of the surface *energy budget*.

Sequestration See *Uptake*.

Shortwave radiation See *Solar radiation*.

Significant wave height The average trough-to-crest height of the highest one third of the wave heights (sea and swell) occurring in a particular time period.

Sink Any process, activity or mechanism that removes a *greenhouse gas*, an *aerosol* or a *precursor* of a greenhouse gas or aerosol from the *atmosphere*.

Slab-ocean model A simplified representation in a *climate model* of the ocean as a motionless layer of water with a depth of 50 to 100 m. Climate models with a slab ocean can be used only for estimating the equilibrium response of *climate* to a given forcing, not the transient evolution of climate. See also *Equilibrium and transient climate experiment*.

Snow cover extent The areal extent of snow covered ground.

Snow water equivalent (SWE) The depth of liquid water that would result if a mass of snow melted completely.

Soil moisture Water stored in the soil in liquid or frozen form.

Soil temperature The temperature of the soil. This can be measured or modelled at multiple levels within the depth of the soil.

Solar activity General term describing a variety of magnetic phenomena on the Sun such as *sunspots*, *faculae* (bright areas), and flares (emission of high-energy particles). It varies on time scales from minutes to millions of years. See also *Solar cycle*.

Solar ('11-year') cycle A quasi-regular modulation of *solar activity* with varying amplitude and a period of between 8 and 14 years.

Solar radiation Electromagnetic radiation emitted by the Sun with a spectrum close to the one of a black body with a temperature of 5770 K. The radiation peaks in visible wavelengths. When compared to the *terrestrial radiation* it is often referred to as *shortwave radiation*. See also *Insolation* and *Total solar irradiance (TSI)*.

Solar Radiation Management (SRM) Solar Radiation Management refers to the intentional modification of the Earth's shortwave radiative budget with the aim to reduce *climate change* according to a given *metric* (e.g., *surface temperature*, precipitation, regional impacts, etc). Artificial injection of stratospheric *aerosols* and cloud brightening are two examples of SRM techniques. Methods to modify some fast-responding elements of the longwave radiative budget (such as cirrus clouds), although not strictly speaking SRM, can be related to SRM. SRM techniques do not fall within the usual definitions of *mitigation* and adaptation (IPCC, 2012, p. 2). See also *Solar radiation*, *Carbon Dioxide Removal (CDR)* and *Geoengineering*.

Solubility pump Solubility pump is an important physicochemical process that transports dissolved inorganic carbon from the ocean's surface to its interior. This process controls the inventory of carbon in the ocean. The solubility of gaseous *carbon dioxide* can alter carbon dioxide concentrations in the oceans and the overlying *atmosphere*. See also *Biological pump*.

Source Any process, activity or mechanism that releases a *greenhouse gas*, an *aerosol* or a *precursor* of a greenhouse gas or aerosol into the *atmosphere*.

Southern Annular Mode (SAM) The leading mode of variability of Southern Hemisphere geopotential height, which is associated with shifts in the latitude of the midlatitude jet. See SAM Index, Box 2.5.

Southern Oscillation See *El Niño-Southern Oscillation (ENSO)*.

South Pacific Convergence Zone (SPCZ) A band of low-level convergence, cloudiness and precipitation ranging from the west Pacific warm pool south-eastwards towards French Polynesia, which is one of the most significant features of subtropical Southern Hemisphere *climate*. It shares some characteristics with the *ITCZ*, but is more extratropical in nature, especially east of the Dateline.

Spatial and temporal scales *Climate* may vary on a large range of spatial and temporal scales. Spatial scales may range from local (less than 100 000 km^2), through regional (100 000 to 10 million km^2) to continental (10 to 100 million km^2). Temporal scales may range from seasonal to geological (up to hundreds of millions of years).

Specific humidity The specific humidity specifies the ratio of the mass of water vapour to the total mass of moist air. See also *Relative humidity*.

SRES scenarios SRES scenarios are *emission scenarios* developed by Nakićenović and Swart (2000) and used, among others, as a basis for some of the *climate projections* shown in Chapters 9 to 11 of IPCC (2001) and Chapters 10 and 11 of IPCC (2007). The following terms are relevant for a better understanding of the structure and use of the set of SRES scenarios:

> **Scenario family** Scenarios that have a similar demographic, societal, economic and technical change storyline. Four scenario families comprise the SRES scenario set: A1, A2, B1 and B2.

Illustrative Scenario A scenario that is illustrative for each of the six scenario groups reflected in the Summary for Policymakers of Nakićenović and Swart (2000). They include four revised *marker scenarios* for the scenario groups A1B, A2, B1, B2 and two additional scenarios for the A1FI and A1T groups. All scenario groups are equally sound.

Marker Scenario A scenario that was originally posted in draft form on the SRES website to represent a given scenario family. The choice of markers was based on which of the initial quantifications best reflected the storyline, and the features of specific models. Markers are no more likely than other scenarios, but are considered by the SRES writing team as illustrative of a particular storyline. They are included in revised form in Nakićenović and Swart (2000). These scenarios received the closest scrutiny of the entire writing team and via the SRES open process. Scenarios were also selected to illustrate the other two scenario groups.

Storyline A narrative description of a scenario (or family of scenarios), highlighting the main scenario characteristics, relationships between key driving forces and the dynamics of their evolution.

Steric See *Sea level change*.

Stock See *Reservoir*.

Storm surge The temporary increase, at a particular locality, in the height of the sea due to extreme meteorological conditions (low atmospheric pressure and/or strong winds). The storm surge is defined as being the excess above the level expected from the tidal variation alone at that time and place.

Storm tracks Originally, a term referring to the tracks of individual cyclonic weather systems, but now often generalized to refer to the main *regions* where the tracks of extratropical disturbances occur as sequences of low (cyclonic) and high (anticyclonic) pressure systems.

Stratosphere The highly stratified region of the *atmosphere* above the *troposphere* extending from about 10 km (ranging from 9 km at high latitudes to 16 km in the tropics on average) to about 50 km altitude.

Streamflow Water flow within a river channel, for example expressed in $m^3 s^{-1}$. A synonym for *river discharge*.

Subduction Ocean process in which surface waters enter the ocean interior from the surface mixed layer through *Ekman pumping* and lateral *advection*. The latter occurs when surface waters are advected to a region where the local surface layer is less dense and therefore must slide below the surface layer, usually with no change in density.

Sunspots Dark areas on the Sun where strong magnetic fields reduce the convection causing a temperature reduction of about 1500 K compared to the surrounding regions. The number of sunspots is higher during periods of higher *solar activity*, and varies in particular with the *solar cycle.*

Surface layer See *Atmospheric boundary layer*.

Surface temperature See *Global mean surface temperature*, *Land surface air temperature* and *Sea surface temperature*.

Talik A layer of year-round unfrozen ground that lies in *permafrost* areas.

Teleconnection A statistical association between climate variables at widely separated, geographically-fixed spatial locations. Teleconnections are caused by large spatial structures such as basin-wide coupled modes of ocean–*atmosphere* variability, Rossby wave-trains, mid-latitude jets and *storm tracks*, etc. See also *Teleconnection pattern*.

Teleconnection pattern A correlation map obtained by calculating the correlation between variables at different spatial locations and a *climate index*. It is the special case of a *climate pattern* obtained for standardized variables and a standardized climate index, that is, the variables and index are each centred and scaled to have zero mean and unit variance. One-point teleconnection maps are made by choosing a variable at one of the locations to be the climate index. See also *Teleconnection*.

Terrestrial radiation Radiation emitted by the Earth's surface, the *atmosphere* and the clouds. It is also known as *thermal infrared* or *longwave radiation*, and is to be distinguished from the near-infrared radiation that is part of the solar spectrum. *Infrared radiation*, in general, has a distinctive range of wavelengths (*spectrum*) longer than the wavelength of the red light in the visible part of the spectrum. The spectrum of terrestrial radiation is almost entirely distinct from that of shortwave or *solar radiation* because of the difference in temperature between the Sun and the Earth–atmosphere system. See also *Outgoing longwave radiation*.

Thermal expansion In connection with sea level, this refers to the increase in volume (and decrease in density) that results from warming water. A warming of the ocean leads to an expansion of the ocean volume and hence an increase in sea level. See also *Sea level change*.

Thermocline The layer of maximum vertical temperature gradient in the ocean, lying between the surface ocean and the abyssal ocean. In subtropical regions, its source waters are typically surface waters at higher latitudes that have *subducted* (see *Subduction*) and moved equatorward. At high latitudes, it is sometimes absent, replaced by a *halocline*, which is a layer of maximum vertical salinity gradient.

Thermohaline circulation (THC) Large-scale circulation in the ocean that transforms low-density upper ocean waters to higher-density intermediate and deep waters and returns those waters back to the upper ocean. The circulation is asymmetric, with conversion to dense waters in restricted regions at high latitudes and the return to the surface involving slow upwelling and diffusive processes over much larger geographic regions. The THC is driven by high densities at or near the surface, caused by cold temperatures and/or high salinities, but despite its suggestive though common name, is also driven by mechanical forces such as wind and tides. Frequently, the name THC has been used synonymously with *Meridional Overturning Circulation*.

Thermokarst The process by which characteristic landforms result from the thawing of ice-rich *permafrost* or the melting of massive ground ice.

Thermosteric See *Sea level change*.

Tide gauge A device at a coastal or deep-sea location that continuously measures the level of the sea with respect to the adjacent land. Time averaging of the sea level so recorded gives the observed secular changes of the *relative sea level*.

Tipping point In *climate*, a hypothesized critical threshold when global or regional *climate changes* from one stable state to another stable state. The tipping point event may be irreversible. See also *Irreversibility*.

Total solar irradiance (TSI) The total amount of *solar radiation* in watts per square metre received outside the Earth's *atmosphere* on a surface normal to the incident radiation, and at the Earth's mean distance from the Sun.

Reliable measurements of solar radiation can only be made from space and the precise record extends back only to 1978. The generally accepted value is 1368 W m^{-2} with an accuracy of about 0.2%. It has recently been estimated to 1360.8 ± 0.5 W m^{-2} for the solar minimum of 2008. Variations of a few tenths of a percent are common, usually associated with the passage of *sunspots* across the solar disk. The *solar cycle* variation of TSI is of the order of 0.1% (AMS, 2000). Changes in the ultraviolet part of the spectrum during a solar cycle are comparatively larger (percent) than in TSI. See also *Insolation*.

Transient climate response See *Climate sensitivity*.

Transient climate response to cumulative CO_2 emissions (TCRE) The transient global average *surface temperature* change per unit cumulated *CO_2* emissions, usually 1000 PgC. TCRE combines both information on the *airborne fraction* of cumulated CO_2 emissions (the fraction of the total CO_2 emitted that remains in the *atmosphere*), and on the *transient climate response* (TCR).

Tree rings Concentric rings of secondary wood evident in a cross section of the stem of a woody plant. The difference between the dense, small-celled late wood of one season and the wide-celled early wood of the following spring enables the age of a tree to be estimated, and the ring widths or density can be related to climate parameters such as temperature and precipitation. See also *Proxy*.

Trend In this report, the word *trend* designates a change, generally monotonic in time, in the value of a variable.

Tropopause The boundary between the *troposphere* and the *stratosphere*.

Troposphere The lowest part of the *atmosphere*, from the surface to about 10 km in altitude at mid-latitudes (ranging from 9 km at high latitudes to 16 km in the tropics on average), where clouds and weather phenomena occur. In the troposphere, temperatures generally decrease with height. See also *Stratosphere*.

Turnover time See *Lifetime*.

Uncertainty A state of incomplete knowledge that can result from a lack of information or from disagreement about what is known or even knowable. It may have many types of sources, from imprecision in the data to ambiguously defined concepts or terminology, or uncertain *projections* of human behaviour. Uncertainty can therefore be represented by quantitative measures (e.g., a *probability density function*) or by qualitative statements (e.g., reflecting the judgment of a team of experts) (see Moss and Schneider, 2000; Manning et al., 2004; Mastrandrea et al., 2010). See also *Confidence* and *Likelihood*.

United Nations Framework Convention on Climate Change (UNFCCC) The Convention was adopted on 9 May 1992 in New York and signed at the 1992 Earth Summit in Rio de Janeiro by more than 150 countries and the European Community. Its ultimate objective is the 'stabilisation of *greenhouse gas* concentrations in the *atmosphere* at a level that would prevent dangerous *anthropogenic* interference with the *climate system*'. It contains commitments for all Parties. Under the Convention, Parties included in Annex I (all OECD countries and countries with economies in transition) aim to return greenhouse gas emissions not controlled by the *Montreal Protocol* to 1990 levels by the year 2000. The convention entered in force in March 1994. In 1997, the UNFCCC adopted the *Kyoto Protocol*.

Uptake The addition of a substance of concern to a *reservoir*. The uptake of carbon containing substances, in particular *carbon dioxide*, is often called (carbon) *sequestration*.

Urban heat island (UHI) The relative warmth of a city compared with surrounding rural areas, associated with changes in *runoff*, effects on heat retention, and changes in surface *albedo*.

Ventilation The exchange of ocean properties with the atmospheric *surface layer* such that property concentrations are brought closer to equilibrium values with the *atmosphere* (AMS, 2000), and the processes that propagate these properties into the ocean interior.

Volatile Organic Compounds (VOC) Important class of organic chemical air pollutants that are volatile at ambient air conditions. Other terms used to represent VOCs are *hydrocarbons* (HCs), *reactive organic gases* (ROGs) and *non-methane volatile organic compounds* (NMVOCs). NMVOCs are major contributors (together with NO_x and CO) to the formation of photochemical oxidants such as *ozone*.

Walker Circulation Direct thermally driven zonal overturning circulation in the *atmosphere* over the tropical Pacific Ocean, with rising air in the western and sinking air in the eastern Pacific.

Warm days/warm nights Days where maximum temperature, or nights where minimum temperature, exceeds the 90th *percentile*, where the respective temperature distributions are generally defined with respect to the 1961–1990 *reference* period. For the corresponding indices, see Box 2.4.

Warm spell A period of abnormally hot weather. For the corresponding indices, see Box 2.4. See also *Heat wave*.

Water cycle See *Hydrological cycle*.

Water mass A body of ocean water with identifiable properties (temperature, salinity, density, chemical tracers) resulting from its unique formation process. Water masses are often identified through a vertical or horizontal extremum of a property such as salinity. North Pacific Intermediate Water (NPIW) and Antarctic Intermediate Water (AAIW) are examples of water masses.

Weathering The gradual removal of atmospheric *CO_2* through dissolution of silicate and carbonate rocks. Weathering may involve physical processes (*mechanical weathering*) or chemical activity (*chemical weathering*).

Well-mixed greenhouse gas See *Greenhouse gas*.

Younger Dryas A period 12.85 to 11.65 ka (thousand years before 1950), during the *deglaciation*, characterized by a temporary return to colder conditions in many locations, especially around the North Atlantic.

References

AMS, 2000: *AMS Glossary of Meteorology*, 2nd ed. American Meteorological Society, Boston, MA, http://amsglossary.allenpress.com/glossary/browse.

Hegerl, G. C., O. Hoegh-Guldberg, G. Casassa, M. P. Hoerling, R. S. Kovats, C. Parmesan, D. W. Pierce, and P. A. Stott, 2010: Good practice guidance paper on detection and attribution related to anthropogenic climate change. In: *Meeting Report of the Intergovernmental Panel on Climate Change Expert Meeting on Detection and Attribution of Anthropogenic Climate Change* [T. F. Stocker, C. B. Field, D. Qin, V. Barros, G.-K. Plattner, M. Tignor, P. M. Midgley and K. L. Ebi (eds.)]. IPCC Working Group I Technical Support Unit, University of Bern, Bern, Switzerland.

IPCC, 1992: *Climate Change 1992: The Supplementary Report to the IPCC Scientific Assessment* [J. T. Houghton, B. A. Callander and S. K. Varney (eds.)]. Cambridge University Press, Cambridge, United Kingdom and New York, NY, USA, 116 pp.

IPCC, 1996: *Climate Change 1995: The Science of Climate Change. Contribution of Working Group I to the Second Assessment Report of the Intergovernmental Panel on Climate Change* [J. T. Houghton., L. G. Meira . A. Callander, N. Harris, A. Kattenberg and K. Maskell (eds.)]. Cambridge University Press, Cambridge, United Kingdom and New York, NY, USA, 572 pp.

IPCC, 2000: *Land Use, Land-Use Change, and Forestry. Special Report of the Intergovernmental Panel on Climate Change* [R. T. Watson, I. R. Noble, B. Bolin, N. H. Ravindranath, D. J. Verardo, and D. J. Dokken (eds.)]. Cambridge University Press, Cambridge, United Kingdom and New York, NY, USA, 377 pp.

IPCC, 2001: *Climate Change 2001: The Scientific Basis. Contribution of Working Group I to the Third Assessment Report of the Intergovernmental Panel on Climate Change* [T. Houghton, Y. Ding, D. J. Griggs, M. Noquer, P. J. van der Linden, X. Dai, K. Maskell and C. A. Johnson (eds.)]. Cambridge University Press, Cambridge, United Kingdom and New York, NY, USA, 881 pp.

IPCC, 2003: Definitions and Methodological Options to Inventory Emissions from Direct Human-Induced Degradation of Forests and Devegetation of Other Vegetation Types [Penman, J., M. Gytarsky, T. Hiraishi, T. Krug, D. Kruger, R. Pipatti, L. Buendia, K. Miwa, T. Ngara, K. Tanabe and F. Wagner (eds.)]. The Institute for Global Environmental Strategies (IGES), Japan, 32 pp.

IPCC, 2007: *Climate Change 2007: The Physical Science Basis. Contribution of Working Group I to the Fourth Assessment Report of the Intergovernmental Panel on Climate Change.* [Solomon, S., D. Qin, M. Manning, Z. Chen, M. Marquis, K. B. Averyt, M. Tignor and H. L. Miller (eds.)]. Cambridge University Press, Cambridge, United Kingdom and New York, NY, USA, 996 pp.

IPCC, 2011: *Workshop Report of the Intergovernmental Panel on Climate Change Workshop on Impacts of Ocean Acidification on Marine Biology and Ecosystems* [C. B. Field, V. Barros, T. F. Stocker, D. Qin, K.J. Mach, G.-K. Plattner, M. D. Mastrandrea, M. Tignor and K. L. Ebi (eds.)]. IPCC Working Group II Technical Support Unit, Carnegie Institution, Stanford, CA, USA, 164 pp.

IPCC, 2012: *Meeting Report of the Intergovernmental Panel on Climate Change Expert Meeting on Geoengineering* [O. Edenhofer, R. Pichs-Madruga, Y. Sokona, C. Field, V. Barros, T. F. Stocker, Q. Dahe, J. Minx, K. Mach, G.-K. Plattner, S. Schlömer, G. Hansen and M. Mastrandrea (eds.)]. IPCC Working Group III Technical Support Unit, Potsdam Institute for Climate Impact Research, Potsdam, Germany, 99 pp.

Manning, M., et al., 2004: *IPCC Workshop on Describing Scientific Uncertainties in Climate Change to Support Analysis of Risk of Options*. Workshop Report. IPCC Working Group I Technical Support Unit, Boulder, CO, USA, 138 pp.

Mastrandrea, M. D., C. B. Field, T. F. Stocker, O. Edenhofer, K. L. Ebi, D. J. Frame, H. Held, E. Kriegler, K. J. Mach, P. R. Matschoss, G.-K. Plattner, G. W. Yohe, and F. W. Zwiers, 2010: *Guidance Note for Lead Authors of the IPCC Fifth Assessment Report on Consistent Treatment of Uncertainties*. Intergovernmental Panel on Climate Change (IPCC). http://www.ipcc.ch.

Moss, R., and S. Schneider, 2000: *Uncertainties in the IPCC TAR: Recommendations to Lead Authors for More Consistent Assessment and Reporting*. In: IPCC Supporting Material: Guidance Papers on Cross Cutting Issues in the Third Assessment Report of the IPCC. [Pachauri, R., T. Taniguchi, and K. Tanaka (eds.)]. Intergovernmental Panel on Climate Change, Geneva, pp. 33–51.

Moss, R., et al., 2008: *Towards new scenarios for analysis of emissions, climate change, impacts and response strategies*. Intergovernmental Panel on Climate Change, Geneva, 132 pp.

Moss, R. et al., 2010: The next generation of scenarios for climate change research and assessment. *Nature*, **463**, 747–756.

Nakićenović, N., and R. Swart (eds.), 2000: *Special Report on Emissions Scenarios*. *A Special Report of Working Group III of the Intergovernmental Panel on Climate Change*. Cambridge University Press, Cambridge, United Kingdom and New York, NY, USA, 599 pp.

Schwartz, S.E., and P. Warneck, 1995: Units for use in atmospheric chemistry. *Pure Appl. Chem.*, **67**, 1377–1406.

AIV

Annex IV: Acronyms

This annex should be cited as:
IPCC, 2013: Annex IV: Acronyms. In: *Climate Change 2013: The Physical Science Basis. Contribution of Working Group I to the Fifth Assessment Report of the Intergovernmental Panel on Climate Change* [Stocker, T.F., D. Qin, G.-K. Plattner, M. Tignor, S.K. Allen, J. Boschung, A. Nauels, Y. Xia, V. Bex and P.M. Midgley (eds.)]. Cambridge University Press, Cambridge, United Kingdom and New York, NY, USA.

µmol	Micromole
20C3M	20th Century Climate in Coupled Models
AABW	Antarctic Bottom Water
AAIW	Antarctic Intermediate Water
AAO	Antarctic Oscillation
AATSR	Advanced Along Track Scanning Radiometer
ABA	AMSR Bootstrap Algorithm
ACC	Antarctic Circumpolar Current
ACCENT	Atmospheric Composition Change: a European Network
aci	Aerosol–Cloud Interactions
ACRIM	Active Cavity Radiometer Irradiance Monitor
ACW	Antarctic Circumpolar Wave
AeroCom	Aerosol Model Intercomparison
AERONET	Aerosol Robotic Network
A-FORCE	Aerosol Radiative Forcing in East Asia Aircraft Campaign
AGAGE	Advanced Global Atmospheric Gases Experiment
AGCM	Atmospheric General Circulation Model
AGTP	Absolute Global Temperature Change Potential
AGWP	Absolute Global Warming Potential
AIC	Aircraft-Induced Cirrus
ALOHA	A Long-term Oligotrophic Habitat Assessment
AMIP	Atmospheric Model Intercomparison Project
AMM	Atlantic Meridional Mode
AMO	Atlantic Multi-decadal Oscillation
AMOC	Atlantic Meridional Overturning Circulation
AMSR	Advanced Microwave Scanning Radiometer
AMSU	Advanced Microwave Sounding Unit
AMV	Atlantic Multi-decadal Variability
AO	Arctic Oscillation
AOD	Aerosol Optical Depth
AOGCM	Atmosphere–Ocean General Circulation Model
APHRODITE	Asian Precipitation – Highly Resolved Observational Data Integration Towards Evaluation
AR4	IPCC Fourth Assessment Report
ARCPAC	Aerosol, Radiation, and Cloud Processes affecting Arctic Climate
ARCTAS	Arctic Research of the Composition of the Troposphere from Aircraft and Satellites
ARFI	Aerosol Radiative Forcing over India
ari	Aerosol–Radiation Interactions
ARM	Atmospheric Radiation Measurement
ARTIST	Arctic Radiation and Turbulence Interaction Study
ATL3	Atlantic 3
ATSR	Along Track Scanning Radiometer
AUSMC	Australian-Maritime Continent
AVHRR	Advanced Very High Resolution Radiometer
AVISO	Archiving, Validation and Interpretation of Satellite Oceanographic Data
BATS	Bermuda Atlantic Time Series Study
BC	Black Carbon
BCC	Beijing Climate Center
BCC-CSM	Beijing Climate Center-Climate System Model
BDC	Brewer–Dobson Circulation
BECCS	Bio-Energy with Carbon-Capture and Storage
BMI	Basin Mean Index
BNF	Biological Nitrogen Fixation
BOM	Bureau of Meteorology
C_2Cl_4	Tetrachloroethene
C^4MIP	Coupled Climate Carbon Cycle Model Intercomparison Project
$CaCO_3$	Calcium Carbonate
CALIOP	Cloud-Aerosol Lidar with Orthogonal Polarization
CALIPSO	Cloud-Aerosol Lidar and Infrared Pathfinder Satellite Observations
CAM	Community Atmosphere Model
CAMS	Climate Anomaly Monitoring System
CanESM	Canadian Earth System Model
CASTNET	Clean Air Status and Trends Network
CCCma	Canadian Centre for Climate Modelling and Analysis
CCl_4	Carbon Tetrachloride
CCM	Chemistry–Climate Model
CCMVal	Chemistry–Climate Model Validation
CCN	Cloud Condensation Nuclei
CCR	Carbon Climate Response
CCSM	Community Climate System Model
CCSR	Centre for Climate System Research
CDD	Consecutive Dry Days

CDIAC	Carbon Dioxide Information Analysis Center
CDR	Carbon Dioxide Removal
CDW	Circumpolar Deep Water
CE	Common Era
CERES	Cloud and the Earth's Radiant Energy System
CESM	Community Earth System Model
CESM1–BGC	Community Earth System Model 1–Biogeochemical
CF_4	Perfluoromethane
CFC	Chlorofluorocarbon
CFC-11	Trichlorofluoromethane ($CFCl_3$)
CFC-113	Trichlorotrifluoroethane ($CF_2ClCFCl_2$)
CFC-12	Dichlorodifluoromethane (CF_2Cl_2)
CFMIP	Cloud Feedback Model Intercomparison Project
CFSRR	Climate Forecast System Reanalysis and Reforecast
CGCM	Coupled General Circulation Model
CH_2Cl_2	Dichloromethane
CH_3Br	Bromomethane
CH_3CCl_3	Methyl Chloroform
CH_3Cl	Chloromethane
CH_4	Methane
CLIMAP	Climate: Long-range Investigation, Mapping, and Prediction
CLIMBER-2	Climate and Biosphere Model
CLIO	Coupled Large-scale Ice-Ocean Model
CLM4C	Community Land Model for Carbon
CLM4CN	Community Land Model for Carbon–Nitrogen
CMAP	CPC Merged Analysis of Precipitation
CMDL	Climate Monitoring and Diagnostics Laboratory (NOAA)
CMIP3	Coupled Model Intercomparison Project Phase 3
CMIP5	Coupled Model Intercomparison Project Phase 5
CNRM	Centre National de Recherches Météorologiques
CO	Carbon Monoxide
CO_2	Carbon Dioxide
CO_3^{2-}	Carbonate
COADS	Comprehensive Ocean–Atmosphere Data Set
COBE-SST	Centennial in situ Observation-Based Estimates of Sea Surface Temperature
COCO	CCSR Ocean Component Model
COHMAP	Cooperative Holocene Mapping Project
CORE	Coordinated Ocean-ice Reference Experiments
COWCLIP	Coordinated Ocean Wave Climate Project
COWL	Cold Ocean/Warm Land
CPC	Climate Prediction Center (NOAA)
CPR	Cloud Profiling Radar
CRE	Cloud Radiative Effect
CRU	Climatic Research Unit
CRUTEM4	Climatic Research Unit Gridded Dataset of Global Historical Near-Surface Air TEMperature Anomalies Over Land Version 4
CS	Complex Ocean Sediment Model
CSFR	Climate Forecast System Reanalysis
CSIRO	Commonwealth Scientific and Industrial Research Organisation
CWC	Cumulative Warming Commitment
DCESS	Danish Center for Earth System Science
DIC	Dissolved Inorganic Carbon
DJF	December, January and February
DMI	Directional Movement Index
DMS	Dimethyl Sulphide
DO	Dissolved Oxygen; also Dansgaard-Oeschger
DOC	Dissolved Organic Carbon
DOE	Department of Energy
DTR	Diurnal Temperature Range
DU	Dobson Units
EAS	East Asian Summer
EASM	East Asian Summer Monsoon
EBC	Equivalent Black Carbon
EBM	Energy Balance Model
ECBILT	Coupled Atmosphere Ocean Model from de Bilt
ECHAM	ECMWF and Hamburg
ECHO-G	ECHAM4+HOPE-G
ECMWF	European Centre for Medium Range Weather Forecasts
ECS	Equilibrium Climate Sensitivity
EDGAR	Emission Database for Global Atmospheric Research
EMIC	Earth System Model of Intermediate Complexity

ENSO	El Niño-Southern Oscillation
EOF	Empirical Orthogonal Function
ERA-40	ECMWF 40-year ReAnalysis
ERBE	Earth Radiation Budget Experiment
ERBS	Earth Radiation Budget Satellite
ERF	Effective Radiative Forcing
ERFaci	Effective Radiative Forcing due to Aerosol–Cloud Interactions
ERFari	Effective Radiative Forcing due to Aerosol–Radiation Interactions
ERS	European Remote Sensing (Satellite)
ERSST	Extended Reconstructed Sea Surface Temperature
ESA	European Space Agency
ESM	Earth System Model
ESMR	Electrically Scanning Microwave Radiometer
ESRL	Earth System Research Library (NOAA)
ESTOC	European Station for Time Series in the Ocean
ETC	Extratropical Cyclone
FACE	Free-Air CO_2 Enrichment
FAO	Food and Agriculture Organization (UN)
FAR	IPCC First Assessment Report
FGOALS1	Flexible Global Ocean Atmosphere Land System Model Version 1
FIO	First Institute of Oceanography
FLUXNET	Global Network of Flux Towers
FTIR	Fourier Transform Infrared Spectroscopy
FTS	Fourier-Transform Spectrometer
FWCC	Freshwater Content Changes
GCAM	Global Change Assessment Model
GCM	General Circulation Model
GCP	Global Cost Potential
GCRM	Global Cloud-Resolving Models
GEISA	Gestion et Etude des Informations Spectroscopiques Atmosphériques
GENIE-1	Grid Enabled Integrated Earth System Model-1
GeoMIP G1	Geoengineering Model Intercomparison Project G1
GFDL	Geophysical Fluid Dynamics Laboratory
GFED	Global Fire Emissions Database
GHCN	Global Historical Climatology Network
GHCNDEX	Global Historical Climatology Network-Daily Gridded Data Set of Climate Extremes
GHCNv3	Global Historical Climatology Network Version 3
GHG	Greenhouse Gas
GI	Greenland Interstadial
GIA	Glacial Isostatic Adjustment
GIS	Greenland Ice Sheet
GISP	Greenland Ice Sheet Project
GISS	Goddard Institute of Space Studies
GISTEMP	Goddard Institute for Space Studies Surface Temperature Analysis
GL	Grounding Line
GLODAP	Global Ocean Data Analysis Project
GLS	Generalized Least Squares
GMA	Global Monsoon Area
GMD	Global Monitoring Division (NOAA)
GMI	Global Monsoon Precipitation Intensity
GMP	Global Monsoon Total Precipitation
GMSL	Global Mean Sea Level
GMST	Global Mean Surface Temperature
GOCCP	GCM-Oriented CALIPSO Cloud Product
GOGA	Global Ocean Global Atmosphere
GOME	Global Ozone Monitoring Experiment
GOMOS	Global Ozone Monitoring by Occultation of Stars
GOSAT	Greenhouse Gases Observing Satellite
GPCC	Global Precipitation Climatology Centre
GPCP	Global Precipitation Climatology Project
GPH	Geopotential Height
GPP	Gross Primary Productivity
GPS	Global Positioning System
GRACE	Gravity Recovery and Climate Experiment
GRISLI	Grenoble Ice Shelf and Land Ice Model
GS	Greenland Stadial
GSFC	Goddard Space Flight Centre
Gt	Gigatonnes
GTP	Global Temperature Change Potential
GUESS	General Ecosystem Simulator
GWD	Gravity-Wave Drag
GWP	Global Warming Potential

HadAT2	Hadley Centre Atmospheric Temperature Data Set 2
HadCM	Hadley Centre Climate Prediction Models
HadCRUT4	Hadley Centre Climatic Research Unit Gridded Surface Temperature Data Set 4
HadEX	Hadley Centre Gridded Data Set Of Temperature And Precipitation Extremes
HadGEM1	Hadley Centre New Global Environmental Model 1
HadGEM2-ES	Hadley Centre New Global Environmental Model 2-Earth System
HadGHCND	Hadley Centre Gridded Daily Temperatures Data Set
HadISST	Hadley Centre Interpolated SST
HadNMAT2	Hadley Centre Night Marine Air Temperatures Data Set Version 2
HadSLP2r	Hadley Centre Sea Level Pressure Data Set 2r
HadSST3	Hadley Centre Sea Surface Temperature Data Set Version 3
HALOE	Halogen Occultation Experiment
HCFC	Hydrochlorofluorocarbon
HCO_3^-	Bicarbonate Ion
HF	Hickey–Frieden (Radiometer)
HFC	Hydrofluorocarbon
HIPPO	HIAPER Pole-to-Pole Observations
HIRHAM5	High-Resolution Hamburg Climate Model 5
HITRAN	High-Resolution Transmission Molecular Absorption
HOAPS	Hamburg Ocean–Atmosphere Parameters and Fluxes from Satellite
HOT	Hawaii Ocean Time Series
HYDE	History Database of the Environment
HY-INT	Hydroclimatic Intensity
HYLAND	Hybrid Land Terrestrial Ecosystem Model
IAM	Integrated Assessment Model
IASI	Infrared Atmospheric Sounder Interferometer
ICE	Ice Cloud and Land Elevation
ICESat	Ice, Cloud and Land Elevation Satellite
ICOADS	International Comprehensive Ocean-Atmosphere Data Set
IGAC	International Global Atmospheric Chemistry
IMAGE	Integrated Model to Assess the Global Environment
IMBIE	Ice-sheet Mass Balance Intercomparison Experiment
IMPROVE	US Interagency Monitoring of Protected Visual Environments
INMCM4	Institute for Numerical Mathematics Coupled Model 4
IOB	Indian Ocean Basin
IOBM	Indian Ocean Basin Mode
IOD	Indian Ocean Dipole
IODM	Indian Ocean Dipole Mode
IPA	International Permafrost Association
IPO	Inter-decadal Pacific Oscillation
IPSL	Institut Pierre Simon Laplace
IPY	International Polar Year
IR	Infrared
IRF	Impulse Response Function
ISCCP	International Satellite Cloud Climatology Project
ITCZ	Inter-Tropical Convergence Zone
ITF	Indonesian Throughflow
IUK	Iterative Universal Kriging
JIMAR	Joint Institute for Marine and Atmospheric Research
JJA	June, July and August
JMA	Japan Meteorological Agency
JPL	Jet Propulsion Laboratory
ka	1000 Years ago
KCM	Knowledge Capture and Modeling
kyr	1000 Years
LAC	Light-Absorbing Carbon
LBIS	Larsen B Ice Shelf
LBL	Line-by-line (models)
LGM	Last Glacial Maximum
LIA	Little Ice Age
LIG	Last Interglacial
LISAM	Large–scale Index for South America Monsoon
LLGHG	Long-Lived Greenhouse Gas
LMM	Late Maunder Minimum
LNADW	Lower North Atlantic Deep Water
LOSU	Level of Scientific Understanding
LOVECLIM	Loch–Vecode-Ecbilt-Clio-Agism Model

LPB	La Plata Basin
LPJ	Lund-Potsdam-Jena Dynamic Global Model
LRF	Long-Range Forecast
LS	Lower Stratosphere
LSAT	Land-Surface Air Temperature
LSW	Labrador Sea Water
LUC	Land Use and Climate
LUCID	Land Use and Climate, Identification of Robust Impacts
LULC	Land Use and Land Cover
LULCC	Land Use and Land Cover Change
LWCRE	Longwave Cloud Radiative Effect
LWR	Longwave Radiation
MAGICC	Model for the Assessment of Greenhouse Gas Induced Climate Change
MAM	March, April and May
MAR	Modèle Atmosphérique Régional
MARGO	Multiproxy Approach for the Reconstruction of the Glacial Ocean Surface
MAT	Marine Air Temperatures
MBT	Mechanical Bathythermograph
MCA	Medieval Climate Anomaly
MDA	Mineral Dust Aerosol
MDT	Mean Dynamic Topography
MEA	Millennium Ecosystem Assessment
MERRA	Modern Era Reanalysis for Research and Applications
MESSAGE	Model for Energy Supply Strategy Alternatives and their General Environmental Impact
MFR	Maximum Feasible Reduction
MHD	Mace Head
MIP	Model Intercomparison Project
MIPAS	Michelson Interferometer for Passive Atmospheric Sounding
MIROC	Model for Interdisciplinary Research on Climate
MISI	Marine Ice Sheet Instability
MISR	Multi-angle Imaging Spectro-Radiometer
MIT	Massachusetts Institute of Technology
MJO	Madden–Julian Oscillation
MLD	Mixed Layer Depth
MLOST	Merged Land–Ocean Surface Temperature (Analysis)
MLS	Microwave Limb Sounder
MME	Multi-Model Ensemble
MMF	Multiscale Modelling Framework
MMM	Multi-Model Mean
MMTS	Maximum–Minimum Temperature Systems
MOC	Meridional Overturning Circulation
MOCAGE	Modèle de Chimie Atmosphérique à Grande Echelle
MODIS	Moderate Resolution Imaging Spectrometer
MOHC	Met Office Hadley Centre
MOPITT	Measurements of Pollutants in the Troposphere
MPI	Max Planck Institute
MPIOM	Max Planck Institute Ocean Model
MPWP	Mid-Pliocene Warm Period
MRI	Meteorological Research Institute of Japan Meteorological Agency
MSL	Mean Sea Level
MSSS	Mean Square Skill Score
MSU	Microwave Sounding Unit
Mt	Megatonnes
MT	Mid-Tropospheric
MTCO	Mean Temperature of the Coldest Month
MTWA	Mean Temperature of the Warmest Month
MW	Microwave
MXD	Maximum Latewood Density
Ma	Million Years ago
Myr	Million Years
N_2O	Nitrous Oxide
NADW	North Atlantic Deep Water
NAM	Northern Annular Mode
NAMP	National Air Quality Monitoring Programme (India)
NAMS	North American Monsoon System
NAO	North Atlantic Oscillation
NASA	National Aeronautics and Space Administration
NCAR	National Center for Atmospheric Research
NCEP	National Centers for Environmental Prediction
NEC	North Equatorial Current

NEEM	North Greenland Eemian Ice Drilling
NEWS	Global Nutrient Export from WaterSheds
NF_3	Nitrogen Trifluoride
NGRIP	North Greenland Ice Core Project
NH	Northern Hemisphere
NIWA	National Institute of Water and Atmospheric Research
NMAT	Nighttime Marine Air Temperature
NMVOC	Non-Methane Volatile Organic Compound
NNR	NCEP–NCAR
NOAA	National Oceanic and Atmospheric Administration
NODC	National Oceanic Data Center
NorESM	Norwegian Earth System Model
NO_x	Reactive Nitrogen Oxides (the Sum of NO and NO_2)
NPI	North Pacific Index
NPIW	North Pacific Intermediate Water
NPP	Net Primary Productivity
NSIDC	National Snow and Ice Data Center
NT1	National Aeronautics and Space Administration (NASA) Team Algorithm, Version 1
NT2	National Aeronautics and Space Administration (NASA) Team Algorithm, Version 2
NTCF	Near-Term Climate Forcer
$O(^1D)$	Oxygen Radical in the 1D Excited State
O_3	Ozone
OA	Ocean–Atmosphere; also Other Anthropogenic (Forcings)
OAC	Ocean–Atmosphere–Carbon Cycle
OAFlux	Objectively Analyzed Air–Sea Heat Fluxes
OAGCMs	Ocean–Atmosphere General Circulation Models
OAV	Ocean–Atmosphere–Vegetation
OC	Organic Carbon
OCN	Oceanic Carbon and Nutrient Cycling (Model)
ODP	Ocean Drilling Program
ODS	Ozone-Depleting Substance
OH	Hydroxyl Radical
OHC	Ocean Heat Content
OHR	Ocean Heating Rate
OLR	Outgoing Longwave Radiation
OLS	Ordinary Least Squares
OMI	Ozone Monitoring Instrument
ONDJFM	October, November, December, January, February and March
ORC	Oceanic Reservoir Correction
PAGES 2k	Past Global Changes 2k
PARASOL	Polarization and Anisotropy of Reflectances for Atmospheric Sciences Coupled with Observations from Lidar
PATMOS-x	Pathfinder Atmospheres Extended Data Set
PBAPs	Primary Biological Aerosol Particles
PCM	Parallel Climate Model
pCO_2	Partial Pressure of Carbon Dioxide
PDF	Probability Density Function
PDO	Pacific Decadal Oscillation
PDSI	Palmer Drought Severity Index
PETM	Paleocene–Eocene Thermal Maximum
PFC	Perfluorocarbon
PG	Peripheral Glacier
Pg	Petagram
PM_{10}	Particulate Matter with Aerodynamic Diameter <10 μm
$PM_{2.5}$	Particulate Matter with Aerodynamic Diameter <2.5 μm
PMEL	Pacific Marine Environmental Laboratory
PMIP3	Paleoclimate Modelling Intercomparison Project Phase III
PMOD	Physikalisch-Meteorologisches Observatorium Davos
PNA	Pacific–North American (Pattern)
POA	Primary Organic Aerosol
POC	Particulate Organic Carbon
POLDER	Polarization and Directionality of the Earth's Reflectance
PPE	Perturbed-Parameter Ensemble
PRCE	Peak Response to Cumulative Emissions
PREMOS	Precision Monitor Sensor
PSA	Pacific–South American (Pattern)
PSMSL	Permanent Service for Mean Sea Level
PSS	Practical Salinity Scale
PSS78	Practical Salinity Scale 1978

PUCCINI	Physical Understanding of Composition-Climate Interactions and Impacts
QBO	Quasi-Biennial Oscillation
R95p (R99p)	Amount of Precipitation from Days >95th (99th) Percentile
RACMO2	Regional Atmospheric Climate Model 2
RAOBCORE	Radiosone Observation Correction using Reanalyses
RAPID/MOCHA	Rapid Climate Change-Meridional Overturning Circulation and Heatflux Array
RATPAC	Radiosonde Atmospheric Temperature Products for Assessing Climate
RCM	Regional Climate Model
RCP	Representative Concentration Pathway
RE	Radiative Efficiency
REMBO	Regional, Moisture-Balance Orographic Model
REML	Restricted Maximum Likelihood
RF	Radiative Forcing
RFaci	Radiative Forcing from Aerosol–Cloud Interactions
RGI	Randolph Glacier Inventory
RH	Relative Humidity
RICH	Radiosonde Innovation Composite Homogenization
RMIB	Royal Meteorological Institute of Belgium
RMS	Root Mean Square
RMSE	Root Mean Square Error
RO	Radio Occultation
RSCA	Relative Snow-Covered Area
RSL	Relative Sea Level
RSS	Remote Sensing System
RX5day/RX1day	Annual Maximum 5-Day/1-Day Precipitation
S/N	Signal-to-Noise (Ratio)
SACZ	South Atlantic Convergence Zone
SAGE	Stratospheric Aerosol and Gas Experiment or Centre for Sustainability and the Global Environment
SAM	Southern Annular Mode
SAMS	South American Monsoon System
SAMW	Sub-Antarctic Mode Water
SAR	IPCC Second Assessment Report
SAT	Surface Air Temperature
SBA	SSM/I Bootstrap Algorithm
SBUV	Solar Backscatter Ultraviolet
SC	Solar Cycle
SCA	Snow-Covered Area
SCD	Snow Cover Duration
SCE	Snow Cover Extent
SCIA	Scanning Imaging Absorption Spectrometer for Atmospheric Chartography
SCIAMACHY	Scanning Imaging Absorption Spectrometer for Atmospheric Chartography
SD	Snow Depth; also Statistical Downscaling
SDGVM	Sheffield Dynamic Global Vegetation Model
SDII	Simple Daily Precipitation Intensity Index
SeaWiFS	Sea-viewing Wide Field-of-view Sensor
SEM	Semi-Empirical Model
SF_6	Sulphur Hexafluoride
SH	Southern Hemisphere
SICOPOLIS	Simulation Code for Polythermal Ice Sheets
SIM	Spectral Irradiance Monitor
SIO	Scripps Institution of Oceanography
SLE	Sea Level Equivalent
SLP	Sea Level Pressure
SLR	Sea Level Rise
SMB	Surface Mass Balance
SMMR	Scanning Multichannel Microwave Radiometer
SMOS	Soil Moisture and Ocean Salinity
SNO	Simultaneous Nadir Overpass
SO_2	Sulphur Dioxide
SO_2F_2	Sulphuryl Fluoride
SO_4^{2-}	Sulfate
SOA	Secondary Organic Aerosol
SOI	Southern Oscillation Index
SOLSTICE	Solar Stellar Irradiance Comparison Experiment
SON	September, October and November
SORCE	Solar Radiation and Climate Experiment
SPARC	Stratospheric Processes and their Role in Climate Chemistry Climate Model Validation
SPCZ	South Pacific Convergence Zone

SPEI	Standardised Precipitation Evapotranspiration Index
SPI	Standardised Precipitation Index
SPRINTARS	Spectral Radiation-Transport Model for Aerosol Species
SRALT	Satellite Radar Altimetry
SRES	IPCC Special Report on Emission Scenarios
SREX	IPCC Special Report on Managing the Risk of Extreme Events and Disasters to Advance Climate Change Adaptation
SRM	Solar Radiation Management
SSH	Sea Surface Height
SSI	Spectral Solar Irradiance
SSM/I	Special Sensor Microwave/Imager
SSR	Surface Solar Radiation
SSS	Sea Surface Salinity
SST	Sea Surface Temperature
SSU	Stratospheric Sounding Unit
STAR	Center for Satellite Applications and Research
STMW	Subtropical Mode Water
SVS	Standard Verification System (WMO)
SWCRE	Shortwave Cloud Radiative Effect
SWE	Snow Water Equivalent
SWH	Significant Wave Height
SWR	Solar Shortwave Radiation
TBO	Tropospheric Biennial Oscillation
Tg	Teragrams
T/P	TOPEX/Poseidon
TANSO	Thermal and Near Infrared Sensor for Carbon Observation
TAR	IPCC Third Assessment Report
TC	Tropical Cyclone; also Total Carbon
TCCON	Total Carbon Column Observing Network
TCR	Transient Climate Response
TCRE	Transient Climate Response to Cumulative CO_2 Emissions
TES	Tropospheric Emission Spectrometer
TIM	Total Irradiance Monitor
TNI	Trans-Niño Index
TOA	Top of the Atmosphere
TOMS	Total Ozone Mapping Spectrometer
TOPEX	Topography Experiment
TRANSCOM	Atmospheric Tracer Transport Model Intercomparison Project
TRIFFID	Top-down Representation of Interactive Foliage and Flora Including Dynamics
TRUTHS	Traceable Radiometry Underpinning Terrestrial and Helio Studies
TRW	Tree-Ring Width
TSI	Total Solar Irradiance
TTD	Transit Time Distribution
TW	Tidewater
UAH	University of Alabama in Huntsville
UARS	Upper Atmosphere Research Satellite
UCI	University of California, Irvine
UHI	Urban Heat Island
UNADW	Upper North Atlantic Deep Water
UNEP	United Nations Environment Programme
UOHC	Upper (0–700 m) Ocean Heat Content
USHCN	US Historical Climatology Network
UTLS	Upper Troposphere/Lower Stratosphere
UV	Ultraviolet
UVic	University of Victoria
VasClimO	Variability Analyses of Surface Climate Observations
VEGAS	Terrestrial Vegetation and Carbon Model
VIIRS	Visible Infrared Imaging Radiometer Suite
VLM	Vertical Land Motion
VOC	Volatile Organic Compound
VOS	Voluntary Observing Ship
W	Watts
WAIS	West Antarctic Ice Sheet
WASWind	Wave- and Anemometer-Based Sea Surface Wind
WCRP	World Climate Research Programme
WMGHG	Well-Mixed Greenhouse Gas
WMO	World Meteorological Organization
WOCE	World Ocean Circulation Experiment
WSG	Western Subarctic Gyre
XBT	Expendable Bathythermograph

AV

Annex V: Contributors to the IPCC WGI Fifth Assessment Report

This annex should be cited as:
IPCC, 2013: Annex V: Contributors to the IPCC WGI Fifth Assessment Report. In: *Climate Change 2013: The Physical Science Basis. Contribution of Working Group I to the Fifth Assessment Report of the Intergovernmental Panel on Climate Change* [Stocker, T.F., D. Qin, G.-K. Plattner, M. Tignor, S.K. Allen, J. Boschung, A. Nauels, Y. Xia, V. Bex and P.M. Midgley (eds.)]. Cambridge University Press, Cambridge, United Kingdom and New York, NY, USA.

Coordinating Lead Authors, Lead Authors, Review Editors and Contributing Authors are listed alphabetically by surname.

AAMAAS, Borgar
Center for International Climate and Environmental Research Oslo
Norway

ABE-OUCHI, Ayako
University of Tokyo
Japan

ABIODUN, Babatunde
University of Cape Town
South Africa

ABRAHAM, Libu
Qatar Meteorological Department
Qatar

ACHUTARAO, Krishna Mirle
Indian Institute of Technology
India

ADEDOYIN, Akintayo John
University of Botswana
Botswana

ADLER, Robert F.
University of Maryland
USA

AHLSTRÖM, Anders
Lund University
Sweden

ALDRIAN, Edvin
Agency for Meteorology, Climatology and Geophysics
Indonesia

ALDRIN, Magne
Norwegian Computing Center and University of Oslo
Norway

ALEXANDER, Lisa V.
University of New South Wales
Australia

ALLAN, Richard P.
University of Reading
UK

ALLAN, Robert
Met Office Hadley Centre
UK

ALLEN, Myles R.
University of Oxford
UK

ALLEN, Simon K.
IPCC WGI TSU, University of Bern
Switzerland

ALLISON, Ian
Antarctic Climate and Ecosystems Cooperative Research Centre
Australia

AMBRIZZI, Tércio
University of Sao Paulo
Brazil

AN, Soon-Il
Yonsei University
Republic of Korea

ANAV, Alessandro
University of Exeter
UK

ANCHUKAITIS, Kevin
Woods Hole Oceanographic Institution
USA

ANDERSON, Bruce
Boston University
USA

ANDREWS, Oliver
University of East Anglia
UK

ANDREWS, Timothy
Met Office Hadley Centre
UK

AOKI, Shigeru
Hokkaido University
Japan

AOYAMA, Michio
Meteorological Research Institute
Japan

ARAKAWA, Osamu
University of Tsukuba
Japan

ARBLASTER, Julie
Bureau of Meteorology
Australia

ARCHER, David
University of Chicago
USA

ARENDT, Anthony A.
University of Alaska Fairbanks
USA

ARORA, Vivek
Environment Canada
Canada

ARRITT, Raymond
Iowa State University
USA

ARTAXO, Paulo
University of Sao Paulo
Brazil

BAEHR, Johanna
University of Hamburg
Germany

BAHR, David B.
University of Colorado Boulder
USA

BALA, Govindasamy
Indian Institute of Science
India

BALAN SAROJINI, Beena
University of Reading
UK

BALDWIN, Mark
University of Exeter
UK

BAMBER, Jonathan
University of Bristol
UK

BARINGER, Molly
National Oceanic and Atmospheric Administration, Atlantic Oceanographic and Meteorological Laboratory
USA

BARLOW, Mathew
University of Massachusetts
USA

BARRIOPEDRO, David
Universidad Complutense de Madrid
Spain

BARTHOLY, Judit
Eötvös Loránd University
Hungary

BARTLEIN, Patrick J.
University of Oregon
USA

BATES, Nicholas R.
Bermuda Biological Station
Bermuda

BEER, Jürg
Eawag - Swiss Federal Institute of Aquatic Science and Technology
Switzerland

BELLOUIN, Nicolas
University of Reading
UK

BENEDETTI, Angela
European Centre for Medium-Range Weather Forecasts
UK

BENITO, Gerardo
Consejo Superior de Investigaciones Cientificas
Spain

BEYERLE, Urs
ETH Zurich
Switzerland

BIASUTTI, Michela
Columbia University
USA

BINDOFF, Nathaniel L.
University of Tasmania
Australia

BINER, Sébastien
Ouranos Consortium on Regional Climatology and Adaptation to Climate Change
Canada

BITZ, Cecilia M.
University of Washington
USA

BLAKE, Donald R.
University of California Irvine
USA

BODAS-SALCEDO, Alejandro
Met Office Hadley Centre
UK

BOER, George J.
Environment Canada
Canada

BOJARIU, Roxana
National Meteorological Administration
Romania

BONAN, Gordon
National Center for Atmospheric Research
USA

BONY, Sandrine
Laboratoire de Météorologie Dynamique, Institut Pierre Simon Laplace
France

BOOTH, Ben B.B.
Met Office Hadley Centre
UK

BOPP, Laurent
Laboratoire des Sciences du Climat et de l'Environnement, Institut Pierre Simon Laplace
France

BORGES, Alberto Vieira
Université de Liège
Belgium

BOUCHER, Olivier
Laboratoire de Météorologie Dynamique, Institut Pierre Simon Laplace
France

BOUSQUET, Philippe
Laboratoire des Sciences du Climat et de l'Environnement, Institut Pierre Simon Laplace
France

BOUWMAN, Lex
PBL Netherlands Environmental Assessment Agency
Netherlands

BOX, Jason E.
Geological Survey of Denmark and Greenland
Denmark

BOYER, Timothy
National Oceanic and Atmospheric Administration, National Oceanographic Data Center
USA

BRACONNOT, Pascale
Laboratoire des Sciences du Climat et de l'Environnement, Institut Pierre Simon Laplace
France

BRAUER, Achim
GFZ German Research Centre for Geosciences
Germany

BRÉON, François-Marie
Laboratoire des Sciences du Climat et de l'Environnement, Institut Pierre Simon Laplace
France

BRETHERTON, Christopher
University of Washington
USA

BROMWICH, David H.
Ohio State University
USA

BRÖNNIMANN, Stefan
University of Bern
Switzerland

BROOKS, Harold E.
National Oceanic and Atmospheric Administration, National Severe Storms Laboratory
USA

BROVKIN, Victor
Max Planck Institute for Meteorology
Germany

BROWN, Josephine
Bureau of Meteorology
Australia

BROWN, Ross
Environment Canada
Canada

BROWNE, Oliver
University of Edinburgh
UK

BRUHWILER, Lori M.
National Oceanic and Atmospheric Administration, Earth System Research Laboratory
USA

BRUTEL-VUILMET, Claire
Laboratoire de Glaciologie et Géophysique de l`Environnement, Université Joseph Fourier
France

BYRNE, Robert H.
University of South Florida
USA

CAI, Wenju
CSIRO Marine and Atmospheric Research
Australia

CALDEIRA, Kenneth
Carnegie Institution for Science
USA

CAMERON-SMITH, Philip
Lawrence Livermore National Laboratory
USA

CAMILLONI, Ines
Universidad de Buenos Aires
Argentina

CAMPOS, Edmo
University of Sao Paulo
Brazil

CANADELL, Josep
CSIRO Marine and Atmospheric Research
Australia

CANE, Mark
Columbia University
USA

CAO, Long
Zhejiang University
China

CARRASCO, Jorge
Direccion Meteorologica de Chile
Chile

CARSON, Mark
University of Hamburg
Germany

CARTER, Tim
Finnish Environment Institute
Finland

CARVALHO, Leila V.
University of California Santa Barbara
USA

CATTO, Jennifer
Monash University
Australia

CAVALCANTI, Iracema F.A.
National Institute for Space Research
Brazil

CAZENAVE, Anny
Laboratoire d'Etudes en Géophysique et Océanographie Spatiales
France

CHADWICK, Robin
Met Office Hadley Centre
UK

CHAMBERS, Don
University of South Florida
USA

CHANG, Ping
Texas A&M University
USA

CHAPPELLAZ, Jérôme
Laboratoire de Glaciologie et Géophysique de l`Environnement, Université Joseph Fourier
France

CHARABI, Yassine Abdul-Rahman
Sultan Qaboos University
Oman

CHEN, Deliang
University of Gothenburg
Sweden

CHEN, Xiaolong
Institute of Atmospheric Physics, Chinese Academy of Sciences
China

CHEVALLIER, Frédéric
Laboratoire des Sciences du Climat et de l'Environnement, Institut Pierre Simon Laplace
France

CHHABRA, Abha
Indian Space Research Organisation
India

CHIKAMOTO, Yoshimitsu
University of Hawaii
USA

CHOI, Jung
Seoul National University
Republic of Korea

CHOU, Sin Chan
National Institute for Space Research
Brazil

CHRISTENSEN, Jens Hesselbjerg
Danish Meteorological Institute
Denmark

CHRISTENSEN, Ole Bøssing
Danish Meteorological Institute
Denmark

CHRISTIDIS, Nikolaos
Met Office Hadley Centre
UK

CHURCH, John A.
CSIRO Marine and Atmospheric Research
Australia

CIAIS, Philippe
Laboratoire des Sciences du Climat et de l'Environnement, Institut Pierre Simon Laplace
France

CLARK, Peter U.
Oregon State University
USA

CLEVELAND, Cory
University of Montana
USA

CLIFTON, Olivia
Columbia University
USA

COGLEY, J. Graham
Trent University
Canada

COLLINS, Matthew
University of Exeter
UK

COLLINS, William
University of Reading
UK

COLLINS, William
Lawrence Berkeley National Laboratory
USA

COMISO, Josefino C.
National Aeronautics and Space Administration, Goddard Space Flight Center
USA

COOK, Edward
Columbia University
USA

COOK, Kerry H.
University of Texas
USA

COOLEY, Sarah
Woods Hole Oceanographic Institution
USA

COOPER, Owen R.
Cooperative Institute for Research in Environmental Sciences
USA

CORTI, Susanna
Institute of Atmospheric Sciences and Climate
Italy

COX, Peter
University of Exeter
UK

CROWLEY, Thomas
Braeheads Institute
UK

CUBASCH, Ulrich
Freie Universität Berlin
Germany

CUNNINGHAM, Stuart
Scottish Association of Marine Science
UK

DAI, Aiguo
University at Albany
USA

DALSØREN, Stig B.
Center for International Climate and Environmental Research Oslo
Norway

DANIEL, John S.
National Oceanic and Atmospheric Administration, Earth System Research Laboratory
USA

DAVIS, Robert E.
University of Virginia
USA

DAVIS, Sean M.
National Oceanic and Atmospheric Administration, Earth System Research Laboratory
USA

DE CASTRO, Manuel
Universidad de Castilla-La Mancha
Spain

DE DECKKER, Patrick
Australian National University
Australia

DE ELÍA, Ramón
Université du Québec à Montréal and Ouranos Consortium
Canada

DE MENEZES, Viviane Vasconcellos
University of Tasmania
Australia

DE VERNAL, Anne
Université du Québec à Montréal
Canada

DEFRIES, Ruth
Columbia University
USA

DEL GENIO, Anthony
National Aeronautics and Space Administration, Goddard Institute for Space Studies
USA

DELCROIX, Thierry
Laboratoire d'Etudes en Géophysique et Océanographie Spatiales
France

DELECLUSE, Pascale
Météo-France
France

DELMONTE, Barbara
University of Milano-Bicocca
Italy

DELSOLE, Tim
George Mason University
USA

DENTENER, Frank J.
European Commission, Joint Research Center
EU

DESER, Clara
National Center for Atmospheric Research
USA

DINEZIO, Pedro
University of Hawaii
USA

DING, Yihui
National Climate Center, China Meteorological Administration
China

DLUGOKENCKY, Edward J.
National Oceanic and Atmospheric Administration, Earth System Research Laboratory
USA

DOBLAS-REYES, Francisco
Institució Catalana de Recerca i Estudis Avançats and Institut Català de Ciències del Clima
Spain

DOKKEN, Trond
Uni Research Norway
Norway

DOMINGUES, Catia M.
Antarctic Climate and Ecosystems Cooperative Research Centre
Australia

DONAT, Markus G.
University of New South Wales
Australia

DONEY, Scott C.
Woods Hole Oceanographic Institution
USA

DONG, Wenjie
Beijing Normal University
China

DORE, John
Montana State University
USA

DOWSETT, Harry J.
U.S. Geological Survey
USA

DRIOUECH, Fatima
Direction de la Météorologie Nationale
Morocco

DUFRESNE, Jean-Louis
Laboratoire de Météorologie Dynamique, Institut Pierre Simon Laplace
France

DURACK, Paul J.
Lawrence Livermore National Laboratory
USA

EASTERLING, David R.
National Oceanic and Atmospheric Administration, Cooperative Institute for Climate and Satellites
USA

EBY, Michael
University of Victoria
Canada

EDWARDS, R. Lawrence
University of Minnesota
USA

ELISEEV, Alexey
Russian Academy of Sciences
Russian Federation

EMANUEL, Kerry
Massachusetts Institute of Technology
USA

EMORI, Seita
National Institute for Environmental Studies
Japan

ENDO, Hirokazu
Meteorological Research Institute
Japan

ENFIELD, David B.
University of Miami
USA

ERISMAN, Jan Willem
Louis Bolk Institute
Netherlands

EUSKIRCHEN, Eugenie S.
University of Alaska Fairbanks
USA

EVAN, Amato
Scripps Institution of Oceanography
USA

EYRING, Veronika
DLR German Aerospace Center
Germany

FACCHINI, Maria Cristina
Institute of Atmospheric Sciences and Climate
Italy

FASULLO, John
National Center for Atmospheric Research
USA

FEELY, Richard A.
National Oceanic and Atmospheric Administration, Pacific Marine Environmental Laboratory
USA

FEINGOLD, Graham
National Oceanic and Atmospheric Administration, Earth System Research Laboratory
USA

FETTWEIS, Xavier
Université de Liège
Belgium

FICHEFET, Thierry
Université catholique de Louvain
Belgium

FINE, Rana
University of Miami
USA

FIOLETOV, Vitali
Environment Canada
Canada

FIORE, Arlene M.
Columbia University and Lamont-Doherty Earth Observatory
USA

FISCHER, Erich M.
ETH Zurich
Switzerland

FISCHER, Hubertus
University of Bern
Switzerland

FLANNER, Mark
University of Michigan
USA

FLATO, Gregory
Environment Canada
Canada

FLEITMANN, Dominik
University of Reading
UK

FOREST, Chris E.
Pennsylvania State University
USA

FORSTER, Piers
University of Leeds
UK

FOSTER, Gavin
University of Southampton
UK

FRAME, David
Victoria University of Wellington
New Zealand

FREELAND, Howard
Fisheries and Oceans Canada
Canada

FRIEDLINGSTEIN, Pierre
University of Exeter
UK

FRÖHLICH, Claus
Physikalisch-Meteorologisches Observatorium Davos, World Radiation Center
Switzerland

FUGLESTVEDT, Jan
Center for International Climate and Environmental Research Oslo
Norway

FUZZI, Sandro
Institute of Atmospheric Sciences and Climate
Italy

FYFE, John
Environment Canada
Canada

GALLOWAY, James
University of Virginia
USA

GANOPOLSKI, Andrey
Potsdam Institute for Climate Impact Research
Germany

GAO, Xuejie
National Climate Center, China Meteorological Administration
China

GARCÍA-SERRANO, Javier
Institut Català de Ciències del Clima
Spain

GARDNER, Alex S.
Clark University
USA

GARZOLI, Silvia
National Oceanic and Atmospheric Administration, Atlantic Oceanographic and Meteorological Laboratory
USA

GATES, Lydia
Freie Universität Berlin
Germany

GBOBANIYI, Emiola
Swedish Meteorological and Hydrological Institute
Sweden

GEHRELS, W. Roland
University of York
UK

GERLAND, Sebastian
Norwegian Polar Institute
Norway

GHAN, Steven
Pacific Northwest National Laboratory
USA

GIANNINI, Alessandra
Columbia University
USA

GIESEN, Rianne
Utrecht University
Netherlands

GILLETT, Nathan
Environment Canada
Canada

GINOUX, Paul
National Oceanic and Atmospheric Administration, Geophysical Fluid Dynamics Laboratory
USA

GLECKLER, Peter J.
Lawrence Livermore National Laboratory
USA

GONZÁLEZ ROUCO, Jesús Fidel
Universidad Complutense de Madrid
Spain

GONZÁLEZ-DÁVILA, Melchor
Universidad de Las Palmas de Gran Canaria
Spain

GOOD, Peter
Met Office Hadley Centre
UK

GOOD, Simon
Met Office Hadley Centre
UK

GOODESS, Clare
University of East Anglia
UK

GOOSSE, Hugues
Université catholique de Louvain
Belgium

GOSWAMI, Prashant
CSIR Centre for Mathematical Modelling and Computer Simulation
India

GOVIN, Aline
MARUM Center for Marine Environmental Sciences
Germany

GRANIER, Claire
Laboratoire Atmosphères, Milieux, Observations Spatiales, Institut Pierre Simon Laplace
France

GRAVERSON, Rune Grand
Stockholm University
Sweden

GRAY, Lesley
University of Oxford
UK

GREGORY, Jonathan M.
University of Reading and Met Office Hadley Centre
UK

GREVE, Ralf
Hokkaido University
Japan

GRIFFIES, Stephen
National Oceanic and Atmospheric Administration, Geophysical Fluid Dynamics Laboratory
USA

GRUBER, Nicolas
ETH Zurich
Switzerland

GRUBER, Stephan
University of Zurich
Switzerland

GUEMAS, Virginie
Institut Català de Ciències del Clima
Spain

GUILYARDI, Eric
Laboratoire d'Océanographie et du Climat, Institut Pierre Simon Laplace
France

GULEV, Sergey
P.P. Shirshov Institute of Oceanology
Russian Federation

GUPTA, Anil K.
Wadia Institute of Himalayan Geology
India

GURNEY, Kevin
Arizona State University
USA

GUTOWSKI, William J.
Iowa State University
USA

GUTZLER, David
University of New Mexico
USA

HAAS, Christian
York University
Canada

HAGEN, Jon Ove
University of Oslo
Norway

HAIGH, Joanna
Imperial College London
UK

HAIMBERGER, Leopold
University of Vienna
Austria

HALL, Alex
University of California Los Angeles
USA

HANNA, Edward
University of Sheffield
UK

HANSINGO, Kabumbwe
University of Zambia
Zambia

HARGREAVES, Julia
Japan Agency for Marine-Earth Science and Technology
Japan

HARIHARASUBRAMANIAN, Annamalai
University of Hawaii
USA

HARRISON, Sandy
Macquarie University
Australia

HARTMANN, Dennis L.
University of Washington
USA

HAWKINS, Ed
University of Reading
UK

HAYWOOD, Alan
University of Leeds
UK

HEGERL, Gabriele C.
University of Edinburgh
UK

HEIMANN, Martin
Max Planck Institute for Biogeochemistry
Germany

HEINZE, Christoph
University of Bergen
Norway

HELD, Isaac
National Oceanic and Atmospheric Administration, Geophysical Fluid Dynamics Laboratory
USA

HEMER, Mark
CSIRO Marine and Atmospheric Research
Australia

HENSE, Andreas
University of Bonn
Germany

HEWITSON, Bruce
University of Cape Town
South Africa

HEZEL, Paul J.
Université catholique de Louvain
Belgium

HO, Shu-Peng (Ben)
National Center for Atmospheric Research
USA

HOCK, Regine
University of Alaska Fairbanks
USA

HODGES, Kevin I.
University of Reading
UK

HODNEBROG, Øivind
Center for International Climate and Environmental Research Oslo
Norway

HOLGATE, Simon J.
Sea Level Research Foundation
UK

HOLLAND, David
New York University
USA

HOLLAND, Elisabeth A.
University of the South Pacific
Fiji

HOLLAND, Greg
National Center for Atmospheric Research
USA

HOLLAND, Marika M.
National Center for Atmospheric Research
USA

HOLLIS, Chris
GNS Science
New Zealand

HOLMES, Christopher
University of California Irvine
USA

HOOSE, Corinna
Karlsruhe Institute of Technology
Germany

HOPWOOD, Brett
Oak Ridge National Laboratory
USA

HORTON, Ben
Rutgers University
USA

HOUGHTON, Richard A.
Woods Hole Research Center
USA

HOUSE, Joanna I.
University of Bristol
UK

HOUWELING, Sander
Utrecht University
Netherlands

HU, Yongyun
Peking University
China

HUANG, Jianping
Lanzhou University
China

HUANG, Ping
Institute of Atmospheric Physics, Chinese Academy of Sciences
China

HUBER, Markus
ETH Zurich
Switzerland

HUNKE, Elizabeth
Los Alamos National Laboratory
USA

HUNTER, John R.
University of Tasmania
Australia

HUNTER, Stephen
University of Leeds
UK

HURRELL, Jim
National Center for Atmospheric Research
USA

HURTT, George
University of Maryland
USA

HUSS, Matthias
University of Fribourg
Switzerland

HUYBRECHTS, Philippe
Vrije Universiteit Brussel
Belgium

HYDES, David
National Oceanography Centre
UK

ILYINA, Tatiana
Max Planck Institute for Meteorology
Germany

IMBERS QUINTANA, Jara
University of Oxford
UK

INFANTI, Johnna
University of Miami
USA

INGRAM, William
University of Oxford
UK

ISHII, Masayoshi
Meteorological Research Institute
Japan

IVANOVA, Detelina
Lawrence Livermore National Laboratory
USA

JACOB, Daniel
Harvard University
USA

JACOBS, Stanley
Columbia University
USA

JACOBSON, Andrew D.
Northwestern University
USA

JAIN, Atul
University of Illinois
USA

JAIN, Suman
University of Zambia
Zambia

JAKOB, Christian
Monash University
Australia

JANSEN, Eystein
University of Bergen
Norway

JANSSEN, Emily
University of Illinois
USA

JEVREJEVA, Svetlana
National Oceanography Centre
UK

JOHN, Jasmin
National Oceanic and Atmospheric Administration, Geophysical Fluid Dynamics Laboratory
USA

JOHNS, Tim
Met Office Hadley Centre
UK

JOHNSON, Gregory C.
National Oceanic and Atmospheric Administration, Pacific Marine Environmental Laboratory
USA

JONES, Andy
Met Office Hadley Centre
UK

JONES, Christopher
Met Office Hadley Centre
UK

JONES, Julie
University of Sheffield
UK

JOOS, Fortunat
University of Bern
Switzerland

JOSEY, Simon A.
National Oceanography Centre
UK

JOSHI, Manoj
University of East Anglia
UK

JOUGHIN, Ian
University of Washington
USA

JOUSSAUME, Sylvie
Laboratoire des Sciences du Climat et de l'Environnement, Institut Pierre Simon Laplace
France

JOUZEL, Jean
Laboratoire des Sciences du Climat et de l'Environnement, Institut Pierre Simon Laplace
France

JUNGCLAUS, Johann
Max Planck Institute for Meteorology
Germany

KAGEYAMA, Masa
Laboratoire des Sciences du Climat et de l'Environnement, Institut Pierre Simon Laplace
France

KANIKICHARLA, Krishna Kumar
Indian Institute of Tropical Meteorology
India

KANYANGA, Joseph Katongo
Zambia Meteorological Department
Zambia

KANZOW, Torsten
GEOMAR Helmholtz Centre for Ocean Research
Germany

KAPLAN, Alexey
Columbia University
USA

KAPLAN, Jed O.
EPFL Lausanne
Switzerland

KARL, David
University of Hawaii
USA

KARUMURI, Ashok
Indian Institute of Tropical Meteorology
India

KASER, Georg
University of Innsbruck
Austria

KASPAR, Frank
Deutscher Wetterdienst
Germany

KATO, Etsushi
National Institute for Environmental Studies
Japan

KATSMAN, Caroline
Royal Netherlands Meteorological Institute
Netherlands

KATTSOV, Vladimir
Voeikov Main Geophysical Observatory
Russian Federation

KATZFEY, Jack
CSIRO Marine and Atmospheric Research
Australia

KAZMIN, Alexander
P.P. Shirshov Institute of Oceanology
Russian Federation

KEELING, Ralph
Scripps Institution of Oceanography
USA

KENNEDY, John J.
Met Office Hadley Centre
UK

KENT, Elizabeth C.
National Oceanography Centre
UK

KERMINEN, Veli-Matti
Finnish Meteorological Institute
Finland

KEY, Robert M.
Princeton University
USA

KHARIN, Viatcheslav
Environment Canada
Canada

KHATIWALA, Samar
Columbia University
USA

KIMOTO, Masahide
University of Tokyo
Japan

KINNE, Stefan
Max Planck Institute for Meteorology
Germany

KIRSCHKE, Stefanie
Laboratoire des Sciences du Climat et de l'Environnement, Institut Pierre Simon Laplace
France

KIRTMAN, Ben
University of Miami
USA

KITOH, Akio
University of Tsukuba
Japan

KJELLSTRÖM, Erik
Swedish Meteorological and Hydrological Institute
Sweden

KLEIN, Stephen A.
Lawrence Livermore National Laboratory
USA

KLEIN GOLDEWIJK, Kees
Utrecht University and PBL Netherlands Environmental Assessment Agency
Netherlands

KLEIN TANK, Albert M.G.
Royal Netherlands Meteorological Institute
Netherlands

KLEYPAS, Joan
National Center for Atmospheric Research
USA

KLIMONT, Zbigniew
International Institute for Applied Systems Analysis
Austria

KLOSTER, Silvia
Max Planck Institute for Meteorology
Germany

KNIGHT, Jeff
Met Office Hadley Centre
UK

KNUTSON, Thomas
National Oceanic and Atmospheric Administration, Geophysical Fluid Dynamics Laboratory
USA

KNUTTI, Reto
ETH Zurich
Switzerland

KOCH, Dorothy
U.S. Department of Energy
USA

KOIKE, Makoto
University of Tokyo
Japan

KONDO, Yutaka
University of Tokyo
Japan

KONIKOW, Leonard
U.S. Geological Survey
USA

KOPP, Robert
Rutgers University
USA

KÖRPER, Janina
Freie Universität Berlin
Germany

KOSSIN, James P.
National Oceanic and Atmospheric Administration, Cooperative Institute for Meteorological Satellite Studies
USA

KOSTIANOY, Andrey
P.P. Shirshov Institute of Oceanology
Russian Federation

KOVEN, Charles
Lawrence Berkeley National Laboratory
USA

KRAVITZ, Ben
Pacific Northwest National Laboratory
USA

KRINNER, Gerhard
Laboratoire de Glaciologie et Géophysique de l`Environnement, Université Joseph Fourier
France

KROEZE, Carolien
Wageningen University and Open Universiteit Nederland
Netherlands

KULKARNI, Ashwini
Indian Institute of Tropical Meteorology
India

KUNDETI, Koteswara Rao
Indian Institute of Tropical Meteorology
India

KUSHNIR, Yochanan
Columbia University
USA

KWOK, Ronald
National Aeronautics and Space Administration, Jet Propulsion Laboratory
USA

KWON, Won-Tae
National Institute of Meteorological Research
Republic of Korea

LAKEN, Benjamin
Instituto de Astrofisica de Canarias
Spain

LAMARQUE, Jean-François
National Center for Atmospheric Research
USA

LAMBECK, Kurt
Australian National University
Australia

LANDAIS, Amaëlle
Laboratoire des Sciences du Climat et de l'Environnement, Institut Pierre Simon Laplace
France

LANDERER, Felix
National Aeronautics and Space Administration, Jet Propulsion Laboratory
USA

LASSEY, Keith
National Institute of Water and Atmospheric Research
New Zealand

LAU, Ngar-Cheung
National Oceanic and Atmospheric Administration, Geophysical Fluid Dynamics Laboratory
USA

LAU, William K.
National Aeronautics and Space Administration, Goddard Institute for Space Studies
USA

LAW, Rachel M.
CSIRO Marine and Atmospheric Research
Australia

LAWRENCE, David M.
National Center for Atmospheric Research
USA

LE BROCQ, Anne
University of Exeter
UK

LE QUÉRÉ, Corinne
University of East Anglia
UK

LEBSOCK, Matthew
National Aeronautics and Space Administration, Jet Propulsion Laboratory
USA

LEE, David
Manchester Metropolitan University
UK

LEE, Kitack
Pohang University of Science and Technology
Republic of Korea

LEE, Robert W.
University of Reading
UK

LEE, Tong
National Aeronautics and Space Administration, Jet Propulsion Laboratory
USA

LEMKE, Peter
Alfred Wegener Institute for Polar and Marine Research
Germany

LENAERTS, Jan
Utrecht University
Netherlands

LENDERINK, Geert
Royal Netherlands Meteorological Institute
Netherlands

LENNARD, Chris
University of Cape Town
South Africa

LENTON, Andrew
CSIRO Marine and Atmospheric Research
Australia

LEULIETTE, Eric
National Oceanic and Atmospheric Administration, Center for Satellite Applications and Research
USA

LEUNG, Lai-yung Ruby
Pacific Northwest National Laboratory
USA

LEVERMANN, Anders
Potsdam Institute for Climate Impact Research
Germany

LI, Camille
University of Bergen
Norway

LI, Hongmei
Max Planck Institute for Meteorology
Germany

LIAO, Hong
Institute of Atmospheric Physics, Chinese Academy of Sciences
China

LIDDICOAT, Spencer
Met Office Hadley Centre
UK

LIGTENBERG, Stefan
Utrecht University
Netherlands

LIN, Renping
Institute of Atmospheric Physics, Chinese Academy of Sciences
China

LITTLE, Christopher M.
Princeton University
USA

LO, Fiona
Cornell University
USA

LOCKWOOD, Mike
University of Reading
UK

LOEB, Norman G.
National Aeronautics and Space Administration, Langley Research Center
USA

LOHMANN, Ulrike
ETH Zurich
Switzerland

LOMAS, Mark R.
University of Sheffield
UK

LOSADA, Teresa
Universidad de Castilla-La Mancha
Spain

LOTT, Fraser
Met Office Hadley Centre
UK

LU, Jian
George Mason University
USA

LUCAS, Christopher
Bureau of Meteorology
Australia

LUCHT, Wolfgang
Potsdam Institute for Climate Impact Research
Germany

LUNT, Daniel J.
University of Bristol
UK

LUO, Yiqi
University of Oklahoma
USA

LUTERBACHER, Jürg
Justus-Liebig University Giessen
Germany

MACKELLAR, Neil C.
University of Cape Town
South Africa

MAGAÑA, Victor
Universidad Nacional Autonoma de Mexico
Mexico

MAHLSTEIN, Irina
Federal Office of Meteorology and Climatology MeteoSwiss
Switzerland

MAHOWALD, Natalie
Cornell University
USA

MAKI, Takashi
Meteorological Research Institute
Japan

MARENGO, José
National Institute for Space Research
Brazil

MARKUS, Thorsten
National Aeronautics and Space Administration, Goddard Space Flight Center
USA

MARLAND, Gregg
Appalachian State University
USA

MAROTZKE, Jochem
Max Planck Institute for Meteorology
Germany

MARSHALL, Gareth
British Antarctic Survey
UK

MARSTON, George
University of Reading
UK

MARZEION, Ben
University of Innsbruck
Austria

MASSOM, Rob
Australian Antarctic Division
Australia

MASSON-DELMOTTE, Valérie
Laboratoire des Sciences du Climat et de l'Environnement, Institut Pierre Simon Laplace
France

MASSONNET, François
Université catholique de Louvain
Belgium

MATTHEWS, H. Damon
Concordia University
Canada

MAURITZEN, Cecilie
Center for International Climate and Environmental Research Oslo
Norway

MAYORGA, Emilio
University of Washington
USA

MCGREGOR, Shayne
University of New South Wales
Australia

MCINNES, Kathleen L.
CSIRO Marine and Atmospheric Research
Australia

MEARNS, Linda
National Center for Atmospheric Research
USA

MEARS, Carl A.
Remote Sensing Systems
USA

MEEHL, Gerald
National Center for Atmospheric Research
USA

MEINSHAUSEN, Malte
Potsdam Institute for Climate Impact Research
Germany

MELTON, Joe R.
Environment Canada
Canada

MENDOZA, Blanca
Universidad Nacional Autonoma de Mexico
Mexico

MENÉNDEZ, Claudio
Universidad de Buenos Aires
Argentina

MENÉNDEZ, Melisa
Universidad de Cantabria
Spain

MENNE, Matthew
National Oceanic and Atmospheric Administration, National Climatic Data Center
USA

MERCHANT, Christopher J.
University of Edinburgh
UK

MERNILD, Sebastian H.
Los Alamos National Laboratory
USA

MERRIFIELD, Mark A.
University of Hawaii
USA

METZL, Nicolas
Laboratoire d'Océanographie et du Climat, Institut Pierre Simon Laplace
France

MILNE, Glenn A.
University of Ottawa
Canada

MIN, Seung-Ki
Pohang University of Science and Technology
Republic of Korea

MITCHELL, Daniel
University of Oxford
UK

MITROVICA, Jerry X.
Harvard University
USA

MOBERG, Anders
Stockholm University
Sweden

MOHOLDT, Geir
Scripps Institution of Oceanography
USA

MOKHOV, Igor I.
A.M. Obukhov Institute of Atmospheric Physics
Russian Federation

MOKSSIT, Abdalah
Direction de la Météorologie Nationale
Morocco

MÖLG, Thomas
Technical University Berlin
Germany

MONSELESAN, Didier
CSIRO Marine and Atmospheric Research
Australia

MONTZKA, Stephen A.
National Oceanic and Atmospheric Administration, Earth System Research Laboratory
USA

MORAK, Simone
University of Reading
UK

MORDY, Calvin
National Oceanic and Atmospheric Administration, Pacific Marine Environmental Laboratory
USA

MORICE, Colin P.
Met Office Hadley Centre
UK

MOTE, Philip
Oregon State University
USA

MOTTRAM, Ruth
Danish Meteorological Institute
Denmark

MSADEK, Rym
National Oceanic and Atmospheric Administration, Geophysical Fluid Dynamics Laboratory
USA

MUDELSEE, Manfred
Alfred Wegener Institute for Polar and Marine Research
Germany

MÜLLER, Stefanie
Freie Universität Berlin
Germany

MUHS, Daniel R.
U.S. Geological Survey
USA

MULITZA, Stefan
MARUM Center for Marine Environmental Sciences
Germany

MUNHOVEN, Guy
Université de Liège
Belgium

MURAKAMI, Hiroyuki
University of Hawaii
USA

MURPHY, Daniel
National Oceanic and Atmospheric Administration, Earth System Research Laboratory
USA

MURRAY, Tavi
Swansea University
UK

MYHRE, Cathrine Lund
Norwegian Institute for Air Research
Norway

MYHRE, Gunnar
Center for International Climate and Environmental Research Oslo
Norway

MYNENI, Ranga B.
Boston University
USA

NAIK, Vaishali
National Oceanic and Atmospheric Administration, Geophysical Fluid Dynamics Laboratory
USA

NAISH, Tim
Victoria University of Wellington
New Zealand

NAKAJIMA, Teruyuki
University of Tokyo
Japan

NATH, Mary Jo
National Oceanic and Atmospheric Administration, Geophysical Fluid Dynamics Laboratory
USA

NEELIN, J. David
University of California Los Angeles
USA

NEREM, R. Steven
Cooperative Institute for Research in Environmental Sciences
USA

NICHOLAS, J.P.
Ohio State University
USA

NICK, Faezeh
UNIS - The University Centre in Svalbard
Norway

NIELSEN, Claus J.
University of Oslo
Norway

NIWA, Yosuke
Meteorological Research Institute
Japan

NOJIRI, Yukihiro
National Institute for Environmental Studies
Japan

NORBY, Richard J.
Oak Ridge National Laboratory
USA

NORRIS, Joel R.
Scripps Institution of Oceanography
USA

NUNN, Patrick D.
University of New England
Australia

O'CONNOR, Fiona
Met Office Hadley Centre
UK

O'DOWD, Colin
National University of Ireland, Galway
Ireland

O'NEILL, Brian C.
National Center for Atmospheric Research
USA

OLAFSSON, Jon
University of Iceland
Iceland

OLESEN, Martin
Danish Meteorological Institute
Denmark

ORR, James
Laboratoire des Sciences du Climat et de l'Environnement, Institut Pierre Simon Laplace
France

ORSI, Alejandro
Texas A&M University
USA

OSBORN, Timothy
University of East Anglia
UK

OTTO, Alexander
University of Oxford
UK

OTTO, Friederike
University of Oxford
UK

OTTO-BLIESNER, Bette
National Center for Atmospheric Research
USA

OVERDUIN, Pier Paul
Alfred Wegener Institute for Polar and Marine Research
Germany

OVERLAND, James
National Oceanic and Atmospheric Administration, Pacific Marine Environmental Laboratory
USA

PAINTER, Jeff
Lawrence Livermore National Laboratory
USA

PALMER, Tim
University of Oxford
UK

PARK, Geun-Ha
Korea Institute of Ocean Science and Technology
Republic of Korea

PARK, Geun-Ha
National Oceanic and Atmospheric Administration, Atlantic Oceanographic and Meteorological Laboratory
USA

PARKER, David E.
Met Office Hadley Centre
UK

PARRENIN, Frédéric
Laboratoire de Glaciologie et Géophysique de l`Environnement, Université Joseph Fourier
France

PATRA, Prabir
Japan Agency for Marine-Earth Science and Technology
Japan

PATRICOLA, Christina M.
Texas A&M University
USA

PAUL, Frank
University of Zurich
Switzerland

PAVLOVA, Tatiana
Voeikov Main Geophysical Observatory
Russian Federation

PAYNE, Antony J.
University of Bristol
UK

PEARSON, Paul N.
Cardiff University
UK

PENNER, Joyce
University of Michigan
USA

PEREGON, Anna
Laboratoire des Sciences du Climat et de l'Environnement, Institut Pierre Simon Laplace
France

PERLWITZ, Judith
Cooperative Institute for Research in Environmental Sciences
USA

PERRETTE, Mahé
Potsdam Institute for Climate Impact Research
Germany

PETERS, Glen P.
Center for International Climate and Environmental Research Oslo
Norway

PETERS, Wouter
Wageningen University
Netherlands

PETERSCHMITT, Jean-Yves
Laboratoire des Sciences du Climat et de l'Environnement, Institut Pierre Simon Laplace
France

PEYLIN, Philippe
Laboratoire des Sciences du Climat et de l'Environnement, Institut Pierre Simon Laplace
France

PFEFFER, W. Tad
University of Colorado Boulder
USA

PHILIPPON-BERTHIER, Gwenaëlle
Laboratoire des Sciences du Climat et de l'Environnement, Institut Pierre Simon Laplace
France

PIAO, Shilong
Peking University
China

PIERCE, David
Scripps Institution of Oceanography
USA

PIPER, Stephen
Scripps Institution of Oceanography
USA

PITMAN, Andy
University of New South Wales
Australia

PLANTON, Serge
Météo-France
France

PLATTNER, Gian-Kasper
IPCC WGI TSU, University of Bern
Switzerland

POLCHER, Jan
Laboratoire de Météorologie Dynamique, Institut Pierre Simon Laplace
France

POLLARD, David
Pennsylvania State University
USA

POLSON, Debbie
University of Edinburgh
UK

POLYAKOV, Igor
University of Alaska Fairbanks
USA

PONGRATZ, Julia
Max Planck Institute for Meteorology
Germany

POULTER, Benjamin
Laboratoire des Sciences du Climat et de l'Environnement, Institut Pierre Simon Laplace
France

POWER, Scott B.
Bureau of Meteorology
Australia

PRABHAT
Lawrence Berkeley National Laboratory
USA

PRATHER, Michael
University of California Irvine
USA

PROWSE, Terry
Environment Canada
Canada

PURKEY, Sarah G.
University of Washington
USA

QIAN, Yun
Pacific Northwest National Laboratory
USA

QIN, Dahe
Co-Chair IPCC WGI, China Meteorological Administration
China

QIU, Bo
University of Hawaii
USA

QUINN, Terrence
University of Texas
USA

RADIĆ, Valentina
University of British Columbia
Canada

RAE, Jamie
Met Office Hadley Centre
UK

RAHIMZADEH, Fatemeh
Islamic Republic of Iran Meteorological Organization
Iran

RAHMSTORF, Stefan
Potsdam Institute for Climate Impact Research
Germany

RÄISÄNEN, Jouni
University of Helsinki
Finland

RAMASWAMY, Venkatachalam
National Oceanic and Atmospheric Administration, Geophysical Fluid Dynamics Laboratory
USA

RAMESH, Rengaswamy
Physical Research Laboratory
India

RANDALL, David
Colorado State University
USA

RANDEL, William J.
National Center for Atmospheric Research
USA

RASCH, Philip
Pacific Northwest National Laboratory
USA

RAUSER, Florian
Max Planck Institute for Meteorology
Germany

RAVISHANKARA, A.R.
National Oceanic and Atmospheric Administration, Earth System Research Laboratory
USA

RAY, Suchanda
CSIR Centre for Mathematical Modelling and Computer Simulation
India

RAYMOND, Peter A.
Yale University
USA

RAYNAUD, Dominique
Laboratoire de Glaciologie et Géophysique de l`Environnement, Université Joseph Fourier
France

RAYNER, Peter
University of Melbourne
Australia

REASON, Chris
University of Cape Town
South Africa

REICH, Katharine Davis
University of California Los Angeles
USA

REID, Jeffrey
U.S. Naval Research Laboratory
USA

REN, Jiawen
Cold and Arid Regions Environmental and Engineering Research Institute, Chinese Academy of Sciences
China

RENWICK, James
Victoria University of Wellington
New Zealand

REVERDIN, Gilles
Laboratoire d'Océanographie et du Climat, Institut Pierre Simon Laplace
France

RHEIN, Monika
University of Bremen
Germany

RIBES, Aurélien
Météo-France
France

RICHTER, Andreas
University of Bremen
Germany

RICHTER, Carolin
World Meteorological Organization
Switzerland

RIDGWELL, Andy
University of Bristol
UK

RIGBY, Matthew
University of Bristol
UK

RIGNOT, Eric
National Aeronautics and Space Administration, Jet Propulsion Laboratory
USA

RILEY, William J.
Lawrence Berkeley National Laboratory
USA

RINGEVAL, Bruno
Utrecht University
Netherlands

RINTOUL, Stephen R.
CSIRO Marine and Atmospheric Research
Australia

ROBINSON, David
Rutgers University
USA

ROBOCK, Alan
Rutgers University
USA

RÖDENBECK, Christian
Max Planck Institute for Biogeochemistry
Germany

RODRIGUES, Luis R.L.
Institut Català de Ciències del Clima
Spain

RODRÍGUEZ DE FONSECA, Belén
Universidad Complutense de Madrid
Spain

RODWELL, Mark
European Centre for Medium-Range Weather Forecasts
UK

ROEMMICH, Dean
Scripps Institution of Oceanography
USA

ROGELJ, Joeri
ETH Zurich
Switzerland

ROHLING, Eelco
Australian National University
Australia

ROJAS, Maisa
Universidad de Chile
Chile

ROMANOU, Anastasia
Columbia University
USA

ROTH, Raphael
University of Bern
Switzerland

ROTSTAYN, Leon
CSIRO Marine and Atmospheric Research
Australia

RUMMUKAINEN, Markku
Swedish Meteorological and Hydrological Institute
Sweden

RUSTICUCCI, Matilde
Universidad de Buenos Aires
Argentina

RUTI, Paolo
Italian National Agency for New Technologies, Energy and Sustainable Economic Development
Italy

SABINE, Christopher
National Oceanic and Atmospheric Administration, Pacific Marine Environmental Laboratory
USA

SAENKO, Oleg
Environment Canada
Canada

SALZMANN, Ulrich
Northumbria University
UK

SAMSET, Bjørn
Center for International Climate and Environmental Research Oslo
Norway

SANTER, Benjamin D.
Lawrence Livermore National Laboratory
USA

SARR, Abdoulaye
National Meteorological Agency of Senegal
Senegal

SATHEESH, S.K.
Indian Institute of Science
India

SAUNOIS, Marielle
Laboratoire des Sciences du Climat et de l'Environnement, Institut Pierre Simon Laplace
France

SAVARINO, Joël
Laboratoire de Glaciologie et Géophysique de l`Environnement, Université Joseph Fourier
France

SCAIFE, Adam A.
Met Office Hadley Centre
UK

SCHÄR, Christoph
ETH Zurich
Switzerland

SCHMIDT, Hauke
Max Planck Institute for Meteorology
Germany

SCHMIDTKO, Sunke
University of East Anglia
UK

SCHMITT, Raymond
Woods Hole Oceanographic Institution
USA

SCHMITTNER, Andreas
Oregon State University
USA

SCHOOF, Christian
University of British Columbia
Canada

SCHULZ, Jörg
EUMETSAT
Germany

SCHULZ, Michael
MARUM Center for Marine Environmental Sciences
Germany

SCHULZ, Michael
Norwegian Meteorological Institute
Norway

SCHULZWEIDA, Uwe
Max Planck Institute for Meteorology
Germany

SCHURER, Andrew
University of Edinburgh
UK

SCHUUR, Edward
University of Florida
USA

SCINOCCA, John
Environment Canada
Canada

SCREEN, James
University of Exeter
UK

SEAGER, Richard
Columbia University
USA

SEBBARI, Rachid
Direction de la Météorologie Nationale
Morocco

SEDLÁČEK, Jan
ETH Zurich
Switzerland

SEIDEL, Dian J.
National Oceanic and Atmospheric Administration, Air Resources Laboratory
USA

SEMENOV, Vladimir
Russian Academy of Sciences
Russian Federation

SEXTON, David
Met Office Hadley Centre
UK

SHAFFREY, Len C.
University of Reading
UK

SHAKUN, Jeremy
Boston College
USA

SHAO, XueMei
Institute of Geographic Sciences and Natural Resources Research, Chinese Academy of Sciences
China

SHARP, Martin
University of Alberta
Canada

SHEPHERD, Theodore
University of Reading
UK

SHERWOOD, Steven
University of New South Wales
Australia

SHIKLOMANOV, Nikolay
George Washington University
USA

SHIMADA, Koji
Tokyo University of Marine Science and Technology
Japan

SHINDELL, Drew
National Aeronautics and Space Administration, Goddard Institute for Space Studies
USA

SHINE, Keith
University of Reading
UK

SHIOGAMA, Hideo
National Institute for Environmental Studies
Japan

SHONGWE, Mxolisi
South African Weather Service
South Africa

SILLMANN, Jana
Environment Canada
Canada

SIMMONS, Adrian
European Centre for Medium-Range Weather Forecasts
UK

SITCH, Stephen
University of Exeter
UK

SLANGEN, Aimée
CSIRO Marine and Atmospheric Research
Australia

SLATER, Andrew
National Snow and Ice Data Center
USA

SMERDON, Jason
Columbia University
USA

SMIRNOV, Dmitry
Russian Academy of Sciences
Russian Federation

SMITH, Doug
Met Office Hadley Centre
UK

SMITH, Sharon
Natural Resources Canada
Canada

SMITH, Steven J.
Pacific Northwest National Laboratory
USA

SMITH, Thomas M.
National Oceanic and Atmospheric Administration, Center for Satellite Applications and Research
USA

SODEN, Brian J.
University of Miami
USA

SOLMAN, Silvina
Universidad de Buenos Aires
Argentina

SOLOMINA, Olga
Russian Academy of Sciences
Russian Federation

SPAHNI, Renato
University of Bern
Switzerland

SPERBER, Kenneth
Lawrence Livermore National Laboratory
USA

STAMMER, Detlef
University of Hamburg
Germany

STAMMERJOHN, Sharon
University of Colorado Boulder
USA

STEFFEN, Konrad
Swiss Federal Institute for Forest, Snow and Landscape Research WSL
Switzerland

STENDEL, Martin
Danish Meteorological Institute
Denmark

STEPHENS, Graeme
National Aeronautics and Space Administration, Jet Propulsion Laboratory
USA

STEPHENSON, David B.
University of Exeter
UK

STEVENS, Bjorn
Max Planck Institute for Meteorology
Germany

STEVENSON, David S.
University of Edinburgh
UK

STEVENSON, Samantha
University of Hawaii
USA

STIER, Philip
University of Oxford
UK

STÖBER, Uwe
University of Bremen
Germany

STOCKER, Benjamin D.
University of Bern
Switzerland

STOCKER, Thomas F.
Co-Chair IPCC WGI, University of Bern
Switzerland

STORELVMO, Trude
Yale University
USA

STOTT, Peter A.
Met Office Hadley Centre
UK

STRAMMA, Lothar
GEOMAR Helmholtz Centre for Ocean Research
Germany

STUBENRAUCH, Claudia
Laboratoire de Météorologie Dynamique, Institut Pierre Simon Laplace
France

SUGA, Toshio
Tohoku University
Japan

SUTTON, Rowan
University of Reading
UK

SWART, Neil
University of Victoria
Canada

TAKAHASHI, Taro
Columbia University
USA

TAKAYABU, Izuru
Meteorological Research Institute
Japan

TAKEMURA, Toshihiko
Kyushu University
Japan

TALLEY, Lynne D.
Scripps Institution of Oceanography
USA

TANGANG, Fredolin
National University of Malaysia
Malaysia

TANHUA, Toste
GEOMAR Helmholtz Centre for Ocean Research
Germany

TANS, Pieter
National Oceanic and Atmospheric Administration, Earth System Research Laboratory
USA

TARASOV, Pavel
Freie Universität Berlin
Germany

TAYLOR, Karl
Lawrence Livermore National Laboratory
USA

TEBALDI, Claudia
Climate Central, Inc.
USA

TETT, Simon
University of Edinburgh
UK

TEULING, Adriaan J. (Ryan)
Wageningen University
Netherlands

THOMPSON, Rona L.
Norwegian Institute for Air Research
Norway

THORNE, Peter W.
Nansen Environmental and Remote Sensing Center
Norway

THORNTON, Peter
Oak Ridge National Laboratory
USA

TIMMERMANN, Axel
University of Hawaii
USA

TJIPUTRA, Jerry
Uni Research Norway
Norway

TRENBERTH, Kevin
National Center for Atmospheric Research
USA

TÜRKEŞ, Murat
Çanakkale Onsekiz Mart University
Turkey

TURNER, John
British Antarctic Survey
UK

UMMENHOFER, Caroline
Woods Hole Oceanographic Institution
USA

UNNIKRISHNAN, Alakkat S.
National Institute of Oceanography
India

VAN ANGELEN, Jan H.
Utrecht University
Netherlands

VAN DE BERG, Willem Jan
Utrecht University
Netherlands

VAN DE WAL, Roderik
Utrecht University
Netherlands

VAN DEN BROEKE, Michiel
Utrecht University
Netherlands

VAN DEN HURK, Bart
Royal Netherlands Meteorological Institute
Netherlands

VAN DER WERF, Guido
VU University Amsterdam
Netherlands

VAN NOIJE, Twan
Royal Netherlands Meteorological Institute
Netherlands

VAN OLDENBORGH, Geert Jan
Royal Netherlands Meteorological Institute
Netherlands

VAN VUUREN, Detlef
PBL Netherlands Environmental Assessment Agency
Netherlands

VAUGHAN, David G.
British Antarctic Survey
UK

VAUTARD, Robert
Laboratoire des Sciences du Climat et de l'Environnement, Institut Pierre Simon Laplace
France

VAVRUS, Steve
University of Wisconsin
USA

VECCHI, Gabriel
National Oceanic and Atmospheric Administration, Geophysical Fluid Dynamics Laboratory
USA

VELICOGNA, Isabella
University of California Irvine
USA

VERNIER, Jean-Paul
National Aeronautics and Space Administration, Langley Research Center
USA

VESALA, Timo
University of Helsinki
Finland

VINTHER, Bo M.
University of Copenhagen
Denmark

VITERBO, Pedro
Instituto de Meteorologia
Portugal

VIZCAÍNO, Miren
Delft University of Technology
Netherlands

VON SCHUCKMANN, Karina
Institut Français de Recherche pour l'Exploitation de la Mer
France

VON STORCH, Hans
University of Hamburg
Germany

VOULGARAKIS, Apostolos
Imperial College London
UK

WADA, Yoshihide
Utrecht University
Netherlands

WADHAMS, Peter
University of Cambridge
UK

WAELBROECK, Claire
Laboratoire des Sciences du Climat et de l'Environnement, Institut Pierre Simon Laplace
France

WALSH, Kevin
University of Melbourne
Australia

WANG, Bin
University of Hawaii
USA

WANG, Chunzai
National Oceanic and Atmospheric Administration, Atlantic Oceanographic and Meteorological Laboratory
USA

WANG, Fan
Institute of Oceanology, Chinese Academy of Sciences
China

WANG, Hui-Jun
Institute of Atmospheric Physics, Chinese Academy of Sciences
China

WANG, Junhong
National Center for Atmospheric Research
USA

WANG, Muyin
National Oceanic and Atmospheric Administration, Joint Institute for the Study of the Atmosphere and Ocean
USA

WANG, Xiaolan L.
Environment Canada
Canada

WANIA, Rita
Austria

WANNER, Heinz
University of Bern
Switzerland

WANNINKHOF, Rik
National Oceanic and Atmospheric Administration, Atlantic Oceanographic and Meteorological Laboratory
USA

WARD, Daniel S.
Cornell University
USA

WATTERSON, Ian
CSIRO Marine and Atmospheric Research
Australia

WEAVER, Andrew J.
University of Victoria
Canada

WEBB, Mark
Met Office Hadley Centre
UK

WEBB, Robert
National Oceanic and Atmospheric Administration, Earth System Research Laboratory
USA

WEHNER, Michael
Lawrence Berkeley National Laboratory
USA

WEISHEIMER, Antje
University of Oxford
UK

WEISS, Ray F.
Scripps Institution of Oceanography
USA

WHITE, Neil J.
CSIRO Marine and Atmospheric Research
Australia

WIDLANSKY, Matthew
University of Hawaii
USA

WIJFFELS, Susan
CSIRO Marine and Atmospheric Research
Australia

WILD, Martin
ETH Zurich
Switzerland

WILD, Oliver
Lancaster University
UK

WILLETT, Kate M.
Met Office Hadley Centre
UK

WILLIAMS, Keith
Met Office Hadley Centre
UK

WINKELMANN, Ricarda
Potsdam Institute for Climate Impact Research
Germany

WINKER, David
National Aeronautics and Space Administration, Langley Research Center
USA

WINTHER, Jan-Gunnar
Norwegian Polar Institute
Norway

WITTENBERG, Andrew
National Oceanic and Atmospheric Administration, Geophysical Fluid Dynamics Laboratory
USA

WOLF-GLADROW, Dieter
Alfred Wegener Institute for Polar and Marine Research
Germany

WOOD, Simon N.
University of Bath
UK

WOODWORTH, Philip L.
National Oceanography Centre
UK

WOOLLINGS, Tim
University of Reading
UK

WORBY, Anthony
CSIRO Marine and Atmospheric Research
Australia

WRATT, David
National Institute of Water and Atmospheric Research
New Zealand

WUEBBLES, Donald
University of Illinois
USA

WYANT, Matthew
University of Washington
USA

XIAO, Cunde
Chinese Academy of Meteorological Sciences, China Meteorological Administration
China

XIE, Shang-Ping
Scripps Institution of Oceanography
USA

YASHAYAEV, Igor
Bedford Institute of Oceanography
Canada

YASUNARI, Tetsuzo
Nagoya University
Japan

YEH, Sang-Wook
Hanyang University
Republic of Korea

YIN, Jianjun
University of Arizona
USA

YOKOYAMA, Yusuke
University of Tokyo
Japan

YOSHIMORI, Masakazu
University of Tokyo
Japan

YOUNG, Paul
Lancaster University
UK

YU, Lisan
Woods Hole Oceanographic Institution
USA

ZACHOS, James
University of California Santa Cruz
USA

ZAEHLE, Sönke
Max Planck Institute for Biogeochemistry
Germany

ZAPPA, Giuseppe
University of Reading
UK

ZENG, Ning
University of Maryland
USA

ZHAI, Panmao
National Climate Center, China Meteorological Administration
China

ZHANG, Chidong
University of Miami
USA

ZHANG, Hua
National Climate Center, China Meteorological Administration
China

ZHANG, Jianglong
University of North Dakota
USA

ZHANG, Lixia
Institute of Atmospheric Physics, Chinese Academy of Sciences
China

ZHANG, Rong
National Oceanic and Atmospheric Administration, Geophysical Fluid Dynamics Laboratory
USA

ZHANG, Tingjun
Cooperative Institute for Research in Environmental Sciences
USA

ZHANG, Xiao-Ye
Chinese Academy of Meteorological Sciences, China Meteorological Administration
China

ZHANG, Xuebin
Environment Canada
Canada

ZHAO, Lin
Cold and Arid Regions Environmental and Engineering Research Institute, Chinese Academy of Sciences
China

ZHAO, Zong-Ci
National Climate Center, China Meteorological Administration
China

ZHENG, Xiaotong
Ocean University of China
China

ZHOU, Tianjun
Institute of Atmospheric Physics, Chinese Academy of Sciences
China

ZICKFELD, Kirsten
Simon Fraser University
Canada

ZOU, Liwei
Institute of Atmospheric Physics, Chinese Academy of Sciences
China

ZWARTZ, Dan
Victoria University of Wellington
New Zealand

ZWIERS, Francis
University of Victoria
Canada

AVI

Annex VI: Expert Reviewers of the IPCC WGI Fifth Assessment Report

This annex should be cited as:
IPCC, 2013: Annex VI: Expert Reviewers of the IPCC WGI Fifth Assessment Report. In: *Climate Change 2013: The Physical Science Basis. Contribution of Working Group I to the Fifth Assessment Report of the Intergovernmental Panel on Climate Change* [Stocker, T.F., D. Qin, G.-K. Plattner, M. Tignor, S.K. Allen, J. Boschung, A. Nauels, Y. Xia, V. Bex and P.M. Midgley (eds.)]. Cambridge University Press, Cambridge, United Kingdom and New York, NY, USA.

AAMAAS, Borgar
Center for International Climate and Environmental Research Oslo
Norway

ABRAHAM, JOHN
University of St. Thomas
USA

ADAM, Hussein
Wad Medani Ahlia College
Sudan

ÅGREN, Göran
Swedish University of Agricultural Sciences
Sweden

ALEXANDER, Lisa
University of New South Wales
Australia

ALEYNIK, Dmitry
Scottish Association for Marine Science
UK

ALLAN, Richard
University of Reading
UK

ALLEN, Simon K.
IPCC WGI TSU, University of Bern
Switzerland

ALLEY, Richard B.
Pennsylvania State University
USA

ALLISON, Ian
Antarctic Climate and Ecosystems Cooperative Research Centre
Australia

ALORY, Gaël
Laboratoire d'Etudes en Géophysique et Océanographie Spatiales
France

ALPERT, Alice
Massachusetts Institute of Technology
USA

AMJAD, Muhammad
Global Change Impact Studies Centre
Pakistan

ANDEREGG, William
Stanford University
USA

ANDERSEN, Bo
Norwegian Space Centre
Norway

ANDREAE, Meinrat O.
Max Planck Institute for Chemistry
Germany

ANDREU-BURILLO, Isabel
Institut Català de Ciències del Clima
Spain

ANDREWS, Oliver David
University of East Anglia
UK

AÑEL CABANELAS, Juan Antonio
University of Oxford
UK

ANENBERG, Susan
U.S. Environmental Protection Agency
USA

ANNAMALAI, H.
University of Hawaii
USA

ANNAN, James
Japan Agency for Marine-Earth Science and Technology
Japan

APITULEY, Arnoud
Royal Netherlands Meteorological Institute
Netherlands

APPENZELLER, Christof
Federal Office of Meteorology and Climatology MeteoSwiss
Switzerland

ARBLASTER, Julie
Bureau of Meteorology
Australia

ARNETH, Almut
Karlsruhe Institute of Technology
Germany

ARORA, Vivek
Environment Canada
Canada

ARTALE, Vincenzo
Italian National Agency for New Technologies, Energy and Sustainable Economic Development
Italy

ARTINANO, Begona
Centro de Investigaciones Energéticas, Medioambientales y Tecnológicas
Spain

ARTUSO, Florinda
Italian National Agency for New Technologies, Energy and Sustainable Economic Development
Italy

ASMI, Ari
University of Helsinki
Finland

AUAD, Guillermo
Bureau of Ocean Energy Management
USA

AUCAMP, Pieter
Ptersa Environmental Management Consultants
South Africa

AZAR, Christian
Chalmers University of Technology
Sweden

BADER, David
Lawrence Livermore National Laboratory
USA

BADIOU, Pascal
Ducks Unlimited Canada
Canada

BAHN, Michael
University of Innsbruck
Austria

BAKAN, Stephan
Max Planck Institute for Meteorology
Germany

BALTENSPERGER, Urs
Paul Scherrer Institute
Switzerland

BAMBER, Jonathan
University of Bristol
UK

BAN-WEISS, George
Lawrence Berkeley National Laboratory and University of Southern California
USA

BARKER, Stephen
Cardiff University
UK

BARNETT, Tim
Scripps Institution of Oceanography
USA

BARRETT, Jack
Imperial College London (retired)
UK

BARRETT, Peter
Victoria University of Wellington
New Zealand

BARRY, Roger
National Snow and Ice Data Center
USA

BATES, J. Ray
University College Dublin
Ireland

BATES, Timothy
National Oceanic and Atmospheric Administration, Pacific Marine Environmental Laboratory
USA

BEKKI, Slimane
Laboratoire Atmosphères, Milieux, Observations Spatiales, Institut Pierre Simon Laplace
France

BELLOUIN, Nicolas
Met Office Hadley Centre
UK

BELTRAN, Catherine
Université Pierre et Marie Curie
France

BENNARTZ, Ralf
University of Wisconsin
USA

BERNHARD, Luzi
Swiss Federal Institute for Forest, Snow and Landscape Research WSL
Switzerland

BERNHARDT, Karl-Heinz
Leibniz Society of Sciences at Berlin
Germany

BERNIER, Pierre
Natural Resources Canada
Canada

BERNTSEN, Terje
University of Oslo
Norway

BERTHIER, Etienne
Laboratoire d'Etudes en Géophysique et Océanographie Spatiales
France

BETTS, Richard
Met Office Hadley Centre
UK

BETZ, Gregor
Karlsruhe Institute of Technology
Germany

BHANDARI, Medani
Syracuse University
USA

BINDOFF, Nathaniel L.
University of Tasmania
Australia

BINTANJA, Richard
Royal Netherlands Meteorological Institute
Netherlands

BLADÉ, Ileana
Universitat de Barcelona
Spain

BLANCO, Juan A.
Universidad Pública de Navarra
Spain

BLATTER, Heinz
ETH Zurich
Switzerland

BLOMQVIST, Sven
Stockholm University
Sweden

BODAS-SALCEDO, Alejandro
Met Office Hadley Centre
UK

BODE, Antonio
Instituto Español de Oceanografia
Spain

BOEHM, Christian Reiner
Imperial College London
UK

BOENING, Carmen
National Aeronautics and Space Administration, Jet Propulsion Laboratory
USA

BOERSMA, Klaas Folkert
Royal Netherlands Meteorological Institute and Eindhoven University of Technology
Netherlands

BOGNER, Jean E.
University of Illinois
USA

BOKO, Michel
Université d'Abomey Calavi
Benin

BOLLASINA, Massimo
National Oceanic and Atmospheric Administration, Geophysical Fluid Dynamics Laboratory
USA

BONNET, Sophie
Université du Québec
Canada

BONY, Sandrine
Laboratoire de Météorologie Dynamique, Institut Pierre Simon Laplace
France

BOOTH, Ben
Met Office Hadley Centre
UK

BOSILOVICH, Michael
National Aeronautics and Space Administration, Goddard Space Flight Center
USA

BOUCHER, Olivier
Laboratoire de Météorologie Dynamique, Institut Pierre Simon Laplace
France

BOULDIN, Jim
University of California Davis
USA

BOURBONNIERE, Richard
Environment Canada
Canada

BOURLES, Bernard
Institut de Recherche pour le Développement
France

BOUSQUET, Philippe
Laboratoire des Sciences du Climat et de l'Environnement, Institut Pierre Simon Laplace
France

BOWEN, Melissa
University of Auckland
New Zealand

BOYER, Timothy
National Oceanic and Atmospheric Administration, National Oceanographic Data Center
USA

BRACEGIRDLE, Thomas
British Antarctic Survey
UK

BRACONNOT, Pascale
Laboratoire des Sciences du Climat et de l'Environnement, Institut Pierre Simon Laplace
France

BRAESICKE, Peter
University of Cambridge
UK

BREGMAN, Abraham
Royal Netherlands Meteorological Institute
Netherlands

BRENDER, Pierre
Laboratoire des Sciences du Climat et de l'Environnement, Institut Pierre Simon Laplace and AgroParisTech
France

BREWER, Michael
National Oceanic and Atmospheric Administration, National Climatic Data Center
USA

BRIERLEY, Christopher
University College London
UK

BRIFFA, Keith
University of East Anglia
UK

BROMWICH, David
Ohio State University
USA

BROOKS, Harold
National Oceanic and Atmospheric Administration, National Severe Storms Laboratory
USA

BROVKIN, Victor
Max Planck Institute for Meteorology
Germany

BROWN, Jaclyn
CSIRO Marine and Atmospheric Research
Australia

BROWN, Josephine
Bureau of Meteorology
Australia

BROWN, Simon
Met Office Hadley Centre
UK

BURKETT, Virginia
U.S. Geological Survey
USA

BURT, Peter
University of Greenwich
UK

BURTON, David
Burton Systems Software
USA

BUTENHOFF, Christopher
Portland State University
USA

BUTLER, James
National Oceanic and Atmospheric Administration, Earth System Research Laboratory
USA

CAESAR, John
Met Office Hadley Centre
UK

CAGNAZZO, Chiara
Institute of Atmospheric Sciences and Climate
Italy

CAI, Rongshuo
Third Institute of Oceanography, State Oceanic Administration
China

CAI, Zucong
Nanjing Normal University
China

CAINEY, Jill
UK

CALVO, Natalia
Universidad Complutense de Madrid
Spain

CAMERON-SMITH, Philip
Lawrence Livermore National Laboratory
USA

CANDELA, Lucila
Universitat Politècnica de Catalunya
Spain

CAO, Jianting
General Institute of Water Resources and Hydropower Planning and Design, Ministry of Water Resources
China

CARDIA SIMÕES, Jefferson
Universidade Federal do Rio Grande do Sul
Brazil

CARDINAL, Damien
Université Pierre et Marie Curie
France

CARTER, Timothy
Finnish Environment Institute
Finland

CASELDINE, Chris
University of Exeter
UK

CASSARDO, Claudio
University of Torino
Italy

CASSOU, Christophe
Centre Européen de Recherche et de Formation Avancée en Calcul Scientifique
France

CEARRETA, Alejandro
Universidad del Pais Vasco
Spain

CERMAK, Jan
Ruhr-Universität Bochum
Germany

CERVARICH, Matthew
University of Illinois
USA

CHADWICK, Robin
Met Office Hadley Centre
UK

CHARLESWORTH, Mark
Keele University
UK

CHARLSON, Robert
University of Washington
USA

CHARPENTIER LJUNGQVIST, Fredrik
Stockholm University
Sweden

CHAUVIN, Fabrice
Météo-France
France

CHAZETTE, Patrick
Laboratoire des Sciences du Climat et de l'Environnement, Institut Pierre Simon Laplace
France

CHE, Tao
Cold and Arid Regions Environmental and Engineering Research Institute, Chinese Academy of Sciences
China

CHEN, Xianyao
First Institute of Oceanography, State Oceanic Administration
China

CHERCHI, Annalisa
Centro Euromediterraneo per i Cambiamenti Climatici and Istituto Nazionale di Geofisica e Vulcanologia
Italy

CHHABRA, Abha
Indian Space Research Organisation
India

CHIKAMOTO, Megumi
University of Hawaii
USA

CHIKAMOTO, Yoshimitsu
University of Hawaii
USA

CHOU, Chia
Academia Sinica
Taiwan, China

CHRISTIAN, James
Fisheries and Oceans Canada
Canada

CHRISTOPHERSEN, Øyvind
Climate and Pollution Agency
Norway

CHRISTY, John
University of Alabama
USA

CHURCH, John
CSIRO Marine and Atmospheric Research
Australia

CHYLEK, Petr
Los Alamos National Laboratory
USA

CIRANO, Mauro
Federal University of Bahia
Brazil

CIURO, Darienne
University of Illinois
USA

CLARK, Robin
Met Office Hadley Centre
UK

CLAUSSEN, Martin
Max Planck Institute for Meteorology
Germany

CLERBAUX, Cathy
Laboratoire Atmosphères, Milieux,
Observations Spatiales, Institut
Pierre Simon Laplace
France

CLIFT, Peter
Louisiana State University
USA

COAKLEY, James
Oregon State University
USA

COFFEY, Michael
National Center for Atmospheric Research
USA

COGLEY, J. Graham
Trent University
Canada

COLE, Julia
University of Arizona
USA

COLLIER, Mark
CSIRO Marine and Atmospheric Research
Australia

COLLINS, Matthew
University of Exeter
UK

COLLINS, William
University of Reading
UK

COLMAN, Robert
Bureau of Meteorology
Australia

COLOSE, Chris
University at Albany
USA

COOPER, Owen
Cooperative Institute for Research
in Environmental Sciences
USA

COPSTEIN WALDEMAR, Celso
Porto Alegre Municipality,
Environmental Department
Brazil

CORTESE, Giuseppe
GNS Science
New Zealand

CORTI, Susanna
European Centre for Medium-Range
Weather Forecasts and Institute of
Atmospheric Sciences and Climate
Italy

COTRIM DA CUNHA, Leticia
Rio de Janeiro State University
Brazil

COUMOU, Dim
Potsdam Institute for Climate
Impact Research
Germany

COVEY, Curt
Lawrence Livermore National Laboratory
USA

CRAWFORD, James
USA

CRIMMINS, Allison
U.S. Environmental Protection Agency
USA

CRISTINI, Luisa
University of Hawaii
USA

CROK, Marcel
Netherlands

CURRY, Charles
University of Victoria
Canada

CURTIS, Jeffrey
University of Illinois
USA

DAI, Aiguo
University at Albany and National
Center for Atmospheric Research
USA

DAIRAKU, Koji
National Research Institute for Earth
Science and Disaster Prevention
Japan

DAMERIS, Martin
DLR German Aerospace Center
Germany

DANIEL, John
National Oceanic and Atmospheric
Administration, Earth System
Research Laboratory
USA

DANIELS, Emma
Wageningen University
Netherlands

DANIS, François
Laboratoire de Météorologie Dynamique,
Institut Pierre Simon Laplace
France

DAUTRAY, Robert
Académie des Sciences
France

DAVIDSON, Eric
Woods Hole Research Center
USA

DAVIES, Michael
Coldwater Consulting Ltd
Canada

DAY, Jonathan
University of Reading
UK

DE ELIA, Ramon
Ouranos Consortium on Regional Climatology and Adaptation to Climate Change
Canada

DE SAEDELEER, Bernard
Université catholique de Louvain
Belgium

DE VRIES, Hylke
Royal Netherlands Meteorological Institute
Netherlands

DEAN, Robert
University of Florida
USA

DEL GENIO, Anthony
National Aeronautics and Space Administration, Goddard Institute for Space Studies
USA

DELPLA, Ianis
Laboratoire d'Etude et de Recherche en Environnement et Santé
France

DELSOLE, Timothy
George Mason University
USA

DELWORTH, Thomas
National Oceanic and Atmospheric Administration, Geophysical Fluid Dynamics Laboratory
USA

DEMORY, Marie-Estelle
University of Reading
UK

DÉQUÉ, Michel
Météo-France
France

DERKSEN, Chris
Environment Canada
Canada

DESIATO, Franco
Institute for Environmental Protection and Research
Italy

DEVARA, Panuganti C.S.
Indian Institute of Tropical Meteorology
India

DEWALS, Benjamin
Université de Liège
Belgium

DEWITT, David G.
Columbia University
USA

DIAZ MOREJON, Cristobal Felix
Ministry of Science, Technology and the Environment
Cuba

DICKENS, Gerald
Rice University
USA

DIEDHIOU, Arona
Institut de Recherche pour le Développement
France

DIMA, Mihai
University of Bucharest
Romania

DING, Yihui
National Climate Center, China Meteorological Administration
China

DING, Yongjian
Cold and Arid Regions Environmental and Engineering Research Institute, Chinese Academy of Sciences
China

DITLEVSEN, Peter
University of Copenhagen
Denmark

DOHERTY, Ruth
University of Edinburgh
UK

DOLE, Randall
National Oceanic and Atmospheric Administration, Earth System Research Laboratory
USA

DOLMAN, Han
VU University Amsterdam
Netherlands

DOMINGUES, Catia M.
Antarctic Climate and Ecosystems Cooperative Research Centre
Australia

DONAHUE, Neil
Carnegie Mellon University
USA

DONNER, Leo
National Oceanic and Atmospheric Administration, Geophysical Fluid Dynamics Laboratory
USA

DOSTAL, Paul
DLR German Aerospace Center
Germany

DOWNES, Stephanie
Australian National University
Australia

DOYLE, Moira Evelina
Universidad de Buenos Aires
Argentina

DRAGONI, Walter
University of Perugia
Italy

DRIJFHOUT, Sybren
Royal Netherlands Meteorological Institute
Netherlands

DU, Enzai
Peking University
China

DUAN, Anmin
Institute of Atmospheric Physics, Chinese Academy of Sciences
China

DUCE, Robert
Texas A&M University
USA

DUDOK DE WIT, Thierry
Université d'Orléans
France

DUNNE, Eimear
Finnish Meteorological Institute
Finland

DUNSTONE, Nick
Met Office Hadley Centre
UK

DURACK, Paul
Lawrence Livermore National Laboratory
USA

DWYER, Ned
University College Cork
Ireland

EASTERBROOK, Don
Western Washington University
USA

EBI, Kristie
Stanford University
USA

EISEN, Olaf
Alfred Wegener Institute for Polar and Marine Research
Germany

EISENMAN, Ian
University of California San Diego
USA

EKHOLM, Tommi
VTT Technical Research Centre of Finland
Finland

ELDEVIK, Tor
University of Bergen
Norway

ELJADID, Ali Geath
Al-Fath University
Libya

EMANUEL, Kerry
Massachusetts Institute of Technology
USA

ENOMOTO, Hiroyuki
National Institute of Polar Research
Japan

ERICKSON, David
Oak Ridge National Laboratory
USA

ESPINOZA, Jhan Carlo
Instituto Geofísico del Perú
Peru

ESSERY, Richard
University of Edinburgh
UK

EVANS, Michael Neil
University of Maryland
USA

EVANS, Wayne
York University
Canada

EXBRAYAT, Jean-François
University of New South Wales
Australia

EYNAUD, Frédérique
Université Bordeaux 1
France

FAHEY, David
National Oceanic and Atmospheric Administration, Earth System Research Laboratory
USA

FAN, Jiwen
Pacific Northwest National Laboratory
USA

FARAGO, Tibor
St. Istvan University
Hungary

FEINGOLD, Graham
National Oceanic and Atmospheric Administration, Earth System Research Laboratory
USA

FEIST, Dietrich
Max Planck Institute for Biogeochemistry
Germany

FERRONE, Andrew
Karlsruhe Institute of Technology
Germany

FESER, Frauke
Helmholtz-Zentrum Geesthacht
Germany

FEULNER, Georg
Potsdam Institute for Climate Impact Research
Germany

FICHEFET, Thierry
Université catholique de Louvain
Belgium

FIELD, Christopher
Carnegie Institution for Science
USA

FISCHER, Andreas
Federal Office of Meteorology and Climatology MeteoSwiss
Switzerland

FISCHER, Hubertus
University of Bern
Switzerland

FISCHLIN, Andreas
ETH Zurich
Switzerland

FISHER, Joshua
National Aeronautics and Space Administration, Jet Propulsion Laboratory
USA

FLORES, José-Abel
Universidad de Salamanca
Spain

FLOSSMANN, Andrea
Université Blaise Pascal
France

FOLBERTH, Gerd
Met Office Hadley Centre
UK

FOLLAND, Christopher
Met Office Hadley Centre
UK

FORBES, Donald
Bedford Institute of Oceanography
Canada

FOREST, Chris
Pennsylvania State University
USA

FORSTER, Piers
University of Leeds
UK

FOSTER, James
National Aeronautics and Space Administration, Goddard Space Flight Center
USA

FOUNTAIN, Andrew
Portland State University
USA

FRANKLIN, James
CLF-Chem Consulting SPRL
Belgium

FRANKS, Stewart
University of Newcastle Australia
Australia

FREDERIKSEN, Carsten
Bureau of Meteorology
Australia

FREDERIKSEN, Jorgen
CSIRO Marine and Atmospheric Research
Australia

FREE, Melissa
National Oceanic and Atmospheric Administration, Air Resources Laboratory
USA

FREELAND, Howard
Fisheries and Oceans Canada
Canada

FREPPAZ, Michele
University of Torino
Italy

FRIEDLINGSTEIN, Pierre
University of Exeter
UK

FROELICHER, Thomas
Princeton University
USA

FRONZEK, Stefan
Finnish Environment Institute
Finland

FRÜH, Barbara
Deutscher Wetterdienst
Germany

FU, Joshua Xiouhua
University of Hawaii
USA

FU, Weiwei
Danish Meteorological Institute
Denmark

FUGLESTVEDT, Jan
Center for International Climate and Environmental Research Oslo
Norway

FUKASAWA, Masao
Japan Agency for Marine-Earth Science and Technology
Japan

FUNG, Inez
University of California Berkeley
USA

FUNK, Martin
ETH Zurich
Switzerland

FYFE, John
Environment Canada
Canada

GAALEMA, Stephen
Black Forest Engineering, LLC
USA

GAGLIARDINI, Olivier
Laboratoire de Glaciologie et Géophysique de l`Environnement, Université Joseph Fourier
France

GAJEWSKI, Konrad
University of Ottawa
Canada

GALDOS, Marcelo
Brazilian Bioethanol Science and Technology Laboratory
Brazil

GALLEGO, David
Universidad Pablo de Olavide
Spain

GANOPOLSKI, Andrey
Potsdam Institute for Climate Impact Research
Germany

GAO, Xuejie
National Climate Center, China Meteorological Administration
China

GARCIA-HERRERA, Ricardo
Universidad Complutense de Madrid
Spain

GARIMELLA, Sarvesh
Massachusetts Institute of Technology
USA

GARREAUD, René
Universidad de Chile
Chile

GATTUSO, Jean-Pierre
Observatoire Océanologique de Villefranche sur Mer, Université Pierre et Marie Curie
France

GAUCI, Vincent
The Open University
UK

GAYO, Eugenia M.
Centro de Investigaciones del Hombre en el Desierto
Chile

GEDNEY, Nicola
Met Office Hadley Centre
UK

GEHRELS, Roland
Plymouth University
UK

GERBER, Stefan
University of Florida
USA

GERLAND, Sebastian
Norwegian Polar Institute
Norway

GERVAIS, François
Université François-Rabelais de Tours
France

GETTELMAN, Andrew
National Center for Atmospheric Research
USA

GHAN, Steven
Pacific Northwest National Laboratory
USA

GHOSH, Sucharita
Swiss Federal Institute for Forest, Snow and Landscape Research WSL
Switzerland

GIFFORD, Roger
CSIRO Plant Industry
Australia

GILBERT, Denis
Fisheries and Oceans Canada
Canada

GILLETT, Nathan
Environment Canada
Canada

GINOUX, Paul
National Oceanic and Atmospheric Administration, Geophysical Fluid Dynamics Laboratory
USA

GIORGETTA, Marco
Max Planck Institute for Meteorology
Germany

GLIKSON, Andrew
Australian National University
Australia

GODIN-BEEKMANN, Sophie
Laboratoire Atmosphères, Milieux, Observations Spatiales, Institut Pierre Simon Laplace
France

GOLAZ, Jean-Christophe
National Oceanic and Atmospheric Administration, Geophysical Fluid Dynamics Laboratory
USA

GONG, Daoyi
Beijing Normal University
China

GONZALEZ, Patrick
U.S. National Park Service
USA

GOOD, Peter
Met Office Hadley Centre
UK

GOOD, Simon
Met Office Hadley Centre
UK

GOODESS, Clare
University of East Anglia
UK

GOOSSE, Hugues
Université catholique de Louvain
Belgium

GORIS, Nadine
University of Bergen and Bjerknes Centre for Climate Research
Norway

GOSWAMI, Santonu
Oak Ridge National Laboratory
USA

GOWER, James
Fisheries and Oceans Canada
Canada

GRAY, Vincent
New Zealand

GREGORY, Jonathan
University of Reading and Met Office Hadley Centre
UK

GREWE, Volker
DLR German Aerospace Center
Germany

GRIFFIES, Stephen
National Oceanic and Atmospheric Administration, Geophysical Fluid Dynamics Laboratory
USA

GRIGGS, David
Monash University
Australia

GRIMM, Alice
Federal University of Parana
Brazil

GRINSTED, Aslak
University of Copenhagen
Denmark

GRUBER, Nicolas
ETH Zurich
Switzerland

GRUBER, Stephan
University of Zurich
Switzerland

GUGLIELMIN, Mauro
University of Insubria
Italy

GUILYARDI, Eric
Laboratoire d'Océanographie et du Climat, Institut Pierre Simon Laplace
France

GUTTORP, Peter
University of Washington and Norwegian Computing Center
USA

GUTZLER, David
University of New Mexico
USA

HAARSMA, Reindert
Royal Netherlands Meteorological Institute
Netherlands

HAEBERLI, Wilfried
University of Zurich
Switzerland

HAFEZ, Yehia
King Abdulaziz University
Saudi Arabia

HAGEN, David L.
AcrossTech
USA

HAGOS, Samson
Pacific Northwest National Laboratory
USA

HAIGH, Joanna
Imperial College London
UK

HAJIMA, Tomohiro
Japan Agency for Marine-Earth Science and Technology
Japan

HALL, Dorothy
National Aeronautics and Space Administration, Goddard Space Flight Center
USA

HALLBERG, Robert
National Oceanic and Atmospheric Administration, Geophysical Fluid Dynamics Laboratory
USA

HALLORAN, Paul
Met Office Hadley Centre
UK

HAN, Dawei
University of Bristol
UK

HANSEN, Bogi
Faroe Marine Research Institute
Faroe Islands

HAO, Aibing
Ministry of Land and Resources
China

HARGREAVES, Julia
Japan Agency for Marine-Earth Science and Technology
Japan

HARNISCH, Jochen
KfW
Germany

HARPER, Joel
University of Montana
USA

HARTMANN, Jens
University of Hamburg
Germany

HASANEAN, Hosny
King Abdulaziz University
Saudi Arabia

HASSLER, Birgit
Cooperative Institute for Research in Environmental Sciences
USA

HAWKINS, Ed
University of Reading
UK

HAYASAKA, Tadahiro
Tohoku University
Japan

HAYWOOD, Jim
Met Office Hadley Centre and University of Exeter
UK

HEGERL, Gabriele
University of Edinburgh
UK

HEIM, Richard
National Oceanic and Atmospheric Administration, National Climatic Data Center
USA

HEINTZENBERG, Jost
Leibniz Institute for Tropospheric Research
Germany

HEINZE, Christoph
University of Bergen and Bjerknes Centre for Climate Research
Norway

HERTWICH, Edgar
Norwegian University of Science and Technology
Norway

HEWITSON, Bruce
University of Cape Town
South Africa

HIGGINS, Paul
American Meteorological Society
USA

HIRST, Anthony
CSIRO Marine and Atmospheric Research
Australia

HISDAL, Hege
Norwegian Water Resources and Energy Directorate
Norway

HOCK, Regine
University of Alaska Fairbanks
USA

HODSON, Dan
University of Reading
UK

HOERLING, Martin
National Oceanic and Atmospheric Administration, Earth System Research Laboratory
USA

HÖGBERG, Peter
Swedish University of Agricultural Sciences
Sweden

HOLGATE, Simon
National Oceanography Centre
UK

HOLLIS, Christopher
GNS Science
New Zealand

HOLTSLAG, Albert A.M.
Wageningen University
Netherlands

HÖNISCH, Bärbel
Columbia University
USA

HOPE, Pandora
Bureau of Meteorology
Australia

HOROWITZ, Larry
National Oceanic and Atmospheric Administration, Geophysical Fluid Dynamics Laboratory
USA

HOURDIN, Frédéric
Laboratoire de Météorologie Dynamique, Institut Pierre Simon Laplace
France

HOUSE, Joanna
University of Bristol
UK

HOUWELING, Sander
Utrecht University
Netherlands

HOVLAND, Martin
University of Bergen
Norway

HOWARD, William
Australian National University
Australia

HREN, Michael
University of Connecticut
USA

HU, Aixue
National Center for Atmospheric Research
USA

HU, Zeng-Zhen
National Oceanic and Atmospheric Administration, National Weather Service
USA

HUANG, Jianping
Lanzhou University
China

HUANG, Lei
National Climate Center, China Meteorological Administration
China

HUANG, Lin
Environment Canada
Canada

HUDSON, James
Desert Research Institute
USA

HUGGEL, Christian
University of Zurich
Switzerland

HUGHES, Malcolm
University of Arizona
USA

HUNTER, John
Antarctic Climate and Ecosystems Cooperative Research Centre
Australia

HURST, Dale
Cooperative Institute for Research in Environmental Sciences
USA

HUYBRECHTS, Philippe
Vrije Universiteit Brussel
Belgium

INCECIK, Selahattin
Istanbul Technical University
Turkey

INGRAM, William
Met Office Hadley Centre and University of Oxford
UK

INOUE, Toshiro
University of Tokyo
Japan

IRVINE, Peter
Institute for Advanced Sustainability Studies
Germany

ISE, Takeshi
University of Hyogo
Japan

ISHII, Masao
Meteorological Research Institute
Japan

ISHIZUKA, Shigehiro
Forestry and Forest Products Institute
Japan

ITO, Akihiko
National Institute for Environmental Studies
Japan

ITO, Takamitsu
Georgia Institute of Technology
USA

ITOH, Kiminori
Yokohama National University
Japan

IVERSEN, Trond
European Centre for Medium-Range Weather Forecasts, UK and Norwegian Meteorological Institute
Norway

JACKSON, Laura
Met Office Hadley Centre
UK

JACOBEIT, Jucundus
University of Augsburg
Germany

JACOBSON, Mark Z.
Stanford University
USA

JAENICKE, Ruprecht
Johannes Gutenberg University Mainz
Germany

JAIN, Sharad K.
Indian Institute of Technology Roorkee
India

JEONG, Myeong-Jae
Gangneung-Wonju National University
Republic of Korea

JIANG, Dabang
Institute of Atmospheric Physics,
Chinese Academy of Sciences
China

JIANG, Jonathan
National Aeronautics and Space
Administration, Jet Propulsion Laboratory
USA

JOHANSSON, Daniel
Chalmers University of Technology
Sweden

JOHN, Jasmin
National Oceanic and Atmospheric
Administration, Geophysical
Fluid Dynamics Laboratory
USA

JOHNS, Tim
Met Office Hadley Centre
UK

JOHNSON, Jennifer
Stanford University
USA

JOHNSON, Nathaniel
University of Hawaii
USA

JONES, Christopher
Met Office Hadley Centre
UK

JONES, Gareth S.
Met Office Hadley Centre
UK

JONES, Philip
University of East Anglia
UK

JOOS, Fortunat
University of Bern
Switzerland

JOSEY, Simon
National Oceanography Centre
UK

JOSHI, Manoj
University of East Anglia
UK

JOUGHIN, Ian
University of Washington
USA

JOUSSAUME, Sylvie
Laboratoire des Sciences du Climat et de
l'Environnement, Institut Pierre Simon Laplace
France

JOYCE, Terrence
Woods Hole Oceanographic Institution
USA

JUCKES, Martin
Science and Technologies Facility Council
UK

JYLHÄ, Kirsti
Finnish Meteorological Institute
Finland

KÄÄB, Andreas
University of Oslo
Norway

KAGEYAMA, Masa
Laboratoire des Sciences du
Climat et de l'Environnement,
Institut Pierre Simon Laplace
France

KAHN, Brian
National Aeronautics and Space
Administration, Jet Propulsion Laboratory
USA

KAHN, Ralph
National Aeronautics and Space
Administration, Goddard Space Flight Center
USA

KALESCHKE, Lars
University of Hamburg
Germany

KANAKIDOU, Maria
University of Crete
Greece

KANAYA, Yugo
Japan Agency for Marine-Earth
Science and Technology
Japan

KANDEL, Robert
Laboratoire de Météorologie Dynamique,
Institut Pierre Simon Laplace
France

KANG, Shichang
Institute of Tibetan Plateau Research,
Chinese Academy of Sciences
China

KANG, Sok Kuh
Korea Ocean Research and
Development Institute
Republic of Korea

KARLSSON, Per Erik
Swedish Environmental Research Institute
Sweden

KAROLY, David
University of Melbourne
Australia

KARPECHKO, Alexey
Finnish Meteorological Institute
Finland

KATBEH-BADER, Nedal
Ministry of Environment Affairs
Palestine

KATO, Etsushi
National Institute for Environmental Studies
Japan

KAUFMANN, Robert
Boston University
USA

KAUPPINEN, Jyrki
University of Turku
Finland

KAVANAGH, Christopher
International Atomic Energy Agency
Monaco

KAWAI, Hiroyasu
Port and Airport Research Institute
Japan

KAWAMIYA, Michio
Japan Agency for Marine-Earth Science
and Technology
Japan

KAWAMURA, Kenji
National Institute of Polar Research
Japan

KAYE, Neil
Met Office Hadley Centre
UK

KEELING, Ralph
Scripps Institution of Oceanography
USA

KEEN, Richard
University of Colorado Boulder (retired)
USA

KEENLYSIDE, Noel
University of Bergen and Bjerknes
Centre for Climate Research
Norway

KELLER, Charles
Los Alamos National Laboratory (retired)
USA

KENDON, Elizabeth
Met Office Hadley Centre
UK

KENNEDY, John
Met Office Hadley Centre
UK

KENT, Elizabeth
National Oceanography Centre
UK

KESKIN, Siddik Sinan
Marmara University
Turkey

KHALIL, Mohammad Aslam Khan
Portland State University
USA

KHESHGI, Haroon
ExxonMobil Research and Engineering
USA

KHMELINSKII, Igor
Universidade do Algarve
Portugal

KHOSRAWI, Farahnaz
Stockholm University
Sweden

KILADIS, George
National Oceanic and Atmospheric Administration, Earth System Research Laboratory
USA

KIM, Daehyun
Columbia University
USA

KIM, Seong-Joong
Korea Polar Research Institute
Republic of Korea

KINDLER, Pascal
University of Geneva
Switzerland

KING, Andrew
University of New South Wales
Australia

KING, Matt
University of Tasmania and Newcastle University
Australia

KINTER, James
Institute of Global Environment and Society, Inc.
USA

KIRCHENGAST, Gottfried
University of Graz
Austria

KIRKEVÅG, Alf
Norwegian Meteorological Institute
Norway

KITOH, Akio
Meteorological Research Institute
Japan

KJELLSTRÖM, Erik
Swedish Meteorological and Hydrological Institute
Sweden

KLEIN TANK, Albert
Royal Netherlands Meteorological Institute
Netherlands

KLINGER, Lee
USA

KLOTZBACH, Philip
Colorado State University
USA

KNUTSON, Thomas
National Oceanic and Atmospheric Administration, Geophysical Fluid Dynamics Laboratory
USA

KNUTTI, Reto
ETH Zurich
Switzerland

KOBASHI, Takuro
National Institute of Polar Research
Japan

KOBAYASHI, Shigeki
Toyota Central R&D Labs., Inc.
Japan

KOBAYASHI, Taiyo
Japan Agency for Marine-Earth Science and Technology
Japan

KOH, Tieh-Yong
Nanyang Technological University
Singapore

KÖHLER, Peter
Alfred Wegener Institute for Polar and Marine Research
Germany

KOMEN, Gerbrand
Royal Netherlands Meteorological Institute and Utrecht University (retired)
Netherlands

KONDO, Yutaka
University of Tokyo
Japan

KONFIRST, Matthew
American Association for the Advancement of Science and National Science Foundation
USA

KONOVALOV, Vladimir
Russian Academy of Sciences
Russian Federation

KOPP, Robert
Rutgers University
USA

KORTELAINEN, Pirkko
Finnish Environment Institute
Finland

KREASUWUN, Jiemjai
Chiang Mai University
Thailand

KREIENKAMP, Frank
Climate & Environment Consulting Potsdam GmbH
Germany

KRINNER, Gerhard
Laboratoire de Glaciologie et Géophysique de l`Environnement, Université Joseph Fourier
France

KRIPALANI, Ramesh
Indian Institute of Tropical Meteorology
India

KRISTJÁNSSON, Jón Egill
University of Oslo
Norway

KRIVOVA, Natalie
Max Planck Institute for Solar System Research
Germany

KUHN, Nikolaus J.
University of Basel
Switzerland

KULSHRESTHA, Umesh
Jawaharlal Nehru University
India

KUSANO, Kanya
Nagoya University
Japan

KUSUNOKI, Shoji
Meteorological Research Institute
Japan

LAGERLOEF, Gary
Earth & Space Research
USA

LAKEN, Benjamin
Instituto de Astrofisíca de Canarias
Spain

LAMBERT, Fabrice
Korea Institute of Ocean
Science and Technology
Republic of Korea

LAMBERT, Francis Hugo
University of Exeter
UK

LANDUYT, William
ExxonMobil Research and Engineering
USA

LANE, Tracy
International Hydropower Association
UK

LANG, Herbert
ETH Zurich
Switzerland

LARTER, Robert
British Antarctic Survey
UK

LAW, Beverly
Oregon State University
USA

LAW, Katharine
Laboratoire Atmosphères, Milieux,
Observations Spatiales, Institut
Pierre Simon Laplace
France

LAWRENCE, Judy
Victoria University of Wellington
New Zealand

LAWRENCE, Mark
Institute for Advanced Sustainability Studies
Germany

LAXON, Seymour
University College London
UK

LE QUÉRÉ, Corinne
University of East Anglia
UK

LEAITCH, Warren Richard
Environment Canada
Canada

LECK, Caroline
Stockholm University
Sweden

LECLERCQ, Paul
Utrecht University
Netherlands

LEE, Arthur
Chevron Corporation
USA

LEE, Jae Hak
Korea Institute of Ocean
Science and Technology
Republic of Korea

LEE, Sai Ming
Hong Kong Observatory
China

LEE, Seoung Soo
National Oceanic and Atmospheric
Administration, Earth System
Research Laboratory
USA

LEE, Tsz-Cheung
Hong Kong Observatory
China

LEGG, Sonya
Princeton University
USA

LEMKE, Peter
Alfred Wegener Institute for
Polar and Marine Research
Germany

LENAERTS, Jan
Utrecht University
Netherlands

LENDERINK, Geert
Royal Netherlands Meteorological Institute
Netherlands

LEROY, Suzanne
Brunel University
UK

LEVIN, Ingeborg
University of Heidelberg
Germany

LEVITUS, Sydney
National Oceanic and Atmospheric
Administration, National
Oceanographic Data Center
USA

LEVY, Julian
Levy Environmental Consulting, Ltd.
USA

LEVY II, Hiram
National Oceanic and Atmospheric
Administration, Geophysical Fluid
Dynamics Laboratory (retired)
USA

LEWIS, Nicholas
UK

LEWITT, Martin
American Geophysical Union
USA

LI, Can
University of Maryland and National
Aeronautics and Space Administration,
Goddard Space Flight Center
USA

LI, Jui-Lin (Frank)
National Aeronautics and Space
Administration, Jet Propulsion Laboratory
USA

LI, Qingxiang
National Meteorological Information Center,
China Meteorological Administration
China

LI, Shenggong
Institute of Geographic Sciences
and Natural Resources Research,
Chinese Academy of Sciences
China

LI, Shuanglin
Institute of Atmospheric Physics,
Chinese Academy of Sciences
China

LI, Weiping
National Climate Center, China
Meteorological Administration
China

LI, Weiwei
University of Illinois
USA

LI, Yueqing
Institute of Plateau Meteorology, China
Meteorological Administration
China

LI, Zhanqing
University of Maryland
USA

LIAO, Hong
Institute of Atmospheric Physics,
Chinese Academy of Sciences
China

LIN, Hai
Environment Canada
Canada

LIN, Jialin
Ohio State University
USA

LINDERHOLM, Hans W.
University of Gothenburg
Sweden

LINDSAY, Ron
University of Washington
USA

LIOU, Kuo-Nan
University of California Los Angeles
USA

LITTLE, Christopher
Princeton University
USA

LIU, Hongyan
Peking University
China

LIU, Ke Xiu
National Marine Data and
Information Service
China

LIU, Qiyong
China CDC
China

LIU, Shaw
Academia Sinica
Taiwan, China

LIU, Xiaohong
Pacific Northwest National Laboratory
USA

LJUNGQVIST, Fredrik
Stockholm University
Sweden

LLOYD, Philip
Cape Peninsula University of Technology
South Africa

LO, Yueh-Hsin
National Taiwan University
Taiwan, China

LOBELL, David
Stanford University
USA

LOEB, Norman
National Aeronautics and Space
Administration, Langley Research Center
USA

LOEW, Alexander
Max Planck Institute for Meteorology
Germany

LOFGREN, Brent
National Oceanic and Atmospheric
Administration, Great Lakes
Environmental Research Laboratory
USA

LOHMANN, Gerrit
Alfred Wegener Institute for
Polar and Marine Research
Germany

LOHMANN, Ulrike
ETH Zurich
Switzerland

LOOKYAT TAYLOR, Helen
World Science Data Base
USA

LÓPEZ MORENO, Juan Ignacio
Instituto Pirenaico de Ecología
Spain

LOUGH, Janice
Australian Institute of Marine Science
Australia

LUCE, Charles
U.S. Forest Service
USA

LÜTHI, Martin
ETH Zurich
Switzerland

LUNT, Daniel
University of Bristol
UK

LUO, Jing-Jia
Bureau of Meteorology
Australia

LUPO, Anthony
University of Missouri
USA

MA, Zhuguo
Institute of Atmospheric Physics,
Chinese Academy of Sciences
China

MACCRACKEN, Michael
Climate Institute
USA

MACGREGOR, Joseph
University of Texas
USA

MÄDER, Claudia
Federal Environment Agency
Germany

MAGGI, Valter
University of Milano-Bicocca
Italy

MAHLSTEIN, Irina
Federal Office of Meteorology and
Climatology MeteoSwiss
Switzerland

MAHOWALD, Natalie
Cornell University
USA

MAKI, Takashi
Meteorological Research Institute
Japan

MANN, Michael
Pennsylvania State University
USA

MANNING, Martin
Victoria University of Wellington
New Zealand

MANZINI, Elisa
Max Planck Institute for Meteorology
Germany

MARAUN, Douglas
GEOMAR Helmholtz Centre
for Ocean Research
Germany

MARBAIX, Philippe
Université catholique de Louvain
Belgium

MARENGO, José
National Institute for Space Research
Brazil

MARINOVA, Dora
Curtin University
Australia

MARIOTTI, Annarita
National Oceanic and Atmospheric
Administration, Climate Program Office
USA

MAROTZKE, Jochem
Max Planck Institute for Meteorology
Germany

MARSH, Robert
University of Southampton
UK

MARTIN, Eric
Météo-France
France

MARTIN, Gill
Met Office Hadley Centre
UK

MARTÍN MÍGUEZ, Belén
Centro Tecnológico del Mar
Spain

MARTIN-VIDE, Javier
Universitat de Barcelona
Spain

MARTY, Christoph
WSL Institute for Snow and
Avalanche Research SLF
Switzerland

MASSONNET, François
Université catholique de Louvain
Belgium

MATEI, Daniela
Max Planck Institute for Meteorology
Germany

MATSUNO, Taroh
Japan Agency for Marine-Earth
Science and Technology
Japan

MATSUOKA, Kenichi
Norwegian Polar Institute
Norway

MATTHEWS, Paul
University of Nottingham
UK

MAURITSEN, Thorsten
Max Planck Institute for Meteorology
Germany

MAY, Wilhelm
Danish Meteorological Institute
Denmark

MCELROY, Charles Thomas
York University
Canada

MCINNES, Kathleen
CSIRO Marine and Atmospheric Research
Australia

MCKAY, Nicholas
University of Arizona
USA

MCKITRICK, Ross
University of Guelph
Canada

MCLEAN, John
James Cook University
Australia

MEEHL, Gerald
National Center for Atmospheric Research
USA

MEIER, Walter
National Snow and Ice Data Center
USA

MEIYAPPAN, Prasanth
University of Illinois
USA

MELSOM, Arne
Norwegian Meteorological Institute
Norway

MÉNDEZ, Carlos
Instituto Venezolano de
Investigaciones Científicas
Venezuela

MENGE, Duncan
Princeton University
USA

MENZEL, W. Paul
University of Wisconsin
USA

MERCHANT, Christopher
University of Edinburgh
UK

MEREDITH, Michael
British Antarctic Survey
UK

MERLIS, Timothy
Princeton University and National
Oceanic and Atmospheric Administration,
Geophysical Fluid Dynamics Laboratory
USA

MERRYFIELD, William
Environment Canada
Canada

MESINGER, Fedor
University of Maryland
USA

METCALFE, Daniel
Swedish University of Agricultural Sciences
Sweden

METELKA, Ladislav
Czech Hydrometeorological Institute
Czech Republic

MEYSSIGNAC, Benoit
Laboratoire d'Etudes en Géophysique
et Océanographie Spatiales
France

MICKLEY, Loretta
Harvard University
USA

MIELIKÄINEN, Kari
Finnish Forest Research Institute
Finland

MILLER, Benjamin R.
Cooperative Institute for Research
in Environmental Sciences
USA

MIMS, Forrest
Geronimo Creek Observatory
USA

MIN, Seung-Ki
CSIRO Marine and Atmospheric Research
Australia

MING, Jing
National Climate Center, China
Meteorological Administration
China

MING, Yi
National Oceanic and Atmospheric
Administration, Geophysical
Fluid Dynamics Laboratory
USA

MINSCHWANER, Kenneth
New Mexico Institute of
Mining and Technology
USA

MITCHELL, John
Met Office Hadley Centre
UK

MOBERG, Anders
Stockholm University
Sweden

MÖHLER, Ottmar
Karlsruhe Institute of Technology
Germany

MOLINIÉ, Gilles
Laboratoire de Glaciologie et Géophysique
de l`Environnement, Université Joseph Fourier
France

MONAHAN, Adam
University of Victoria
Canada

MONCKTON OF BRENCHLEY, Christopher
Science and Public Policy Institute
UK

MONTZKA, Stephen
National Oceanic and Atmospheric Administration, Earth System Research Laboratory
USA

MOORTHY, K. Krishna
Indian Space Research Organisation
India

MOOSDORF, Nils
University of Hamburg
Germany

MORGENSTERN, Olaf
National Institute of Water and Atmospheric Research
New Zealand

MORI, Nobuhito
Kyoto University
Japan

MORICE, Colin
Met Office Hadley Centre
UK

MORRISON, Hugh
National Center for Atmospheric Research
USA

MOTE, Philip
Oregon State University
USA

MSADEK, Rym
National Oceanic and Atmospheric Administration, Geophysical Fluid Dynamics Laboratory
USA

MUDELSEE, Manfred
Alfred Wegener Institute for Polar and Marine Research
Germany

MUELLER, Christoph
Justus Leibig University Giessen
Germany

MÜLLER, Rolf
Forschungszentrum Jülich
Germany

MÜLLER, Wolfgang
Max Planck Institute for Meteorology
Germany

MULLER, Christian
Belgian Institute for Space Aeronomy
Belgium

MURATA, Akihiko
Japan Agency for Marine-Earth Science and Technology
Japan

MURPHY, Brad
Bureau of Meteorology
Australia

MURPHY, Daniel
National Oceanic and Atmospheric Administration, Earth System Research Laboratory
USA

MUSCHELER, Raimund
Lund University
Sweden

MUTHALAGU, Ravichandran
Indian National Centre for Ocean Information Services
India

MYHRE, Gunnar
Center for International Climate and Environmental Research Oslo
Norway

NABBEFELD, Birgit
DLR German Aerospace Center
Germany

NAIK, Vaishali
National Oceanic and Atmospheric Administration, Geophysical Fluid Dynamics Laboratory
USA

NAKAEGAWA, Tosiyuki
Meteorological Research Institute
Japan

NAKAJIMA, Teruyuki
University of Tokyo
Japan

NASSAR, Ray
Environment Canada
Canada

NAUELS, Alexander
IPCC WGI TSU, University of Bern
Switzerland

NEELIN, J. David
University of California Los Angeles
USA

NESJE, Atle
University of Bergen and Bjerknes Centre for Climate Research
Norway

NEU, Urs
Swiss Academy of Sciences
Switzerland

NEVISON, Cynthia
University of Colorado Boulder
USA

NEWBERY, David
University of Bern
Switzerland

NEWBURY, Thomas Dunning
Amercian Association for the Advancement of Science and U.S. Department of the Interior (retired)
USA

NICHOLLS, Robert
University of Southampton
UK

NITSCHE, Helga
Deutscher Wetterdienst
Germany

NODA, Akira
Japan Agency for Marine-Earth Science and Technology
Japan

OBBARD, Jeffrey
National University of Singapore
Singapore

OBROCHTA, Stephen
University of Tokyo
Japan

O'CONNOR, Fiona
Met Office Hadley Centre
UK

OGREN, John
National Oceanic and Atmospheric Administration, Earth System Research Laboratory
USA

OGURA, Tomoo
National Institute for Environmental Studies
Japan

OHBA, Masamichi
Central Research Institute of Electric Power Industry
Japan

OHMURA, Atsumu
ETH Zurich
Switzerland

OHNEISER, Christian
Shell International B.V.
Netherlands

O'ISHI, Ryouta
University of Tokyo
Japan

OLIVIÉ, Dirk
University of Oslo
Norway

OLIVIER, Jos
Netherlands Environmental Assessment Agency
Netherlands

OOUCHI, Kazuyoshi
Japan Agency for Marine-Earth Science and Technology
Japan

OPPENHEIMER, Michael
Princeton University
USA

OREOPOULOS, Lazaros
National Aeronautics and Space Administration, Goddard Space Flight Center
USA

ORLIC, Mirko
University of Zagreb
Croatia

ORLOWSKY, Boris
ETH Zurich
Switzerland

OSBORN, Timothy
University of East Anglia
UK

OSTROM, Nathaniel
Michigan State University
USA

OVERPECK, Jonathan
University of Arizona
USA

OWENS, John
3M Company
USA

PABÓN-CAICEDO, José Daniel
Universidad Nacional de Colombia
Colombia

PADMAN, Laurence
Earth & Space Research
USA

PALMER, Matthew
Met Office Hadley Centre
UK

PAN, Genxing
Nanjing Agricultural University
China

PANDEY, Dhananjai Kumar
National Centre for Antarctic and Ocean Research
India

PARKER, Albert
University of Ballarat
Australia

PARKER, David
Met Office Hadley Centre
UK

PARRISH, David
National Oceanic and Atmospheric Administration, Earth System Research Laboratory
USA

PASSCHIER, Sandra
Montclair State University
USA

PATTYN, Frank
Université libre de Bruxelles
Belgium

PAUL, Frank
University of Zurich
Switzerland

PAVAN, Valentina
Environmental Agency of Emilia-Romagna
Italy

PAVELSKY, Tamlin
University of North Carolina
USA

PAYNE, Antony
University of Bristol
UK

PAYNTER, David
National Oceanic and Atmospheric Administration, Geophysical Fluid Dynamics Laboratory
USA

PEARSON, David
Met Office Hadley Centre
UK

PEDERSEN, Jens Olaf Pepke
Technical University of Denmark
Denmark

PELEJERO, Carles
Institució Catalana de Recerca i Estudis Avançats and Institut de Ciències del Mar
Spain

PELLIKKA, Hilkka
Finnish Meteorological Institute
Finland

PERLWITZ, Judith
Cooperative Institute for Research in Environmental Sciences
USA

PEROVICH, Donald
Cold Regions Research and Engineering Laboratory
USA

PETERS, Glen
Center for International Climate and Environmental Research Oslo
Norway

PETERS, Karsten
Monash University
Australia

PETIT, Michel
Conseil général de l'Economie,de l'Industrie, de l'Energie et des Technologies
France

PFEFFER, W. Tad
University of Colorado Boulder
USA

PHILIPONA, Rolf
Federal Office of Meteorology and Climatology MeteoSwiss
Switzerland

PIACENTINI, Rubén D.
Universidad Nacional de Rosario
Argentina

PINCUS, Robert
University of Colorado Boulder
USA

PLANTON, Serge
Météo-France
France

PLATTNER, Gian-Kasper
IPCC WGI TSU, University of Bern
Switzerland

PLUMMER, David
Environment Canada
Canada

POERTNER, Hans
Alfred Wegener Institute for Polar and Marine Research
Germany

POHLMANN, Holger
Max Planck Institute for Meteorology
Germany

POITOU, Jean
Laboratoire des Sciences du Climat et de l'Environnement, Institut Pierre Simon Laplace and Société Française de Physique
France

POKHREL, Samir
Indian Institute of Tropical Meteorology
India

POLLACK, Henry
University of Michigan
USA

POLONSKY, Alexander
Marine Hydrophysical Institute
Ukraine

PONGRATZ, Julia
Max Planck Institute for Meteorology
Germany

PORTMANN, Robert
National Oceanic and Atmospheric Administration, Earth System Research Laboratory
USA

POULTER, Benjamin
Laboratoire des Sciences du Climat et de l'Environnement, Institut Pierre Simon Laplace
France

POWER, Scott
Bureau of Meteorology
Australia

PRATHER, Michael
University of California Irvine
USA

PRENTICE, Iain Colin
Macquarie University and Imperial College
Australia

PRINN, Ronald
Massachusetts Institute of Technology
USA

PUEYO, Salvador
Institut Català de Ciències del Clima
Spain

QIAO, Bing
China Waterborne Transport Research Institute
China

QUAAS, Johannes
University of Leipzig
Germany

QUINN, Patricia
National Oceanic and Atmospheric Administration, Pacific Marine Environmental Laboratory
USA

RABATEL, Antoine
Laboratoire de Glaciologie et Géophysique de l`Environnement, Université Joseph Fourier
France

RADIĆ, Valentina
University of British Columbia
Canada

RADUNSKY, Klaus
Umweltbundesamt
Austria

RAHAMAN, Hasibur
Indian National Centre for Ocean Information Services
India

RAHIMZADEH, Fatemeh
Islamic Republic of Iran Meteorological Organization
Iran

RAHMSTORF, Stefan
Potsdam Institute for Climate Impact Research
Germany

RAIBLE, Christoph
University of Bern
Switzerland

RÄISÄNEN, Jouni
University of Helsinki
Finland

RÄISÄNEN, Petri
Finnish Meteorological Institute
Finland

RAJEEVAN, Madhavan Nair
Government of India, Ministry of Earth Sciences
India

RAMASWAMY, Venkatachalam
National Oceanic and Atmospheric Administration, Geophysical Fluid Dynamics Laboratory
USA

RAMSTEIN, Gilles
Laboratoire des Sciences du Climat et de l'Environnement, Institut Pierre Simon Laplace
France

RANDALL, David
Colorado State University
USA

RAPER, Sarah
Manchester Metropolitan University
UK

RASCH, Philip
Pacific Northwest National Laboratory
USA

RAUPACH, Michael
CSIRO Marine and Atmospheric Research
Australia

RAVISHANKARA, A.R.
National Oceanic and Atmospheric Administration, Earth System Research Laboratory
USA

RAWLS, Alec
USA

RAYNER, Nick
Met Office Hadley Centre
UK

RAYNER, Peter
University of Melbourne
Australia

REAY, David
University of Edinburgh
UK

REIS, Stefan
Centre for Ecology & Hydrology
UK

REISINGER, Andy
New Zealand Agricultural GHG Research Centre
New Zealand

REISMAN, John P.
OSS Foundation
USA

REMEDIOS, John
University of Leicester
UK

REMER, Lorraine
National Aeronautics and Space Administration, Goddard Space Flight Center
USA

REN, Guoyu
National Climate Center, China Meteorological Administration
China

RENWICK, James
Victoria University of Wellington
New Zealand

REUTEN, Christian
RWDI AIR Inc.
Canada

RIAHI, Keywan
International Institute for Applied Systems Analysis
Austria

RIBES, Aurélien
Météo-France
France

RIDDICK, Stuart
Cornell University
USA

RIDLEY, Jeff
Met Office Hadley Centre
UK

RIGNOT, Eric
University of California Irvine
USA

RIGOR, Ignatius
University of Washington
USA

RINGEVAL, Bruno
Utrecht University
Netherlands

RITZ, Christoph
Swiss Academy of Sciences
Switzerland

RIVERA, Andrés
Centro de Estudios Científicos
Chile

ROBAA, S.M.
Cairo University
Egypt

ROBERTS, Chris
Met Office Hadley Centre
UK

ROBERTSON, Iain
Swansea University
UK

ROBOCK, Alan
Rutgers University
USA

ROBSON, Jonathan
University of Reading
UK

RODHE, Henning
Stockholm University
Sweden

ROGELJ, Joeri
ETH Zurich
Switzerland

ROHLING, Eelco Johan
National Oceanography Centre
UK

ROJAS, Maisa
Universidad de Chile
Chile

ROMANOVSKY, Vladimir
University of Alaska Fairbanks
USA

RONCHAIL, Josyane
Laboratoire d'Océanographie et du Climat, Institut Pierre Simon Laplace
France

ROSEN, Sergiu Dov
Israel Oceanographic and Limnological Research
Israel

ROSENFELD, Daniel
Hebrew University of Jerusalem
Israel

ROSENLOF, Karen
National Oceanic and Atmospheric Administration, Earth System Research Laboratory
USA

ROTSTAYN, Leon
CSIRO Marine and Atmospheric Research
Australia

ROTT, Helmut
University of Innsbruck
Austria

ROWELL, David
Met Office Hadley Centre
UK

ROY, Indrani
University of Exeter
UK

ROY, Shouraseni
University of Miami
USA

RUMMUKAINEN, Markku
Swedish Meteorological and Hydrological Institute and Lund University
Sweden

RUPP, David
Oregon State University
USA

RUSSELL, Andrew
Brunel University
UK

RUTI, Paolo Michele
Italian National Agency for New Technologies, Energy and Sustainable Economic Development
Italy

SAHU, Lokesh Kumar
Physical Research Laboratory
India

SAKAGUCHI, Koichi
University of Arizona
USA

SALAS Y MELIA, David
Météo-France
France

SALZMANN, Nadine
University of Zurich and University of Fribourg
Switzerland

SAMANTA, Arindam
Atmospheric and Environmental Research
USA

SANCHEZ GOÑI, Maria Fernanda
Université Bordeaux 1
France

SANDERSON, Benjamin
National Center for Atmospheric Research
USA

SANYAL, Swarnali
University of Illinois
USA

SAROFIM, Marcus
U.S. Environmental Protection Agency
USA

SATHEESH, S.K.
Indian Institute of Science
India

SATOH, Masaki
University of Tokyo
Japan

SAUCHYN, David
University of Regina
Canada

SAULO, Celeste
Universidad de Buenos Aires
Argentina

SAUNDERS, Roger
Met Office Hadley Centre
UK

SAUSEN, Robert
DLR German Aerospace Center
Germany

SAVOLAINEN, Ilkka
VTT Technical Research Centre of Finland
Finland

SCAIFE, Adam
Met Office Hadley Centre
UK

SCHMID, Beat
Pacific Northwest National Laboratory
USA

SCHMIDT, Gavin
National Aeronautics and
Space Administration, Goddard
Institute for Space Studies
USA

SCHNEEBELI, Martin
WSL Institute for Snow and
Avalanche Research SLF
Switzerland

SCHNEIDER, Johannes
Max Planck Institute for Chemistry
Germany

SCHOENWIESE, Christian-D.
Goethe University
Germany

SCHOLES, Robert
Council for Scientific and Industrial Research
South Africa

SCHRAMA, Ernst
Delft University of Technology
Netherlands

SCHULZ, Michael
Norwegian Meteorological Institute
Norway

SCHUMANN, Ulrich
DLR German Aerospace Center
Germany

SCHUSTER, Gregory
National Aeronautics and Space
Administration, Langley Research Center
USA

SCHUUR, Edward
University of Florida
USA

SCHWARTZ, Stephen E.
Brookhaven National Laboratory
USA

SCHWARZKOPF, M. Daniel
National Oceanic and Atmospheric
Administration, Geophysical
Fluid Dynamics Laboratory
USA

SCHWEIGER, Axel
University of Washington
USA

SEDLÁČEK, Jan
ETH Zurich
Switzerland

SEHAT KASHANI, Saviz
Islamic Azad University
Iran

SEIBERT, Petra
University of Vienna
Austria

SEIDEL, Dian
National Oceanic and Atmospheric
Administration, Air Resources Laboratory
USA

SELVARAJ, Kandasamy
Xiamen University
China

SEN, Omer L.
Istanbul Technical University
Turkey

SENEVIRATNE, Sonia
ETH Zurich
Switzerland

SENSOY, Serhat
Turkish State Meteorological Service
Turkey

SENTMAN, Lori
National Oceanic and Atmospheric
Administration, Geophysical
Fluid Dynamics Laboratory
USA

SERPIL, Yaäžan
Turkish State Meteorological Service
Turkey

SETH, Anji
University of Connecticut
USA

SEXTON, David
Met Office Hadley Centre
UK

SHAO, Andrew
University of Washington
USA

SHAO, XueMei
Institute of Geographic Sciences
and Natural Resources Research,
Chinese Academy of Sciences
China

SHELL, Karen
Oregon State University
USA

SHERWIN, Toby
Scottish Association for Marine Science
UK

SHERWOOD, Steven
University of New South Wales
Australia

SHEVLIAKOVA, Elena
Princeton University
USA

SHI, Zongbo
University of Birmingham
UK

SHIBATA, Kiyotaka
Meteorological Research Institute
Japan

SHINDELL, Drew
National Aeronautics and
Space Administration, Goddard
Institute for Space Studies
USA

SHINE, Keith
University of Reading
UK

SHIOGAMA, Hideo
National Institute for Environmental Studies
Japan

SHKOLNIK, Igor
Voeikov Main Geophysical Observatory
Russian Federation

SHMAKIN, Andrey
Russian Academy of Sciences
Russian Federation

SHUMAN, Bryan
University of Wyoming
USA

SICRE, Marie-Alexandrine
Laboratoire des Sciences du Climat et de
l'Environnement, Institut Pierre Simon Laplace
France

SIDDALL, Mark
University of Bristol
UK

SIEGLE, Eduardo
Universidade de São Paulo
Brazil

SIEVERING, Herman
National Oceanic and Atmospheric Administration, Earth System Research Laboratory and University of Colorado Boulder
USA

SILLMANN, Jana
Environment Canada
Canada

SIMMONDS, Ian
University of Melbourne
Australia

SIMMONS, Adrian
European Centre for Medium-Range Weather Forecasts
UK

SINGER, S. Fred
University of Virginia
USA

SLANGEN, Aimée
Utrecht University
Netherlands

SMEDSRUD, Lars Henrik
Bjerknes Centre for Climate Research
Norway

SMITH, Doug
Met Office Hadley Centre
UK

SMITH, Ian
CSIRO Marine and Atmospheric Research
Australia

SMITH, Leonard
London School of Economics and Political Science
UK

SMITH, Sharon
Natural Resources Canada
Canada

SMITH, Stephen
Committee on Climate Change
UK

SMITH, Stephen G.G.
UK

SMITH, Steven
Pacific Northwest National Laboratory
USA

SNIDERMAN, Kale
University of Melbourne
Australia

SOLOMINA, Olga
Russian Academy of Sciences
Russian Federation

SOLOMON, Susan
Massachusetts Institute of Technology
USA

SOMERVILLE, Richard
Scripps Institution of Oceanography
USA

SONG, Shaojie
Massachusetts Institute of Technology
USA

SPAHNI, Renato
University of Bern
Switzerland

SPARRENBOM, Charlotte
Lund University
Sweden

SPARROW, Michael
Scientific Committee on Antarctic Research
UK

SPORYSHEV, Petr
Voeikov Main Geophysical Observatory
Russian Federation

SRIKANTHAN, Ramachandran
Physical Research Laboratory
India

SRIVER, Ryan
University of Illinois
USA

SROKOSZ, Meric
National Oceanography Centre
UK

STAGER, Jay Curt
Paul Smith's College
USA

STAHLE, David
University of Arkansas
USA

STAINFORTH, David
London School of Economics and Political Science
UK

STEBLER, Oliver
ETH Zurich
Switzerland

STEIG, Eric
University of Washington
USA

STEINFELDT, Reiner
University of Bremen
Germany

STENDEL, Martin
Danish Meteorological Institute
Denmark

STEPEK, Andrew
Royal Netherlands Meteorological Institute
Netherlands

STEPHENS, Graeme
National Aeronautics and Space Administration, Jet Propulsion Laboratory
USA

STEPHENSON, David
University of Exeter
UK

STERL, Andreas
Royal Netherlands Meteorological Institute
Netherlands

STERN, Harry
University of Washington
USA

STEVENSON, David
University of Edinburgh
UK

STEWART, Ronald
University of Manitoba
Canada

STIER, Philip
University of Oxford
UK

STÖBER, Uwe
University of Bremen
Germany

STOCKDALE, Timothy
European Centre for Medium-Range Weather Forecasts
UK

STOCKER, Benjamin
University of Bern
Switzerland

STOCKER, Thomas F.
Co-Chair IPCC WGI, University of Bern
Switzerland

STONE, Dáithí
Lawrence Berkeley National Laboratory
USA

STONE, Reynold
University of the West Indies
Trinidad and Tobago

STOTT, Peter
Met Office Hadley Centre
UK

STOUFFER, Ronald
National Oceanic and Atmospheric Administration, Geophysical Fluid Dynamics Laboratory
USA

STOY, Paul
Montana State University
USA

STRAUSS, Benjamin
Climate Central
USA

STUBENRAUCH, Claudia
Laboratoire de Météorologie Dynamique, Institut Pierre Simon Laplace
France

STUMM, Dorothea
International Centre for Integrated Mountain Development
Nepal

SU, Hui
National Aeronautics and Space Administration, Jet Propulsion Laboratory
USA

SUBRAMANIAN, Aneesh
Scripps Institution of Oceanography
USA

SUGI, Masato
Japan Agency for Marine-Earth Science and Technology
Japan

SUGIYAMA, Masahiro
Central Research Institute of Electric Power Industry
Japan

SUN, Jianqi
Institute of Atmospheric Physics, Chinese Academy of Sciences
China

SUN, Junying
Chinese Academy of Meteorological Sciences, China Meteorological Administration
China

SUNDQUIST, Eric
U.S. Geological Survey
USA

SUTTON, Rowan
University of Reading
UK

SVENSSON, Gunilla
Stockholm University
Sweden

SWEENEY, Conor
University College Dublin
Ireland

SWIETLICKI, Erik
Lund University
Sweden

SWINGEDOUW, Didier
Laboratoire des Sciences du Climat et de l'Environnement, Institut Pierre Simon Laplace
France

TACHIIRI, Kaoru
Japan Agency for Marine-Earth Science and Technology
Japan

TAKAHASHI, Ken
Instituto Geofísico del Perú
Peru

TAKAHASHI, Kiyoshi
National Institute for Environmental Studies
Japan

TAKAYABU, Izuru
Meteorological Research Institute
Japan

TAKAYABU, Yukari
University of Tokyo
Japan

TAKEMURA, Toshihiko
Kyushu University
Japan

TALARICO, Franco
University of Siena
Italy

TALLAKSEN, Lena M.
University of Oslo
Norway

TAMISIEA, Mark
National Oceanography Centre
UK

TANAKA, Hiroshi
University of Tsukuba
Japan

TANAKA, Katsumasa
ETH Zurich
Switzerland

TANG, Qi
Cornell University
USA

TAPIADOR, Francisco J.
Universidad de Castilla-La Mancha
Spain

TARASOV, Lev
Memorial University of Newfoundland
Canada

TAYLOR, Jeffrey
National Ecological Observatory Network
USA

TELFORD, Richard
University of Bergen
Norway

TERRAY, Laurent
Centre Européen de Recherche et de Formation Avancée en Calcul Scientifique
France

TETT, Simon
University of Edinburgh
UK

THIELEN, Dirk
Instituto Venezolano de Investigaciones Científicas
Venezuela

THOMAS, Robert
SIGMA Space
USA

THOMASON, Larry
National Aeronautics and Space Administration, Langley Research Center
USA

THOMPSON, Erica
London School of Economics and Political Science
UK

THOMPSON, Rona
Norwegian Institute for Air Research
Norway

THORNE, Peter
National Oceanic and Atmospheric Administration, National Climatic Data Center
USA

TIAN, Jian
University of Illinois
USA

TIGNOR, Melinda
IPCC WGI TSU, University of Bern
Switzerland

TILYA, Faustine Fidelis
Tanzania Meteorological Agency
United Republic Of Tanzania

TITUS, James G.
U.S. Environmental Protection Agency
USA

TKALICH, Pavel
National University of Singapore
Singapore

TOKINAGA, Hiroki
University of Hawaii
USA

TOMASEK, Bradley
University of Illinois
USA

TOMOZEIU, Rodica
Environmental Agency of Emilia-Romagna
Italy

TONITTO, Christina
Cornell University
USA

TOTTERDELL, Ian
Met Office Hadley Centre
UK

TRAINER, Michael
National Oceanic and Atmospheric Administration, Earth System Research Laboratory
USA

TRANVIK, Lars
Uppsala University
Sweden

TRENBERTH, Kevin
National Center for Atmospheric Research
USA

TROUET, Valerie
University of Arizona
USA

TSUSHIMA, Yoko
Met Office Hadley Centre
UK

TSUTSUI, Junichi
Central Research Institute of Electric Power Industry
Japan

TURCQ, Bruno
Institut de Recherche pour le Développement
France

TURNER, Andrew
University of Reading
UK

TZEDAKIS, Chronis
University College London
UK

UNNINAYAR, Sushel
National Aeronautics and Space Administration, Goddard Space Flight Center
USA

URREGO, Dunia H.
Université Bordeaux 1
France

VAN DEN HURK, Bart
Royal Netherlands Meteorological Institute
Netherlands

VAN DER LINDEN, Paul
Met Office Hadley Centre
UK

VAN DER WERF, Guido
VU University Amsterdam
Netherlands

VAN HUISSTEDEN, Ko
VU University Amsterdam
Netherlands

VAN KESTEREN, Line
IPCC Synthesis Report TSU
Netherlands

VAN NOIJE, Twan
Royal Netherlands Meteorological Institute
Netherlands

VAN OLDENBORGH, Geert Jan
Royal Netherlands Meteorological Institute
Netherlands

VAN OMMEN, Tasman
Australian Antarctic Division
Australia

VAN VELTHOVEN, Peter
Royal Netherlands Meteorological Institute
Netherlands

VAN WEELE, Michiel
Royal Netherlands Meteorological Institute
Netherlands

VAN YPERSELE, Jean-Pascal
Université catholique de Louvain
Belgium

VANAGS, Andrejs
The Space Exploration Society
USA

VAQUERO, José Manuel
Universidad de Extremadura
Spain

VAUGHAN, David
British Antarctic Survey
UK

VAUGHAN, Naomi
University of East Anglia
UK

VELDERS, Guus
National Institute for Public Health and the Environment
Netherlands

VERHEGGEN, Bart
ECN Energy Research Institute of the Netherlands
Netherlands

VERHOEF, Anne
University of Reading
UK

VERLEYEN, Elie
Ghent University
Belgium

VIDAL, Jean-Philippe
Institut National de Recherche en Sciences et Technologies pour l'Environnement et l'Agriculture
France

VIGNATI, Elisabetta
European Commission Joint Research Centre
Italy

VINITNANTHARAT, Soydoa
King Mongkut's University of Technology Thonburi
Thailand

VISSER, Hans
PBL Netherlands Environmental Assessment Agency
Netherlands

VOIGT, Thomas
Federal Environment Agency
Germany

VOLLMER, Martin
Swiss Federal Laboratories for Materials Science and Technology EMPA
Switzerland

VON SCHUCKMANN, Karina
Institut Français de Recherche pour l'Exploitation de la Mer
France

WAGNON, Patrick
Laboratoire de Glaciologie et Géophysique de l`Environnement, Université Joseph Fourier
France

WAHL, Eugene
National Oceanic and Atmospheric Administration, National Climatic Data Center
USA

WAHL, Terje
Norwegian Space Centre
Norway

WAHL, Thomas
University of Siegen
Germany

WALISER, Duane
National Aeronautics and Space Administration, Jet Propulsion Laboratory
USA

WALLINGTON, Timothy
Ford Motor Company
USA

WALTER, Andreas
Deutscher Wetterdienst
Germany

WANG, Bin
Institute of Atmospheric Physics, Chinese Academy of Sciences and Tsinghua University
China

WANG, Chien
Massachusetts Institute of Technology
USA

WANG, Dongxiao
South China Sea Institute of Oceanology, Chinese Academy of Sciences
China

WANG, Hailong
Pacific Northwest National Laboratory
USA

WANG, Junye
Rothamsted Research
UK

WANG, Kaicun
Beijing Normal University
China

WANG, Minghuai
Pacific Northwest National Laboratory
USA

WANG, Pinxian
Tongji University
China

WANG, Shaowu
Peking University
China

WANG, Tijian
Nanjing University
China

WANG, Ting
Lehigh University
USA

WANG, Xiaolan
Environment Canada
Canada

WANG, Xuemei
Sun Yat-sen University
China

WANG, Yingping
CSIRO Marine and Atmospheric Research
Australia

WANG, Yongguang
National Climate Center, China Meteorological Administration
China

WANG, Zhaomin
Nanjing University of Information Science and Technology
China

WANLISS, James
Presbyterian College
USA

WANNER, Heinz
University of Bern
Switzerland

WATERLAND, Robert
E. I. du Pont de Nemours & Co. Inc.
USA

WATSON, Phil
NSW Government Office of Environment and Heritage
Australia

WATSON, Thomas
Australia

WATTERSON, Ian
CSIRO Marine and Atmospheric Research
Australia

WEBB, David
National Oceanography Centre
UK

WEBB, Mark
Met Office Hadley Centre
UK

WEBB, Robert
National Oceanic and Atmospheric Administration, Earth System Research Laboratory
USA

WEEDON, Graham
Met Office Hadley Centre
UK

WEISHEIMER, Antje
European Centre for Medium-Range Weather Forecasts
UK

WEISS, Jérôme
Laboratoire de Glaciologie et Géophysique de l`Environnement, Université Joseph Fourier
France

WEISSE, Ralf
Helmholtz-Zentrum Geesthacht
Germany

WENDISCH, Manfred
University of Leipzig
Germany

WESTRA, Seth
University of Adelaide
Australia

WEYHENMEYER, Gesa
Uppsala University
Sweden

WHETTON, Penny
CSIRO Marine and Atmospheric Research
Australia

WHITE, Neil
CSIRO Marine and Atmospheric Research
Australia

WIELICKI, Bruce
National Aeronautics and Space Administration, Langley Research Center
USA

WILD, Oliver
Lancaster University
UK

WILLETT, Kate
Met Office Hadley Centre
UK

WILLIAMS, Keith
Met Office Hadley Centre
UK

WILLIAMS, Paul
University of Reading
UK

WILLIAMS, Richard G.
Liverpool University
UK

WILLIAMS, S. Jeffress
U.S. Geological Survey
USA

WILSON, Rob
University of St Andrews
UK

WITTENBERG, Andrew
National Oceanic and Atmospheric Administration, Geophysical Fluid Dynamics Laboratory
USA

WOLFF, Eric
British Antarctic Survey
UK

WOOD, Richard
Met Office Hadley Centre
UK

WOOD, Robert
University of Washington
USA

WOODS, Thomas
University of Colorado Boulder
USA

WOODWORTH, Philip
National Oceanography Centre
UK

WORDEN, Helen
National Center for Atmospheric Research
USA

WRATT, David
National Institute of Water and Atmospheric Research
New Zealand

WU, Tonghua
Cold and Arid Regions Environmental and Engineering Research Institute, Chinese Academy of Sciences
China

WURZLER, Sabine
Landesamt für Natur, Umwelt und Verbraucherschutz NRW
Germany

XIA, Chaozong
State Forestry Administration
China

XIA, Yu
IPCC WGI TSU, University of Bern
Switzerland

XIE, Shang-Ping
Scripps Institution of Oceanography
USA

XU, Chong-Yu
University of Oslo
Norway

XU, Kuan-Man
National Aeronautics and Space Administration, Langley Research Center
USA

XU, Xiaobin
Chinese Academy of Meteorological Sciences, China Meteorological Administration
China

XU, Ying
National Climate Center, China Meteorological Administration
China

XU, Yongfu
Institute of Atmospheric Physics, Chinese Academy of Sciences
China

YABI, Ibouraïma
Université d'Abomey Calavi
Benin

YASUNARI, Tetsuzo
Nagoya University
Japan

YDE, Jacob Clement
Sogn og Fjordane University College
Norway

YOKOUCHI, Yoko
National Institute for Environmental Studies
Japan

YOSHIMORI, Masakazu
University of Tokyo
Japan

YU, Rucong
China Meteorological Administration
China

YU, Zicheng
Lehigh University
USA

YUKIMOTO, Seiji
Meteorological Research Institute
Japan

ZAEHLE, Sönke
Max Planck Institute for Biogeochemistry
Germany

ZAHN, Matthias
University of Reading
UK

ZAPPA, Giuseppe
University of Reading
UK

ZEMP, Michael
University of Zurich
Switzerland

ZENG, Xubin
University of Arizona
USA

ZHANG, Chengyi
National Climate Center, China Meteorological Administration
China

ZHANG, De-er
National Climate Center, China Meteorological Administration
China

ZHANG, Gan
University of Illinois
USA

ZHANG, Guang
Scripps Institution of Oceanography
USA

ZHANG, Hua
National Climate Center, China Meteorological Administration
China

ZHANG, Rong
National Oceanic and Atmospheric Administration, Geophysical Fluid Dynamics Laboratory
USA

ZHANG, Tianyu
National Marine Environmental Forecasting Center
China

ZHANG, Xiangdong
University of Alaska Fairbanks
USA

ZHANG, Xuebin
CSIRO Marine and Atmospheric Research
Australia

ZHANG, Xuebin
Environment Canada
Canada

ZHAO, Xuepeng (Tom)
National Oceanic and Atmospheric Administration, National Climatic Data Center
USA

ZHAO, Zong-Ci
National Climate Center, China Meteorological Administration
China

ZHENG, Jingyun
Institute of Geographic Sciences and Natural Resources Research, Chinese Academy of Sciences
China

ZHOU, Guangsheng
Chinese Academy of Meteorological Sciences, China Meteorological Administration
China

ZHOU, Limin
East China Normal University
China

ZHOU, Tianjun
Institute of Atmospheric Physics, Chinese Academy of Sciences
China

ZHU, Bin
Nanjing University of Information Science and Technology
China

ZICKFELD, Kirsten
Simon Fraser University
Canada

ZORITA, Eduardo
Helmholtz-Zentrum Geesthacht
Germany

ZUIDEMA, Paquita
University of Miami
USA

ZUO, Juncheng
HoHai University
China

ZWEIFEL, Roman
Swiss Federal Institute for Forest, Snow and Landscape Research WSL
Switzerland

ZWIERS, Francis
University of Victoria
Canada

Index

This index should be cited as:
IPCC, 2013: Index. In: *Climate Change 2013: The Physical Science Basis. Contribution of Working Group I to the Fifth Assessment Report of the Intergovernmental Panel on Climate Change* [Stocker, T.F., D. Qin, G.-K. Plattner, M. Tignor, S.K. Allen, J. Boschung, A. Nauels, Y. Xia, V. Bex and P.M. Midgley (eds.)]. Cambridge University Press, Cambridge, United Kingdom and New York, NY, USA.

*Note: * indicates the term also appears in the Glossary (Annex III). Bold page numbers indicate page spans for entire chapters. Italicized page numbers denote tables, figures and boxed material.*

A

D

O

P

Q

R

T